frontiers | Research Topics

Emerging talents in pharmacology of anti-cancer drugs 2022

Edited by
Husain Yar Khan, Khuloud Bajbouj and Mai F. Tolba

Published in
Frontiers in Pharmacology
Frontiers in Oncology

ISSN 1664-8714
ISBN 978-2-8325-2330-8
DOI 10.3389/978-2-8325-2330-8

About Frontiers

Frontiers is more than just an open access publisher of scholarly articles: it is a pioneering approach to the world of academia, radically improving the way scholarly research is managed. The grand vision of Frontiers is a world where all people have an equal opportunity to seek, share and generate knowledge. Frontiers provides immediate and permanent online open access to all its publications, but this alone is not enough to realize our grand goals.

Frontiers journal series

The Frontiers journal series is a multi-tier and interdisciplinary set of open-access, online journals, promising a paradigm shift from the current review, selection and dissemination processes in academic publishing. All Frontiers journals are driven by researchers for researchers; therefore, they constitute a service to the scholarly community. At the same time, the *Frontiers journal series* operates on a revolutionary invention, the tiered publishing system, initially addressing specific communities of scholars, and gradually climbing up to broader public understanding, thus serving the interests of the lay society, too.

Dedication to quality

Each Frontiers article is a landmark of the highest quality, thanks to genuinely collaborative interactions between authors and review editors, who include some of the world's best academicians. Research must be certified by peers before entering a stream of knowledge that may eventually reach the public - and shape society; therefore, Frontiers only applies the most rigorous and unbiased reviews. Frontiers revolutionizes research publishing by freely delivering the most outstanding research, evaluated with no bias from both the academic and social point of view. By applying the most advanced information technologies, Frontiers is catapulting scholarly publishing into a new generation.

What are Frontiers Research Topics?

Frontiers Research Topics are very popular trademarks of the *Frontiers journals series*: they are collections of at least ten articles, all centered on a particular subject. With their unique mix of varied contributions from Original Research to Review Articles, Frontiers Research Topics unify the most influential researchers, the latest key findings and historical advances in a hot research area.

Find out more on how to host your own Frontiers Research Topic or contribute to one as an author by contacting the Frontiers editorial office: frontiersin.org/about/contact

Emerging talents in pharmacology of anti-cancer drugs 2022

Topic editors

Husain Yar Khan — Wayne State University, United States

Khuloud Bajbouj — University of Sharjah, United Arab Emirates

Mai F. Tolba — Ain Shams University, Egypt

Citation

Khan, H. Y., Bajbouj, K., Tolba, M. F., eds. (2023). *Emerging talents in pharmacology of anti-cancer drugs 2022*. Lausanne: Frontiers Media SA.

doi: 10.3389/978-2-8325-2330-8

Table of contents

frontiers | Frontiers in Pharmacology

TYPE Editorial
PUBLISHED 19 April 2023
DOI 10.3389/fphar.2023.1191321

OPEN ACCESS

EDITED AND REVIEWED BY
Olivier Feron,
Université catholique de Louvain,
Belgium

*CORRESPONDENCE
Mai F. Tolba,
tolba.mf@pharma.asu.edu.eg

SPECIALTY SECTION
This article was submitted to Pharmacology of Anti-Cancer Drugs, a section of the journal Frontiers in Pharmacology

RECEIVED 21 March 2023
ACCEPTED 27 March 2023
PUBLISHED 19 April 2023

CITATION
Khan HY, Bajbouj K and Tolba MF (2023), Editorial: Emerging talents in pharmacology of anti-cancer drugs 2022.
Front. Pharmacol. 14:1191321.
doi: 10.3389/fphar.2023.1191321

Editorial: Emerging talents in pharmacology of anti-cancer drugs 2022

Husain Yar Khan[1], Khuloud Bajbouj[2,3] and Mai F. Tolba[4,5]*

[1]Karmanos Cancer Institute, Wayne State University School of Medicine, Detroit, MI, United States, [2]College of Medicine, University of Sharjah, Sharjah, United Arab Emirates, [3]Research Institute for Medical and Health Sciences, University of Sharjah, Sharjah, United Arab Emirates, [4]CNIO-Spanish National Cancer Research Center, Melchor Fernandez Almagro, Madrid, Spain, [5]Department of Pharmacology and Toxicology, Faculty of Pharmacy, Ain Shams University, Cairo, Egypt

KEYWORDS

breast cancer, hepatocellular carcinoma, colon cancer, pancreatic cancer, lung cancer

Editorial on the Research Topic
Emerging talents in pharmacology of anti-cancer drugs 2022

Continuous research efforts have significantly unraveled fundamental molecular pathways that have contributed to paving the way for the development of a multitude of therapeutic strategies, which have and expanded the arsenal of weapons against cancer. This has been tremendously reflected on the uplifting of the cancer survival curve and the improvement of the quality of life of cancer patients. The Research Topic herein was dedicated to highlighting the emerging talents of student researchers pursuing studies in the area of pharmacology of anticancer drugs. The articles in this Research Topic have shed light on the quality and diversity of student researchers across this field and focused on three main themes: 1) Remodeling Cancer Epigenome: Therapeutic Advances; 2) Cancer Immunosurveillance: From Mechanisms to Therapy; 3) Anticancer Drug Discovery and Translational Oncology. The studies herein include two reports of clinical trials by Tan et al. and Zhu et al. A diversity of preclinical/translational research studies were also presented in the Research Topic. Lozon et al. presented a novel chemotherapy combination that was validated *in vitro* in colon cancer and lung cancer cell lines. Abdollah et al., Yang et al., and Lee et al. highlighted a promising anticancer activity for a variety of natural products against hepatocellular carcinoma. On the other hand, the work of Lee et al., Lin et al., Irshad et al., and Kuttikrishnan et al. presented mechanistic insights in pancreatic cancer, breast cancer, non-small-cell lung cancer, and leukemia. The Research Topic also encompasses two literature reviews by Bannoura et al. and Yuan et al.

Trastuzumab deruxtecan (T-DXd), an antibody–drug conjugate, has shown antitumor activity in patients with HER2-low advanced breast cancer (ABC) in clinical trials. However, the cost-effectiveness of T-DXd was not clearly established. In order to determine whether the benefits of this treatment outweigh its costs, Zhu et al. employed a Markov decision-analytic model to compare the cost-effectiveness of T-DXd with chemotherapy in HER2-low ABC patients. While T-DXd showed improved quality-adjusted life years (QALYs), its incorporation led to increased costs and an unfavorable incremental cost-effectiveness ratio (ICER) compared to chemotherapy, making it devoid of cost-effectiveness in HER2-low ABC patients in the United States. The authors, however, believe that it may still provide health benefits to patients with HR+/HER2-low ABC.

In their case report, Tan et al. suggested that pembrolizumab plus nab-paclitaxel might be a potential treatment option for patients with cholangiocarcinoma (CCA), which is a

highly aggressive malignancy with poor overall survival. In this report, a metastatic extrahepatic CCA patient achieved durable response and good tolerance to a combination treatment of pembrolizumab plus nab-paclitaxel following progression on a chemotherapy of gemcitabine and capecitabine.

Lozon et al. contributed an original article highlighting the importance of safranal (SAF) as a promising candidate-sensitizing agent of human colon cancer cells (HCT116) and lung cancer cells (A549) to the cytotoxic effect of the topoisomerase inhibitor topotecan (TPT). The combination augmented TPT-induced alterations in DNA repair and boosted the incidence of double-strand breaks with subsequent induction of apoptosis. The sensitization only occurred when the cells were pretreated with SAF 24 h before TPT treatment. However, simultaneous exposure or adding SAF 24 h after TPT did not recapitulate the same results. Hence, the effect was sequence dependent.

An article by Abdollah et al. aimed to determine whether fucoidan's chemomodulatory benefits may be enhanced by using it in combination with the FDA-approved antiangiogenic drugs sorafenib and Avastin (bevacizumab) in order to augment their anticancer activity in hepatocellular carcinoma (HCC) cells. The authors reported that the combination treatment inhibited the PI3K/AKT/mTOR and KRAS/BRAF/MAPK pathways in addition to apoptosis induction in HCC both *in vitro and in vivo*.

Yang et al. identified a potential pharmacological mechanism by which Ganji Fang (GJF) can treat HCC at the systemic level. The underlying mechanisms were shown to involve immune control, cell migration, cell proliferation, apoptosis, and inflammation induction. Furthermore, it was demonstrated that the G0/G1 phase cycle arrest subsequent to the apoptosis after GJF treatment in liver cancer cells was triggered by blocking the PI3K/Akt signaling pathway. Pachymic acid has been shown to be the significant active component of GJF that exhibits anticancer action, and EPHA2 may be a potential key target for GJF in HCC.

It was previously found that white genius mushroom (WGM), a popular edible mushroom in Taiwan, mediates strong antiproliferative activities against human Hep3B liver cancer cells. However, the underlying mechanisms have not been fully investigated. Lee et al. reported that WGM extracts induced cell death by targeting mTOR and MAPK signaling pathways in liver cancer cells, suggesting that they could be used as a pharmacologically safe natural dietary chemopreventive agent for HCC treatment.

The article by Lee et al. investigated the efficacy and molecular mechanisms of ivermectin/gemcitabine combination in pancreatic cancer. They observed that a combination treatment of ivermectin and gemcitabine suppressed pancreatic cancer both *in vitro* and *in vivo* more effectively than gemcitabine alone. Mechanistically, this combination was found to exert its effects by inhibiting cell proliferation *via* G1 cell cycle arrest and augmenting apoptosis by inducing mitochondrial dysfunction. Based on these findings, the study concluded that ivermectin, an antiparasitic drug, can exhibit synergistic effects with gemcitabine and may be repurposed to serve as a promising therapeutic agent for pancreatic cancer therapy.

Lin et al. demonstrated the anticancer effects of gallic acid, a phenolic acid known for its antioxidant properties, against triple-negative breast cancer cells *in vitro*. The study showed that gallic acid was able to inhibit the growth of HCC1806 cells and stimulate their apoptosis by triggering the production of reactive oxygen species, which modulate the PI3K/AKT/EGFR and MAPK signaling pathways.

Irshad et al. employed integrative network pharmacology, molecular docking, and *in vitro* experiments to elucidate the mechanism of action of glycyrrhetinic acid (18α-GA), a triterpenoid found in licorice against non-small-cell lung cancer (NSCLC). Their network pharmacology study identified EGFR, AKT1, PI3KR1, MAPK1, IGF1, and SRC as crucial hub targets for 18α-GA against NSCLC. The authors further showed that 18α-GA augmented G1 cell cycle arrest, triggered apoptosis, reduced the migratory potential, and inhibited the EGFR-PI3K/AKT pathway in NSCLC cell lines.

Kuttikrishnan et al. explored the role of neosetophomone-B (NSP-B), a meroterpenoid fungal secondary metabolite, on the FOXM1/BUB1B signaling pathway. The development and progression of various types of cancer, including chronic myelogenous leukemia, have been linked to the abnormal expression of FOXM1 and BUB1B genes. A TCGA data analysis elaborated that BUB1B is overexpressed in most cancers and linked with poor prognosis. Using gene expression profiling, the authors showed the significant downregulation of BUB1B in leukemia cells treated with NSP-B. In addition, they validated their *in silico* findings *in vitro* by showing that NSP-B suppresses the expression of FOXM1 and BUB1B in a dose-dependent manner, leading to compromised cell viability and apoptosis induction in leukemia cells.

The minireview by Bannoura et al. summarized the recent data on targeting KRAS G12D, which is among the most common mutations (45%) in pancreatic cancer that are associated with poor prognosis. The article discussed several modalities under development for targeting KRAS G12D, including small molecule inhibitors and immunotherapy.

Yuan et al. contributed a bibliometric article of the literature from the Web of Science Core Research Topic (2002–2021) on the emerging trends and research foci of the natural compound berberine in cancer. Berberine is a multitarget Chinese medicine monomer compound that is extensively studied for its antitumor/antiproliferative effects and its capacity to sensitize cancer cells to chemotherapy. The collected data showed that berberine exhibits anticancer capacity through a diversity of mechanisms, including halting the cell cycle, inhibition of tumor cell invasion and migration, and inducing autophagy and apoptotic cell death.

Author contributions

All authors listed have made a substantial, direct, and intellectual contribution to the work and approved it for publication.

Conflict of interest

The authors declare that the research was conducted in the absence of any commercial or financial relationships that could be construed as a potential conflict of interest.

Publisher's note

frontiers | Frontiers in Oncology

ORIGINAL RESEARCH
published: 01 July 2022
doi: 10.3389/fonc.2022.929996

Bioinformatics Analysis Reveals FOXM1/BUB1B Signaling Pathway as a Key Target of Neosetophomone B in Human Leukemic Cells: A Gene Network-Based Microarray Analysis

Shilpa Kuttikrishnan[1,2†], Tariq Masoodi[3†], Gulab Sher[1], Ajaz A. Bhat[3], Kalyani Patil[1], Tamam El-Elimat[4], Nicholas H. Oberlies[5], Cedric J. Pearce[6], Mohmmad Haris[3,7], Aamir Ahmad[1,8], Feras Q. Alali[2] and Shahab Uddin[1,7,8]*

[1] Translational Research Institute, Academic Health System, Hamad Medical Corporation, Doha, Qatar, [2] College of Pharmacy, Qatar University, Doha, Qatar, [3] Laboratory of Molecular and Metabolic Imaging, Cancer Research Department, Sidra Medicine, Doha, Qatar, [4] Department of Medicinal Chemistry and Pharmacognosy, Faculty of Pharmacy, Jordan University of Science and Technology, Irbid, Jordan, [5] Department of Chemistry and Biochemistry, University of North Carolina at Greensboro, Greensboro, NC, United States, [6] Mycosynthetix, Inc., Hillsborough, NC, United States, [7] Laboratory of Animal Research Center, Qatar University, Doha, Qatar, [8] Dermatology Institute, Academic Health System, Hamad Medical Corporation, Doha, Qatar

OPEN ACCESS

Edited by:
Husain Yar Khan,
Wayne State University, United States

Reviewed by:
Nagaraj Nagathihalli,
University of Miami Health System, United States
Mohd Wasim Nasser,
University of Nebraska Medical Center, United States

***Correspondence:**
Shahab Uddin
SKhan34@hamad.qa

[†]These authors have contributed equally to this work

Specialty section:
This article was submitted to Pharmacology of Anti-Cancer Drugs, a section of the journal Frontiers in Oncology

Received: 27 April 2022
Accepted: 16 May 2022
Published: 01 July 2022

Citation:
Kuttikrishnan S, Masoodi T, Sher G, Bhat AA, Patil K, El-Elimat T, Oberlies NH, Pearce CJ, Haris M, Ahmad A, Alali FQ and Uddin S (2022) Bioinformatics Analysis Reveals FOXM1/BUB1B Signaling Pathway as a Key Target of Neosetophomone B in Human Leukemic Cells: A Gene Network-Based Microarray Analysis. Front. Oncol. 12:929996. doi: 10.3389/fonc.2022.929996

Abnormal expression of Forkhead box protein M1 (FOXM1) and serine/threonine kinase Budding uninhibited by benzimidazoles 1 (BUB1B) contributes to the development and progression of several cancers, including chronic myelogenous leukemia (CML). However, the molecular mechanism of the FOXM1/BUB1B regulatory network and the role of Neosetophomone-B (NSP-B) in leukemia remains unclear. NSP-B, a meroterpenoid fungal secondary metabolite, possesses anticancer potential in human leukemic cells lines; however, the underlying mechanism has not been elucidated. The present study aimed to explore the role of NSP-B on FOXM1/BUB1B signaling and the underlying molecular mechanism of apoptosis induction in leukemic cells. We performed gene expression profiling of NSP-B-treated and untreated leukemic cells to search for differentially expressed genes (DEGs). Interestingly *BUB1B* was found to be significantly downregulated (logFC -2.60, adjusted p = 0.001) in the treated cell line with the highest connectivity score among cancer genes. Analysis of TCGA data revealed overexpression of *BUB1B* compared to normal in most cancers and overexpression was associated with poor prognosis. *BUB1B* also showed a highly significant positive correlation with *FOXM1* in all the TCGA cancer types. We used human leukemic cell lines (K562 and U937) as an *in vitro* study model to validate our findings. We found that NSP-B treatment of leukemic cells suppressed the expression of FOXM1 and BUB1B in a dose-dependent manner. In addition, NSP-B also resulted in the downregulation of FOXM1-regulated genes such as Aurora kinase A, Aurora kinase B, CDK4, and CDK6. Suppression of FOXM1 either by siRNA or NSP-B reduced BUB1B expression and enhanced cell survival inhibition and induction of apoptosis. Interestingly combination treatment of thiostrepton and NSP-B

suppressed of cell viability and inducted apoptosis in leukemic cells *via* enhancing the activation of caspase-3 and caspase-8 compared with single-agent treatment. These results demonstrate the important role of the FOXM1/BUB1B pathway in leukemia and thus a potential therapeutic target.

Keywords: fungal metabolites, Neosetophomone B, FOXM1, BUB1B, apoptosis, leukemia, cell-cycle checkpoints, TCGA

INTRODUCTION

Leukemia is a type of blood cancer characterized by the uncontrolled proliferation and lack of proper differentiation of hematopoietic cells causing the accumulation of non-functional leukocytes and their progenitors, primarily in the bone marrow and lymphatic system (1). According to GLOBOCAN 2020 statistics, leukemia was the 11th leading cause of cancer-related mortality worldwide (1). Leukemia accounted for approximately 3.4% (474,519) of all new cancer cases and 3.8% (311,549) of all cancer deaths in 2020, representing 2.5% of all cancer sites/types reported (2). The most common type of leukemia, acute myeloid leukemia (AML), has a high mortality rate and is difficult to treat (3). Currently, the mainstay treatment of AML includes chemotherapy, radiotherapy, and bone marrow transplantation. Even though these therapies have increased patient survival rates, some patients develop resistance and relapse (4). As a result, finding new strategies to treat leukemia with minimal side effects remains a significant therapeutic problem. Recently, natural compounds have gained considerable interest as abundant and emerging sources for developing novel anticancer therapies due to improved efficacy and reduced side effects (5). In recent years combinational therapeutic regimen involving the use of chemotherapeutic drugs and natural compounds is now considered a new innovative approach for overcoming multidrug resistance and normal cell toxicity (6).

Natural products and their derivatives, endowed with structural diversity and a range of pharmacological and molecular properties have shown great promise in the development of cancer therapies (7). Neosetophomone B (NSP-B), a meroterpenoid fungal secondary metabolite, isolated from a *Neosetophoma sp*. has been reported to be cytotoxic even at micromolar concentrations in breast and ovarian cancer cell lines (8). Recently NSP-B has been shown to cause cell death in leukemic cells *via* inhibition of AKT/SKP2 axis and activation of mitochondrial and caspase signaling cascades (9).

Budding uninhibited by benzimidazoles 1 (BUB1B), a mitotic checkpoint serine/threonine kinase, that serves an important role in chromosome alignment, has been shown to act as a tumor promoter in many cancers (10–12). It has been shown that complete deletion of BUB1B in the mouse germline causes early embryonic mortality (13). Furthermore, lowering BUB1B levels or inhibiting BUB1B kinase activity in human cancer cells causes significant chromosomal loss and apoptotic cell death (14). Knockdown of BUB1B has been shown to reduce tumor growth *in vivo* (15). It has been demonstrated that Forkhead box protein M1 (FOXM1) regulates BUB1B expression through transcriptional regulation by binding to and activating the BUB1B promoter (16). FOXM1 is a transcription factor also known as a master regulator of tumor metastasis and has been reported to regulate a wide range of biological activities, including cell proliferation, cell cycle progression, cell differentiation, DNA damage repair, tissue homeostasis, angiogenesis, and apoptosis, among others (17, 18). Gene silencing of FOXM1 or suppression of its expression with siomycin A reduced BUB1B expression and decreased cell growth (15). This study suggests that the crosstalk between FOXM1 and BUB1B plays an essential role in the growth and survival of cancer cells. Co-targeting these signaling pathways may be a viable strategy to induce cancer cell death.

In our recent study, we explored the effect of NSP-B on cell proliferation, cell cycle, and apoptosis in leukemic cells (9). In the present study, we performed bioinformatic analysis to screen the targets of NSP-B in leukemic cells. Furthermore, we validated these screened targets with gene profiles of leukemia patients, to understand the underlying mechanism of pathogenesis of leukemia.

MATERIALS AND METHODS

Reagents and Antibodies

Cell Counting Kit-8(CCK-8), methanol, dimethylsulfoxide (DMSO),thiostrepton were obtained from Sigma-Aldrich (St. Louis, MO, USA). Antibodies against FOXM1, Aurora Kinase A,B,CDK-6,-4, PARP, cleaved caspase-8,-3, and β-actin were obtained from Cell Signaling Technologies (Beverly, MA, USA).BUB1B, HSP60, p-H2AX, Bax, Bcl2 were obtained from Santa Cruz Biotechnology, Inc., (CA, USA). AllPrep DNA/RNA Mini Kit was purchased from Qiagen (Hilden, Germany). Live and Dead assay kit, RPMI 1640 medium, fetal bovine serum (FBS), penicillin and streptomycin were obtained from Life Technologies, Inc. (Carlsbad, CA).

Cell Culture and The Natural Compound NSP-B

Leukemic cell lines K562 and U937 were purchased from ATCC (Manassas, Virginia, USA), and maintained in RPMI 1640 medium supplemented with 10% fetal bovine serum,100 U/ml penicillin, and 100 U/ml streptomycin at 37°C in humidified incubator comprising of 5% CO_2 (19).The natural compound NSP-B was isolated from the fungal strain *Neosetophoma* sp. [strain MSX50044], as mentioned earlier (8).

Expression Profiling

We investigated gene expression in NSP-B treated K562 cells by comprehensive transcriptome analysis using the high-resolution Human Transcriptome Array 2.0 (HTA 2.0) (Applied Biosystems™) containing >6.0 million distinct probes covering >285,000 transcripts. K562 cells were treated with NSP-B (10 μM) in duplicate for 48 hours. Total RNA was extracted from the cell lines using AllPrep DNA/RNA Mini Kit (Hilden, Germany). The quantity and quality of the RNA was checked by NanoDrop®; Spectrophotometer (Thermo Scientific™), Qubit RNA HS Assay Kit (Invitrogen™), and Qubit RNA IQ Assay Kit (Invitrogen™). GeneChip™ WT PLUS Reagent Kit (Applied Biosystems™) was used to prepare samples for hybridization on the HTA 2.0 arrays. In brief, 100 ng of total RNA was reverse transcribed to cDNA. cRNA was prepared from the cDNA and purified with purification beads. ss-cDNA was synthesized from the cRNA and purified by the beads. The ss-cDNA was fragmented, labeled, and added to the hybridization master mix to prepare a hybridization cocktail. 200 μL of the cocktail was added to the probe array cartridge and incubated with rotation at 60 rpm for 16 hours at 45°C in the hybridization oven. GeneChip™ Hybridization, Wash and Stain Kit (Applied Biosystems™) was used to process the arrays on the Fluidics Station 450. Finally, the arrays were scanned with the Scanner 3000 7G to generate CEL files (raw data).

Dysregulated Genes, Network, and Pathway Analysis

Treated and untreated CEL files in duplicates were processed and analyzed by different packages in R version 4.1.1 (https://www.R-project.org). Quality control (QC) metrics were generated and differentially expressed genes (DEGs) between untreated and treated cell lines were analyzed using limma R package (20). Log2 values with a fold change (FC) ≥ 1.5 and ≤ -1.5 with $p < 0.05$ were used to identify upregulated and downregulated genes, respectively. Statistically significant DEGs were inputted to Ingenuity Pathway Analysis (IPA) for the identification of key activated and inhibited signaling pathways, gene networks, molecular and cellular biological functions. Further, activated or inhibited upstream regulators were identified with an inactivation or inhibition score of ±2 using IPA. Protein-protein interaction (PPI) analysis of DEGs was performed using STRING tool (21) and results were visualized by Cytoscape. An interaction score of ≥0.4 was used as the cut-off for the network and all the interactions below the cut-off were termed as weak and removed. Genes in the PPI network having a connectivity score >20 was referred as potential hub genes.

The PPI interactions from the STRING were used as input to Cytoscape version v3.9.0 to visualize the interactions and identify the hub genes (22). High confidence clusters were identified by setting kappa score (K-score) to 5, degree to 2, maximum depth to 100, and node score to 0.2 in the network (23). In order to find biological relevance of hub genes, cancer gene annotation was performed, and key tumor suppressors and oncogenes were identified.

Expression and Correlation of Hub Genes

Expression data of key hub genes was downloaded from Genomic Data Commons (GDC) of The Cancer Genome Atlas (TCGA) for AML and Lymphoid Neoplasm Diffuse Large B-cell Lymphoma (DLBC). Expressed data was further supplemented with clinical data of the patients to perform clinical associations for diagnosis and prognosis. In order to identify importance of cancer hub genes, we extended our analysis to include the entire solid tumor in TCGA and differential expression analysis was performed. Further, Spearman correlation analysis was carried out to identify key co-expressing genes with our gene of interest.

Prognosis of Key Hub Genes

To derive biological relevance, clinical associations of cancer hub genes was performed using clinical and expression data from TCGA. ANOVA and Mann–Whitney U test were applied to see the differences between different clinical subtypes and groups wherever appropriate. Survival curves were obtained using the survival package in R by dividing the patients into low and high expression groups. The log-rank p-value and hazard ratio (HR) with 95% confidence interval (CI) were obtained for clinical interpretations.

Cell Viability Assay

Leukemic cell lines K562 and U937 were treated in the presence and absence of NSP-B and thiostrepton, and the cell viability was measured using CCK-8 colorimetric method as mentioned earlier (19).

Live/Dead Assay

Leukemic cells K562 and U937 were treated with various doses of NSP-B and thiostrepton and the stain was prepared according to the protocol. The cells were stained and visualized by EVOS FLoid Cell Imaging System from Invitrogen (Thermo Fisher Scientific) (19).

Cell Lysis and Immunoblotting

Leukemic cells K562 and U937 were treated with NSP-B and thiostrepton and the cells were lysed as described previously (19).An equal amount of protein was separated by SDS-page, transferred into the PVDF membrane, and then immunoblotted with various antibodies and visualized.

Gene Silencing

Leukemic cells K562 were transfected with FOXM1 siRNA (Cat no: SI00421050, Qiagen, Germany) and Control siRNA (Cat no: 1027281, Qiagen) using SF Cell Line-4D-Nucleofector™ System (Lonza) as per the protocol. After incubation, cells were harvested, lysed and probed with anti- FOXM1 and other different antibodies (19).

Synergism Analyses

Synergy was quantified using the Chou–Talalay method using the CalcuSyn software to calculate the values of the combination index (http://www.biosoft.com/w/calcusyn.htm, Biosoft) (24). The dose–effect curve for each drug alone is determined on the

basis of experimental observations using the median-effect principle and is compared with the effect achieved with a combination of the two drugs to derive a combination index (CI) value. The CI indicates the level of synergism or antagonism: <0.9 indicates synergism (0.3–0.7 strong; 0.7–0.85 moderate; 0.85–0.9 slight), 0.9–1.1 nearly additive effect, and >1.1 antagonism (25).

Statistical Analysis

All statistical analyses were performed in R version 4.1.1. The Mann–Whitney U Test, the Chi-Squared Test or Fisher's Exact Test were executed to compare the continuous and categorical variables. Correlation analysis was performed using Spearman's rank correlation method. All the statistical tests were two-tailed with $p < 0.05$ considered statistically significant. For differential expression of genes, the p-values were adjusted with false discovery rate (FDR) of <10%.

RESULTS

Differentially Expressed Genes and Pathways

K562 cells were treated with NSP-B (10μM) in duplicate for 48 h, and transcript expressions were analyzed using the HTA 2.0 array containing >6.0 million distinct probes covering >85,000 transcripts. The data was analyzed using different R packages, including ArrayExpress, Oligo, arrayQualityMetrics, limma and ggplot2. Quality metrics of the data was obtained, data preprocessed and DEGs were identified (**Figure 1A**). For identifying DEGs, the logFC of ≥ 1.5 and ≤ -1.5 with statistically significant p value ($p < 0.05$) were used for up-regulated and down-regulated genes, respectively. The p values were adjusted with FDR of 10%. Overall, 2,079 significant DEGs were identified with $p < 0.05$ in the NSP-B treated cell line. This included 2,072 down-regulated genes and only 7 genes were found to be up-regulated (**Supplementary Table 1**). The volcano plot and heatmap of the expression data were obtained with heatmap restricted to only cancer genes (**Figures 1B, C**). Genes with logFC ≥ 1.5 and ≤ -1.5 were submitted to IPA to identify pathways and gene ontologies (GO) associated with DEGs. The highly significant pathways associated with treatment were inhibition of ERBB Signaling, EGF Signaling, PI3K Signaling, JAK/STAT Signaling, VEGF Signaling, TGF-β Signaling and likely activation of PTEN Signaling. (**Figure 2A**). The significant GOs found in molecular and cellular functions category were inhibition of cell cycle progression and DNA replication (**Figure 2B**).

PPI Network Analysis and Functional Annotations of the Selected Potential Targets

The PPI network was constructed for the DEGs using STRING with a confidence interaction score of ≥ 0.4. The interaction scores were analyzed and visualized in Cytoscape to identify hub genes and clusters (**Figure 3A**). We found approximately 37 hub genes having a degree value of over 200 including down-regulation of two oncogenes (*BUB1B* and *XPO1)*, with *BUB1B* comparatively having a higher number of connections (**Supplementary Table 1**). The hub genes are displayed as darker color in the figure, and color intensity depends on the number of connections (**Figure 3A**). *FOXM1* regulates *BUB1B* expression through transcriptional regulation by binding to and activating the BUB1B promoter (15). IPA analysis showed many targets of *FOXM1* are down-regulated (green color), which likely inhibits *FOXM1* (blue color; predicted inhibition by IPA), thus likely inhibiting cell cycle progression (**Figure 3B**).

Co-Expression and Clinical Correlation of Selected Genes

We investigated the co-expression of *BUB1B* with *FOXM1* using expression data from TCGA. *BUB1B* is positively correlated with *FOXM1* in all the cancer types from TCGA. It showed highly significant positive correlation in AML (spearman r = 0.8377; p = 2.26e-48) (**Figure 4A**) and Lymphoid Neoplasm DLBC (spearman r = 0.8705; p = 9.25e-16) (**Figure 4B**). We further extended this to other solid tumors in TCGA, and interestingly a highly significant correlation was observed between *BUB1B* and *FOXM1* (**Supplementary Figure 1**).

To see if the high expression of *BUB1B* has any prognostic importance, we investigated its clinical association and overall survival in AML and DLBC from TCGA. We found high expression of *BUB1B* in M6 and M7 subtypes of AML, however the association was not statistically significant due to small number of samples (**Figure 4C**). The median overall survival for AML patients with high BUB1B expression was ~10 months in comparision to ~19 months for patients exhibiting low expression of BUB1B; however the association was not statistically significant (HR 1.35, CI 0.88-2.05; logrank p=0.16) (**Figure 4D**). In DLBC, high expression of *BUB1B* was found to be associated with higher tumor stage (Stage1 vs 2, p=0.038; Stage1 vs 4, p=0.024. **Figure 4E**). Overall survival was not calculated in DLBC due to fewer patients and survival events. Further, *BUB1B* was found to be significantly overexpressed in most TCGA tumor types (**Figure 4F**). We performed overall survival analysis of *BUB1B* in other solid tumors in TCGA and found that high expression of *BUB1B* is associated with poor overall survival in six different cancer types (**Supplementary Figure 2**).

Effect of NSP-B on FOXM1, BUB1B and Downstream Key Targets: Validation of Microarray Data

To substantiate the results of the microarray studies, immunoblotting was performed to assess the protein expression of FOXM1, BUB1B and downstream targets such as Aurora kinase A, Aurora kinase AB, CDK4, and CDK6. We found that NSP-B treatment of K562 and U937 cells inhibited the expression of FOXM1 and BUB1B in a dose dependent manner confirming the reliability of our microarray results at the protein level (**Figure 5**). In addition, NSP-B also suppressed the expression of Aurora kinase A, Aurora kinase B, CDK4 and CDK6 (**Figure 5**).

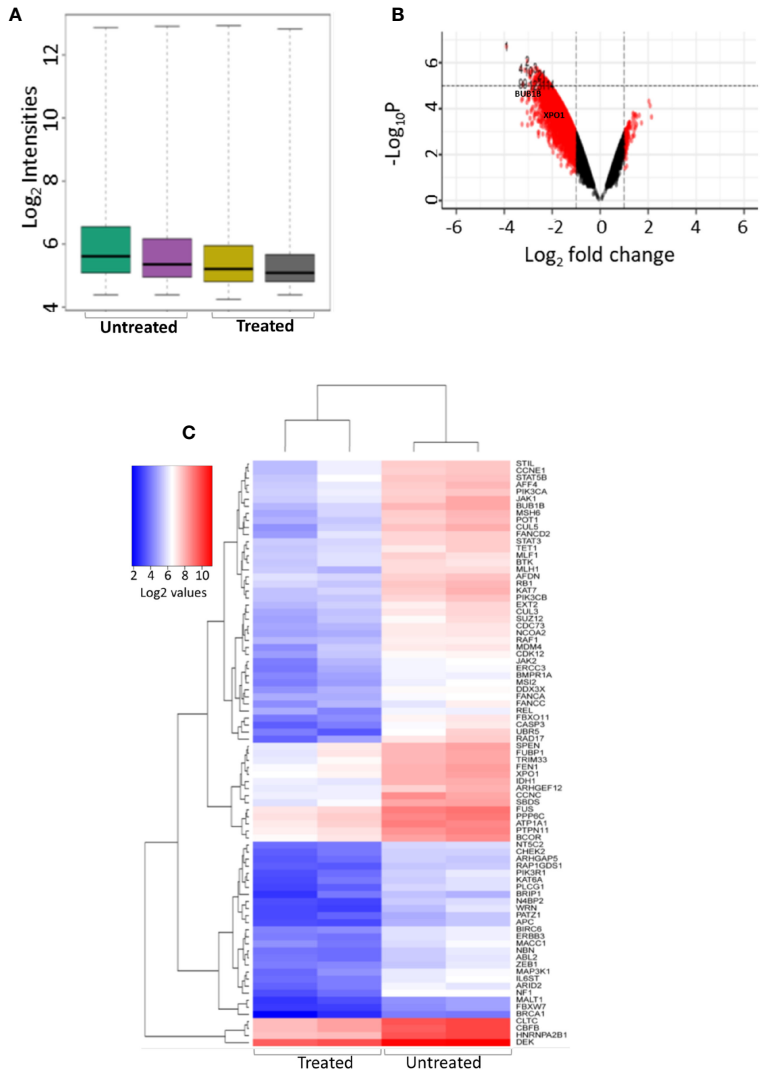

FIGURE 1 | Differential gene expression of treated and untreated K562 cell line using microarray. **(A)** Intensity plot displaying the quality of the microarray CELL data **(B)** Volcano plot showing the differentially expressed genes between K562 cell line treated with NSP-B (10μM) and untreated K652 cells, A $\log_2$ fold change (FC) cutoff of ± 1.5 was used for significant differentially expressed genes with $p < 0.05$. **(C)** Heatmap displaying the expression of significant differentially expressed cancer genes between treated and untreated K562 cells.

Knockdown of FOXM1 Resulted in Growth Inhibition, Suppression of BUB1B and Activation of Caspase-Cascade

To investigate that FOXM1 regulates cell proliferation and BUB1B expression in leukemic cells, we silenced the FOXM1 expression in K562 cells using specific siRNA against FOXM1. As shown in **Figure 6A**, the siRNA knockdown of FOXM1 resulted in the increased level of red floresence,which is a measure of dead cells. Immunoblotting data furher showed that gene silencing of FOXM1 in leukemic cells down regulated the expression of BUB1B as well as Aurora kinase A, a downstream target of FOXM1 (**Figure 6B**). Interestingly, apoptotic markers including p-H2AX, caspase-8, and PARP were also found to be activated after FOXM1 knockdown (**Figure 6B**). These results suggest that the knockdown of FOXM1 inhbits cell growth and triggers apoptosis *via* supression of BUB1B in leukemic cells.

Synergistic Activity Between Thiostrepton and NSP-B in Leukemic Cells

As we showed that NSP-B inhibits FOXM1 expression in leukemic cells cells, next we wanted to investigate if thiostrepton, a specific and direct inhibitor of the FOXM1 protein, could act synergistically with NSP-B in inhibiting cell proliferation and inducing apoptosis. To determine the combination dose of thiostrepton and NSP-B that posseses maximal cytotoxic effects, K562 and U937 cells were treated with various combinations of thiostrepton and NSP-B and cell viability was determined. The combination index (CI) values of

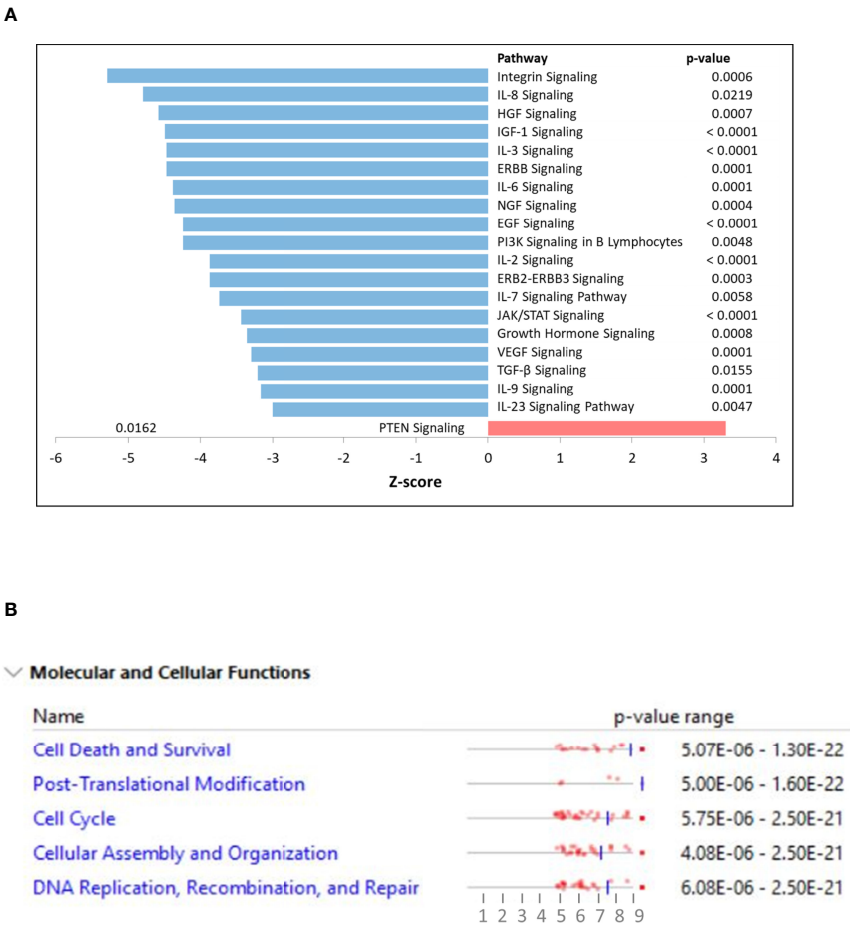

FIGURE 2 | **(A)** Ingenuity pathway analysis (IPA) displaying top affected signaling pathways with their z-scores. Positive z-score is predicted to be activated whereas negative z-score as inhibition of the pathway. **(B)** Ingenuity pathway analysis (IPA) displaying top affected molecular and cellular functions using differentially expressed genes as input.

sub toxic doses of thiostrepton and NSP-B were calculated using Calcusyn software of Chou- Talalay method (26, 27). CI represents the quantitative interaction between drugs and CI values < 1 (synergy), = 1 (additive effect), and >1 (antagonism), as explained by Chou and Talalay (27). The synergistic effects of GS and thiostrepton on cell viability in K562 and U937 cell lines were found at 1 μM of GS and 1 μM of thiostrepton with a CI index of 0.328 and 0.437 respectively. (**Supplementary Tables 2, 3**) (**Supplementary Figures 3A, B**).

Co-Treatment With Thiostrepton and NSP-B Augmented Inhibition of Cell Viability and Induced Apoptosis *Via* Mitochondrial Apoptotic Pathway in Leukemic Cells

Using the Chou-Talalay isobologram equation, we optimized the doses of thiostrepton and NSP-B at 1 μM each for maximal synergistic effects. We performed several experiments in K562 and U937 cells to assess the combination effects of thiostrepton and NSP-B, as compared with single agent treatments. We first performed a live and dead cell assay using LIVE/DEAD®; Cell Imaging Kit as described in Materials and Methods. We found that the combination of thiostrepton and NSP-B in K562 and U937 cells triggered cell death to a greater extent than individual treatments (**Figures 7A, B**). Next CCK-8 assay was performed in K562 and U937 cells to determine the number of viable cells upon treatment. We found that the combination of thiostrepton and NSP-B siginificatly ($p<0.001$) inhibited the proliferation of K562 and U937 cells compared to single agent treatment, as shown in **Figure 7C**. The results demonstrated that co-treatment with thiostrepton and NSP-B exerts synergistic effects on the inhibition of cell viability in leukemic cells. To further examine whether the observed suppression of cell viability involved apoptosis, K562 and U937 cells were treated with 1 μM of thiostrepton or 1μM of NSP-B or both, for 24 *h* prior to the determination of caspase-3 and caspase-8 activities. As shown in **Figure 7D**, the combination of thiostrepton and NSP-B showed a significant increase in the activation of capase 8, caspase3 and PARP as compared to individual treatments. Combination of thiostrepton and NSP-B also increased expression levels of p-H2AX, a marker of double strand breaks (**Figure 7D**). Finally,

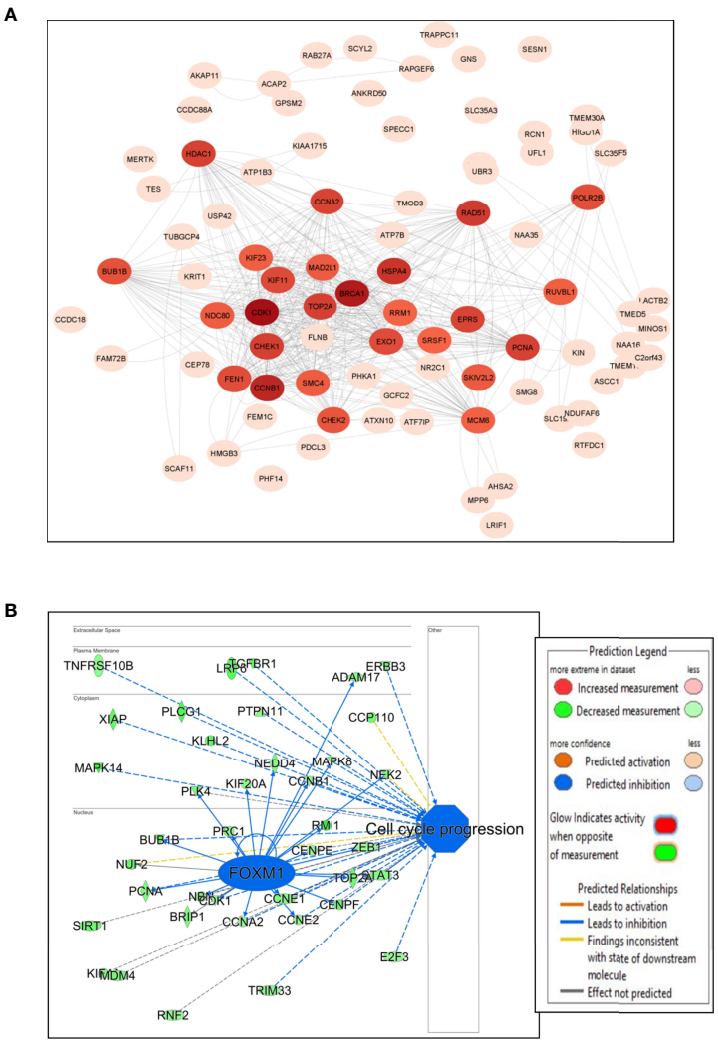

FIGURE 3 | Network and pathway analysis. **(A)** Protein-protein interaction network using Cytoscape. The color intensity of the circles with genes depends on the number of connections with intense color (hub genes) having large number of connections and light color with less connections. **(B)** IPA transcriptional analysis of *FOXM1* and its interaction and connectivity with other differentially expressed genes in the network. The predicted inhibition of *FOXM1* likely inhibits cell cycle progression.

cotreated cells showed an increase in the expression levels of Bax and a decrease in the Bcl-2 levels leading to an increased ratio of Bax/Bcl2 in leukemic cells suggesting mitochondrial mediated apoptosis. These results indicate the synergistic cytotoxicity of thiostrepton and NSP-B, and that the apoptotic mechanism was caspase-3/-8-dependent in leukemic cells.

DISCUSSION

Natural compounds have increasingly become important as anticancer agents against several cancers. A number of bioactive natural substances have been demonstrated to be effective in preventing and treating cancer *via* targeting diverse signaling molecules and pathways (28, 29). In addition, increasing evidence suggests that many naturally occurring compounds improve the efficacy of chemotherapy (7). NSP-B, a meroterpenoid fungal secondary metabolite, isolated from an undescribed *Neosetophoma sp* (8) has recently been shown to induce cytotoxicity *via* triggering apoptosis in leukemic cell lines (9). These encouraging results prompted us to investigate the more detailed anti-proliferative and proapoptotic mechanism of NSP-B in leukemic cells. In the present study, we screened and verified several novel and promising NSP-B target genes in leukemia cells *via* bioinformatics analysis approach. We investigated gene expression in NSP-B treated K562 cells by comprehensive transcriptome analysis using the high-resolution Human Transcriptome Array 2.0 (HTA 2.0). Pathway analysis of DEGs using IPA revealed inhibition (z-score < -2.0) of ERBB Signaling, EGF Signaling, PI3K Signaling, JAK/STAT Signaling,

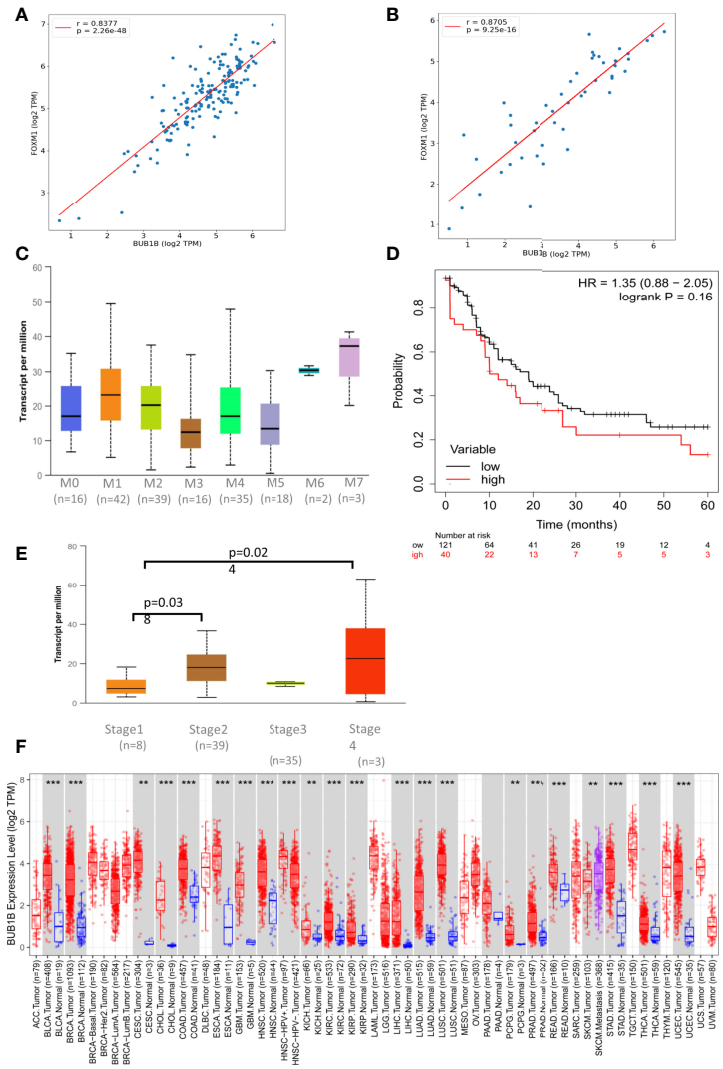

FIGURE 4 | *BUB1B* expression and association in TCGA: **(A)** Spearman correlation between *BUB1B* and *FOXM1* in AML plotted using log2 Transcript Count Per Million (TPM) expression values. **(B)** Spearman correlation between *BUB1B* and *FOXM1* in DLBC plotted using log2 TPM expression values. **(C)** Expression of *BUB1B* in different subtypes of Acute Myeloid Leukemia (AML). The expression values are normalized in TPM. **(D)** Kaplan Meier Curve showing overall survival between *BUB1B* high and low expression patients in AML. **(E)** Expression of *BUB1B* in different stages of DLBC. The expression values are normalized and plotted as Log2 TPM. **(F)** Log2 TPM expression of *BUB1B* in TCGA hematological and solid malignancies. Significant differential expression between tumor and normal tissues or between tumor subtypes is calculated using Wilcoxon test and the significance level is annotated by the number of stars on top of box plots (**p < 0.01; ***p < 0.001). This figure was generated using TIMER2.0 (http://timer.cistrome.org/) TCGA abbreviations are expanded in **Supplementary Figure 1**.

VEGF Signaling, TGF-β Signaling, and likely activation (z-score > 2.0) of PTEN Signaling. Activation of these pathways play a significant role in the development and aggressiveness of various cancers and inhibiting them is an effective treatment for different types of hematological and solid tumors (30, 31). Hence, NSP-B mediated inhibition and activation of these key signaling pathways highlight the anti-leukemic mechanism. Protein-protein interaction (PPI) analysis revealed key hub genes with high connectivity scores, including down-regulation of BUB1B among the top candidates. The BUB1B plays an oncogenic role in a variety of cancers. Increased expression of BUB1B in glioblastoma is associated with tumor proliferation both *in vitro* and *in vivo*. Reduced expression of BUB1B or suppression of its kinase activity resulted in apoptotic cell death in cancer cells (14). In addition, BUB1B expression is associated with poor prognosis in GBM patients (16). BUB1B expression is regulated by FOXM1 transcription factor through direct binding to BUB1B promoter (15). FOXM1 is a master regulator of cell cycle controlling G1/S transition and mitotic progression; however, its mechanism in cell cycle progression is unknown. It has been reported that FOXM1-BUB1B axis is important for the growth and survival of rhabdomyosarcoma

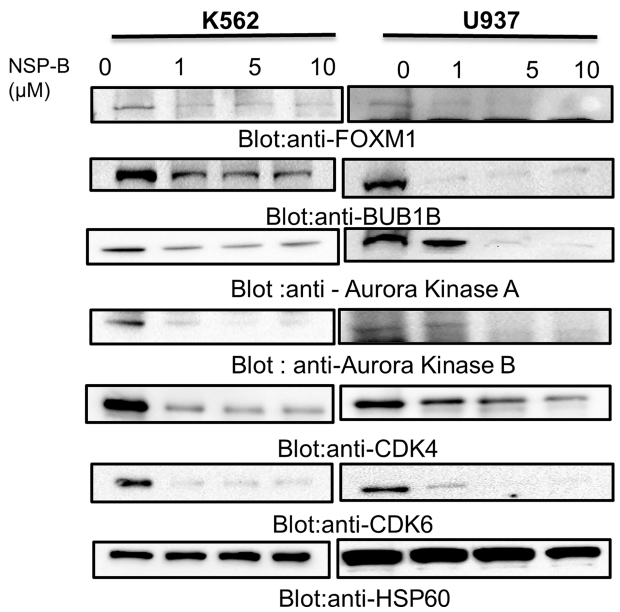

FIGURE 5 | NSP-B mediated downregulation of FOXM1 and its downstream targets in leukemic cells. K562 and U937 cells were treated with increasing doses of NSP-B and equal amount of proteins were immunoblotted against various antibodies such as FOXM1, BUB1B,Aurora Kinases A and B, CDK 4 and 6 and HSP60.NSP-B treatment caused the downregulation of FOXM1 and its downstream targets BUB1B, Aurora Kinases A and B, CDKs 4 and 6.

cells (15). This corroborates well with our findings where we show that siRNA knockdown or NSP-B mediated inhibition of FOXM1 downregulates BUB1B expression causing suppression of cell proliferation and induction of apoptosis. Down-regulation of key genes and IPA prediction also revealed inhibition of many targets of *FOXM1*, including *BUB1B*. This likely inhibits *FOXM1*, which in turn inhibits cell cycle progression as predicted by IPA. These findings are in agreement with our recent study where we have shown that the NSP-B treatment of leukemic cells caused cell cycle arrest and apoptosis (9). We further found that K562 and U937 cells co-expressed FOXM1 and BUB1B and treatment with NSP-B downregulated the expression of FOXM1 and BUB1B in a dose-dependent manner. NSP-B also downregulated the FOXM1 regulated target molecules, including Aurora kinase A and B. Interestingly, NSP-B treatment suppressed the expression of cell cycle regulated genes CDK4 and CDK6, further supporting our prediction model findings that FOXM1 and BUB1B are linked and together affects the cell cycle progression.

We also found that expression of *BUB1B* is positively correlated with *FOXM1* in all hematological and solid cancers using TCGA data. To see if the high expression of *BUB1B* has any prognostic importance, we investigated the overall survival in AML from TCGA data. The median overall survival in patients exhibiting higher BUB1B expression was ~10 months compared to ~19 months in those exhibiting lower expression profile; however, the association was not statistically significant (HR 1.35, CI 0.88-2.05; logrank p=0.16). We extended the overall survival analysis of *BUB1B* in other solid tumors in TCGA and found that high expression of *BUB1B* is associated with poor overall survival in most cancer types. Cross-talk between survival pathways is gradually emerging as one of the major reasons for drug resistance in cancer treatment. Resistance to chemotherapy, in many instances occurs due to reactivation of the upstream target molecule *via* a negative feedback mechanism (32). Recently it has been shown that targeting of multiple survival pathways with a combination of specific drugs is more effective

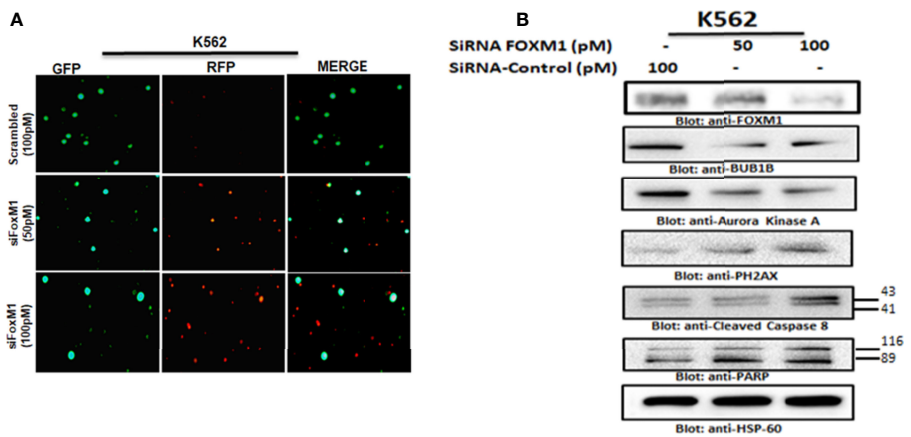

FIGURE 6 | Gene silencing of FOXM1 suppressed BUB1B expression. **(A)** K562 cells were transfected with control (100 pM) and FOXM1 siRNA (50 and 100 pM) as indicated. After 48 hours of transfection Live and dead assay was performed for detection of live and dead cells after FOXM1 knockdown. **(B)** K562 cells were transfected with control (100 pM) and FOXM1 siRNA (50 and 100 pM) as indicated in Materials and Methods. Immunoblot analysis of K562 cells transfected with control (100 pM) and FOXM1 siRNA (50 and 100 pM). Cells were lysed, and an equal amount of proteins for each sample were loaded onto the SDS-polyacrylamide gel. Membranes were blotted against against FOXM1, BUB1B, Aurora Kinase A, p-H2AX, Cleaved caspase-8, PARP and HSP60.

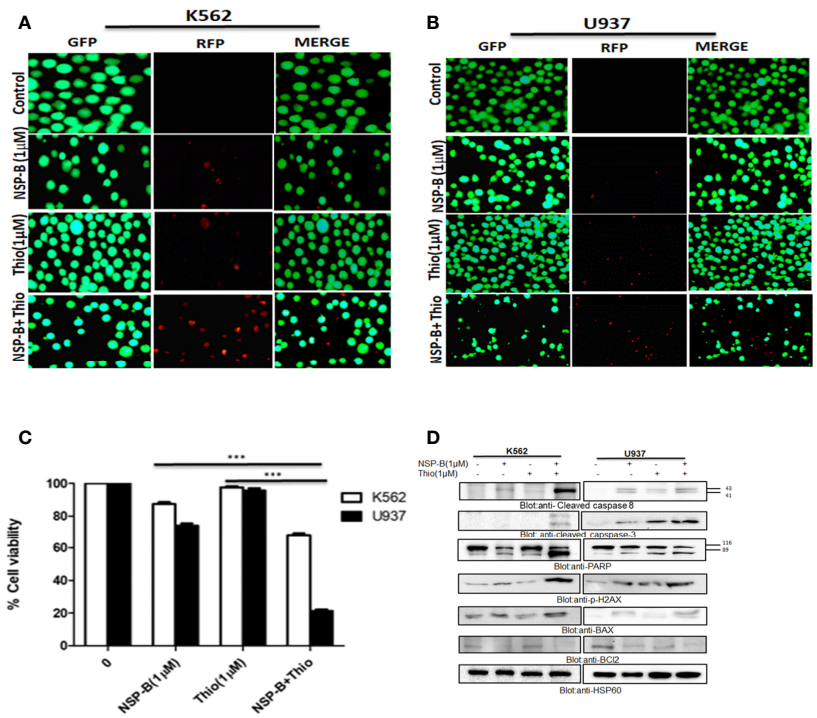

FIGURE 7 | Cotreatment of NSP-B and thiostrepton augmented the inhibition of cell viability and induces apoptosis in leukemic cells. **(A)** K562 and **(B)** U937 were treated with NSP-B and thiostrepton alone and in combination for 48 hours. After incubation the cells were stained with live and dead reagent and visualized under a fluorescent microscope. **(C)** K562 and U937 cells cells were treated with 1μM of NSP-B and 1μM of thiostrepton for 48 hours and cell viability assay was performed as mentioned in Materials and Methods. The graph displays the mean ± SD (standard deviation) of three independent experiments. ***$p < 0.001$. **(D)** K562 and U937 were treated with 1 μM of NSP-B and thiostrepton alone and in combination and cells were lysed and separated using SDS-PAGE, transferred to a PVDF membrane, and immunoblotted with antibodies such as PARP, cleaved caspase-8, cleaved caspase-3, BAX, Bcl-2, P-H2AX, and HSP60.

than treating with a single drug alone in overcoming cancer resistance (25, 33). Therefore, the combinational therapy is advantageous as each drug's concentration is significantly reduced when administered together, reducing the toxic effects on normal cells. The thiazole antibiotic siomycin also known as thiostrepton is a potent inhibitor of FOXM1 (34). Cotreatment of leukemic cells with subtoxic doses of thiostrepton and NSP-B caused suppression of cell viability. The combination of thiostrepton and NSP-B treatment of K562 and U937 cells further activated caspase-cascades. Indeed, our study demonstrated that NSP-B significantly reduced cell viability and together with thiostrepton exhibited survival-inhibitory effect that is associated with decreased FOXM1 and BUB1B expression in leukemic cells. The activation of the mitochondrial apoptotic pathway is initiated by Bax conformational changes and translocation to the mitochondrial membrane, thereby leading to changes in the mitochondrial membrane potential and, finally activation and cleavage of caspases. Once caspases are activated, there is cleavage of PARP; an essential enzyme that is required for repairing single-stranded breaks in DNA and is a hallmark of cells undergoing apoptosis. Our results go well with these studies as we have also shown that NSP-B treatment of leukemic cells increased Bax, cleaved PARP and p-H2AX expression and downregulated antiapoptotic protein BCl2 together leading to increased apoptosis. Taken together, the present study provides a novel insight into the mechanism of NSP-B mediated apoptosis in leukemic cells and opens a new window for more research.

CONCLUSIONS

The bioinformatic analysis results revealed several novel and promising NSP-B target genes in leukemia cells. Downregulation of ERBB Signaling, EGF Signaling, PI3K Signaling, JAK/STAT Signaling, VEGF Signaling, TGF-β Signaling, and activation of PTEN Signaling were observed in NSP-B treated leukemic cells. *BUB1B* was among the top candidate hub genes and was significantly correlated with *FOXM1* in TCGA data. *In vitro*, we confirmed that NSP-B significantly downregulates the expression of FOXM1 and BUB1B along with other targets such as AURK A, AURK B CDK4, and CDK6. FOXM1 silencing caused downregulation of BUB1B, and AURK A while significantly upregulating the expression of p-H2AX, cleaved caspase 8 and cleaved PARP. We also found synergistic activity between NSP-B and thiostrepton in inhibiting cell proliferation and inducing apoptosis. Further in-depth investigations are warranted to elucidate the potential significance of combination treatment of NSP-B together with FOXM1 targeting agents in preclinical animal models for the successful treatment of leukemia.

DATA AVAILABILITY STATEMENT

The datasets presented in this study can be found in online repositories. The names of the repository/repositories and accession number(s) can be found in the article/**Supplementary Material**.

AUTHOR CONTRIBUTIONS

SK; data curation, writing—review and editing, TM; data curation, Analysis, writing—review and editing, GS; data curation, writing—review and editing, AB; writing—review and editing, KP; review and editing, NO; review and editing, CP; review and editing, MH; review and editing, AA; Conceptualization, writing—review and editing, FA; writing—review and editing, TE-E; writing—review and editing, SU; Conceptualization, supervision, writing—original draft preparation. All authors contributed to the article and approved the submitted version.

FUNDING

Medical Research Center Grant no; MRC-01-21-301 (SU), Hamad Medical Corporation, Doha Qatar.

ACKNOWLEDGMENTS

The publication of this article was funded by the Qatar National Library.

SUPPLEMENTARY MATERIAL

The Supplementary Material for this article can be found online at: https://www.frontiersin.org/articles/10.3389/fonc.2022.929996/full#supplementary-material

Supplementary Figure 1 | Spearman correlation between BUB1B and FOXM1 in TCGA cancers plotted using log2 TPM expression values. Correlation score (r) and p values (p) are plotted on top left. LAML, Acute Myeloid Leukemia; ACC, Adrenocortical carcinoma; BLCA, Bladder Urothelial Carcinoma; LGG, Brain Lower Grade Glioma; BRCA, Breast invasive carcinoma; CESC, Cervical squamous cell carcinoma and endocervical adenocarcinoma; CHOL, Cholangiocarcinoma; LCML, Chronic Myelogenous Leukemia; COAD, Colon adenocarcinoma; ESCA, Esophageal carcinoma; GBM, Glioblastoma multiforme; HNSC, Head and Neck squamous cell carcinoma; KICH, Kidney Chromophobe; KIRC, Kidney renal clear cell carcinoma; KIRP, Kidney renal papillary cell carcinoma; LIHC, Liver hepatocellular carcinoma; LUAD, Lung adenocarcinoma; LUSC, Lung squamous cell carcinoma; DLBC, Lymphoid Neoplasm Diffuse Large B-cell Lymphoma; MESO, Mesothelioma; MISC, Miscellaneous; OV, Ovarian serous cystadenocarcinoma; PAAD, Pancreatic adenocarcinoma; PCPG, Pheochromocytoma and Paraganglioma; PRAD, Prostate adenocarcinoma; READ, Rectum adenocarcinoma; SARC, Sarcoma; SKCM, Skin Cutaneous Melanoma; STAD, Stomach adenocarcinoma; TGCT, Testicular Germ Cell Tumors; THYM, Thymoma; THCA, Thyroid carcinoma; UCS, Uterine Carcinosarcoma; UCEC, Uterine Corpus Endometrial Carcinoma; UVM, Uveal Melanoma.

Supplementary Figure 2 | Overall survival BUB1B for the solid tumors from TCGA. Higher expression of BUB1B is associated with poor overall survival in six different cancers.

Supplementary Figure 3 | NSP-B synergistically enhanced the antiproliferative response of thiostrepton in leukemic cells. K562 **(A)** and U937 **(B)** cells were treated with various combinations of NSP-B and thiostrepton for 48 hours and graphs were generated.K562 and U937 cells were treated with different combinations of NSP-B and thiostrepton for 48 hours and cell viability assay were performed as mentioned in the method section. Different types of graphs were prepared using Calcusyn software as described by Chou and Talay.

REFERENCES

1. Juliusson G, Hough R. Leukemia. *Prog Tumor Res* (2016) 43:87–100. doi: 10.1159/000447076
2. Sung H, Ferlay J, Siegel RL, Laversanne M, Soerjomataram I, Jemal A, et al. GLOBOCAN Estimates of Incidence and Mortality Worldwide for 36 Cancers in 185 Countries. *CA Cancer J Clin* (2021) 71:209–49. doi: 10.3322/caac.21660
3. O'Donnell MR, Tallman MS, Abboud CN, Altman JK, Appelbaum FR, Arber DA, et al. Acute Myeloid Leukemia, Version 2.2013. *J Natl Compr Canc Netw* (2013) 11:1047–55. doi: 10.6004/jnccn.2013.0127
4. Cannas G, Thomas X. Supportive Care in Patients With Acute Leukaemia: Historical Perspectives. *Blood Transfus* (2015) 13:205–20. doi: 10.2450/2014.0080-14
5. Lucas DM, Still PC, Pérez LB, Grever MR, Kinghorn AD. Potential of Plant-Derived Natural Products in the Treatment of Leukemia and Lymphoma. *Curr Drug Targets* (2010) 11:812–22. doi: 10.2174/138945010791320809
6. Bayat Mokhtari R, Homayouni TS, Baluch N, Morgatskaya E, Kumar S, Das B, et al. Combination Therapy in Combating Cancer. *Oncotarget* (2017) 8:38022–43. doi: 10.18632/oncotarget.16723
7. Mondal A, Gandhi A, Fimognari C, Atanasov AG, Bishayee A. Alkaloids for Cancer Prevention and Therapy: Current Progress and Future Perspectives. *Eur J Pharmacol* (2019) 858:172472. doi: 10.1016/j.ejphar.2019.172472
8. El-Elimat T, Raja HA, Ayers S, Kurina SJ, Burdette JE, Mattes Z, et al. Meroterpenoids From Neosetophoma Sp.: A Dioxa[4.3.3]propellane Ring System, Potent Cytotoxicity, and Prolific Expression. *Organic Lett* (2019) 21:529–34. doi: 10.1021/acs.orglett.8b03769
9. Kuttikrishnan S, Bhat AA, Mateo JM, Ahmad F, Alali FQ, El-Elimat T, et al. Anticancer Activity of Neosetophomone B by Targeting AKT/SKP2/MTH1 Axis in Leukemic Cells. *Biochem Biophys Res Commun* (2022) 601:59–64. doi: 10.1016/j.bbrc.2022.02.071
10. Piao J, Zhu L, Sun J, Li N, Dong B, Yang Y, et al. High Expression of CDK1 and BUB1 Predicts Poor Prognosis of Pancreatic Ductal Adenocarcinoma. *Gene* (2019) 701:15–22. doi: 10.1016/j.gene.2019.02.081
11. Fu X, Chen G, Cai ZD, Wang C, Liu ZZ, Lin ZY, et al. Overexpression of BUB1B Contributes to Progression of Prostate Cancer and Predicts Poor Outcome in Patients With Prostate Cancer. *Onco Targets Ther* (2016) 9:2211–20. doi: 10.2147/OTT.S101994
12. Ricke RM, Jeganathan KB, van Deursen JM. Bub1 Overexpression Induces Aneuploidy and Tumor Formation Through Aurora B Kinase Hyperactivation. *J Cell Biol* (2011) 193:1049–64. doi: 10.1083/jcb.201012035
13. Baker DJ, Jeganathan KB, Cameron JD, Thompson M, Juneja S, Kopecka A, et al. BubR1 Insufficiency Causes Early Onset of Aging-Associated Phenotypes and Infertility in Mice. *Nat Genet* (2004) 36:744–9. doi: 10.1038/ng1382
14. Kops GJ, Foltz DR, Cleveland DW. Lethality to Human Cancer Cells Through Massive Chromosome Loss by Inhibition of the Mitotic Checkpoint. *Proc Natl Acad Sci U S A* (2004) 101:8699–704. doi: 10.1073/pnas.0401142101
15. Wan X, Yeung C, Kim SY, Dolan JG, Ngo VN, Burkett S, et al. Identification of FoxM1/Bub1b Signaling Pathway as a Required Component for Growth and Survival of Rhabdomyosarcoma. *Cancer Res* (2012) 72:5889–99. doi: 10.1158/0008-5472.CAN-12-1991
16. Ma Q, Liu Y, Shang L, Yu J, Qu Q. The FOXM1/BUB1B Signaling Pathway is Essential for the Tumorigenicity and Radioresistance of Glioblastoma. *Oncol Rep* (2017) 38:3367–75. doi: 10.3892/or.2017.6032

17. Monteiro LJ, Khongkow P, Kongsema M, Morris JR, Man C, Weekes D, et al. The Forkhead Box M1 Protein Regulates BRIP1 Expression and DNA Damage Repair in Epirubicin Treatment. *Oncogene* (2013) 32:4634–45. doi: 10.1038/onc.2012.491
18. Raychaudhuri P, Park HJ. FoxM1: A Master Regulator of Tumor Metastasis. *Cancer Res* (2011) 71:4329–33. doi: 10.1158/0008-5472.CAN-11-0640
19. Kuttikrishnan S, Prabhu KS, Khan AQ, Alali FQ, Ahmad A, Uddin S. Thiostrepton Inhibits Growth and Induces Apoptosis by Targeting FoxM1/SKP2/MTH1 Axis in B-Precursor Acute Lymphoblastic Leukemia Cells. *Leuk Lymphoma* (2021) 62:3170–80. doi: 10.1080/10428194.2021.1957873
20. Ritchie ME, Phipson B, Wu D, Hu Y, Law CW, Shi W. Smyth, G.K. Limma Powers Differential Expression Analyses for RNA-Sequencing and Microarray Studies. *Nucleic Acids Res* (2015) 43:e47. doi: 10.1093/nar/gkv007
21. Szklarczyk D, Gable AL, Lyon D, Junge A, Wyder S, Huerta-Cepas J, et al. STRING V11: Protein-Protein Association Networks With Increased Coverage, Supporting Functional Discovery in Genome-Wide Experimental Datasets. *Nucleic Acids Res* (2019) 47:D607–13. doi: 10.1093/nar/gky1131
22. Shannon P, Markiel A, Ozier O, Baliga NS, Wang JT, Ramage D, et al. Cytoscape: A Software Environment for Integrated Models of Biomolecular Interaction Networks. *Genome Res* (2003) 13:2498–504. doi: 10.1101/gr.1239303
23. Bader GD, Hogue CW. An Automated Method for Finding Molecular Complexes in Large Protein Interaction Networks. *BMC Bioinf* (2003) 4:2. doi: 10.1186/1471-2105-4-2
24. Chou TC, Talalay P. Quantitative Analysis of Dose-Effect Relationships: The Combined Effects of Multiple Drugs or Enzyme Inhibitors. *Adv Enzyme Regul* (1984) 22:27–55. doi: 10.1016/0065-2571(84)90007-4
25. Ahmed M, Hussain AR, Siraj AK, Uddin S, Al-Sanea N, Al-Dayel F, et al. Co-Targeting of Cyclooxygenase-2 and FoxM1 Is a Viable Strategy in Inducing Anticancer Effects in Colorectal Cancer Cells. *Mol Cancer* (2015) 14:131. doi: 10.1186/s12943-015-0406-1
26. Khan AQ, Ahmed EI, Elareer N, Fathima H, Prabhu KS, Siveen KS, et al. Curcumin-Mediated Apoptotic Cell Death in Papillary Thyroid Cancer and Cancer Stem-Like Cells Through Targeting of the JAK/STAT3 Signaling Pathway. *Int J Mol Sci* (2020) 21(2):438. doi: 10.3390/ijms21020438
27. Chou TC. Drug Combination Studies and Their Synergy Quantification Using the Chou-Talalay Method. *Cancer Res* (2010) 70:440–6. doi: 10.1158/0008-5472.CAN-09-1947
28. Boulos JC, Rahama M, Hegazy MF, Efferth T. Shikonin Derivatives for Cancer Prevention and Therapy. *Cancer Lett* (2019) 459:248–67. doi: 10.1016/j.canlet.2019.04.033
29. Yuan R, Hou Y, Sun W, Yu J, Liu X, Niu Y, et al. Natural Products to Prevent Drug Resistance in Cancer Chemotherapy: A Review. *Ann N Y Acad Sci* (2017) 1401:19–27. doi: 10.1111/nyas.13387
30. Owen KL, Brockwell NK, Parker BS. JAK-STAT Signaling: A Double-Edged Sword of Immune Regulation and Cancer Progression. *Cancers (Basel)* (2019) 11(12):2002. doi: 10.3390/cancers11122002
31. Huang CY, Chung CL, Hu TH, Chen JJ, Liu PF, Chen CL. Recent Progress in TGF-Beta Inhibitors for Cancer Therapy. *BioMed Pharmacother* (2021) 134:111046. doi: 10.1016/j.biopha.2020.111046
32. Chandarlapaty S. Negative Feedback and Adaptive Resistance to the Targeted Therapy of Cancer. *Cancer Discovery* (2012) 2:311–9. doi: 10.1158/2159-8290.CD-12-0018
33. Seitz C, Hugle M, Cristofanon S, Tchoghandjian A, Fulda S. The Dual PI3K/mTOR Inhibitor NVP-BEZ235 and Chloroquine Synergize to Trigger Apoptosis *via* Mitochondrial-Lysosomal Cross-Talk. *Int J Cancer* (2013) 132:2682–93. doi: 10.1002/ijc.27935
34. Radhakrishnan SK, Bhat UG, Hughes DE, Wang IC, Costa RH, Gartel AL. Identification of a Chemical Inhibitor of the Oncogenic Transcription Factor Forkhead Box M1. *Cancer Res* (2006) 66:9731–5. doi: 10.1158/0008-5472.CAN-06-1576

Conflict of Interest: Authors SK, GS, KP, and SU were employed by Hamad Medical Corporation. CP is employed by Mycosynthetix, Inc.

The remaining authors declare that the research was conducted in the absence of any commercial or financial relationships that could be construed as a potential conflict of interest.

Publisher's Note: All claims expressed in this article are solely those of the authors and do not necessarily represent those of their affiliated organizations, or those of the publisher, the editors and the reviewers. Any product that may be evaluated in this article, or claim that may be made by its manufacturer, is not guaranteed or endorsed by the publisher.

frontiers | Frontiers in Pharmacology

TYPE Original Research
PUBLISHED 26 August 2022
DOI 10.3389/fphar.2022.934746

OPEN ACCESS

EDITED BY
Husain Yar Khan,
Wayne State University, United States

REVIEWED BY
Alejandro Schcolnik-Cabrera,
Hôpital Maisonneuve-Rosemont, Canada
Liang Chen,
Henan University, China

*CORRESPONDENCE
Hyo Jung Kim,
hjkim17@yuhs.ac
Joon Seong Park,
jspark330@yuhs.ac

SPECIALTY SECTION
This article was submitted to Pharmacology of Anti-Cancer Drugs, a section of the journal Frontiers in Pharmacology

RECEIVED 03 May 2022
ACCEPTED 02 August 2022
PUBLISHED 26 August 2022

CITATION
Lee DE, Kang HW, Kim SY, Kim MJ, Jeong JW, Hong WC, Fang S, Kim HS, Lee YS, Kim HJ and Park JS (2022), Ivermectin and gemcitabine combination treatment induces apoptosis of pancreatic cancer cells via mitochondrial dysfunction. *Front. Pharmacol.* 13:934746. doi: 10.3389/fphar.2022.934746

Ivermectin and gemcitabine combination treatment induces apoptosis of pancreatic cancer cells *via* mitochondrial dysfunction

Da Eun Lee[1,2], Hyeon Woong Kang[1,2], So Yi Kim[1,2], Myeong Jin Kim[1,2], Jae Woong Jeong[3], Woosol Chris Hong[1,2], Sungsoon Fang[2], Hyung Sun Kim[1], Yun Sun Lee[1,2], Hyo Jung Kim[1]* and Joon Seong Park[1]*

[1]Department of Surgery, Gangnam Severance Hospital, Yonsei University College of Medicine, Seoul, South Korea, [2]Department of Medical Science, Graduate School of Medical Science, Brain Korea 21 Project, Yonsei University College of Medicine, Seoul, South Korea, [3]Department of Medicine, Yonsei University College of Medicine, Seoul, South Korea

Pancreatic cancer is an aggressive cancer characterized by high mortality and poor prognosis, with a survival rate of less than 5 years in advanced stages. Ivermectin, an antiparasitic drug, exerts antitumor effects in various cancer types. This is the first study to evaluate the anticancer effects of the combination of ivermectin and gemcitabine in pancreatic cancer. We found that the ivermectin–gemcitabine combination treatment suppressed pancreatic cancer more effectively than gemcitabine alone treatment. The ivermectin–gemcitabine combination inhibited cell proliferation *via* G1 arrest of the cell cycle, as evidenced by the downregulation of cyclin D1 expression and the mammalian target of rapamycin (mTOR)/signal transducer and activator of transcription 3 (STAT-3) signaling pathway. Ivermectin–gemcitabine increased cell apoptosis by inducing mitochondrial dysfunction *via* the overproduction of reactive oxygen species and decreased the mitochondrial membrane potential. This combination treatment also decreased the oxygen consumption rate and inhibited mitophagy, which is important for cancer cell death. Moreover, *in vivo* experiments confirmed that the ivermectin–gemcitabine group had significantly suppressed tumor growth compared to the gemcitabine alone group. These results indicate that ivermectin exerts synergistic effects with gemcitabine, preventing pancreatic cancer progression, and could be a potential antitumor drug for the treatment of pancreatic cancer.

KEYWORDS

pancreatic cancer, gemcitabine, ivermectin, apoptosis, reactive oxygen species, mitochondrial dysfunction

Introduction

Pancreatic cancer is the fourth leading cause of cancer-related deaths in the world. In addition, the 5-year survival rate is less than 10% (Jia et al., 2019; Hyatt and Powers, 2021; Lee et al., 2021) owing to late diagnosis, frequent metastases, and limited treatment options (Liang et al., 2017). Currently, gemcitabine is one of the standard chemotherapeutic drugs used for treating patients with pancreatic cancer. However, its contribution to increasing the overall survival is negligible due to its low efficacy (Rawla et al., 2019). Therefore, it is necessary to discover novel chemotherapeutic agents and develop effective therapeutic strategies to enhance the tumor susceptibility of gemcitabine to reduce the tumor growth in pancreatic cancer.

Mitochondria play an important role in tumorigenesis by regulating ATP production and apoptosis (Masoud et al., 2020; Fu et al., 2021). Reactive oxygen species (ROS) generation occurs in the mitochondria of cancer cells to support tumor initiation *via* oncogenic changes, such as abnormal cell proliferation, metastasis, and angiogenesis, to avoid apoptosis and overcome hypoxia (Muz et al., 2015). However, excessive accumulation of ROS induces oxidative damage in mitochondria, reduces the mitochondrial membrane potential (MMP), and leads to mitochondrial dysfunction (Aggarwal et al., 2019). Mitochondrial dysfunction promotes apoptosis *via* the release of cytochrome c, which activates the caspase cascade (Lin et al., 2012; Wallace, 2012). In addition, mitochondrial dysfunction induces the excessive production of ROS and bioenergetic failure (Bhatti et al., 2017; Millichap et al., 2021). Thus, cells eliminate dysfunctional mitochondria *via* mitophagy to maintain cellular fitness (Ponraj et al., 2018).

Ivermectin is a U.S. Food and Drug Administration (FDA)-approved antiparasitic drug that is widely used in clinical practice (Zhang et al., 2015). Ivermectin is as a potential anticancer agent against colon cancer, breast cancer, ovarian cancer, melanoma, and leukemia (Wang et al., 2016). It reverses multidrug resistance, inhibits angiogenesis, and decreases mitochondrial biogenesis (Juarez et al., 2018). It also increases ROS generation to induce apoptosis in esophageal squamous cell carcinoma (Xu et al., 2021). Moreover, ivermectin inhibits the serine/threonine kinase (AKT)/mammalian target of rapamycin (mTOR) signaling pathway in breast cancer (Wang et al., 2016). However, the effect of ivermectin on pancreatic cancer and its underlying mechanism are not well understood.

In this study, we investigated the antitumor effects of ivermectin in pancreatic cancer. Interestingly, we found that co-administration of ivermectin and gemcitabine had a significantly more suppressive effect than gemcitabine alone on pancreatic cancer. We also confirmed that the ivermectin–gemcitabine combination induced apoptosis *via* mitochondrial dysfunction and inhibited mitophagy. Moreover, the ivermectin–gemcitabine combination effectively inhibited tumor growth *in vivo*, similar to the gemcitabine alone group. Taken together, the present study suggests that ivermectin, in combination with gemcitabine, could be a promising therapeutic candidate for patients with pancreatic cancer.

Materials and methods

Ethics statement

Experiments involving human participants were reviewed by the ethics committee of Gangnam Severance Hospital. All patients provided written informed consent to participate in the study. The animal study protocol was reviewed and approved by the Gangnam Severance Hospital of Yonsei University.

Cell culture and treatment

Human pancreatic cancer cell lines (MIA PaCa-2 and PANC-1) were purchased from the American Type Culture Collection (ATCC, MD, VA, United States). MIA PaCa-2 and PANC-1 cells were cultured in Dulbecco's modified Eagle's medium (DMEM) supplemented with 10% fetal bovine serum (Biowest, MO, United States) and 1% antibiotic-antimycotic reagent (Gibco, MA, United States) at 37°C and 5% CO_2. Cells were treated with different concentrations of gemcitabine (Yuhan, Seoul, Korea) and ivermectin (Selleckchem, PA, United States).

Cell viability assay

The cells were seeded in a 96-well plate at a density of 3×10^3 per well and incubated for 24 h. Then, the cells were treated with the indicated concentrations of gemcitabine and ivermectin for 72 h. The growth medium was replaced with 10% water-soluble tetrazolium (WST)-1 reagent (DoGenBio, Seoul, Korea) and incubated for 1 h at 37°C in the dark. The absorbance of each well was measured at 450 nm wavelength using a VersaMax microplate reader (Molecular Devices, CA, United States).

Patient-derived organoids

Pancreatic tissues were obtained from patients diagnosed with pancreatic cancer at the Gangnam Severance Hospital from 2018 to 2019. Written informed consent was obtained from all patients, and this study was approved by the Institutional Review Board (3-2018-0241). The tissues were chopped and washed with advanced DMEM/F12 (Gibco) supplemented with 1% penicillin-streptomycin (Welgene, Gyeongsan, Korea) and then

enzymatically digested with advanced DMEM/F12 supplemented with 0.125 mg/ml dispase II (Wako, VA, United States), 0.1 mg/ml DNase I (Millipore, MA, United States), 0.125 mg/ml collagenase II (Gibco), and 1% penicillin-streptomycin for 1 h at 37°C with shaking (150 rpm). After digestion, the supernatant was filtered through a 70-μm cell strainer (SPL, Gyeonggi-do, Korea) and pelleted *via* centrifugation at 200 × g for 5 min. The pellet was resuspended and mixed with Matrigel (Corning, NY, United States) at a ratio of 1:1 and incubated at 37°C for 10 min to polymerize the matrices. Ivermectin at 4 and 8 μM concentrations was used to treat the cells for 72 h.

Cell cycle analysis

MIA PaCa-2 cells were seeded in a 6-well-plate at a density of 3×10^5 per well and incubated for 24 h. Then, cells were treated with ivermectin and gemcitabine for 48 h. Treated cells were harvested, fixed in 70% ethanol, and stained with propidium iodide (PI; Sigma-Aldrich, MO, United States) and RNase A (Sigma-Aldrich) for 30 min in the dark. The fluorescence intensity was measured using an FACScanto II flow cytometer (BD Biosciences, NJ, United States). A minimum of 10,000 events were collected on each sample. Cell cycle analysis of DNA histograms was performed with FCS Express Flow Cytometry Software.

Apoptosis analysis

MIA PaCa-2 cells were seeded in a 6-well-plate at a density of 3×10^5 per well and incubated for 24 h. Then, cells were treated with the indicated concentrations of gemcitabine and ivermectin for 48 h, and stained with the fluorescein isothiocyanate (FITC)-Annexin V Apoptosis Detection Kit I (BD Biosciences), following the manufacturer's protocols. Briefly, the cells were stained with PI and FITC for 15 min in the dark, and cell apoptosis was analyzed using an FACScanto II flow cytometer (BD Biosciences) and BD FACSDiva Software (version 8.0.3). A minimum of 10,000 events were collected on each sample.

Reactive oxygen species measurement

MIA PaCa-2 cells were plated on a 6-well-plate at a density of 3×10^5 per well and incubated for 24 h. Then, cells were treated with the indicated concentrations of gemcitabine and ivermectin for 48 h. After treatment, MIA PaCa-2 cells were incubated with 20 μM 2′7′-dichlorodihydrofluorescein diacetate (DCF-DA; Sigma-Aldrich) for 20 min at 37°C in the dark. Cells were washed with PBS twice, and ROS levels were measured by measuring DCF fluorescence using an FACScanto II flow cytometer (BD Biosciences).

JC-10 staining

MIA PaCa-2 cells were seeded in a 6-well confocal plate at a density of 3×10^5 per well. MMP was assessed using the Mitochondrial Membrane Potential Kit (Sigma-Aldrich), following the manufacturer's protocols. Briefly, drug-treated cells were stained with JC-10 dye for 30 min at 37°C in the dark. Buffer B was added, and the cells were then visualized with Confocal Laser Scanning Microscope (Zeiss LSM 780) and ImageJ software.

Oxygen consumption rate measurement

The Oxygen consumption rate (OCR) was measured using a Seahorse XF24 extracellular flux analyzer (Seahorse Bioscience, MA, United States). MIA PaCa-2 cells were seeded into XF-24 plates at a density of 3×10^5 per well for 24 h and treated with ivermectin and gemcitabine. Then, the cells were incubated XF assay media for 1 h at 37°C in a non-CO_2 incubator and stressed with sequential addition of 1 μM oligomycin, 2 μM carbonyl cyanide p-(trifluoromethoxy) phenylhydrazone, and a 0.5 μM cocktail of rotenone/antimycin A. The OCR was normalized to total cellular protein concentration.

Reverse transcription-polymerase chain reaction

MIA PaCa-2 cells were seeded in a 6-well-plate at a density of 3×10^5 per well and incubated for 24 h. Then, cells were treated with the indicated concentrations of gemcitabine and ivermectin for 48 h. RNA was isolated using the TRIZOL reagent (Sigma-Aldrich). Total RNA isolated samples were analyzed *via* RT-PCR using the Maxime RT-PCR premix kit (Intron, Gyeonggi-do, Korea).

Western blotting analysis

MIA PaCa-2 cells were seeded in a 6-well-plate at a density of 3×10^5 per well and incubated for 24 h. Then, cells were treated with the indicated concentrations of gemcitabine and ivermectin for 48 h. Then, treated cells were lysed using the radioimmunoprecipitation assay buffer. Cell lysates were separated using sodium dodecyl sulfate-polyacrylamide gel electrophoresis and transferred onto polyvinylidene fluoride membranes. After blocking with 5% skim milk for 1 h, the membranes were incubated with the primary antibodies (1:1000) at 4°C overnight, followed by incubation with the horseradish peroxidase (HRP)-conjugated secondary antibodies (1:5000) for 1 h. The protein bands were then exposed to an enhanced chemiluminescent HRP substrate (Thermo Fisher Scientific, United States) and detected on X-ray films. The primary antibodies: Anti-cleaved/pro-caspase 9 (# 56076), anti-

cleaved/pro-caspase 3 (# 9662/9661), anti-Bcl2 (# 509), anti-p21 (# 6246), anti-CDK4 (# 601), and anti-CDK6 (# 7961) were purchased from Santa Cruz Biotechnology (Dallas, TX, United States). Anti-Cyclin D1 (# 2922S), anti-PI3Kinase p110 alpha (# 4249T), anti-mTOR (# 2972S), anti-Phospho-mTOR (# 5536S), anti-Phospho-Akt (# 9275S), anti-Akt (# 9272S), anti-Bax (# 2772T), anti-Phospho-STAT3 (# 9145S), anti-STAT3 (# 9139S), were purchased from Cell Signaling Technology (Danvers, MA, United States). Anti-γ-tubulin (#T6557) was purchased from Sigma-Aldrich (St. Louis, MO, United States). HRP-conjugated goat anti-mouse secondary (# 7076S) and HRP-conjugated goat anti-rabbit secondary (# 7074S) antibodies were obtained from Cell Signaling Technology (Danvers, MA, United States).

Xenograft tumor model

Five-week-old male BALB/c nude mice were purchased from the Model Animal Research Center of Yonsei University (Seoul, Korea). 4×10^6 PANC-1 cells were subcutaneously injected into the left flank of each mouse. When tumors reached approximately 150 mm^3, mice were randomized into four groups ($n = 6$). Gemcitabine (10 mg/kg) and ivermectin (5 mg/kg) were intraperitoneally injected twice a week for 21 days. Tumor volume was measured using calipers and calculated using the following formula = 0.5 × length × $width^2$. On the 21st day, the tumors were harvested, weighed, and fixed in 4% paraformaldehyde. All animal experimental procedures followed the National Institutes of Health Guide for the Care and Use of Laboratory Animals and were performed in accordance with the protocols approved by the Institutional Animal Care and Use Committee of the Seoul Yonsei Pharmaceutical University Experimental Animal Center.

Statistical analysis

Statistical analysis was evaluated by one-way or two-way ANOVA using GraphPad Prism version 8.0 (GraphPad Software, CA, United States). Data are presented as the mean ± standard deviation. Statistical significance was indicated (*$p < 0.05$; **$p < 0.01$).

Results

Ivermectin exerts synergistic effects with gemcitabine and inhibits pancreatic cancer growth

Ivermectin exerts antitumor effects in various cancer types (Juarez et al., 2018). However, the mechanism underlying its antitumor effect on pancreatic cancer remains unclear. To elucidate the effects of ivermectin and the underlying molecular mechanisms, we first tested the effect of ivermectin on pancreatic cancer proliferation using patient-derived organoids. Ivermectin significantly inhibited the growth of organoids in a concentration-dependent manner compared to the control group (Figure 1A), indicating that ivermectin inhibits the growth of pancreatic cancer.

Next, to determine whether the gemcitabine and ivermectin combination affected pancreatic cancer cell proliferation, pancreatic cancer cells were treated with either gemcitabine or ivermectin, and the viability of PANC-1 and MIA PaCa-2 cells were determined using the WST-1 assay. Ivermectin–gemcitabine combination significantly reduced the cell viability compared to gemcitabine alone (Figure 1B). Also, the median inhibitory concentration (IC_{50}) value of each drug was calculated *via* IC_{50} analysis to decide the optimal concentrations of both drugs to treat pancreatic cancer (Figure 1C). The treatment concentration of gemcitabine for pancreatic cancer was determined as 5 μM, and gemcitabine was co-administered with various concentrations of ivermectin to pancreatic cancer cells. The cell viability decreased in a dose-dependent manner after 48 h (Figure 1D). We confirmed that the co-administration of ivermectin and gemcitabine significantly inhibited the cell proliferation in a concentration- and time-dependent manner (Figure 1E). We also examined cell proliferation-related genes following treatment with the indicated concentrations of gemcitabine and ivermectin (Figure 1F). The expression levels of cell proliferation-related genes were significantly reduced in the ivermectin–gemcitabine group than in the gemcitabine alone group. These results suggest that ivermectin significantly enhances the anti-proliferative effects of gemcitabine on cell growth.

Ivermectin–gemcitabine combination induces cell cycle arrest in pancreatic cancer

Gemcitabine is a DNA-damaging drug that induces S/G2 phase arrest in bladder cancer (Montano et al., 2017), while ivermectin induces G1/S phase arrest in cervical cancer (Zhang et al., 2019). As ivermectin and gemcitabine treatment decreased cell viability, we performed cell cycle analysis using flow cytometry to confirm whether ivermectin and gemcitabine induced cell cycle arrest in pancreatic cancer. Gemcitabine induced S phase arrest, whereas ivermectin–gemcitabine combination treatment increased the percentage of G1 phase arrest cells in a dose-dependent manner (Figures 2A,B). These data suggest that the ivermectin–gemcitabine combination inhibits cell proliferation by inducing G1 arrest in pancreatic cancer cells.

Consistently, the ivermectin–gemcitabine combination affected the expression of cell cycle-related genes.

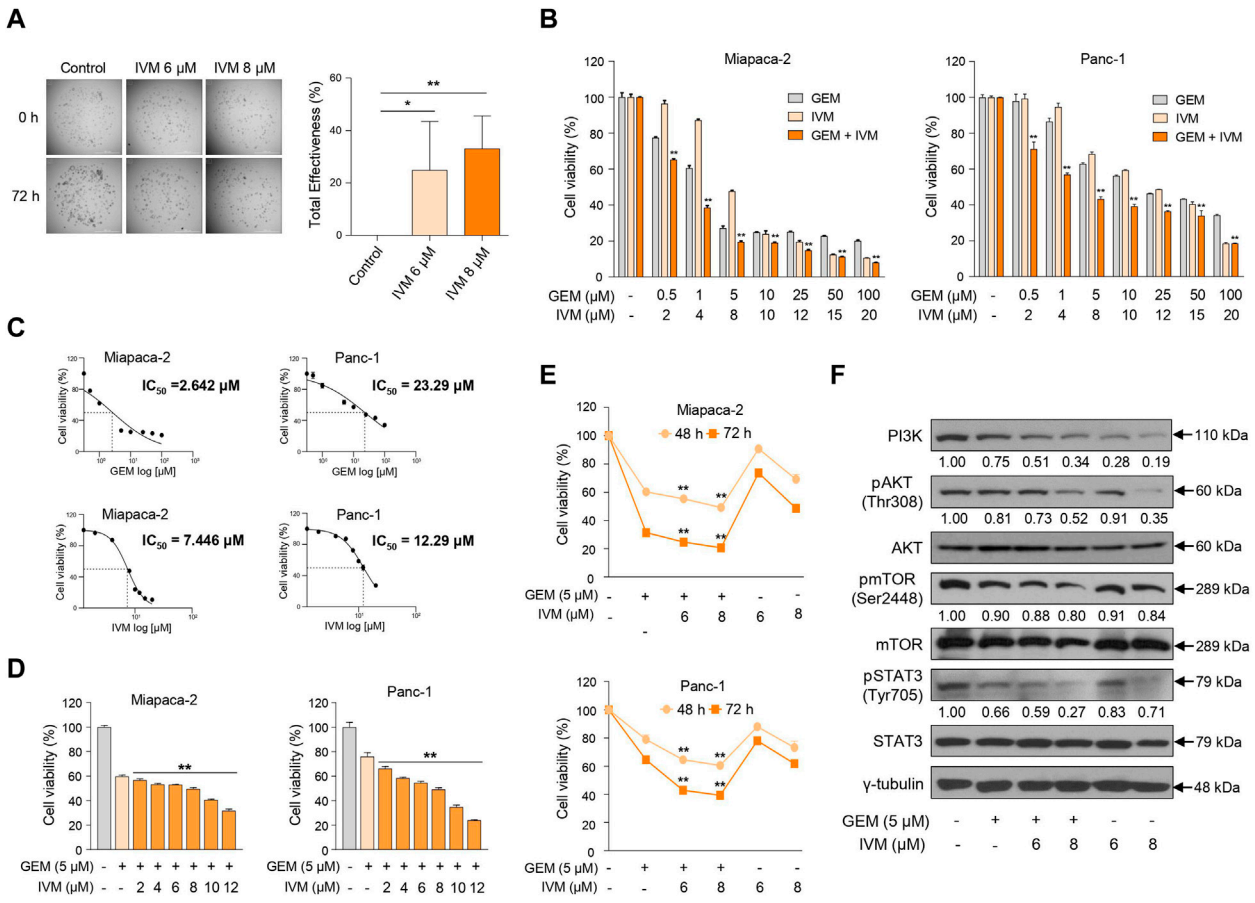

FIGURE 1
Ivermectin inhibits the proliferation of pancreas cancer cells. **(A)** Morphological changes in patient-derived organoids were monitored for 72 h after treatment with ivermectin at 6 and 8 μM concentrations. Total inhibiting effectiveness of ivermectin was calculated. Data represents the mean ± standard deviation (SD) (n = 5). *$p < 0.05$; **$p < 0.01$ compared with the control group. Scale bar = 1000 μm. **(B)** MIA PaCa-2 and PANC-1 cells were seeded in a 96-well plate and treated with increasing doses of gemcitabine and ivermectin for 72 h. Cell viability was determined using the water-soluble tetrazolium (WST) assay. **(C)** Median inhibitory concentration (IC_{50}) values of gemcitabine and ivermectin for each cell line are shown. **(D)** MIA PaCa-2 and PANC-1 cells were treated with 5 μM gemcitabine and increasing doses of ivermectin for 48 h **(E)** MIA PaCa-2 and PANC-1 cells were treated with the indicated concentrations of gemcitabine and ivermectin for 48 and 72 h **(F)** MIA PaCa-2 cells were treated with gemcitabine and ivermectin at the indicated concentrations, and the protein expression levels were determined using western blotting. **(B,D,E)** Data represents the mean ± SD ($n = 3$). *$p < 0.05$ and **$p < 0.01$ compared with the gemcitabine alone group.

Ivermectin–gemcitabine combination treatment increased p21 expression and decreased cyclin D1 expression more effectively than gemcitabine or ivermectin alone. However, there was no difference in the mRNA expression levels of cyclin-dependent kinase (CDK)-4, cyclin E1, and CDK2 (Figure 2C). Western blotting analysis was performed to confirm the regulation of genes at the protein level. The results showed that the combination treatment further reduced the expression levels of CDK4 and CDK6 compared to gemcitabine treatment alone (Figure 2D). These results indicate that the ivermectin–gemcitabine combination inhibits the formation of cyclin D1 and CDK4/6 complexes in pancreatic cancer, inhibits G1-S cell cycle transition, and induces G1 phase arrest.

Ivermectin–gemcitabine combination enhances apoptosis more than gemcitabine alone

To investigate whether the ivermectin–gemcitabine combination promotes apoptosis, we performed fluorescence-activated cell sorting (FACS) analysis using Annexin V/PI dual staining after treatment with the indicated concentrations of ivermectin and gemcitabine. The ivermectin–gemcitabine combination showed a significantly higher rate of apoptosis than gemcitabine alone (Figures 3A,B). We then confirmed the expression of apoptosis-related genes at both the mRNA and protein levels. The ivermectin–gemcitabine combination significantly increased the expression levels of B-cell

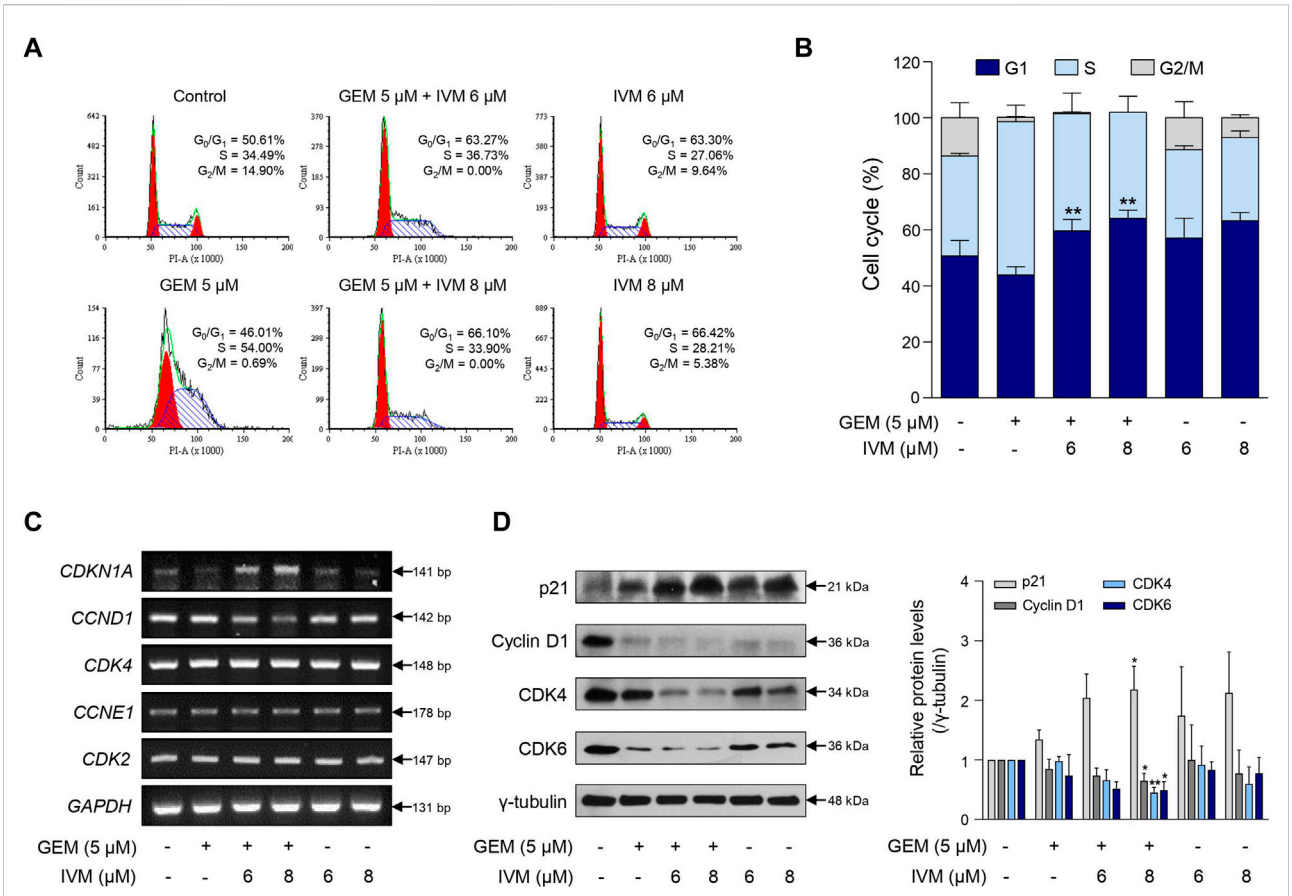

FIGURE 2
Ivermectin–gemcitabine combination induces G1 phase arrest. **(A)** MIA PaCa-2 cells were treated with the indicated concentrations of gemcitabine and ivermectin for 48 h and monitored by propidium iodide (PI) staining and flow cytometry. **(B)** Graph showing the percentage of cells at each stage of the cell cycle. Data represents the mean ± SD (n = 3). *p < 0.05 and **p < 0.01 compared with the gemcitabine alone group. **(C)** After the treatment of MIA PaCa-2 cells with gemcitabine and ivermectin, the mRNA expression levels of p21, cyclin D1, cyclin-dependent kinase (CDK)-4, cyclin E1, and CDK2 were estimated *via* polymerase chain reaction (PCR). **(D)** Protein levels of p21, cyclin D1, CDK4, and CDK6 were determined *via* western blotting of gemcitabine and ivermectin-treated cells. Data represents the mean ± SD (n = 3). *p < 0.05 and **p < 0.01 compared with the gemcitabine alone group.

lymphoma-associated X, caspase 3, and caspase 9 and decreased the levels of B-cell lymphoma-extra-large and B-cell lymphoma-2 compared to gemcitabine alone (Figures 3C,D). These results suggest that the combination of ivermectin and gemcitabine synergistically increases apoptosis by regulating the proapoptotic factors in pancreatic cancer.

Ivermectin–gemcitabine combination enhances apoptosis *via* mitochondrial dysfunction

As various anticancer drugs have been reported to induce apoptosis due to overproduction of the oxidative stress cascade (Ding et al., 2016; Arfin et al., 2021), we measured cellular ROS production in ivermectin–gemcitabine combination-treated cells to confirm the status of oxidative stress. As expected, ivermectin–gemcitabine increased the fluorescence intensity of DCF-DA, indicating increased ROS generation (Figure 4A).

A high level of ROS increases membrane permeability and induces disruption of MMP (Li et al., 2013). MMP, a consequence of the electrochemical proton gradient maintained for ATP synthesis, is an important indicator of functional mitochondria (Perry et al., 2011). Therefore, we monitored the MMP levels in pancreatic cancer cells treated with ivermectin and gemcitabine. In normal cells, red fluorescence was detected by the JC-10 aggregates, whereas in apoptotic cells, green fluorescence was detected by the JC-10 monomer. The co-treatment group showed increased green fluorescence compared to gemcitabine alone (Figure 4B), suggesting that the ivermectin–gemcitabine combination treatment induces mitochondrial dysfunction with decreased levels of MMP due to increased levels of ROS.

As ROS impair the mitochondrial respiratory chain (Wang et al., 2015), we confirmed whether ROS produced by ivermectin and

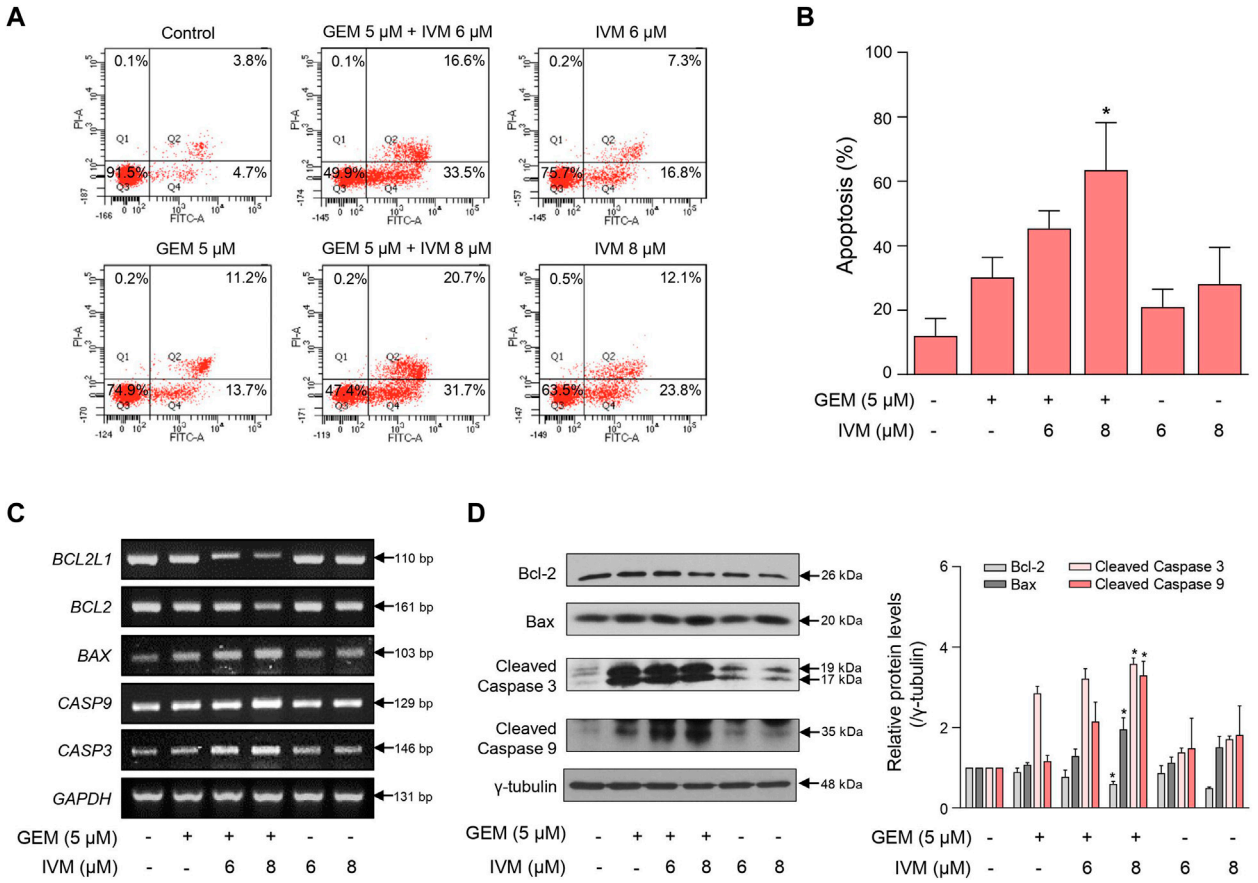

FIGURE 3
Ivermectin and gemcitabine combination increases cell apoptosis. **(A)** MIA PaCa-2 cells were treated with the indicated concentrations of gemcitabine and ivermectin for 48 h. Apoptosis of MIA PaCa-2 cells was analyzed using fluorescence-activated cell sorting (FACS) after Annexin V-fluorescein isothiocyanate (FITC) staining. **(B)** Graph showing the percentage of cells in early and late apoptosis Data represents the mean ± SD (n = 3). *p < 0.05 and **p < 0.01 compared with the gemcitabine alone group. **(C)** mRNA expression levels in cells treated with the ivermectin and gemcitabine combination for 48 h were determined using PCR. **(D)** Protein expression levels were determined using western blotting after ivermectin and gemcitabine treatment. Data represents the mean ± SD (n = 3). *p < 0.05 and **p < 0.01 compared with the gemcitabine alone group.

gemcitabine reduced OCR. As expected, ivermectin–gemcitabine co-administration significantly reduced mitochondrial respiration compared with gemcitabine alone (Figure 4C). Taken together, we found that the ivermectin–gemcitabine combination significantly induced apoptosis by activating pro-apoptotic factors through mitochondrial dysfunction caused by excessive ROS production compared to gemcitabine alone in pancreatic cancer.

Ivermectin–gemcitabine combination inhibits mitophagy

During cancer progression, mitophagy can be more easily detected in cancer cells than in normal cells to manage the elevated ROS levels that cause apoptosis (Chiu et al., 2019; Wang Y. et al., 2020). Damaged mitochondria are usually detected as targets of mitophagy, which promotes mitochondrial fission (Wu et al., 2019). To determine whether ivermectin and gemcitabine affected mitophagy activation in pancreatic cancer, we investigated the expression of mitochondrial fusion- and fission-related genes. We found that the ivermectin–gemcitabine combination significantly reduced mitochondrial fusion- and fission-related gene expression compared with gemcitabine alone (Figure 4D). These data suggest that the two chemical compounds synergistically inhibited mitophagy by decreasing the expression of mitochondrial fission-related genes to induce apoptosis.

Ivermectin–gemcitabine combination effectively suppresses the tumor growth

To evaluate the anti-proliferative effect of ivermectin–gemcitabine combination treatment *in vivo*, PANC-1 cells were injected subcutaneously into BALB/c nude mice and allowed to reach

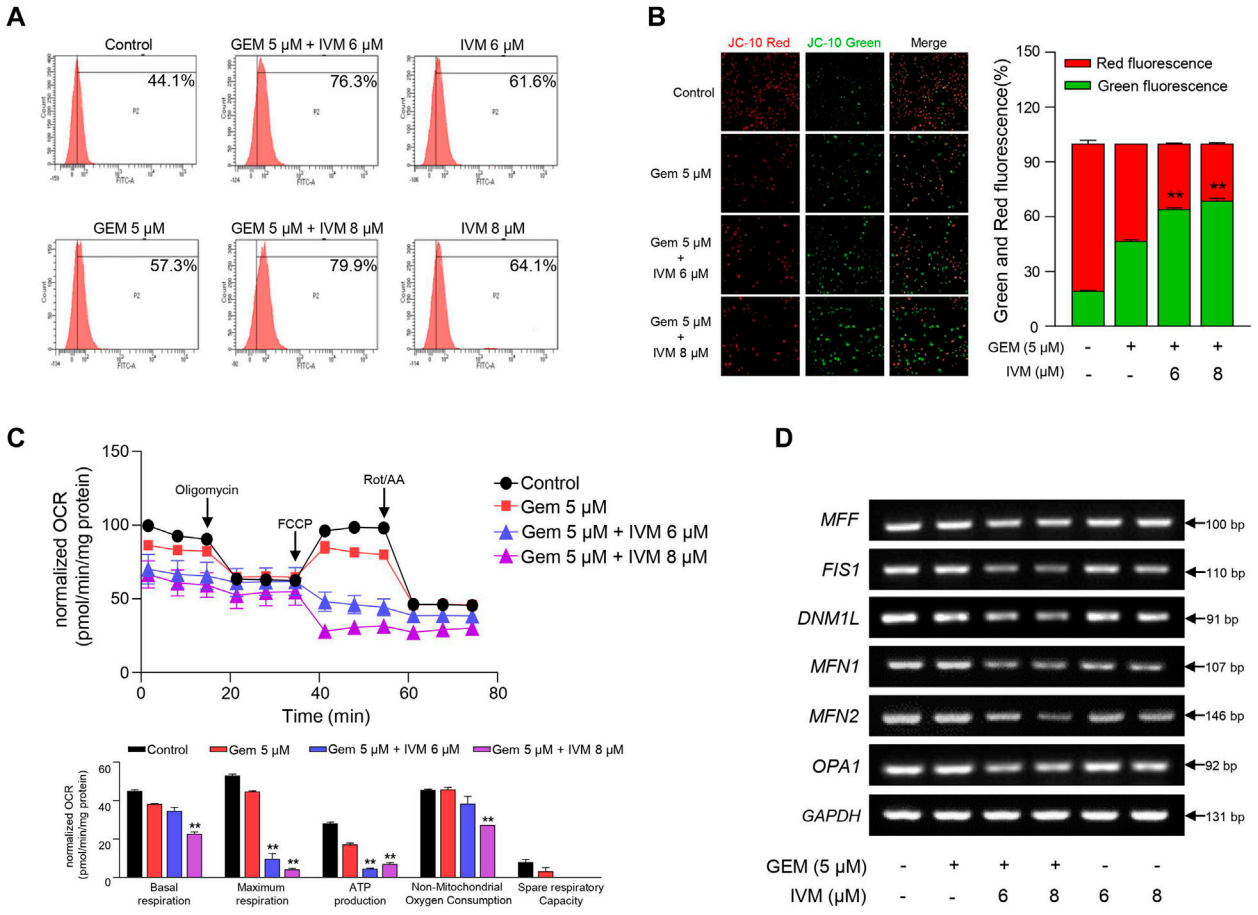

FIGURE 4
Combination of ivermectin and gemcitabine induces mitochondrial dysfunction *via* reactive oxygen species (ROS) generation. **(A)** Relative ROS production in MIA PaCa-2 cells treated with gemcitabine and ivermectin was analyzed using flow cytometry after dichlorofluorescein (DCF)-staining. **(B)** After JC-10 staining, mitochondrial membrane potential (MMP) was measured *via* fluorescence microscopy. Data represents the mean ± SD (n = 3). *p < 0.05 and **p < 0.01 compared with the gemcitabine alone group. **(C)** Oxygen consumption rate (OCR) was determined after treatment with ivermectin and gemcitabine and calculated under oligomycin, carbonyl cyanide p-(trifluoromethoxy) phenylhydrazone (FCCP), and Rot/antimycin A treatments. Data represents the mean ± SD (n = 3). *p < 0.05 and **p < 0.01 compared with the gemcitabine alone group. **(D)** mRNA expression levels of mitochondria fusion and fission genes were determined *via* PCR.

150 mm^3. Mice were randomly divided into four groups and ivermectin and/or gemcitabine were administered intraperitoneally twice a week (Figure 5A). There were no significant differences in body weight (Figure 5B). The combination of ivermectin and gemcitabine significantly suppressed tumor growth compared to the treatment with gemcitabine alone (Figure 5C). Both tumor size and weight were lower in the co-treatment group than in the gemcitabine alone group (Figures 5D,E). These results indicate that the ivermectin–gemcitabine combination has a synergistic effect in inhibiting the growth of pancreatic cancer.

Discussion

Although gemcitabine is the first-line anticancer drug for pancreatic cancer, it does not significantly improve the survival rate of patients with pancreatic cancer. Therefore, gemcitabine-based combination therapies are being investigated to improve the treatment of patients with pancreatic cancer. Only a few known drugs can be used in combination with gemcitabine (Ramaswamy et al., 2017). Drug repurposing, a strategy that utilizes a drug that is already approved by the FDA by switching its original purpose to a new one, is also being actively studied as it is more cost-effective than creating new anticancer drugs (Zhang et al., 2020). Ivermectin, an antiparasitic drug, is being repurposed as an anticancer drug, and has been shown to synergize with doxycycline or tamoxifen in breast and prostate cancer (Juarez et al., 2020; Pfab et al., 2021). However, the exact role of ivermectin in pancreatic cancer has not yet been elucidated. In addition, the combined effects of ivermectin and gemcitabine have not yet been studied. In this study, we demonstrated that ivermectin can be used as an

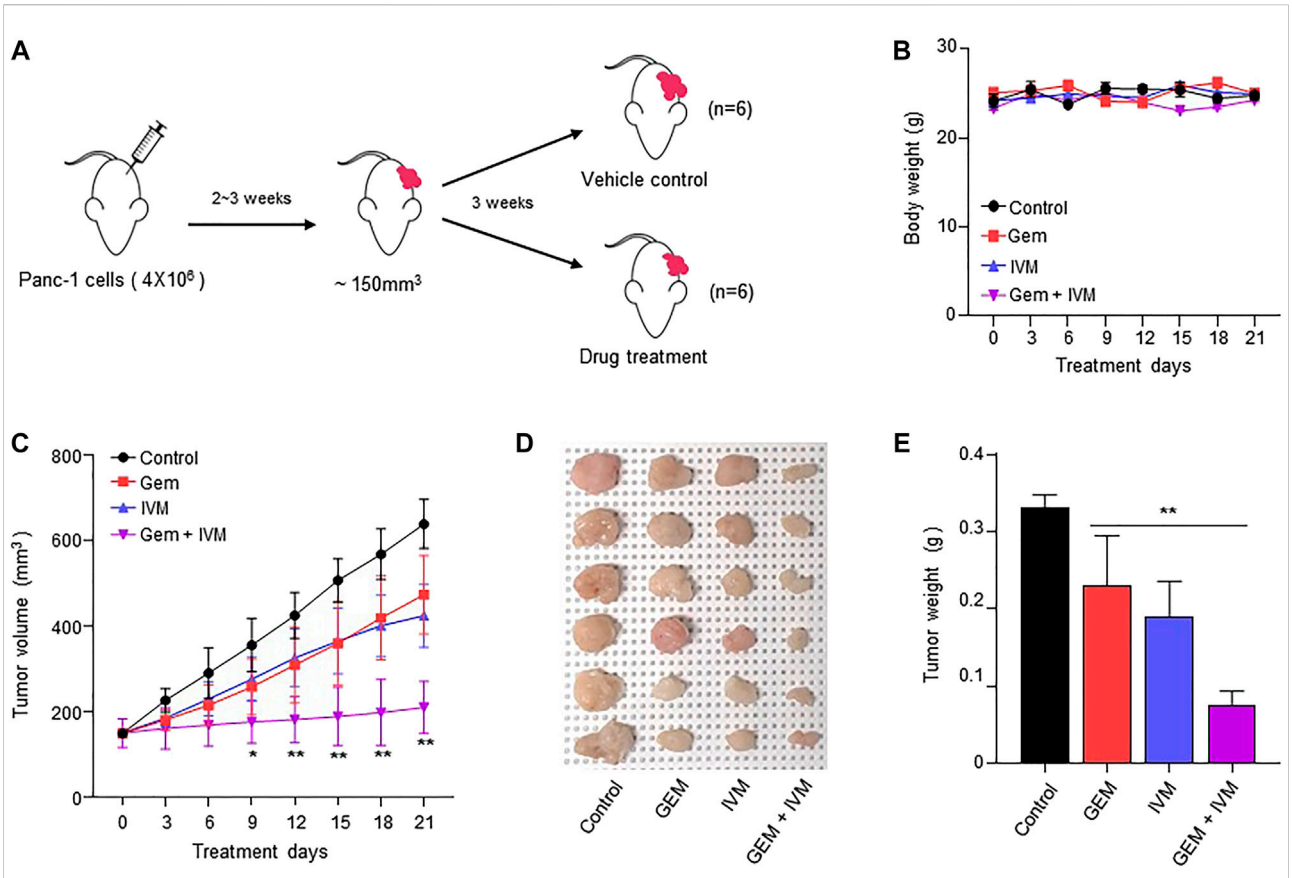

FIGURE 5
Combination of ivermectin and gemcitabine synergistically inhibits the tumor growth *in vivo*. **(A)** BALB/c nude mice were xenografted with PANC-1 cells (4×10^6 cells). Then, the mice were intraperitoneally injected with dimethyl sulfoxide (DMSO) or gemcitabine (10 mg/kg) or ivermectin (5 mg/kg) twice a week for 21 days. **(B)** Mice body weights. **(C)** Tumor volume was measured every 3 days. Data represents the mean ± SD ($n = 6$). *$p <$ 0.05 and **$p < 0.01$ compared with the gemcitabine alone group. **(D)** Representative image of tumors on day 21. **(E)** Tumor weights. Data represents the mean ± SD ($n = 6$). *$p < 0.05$ and **$p < 0.01$ compared with the gemcitabine alone group.

antitumor agent for pancreatic cancer. Moreover, combination treatment with gemcitabine suppressed the growth of cancer cells more effectively than gemcitabine alone.

Ivermectin inhibits cell proliferation *via* Akt/mTOR phosphorylation and induces G1 arrest in glioblastoma and cervical cancer (Liu et al., 2016; Juarez et al., 2018; Zhang et al., 2019). It synergistically increases the antitumor effects in colorectal cancer with vincristine, an anticancer agent, compared to ivermectin or vincristine alone (Jiang et al., 2019). Cell viability tests and FACS analysis suggested that ivermectin has an anti-proliferative effect and inhibits the cell cycle in pancreatic cancer. We investigated whether ivermectin synergistically enhances the anticancer effects of gemcitabine. We found that the combination treatment of ivermectin and gemcitabine significantly enhanced the antitumor effects *via* the phosphatidylinositol 3-kinase/mTOR/STAT3 pathway compared to gemcitabine treatment alone (Figure 1F).

Oxidative stress plays a predominant role in various cancers (Arfin et al., 2021) as the excessive accumulation of ROS can induce mitochondrial dysfunction and apoptosis (Garrido et al., 2006; Zhang et al., 2016). Ivermectin promotes programmed cell death *via* ROS production (Tang et al., 2021; Zhou et al., 2021), and gemcitabine induces DNA damage *via* ROS (Wang X. et al., 2020). In renal cancer, ivermectin promotes programmed cell death *via* mitochondrial dysfunction caused by ROS generation (Zhu et al., 2017). Ivermectin increases cell apoptosis (Figure 3); however, this function has not yet been elucidated in pancreatic cancer. Thus, in this study, oxidative stress induced by ivermectin and/or gemcitabine was confirmed by ROS production. To the best of our knowledge, this is the first report to demonstrate the function of ivermectin in pancreatic cancer. Ivermectin–gemcitabine combination significantly increased the ROS levels compared to gemcitabine alone (Figure 4A). This result indicates that oxidative stress contributes to pancreatic cancer apoptosis, suggesting that ivermectin may represent a therapeutic alternative for pancreatic cancer. As ROS reduce MMP and OCR by damaging mitochondria (Yang et al., 2021), the MMP and OCR values in the combination treatment group and gemcitabine alone group

were compared. The ivermectin–gemcitabine combination further decreased MMP and OCR compared to gemcitabine alone (Figures 4B,C), indicating that the combination treatment promotes apoptosis in pancreatic cancer *via* mitochondrial dysfunction caused by ROS generation.

Mitochondrial biosynthesis is important for maintaining mitochondrial homeostasis, which is crucial for cell survival (Ma et al., 2020). Cancer induces mitochondrial fission and mitophagy to eliminate dysfunctional mitochondria, which can lead to cell death (Martinez-Outschoorn et al., 2011; Chourasia et al., 2015). Ivermectin–gemcitabine combination treatment significantly reduced the expression levels of the mitochondrial fission- and fusion-related genes compared to gemcitabine alone (Figure 4D). These results suggest that co-treatment with ivermectin and gemcitabine can inhibit the survival rate of cancer cells by blocking mitophagy.

Overall, our study showed that the combination of ivermectin and gemcitabine has a stronger antitumor effect on pancreatic cancer than gemcitabine alone. The ivermectin–gemcitabine combination increased apoptosis of pancreatic cancer cells *via* ROS-induced mitochondrial dysfunction. Moreover, the combination treatment reduced mitophagy, leading to cancer cell death, and further inhibited tumor growth *in vivo*. Therefore, the ivermectin–gemcitabine combination may be a promising therapeutic agent for improving the survival rate of patients with pancreatic cancer.

Data availability statement

The original contributions presented in the study are included in the article/Supplementary Material, further inquiries can be directed to the corresponding author.

Ethics statement

The studies involving human participants were reviewed and approved by the Gangnam Severance Hospital of Yonsei University. The patients/participants provided their written informed consent to participate in this study. The animal study was reviewed and approved by the Institutional Animal Care and Use Committee of the Seoul Yonsei Pharmaceutical University Experimental Animal Center.

Author contributions

DL, HJK, and JP conceived the study and designed the experiments. DL, MK, SK, JJ, SF, WC, YL, and HSK performed the experiments. DL and HJK analyzed the data. DL, HJK, and JP wrote the manuscript.

Funding

This work was supported by a National Research Foundation of Korea (NRF) grant funded by the Korean Government, Ministry of Science, and ICT (MSIT) (NRF 2022R1A2C1004141) and the Industrial Strategic Technology Development Program (20009773, Commercialization of 3D Multifunction Tissue Mimetics Based Drug Evaluation Platform) funded by the Ministry of Trade, Industry and Energy (MOTIE, South Korea). This work was supported by faculty research grant of Yonsei University College of Medicine for (6-2019-0084).

Conflict of interest

The authors declare that the research was conducted in the absence of any commercial or financial relationships that could be construed as a potential conflict of interest.

Publisher's note

All claims expressed in this article are solely those of the authors and do not necessarily represent those of their affiliated organizations, or those of the publisher, the editors and the reviewers. Any product that may be evaluated in this article, or claim that may be made by its manufacturer, is not guaranteed or endorsed by the publisher.

Supplementary material

The Supplementary Material for this article can be found online at: https://www.frontiersin.org/articles/10.3389/fphar.2022.934746/full#supplementary-material

References

Aggarwal, V., Tuli, H. S., Varol, A., Thakral, F., Yerer, M. B., Sak, K., et al. (2019). Role of reactive oxygen species in cancer progression: molecular mechanisms and recent advancements. *Biomolecules* 9, E735. doi:10.3390/biom9110735

Arfin, S., Jha, N. K., Jha, S. K., Kesari, K. K., Ruokolainen, J., Roychoudhury, S., et al. (2021). Oxidative stress in cancer cell metabolism. *Antioxidants (Basel)* 10, 642. doi:10.3390/antiox10050642

Bhatti, J. S., Bhatti, G. K., and Reddy, P. H. (2017). Mitochondrial dysfunction and oxidative stress in metabolic disorders — a step towards mitochondria based therapeutic strategies. *Biochim. Biophys. Acta. Mol. Basis Dis.* 1863, 1066–1077. doi:10.1016/j.bbadis.2016.11.010

Chiu, H. Y., Tay, E. X. Y., Ong, D. S. T., and Taneja, R. (2019). Mitochondrial dysfunction at the center of cancer therapy. *Antioxid. Redox Signal.* 32, 309–330. doi:10.1089/ars.2019.7898

Chourasia, A. H., Boland, M. L., and Macleod, K. F. (2015). Mitophagy and cancer. *Cancer Metab.* 3, 4. doi:10.1186/s40170-015-0130-8

Ding, Y., Wang, H., Niu, J., Luo, M., Gou, Y., Miao, L., et al. (2016). Induction of ROS overload by alantolactone prompts oxidative DNA damage and apoptosis in colorectal cancer cells. *Int. J. Mol. Sci.* 17, 558. doi:10.3390/ijms17040558

Fu, Y., Ricciardiello, F., Yang, G., Qiu, J., Huang, H., Xiao, J., et al. (2021). The role of mitochondria in the chemoresistance of pancreatic cancer cells. *Cells* 10, 497. doi:10.3390/cells10030497

Garrido, C., Galluzzi, L., Brunet, M., Puig, P. E., Didelot, C., and Kroemer, G. (2006). Mechanisms of cytochrome c release from mitochondria. *Cell Death Differ.* 13, 1423–1433. doi:10.1038/sj.cdd.4401950

Hyatt, H. W., and Powers, S. K. (2021). Mitochondrial dysfunction is a common denominator linking skeletal muscle wasting due to disease, aging, and prolonged inactivity. *Antioxidants* 10, 588. doi:10.3390/antiox10040588

Jia, Y., Gu, D., Wan, J., Yu, B., Zhang, X., Chiorean, E. G., et al. (2019). The role of GLI-SOX2 signaling axis for gemcitabine resistance in pancreatic cancer. *Oncogene* 38, 1764–1777. doi:10.1038/s41388-018-0553-0

Jiang, L., Wang, P., Sun, Y.-J., and Wu, Y.-J. (2019). Ivermectin reverses the drug resistance in cancer cells through EGFR/ERK/Akt/NF-κB pathway. *J. Exp. Clin. Cancer Res.* 38, 265. doi:10.1186/s13046-019-1251-7

Juarez, M., Schcolnik-Cabrera, A., Dominguez-Gomez, G., Chavez-Blanco, A., Diaz-Chavez, J., and Duenas-Gonzalez, A. (2020). Antitumor effects of ivermectin at clinically feasible concentrations support its clinical development as a repositioned cancer drug. *Cancer Chemother. Pharmacol.* 85, 1153–1163. doi:10.1007/s00280-020-04041-z

Juarez, M., Schcolnik-Cabrera, A., and Dueñas-Gonzalez, A. (2018). The multitargeted drug ivermectin: from an antiparasitic agent to a repositioned cancer drug. *Am. J. Cancer Res.* 8, 317–331.

Lee, K.-H., Chie, E. K., Im, S.-A., Kim, J. H., Kwon, J., Han, S.-W., et al. (2021). Phase II trial of postoperative adjuvant gemcitabine and cisplatin chemotherapy followed by chemoradiotherapy with gemcitabine in patients with resected pancreatic cancer. *Cancer Res. Treat.* 53, 1096–1103. doi:10.4143/crt.2020.928

Li, X., Fang, P., Mai, J., Choi, E. T., Wang, H., and Yang, X.-f. (2013). Targeting mitochondrial reactive oxygen species as novel therapy for inflammatory diseases and cancers. *J. Hematol. Oncol.* 6, 19. doi:10.1186/1756-8722-6-19

Liang, C., Shi, S., Meng, Q., Liang, D., Ji, S., Zhang, B., et al. (2017). Complex roles of the stroma in the intrinsic resistance to gemcitabine in pancreatic cancer: where we are and where we are going. *Exp. Mol. Med.* 49, e406. doi:10.1038/emm.2017.255

Lin, T.-K., Cheng, C.-H., Chen, S.-D., Liou, C.-W., Huang, C.-R., and Chuang, Y.-C. (2012). Mitochondrial dysfunction and oxidative stress promote apoptotic cell death in the striatum via cytochrome c/caspase-3 signaling cascade following chronic rotenone intoxication in rats. *Int. J. Mol. Sci.* 13, 8722–8739. doi:10.3390/ijms13078722

Liu, Y., Fang, S., Sun, Q., and Liu, B. (2016). Anthelmintic drug ivermectin inhibits angiogenesis, growth and survival of glioblastoma through inducing mitochondrial dysfunction and oxidative stress. *Biochem. Biophys. Res. Commun.* 480, 415–421. doi:10.1016/j.bbrc.2016.10.064

Ma, K., Chen, G., Li, W., Kepp, O., Zhu, Y., and Chen, Q. (2020). Mitophagy, mitochondrial homeostasis, and cell fate. *Front. Cell Dev. Biol.* 8, 467. doi:10.3389/fcell.2020.00467

Martinez-Outschoorn, U. E., Pavlides, S., Sotgia, F., and Lisanti, M. P. (2011). Mitochondrial biogenesis drives tumor cell proliferation. *Am. J. Pathol.* 178, 1949–1952. doi:10.1016/j.ajpath.2011.03.002

Masoud, R., Reyes-Castellanos, G., Lac, S., Garcia, J., Dou, S., Shintu, L., et al. (2020). Targeting mitochondrial complex I overcomes chemoresistance in high OXPHOS pancreatic cancer. *Cell Rep. Med.* 1, 100143. doi:10.1016/j.xcrm.2020.100143

Millichap, L. E., Damiani, E., Tiano, L., and Hargreaves, I. P. (2021). Targetable pathways for alleviating mitochondrial dysfunction in neurodegeneration of metabolic and non-metabolic diseases. *Int. J. Mol. Sci.* 22, 11444. doi:10.3390/ijms222111444

Montano, R., Khan, N., Hou, H., Seigne, J., Ernstoff, M. S., Lewis, L. D., et al. (2017). Cell cycle perturbation induced by gemcitabine in human tumor cells in cell culture, xenografts and bladder cancer patients: Implications for clinical trial designs combining gemcitabine with a Chk1 inhibitor. *Oncotarget* 8, 67754–67768. doi:10.18632/oncotarget.18834

Muz, B., de la Puente, P., Azab, F., and Azab, A. K. (2015). The role of hypoxia in cancer progression, angiogenesis, metastasis, and resistance to therapy. *Hypoxia (Auckl)* 3, 83–92. doi:10.2147/HP.S93413

Perry, S. W., Norman, J. P., Barbieri, J., Brown, E. B., and Gelbard, H. A. (2011). Mitochondrial membrane potential probes and the proton gradient: a practical usage guide. *Biotechniques* 50, 98–115. doi:10.2144/000113610

Pfab, C., Schnobrich, L., Eldnasoury, S., Gessner, A., and El-Najjar, N. (2021). Repurposing of antimicrobial agents for cancer therapy: what do we know? *Cancers (Basel)* 13, 3193. doi:10.3390/cancers13133193

Ponraj, T., Vivek, R., Paulpandi, M., Rejeeth, C., Nipun Babu, V., Vimala, K., et al. (2018). Mitochondrial dysfunction-induced apoptosis in breast carcinoma cells through a pH-dependent intracellular quercetin NDDS of PVPylated-TiO2NPs. *J. Mat. Chem. B* 6, 3555–3570. doi:10.1039/C8TB00769A

Ramaswamy, A., Ostwal, V., Pinninti, R., Kannan, S., Bhargava, P., Nashikkar, C., et al. (2017). Gemcitabine-cisplatin versus gemcitabine-oxaliplatin doublet chemotherapy in advanced gallbladder cancers: a match pair analysis. *J. Hepatobiliary. Pancreat. Sci.* 24, 262–267. doi:10.1002/jhbp.439

Rawla, P., Sunkara, T., and Gaduputi, V. (2019). Epidemiology of pancreatic cancer: global trends, etiology and risk factors. *World J. Oncol.* 10, 10–27. doi:10.14740/wjon1166

Tang, M., Hu, X., Wang, Y., Yao, X., Zhang, W., Yu, C., et al. (2021). Ivermectin, a potential anticancer drug derived from an antiparasitic drug. *Pharmacol. Res.* 163, 105207. doi:10.1016/j.phrs.2020.105207

Wallace, D. C. (2012). Mitochondria and cancer. *Nat. Rev. Cancer* 12, 685–698. doi:10.1038/nrc3365

Wang, K., Gao, W., Dou, Q., Chen, H., Li, Q., Nice, E. C., et al. (2016). Ivermectin induces PAK1-mediated cytostatic autophagy in breast cancer. *Autophagy* 12, 2498–2499. doi:10.1080/15548627.2016.1231494

Wang, L., Duan, Q., Wang, T., Ahmed, M., Zhang, N., Li, Y., et al. (2015). Mitochondrial respiratory chain inhibitors involved in ROS production induced by acute high concentrations of iodide and the effects of SOD as a protective factor. *Oxid. Med. Cell. Longev.* 2015, 217670. doi:10.1155/2015/217670

Wang, X., Chen, F., and Gou, S. (2020). Combination of DN604 with gemcitabine led to cell apoptosis and cell motility inhibition via p38 MAPK signaling pathway in NSCLC. *Bioorg. Chem.* 104, 104234. doi:10.1016/j.bioorg.2020.104234

Wang, Y., Liu, H.-H., Cao, Y.-T., Zhang, L.-L., Huang, F., and Yi, C. (2020). The role of mitochondrial dynamics and mitophagy in carcinogenesis, metastasis and therapy. *Front. Cell Dev. Biol.* 8, 413. doi:10.3389/fcell.2020.00413

Wu, N. N., Zhang, Y., and Ren, J. (2019). Mitophagy, mitochondrial dynamics, and homeostasis in cardiovascular aging. *Oxid. Med. Cell. Longev.* 2019, 9825061. doi:10.1155/2019/9825061

Xu, N., Lu, M., Wang, J., Li, Y., Yang, X., Wei, X., et al. (2021). Ivermectin induces apoptosis of esophageal squamous cell carcinoma via mitochondrial pathway. *BMC Cancer* 21, 1307. doi:10.1186/s12885-021-09021-x

Yang, H., van der Stel, W., Lee, R., Bauch, C., Bevan, S., Walker, P., et al. (2021). Dynamic modeling of mitochondrial membrane potential upon exposure to mitochondrial inhibitors. *Front. Pharmacol.* 12, 679407. doi:10.3389/fphar.2021.679407

Zhang, J., Yan, Y.-J., An, J., Huang, S.-X., Wang, X.-J., and Xiang, W.-S. (2015). Designed biosynthesis of 25-methyl and 25-ethyl ivermectin with enhanced insecticidal activity by domain swap of avermectin polyketide synthase. *Microb. Cell Fact.* 14, 152. doi:10.1186/s12934-015-0337-y

Zhang, L., Li, J., Zong, L., Chen, X., Chen, K., Jiang, Z., et al. (2016). Reactive oxygen species and targeted therapy for pancreatic cancer. *Oxid. Med. Cell. Longev.* 2016, 1616781. doi:10.1155/2016/1616781

Zhang, P., Zhang, Y., Liu, K., Liu, B., Xu, W., Gao, J., et al. (2019). Ivermectin induces cell cycle arrest and apoptosis of HeLa cells via mitochondrial pathway. *Cell Prolif.* 52, e12543. doi:10.1111/cpr.12543

Zhang, Z., Zhou, L., Xie, N., Nice, E. C., Zhang, T., Cui, Y., et al. (2020). Overcoming cancer therapeutic bottleneck by drug repurposing. *Signal Transduct. Target. Ther.* 5, 113. doi:10.1038/s41392-020-00213-8

Zhou, S., Wu, H., Ning, W., Wu, X., Xu, X., Ma, Y., et al. (2021). Ivermectin has new application in inhibiting colorectal cancer cell growth. *Front. Pharmacol.* 12, 717529. doi:10.3389/fphar.2021.717529

Zhu, M., Li, Y., and Zhou, Z. (2017). Antibiotic ivermectin preferentially targets renal cancer through inducing mitochondrial dysfunction and oxidative damage. *Biochem. Biophys. Res. Commun.* 492, 373–378. doi:10.1016/j.bbrc.2017.08.097

frontiers | Frontiers in Pharmacology

TYPE Original Research
PUBLISHED 02 September 2022
DOI 10.3389/fphar.2022.938471

OPEN ACCESS

EDITED BY
Mai F. Tolba,
Ain Shams University, Egypt

REVIEWED BY
Alexander Tikhomirov,
Russian Academy of Medical Sciences, Russia
Nadezhda Dyrkheeva,
Institute of Chemical Biology and Fundamental Medicine (RAS), Russia

*CORRESPONDENCE
Raafat El-Awady,
relawady@sharjah.ac.ae,

SPECIALTY SECTION
This article was submitted to Pharmacology of Anti-Cancer Drugs, a section of the journal Frontiers in Pharmacology

RECEIVED 07 May 2022
ACCEPTED 08 August 2022
PUBLISHED 02 September 2022

CITATION
Lozon L, Saleh E, Menon V, Ramadan WS, Amin A and El-Awady R (2022), Effect of safranal on the response of cancer cells to topoisomerase I inhibitors: Does sequence matter?
Front. Pharmacol. 13:938471.
doi: 10.3389/fphar.2022.938471

Effect of safranal on the response of cancer cells to topoisomerase I inhibitors: Does sequence matter?

Lama Lozon[1,2], Ekram Saleh[3], Varsha Menon[1], Wafaa S. Ramadan[1], Amr Amin [4] and Raafat El-Awady [1,5]*

[1]Sharjah Institute of Medical Research, University of Sharjah, Sharjah, United Arab Emirates, [2]College of Medicine, University of Sharjah, Sharjah, United Arab Emirates, [3]Clinical Biochemistry and Molecular Biology Unit, Cancer Biology Department, National Cancer Institute, Cairo University, Giza, Egypt, [4]Department of Biology, College of Science, UAE University, Al Ain, United Arab Emirates, [5]College of Pharmacy, University of Sharjah, Sharjah, United Arab Emirates

Lung and colorectal cancers are among the leading causes of death from cancer worldwide. Although topotecan (TPT), a topoisomerase1 inhibitor, is a first- and second-line drug for lung and colon cancers, the development of drug resistance and toxicity still remain as a major obstacle to chemotherapeutic success. Accumulating evidence indicates increased efficacy and reduced toxicity of chemotherapeutic agents upon combining them with natural products. We aimed to investigate the possible interaction of safranal (SAF), a natural compound obtained from *Crocus sativus* stigma, with TPT when used in different sequences in colon and lung cancer cell lines. The growth inhibitory effect of the proposed combination given in different sequences was assessed using the colony formation assay. The comet assay, cell cycle distribution, Annexin-V staining, and expression of proteins involved in DNA damage/repair were utilized to understand the mechanism underlying the effect of the combination. SAF enhanced the growth inhibitory effects of TPT particularly when it was added to the cells prior to TPT. This combination increased the double-strand break induction and dysregulated the DNA repair machinery, particularly the tyrosyl-DNA phosphodiesterase 1 enzyme. In addition, the SAF + TPT combination increased the fraction of cells arrested at the G2/M checkpoint as well as enhanced the induction of apoptosis. The current study highlights the status of SAF as a natural product sensitizing the lung and colon cancer cells to the cytotoxic effects of the anticancer drug TPT. In addition, it emphasizes the importance of sequence-dependent interaction which can affect the overall outcome.

KEYWORDS

safranal, topotecan, TDP1, topoisomerase, lung cancer and colon cancer

Introduction

Colorectal (CRC) and lung cancers are among the most prevalent cancer subtypes, together they account for approximately 2.8 million deaths from cancer annually (Sung et al., 2021). Chemotherapy is a principal option in the treatment of both types. However, its use is associated with various problems that limit its usefulness. First, they lack selectivity toward cancer cells, thus they can damage rapidly dividing normal cells including gastrointestinal tract epithelial cells and the bone marrow (Zugazagoitia et al., 2016; Falzone et al., 2018). Second, the development of resistance which can cause therapy failure (El-Awady et al., 2017; Mansoori et al., 2017). Combination treatment with different anticancer agents remains the core practice to overcome drawbacks of conventional cancer therapy. It allows the use of more than one agent in a reduced dosage which enhances the efficacy and reduces the likelihood of severe adverse events (Chabner and Longo, 2018). Recently, a new option of cancer therapy has emerged, which involves combining traditional chemotherapy with a naturally derived chemical that is showing evidence of cytotoxicity to cancer cells and limited damage toward normal cells (Huang et al., 2017, 2019; Rejhová et al., 2018). The sequence by which the combined agents are administered is as important as the choice of the agents themselves. This decision is based on understanding the pharmacodynamics and pharmacokinetics of the combined drugs (Mancini and Modlin, 2011; Poggio et al., 2017).

Topoisomerase I (TOPOI) inhibitors are an important class of chemotherapy, which include topotecan (TPT) and irinotecan. They are used in the management of different types of cancers such as colon, lung, and ovarian (Vennepureddy et al., 2015; Bailly, 2019). They exert their effect on TOPOI, which controls the topology of DNA and is usually required to relieve the DNA supercoiling to allow a flawless DNA replication and transcription. TOPOI works by generating a nick in a single strand of DNA double helix, rotating one strand over the other, and then it re-ligates the nick. TOPOI inhibitors stabilize the TOPOI–DNA cleavage complex (TOPcc) thus preventing DNA re-ligation, which results in a DNA single-strand break (SSBs). This will activate the SSB repair response that involves a cascade of proteins, among which is tyrosyl-DNA phosphodiesterase 1 (TDP1).

Human TDP1 is a member of the phospholipase D (PLD) superfamily and is described as a repair enzyme of TOPcc (Interthal et al., 2001). TDP1 repairs trapped TOPcc, caused by TOPOI inhibitors, by catalyzing the hydrolysis of 3̀-phosphotyrosyl bond located in that complex, to make DNA ends suitable for ligation (Pommier et al., 2014; Kawale and Povirk, 2018). Targeting TDP1 catches the attention of many scientists, suggesting that inhibiting TDP1 has the potential to augment the anticancer activity of TOPOI inhibitors by decreasing the repair of the stable complex caused by these drugs (Dean et al., 2014). This was supported by the finding that TDP1 knockout mice are hypersensitive to TOPOI inhibitors (Miao et al., 2006). It was reported that TDP1 tends to be overexpressed in non–small–cell lung cancer (NSCLC) and CRC, which confers resistance to TPT and other TOPOI inhibitors (Liu et al., 2007; Gilbert et al., 2012). The mutations in TDP1 that result in reduction of its catalytic activity sensitizes cancer cells to the cytotoxic effects of TOPOI inhibitors (Miao et al., 2006). These pieces of evidences suggest the importance of TDP1 in predicting the response to TOPOI inhibitors, and thus highlighting the significance of developing inhibitors to block its activity.

Safranal (SAF) constitutes the volatile fraction of *Crocus sativus* stigma (Leone et al., 2018). It has been shown to exert anticonvulsant, antidepressant, antihypertensive, antioxidant, and cytotoxic activities. These valuable effects illustrate its importance as a potential drug in future (Rezaee and Hosseinzadeh, 2013). In cancer, SAF shows a promising cytotoxic effect that is specific to cancer cells. This tumoricidal observation was seen even at low concentrations where it shows no toxicities (Riahi-Zanjani et al., 2015; Milajerdi et al., 2016). The mechanisms by which SAF is excreting its cytotoxicity on several cancer cell lines have been a hot area of research. In oral squamous cell carcinoma HSC-3 cells, SAF was able to reduce the invasiveness and migration of those cells by reducing the expression of mesenchymal markers and increasing those of epithelial cells (Zhang et al., 2017). In hepatocellular carcinoma cell HepG2, SAF shows ability to induce ER stress, to increase the extent of DNA double-strand breaks, and to increase apoptosis (Al-Hrout et al., 2018).

Inspired by the ability of SAF to potentially interfere with the function of TDP1 (Al-Hrout et al., 2018), we explored, in the present study, the effect of a new combination involving the TOPOI inhibitor TPT and SAF against HCT116 and A549 cell lines. The sequence-dependent effects of this combination and the mechanism of their cytotoxicity were also investigated.

Materials and methods

Cell lines and culture conditions

Two cancer cell lines (CRC: HCT116 and NSCLC: A549) were used in this study. The two cell lines were a generous gift from the Radiobiology and Experimental Radio-Oncology laboratory, University Cancer Center, Hamburg University, Hamburg, Germany. All cell lines were maintained in a RPMI (A549) or DMEM (HCT116) medium supplemented with 10% fetal bovine serum and 1% penicillin/streptomycin (Sigma-Aldrich, St. Louis, MO, United States) and are kept in a 37□C humidified incubator and an atmosphere of 5% CO_2.

Chemicals and antibodies

Topotecan hydrochloride (TPT) and safranal (SAF) (Sigma-Aldrich, Missouri, United States) were dissolved in dimethyl sulfoxide (DMSO) (Sigma-Aldrich, Missouri, United States), the stock solution of TPT was kept at −20°C. In preparation for an experiment, a serial dilution of TPT was prepared in the medium to achieve a concentration range of 0.001–1 μM and the concentration of DMSO in all samples was 0.02%. Primary monoclonal antibodies against γ-H2AX and TDP1 and secondary antibodies (anti-rabbit and anti-mouse) were obtained from Cell Signaling Technology (Danvers, MA, United States). In addition, propidium iodide (PI), RNAase, and crystal violet were purchased from (Sigma-Aldrich, Missouri, United States).

Colony formation assay

SAF IC50 for each cell line was determined by CFA (El-Awady et al., 2010), and the cells were seeded in T25 cm^2 culture flasks in densities ranging from 50 to 1,200 cells per flask. This was decided based on the SAF concentration used and the doubling time of the cells. After 24 h, the cells were treated with different SAF concentrations (10–200 μM) and the control group was treated with DMSO. All treatments were incubated for the whole period of colony formation. CFA was also used to assess the effect of the combination TPT/SAF in different sequences. The first sequence involves the addition of SAF IC50/IC25 24 h before TPT (0.001–1.0 μM) and the combination was incubated for 24 h. The second is where SAF IC50/IC25 is given simultaneously with TPT (0.001–1.0 μM) and the combination was incubated for 48 h. Last, SAF IC50/IC25 was introduced 24 h after TPT (0.001–1.0 μM) and incubated for another 24 h. In this experiment, the cells were seeded in T25 cm^2 culture flasks with seeding densities ranging from 50 to 20,000 cells per flask. After 24 h, the cells were treated with SAF/TPT in different sequences. After 12–14 days when colonies of ≥50 cells were observed, the cells were fixed with 70% of ethanol for 30 min. After dryness, the flasks were stained with 1% crystal violet for 5 min at room temperature (RT), and then left to dry. The number of colonies at each treatment was counted using the microscope for the calculation of both plating efficiency (counted colonies/seeding number) and surviving fraction (plating efficiency of treated/plating efficiency of control). The IC50 values were calculated by sigmoidal curve fitting models using GraphPad Prism 3 software (GraphPad Software, San Diego, CA, United States). To assess the type of pharmacological interaction, the following isobologram equation was used (Berenbaum, 1989): $I = d1/D1 + d2/D2$, where I is the interaction index, d1 and d2 are the respective concentrations of SAF and TPT used in the combination required to produce 50% inhibition of cell growth. D1 and D2 are the concentrations of each agent alone that are able to yield the same degree of effect (50% inhibition of cell growth). If interaction index (I) < 1, the combination is synergistic, whereas if I = 1, it is additive and if I > 1, the effect is antagonistic.

Neutral comet assay

To investigate the effect of SAF, TPT, and their combination on DNA damage, the neutral comet assay was performed according to the manufacturer's protocol (Trevigen Inc, Gaithersburg, MD) following treatment with the most effective sequence, SAF IC25/IC50 added before TPT IC50. The cells were seeded in T25 cm^2 flasks at a density of 0.5–0.8 million cells, after 24 h; they were treated with SAF IC25/IC50, and TPT was introduced 24 h thereafter. The combination was kept for 24 h, and then the cells were washed, harvested gently with a scraper, and counted to obtain 10^5 cells/sample to be mixed with low melting point agarose (Trevigen Inc) at a proportion of 1:10. The cells/agarose mixture was evenly distributed on the comet slides and allowed to solidify before being immersed in lysis buffer (Trevigen Inc) at 4°C overnight. The next day, the slides were washed with the neutral buffer (Tris-base, sodium acetate, pH of 9), followed by 30 min/35 V electrophoresis at 4°C. The slides were submerged in a precipitation solution (7.5 M ammonium acetate) followed by 70% ethanol for 30 min each. The dry slides were then stained with SYBER Gold (Invitrogen, CA, United States) in TE buffer for 30 min, washed, dried, and covered. Images were captured at ×20 magnification using a confocal microscope (Olympus, Japan). The tail length and the intensity of the fluorescence signal in the tail area were measured using ImageJ (NIH, United States) for at least 70 cells/sample to calculate the tail moment (tail length + tail area).

Western blot

The cells were seeded, treated as mentioned in the comet assay, and the total cell lysate was obtained by incubation with lysis buffer (Glycerol, 20% SDS and 1 M Tris, pH 6.8) containing the protease inhibitor cocktail (Sigma-Aldrich, United States). The protein was quantified using the DC™ protein assay kit (Bio-Rad, United States) and Western blot was performed as described previously (Ramadan et al., 2021). The samples containing equal amounts of protein (15–30 μg) were loaded into the gels to be separated on either 8% or 12% SDS polyacrylamide gel and transblotted onto the nitrocellulose membrane (Bio-Rad, United States). The membranes were blocked with 5% non-fat dried milk/1X TBS-Tween 20 and incubated with primary monoclonal antibodies (1:1,000) against γ-H2AX and TDP1 and β-actin overnight at 4°C, and then the membranes were blocked with 1X TBS-T. The secondary antibodies were

prepared at a dilution of (1:2,000) and incubated with the membrane at RT for 1 h. Chemiluminescence was detected using the ECL method (Thermo Fisher Scientific, Massachusetts, United States) and developed using the ChemiDoc™ imaging system (Bio-Rad, United States). Quantification and analysis of the bands were performed using ImageLab™ software (Bio-Rad, United States).

Cell cycle distribution analysis

The effect of SAF, TPT, and their combination on cell cycle progression was elucidated by flow cytometry (Saleh et al., 2009). The cells were seeded in T75 cm^2 culture flasks at variable densities for each time point (0.5–1.5 million cells/flask). After 24 h, the cells were treated with DMSO, TPT IC50, SAF IC25/IC50, and a combination of them. The combinations were performed in three different sequences where SAF was given before TPT, concurrent or after TPT treatment for HCT116. However, for A549, only SAF before TPT was assessed. The flasks were incubated for different time intervals (12, 24, and 48 h). At each time interval, the cells were harvested and washed and fixed in 70% ethanol at 4°C. The fixed cells were washed two times with 1X PBS, counted and resuspended in 1X PBS containing RNAase (100 µg/ml), and incubated for 30 min at 37°C on a shaker. The cells were stained with propidium iodide (PI) (50 µg/ml) and analyzed using an Accuri C6 flow cytometer (Becton Dickenson, United States). DNA histograms were obtained using FlowJo V.10 software (Tree Star, Inc-Oregon, United States).

Apoptosis assay

The induction of apoptosis in HCT116 and A549 cells after treatment with DMSO, TPT IC50, and SAF IC25/IC50 alone or in combination (SAF plus TPT) was assessed for the percentage of cells positive for either Annexin-V, PI or both. The cells were prepared according to the manufacturer's protocol FITC Annexin-V Apoptosis Detection Kit (BD Biosciences, United States). A measure of 5 µl of FITC Annexin-V and 10 µl PI (500 mg/ml) was added and the samples were incubated for 15 min in the dark at RT. Binding buffer (400 µl) was then added and cell staining was analyzed using an Accuri C6 flow cytometer (Becton Dickenson, United States).

Statistical analysis

All experiments were carried out in triplicate and repeated at least three times. Data are expressed as means ± SEM. Statistical analysis was performed by unpaired student's *t*-test using GraphPad Prism 3 (CA, United States) software (GraphPad Software). $p < 0.05$ was considered statistically significant.

Results

Effect of SAF on the survival of HCT116 and A549 cells

The growth inhibition of HCT116 and A549 cells by SAF treatment was assessed using the colony formation assay. SAF treatment caused concentration-dependent reduction in survival of both cell lines (Figure 1A). The IC50 of SAF was determined for each cell line using the best fitting curve method in prism software. Based on the calculated IC50 value, HCT116 is more sensitive to SAF with IC50 of 49.3 µM while A549 is more resistant with IC50 of 92.5 µM.

Effect of SAF on the cytotoxic effect of TPT on HCT116 and A549 cells

The effect of SAF and TPT combination treatment given in three different sequences on the survival of the HCT116 and A549 cells was evaluated using the colony formation assay, where the IC25 and IC50 of SAF equivalent to (24.7/49.3 µM) for HCT116 and to (46.3/92.5 µM) for A549 cells were used in combination with different concentrations (0.0–1.0 µM) of TPT. This treatment scheme was applied for three different sequences: SAF 24 h before TPT, SAF, and TPT were added simultaneously and SAF 24 h after TPT. IC50 of TPT was 0.01 µM for HCT116 cells and 0.05 µM for A549 cells. This indicates that A549 cells are more resistant to TPT compared to HCT116 cells. The combined treatment of SAF and TPT was able to decrease the IC50 of TPT in all treatment sequences in HCT116 cells (Figure 1B and Table 1) while in A549, only when SAF was given before TPT there was a significant reduction in the IC50 of TPT (Figure 1C and Table 1). It is worth mentioning that incubation of HCT116 cells with SAF 24 h before the addition of TPT resulted in 16.8 fold increase in the sensitivity of the cells to TPT (IC50 of TPT alone is 0.01 µM compared to 0.00069 µM for SAF + TPT) (Figure 1B) (Table 1). The type of pharmacological interaction between SAF and TPT was determined using the isobologram equation. In HCT116 cells, the interaction between SAF IC25 and TPT in all treatment sequences was synergistic, while the interaction of SAF IC50 with TPT was additive when SAF was given before TPT. For A549 cells, the interaction of SAF IC25/IC50 was additive when SAF was added before TPT, while the other sequences showed an antagonistic interaction (Table 2).

Effect of SAF, TPT, and their combination on the induction of DNA damage

TPT exerts its cytotoxic effect via induction of single-strand breaks (SSBs) which are converted to double-strand breaks

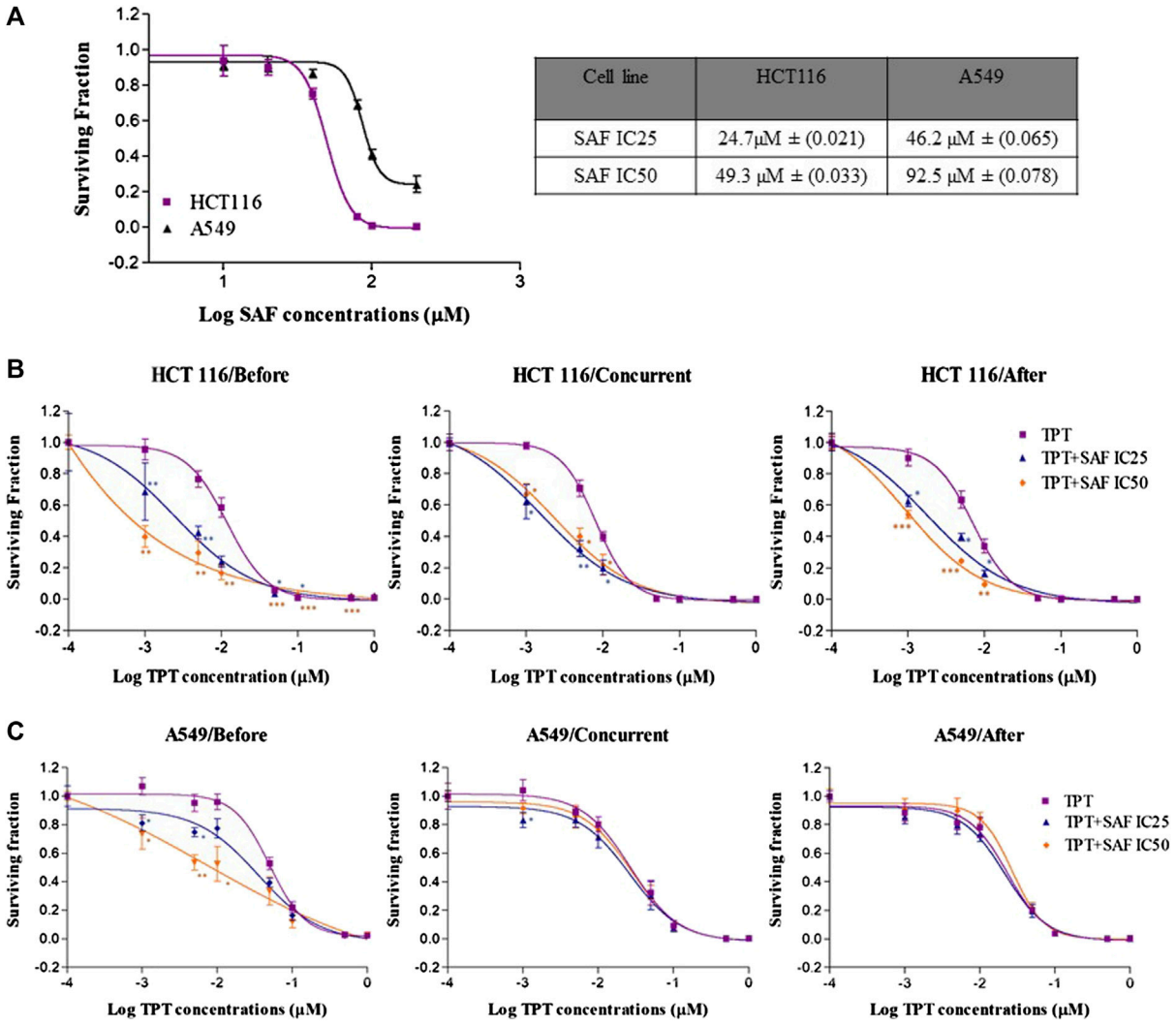

Cell line	HCT116	A549
SAF IC25	24.7μM ± (0.021)	46.2 μM ± (0.065)
SAF IC50	49.3 μM ± (0.033)	92.5 μM ± (0.078)

FIGURE 1
Effect of SAF IC25/IC50 on the sensitivity of both HCT116 and A549 cells to topotecan treatment by using different sequences. **(A)** Colony formation assay was used to measure the sensitivity of HCT116 and A549 cancer cell lines to different concentrations of SAF (μM). **(B–C)** HCT116 and A549 cells were treated with IC25/IC50 concentrations of SAF either 24 h before, concurrently or 24 h after treatment with different concentrations of TPT (μM). Surviving fraction is calculated by dividing the plating efficiency (PE) of treated cells by the (PE) of control cells. The means ± SEM of at least two independent experiments are shown. *$p < 0.05$, **$p < 0.005$, and ***$p < 0.0005$ vs TPT group.

(DSBs) during DNA replication. So, we next investigated the contribution of SAF to the overall seen DNA damage upon combination given in the most effective sequence using the neutral comet assay. Both HCT116 and A549 cells were treated with SAF IC25/IC50 24 h before the addition of TPT IC50, then the combined therapy was incubated for another 24 h. HCT116 cells showed a significant increase in the extent of DNA damage (DSBs) in the combined treatment compared to TPT 0.01 μM alone with both SAF IC25/IC50 (Figures 2A–D). However, the effect was more pronounced with SAF IC50 combination (Figure 2C). In A549 cells, both SAF IC25/IC50 combined with TPT 0.05 μM caused a similar increase in DSBs induced compared to TPT alone (Figures 2E–H). The phosphorylated H2AX histone protein (γH2AX) normally forms nuclear foci at DNA break sites in cells experiencing DNA damage. It is, therefore, used as a DNA damage marker and was used in the current study to confirm the finding from the comet assay. HCT116 cells were treated with SAF IC25/IC50 given 24 h before TPT 0.01 μM. There was a significant increase in the level of γH2AX after the combined treatment with SAF IC50 and TPT 0.01 μM (Figure 3A). A similar pattern of increase in γH2AX was also seen in A549 cells (Figure 3B).

TABLE 1 IC50 values after treatment of HCT116 and A549 cell lines with TPT and TPT + SAF at different sequences. IC25 (μM): the concentration of the drug necessary to produce 25% inhibition of cell growth. IC50 (μM): the concentration of the drug necessary to produce 50% inhibition of cell growth. Represented data are means ± SEM of at least three independent experiments.

	IC50 (μM)	
Cell line	HCT116	A549
TPT alone	0.0100 ± (0.0013)	0.0496 ± (0.0067)
SAF IC25+TPT		
Before	0.0028 ± (0.0004)	0.0280 ± (0.0077)
Concurrent	0.0018 ± (0.0010)	0.0226 ± (0.0194)
After	0.0021 ± (0.0002)	0.0191 ± (0.0033)
SAF IC50+TPT		
Before	0.0007 ± (0.0006)	0.0098 ± (0.0184)
Concurrent	0.0025 ± (0.0017)	0.0257 ± (0.0103)
After	0.0012 ± (0.0002)	0.0258 ± (0.0009)

Effect of the combined treatment of SAF and TPT on the modulation of DNA repair

TDP1 is a key enzyme required to repair SSBs induced by TPT. SAF was reported to bind to TDP1 in an inhibitory manner (Al-Hrout et al., 2018). Thus, we investigated the changes in the expression level of TDP1 following treatment with SAF IC25/IC50 given before TPT IC50. In both cell lines (HCT116 and A549), the combined treatment of SAF IC50 and TPT IC50 significantly reduced the expression of TDP1 (Figures 3A,B). However, the combination IC25 SAF with TPT reduced the expression of TDP1 in HCT116 only (Figure 3A).

Effect of the combined treatment of SAF plus TPT on the cell cycle progression

Cell cycle distribution analyses of both cell lines at 12, 24, and 48 h intervals were performed to determine the effect of combining SAF IC25/IC50 with TPT at the sequences that showed a significant reduction in the IC50 of TPT in the proliferative assay. The combination of SAF IC50 and TPT 0.01 μM in HCT116 cells caused an increase in the fraction of cells arrested at the G2/M checkpoint at 12, 24, and 48 h when SAF was given before TPT (Figure 4A and Supplementary Figure S1A). The same effect was achieved at 48 h only in the treatment sequence where SAF is given simultaneously with TPT (Figure 4B and Supplementary Figure S1B). SAF IC25 was only able to increase in the S phase arrest when given after TPT 0.01 μM at the 12 h interval (Figure 4C and Supplementary Figure S1C). For A549 cells, treatment with SAF IC25/IC50 before 0.05 μM of TPT showed a statistically significant increase in the fraction of cells arrested at the G2/M checkpoint at 24 h post-treatment compared to TPT 0.05 μM alone only (Figure 4D and Supplementary Figure S1D). Other time points did not show any change in the cell cycle distribution among single or combination treatments (Figure 4D).

SAF enhances induction of apoptosis when combined with TPT

The main proposed mechanism of safranal's cytotoxicity is its ability to induce apoptosis. So, we performed Annexin-V staining for HCT116 cells which revealed an increase in Annexin+/PI + cells at 24 and 48 h with SAF IC25/IC50 combined with TPT which indicates late apoptosis

TABLE 2 Effect of SAF on TPT cytotoxicity in HCT116 and A549 cells and the type of interaction after each treatment and sequence. Interaction index: *I* = d1/D1 + d2/D2, where d1 and d2 are the respective concentrations of TPT and SAF used in the combination required to produce a fixed level of inhibition IC25/IC50. While D1 and D2 represent concentrations of each TPT and SAF alone to produce the same magnitude of effect (IC25/IC50). Values presented are means ± SEM of at least three independent experiments.

	IC50 (μM)			
Cell line	**HCT116**		**A549**	
SAF IC25+TPT	**Interaction index (I)**	**Type of interaction**	**Interaction index (I)**	**Type of interaction**
Before	0.76 ± (0.03)	Synergy	1.04 ± (0.069)	Additivity
Concurrent	0.73 ± (0.04)	Synergy	1.33 ± (0.068)	Antagonistic
After	0.80 ± (0.1)	Synergy	1.40 ± (0.058)	Antagonistic
SAF IC50+TPT				
Before	1.00 ± (0.038)	Additivity	1.05 ± (0.013)	Additivity
Concurrent	1.32 ± (0.07)	Antagonistic	1.95 ± (0.085)	Antagonistic
After	1.17 ± (0.1)	Antagonistic	2.21 ± (0.102)	Antagonistic

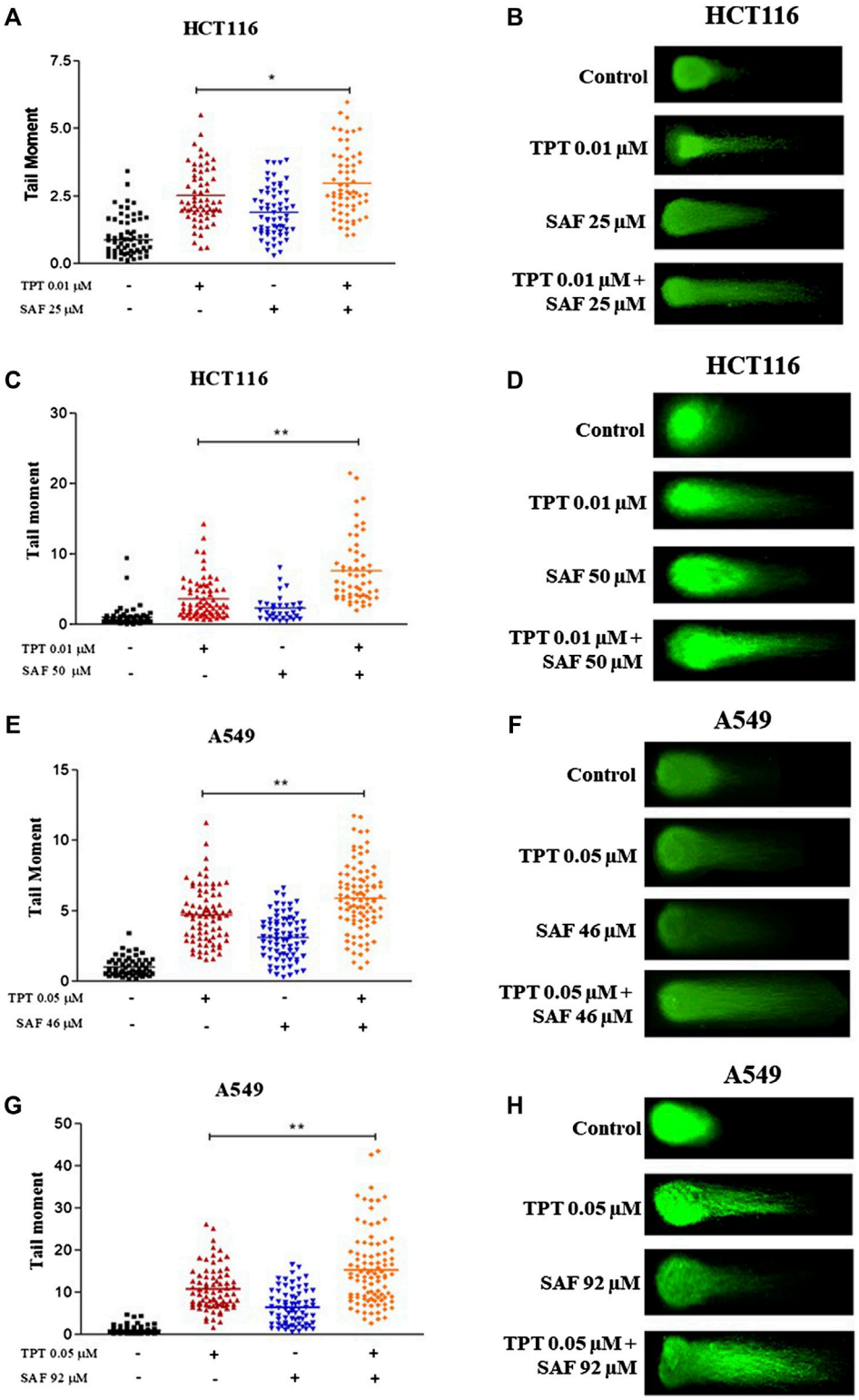

FIGURE 2
Neutral comet assay of HCT116 and A549 cells treated with SAF IC25/IC50 before TPT IC50 treatment for 24 h. **(A–D)** Tail moment and fluorescence microscopic images of HCT116 cells treated with SAF IC25/IC50, 24 h before TPT 0.01 μM, the combined treatment was incubated for 24 h. **(E–H)** Tail moment and florescence microscopic images of A549 cells treated with SAF IC25/IC50, 24 h before TPT 0.05 μM and the combined treatment was incubated for 24 h. The means ± SEM of at least two independent experiments are shown. *$p < 0.05$, **$p < 0.005$ vs TOP group.

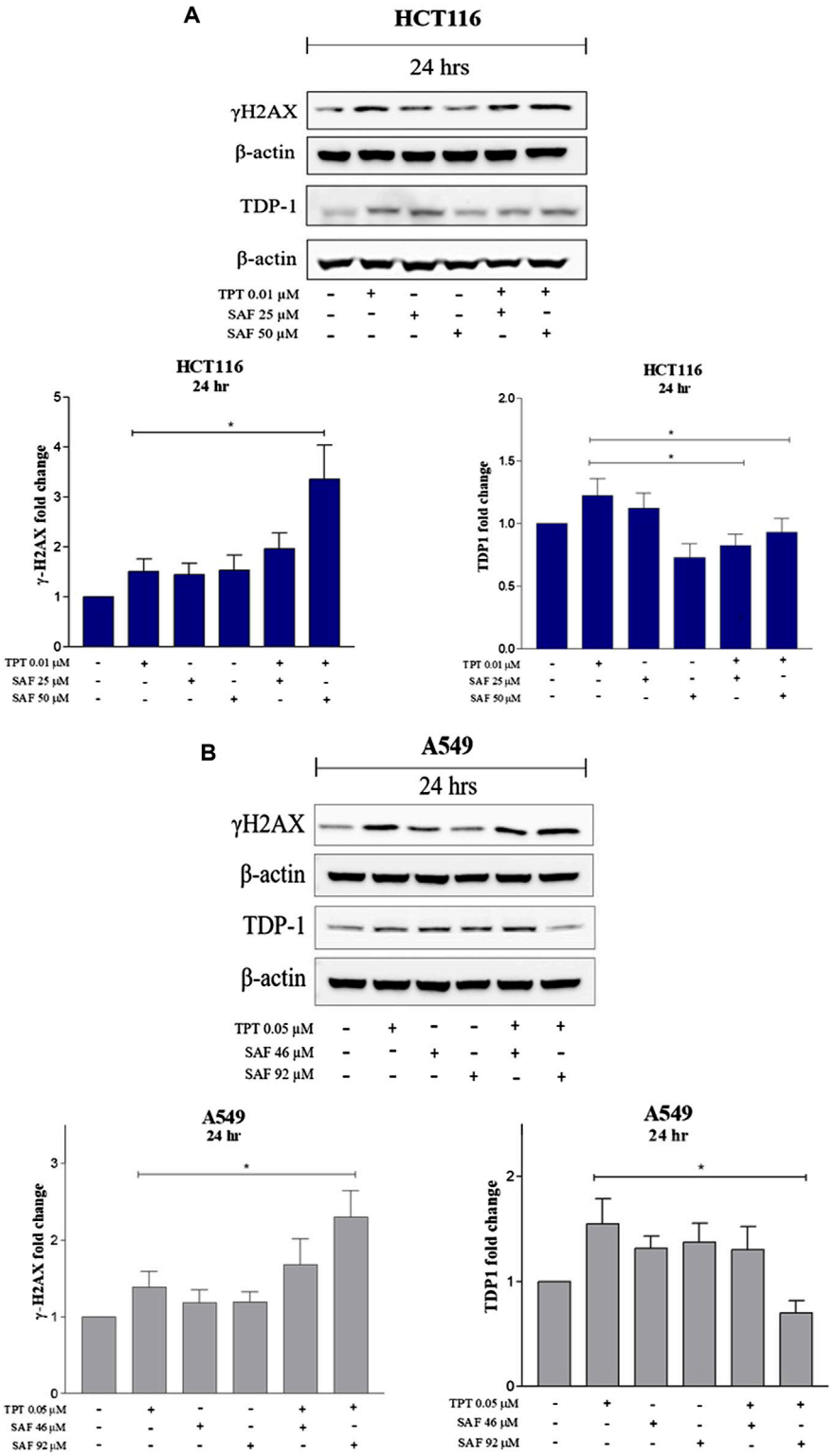

FIGURE 3
Expression of γH2AX and TDP1 in HCT116 and A549 cells after treatment with SAF IC25/IC50 before TPT IC50 treatment Western blot analysis for HCT116 **(A)** and A549 **(B)** was performed by loading the whole cell lysates treated with SAF IC25/IC50 before TPT 0.01 μM for 24 and 48 h in HCT116 cells and treated with SAF IC25/IC50 before TPT 0.05 μM for 24 and 48 h in A549 cells. Bar graphs represent densitometric quantifications of Western blot bands normalized to β-actin and vehicle-treated control. The means ± SEM of at least three independent experiments are shown. *$p < 0.05$ vs. TPT group.

10.3389/fphar.2022.938471

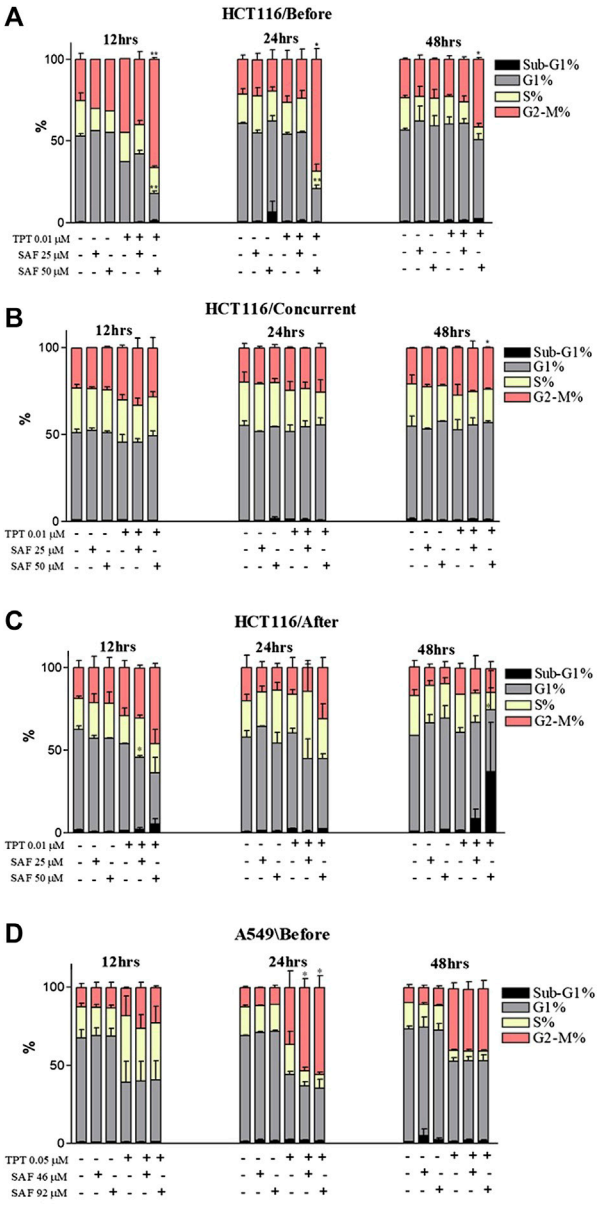

FIGURE 4
Cell cycle distribution analysis of HCT116 and A549 cells treated with SAF IC25/IC50 and TPT IC50 μM for different time intervals and sequences. **(A–C)** HCT116 cells treated with SAF IC25/IC50 24 h before TPT 0.01 μM **(A)**, concurrently with TPT 0.01 μM **(B)**, and 24 h after TPT 0.01 μM **(C)**, the combined treatment was incubated for 12, 24, and 48 h. **(D)** A549 cells treated with SAF IC25/IC50 24 h before TPT 0.05 μM, the combined treatment was incubated for different time intervals of 12, 24, and 48 h. The means ± SEM of at least two independent experiments are shown. *$p < 0.05$, **$p < 0.005$ vs TPT group.

(Figure 5A and Supplementary Figure S2A). The same results were observed when A549 cells were treated with SAF IC50 given before TPT at 48 h (Figure 5B and Supplementary Figure S2A).

Discussion

Resistance of cancer cells and the low safety profile of anticancer drugs are two major factors limiting the success of cancer therapy. Combining natural products with current anticancer drugs is one strategy to overcome this problem. Due to their high safety profile, natural products will not add to the toxicity of anticancer drugs, yet they might enhance their anticancer activity by allowing the use of smaller doses and enhancing the therapeutic index of anticancer drugs. The clinical applications of TOPO1 inhibitors are limited to confined tumor subtypes due to profound neutropenia and bone marrow suppression associated with the effective dose (Chabner and Longo, 2018). Recent data have shown that high levels/activity of TDP1 can negatively impact the success of therapy with TOPO1 inhibitors as there is a higher degree of TOPO1-damage reversal thus negating the ensuing DNA damages and cell death signal imparted in the cancer cell. TOPO1 vs. TDP1 ratio has recently become an important indicator/predictor of response to TOPO1 inhibitors (Meisenberg et al., 2014). High TOPO1 levels with low TDP1 levels/activity are an ideal scenario for the enhanced use of TOPO1 inhibitors as an effective anticancer strategy. Identifying TDP1 inhibitors to reduce the denominator in this ratio would extend the therapeutic benefit of the TOPO1 inhibitors. A recent study has revealed that using an *in silico* molecular docking can help SAF bind to the active site of TDP1 suggesting its ability to prevent TDP1 to correct single-strand breaks induced in the DNA. The same study showed that SAF can reduce the expression levels of TDP1 in HepG2 cells (Al-Hrout et al., 2018). In the present study, we tested the effect of the natural product SAF on the anticancer activity of the TOPOI inhibitor TPT. Moreover, the effect of combining SAF with TPT in different sequences was investigated.

In the current study, incubation of the colon cancer cell line (HCT116) or the non–small–cell lung cancer cell line (A549) with SAF (IC25 or IC50) 24 h prior to TPT increased the amount of DNA double-strand breaks compared to cells treated with TPT alone as indicated by the increased tail moment (Figure 2) and the increased γ–H2AX formation (Figure 3). This may be attributed to additional induction of DNA DSB by SAF or due to the ability of SAF to inhibit the repair of TPT-induced DSBs or both.

Our results show that treatment of both cell lines with TPT alone increases the expression of TDP1, whereas combination of SAF + TPT (SAF IC25/IC50 followed by TPT IC50) reduced the expression of TDP1. This may explain the increased sensitivity of both cell lines to TPT when cells were treated with SAF followed by TPT. The reduced expression of TDP1 in combined treatment decreases the repair of TPT-induced DNA lesions and results in accumulation of more DNA lesions leading to enhanced cell death.

It is noteworthy that the sequence of adding SAF and TPT to the cells significantly affected the type of pharmacological interaction between the two compounds. Incubating the cells with SAF before TPT showed the best interaction (synergistic or

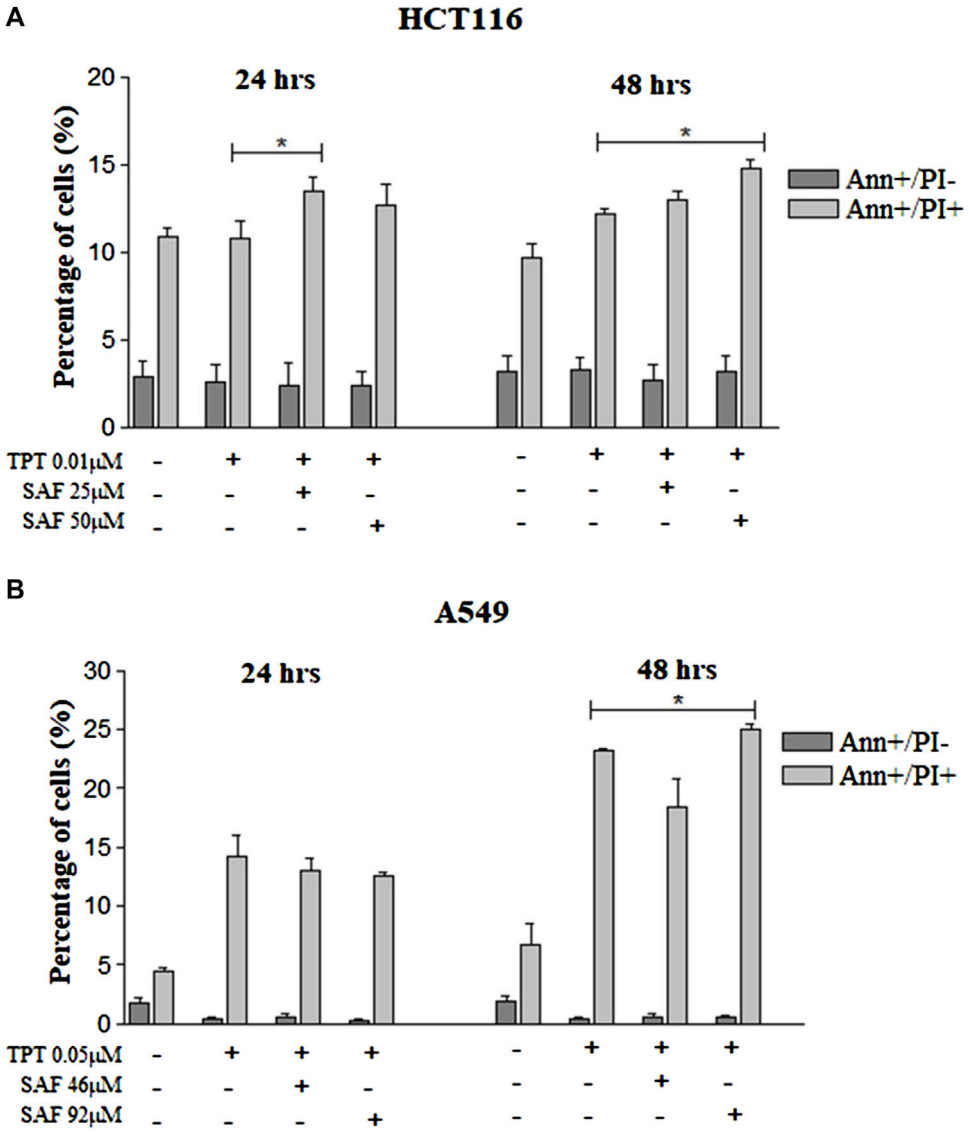

FIGURE 5
Annexin-V/PI flow cytometry of HCT116 and A549 cells treated with SAF IC25/IC50 before TPT IC50 treatment. Annexin-V/PI analysis of apoptosis in HCT116 cells **(A)** treated with SAF IC25/IC50 24 h before TPT 0.01 μM treatment. The combined treatment was incubated for 24 and 48 h. The cells were stained with fluorescein-conjugated Annexin-V and propidium iodide (PI) and analyzed by flow cytometry. The same analysis was performed for A549 cells **(B)** treated with SAF IC25/IC50 24 h before TPT 0.05 μM treatment. The means ± SEM of at least three independent experiments are shown. *$p < 0.05$ vs. TPT group.

additive), whereas other sequences (concurrent treatment or TPT followed by SAF) resulted in antagonistic interaction in most cases. The sequence-dependent type of pharmacological interaction of anticancer drugs with other compounds has been previously reported (El-Awady et al., 2011).

The inability of cancer cells to efficiently repair drug-induced DNA damage stimulates cell cycle checkpoints. The main aim was to prevent cells from entering the S and M phases of the cell cycle with damaged DNA (El-Awady et al., 2011). In the present investigation, incubation of cells with SAF, especially before TPT resulted in an increased fraction of cells arrested at the G2 phase of the cell cycle compared to cells treated with TPT alone. TOPOI inhibitors are known to be most toxic to actively dividing cells and to induce lethal DNA lesions during the S phase of the cell cycle (Pommier, 2006). This explains the high fraction of cells arrested at the G2 phase upon treatment with SAF + TPT. Inhibition of TDP1 by SAF reduces the repair of TPT-induced DNA damage and activates the G2/M checkpoint to prevent cells from entering the M phase with damaged DNA. The cells arrested at the G2 phase are given more time to repair their DNA lesions or to be removed by different cell

death pathways such as apoptosis. Combined treatment with SAF followed by TPT increased the fraction of apoptotic and necrotic cells in both cell lines indicating the stimulation of apoptosis/necrosis pathways upon combining SAF with TPT. This is in line with previous studies showing activation of apoptosis upon treatment of cells with topoisomerase inhibitors (El-Awady et al., 2008).

In conclusion, our results emphasize the importance of SAF as a candidate-sensitizing agent of colon and lung cancer cells to the effect of topotecan. This sensitization showed to be sequence-dependent with the most profound effects when SAF is given before TPT. Furthermore, it gives an insight into understanding the mechanism of the potentiated growth inhibitory effects seen with combination treatment that involves DNA damage, DNA repair machinery, cell cycle, and apoptosis. Patients with colon or lung cancer can greatly benefit from the results of this study by combining SAF with TOPOI inhibitors to enhance the anticancer effect and to improve the safety profile of the TOPOI inhibitors.

Data availability statement

The original contributions presented in the study are included in the article/Supplementary Material; further inquiries can be directed to the corresponding author.

Author contributions

LL: methodology, data curation, writing—original draft, and validation. ES: writing—original draft, review, and editing. VM: data curation and methodology. WR: data curation and methodology. AA: conceptualization. RE: conceptualization, supervision, methodology, data curation, writing, review, and editing. All authors read and approved the final manuscript.

Funding

This work was supported by the Research Funding Department, University of Sharjah, United Arab Emirates, under grant number 2001110343.

Acknowledgments

This work appeared as a preprint (Lozon et al., 2022).

Conflict of interest

The authors declare that the research was conducted in the absence of any commercial or financial relationships that could be construed as a potential conflict of interest.

Publisher's note

Supplementary material

The Supplementary Material for this article can be found online at: https://www.frontiersin.org/articles/10.3389/fphar.2022.938471/full#supplementary-material

References

Al-Hrout, A., Chaiboonchoe, A., Khraiwesh, B., Murali, C., Baig, B., El-Awady, R., et al. (2018). Safranal induces DNA double-strand breakage and ER-stress-mediated cell death in hepatocellular carcinoma cells. *Sci. Rep.* 8, 16951. doi:10.1038/s41598-018-34855-0

Bailly, C. (2019). Irinotecan: 25 years of cancer treatment. *Pharmacol. Res.* 148, 104398. doi:10.1016/J.PHRS.2019.104398

Berenbaum, M. C. (1989). What is synergy? *Pharmacol. Rev.* 41, 93. Available at: http://pharmrev.aspetjournals.org/content/41/2/93.abstract.

Chabner, B. A., and Longo, D. L. (2018). *Cancer chemotherapy, immunotherapy and biotherapy: Principles and practice*. Philadelphia: Wolters Kluwer, sixth edition

Dean, R. A., Fam, H. K., An, J., Choi, K., Shimizu, Y., Jones, S. J. M., et al. (2014). Identification of a putative tdp1 inhibitor (CD00509) by *in vitro* and cell-based assays. *J. Biomol. Screen.* 19, 1372–1382. doi:10.1177/1087057114546551

El-Awady, R. A., Ali, M. M., Saleh, E. M., and Ghaleb, F. M. (2008). Apoptosis is the most efficient death-pathway in tumor cells after topoisomerase II inhibition. *Saudi Med. J.* 29, 558.

El-Awady, R. A., Saleh, E. M., and Dahm-Daphi, J. (2010). Targeting DNA double-strand break repair: Is it the right way for sensitizing cells to 5-fluorouracil? *Anticancer. Drugs* 21, 277–287. doi:10.1097/CAD.0b013e328334b0ae

El-Awady, R. A., Saleh, E. M., Ezz, M., and Elsayed, A. M. (2011). Interaction of celecoxib with different anti-cancer drugs is antagonistic in breast but not in other cancer cells. *Toxicol. Appl. Pharmacol.* 255, 271–286. doi:10.1016/j.taap.2011.06.019

El-Awady, R., Saleh, E., Hashim, A., Soliman, N., Dallah, A., Elrasheed, A., et al. (2017). The role of eukaryotic and prokaryotic ABC transporter family in failure of chemotherapy. *Front. Pharmacol.* 7, 535–615. doi:10.3389/fphar.2016.00535

Falzone, L., Salomone, S., and Libra, M. (2018). Evolution of cancer pharmacological treatments at the turn of the third millennium. *Front. Pharmacol.* 9, 1300. doi:10.3389/fphar.2018.01300

Gilbert, D. C., Chalmers, A. J., and El-Khamisy, S. F. (2012). Topoisomerase i inhibition in colorectal cancer: Biomarkers and therapeutic targets. *Br. J. Cancer* 106, 18–24. doi:10.1038/bjc.2011.498

Huang, C. Y., Ju, D. T., Chang, C. F., Muralidhar Reddy, P., and Velmurugan, B. K. (2017). A review on the effects of current chemotherapy drugs and natural agents in treating non-small cell lung cancer. *Biomedicine* 7, 23. doi:10.1051/bmdcn/2017070423

Huang, X., Yang, Z., Xie, Q., Zhang, Z., Zhang, H., and Ma, J. (2019). Natural products for treating colorectal cancer: A mechanistic review. *Biomed. Pharmacother.* 117, 109142. doi:10.1016/j.biopha.2019.109142

Interthal, H., Pouliot, J. J., and Champoux, J. J. (2001). The tyrosyl-DNA phosphodiesterase Tdp1 is a member of the phospholipase D superfamily. *Proc. Natl. Acad. Sci. U. S. A.* 98, 12009–12014. doi:10.1073/PNAS.211429198

Kawale, A. S., and Povirk, L. F. (2018). Tyrosyl-DNA phosphodiesterases: Rescuing the genome from the risks of relaxation. *Nucleic Acids Res.* 46, 520–537. doi:10.1093/nar/gkx1219

Leone, S., Recinella, L., Chiavaroli, A., Orlando, G., Ferrante, C., Leporini, L., et al. (2018). Phytotherapic use of the Crocus sativus L. (saffron) and its potential applications: A brief overview. *Phytother. Res.* 32, 2364–2375. doi:10.1002/ptr.6181

Liu, C., Zhou, S., Begum, S., Sidransky, D., Westra, W. H., Brock, M., et al. (2007). Increased expression and activity of repair genes TDP1 and XPF in non-small cell lung cancer. *Lung Cancer* 55, 303–311. doi:10.1016/j.lungcan.2006.10.019

Lozon, L., Saleh, E., Menon, V., Ramadan, W., and Amin, A. (2022). *Effect of safranal on the response of cancer cells to topoisomerase I inhibitors*. Philadelphia: Wolters Kluwer. Dose sequence

Mancini, R., and Modlin, J. (2011). Chemotherapy administration sequence: A review of the literature and creation of a sequencing chart. *J. Hematol. Oncol. Pharm.* 1 (1), 17–25.

Mansoori, B., Mohammadi, A., Davudian, S., Shirjang, S., and Baradaran, B. (2017). The different mechanisms of cancer drug resistance: A brief review. *Adv. Pharm. Bull.* 7, 339–348. doi:10.15171/apb.2017.041

Meisenberg, C., Ward, S. E., Schmid, P., and El-Khamisy, S. F. (2014). TDP1/TOP1 ratio as a promising indicator for the response of small cell lung cancer to topotecan. *J. Cancer Sci. Ther.* 6, 258–267. doi:10.4172/1948-5956.1000280

Miao, Z. H., Agama, K., Sordet, O., Povirk, L., Kohn, K. W., and Pommier, Y. (2006). Hereditary ataxia SCAN1 cells are defective for the repair of transcription-dependent topoisomerase I cleavage complexes. *DNA Repair (Amst)* 5, 1489–1494. doi:10.1016/j.dnarep.2006.07.004

Milajerdi, A., Djafarian, K., and Hosseini, B. (2016). The toxicity of saffron (Crocus sativus L.) and its constituents against normal and cancer cells. *J. Nutr. Intermed. Metab.* 3, 23–32. doi:10.1016/j.jnim.2015.12.332

Poggio, F., Ceppi, M., Lambertini, M., Bruzzi, P., Ugolini, D., Bighin, C., et al. (2017). Concurrent versus sequential adjuvant chemo-endocrine therapy in hormone-receptor positive early stage breast cancer patients: A systematic review and meta-analysis. *Breast* 33, 104–108. doi:10.1016/j.breast.2017.03.011

Pommier, Y., Huang, S., yin, N., Gao, R., Das, B. B., Murai, J., et al. (2014). Tyrosyl-DNA-phosphodiesterases (TDP1 and TDP2). *DNA Repair* 19, 114–129. doi:10.1016/J.DNAREP.2014.03.020

Pommier, Y. (2006). Topoisomerase I inhibitors: Camptothecins and beyond. *Nat. Rev. Cancer* 6, 789–802. doi:10.1038/nrc1977

Ramadan, W. S., Talaat, I. M., Hachim, M. Y., Lischka, A., Gemoll, T., and El-Awady, R. (2021). The impact of CBP expression in estrogen receptor-positive breast cancer. *Clin. Epigenetics* 13, 72–18. doi:10.1186/s13148-021-01060-2

Rejhová, A., Opattová, A., Čumová, A., Slíva, D., and Vodička, P. (2018). Natural compounds and combination therapy in colorectal cancer treatment. *Eur. J. Med. Chem.* 144, 582–594. doi:10.1016/j.ejmech.2017.12.039

Rezaee, R., and Hosseinzadeh, H. (2013). Safranal: From an aromatic natural product to a rewarding pharmacological agent. *Iran. J. Basic Med. Sci.* 16, 12–26. doi:10.22038/ijbms.2013.244

Riahi-Zanjani, B., Balali-Mood, M., Mohammadi, E., Badie-Bostan, H., Memar, B., and Karimi, G. (2015). Safranal as a safe compound to mice immune system. *Avicenna J. Phytomed.* 5, 441–449. doi:10.22038/ajp.2015.4504

Saleh, E. M., El-Awady, R. A., Abdel Alim, M. A., and Abdel Wahab, A. H. A. (2009). Altered expression of proliferation-inducing and proliferation-inhibiting genes might contribute to acquired doxorubicin resistance in breast cancer cells. *Cell biochem. Biophys.* 55, 95–105. doi:10.1007/s12013-009-9058-3

Sung, H., Ferlay, J., Siegel, R. L., Laversanne, M., Soerjomataram, I., Jemal, A., et al. (2021). Global cancer statistics 2020: GLOBOCAN estimates of incidence and mortality worldwide for 36 cancers in 185 countries. *Ca. Cancer J. Clin.* 71, 209–249. doi:10.3322/caac.21660

Vennepureddy, A., Atallah, J.-P., and Terjanian, T. (2015). Role of topotecan in non-small cell lung cancer: A review of literature. *World J. Oncol.* 6, 429–436. doi:10.14740/wjon950e

Zhang, S. P., Huang, J. N., Jin, N., Wang, X. L., and Jin, C. C. (2017). Safranal inhibits the migration and invasion of human oral squamous cell carcinoma cells by overcoming epithelial-mesenchymal transition. *Biomed. Res.* 28, 817

Zugazagoitia, J., Guedes, C., Ponce, S., Ferrer, I., Molina-Pinelo, S., and Paz-Ares, L. (2016). Current challenges in cancer treatment. *Clin. Ther.* 38, 1551–1566. doi:10.1016/j.clinthera.2016.03.026

frontiers | Frontiers in Pharmacology

TYPE Original Research
PUBLISHED 12 October 2022
DOI 10.3389/fphar.2022.1018974

OPEN ACCESS

EDITED BY
Husain Yar Khan,
Wayne State University, United States

REVIEWED BY
Shahab Uddin,
Hamad Medical Corporation, Qatar
Qin Wan Huang,
Chengdu University of Traditional Chinese Medicine, China

*CORRESPONDENCE
Mohammad Husain,
mhusain2@jmi.ac.in

SPECIALTY SECTION
This article was submitted to Pharmacology of Anti-Cancer Drugs, a section of the journal Frontiers in Pharmacology

RECEIVED 14 August 2022
ACCEPTED 28 September 2022
PUBLISHED 12 October 2022

CITATION
Irshad R, Raj N, Gabr GA, Manzoor N and Husain M (2022), Integrated network pharmacology and experimental analysis unveil multi-targeted effect of 18α- glycyrrhetinic acid against non-small cell lung cancer.
Front. Pharmacol. 13:1018974.
doi: 10.3389/fphar.2022.1018974

Integrated network pharmacology and experimental analysis unveil multi-targeted effect of 18α- glycyrrhetinic acid against non-small cell lung cancer

Rasha Irshad[1], Nafis Raj[2], Gamal A. Gabr[3], Nikhat Manzoor[2] and Mohammad Husain[1]*

[1]Virology and Oncology Lab, Department of Biotechnology, Jamia Millia Islamia, New Delhi, India, [2]Medical Mycology Lab, Department of Biosciences, Jamia Millia Islamia, New Delhi, India, [3]Department of Pharmacology and Toxicology, College of Pharmacy, Prince Sattam Bin Abdulaziz University, Al- Kharj, Saudi Arabia

Non-small cell lung cancer (NSCLC) is one of the most malignant types of cancer with soaring incidence rates worldwide, attributed to its heterogeneity and complex etiology. Evidently, alternative anti-cancer therapies comprising traditional medicines and natural products have gained attention for their ability to act as chemopreventive agents with minimal toxicities, either alone or in combination. Accumulating studies have substantiated the inevitability of network pharmacology studies for effectively mapping molecular targets of natural products against multifaceted diseases, including cancer. The 18α-Glycyrrhetinic acid (18α-GA), a triterpenoid found in licorice plants, has shown promising medicinal properties, although, its mechanism of action against NSCLC yet remains elusive. The present study was conducted to explore the anti- NSCLC potential of 18α-GA, employing integrative network pharmacology, molecular docking, and experimental research. Initially, network analysis revealed 181 common targets of 18α-GA in NSCLC as shown in the "compound-target- disease" network employing *Cytoscape 3.8.2*. Further analyses identified EGFR, AKT1, PI3KR1, MAPK1, IGF1, and SRC as the most crucial hub targets of 18α-GA against NSCLC. Moreover, molecular docking simulations and functional enrichment analyses indicated the involvement of multiple signaling pathways in suppressing NSCLC. Subsequent *in-vitro* studies verified the antiproliferative effect of 18α-GA on two NSCLC cancer cell lines, H1299 and A549. Mechanistically, 18α-GA arrested cell cycle at the G1 phase, induced apoptosis, decreased migratory potential, and protein expression levels of EGFR-PI3K/AKT, as examined by flow cytometry, morphological assessment, RT-PCR, and western blot. In conclusion, this study delineates the therapeutic potential and underlying mechanism(s) of 18α-GA as a putative novel drug against NSCLC. However, further studies are warranted to elucidate the complete molecular mechanism(s) using animal models of NSCLC.

KEYWORDS

18α-Glycyrrhetinic acid, triterpenoid, NSCLC, network pharmacology, apoptosis, EGFR-PI3K/AKT pathway, survival analysis

1 Introduction

NSCLC is the most frequently diagnosed type of lung cancer worldwide comprising approximately 85% of all new cases with a mortality rate of 18% (Sung et al., 2021). The absence of clinical symptoms and inadequate prognosis eventually cause a delay in diagnosis, which impedes the therapeutic success of the patients. Owing to its heterogeneous nature, the treatment regime of NSCLC is personalized based on cell type, molecular profile, stage of disease and ranges from lobectomy, adjuvant immunotherapy, radiotherapy to standard platinum-based chemotherapy (Gridelli et al., 2015) However, severe toxicity, resistance, frequent recurrence, and metastasis are associated with less than five years of overall survival rate rendering these curative treatment options insufficient. Therefore, cancer therapy has been continually evolving toward its prevention in recent years, and alternative therapeutic strategies are gaining attention in lowering cancer initiation and progression rates. In this pursuit, the development of complementary strategies including the use of phytochemicals has been envisioned due to their low toxicity, effectiveness, diverse structure, affordability, and multi-targeted impact (Mustafa et al., 2021). The preventive prospects of natural products are multidimensional and can be utilized for targeting cancer in multiple ways. This aids in coping with the heterogeneity that exists among cancer cells of the same type and contributes to the restriction of tumor growth. In this direction, several phytochemicals are being routinely examined for their anti-NSCLC potential, either as a stand-alone drug or as adjuvants to standard chemotherapy.

The 18α-Glycyrrhetinic acid (18α-GA) is one such bioactive triterpenoid compound isolated from licorice (*Glycyrrhiza sp.*) roots, a perennial herb found in warm countries like India, other parts of Asia, and the Mediterranean region (Tiboni et al., 2020). Licorice is approved by the FDA to be used as a flavoring agent. The 18α-stereoisomeric form of aglycone glycyrrhetinic acid (18α-GA) is metabolically formed by partial hydrolysis of glucuronidase present in glycyrrhizin which is the primary metabolite of licorice plants (Ha et al., 1991). It demonstrates remarkable antioxidant, anti-tumor (Shetty et al., 2011), anti-viral, anti-inflammatory, hepatoprotective, and ulcer healing properties (Zong et al., 2013; Li et al., 2020). The 18α-GA is reported to have inhibited cancer cell progression in various cancer types by eliciting modifications like cell cycle arrest (Sathya et al., 2014), apoptotic induction (Pirzadeh et al., 2014), and restriction of epithelial-mesenchymal transition among others (Takeuchi et al., 2016). It has been illustrated to deregulate the Beclin-1/Bcl-2 complex and induce apoptosis *via* inhibition of MAP Kinases in neuroblastoma cells (Rahman et al., 2016). In addition, 18α-GA was shown to suppress hepatic fibrosis and subsequent suppression of hepatocellular carcinoma by modulating the TGF-β1/Smad Signaling Pathway (Zong et al., 2012). Even though a few studies have been carried out on elucidating the mechanism of action of 18α-GA against cancer, it is still in infancy, particularly in NSCLC, and needs to be evaluated for reaping its wide-ranging pharmacological advantages.

Recently, network pharmacology has emerged as a holistic tool to unveil the putative molecular bio-targets, signaling pathway intricacies, and protein-protein interactions of natural compounds/medicinal plants against various diseases by utilizing extensive databases, pharmaco-mapping, and computational strategies (Chandran et al., 2017). It has been successfully employed to describe the molecular mechanisms of various phytochemicals and drugs in targeting various diseases. Therefore, in this study, we aimed to unveil the mechanism of action and the molecular pathways affected by 18α-GA against NSCLC by network pharmacology, which was further corroborated by molecular docking studies, and the core target genes were identified. We also evaluated the potential of 18α-GA in regulating various hallmarks/phenotypes of NSCLC through *in-vitro* validation on two NSCLC cell lines.

Our findings highlight the multi-targeted effect of 18α-GA in reducing NSCLC tumorigenesis as seen by network pharmacological studies. Further, it provides evidence that 18α-GA treatment suppresses cell proliferation, induces G1 phase cell cycle arrest, represses metastasis, exhibits apoptotic cell death, and regulates EGFR- PI3K/AKT signaling in NSCLC cells. The framework of this study is described in Supplementary Figure S1.

2 Materials and methods

2.1 Bioinformatics study

2.1.1 Evaluation of pharmacokinetics and physicochemical parameters of 18-αGA

The canonical SMILES of 18α-GA were input into SwissADME, a free-to-access web tool (http://www.swissadme.ch/) for instant and robust prediction of physicochemical properties and pharmacokinetic descriptors including ADME parameters. The SwissADME tool utilizes the most relevant computational methods for efficient calculation of Drug likeness (DL), Oral Bioavailability (OB), Caco-2 permeability, lipophilicity, and other features of naturally occurring small molecules. The estimation of the drug-likeness of the compound was calculated by Lipinski and other rules (Daina et al., 2017).

2.1.2 Identification of 18α-GA-related targets

The chemical structure of 18α-GA as an SDF file was obtained from the PubChem database (https://pubchem.ncbi.nlm.nih.gov/). The structure of 18α-GA was imported into PharmMapper (http://lilab.ecust.edu.cn/pharmmapper/) (Wang et al., 2017) and SwissTarget (Daina et al., 2019) database for identifying related target genes. The list of putative target genes was downloaded as a CSV file and the gene names were changed to standard gene symbols utilizing the UniProt database (http://www.uniprot.org/).

2.1.3 Collection of gene targets specific to Non-small cell lung cancer

The pathogenic gene targets of NSCLC were extracted from DisGeNET (version 6.0) database after setting the species as homosapiens. DisGeNET is the largest platform linking human genes to diseases by integrating data from scientific literature, expert-curated repositories, and the genome-wide association study (GWAS) catalogs.

All overlapping gene targets shared by 18α-GA and NSCLC simultaneously were obtained by Venny 2.1.0 (http://bioinfo.cnb.csic.es/tools/venny/index.html) software and chosen as the expected target of 18α-GA compound for the treatment of NSCLC.

2.1.4. Protein-protein interaction and network construction

The common target genes of 18α-GA and NSCLC were used to analyze the underlying mechanism of interacting genes and the protein-protein interaction network was constructed by importing the data to the STRING (Search Tool for the Retrieval of Interacting Genes 11.0) database (https://string-db.org/) (Szklarczyk et al., 2019). The species was specified as "*Homo sapiens*" and the cut-off confidence score of ≥0.9 was considered significant to assure robustness of the interaction. Further, the PPI network was visualized using the Cytoscape (version 3.8.2) (http://www.cytoscape.org/) software, and a Compound-Target- Disease ("C-T-D") network was constructed (Shannon et al., 2003). The network nodes represent proteins whereas the edge represents associated protein-protein interaction.

2.1.5 Prediction and validation of hub/core targets

The CytoHubba plugin of Cytoscape was utilized to analyze the highly interconnected nodes in the PPI network that represents the most important interacting genes of a network. The top overlapping genes among important topological features like Degree, Betweenness, Closeness, and Maximal Clique Centrality (MCC) were considered to filter core genes in the network.

2.1.6 Molecular docking

Next, the molecular docking approach was applied to confirm the interaction strength between the compound 18α-GA and the predicted core targets. The 3D structures of core proteins were obtained from the RCSB PDB database (https://www.rcsb.org/) and the structure of the compound was taken from the PubChem database and converted to PDB format through Pymol software (version 2.2). During the receptor preparation module, a PDBQT file of our target receptors was generated that consisted of atoms of hydrogen along with partial charges. There are multiple ways to estimate partial charges but we used "Kollman charges" which provide a quick and simple calculation of receptor topology. Furthermore, we added hydrogen atoms to the PDB receptor files as well as deleted water molecules and converted them into the PDBQT format for docking calculations. In proteins, the active site has been predicted through the CASTp 3.0 (Computed Atlas of Surface Topography) online server (Tian et al., 2018). CASTp is a good platform to predict and characterize the active site based on algorithmic computational geometry and identify the pocket and cavities analytically. Additionally, the grid was made around the active site (catalytic pocket). InstaDock has been used for molecular docking calculation (Mohammad et al., 2021) and the results were evaluated from log files generated by docking performance. After molecular docking, the docked conformations were analyzed by Discovery Studio 2019 for 3D and 2D interaction analysis.

2.1.7 Functional enrichment analysis

The GO and KEGG signaling pathways enrichment analyses of screened gene targets were done by entering targets of 18α-GA in the DAVID database (Huang et al., 2007). The Gene Ontology terms like biological process (BP), cellular component (CC), and molecular function (MF) were analyzed and the results with values of $p < 0.05$ and FDR <0.05 were considered to be statistically significant. The Top 15 terms were plotted into graphs using GraphPad.

2.1.8 Survival analysis

The association between the survival rates of NSCLC patients and the expression levels of the core targets was analyzed using the Kaplan-Meier Plotter (https://kmplot.com) (Lánczky and Győrffy, 2021). Furthermore, the Gene Expression Profiling Interactive Analysis (GEPIA2) webserver (http://gepia2.cancer-pku.cn) was used for performing tumor/normal differential core gene expression analysis.

Besides, the Human Protein Atlas (http://www.proteinatlas.org) database was used to observe the distribution of hub proteins in the lung cancer cells and normal lung cells.

2.2 Experimental verification

2.2.1 Chemicals and reagents

High-glucose Dulbecco's Modified Eagles Medium (DMEM), Fetal Bovine Serum (FBS), and the penicillin-streptomycin mixed

solution were procured from Gibco-life technologies, Thermo Fischer Scientific (USA). MTT (3-[4,5-dimethylthiazol-2-yl]-2,5-diphenyltetrazolium bromide), propidium iodide (PI), DAPI, Acridine orange were acquired from Sigma. Bax, β-actin, and Bcl-2 primary antibodies were purchased from Novus Biologicals (Centennial, CO, USA). FITC/Annexin V apoptosis detection kit was purchased from BD Bioscience. The compound 18α-GA was purchased from Sigma-Aldrich with purity ≥95% and stock solutions were dissolved in DMSO and stored at −20°C. All other reagents were of analytical grade and purchased from local suppliers. All the experiments were repeated at least three times.

2.2.2 Cell culture

The NSCLC cell lines H1299 and A549 were procured from National Centre for Cell Sciences (NCSS), Pune, India. All the cell lines were cultured in DMEM, supplemented with 1% 1X penicillin/streptomycin and 10% heat-inactivated FBS at 37°C and 5% CO_2 under 95% humidified conditions in a cell culture incubator (Shell labs) (Alam et al., 2022). Cell cultures were maintained regularly, not more than 30 passages. The compound 18α-GA was dissolved in DMSO with a concentration not more than 0.2% and used as a vehicle in all the experiments.

2.2.3 Cell Cytotoxicity assay

Cytotoxic potential of 18α-GA on NSCLC cell lines; H1299 and A549 were evaluated by MTT assay. Briefly, 6,000–7,000 cells were seeded per well in a 96-well plate and were allowed to grow overnight, the cells were then treated with increasing concentrations (0–200 μm) of 18α-GA for 24 and 48 h at 37°C in a CO_2 incubator. After treatment, 10 μl MTT was added (5 mg/ml, PBS, pH 7.4) to each well, and incubated for 4–5 h at 37°C in a CO_2 incubator in dark. The supernatant from each well was then discarded and 100 μl of DMSO was added. The absorbance was measured using a microplate reader (BioRad) at 570 nm. The IC_{50} values were calculated by GraphPad Prism 9.0 and percent cell inhibition was plotted for H1299 and A549 cells.

2.2.4 Observation of morphological changes

H1299 and A549 cells were seeded 18α-GA at a density of 4×10^5 cells per well in a 6-well culture plate and allowed to grow up to 70% confluency. Later, cells were treated with distinct concentrations of (0, 40, 80 μM) and incubated for 48 h. The cell morphology was observed and captured by using an inverted microscope (LMI microscopes, United Kingdom).

2.2.4.1 DAPI staining

As previously described (Sun et al., 2022), H1299 and A549 cells were seeded at the density of 1×10^5 cells/well in a 6-well plate overnight and treated with different doses of 18-αGA. After 48 h, the treated cells were washed with 1X PBS, followed by fixing using 3.7% paraformaldehyde for at least 10 min at RT. The fixed cells were further washed with PBS, stained by DAPI (300 nM)) and imaged under a fluorescence microscope (Bio-Rad).

2.2.5 Colony formation assay

Briefly, 200–300 cells per well were grown overnight and treated with different doses of 18-αGA and allowed to form colonies in a serum-deprived medium (2%) for 10–14 days in a six-well cell culture plate. Subsequently, colonies were fixed (acetic acid/methanol; 1:3) and stained with 0.5% crystal violet in 100% methanol for 30 min, and then counted.

2.2.6 Cell cycle assessment

Cells were treated as described above and then harvested, washed twice with 1×PBS, and fixed with 70% ethanol at 4°C for 24 h. Next, cells were washed with PBS and incubated with PI staining solution (50 μg/ml PI and 100 μg/ml RNAase A) for 30–40 min at 37°C in dark. The percentage of cell count in the G0, G1, S, and G2/M phases of the cell cycle was determined by BD FACS Aria BD FACS Aria™ III (BD Biosciences, United States). A total of 10,000 events for all samples were taken to ensure adequate data.

2.2.7 Acridine orange/ethidium bromide staining

In addition to DAPI staining, acridine orange (AO) and ethidium bromide (EB) staining were carried out to detect apoptotic cell formation. The assay was performed as described previously with slight modifications (Kasibhatla et al., 2006). Briefly, cells were treated as described above and then spent media was collected, cells harvested, and centrifuged. After washing with PBS, 25 μl of cell suspension was stained with 1 μl of AO/EB solution (1:1) and incubated for 1–2 min. Subsequently, fluorescence images were captured under a fluorescence microscope (Bio-Rad).

2.2.8 FITC annexin V/propidium iodide apoptosis assay

FITC Annexin V Detection Kit I (BD-Biosciences, USA) was used to measure the apoptotic changes in both the cell lines according to manufacturers' instructions. Briefly, 1×10^6 cells/mL were seeded in a 6-well plate and treated with different concentrations of 18α-GA for 48 h. After harvesting, the cells were suspended in 500 μl of binding buffer. 100 μl of this cell suspension were mixed with 5 ml of Annexin V and propidium iodide (PI) for 15–20 min at RT in dark. The percentage of live and dead cells was determined using FITC/PI channel, and 10,000 events for each sample were recorded by BD FACS Aria™ III (BD Biosciences, USA) using BD FACS Diva software.

2.2.9 Mitochondrial membrane potential measurement

We assessed the mitochondrial transmembrane potential using the Tetramethylrhodamine, methyl ester

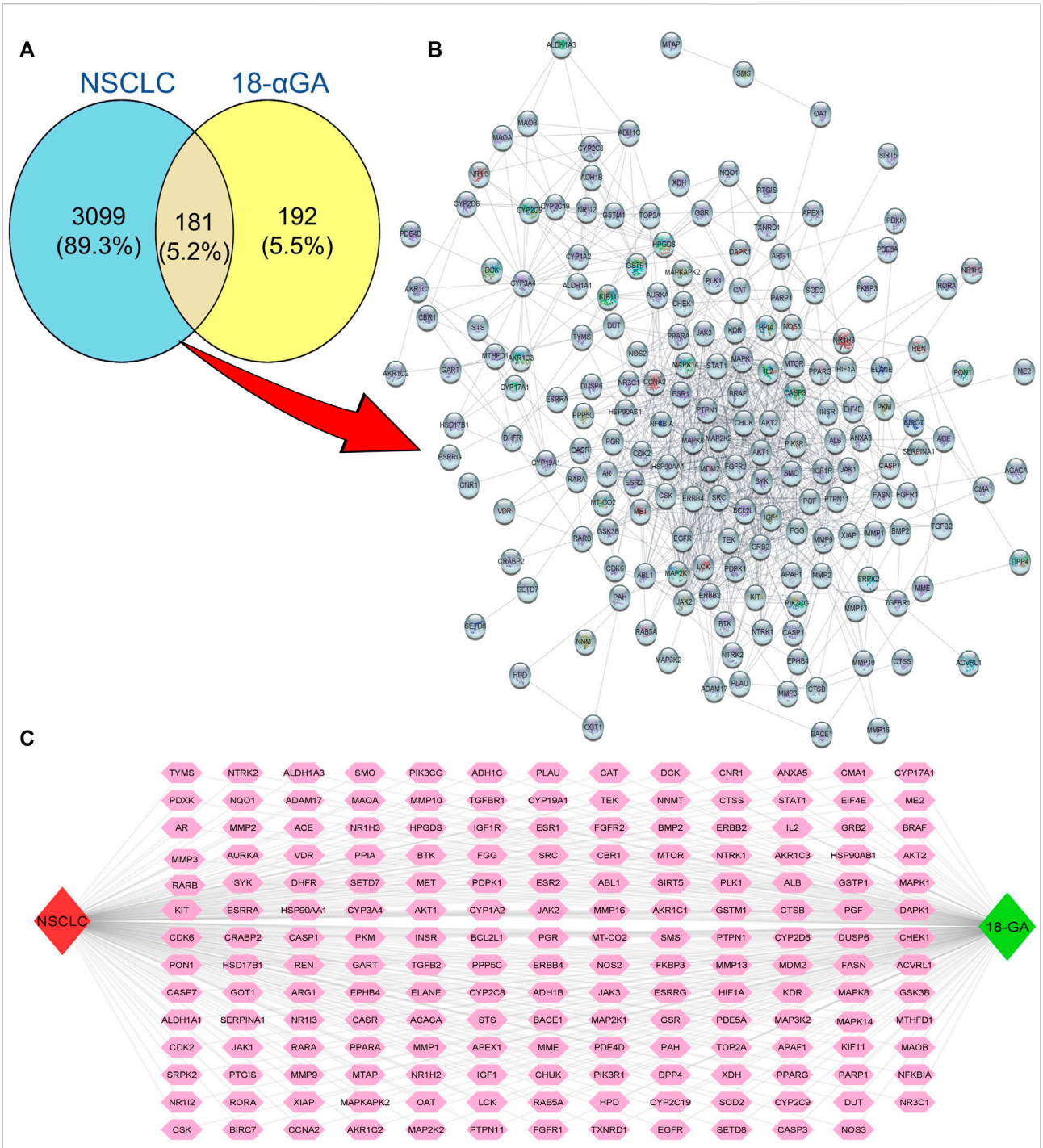

FIGURE 1
Putative targets of 18-αGA against NSCLC. **(A)** Venn Diagram showing 181 overlapping targets between 18-αGA and NSCLC by Venny 2.1.0. **(B)** Protein-protein interaction (PPI) network of 181 nodes and 964 edges of 18-αGA and NSCLC as visualised by *Cytoscape v 3.9.0*. **(C)** The "Compound-Target-Disease" Network constructed by Cytoscape v.3.8.2, the Green diamond represents the compound name, the Red diamond represents the disease name, and Pink hexagons show common targets between 18-αGA and NSCLC.

(TMRM, Invitrogen) fluorescent dye (Creed and McKenzie, 2019). After being treated with different concentrations, H1299 and A549 cells were incubated with 200 nM TMRM in DMEM for 30 min at 37°C in dark. After washing three times with PBS, the cell monolayer was imaged under a fluorescence microscope.

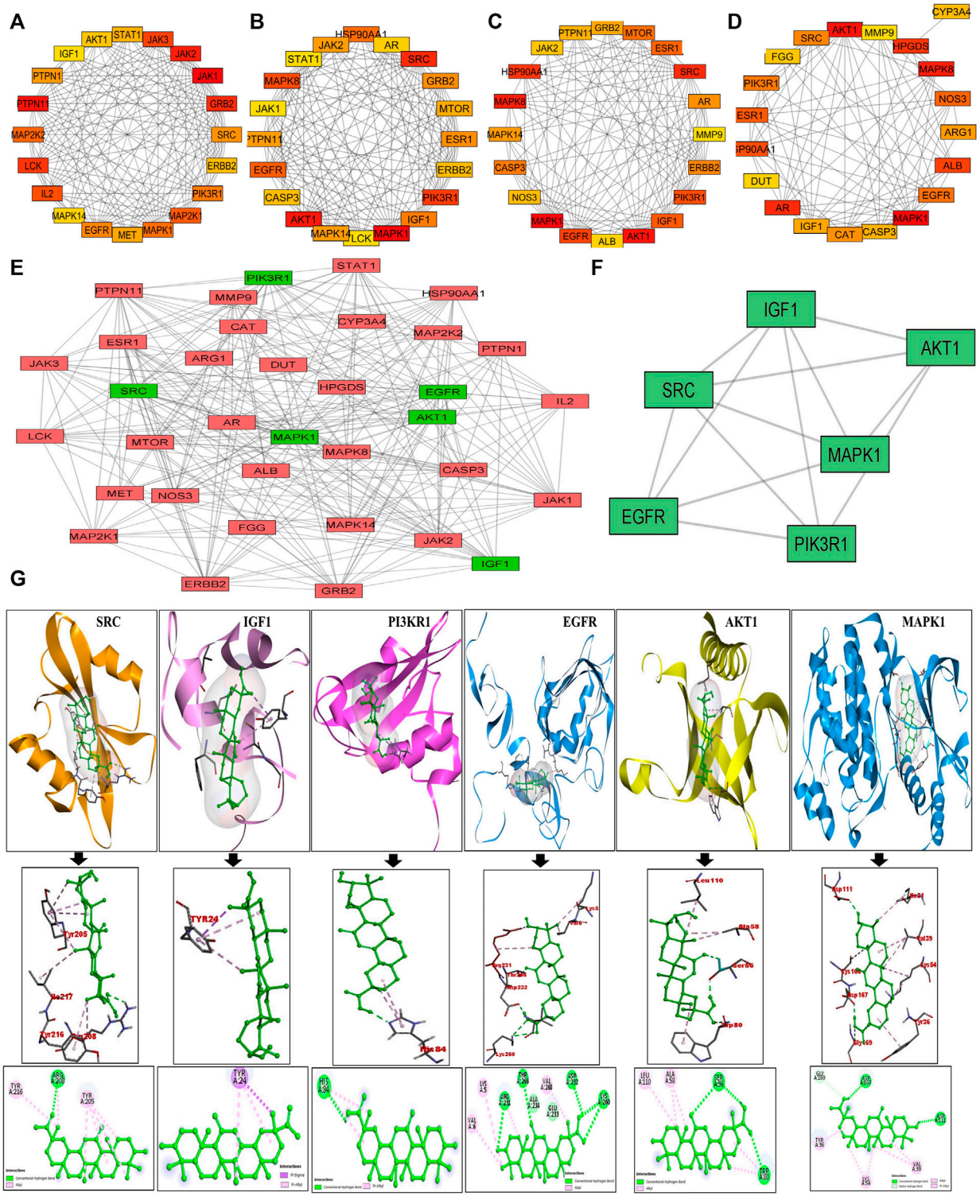

FIGURE 2
Identification of Top 6 hub/core targets of 18-αGA against NSCLC. **(A)** Top 20 targets based on MCC visualized by CytoHubba plugin. **(B)** Top 20 targets based on Degree as visualized by CytoHubba plugin. **(C)** Top 20 targets based on Betweenness as visualized by the CytoHubba plugin **(D)** Top 20 targets based on Closeness as visualized by the CytoHubba plugin. **(E)** The PPI network of identified hub/core targets of 18-αGA against NSCLC constructed by merging top 20 targets obtained from CytoHubba plugin visualized by Cytoscape v 3.8.2; green rectangles represent the highly enriched target nodes and pink boxes show less enriched nodes. **(F)** Top 6 hub nodes interactive PPI network visualized and constructed by Cytoscape v3.8.2.**(G)** Molecular docking verification of the crucial hub targets of 18-αGA against NSCLC. The three-dimensional structure of 18-αGA docked against the structure of the targets is shown along with the interaction diagram. The arrow represents the docking complexes in 3D and 2D poses respectively.

2.2.10 Wound healing assay

The assay was performed as previously described with minor changes. In brief, 1×10^5 cells were allowed to form a monolayer in a 12-well plate, then a scratch was made using a 10 µl pipette tip. After thorough and gentle washing, the cells were treated accordingly under serum-starved conditions for different time -points. Images were obtained at 0, 24, and 48 h to analyze the movement of the cells to close the wound. ImageJ software (National Institutes of Health, Bethesda, MD, United States) was used to analyze the migration distance.

2.2.11 Semi-quantitative RT-PCR

Total RNA was extracted from treated cells using Trizol reagent (Invitrogen). Next, cDNA was transcribed using an iScript cDNA synthesis kit (Bio-Rad) according to the manufacturer's protocol. RT-PCR analyses for mRNA of p53, p27, cyclin E1, E-cadherin, vimentin, and snail, were performed by using the GoTaq Green PCR master mix (Promega). GAPDH was used as the endogenous control for data normalization. The PCR amplicons were run on 1.8% agarose gel and visualized on the ChemiDoc imaging system (Bio-Rad) and the bands were quantified using ImageJ (Bethesda, Maryland, MD, United States) software.

2.2.12 Western blot

The experiment was performed as described previously (Padder et al., 2021). Briefly, H1299 and A549 cells were treated with different concentrations of 18α-GA for 48 h, trypsinized, and lysed in RIPA lysis buffer supplemented with 1x Phos stop and Sigma fast (Sigma Aldrich) for 10–15 min on ice. The lysates were centrifuged at 10,000 rpm for 10 min at 4°C; the supernatant was taken and total protein was quantified using a BCA kit (Thermo Scientific). Equal amounts of protein (20–50 µg) were resolved on SDS-PAGE gels, followed by transfer of the resolved proteins onto PVDF membrane (Bio-Rad) using a wet transfer system at 60 V–80 V for 1 h. The membranes were then blocked with 5% non-fat milk in TBST for 40 min and probed overnight with indicated primary antibodies at 4°C and later probed with appropriate HRP conjugated secondary antibodies at room temperature for 1 h. The protein bands were then developed onto x-ray film (kodak) and the ChemiDoc imaging system. The primary antibodies used were against, beta-actin, caspase-3, Bax, and Bcl_2 (Novus Biologicals), EGFR and pPKBa (Cloud Clone), pPI3K (CST), and the corresponding secondary antibodies used were either goat anti-rabbit IgGHRP (Novus Biologicals) or goat anti-mouse IgGHRP, (Novus Biologicals).

2.2.13 Statistical analysis

Data analysis was performed using Graph Pad prism 9.0. All experiments were repeated at least three times independently. Data are presented as the mean ± SD. Differences between groups were analyzed by two-way ANOVA as applicable with appropriate post hoc tests as indicated. p values corresponding to $p \leq 0.05$ were considered statistically significant.

3 Results

3.1 Bioinformatic study

3.1.1 Putative targets of 18α-GA against non-small cell lung cancer

Natural products have the characteristic ability to act on multiple molecular targets and hence can be utilized to harness multi-targeted therapeutic strategies against various diseases. The PharmMapper and SwissTarget online tools are online databases that match the query compound against a huge internal pharmacophore model database for potential drug target identification *via* a reverse pharmacophore alignment. Thus, 305 and 100 putative targets associated with 18α-GA were identified using PharmMapper and SwissTarget, respectively. Later, the DisGeNET database predicted a total of 3926 NSCLC-related genes, which, when overlapped using a Venn diagram, produced 181 potential targets of 18α-GA against NSCLC (Figure 1A). These predicted targets were subjected to further exploration.

3.1.2 "C-T-D network" construction and hub/core targets identification

The putative targets obtained were imported to the STRING platform and a PPI network was retrieved (Supplementary Figure S2) and visualised by *Cytoscape v3.9.0* (Figure 1B). The PPI network reveals the interaction among the targets with more interacting lines between proteins representing highly connected proteins in the network. A"Compound-Target-Disease" network was constructed using the *Cytoscape 3.8.2* software (Figure 1C). The resultant "C-T-D" network contained 181 nodes and 964 edges representing proteins and the interaction among them respectively. The red and green diamonds represent NSCLC and 18α-GA respectively, whereas the pink hexagons represent the putative protein targets of 18α-GA acting against NSCLC. To further understand the above network comprehensively, topological analysis was done by a Cytoscape plugin, Cytohubba, which exhibited the top 20 proteins related to degree, betweenness centrality, closeness centrality, and maximum clique centrality as shown in (Figures 2A–D). Furthermore, these top-rated proteins were merged and intersected revealing the 6 most important and highly connected proteins the Merge tool of Cytoscape 3.8.2. Figure 2E represents the merged PPI network with green boxes illustrating the most crucial proteins in the network that signifies the hub/core targets of 18α-GA effective against NSCLC. The 6 core hub proteins identified as therapeutic targets were; EGFR, IGF1, MAPK1, AKT1, PIK3R1, and SRC (Figure 2F).

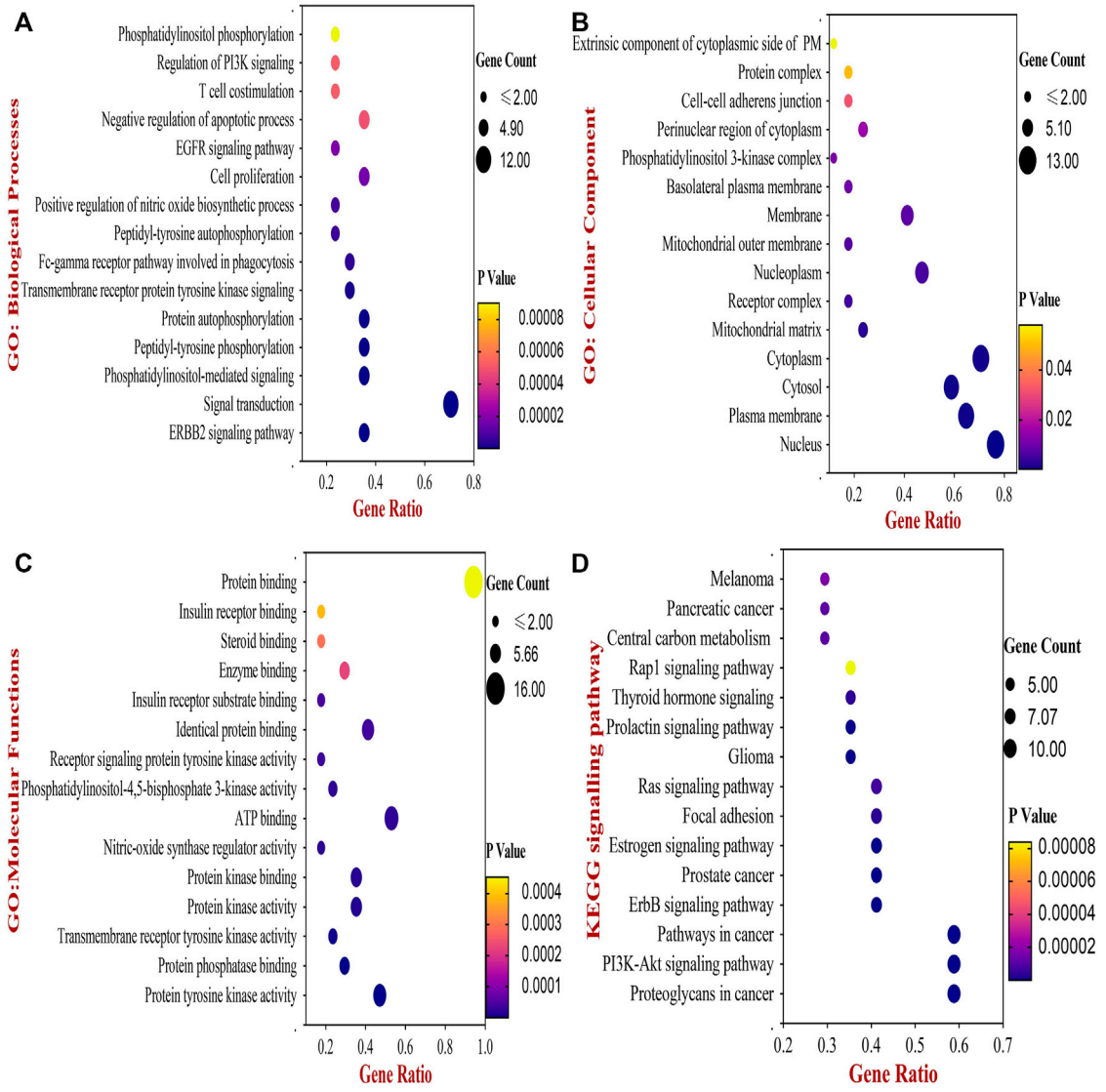

FIGURE 3
The Bubble chart of Gene Ontology (GO) and KEGG pathway analyses by DAVID database. **(A)** Top 15 GO- Biological Processes of 18-αGA targets. **(B)** Top 15 GO- Cellular Component of 18-αGA targets. **(C)** Top 15 GO- Molecular Functions; *p*-value < 0.05 in all three GO terms **(D)** Bubble plot of Top 15 highly enriched KEGG pathways of 18- αGA targets, *p*-value < 0.05. Bubble size represents the number of enriched genes, and bubble color difference represents the significance of target gene enrichment.

3.1.3 Molecular docking of core targets

These hub proteins were docked against 18α-GA to understand the binding interactions among them. When subjected to molecular docking analysis, the binding energies of hub targets from PPI network analysis demonstrated high affinities towards 18α-GA with EGFR, MAPK1, and AKT1 having the lowest binding energies of -8.8 kcal/mol, −8.2 kcal/mol, and −7.9 kcal/mol respectively and the number of interacted bonds (polar and non-polar) showed the ligand is stable in the binding pocket (Supplementary Table S2). The docking conformations of hub targets are shown in Figure 2G, highlighting the stable ligand-receptor binding and greater interaction. Most of the docked targets with high binding affinities were distributed in crucial pathways revealed from GO and KEGG analysis, hence validating the role of ErbB and PI3K signaling pathways.

3.1.4 Functional enrichment analysis

Next, the biological functions and pathways of anti- NSCLC targets of 18α-GA were elucidated by enriching KEGG pathways and acquiring GO terms by DAVID software. After correcting the *p*-values, the top 20 most significant GO terms associated

with Biological Processes (GO_BP), Cellular components (GO_CC), and Molecular Functions (GO_MF) were visualized in Figures 3A–C. According to the GO analysis, the most vital biological processes involved in the anti-NSCLC activity of 18α-GA were attributed to the ERBB2 signaling pathway, signal transduction, PI-mediated signaling, cell proliferation, negative regulation of apoptosis, regulation of phosphatidylinositol 3-kinase (PI3K) mediated signaling and peptidyl-tyrosine phosphorylation among others. The most valued GO_CC terms involved, were the nucleus, cytoplasm, plasma membrane, cytosol, and nucleoplasm. In GO_MF, the most important terms included were protein tyrosine kinase activity, protein phosphatase binding, identical protein binding, transmembrane receptor protein tyrosine kinase activity, and phosphatidylinositol-4,5-bisphosphate 3-kinase activity among others.

Following this, enrichment of the KEGG pathway disclosed a total of 56 pathways involved in the anti- NSCLC effect of 18-αGA. After adjustment of the *p*-value, the top 15 pathways encompassed proteoglycans in cancer, PI3K-Akt signaling pathway, ErbB signaling pathway, Pathways in cancer, Estrogen signaling pathway, Focal adhesion, Ras signaling pathway, and Prolactin signaling pathway (Figure 3D). The integration of the above GO and KEGG data indicates that the 6 hub targets are mainly enriched in the ErbB signaling pathway and PI3K-Akt signaling pathway, thereby associating significantly with the anti-lung cancer activity of 18-αGA. To this conjecture, we sought to perform further external validation of the hub/core targets by molecular docking, expression, and survival analysis.

3.1.5 External validation by mRNA and protein expression of core targets

To validate the prognostic and clinical significance of the core targets, we used the GEPIA database to examine the differential expression of mRNA levels between NSCLC and normal lung tissues. The red and grey boxplots represent the lung cancer tissues and normal lung tissues respectively. It was observed that the mRNA expression of EGFR, MAPK1, Akt1, and SRC were upregulated in the lung cancer tissues whereas the expression of IGF1 and PI3KR1 was reduced as compared to the normal lung tissues (Supplementary Figure S3A).

Furthermore, protein expression levels of hub/core proteins by immunohistochemical staining images were studied from the HPA database. As shown in Supplementary Figure S3B, the staining indicating expression levels were moderate to strong in all hub proteins except for IGF1, which was undetectable in lung cancer tissues compared to normal lung tissue.

These assessments suggested that the expression levels of these hub genes/proteins are possibly correlated with NSCLC progression and could prove as potential biomarkers clinically for the detection and treatment of NSCLC.

3.1.6 Survival analysis and prognostic value of the hub genes

Subsequently, to validate the clinical significance of targeting the hub genes, the association of NSCLC patients' survival outcomes was co-related with the expression levels of these hub targets. The Kaplan-Meier plot (Supplementary Figure S3C) shows that high expression of EGFR, AKT1, MAPK, IGF1, and SRC significantly worsened the overall survival of patients while higher expression of PIK3R1 did not reduce the survival probability.

Collectively, the identification of hub targets of 18α-GA against NSCLC by network analysis and subsequent KEGG, GO, molecular docking, external expression analysis, and survival analysis verify the importance of particularly EGFR and AKT1 as the core therapeutic targets of 18α-GA among other hub genes. These findings confirm the prognostic and clinical significance of targeting these genes for restraining the pathogenesis of NSCLC by 18-αGA.

Taking into consideration these bioinformatics conclusions, further *in-vitro* experiments were performed to validate 18α-GA as an anti- NSCLC agent by modulating different hallmarks of cancer in a multi-targeted and multi-step manner. Therefore, it may be speculated that EGFR/AKT signaling pathway may be associated with the therapeutic mechanism of 18α-GA against NSCLC.

3.2 *In-vitro* verification-

3.2.1 18α-GA inhibits cell proliferation in non-small cell lung cancer cells

To prove the data obtained through bioinformatics, further study was done by performing experiments in cell culture. First, the growth-suppressive effects of 18α-GA were assessed with different concentrations of 18α-GA at 2 different time points (24 h and 48 h). At 24 h, the MTT assay revealed that in H1299 cells, the inhibition was prominent whereas, in the A549 cells, the viability was not significantly affected up to 200 μM. Besides, H1299 and A549 cell proliferation were significantly inhibited at 48 h in a dose and time-dependent manner with more than 80% inhibition at higher concentrations (Figure 4A). The IC50 values as calculated by Microsoft Excel and were found to be 111.17 μM and >200 μM for H1299 and A549 cells respectively at 24 h. Similarly, at 48 h, the IC50 values were found to be 73.45 μM and 91.20 μM and it was noted that H1299 cells were more responsive to 18α-GA than A549 cells at both time points. Accordingly, 40 μM and 80 μM treatments for 48 h were chosen to carry out further experiments in both the cell lines.

The cell viability of non-cancer cell line HEK-293 at different concentrations of 18α-GA at 24 and 48 h was also measured, which showed negligible effect and the cells were viable even after

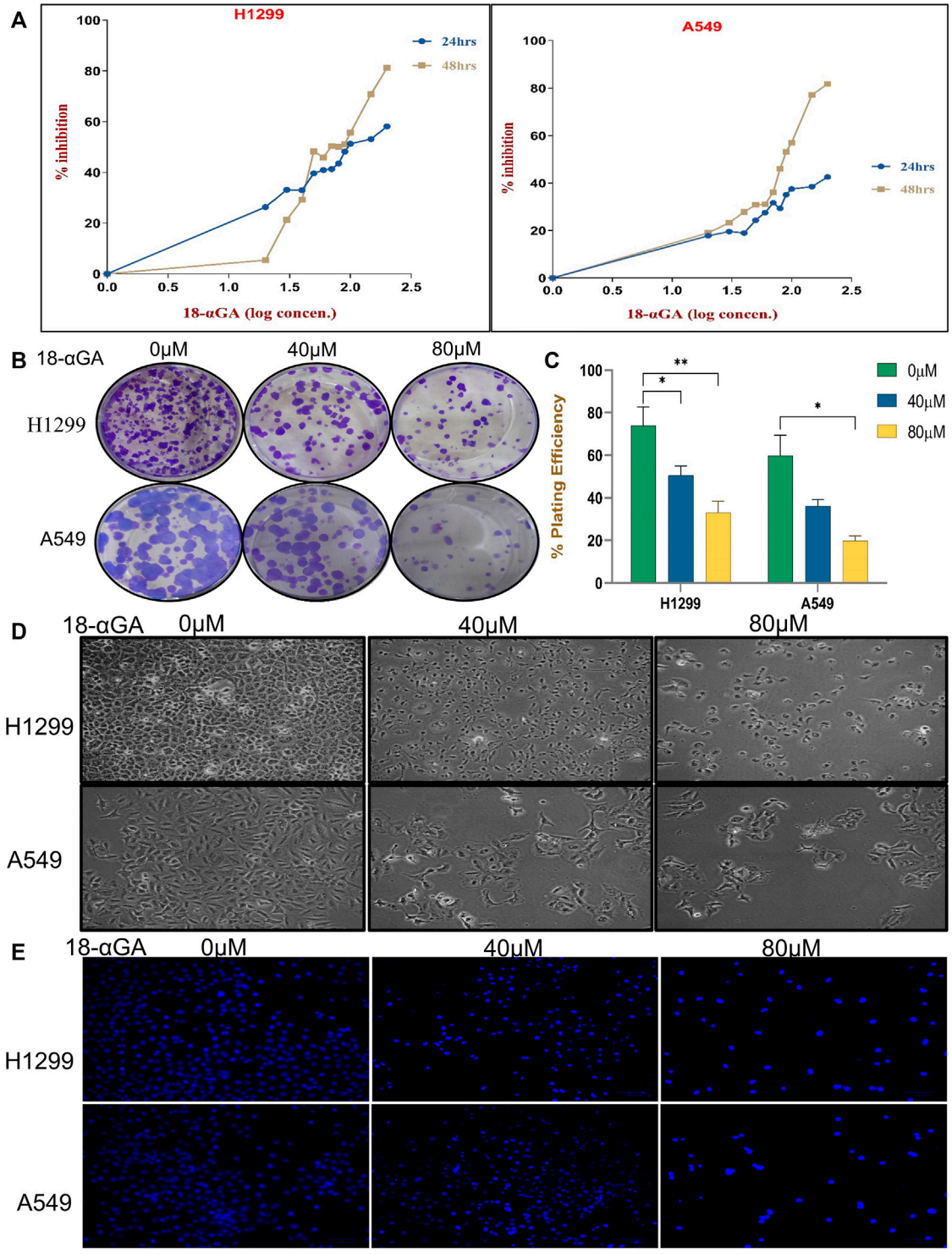

FIGURE 4
(A) Effect of 18-αGA on the viability and proliferation of NSCLC cells. **(A)** Growth inhibition assessment by the MTT assay upon treatment with various concentrations (0, 10, 20, 30,40, 50, 60, 70,80, 90, 100, 150, and 200 μM) of 18-αGA at two different time intervals of 24 h and 48 h on NSCLC cell lines; H1299 and A549. **(B)** Images showing colonies appeared after treatment at two different concentrations in both cell lines. **(C)** % plating efficiency after treatment with 18-αGA, colonies counted by ImageJ (n = 3, mean ± SD), statistical analysis was done by 2-way Anova followed by Tukey's Post-hoc multiple comparison test. *$p < 0.05$, **$p < 0.01$, ***$p < 0.001$, ****$p < 0.0001$. **(D)** Cell morphological and cytoplasmic changes in H1299 and A549 cells in the different treatment groups after 48 h **(E)** DAPI staining shows changes in the fluorescence levels of cells in different 18-αGA treatment groups (original magnification, × 20).

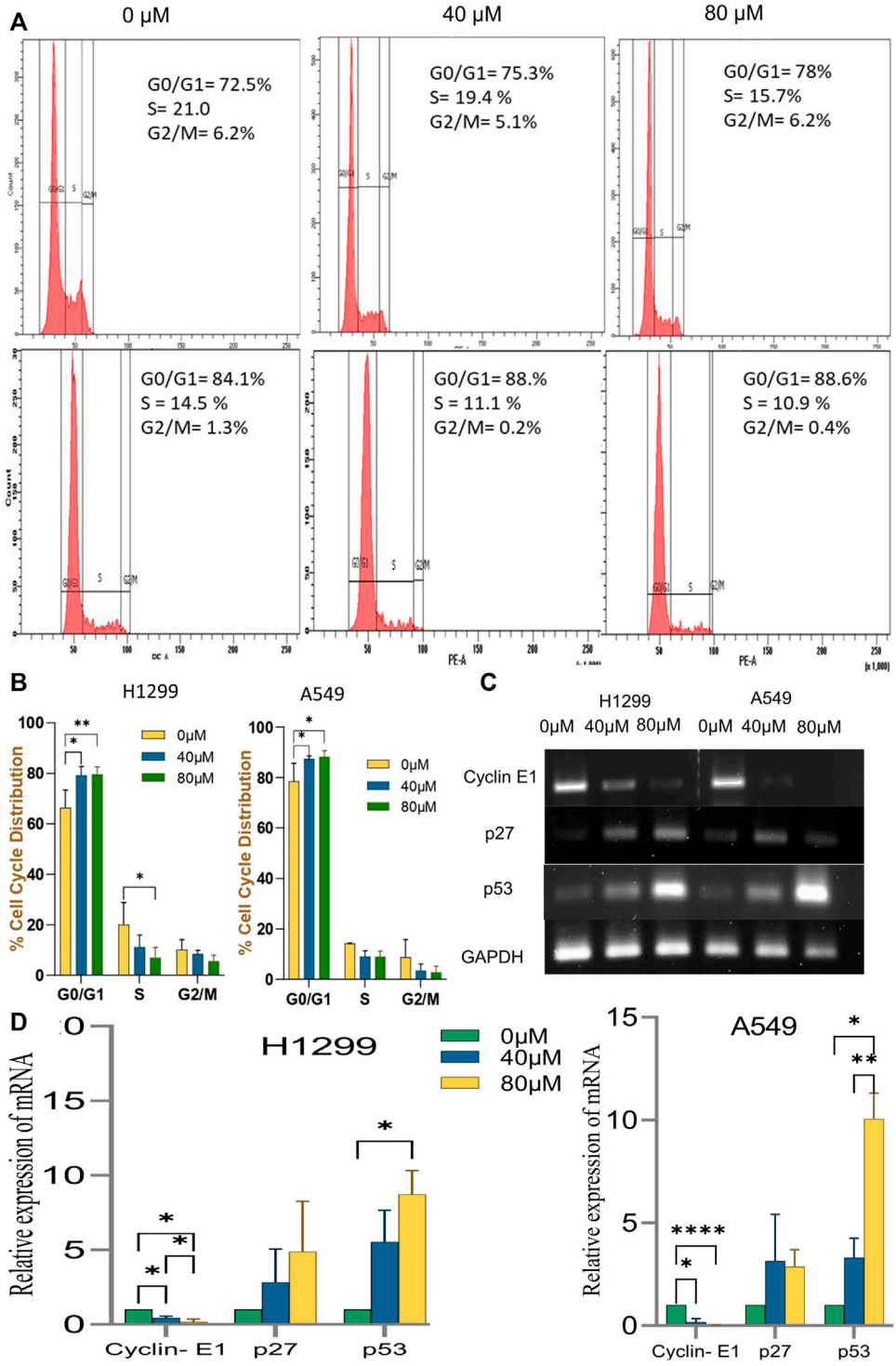

FIGURE 5
Effect of Cell Cycle progression after treatment with 18α-GA. **(A)** Flow cytometric images represent the distribution of H1299 and A549 cells at different stages of the cell cycle. **(B)** % cell cycle distribution measured by FACS (n = 3, mean ± SD), statistical analysis was done by 2-way Anova followed by Tukey's Post-hoc multiple comparison test. *p < 0.05, **p < 0.01, ***p < 0.001, ****p < 0.0001. **(C)** The mRNA expression of related genes after treatment with 18α-GA by RT-PCR. **(D)** Graph representing mRNA expression levels of genes with respect to GAPDH, statistical analysis was done by 2-way ANOVA followed by Tukey's Post-hoc multiple comparison test, *p < 0.05, **p < 0.01, ***p < 0.001, ****p < 0.0001.

48 h of treatment at the highest dose of 18α-GA (Supplementary Figure S4).

Further, the long-term effect of 18α-GA on the proliferation of NSCLC cell lines was assessed by colony formation assay. A significant reduction in the number of colonies was observed with a concomitant decrease in the size of the cell colonies (more prominent in A549 cells) as compared to the untreated group, indicating the growth inhibitory potential of 18α-GA in both the cell lines with increasing concentrations (Figures 4B,C).

3.2.2 18α-GA causes morphological changes in non-small cell lung cancer cells

For evaluating the effects of 18α-GA as predicted by bioinformatic, two NSCLC cell lines; H1299 and A549 were exposed to two different concentrations of 18α-GA, and the morphological changes in the cells were observed under an inverted microscope. After 48 h, a disrupted monolayer with cells floating in the media along with rounding, shrinkage, and loss of characteristic size and shape of the cells was observed as shown in Figure 4D. To further evaluate these changes, DAPI staining was done. It revealed that with increasing concentration, cells became more and more sparse with a decrease in the cell numbers and density. Although, a significant increase in blue fluorescence of the treated cells was observed clearly indicating permeabilization of the membrane marking cell death (Figure 4E).

3.2.3 Cell cycle progression was arrested at G0/G1 stage

Disruption of the cell cycle process is a hallmark of cancer cells. After treatment with 18-αGA, cell cycle analysis by flow cytometry revealed that the cells remained significantly at the G1 stage at both concentrations in H1299 and A549 cells (Figures 5A,B). This increase in cell number suggests that the cell cycle was arrested at the G1 phase. To know the possible molecular mechanisms implicated with growth arrest in NSCLC cells, regulatory proteins of the cell cycle were examined by RT-PCR. The cell cycle is a complex mechanism regulated by the coordination of several markers and the mRNA expression analysis of G1/S transition markers Cyclin E1, p27, and p53 were analyzed (Figures 5C,D). It was observed that the mRNA expression of p53 and p27 were increased significantly in the treated cells whereas the expression of the cyclin E1 gene was decreased significantly in a representing cell cycle arrest at the G1 phase.

3.2.4 18α-GA induces apoptosis in non-small cell lung cancer cells

It was speculated that the morphological changes and growth inhibition observed may be due to apoptotic induction in the cells. Accordingly, AO/EB fluorescent imaging revealed that the exposure of cells to 18α-GA caused in reduction of bright green fluorescence and an increase in red fluorescence indicating a decrease in healthy viable cells and an increase in dead late apoptotic cells respectively as compared to the control group. Additionally, orange-red fluorescence in the treated groups of H1299 cells was more prominent indicating that these cells were undergoing early apoptotic changes (Figure 6A).

The above results were substantiated by flow cytometric analysis after Annexin V/PI double staining. The FACS analysis exhibited a significant increase in the percentage of cells undergoing early and late apoptotic stages. It was 47.3% and 53.8% in treated H1299 cells in their respective concentration when compared to control cells, which was 21.2%. Similarly, in treated A549 cells, it was 34.2 and 53.8% in their respective concentration as compared to 19.8% in control cells. (Figures 6B,C). Also, a shift of cells from the early apoptotic stage to the late apoptotic stage was observed at higher concentrations in both H1299 and A549 cell lines indicating cell death.

To confirm the induction of apoptosis after exposure to 18-αGA, protein expression levels of apoptotic-related markers i.e., Caspase-3, Bcl2, and Bax were analyzed by western blotting.

The results in Figures 6D,E demonstrated that pro-apoptotic marker Bax and cleaved caspase-3 expressions were increased markedly in the treated groups as compared to the untreated one in H1299 cells. In A549 cells, the expression of these proteins was slightly less. Expectedly, the expression of anti-apoptotic protein Bcl_2 was significantly diminished in both the cell lines at both concentrations as compared to the control group. A fine balance among Bcl-2 family proteins leads to apoptotic regulation in cancer cells, as noted above, the simultaneous increase and decrease of Bax and Bcl-2 proteins respectively led to an almost 70% increase in the A549 cel lines whereas the increase was nearly 20% in H1299 cells in the Bax/Bcl-2 ratio (Figure 6E) at 80 μM as compared to control cells validating the induction of apoptosis after exposure to 18-αGA (Zhu et al., 2015).

3.2.5 18α-GA causes loss of mitochondrial membrane potential in non-small cell lung cancer cells

To understand the involvement of mitochondria in the apoptotic effect of 18α-GA on H1299 and A549 cells, mitochondrial membrane potential analysis was done. In early apoptotic cells, depolarization of the mitochondrial membrane occurs, and the MMP decreases. TMRM is a cell-permeant, cationic, and red-orange fluorescent dye readily sequestered by active mitochondria. In apoptotic cells, TMRM leaves mitochondria and dye dispersion occurs.

As presented in Figure 6F, it was observed that in both the cell lines, the treated cells have significantly decreased red fluorescence cells compared to untreated ones, indicating malfunctioning of the mitochondrial membrane potential. This decrease in the MMP and disruption of membrane potential gradient indicates that the 18α-GA induces apoptosis at both concentrations in both cell lines.

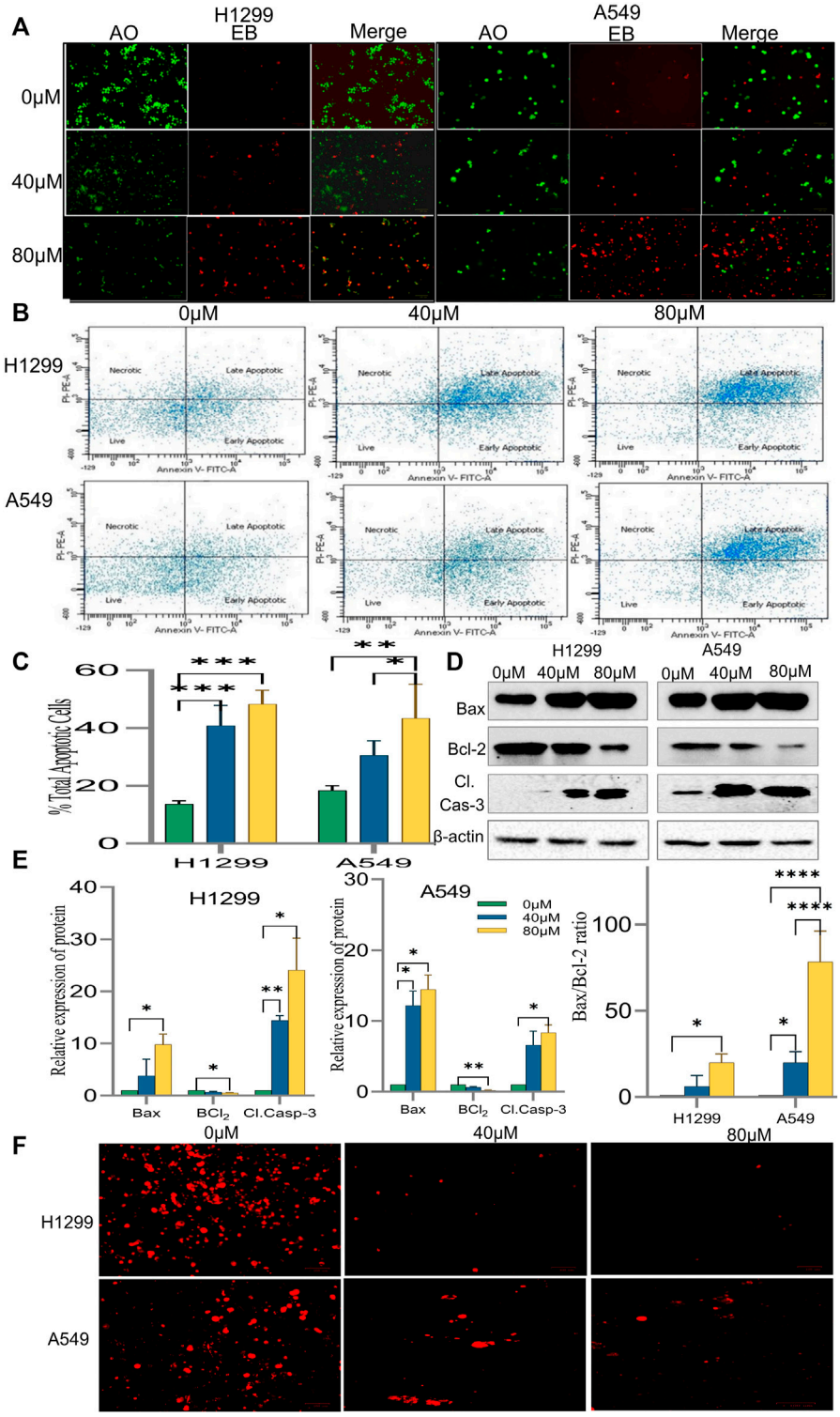

FIGURE 6
Induction of apoptosis by 18α-GA in H1299 and A549 cells. **(A)** Images of AO/EB staining by fluorescence microscopy; Green fluorescence represents healthy cells, Red cells represents cells undergoing late apoptotic stage. **(B)** Fluorescent images showing cell distribution in different stages of apoptosis detected by FACS. **(C)** % total apoptotic cells found after treatment with 18-αGA; (n = 3, mean ± SD), statistical analysis was done by 2-way ANOVA followed by Sidak's Post-hoc multiple comparison test. *$p < 0.05$, **$p < 0.01$, ***$p < 0.001$, ****$p < 0.0001$. **(D)** Western blots showing expressions of apoptotic-related proteins. **(E)** Graphs representing protein expression levels after normalisation with beta-actin, statistical analysis was done by 2-way ANOVA followed by Tukey's Post-hoc multiple comparison test, *$p < 0.05$, **$p < 0.01$, ***$p < 0.001$, ****$p < 0.0001$. Graph representing calculated Bax/Bcl-2 ratio, Sidak's multiple comparison test was used. **(F)** Fluorescent images show TMRM staining for mitochondrial membrane potential.

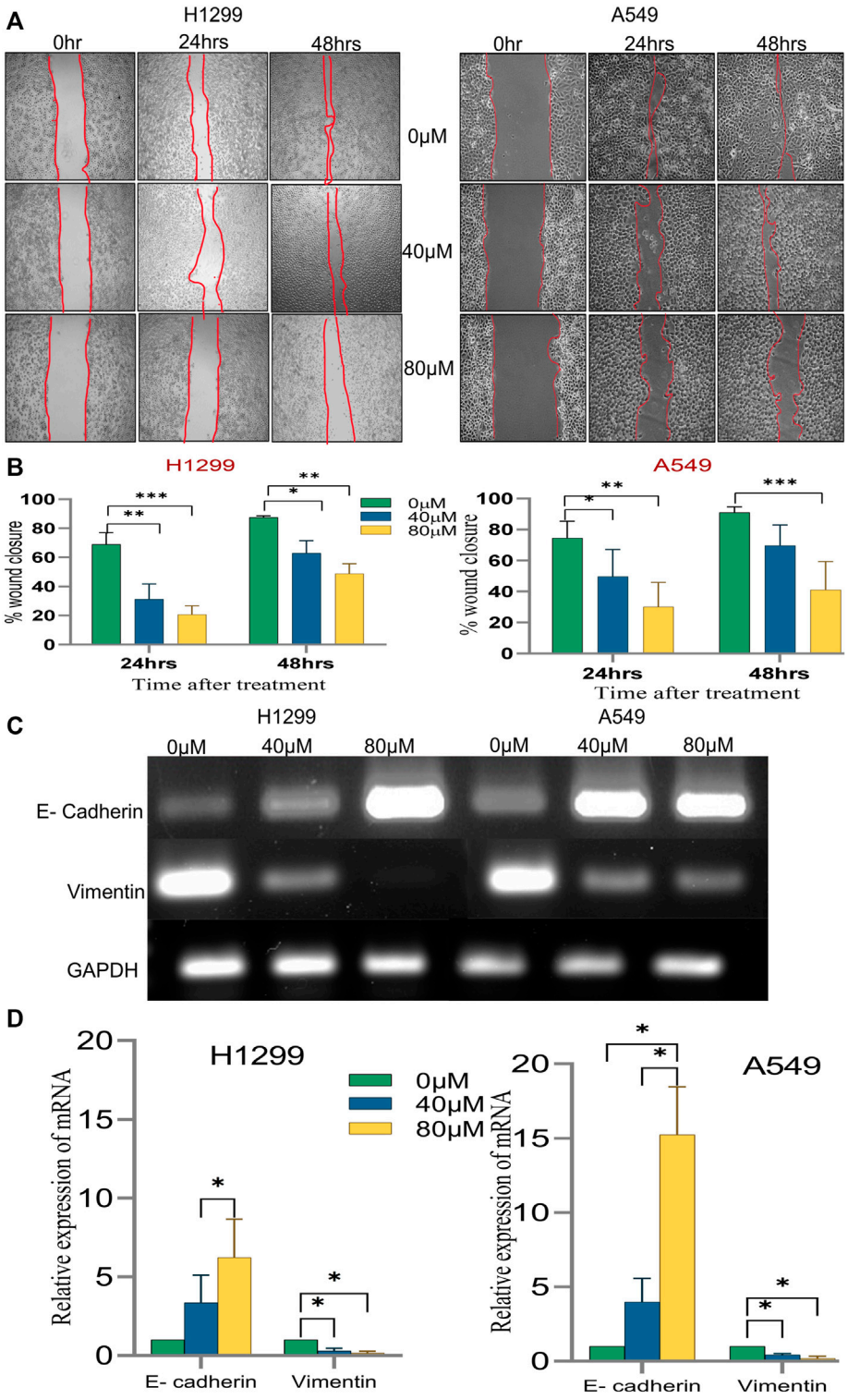

FIGURE 7
The effect of different concentrations of 18α-GA on the migration of NSCLC cells. **(A)** Images representing wound healing assay at two different time points, the wound area was calculated by ImageJ. **(B)** % wound closure calculated after treatment with 18α-GA (n = 3, mean ± SD), statistical analysis was done by 2-way ANOVA followed by Bonferroni's Post-hoc multiple comparison test, *p < 0.05, **p < 0.01, ***p < 0.001, ****p < 0.0001 **(C)** The mRNA expression of related genes after treatment with 18α-GA by RT-PCR. **(D)** Graph representing mRNA expression levels of genes with respect to GAPDH, statistical analysis was done by 2-way ANOVA followed by Tukey's Post-hoc multiple comparison test, *p < 0.05, **p < 0.01, ***p < 0.001, ****p < 0.0001.

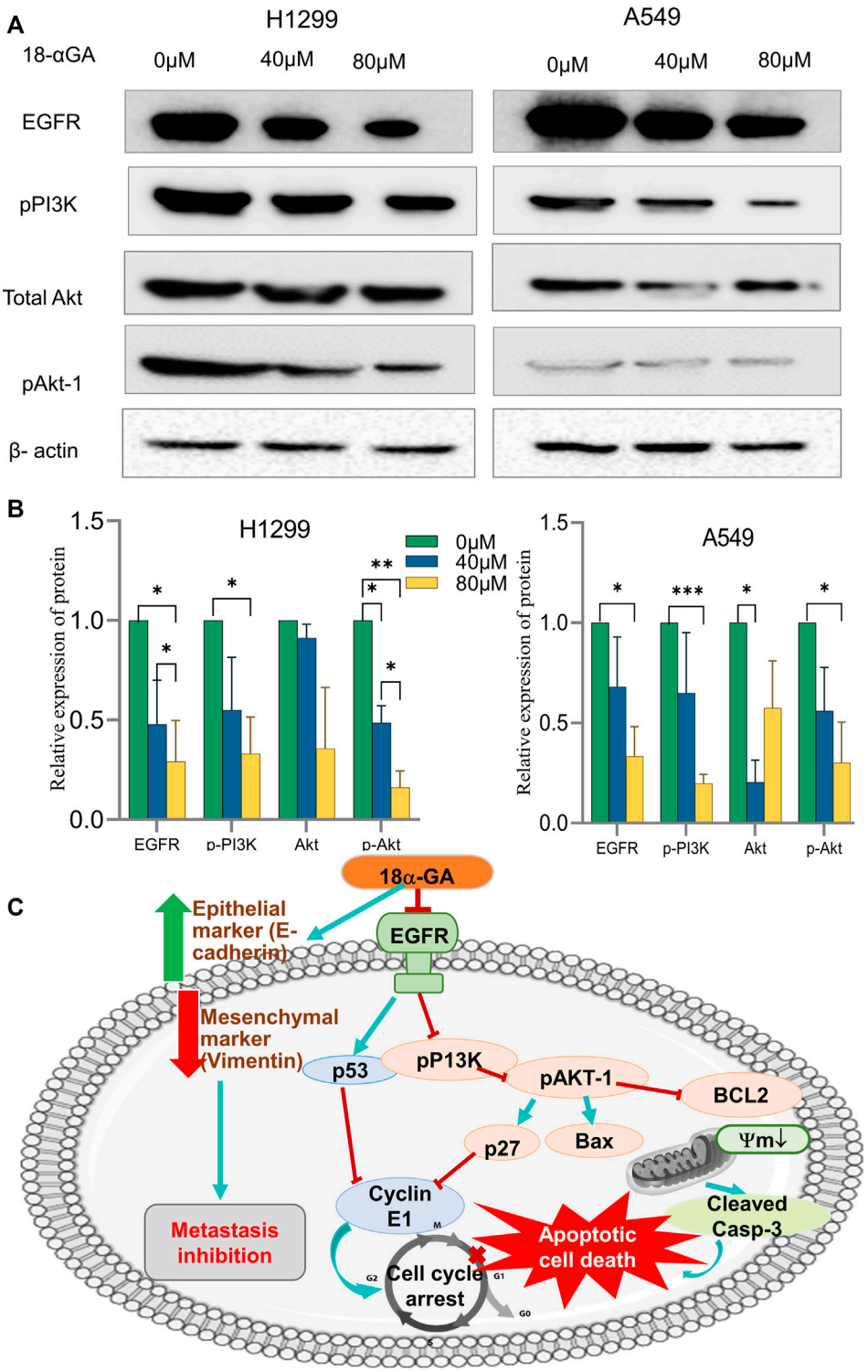

FIGURE 8
(A) Effect of different concentrations of 18α-GA treatment on the protein expression of EGFR, pPI3K, pan-Akt and pAKT1 in H1299 and A549 cells. **(B)** Graph representing relative expression of protein with respect to beta-actin in treated and untreated groups, statistical analysis was done by 2-way ANOVA followed by Tukey's Post-hoc multiple comparison test, *$p < 0.05$, **$p < 0.01$, ***$p < 0.001$, ****$p < 0.0001$. **(C)** Depiction of the overall mechanism of action of 18α-GA against NSCLC as predicted by combining key targets found in the bioinformatics and *in-vitro* analysis.

3.2.6 18α-GA confers a reduction in the migratory potential of non-small cell lung cancer cells

Since the migratory potential of tumor cells is essential for metastatic dissemination and tumorigenesis, the effect of 18α-GA on H1299 and A549 cancer cells was evaluated for metastatic propensity. The results of the wound-healing assay (Figure 7A) exhibited a significant dose-dependent decrease in the wound closure ability of the cells in the treated groups compared to the untreated ones. The cell migration in the wound healing assay showed reduced migration of cells in the wound as compared to the control group at both concentrations in both the cell lines suggesting abrogation of the wound healing capacity of the cells after pre-treatment with 18-αGA (Figure 7B).

Next, it was sought to check the key EMT markers at the molecular level. It was found that the mRNA expression of E-cadherin was intensified significantly in the treated groups with a concomitant decrease in the vimentin mRNA expression (Figures 7C,D). These outcomes at least in part suggest that 18α-GA could significantly inhibit the EMT ability of H1299 and A549 cells.

3.2.7 18α-GA inhibits EGFR-phosphatidylinositol 3-kinase/AKT pathway

The network pharmacology and pathway enrichment analysis predicted that EGFR, PI3K, and AKT1 was increasingly associated pathway with the anti-tumor properties of 18α-GA in NSCLC. Therefore, to confirm the *in-silico* findings, the protein expression levels of these targets were examined by western blotting. As shown in Figures 8A,B, the expression level of EGFR was apparently reduced in both the cell lines with increasing dose but the effect was more significant in H1299 cells as compared to A549 cells. Additionally, the phosphorylation levels of PI3K and Akt1 were significantly decreased after treatment with two concentrations of 18α-GA. These results validated that the highly expressed hub targets are repressed on treatment by 18α-GA and might regulate NSCLC proliferation and tumorigenesis *via* the EGFR-PI3K-Akt signaling pathway.

4 Discussion

The NSCLC, comprising adenocarcinoma, squamous cell carcinoma, and large-cell carcinoma subtypes, is the most aggressive and highly metastatic kind of lung cancer, leading to higher overall death rates than combined mortality rates of breast cancer, prostate cancer, colorectal cancer, and leukemia (Alexander et al., 2020). In an attempt to reduce lung cancer incidences and improve patients' survival rates, great efforts are being made, including refinement of early-stage screening methods, understanding lung cancer etiology, and introducing newer state-of-the-art treatment regimens (Bade and dela Cruz, 2020). Recently neoadjuvant and adjuvant chemotherapy in conjunction with the current standard drug regimen (vandetanib, pazopanib, and axitinib) and radiotherapy have been instituted (Chen et al., 2020). However, these attempts are futile and somewhat ineffective in ameliorating the clinical outcome of NSCLC patients. To address this challenge, complementary therapeutic approaches have been the focus for the last few decades, including the use of natural compounds or medicinal plants to find novel therapeutic agents and new leads for synthetic or semi-synthetic chemotherapeutic drugs (Irshad and Husain, 2021; Yang et al., 2021). Not to forget, the lesser side-effects and toxicity associated with utilizing these agents in clini cal settings enhance patients' quality of life and overall treatment outcomes. Countless such natural products have been under scrutiny for their chemopreventive properties, e.g., Curcumin and curcumin-derived semi-synthetic derivatives being administered to cancer patients that are proving as an adequate adjuvant remedy (Salehi et al., 2020; Ali et al., 2021). Nevertheless, there is always room to search for newer and better natural products from nature's diverse sources that can be utilized to harness their chemopreventive capacities.

Although pentacyclic triterpenoids have a significant history of showing great potential as anti-cancer agents, there is still a gap in screening numerous triterpenoids present in nature (Markov et al., 2017; Salvador et al., 2017; Ghante and Jamkhande, 2019). Accordingly, in this study, the effect and mechanism of action of a pentacyclic triterpenoid compound-18α-GA were evaluated on the growth, proliferation, metastasis, and survival of NSCLC by utilizing network pharmacology and *in-vitro* approaches. Systems pharmacology has become apparent as one of the most exciting approaches in investigating the mechanistic underpinnings ranging from molecular to tissue level of the natural products, medicinal plants, and traditional Chinese medicine against various diseases, including cancer (Kibble et al., 2015; Fang et al., 2017). Network pharmacology is a multi-disciplinary method and acts as the converging point of pharmacokinetics and pharmaco-mapping analysis, high-throughput omics data analysis, biological database retrieval, systems biology, drug repurposing, and structure-based drug designing (Chandran et al., 2017). It is a novel methodology that helps in creating and establishing "compound-target- pathway-disease" network models that aid in the prediction of disease targets, thereby increasing the efficiency of drug discovery and, in turn, snowballing the success rate of clinical trials with a simultaneous reduction in the expenditure associated with drug discovery (Li and Zhang, 2013).

Recently, targeted therapies have shown promise in chemoprevention and treatment, yet it has only been successfully utilized in a few cancer types (Charmsaz et al., 2018). The curative outcomes of single-target therapies are often counterweighed by either acquiring resistance or

establishing compensatory signaling pathways in cancer cells. Network pharmacology breaks such limitations by deciphering the underlying putative multi-targeted, multi-channel therapeutic abilities of natural products and medicinal plants in treating heterogeneous diseases like cancer (Kibble et al., 2015). Thus, network pharmacology was utilized to systematically elucidate the mechanism of 18α-GA against NSCLC and further corroborate it by extensive *in-vitro* experiments. To the best of our knowledge, this study has first time delineated the anti-tumor effects of 18α-GA by reducing proliferation, inducing apoptosis, and inhibiting cell cycle progression as well as migration and metastasis in NSCLC cells.

At the outset of this study, the pharmacokinetics evaluation of the absorption, distribution, metabolism, excretion, and toxicity (ADME/T) confirmed the excellent druggability of 18α-GA *in vivo* (Supplementary Figure S5). The absorption parameter confirmed that 18α-GA is absorbed easily, and it follows Lipinski's rule of drug-likeness hence, it is believed that 18α-GA has the characteristics to be developed into a drug. Subsequently, the MTT assay result verified that 18α-GA did not have a cytotoxic effect on HEK- 293 cells and had a negligible effect on its proliferative capacity. Meanwhile, network pharmacological analysis established at least 181 potential targets of 18α-GA against NSCLC. Further evaluation of PPI network that had 181 nodes and 964 edges was done by recognising the Top 20 targets on the basis of Degree, Betweenness, Closeness and MCC values. According to these network topological properties, EGFR, PI3KR1, AKT1, MAPK1, SRC, and IGF1 were identified as the core targets of anti-NSCLC effects of 18α-GA; most of these targets have critical roles in cell proliferation, survival, cell cycle regulation, metastasis, and invasion.

These targets were chosen as they were the key nodes of the PPI network and the binding energies confirmed that among these 6 key targets, EGFR and AKT1 had the most excellent affinity toward our compound. In the docking studies, lower scores correspond to lower matching energies, which means that there is a higher likelihood of contact and a more stable conformation of ligand-receptor binding. The results showed that the binding energy of these two proteins specifically were less than −7.5 kcal/mol indicating strong binding activity.

Consistent with this result, the GO analysis of common targets of 18α-GA and NSCLC displayed several important biological processes, molecular functions and cellular compartments. The highly significant biological processes when screened included ErbB (EGFR) signaling pathway, cell proliferation, regulation of PI3K signalling, protein tyrosine kinase signalling, regulation of apoptosis and phosphatidyl-inositol signalling. Similarly, the nucleus, plasma membrane, mitochondrial matrix, cytoplasm are the few important cellular components that are involved. The molecular functions gene ontology disclosed the contribution protein kinase binding, protein kinase activity, protein phosphatase binding, insulin receptor binding, phosphatidylinositol-4,5-bisphosphate 3-kinase activity as the crucial effecters of 18α-GA targets. The results of KEGG analysis revealed that the highly enriched top pathways involved were the PI3K-Akt signaling pathway, ErbB (EGFR) signaling pathway, pathways in cancer, estrogen signaling pathway, and Ras signaling pathway, among other closely related cancer signaling pathways associated with targets of 18α-GA against NSCLC. The GO terms and KEGG pathways allow for concrete prediction of the mechanisms involved in anti-cancer activity of the compound by taking into considerations the large-scale molecular datasets produced by genome sequencing and other high-throughput experimental techniques. Taken together result of the above *in-silico* analysis, it can be inferred that 18α-GA may exert its therapeutic effects on NSCLC by regulating ErbB signaling and PI3K/AKT signaling pathway, which is widely involved in tumor proliferation, apoptosis, and metastasis regulation. EGFR belongs to the protein kinase superfamily, a member of the ErbB family, and is a transmembrane glycoprotein and a receptor of epidermal growth factor. Mostly NSCLC harbors EGFR mutations and is widely involved in causing tumorigenesis (da Cunha Santos et al., 2011). EGFR is a vital driver mutation because it regulates a multitude of intracellular signaling networks. Overexpression of EGFR can lead to unregulated activation of its downstream signaling pathways, which include PI3K/AKT, Ras-ERK/MAP kinase, Src, JAK/STAT, and PKC, thereby leading to uncontrolled proliferation, survival, migration of invasion of cancer cells (Seshacharyulu et al., 2012). Similarly, PI3K/AKT is correlated with the initiation and development of cancer which is conducive to the proliferation, cell cycle progression, migration, and invasion of cancer cells. This pathway is most commonly and consistently activated in human cancers and is closely associated with tumorigenesis, proliferation, apoptosis, metastasis, epithelial-mesenchymal transition (EMT), metabolism, and chemoresistance. Hence, it is no surprise that these pathways have been attractive targets for anti-cancer therapies (Chang et al., 2003). Thus, this indicates that inhibition of these signaling molecules might help in suppressing cancer cell growth and tumorigenesis.

The data obtained as stated above was validated in cell culture to confirm the effect of 18α-GA on NSCLC cancer cell lines; H1299 and A549. It was observed that 18α-GA could inhibit cell growth and was found to be cytotoxic for both the cell lines at 24 and 48 h of treatment. Although, the growth inhibitory effect was more pronounced at 48 h. Thus, two fixed dosages were adopted for the treatment of 48 h in this study. As uncontrolled cell cycle progression supports the growth of cancer cells, the effect of 18α-GA was found that it was able to arrest the cell cycle at the G1 phase, hence inhibiting the G1-S transition. This was in accordance with the expressions of key regulatory genes p27, Cyclin E1, and p53 of this transition (Raghunandhakumar et al., 2013). It is important to note here that these genes are also a part of the signaling network identified by bioinformatics analysis in

this study. EGFR stimulates the PI3K/AKT axis which directly affects the expression of p27 and p21 which in turn regulated cyclin E1 expression and act in the G1/S transition (Chang et al., 2003). The activated Akt negatively regulates p27 and p21 decreasing their expression and promoting the cell cycle. Accordingly, it was observed that the expression of p27 was increased with a concomitant decrease in Cyclin E1.

The FACS and morphological analysis (AO/EB) in this study suggested that the anti-tumor effect of 18α-GA against NSCLC cell lines, H1299 and A549 was found to be associated with the induction of apoptotic cell death. Additionally, the protein expression analysis by western blotting revealed that apoptosis was induced after treatment with 18α-GA due to a decrease in the expression of Bcl-2 with a concomitant increase in the expressions of Bax and cleaved caspase- 3 proteins. The Bcl2 family of proteins maintains a balance between pro and anti-apoptotic proteins and is downstream of PI3K/AKT signaling pathway, hence, the unchecked pathway disturbs this balance and causes the uncontrolled proliferation (Pilling and Hwang, 2019). Bcl-2 and Bax are two distinct members of Bcl-2 family that regulates cellular apoptosis and an elevated ratio of Bax/Bcl-2 is known to induce apoptosis (Perlman et al., 1999) which was seen in our data too. There are other reports suggesting that the increased ratio of Bax/Bcl-2 could also increase caspase- 3 activation and irreversibly activate the process of apoptosis in cells (Salakou et al., 2007). It has been reported that the overactive EGFR- PI3K/AKT pathway plays a vital role in perturbing the apoptotic system of cancer cells and thus evading this process altogether and targeting these pathway proteins can induce apoptosis (Nicholson and Anderson, 2002; Jeon et al., 2016).

Metastatic dissemination is an important hallmark of cancer transformation which involves Epithelial to Mesenchymal transition (EMT) causing the cells to lose epithelial markers and gain mesenchymal properties (Huber et al., 2005; Bhat et al., 2014; Duan et al., 2014). Congruently, this study showed increased expression of E-cadherin, an epithelial marker with a simultaneous decrease of Vimentin expression which is a mesenchymal marker after treatment with 18α-GA. Moreover, a significant reduction in the wound healing process was evident in NSCLC cell lines after 18α-GA incubation, therefore it may be speculated that 18α-GA could inhibit EMT and hence metastasis. In addition, the protein expression levels of key signaling molecules i.e., EGFR, pPI3K, and pAkt-1 were validated through western blotting. It was observed that 18α-GA treated NSCLC cells showed significantly reduced expression of these targets indicating that NSCLC inhibition was mainly *via* the regulation of cell proliferation and survival through the EGFR-PI3K/Akt signaling pathways.

In summary, the therapeutic efficacy of 18α-GA against NSCLC was explored by bio-informatics and confirmed using *in-vitro* studies. The present study confirms the anti-tumorigenic effects of 18α-GA on NSCLC, thereby inhibiting proliferation and metastasis of lung cancer cells by inducing apoptosis and inhibiting cell cycle progression, EMT, and regulating EGFR-PI3K/AKT signaling pathway. It was also reported that other closely related pathways may be modulated by 18α-GA to suppress NSCLC growth as assessed by network pharmacological and functional enrichment studies that need future *in-vitro* investigations. The predicted model of the mechanism of action of 18α-GA in restraining NSCLC growth and progression has been elucidated in Figure 8C.

Conclusion

In this study, an integrative approach involving network pharmacology and experimental assays was utilized to explore the underlying anti-NSCLC mechanisms of a natural compound, 18α-GA for the first time. The antiproliferative effect of 18α-GA on two NSCLC cell lines was due to inhibition of cell growth by induction of apoptosis, arrest of cell cycle progression, reduction in the migratory potential, and regulation of EGFR- PI3K/Akt pathway. Moreover, network pharmacology analysis suggested the involvement of multiple pathways and molecular targets of 18α-GA, hence forming a base of its multi-targeted efficacy against NSCLC. Although a comprehensive approach was utilized in this study, further investigation may provide more insight using animal models.

Data availability statement

The original contributions presented in the study are included in the article/Supplementary Material. Further inquiries can be directed to the corresponding author.

Author contributions

RI and MH conceptualized the idea and designed the experiments. RI performed experiments and acquired the data. NR performed Molecular Docking simulations. NR and NM helped with software resources and data analysis. RI wrote the manuscript and sketched the mechanistic interpretation under the supervision of MH. RI, GG, and MH did final reviewing and editing All the infrastructure and reagents were provided by MH to conduct the research. GG and MH assisted in funding acquisition. All the authors contributed to the article and approved the submitted version.

Funding

The research received no external funding support; however, some support was utilized from the extramural funding grant of

MH (Ministry of AYUSH, Government of India grant no. 3-7/2009-CCRUM/EMR).

Acknowledgments

The University Grants Commission (UGC) is highly acknowledged for providing fellowship to RI.

Conflict of interest

The authors declare that the research was conducted in the absence of any commercial or financial relationships that could be construed as a potential conflict of interest.

Publisher's note

Supplementary material

The Supplementary Material for this article can be found online at: https://www.frontiersin.org/articles/10.3389/fphar.2022.1018974/full#supplementary-material

References

Alam, S., Mohammad, T., Padder, R. A., Hassan, M. I., and Husain, M. (2022). Thymoquinone and quercetin induce enhanced apoptosis in non-small cell lung cancer in combination through the Bax/Bcl2 cascade. *J. Cell Biochem.* 123, 259–274. doi:10.1002/jcb.30162

Alexander, M., Kim, S. Y., and Cheng, H. (2020). Update 2020: Management of non-small cell lung cancer. *Lung* 198, 897–907. doi:10.1007/s00408-020-00407-5

Ali, R., Tabrez, S., Akand, S. K., Rahman, F., Husein, A., Arish, M., et al.fnm (2021). Sesamol induces apoptosis-like cell death in leishmania donovani. *Front. Cell Infect. Microbiol.* 11. 749420. doi:10.3389/fcimb.2021.749420

Bade, B. C., and dela Cruz, C. S. (2020). Lung cancer 2020: Epidemiology, etiology, and prevention. *Clin. Chest Med.* 41, 1–24. doi:10.1016/j.ccm.2019.10.001

Bhat, F. A., Sharmila, G., Balakrishnan, S., Arunkumar, R., Elumalai, P., Suganya, S., et al. (2014). Quercetin reverses EGF-induced epithelial to mesenchymal transition and invasiveness in prostate cancer (PC-3) cell line via EGFR/PI3K/Akt pathway. *J. Nutr. Biochem.* 25, 1132–1139. doi:10.1016/j.jnutbio.2014.06.008

Chandran, U., Mehendale, N., Patil, S., Chaguturu, R., and Patwardhan, B. (2017). "Chapter 5 - network pharmacology," in *Innovative approaches in drug discovery*, 1.

Chang, F., Lee, J. T., Navolanic, P. M., Steelman, L. S., Shelton, J. G., Blalock, W. L., et al. (2003). Involvement of PI3K/Akt pathway in cell cycle progression, apoptosis, and neoplastic transformation: A target for cancer chemotherapy. *Leukemia* 17, 590–603. doi:10.1038/sj.leu.2402824

Charmsaz, S., Prencipe, M., Kiely, M., Pidgeon, G. P., and Collins, D. M. (2018). Innovative technologies changing cancer treatment. *Cancers (Basel)* 10, 208. doi:10.3390/cancers10060208

Chen, R., Manochakian, R., James, L., Azzouqa, A. G., Shi, H., Zhang, Y., et al. (2020). Emerging therapeutic agents for advanced non-small cell lung cancer. *J. Hematol. Oncol.* 13, 138. doi:10.1186/s13045-020-00881-7

Creed, S., and McKenzie, M. (2019). "Measurement of mitochondrial membrane potential with the fluorescent dye tetramethylrhodamine methyl ester (TMRM)," in *Methods in molecular biology*, 1. doi:10.1007/978-1-4939-9027-6_5

da Cunha Santos, G., Shepherd, F. A., and Tsao, M. S. (2011). EGFR mutations and lung cancer. *Annu. Rev. Pathology Mech. Dis.* 6, 49–69. doi:10.1146/annurev-pathol-011110-130206

Daina, A., Michielin, O., and Zoete, V. (2017). SwissADME: A free web tool to evaluate pharmacokinetics, drug-likeness and medicinal chemistry friendliness of small molecules. *Sci. Rep.* 7, 42717. doi:10.1038/srep42717

Daina, A., Michielin, O., and Zoete, V. (2019). SwissTargetPrediction: Updated data and new features for efficient prediction of protein targets of small molecules. *Nucleic Acids Res.* 47, W357–W364. doi:10.1093/nar/gkz382

Duan, H., Qu, L., and Shou, C. (2014). Activation of EGFR-PI3K-AKT signaling is required for Mycoplasma hyorhinis-promoted gastric cancer cell migration. *Cancer Cell Int.* 14, 135. doi:10.1186/s12935-014-0135-3

Fang, J., Cai, C., Wang, Q., Lin, P., Zhao, Z., and Cheng, F. (2017). Systems pharmacology-based discovery of natural products for precision oncology through targeting cancer mutated genes. *CPT Pharmacometrics Syst. Pharmacol.* 6, 177–187. doi:10.1002/psp4.12172

Ghante, M. H., and Jamkhande, P. G. (2019). Role of pentacyclic triterpenoids in chemoprevention and anticancer treatment: An overview on targets and underling mechanisms. *J. Pharmacopuncture* 22, 55–67. doi:10.3831/KPI.201.22.007

Gridelli, C., Rossi, A., Carbone, D. P., Guarize, J., Karachaliou, N., Mok, T., et al. (2015). Non-small-cell lung cancer. *Nat. Rev. Dis. Prim.* 1, 1. doi:10.1038/nrdp.2015.9

Ha, Y. M., Cheung, A. P., and Lim, P. (1991). Chiral separation of glycyrrhetinic acid by high-performance liquid chromatography. *J. Pharm. Biomed. Anal.* 9, 805–809. doi:10.1016/0731-7085(91)80005-t

Huang, D. W., Sherman, B. T., Tan, Q., Kir, J., Liu, D., Bryant, D., et al. (2007). DAVID Bioinformatics Resources: Expanded annotation database and novel algorithms to better extract biology from large gene lists. *Nucleic Acids Res.* 35, W169–W175. doi:10.1093/nar/gkm415

Huber, M. A., Kraut, N., and Beug, H. (2005). Molecular requirements for epithelial–mesenchymal transition during tumor progression. *Curr. Opin. Cell Biol.* 17, 548–558. doi:10.1016/J.CEB.2005.08.001

Irshad, R., and Husain, M. (2021). Natural products in the reprogramming of cancer epigenetics. *Toxicol. Appl. Pharmacol.* 417, 115467. doi:10.1016/j.taap.2021.115467

Jeon, Y. J., Cho, J. H., Lee, S. Y., Choi, Y. H., Park, H., Jung, S., et al. (2016). Esculetin induces apoptosis through EGFR/PI3K/Akt signaling pathway and nucleophosmin relocalization. *J. Cell Biochem.* 117, 1210–1221. doi:10.1002/jcb.25404

Kasibhatla, S., Amarante-Mendes, G. P., Finucane, D., Brunner, T., Bossy-Wetzel, E., and Green, D. R. (2006). Acridine orange/ethidium bromide (AO/EB) staining to detect apoptosis. *Cold Spring Harb. Protoc.* 2006, 1. doi:10.1101/pdb.prot4493

Kibble, M., Saarinen, N., Tang, J., Wennerberg, K., Mäkelä, S., and Aittokallio, T. (2015). Network pharmacology applications to map the unexplored target space and therapeutic potential of natural products. *Nat. Prod. Rep.* 32, 1249–1266. doi:10.1039/c5np00005j

Lánczky, A., and Győrffy, B. (2021). Web-based survival analysis tool tailored for medical research (KMplot): Development and implementation. *J. Med. Internet Res.* 23, e27633. doi:10.2196/27633

Li, J., Tang, F., Li, R., Chen, Z., Lee, S. M. Y., Fu, C., et al. (2020). Dietary compound glycyrrhetinic acid suppresses tumor angiogenesis and growth by modulating antiangiogenic and proapoptotic pathways *in vitro* and *in vivo*. *J. Nutr. Biochem.* 77, 108268. doi:10.1016/j.jnutbio.2019.108268

Li, S., and Zhang, B. (2013). Traditional Chinese medicine network pharmacology: Theory, methodology and application. *Chin. J. Nat. Med.* 11, 110–120. doi:10.1016/S1875-5364(13)60037-0

Markov, A. v., Zenkova, M. A., and Logashenko, E. B. (2017). Modulation of tumour-related signaling pathways by natural pentacyclic triterpenoids and their semisynthetic derivatives. *Curr. Med. Chem.* 24, 1277–1320. doi:10.2174/0929867324666170112115313

Mohammad, T., Mathur, Y., and Hassan, M. I. (2021). InstaDock: A single-click graphical user interface for molecular docking-based virtual high-throughput screening. *Brief. Bioinform* 22, bbaa279. doi:10.1093/bib/bbaa279

Mustafa, S., Pawar, J. S., and Ghosh, I. (2021). Fucoidan induces ROS-dependent epigenetic modulation in cervical cancer HeLa cell. *Int. J. Biol. Macromol.* 181, 180–192. doi:10.1016/j.ijbiomac.2021.03.110

Nicholson, K., and Anderson, N. (2002). Nicholson KM, Anderson NG. The protein kinase B/Akt signaling pathway in human malignancy. *Cell Signal* 14, 381–395. doi:10.1016/S0898-6568(01)00271-6

Padder, R. A., Bhat, Z. I., Ahmad, Z., Singh, N., and Husain, M. (2021). DRP1 promotes brafv600e-driven tumor progression and metabolic reprogramming in colorectal cancer. *Front. Oncol.* 10, 592130. doi:10.3389/fonc.2020.592130

Perlman, H., Zhang, X., Chen, M. W., Walsh, K., and Buttyan, R. (1999). An elevated bax/bcl-2 ratio corresponds with the onset of prostate epithelial cell apoptosis. *Cell Death Differ.* 6, 48–54. doi:10.1038/sj.cdd.4400453

Pilling, A. B., and Hwang, C. (2019). Targeting prosurvival BCL2 signaling through Akt blockade sensitizes castration-resistant prostate cancer cells to enzalutamide. *Prostate* 79, 1347–1359. doi:10.1002/pros.23843

Pirzadeh, S., Fakhari, S., Jalili, A., Mirzai, S., Ghaderi, B., and Haghshenas, V. (2014). Glycyrrhetinic acid induces apoptosis in leukemic HL60 cells through upregulating of CD95/CD178. *Int. J. Mol. Cell. Med.* 3 (4), 272–278.

Raghunandhakumar, S., Paramasivam, A., Senthilraja, S., Naveenkumar, C., Asokkumar, S., Binuclara, J., et al. (2013). Thymoquinone inhibits cell proliferation through regulation of G1/S phase cell cycle transition in N-nitrosodiethylamine-induced experimental rat hepatocellular carcinoma. *Toxicol. Lett.* 223, 60–72. doi:10.1016/J.TOXLET.2013.08.018

Rahman, M. A., Bishayee, K., Habib, K., Sadra, A., and Huh, S. O. (2016). 18α-Glycyrrhetinic acid lethality for neuroblastoma cells via de-regulating the Beclin-1/Bcl-2 complex and inducing apoptosis. *Biochem. Pharmacol.* 117, 97–112. doi:10.1016/j.bcp.2016.08.006

Salakou, S., Kardamakis, D., Tsamandas, A. C., Zolota, V., Apostolakis, E., Tzelepi, V., et al. (2007). "Increased bax/bcl-2 ratio up-regulates caspase-3 and increases apoptosis in the thymus of patients with Myasthenia gravis," *in Vivo(brooklyn)*, 21.

Salehi, M., Movahedpour, A., Tayarani, A., Shabaninejad, Z., Pourhanifeh, M. H., Mortezapour, E., et al. (2020). Therapeutic potentials of curcumin in the treatment of non-small-cell lung carcinoma. *Phytotherapy Res.* 34, 2557–2576. doi:10.1002/ptr.6704

Salvador, J. A. R., Leal, A. S., Valdeira, A. S., Gonçalves, B. M. F., Alho, D. P. S., Figueiredo, S. A. C., et al. (2017). Oleanane-, ursane-, and quinone methide friedelane-type triterpenoid derivatives: Recent advances in cancer treatment. *Eur. J. Med. Chem.* 142, 95–130. doi:10.1016/j.ejmech.2017.07.013

Sathya, S., Sudhagar, S., Sarathkumar, B., and Lakshmi, B. S. (2014). EGFR inhibition by pentacyclic triterpenes exhibit cell cycle and growth arrest in breast cancer cells. *Life Sci.* 95, 53–62. doi:10.1016/j.lfs.2013.11.019

Seshacharyulu, P., Ponnusamy, M. P., Haridas, D., Jain, M., Ganti, A. K., and Batra, S. K. (2012). Targeting the EGFR signaling pathway in cancer therapy. *Expert Opin. Ther. Targets* 16, 15–31. doi:10.1517/14728222.2011.648617

Shannon, P., Markiel, A., Ozier, O., Baliga, N. S., Wang, J. T., Ramage, D., et al. (2003). Cytoscape: A software environment for integrated models of biomolecular interaction networks. *Genome Res.* 13, 2498–2504. doi:10.1101/gr.1239303

Shetty, A. v., Thirugnanam, S., Dakshinamoorthy, G., Samykutty, A., Zheng, G., Chen, A., et al. (2011). 18α-glycyrrhetinic acid targets prostate cancer cells by down-regulating inflammation-related genes. *Int. J. Oncol.* 39, 635–640. doi:10.3892/ijo.2011.1061

Sun, H., Wang, F., Huang, Y., Wang, J., Zhang, L., Shen, Y., et al. (2022). Targeted inhibition of ACLY expression to reverse the resistance of sorafenib in hepatocellular carcinoma. *J. Cancer* 13, 951–964. doi:10.7150/jca.52778

Sung, H., Ferlay, J., Siegel, R. L., Laversanne, M., Soerjomataram, I., Jemal, A., et al. (2021). Global cancer statistics 2020: GLOBOCAN estimates of incidence and mortality worldwide for 36 cancers in 185 countries. *CA Cancer J. Clin.* 71, 209–249. doi:10.3322/caac.21660

Szklarczyk, D., Gable, A. L., Lyon, D., Junge, A., Wyder, S., Huerta-Cepas, J., et al. (2019). STRING v11: Protein-protein association networks with increased coverage, supporting functional discovery in genome-wide experimental datasets. *Nucleic Acids Res.* 47, 1. doi:10.1093/nar/gky1131

Takeuchi, R., Hiratsuka, K., Arikawa, K., Ono, M., Komiya, M., Akimoto, Y., et al. (2016). Possible pharmacotherapy for nifedipine-induced gingival overgrowth: 18α-glycyrrhetinic acid inhibits human gingival fibroblast growth. *Br. J. Pharmacol.* 173, 913–924. doi:10.1111/bph.13410

Tian, W., Chen, C., Lei, X., Zhao, J., and Liang, J. (2018). CASTp 3.0: Computed atlas of surface topography of proteins. *Nucleic Acids Res.* 46, W363–W367. doi:10.1093/nar/gky473

Tiboni, M., Benedetti, S., Skouras, A., Curzi, G., Perinelli, D. R., Palmieri, G. F., et al. (2020). 3D-printed microfluidic chip for the preparation of glycyrrhetinic acid-loaded ethanolic liposomes. *Int. J. Pharm.* 584, 119436. doi:10.1016/j.ijpharm.2020.119436

Wang, X., Shen, Y., Wang, S., Li, S., Zhang, W., Liu, X., et al. (2017). PharmMapper 2017 update: A web server for potential drug target identification with a comprehensive target pharmacophore database. *Nucleic Acids Res.* 45, W356–W360. doi:10.1093/nar/gkx374

Yang, Y., Li, N., Wang, T.-M., and Di, L. (2021). Natural products with activity against lung cancer: A review focusing on the tumor microenvironment. *Int. J. Mol. Sci.* 22, 10827. doi:10.3390/ijms221910827

Zhu, L., Han, M. B., Gao, Y., Wang, H., Dai, L., Wen, Y., et al. (2015). Curcumin triggers apoptosis via upregulation of Bax/Bcl-2 ratio and caspase activation in SW872 human adipocytes. *Mol. Med. Rep.* 12, 1151–1156. doi:10.3892/mmr.2015.3450

Zong, L., Qu, Y., Xu, M., Dong, Y., and Lu, L. (2012). 18α-glycyrrhetinic acid down-regulates expression of type I and III collagen via TGF-B1/Smad signaling pathway in human and rat hepatic stellate cells. *Int. J. Med. Sci.* 9, 370–379. doi:10.7150/ijms.4395

Zong, L., Qu, Y., Xu, M. Y., Dong, Y. W., and Lu, L. G. (2013). 18α-glycyrrhetinic acid extracted from Glycyrrhiza radix inhibits proliferation and promotes apoptosis of the hepatic stellate cell line. *J. Dig. Dis.* 14, 328–336. doi:10.1111/1751-2980.12041

frontiers | Frontiers in Pharmacology

TYPE Original Research
PUBLISHED 28 October 2022
DOI 10.3389/fphar.2022.1025243

OPEN ACCESS

EDITED BY
Husain Yar Khan,
Wayne State University, United States

REVIEWED BY
Lamia M. El Wakeel,
Ain Shams University, Egypt
Osama Badary,
British University in Egypt, Egypt

*CORRESPONDENCE
Hong Zhu,
zhuhong0719@126.com
Qun Qin,
qinqun8087@hotmail.com

SPECIALTY SECTION
This article was submitted to Pharmacology of Anti-Cancer Drugs, a section of the journal Frontiers in Pharmacology

RECEIVED 22 August 2022
ACCEPTED 13 October 2022
PUBLISHED 28 October 2022

CITATION
Zhu Y, Liu K, Zhu X, Qin Q and Zhu H (2022), Trastuzumab deruxtecan versus chemotherapy for patients with HER2-low advanced breast cancer: A US-based cost-effectiveness analysis. *Front. Pharmacol.* 13:1025243. doi: 10.3389/fphar.2022.1025243

Trastuzumab deruxtecan *versus* chemotherapy for patients with HER2-low advanced breast cancer: A US-based cost-effectiveness analysis

Youwen Zhu[1,2], Kun Liu[1,2], Xiaolu Zhu[1,2], Qun Qin[2,3]* and Hong Zhu[1,2]*

[1]Department of Oncology, Xiangya Hospital, Central South University, Changsha, China, [2]National Clinical Research Center for Geriatric Disorders, Xiangya Hospital, Central South University, Changsha, China, [3]National Institution of Drug Clinical Trial, Xiangya Hospital, Central South University, Changsha, China

Background: In recent years, the rise of antibody–drug conjugates (ADCs) has changed the treatment paradigm for patients with HER2-low advanced breast cancer (ABC). DESTINY-Breast04 (NCT03734029) has demonstrated the antitumor activity of trastuzumab deruxtecan (T-DXd). However, the balance between the efficacy and cost of T-DXd remains undefined. Consequently, there is a great need to assess the cost-effectiveness of T-DXd for patients with HER2-low ABC when compared with chemotherapy.

Methods: A Markov decision-analytic model with a time horizon of 15 years was employed to estimate the costs and clinical efficacy of trials with the administration of T-DXd in contrast to chemotherapy alone as a later-line therapy in a group of patients with hormone receptor-positive (HR+) or negative (HR-) HER2-low ABC. The US payer perspective was taken into account when factors such as medical lifetime expenditure, incremental cost-effectiveness ratios (ICERs), and quality-adjusted life years (QALYs) were calculated. Sensitivity analyses were used to determine the model's stability. A subgroup analysis was also conducted on the HR+/HER2-low cohort.

Results: T-DXd was associated with an improvement of 0.543, 0.558, and 0.789 QALYs when compared with treatment with chemotherapy for overall, HR+, and HR- HER2-low patients, respectively. However, incorporating T-DXd into later-line therapy led to increased costs ($161,406, $177,907, and $155,757), which causes the ICER for T-DXd to be $296,873, $318,944, and $197,355 per QALY. The cost of T-DXd and the patient's weight were the most influential factors for ICER. T-DXd being the dominant strategy is about 1.5%, 0.5%, and 28.0% in overall, HR+, and HR- HER2-low ABC patients, respectively. In addition, the T-DXd regimen was not cost-effective in all subgroups.

Conclusion: Compared with chemotherapy, T-DXd was not cost-effective for patients with HER2-low ABC in the United States. However, it can provide more health benefits to patients with HR+/HER2-low ABC.

KEYWORDS

HER2-low advanced breast cancer, trastuzumab-deruxtecan, cost-effectiveness analysis, quality-adjusted life years, Markov model

Introduction

Breast cancer (BC) is one of the most common diseases and was the fifth most common cause of death across the globe in 2020, with a slightly increased incidence rate (by 0.5% annually) (Siegel et al., 2022; World Health Organization, 2022). In 2020, it is expected that there will be approximately 290,560 new cases diagnosed with BC in the United States, with 43,780 people dying from BC (Siegel et al., 2022). Among the women diagnosed with BC, 80–90% were diagnosed with an HER-2 (human epidermal growth factor receptor 2) negative tumor, which is characterized by a downregulated expression of the *HER2* gene (Slamon et al., 1987; Schettini et al., 2021). In HER2-negative tumors, hormone receptor-positive (HR+) and hormone receptor-negative (HR-) showcase substantial heterogeneity in terms of treatment sensitivity and prognosis, with a 0.8-fold difference in the 5-year relative survival (Burris et al., 2011; Fehrenbacher et al., 2020; Tarantino et al., 2020; National Cancer Institute, 2021; Schettini et al., 2021).

HER2-low expression has been defined as an immunohistochemical (IHC) assay score of 1+, or an IHC score of 2+ and a negative result *in situ* hybridization (ISH) (Fehrenbacher et al., 2020; Tarantino et al., 2020; Schettini et al., 2021). Although the NSABP B-47 (NCT01275677) study evaluated the efficacy of adjuvant chemotherapy with or without the monoclonal antibody trastuzumab in the treatment of subjects with HER2-low BC, the results were not satisfactory (Fehrenbacher et al., 2020). In particular, this study found that the addition of trastuzumab to adjuvant chemotherapy did not improve invasive disease-free survival (hazard ratio [HR], 0.98; 95% confidence interval (CI), 0.76 to 1.25; $p = 0.85$) (Fehrenbacher et al., 2020). For the moment, there is skepticism about the therapeutic prospect for patients with HER2-low because they cannot benefit from the traditional treatment of HER2, and therefore innovative treatment options must be developed.

Trastuzumab deruxtecan (T-DXd) is an ADC conjugated with anti-HER2 humanized monoclonal antibody (mAB) of tumor-associated antigen coupled with topoisomerase I inhibitor (DXd), which are connected by an enzyme-cleavable linker (Doi et al., 2017). With the improvement of T-DXd and its drug pharmaceutical properties, along with the increased bystander effect, clinicians have now turned their attention to T-DXd (Doi et al., 2017). The DESTINY-Breast04 (NCT03734029) phase III trial found that T-DXd treatment for patients with HER2-low ABC significantly improved the median overall survival (mOS, 23.4 *versus* 16.8 months; HR, 0.64; 95% CI, 0.49 to 0.84; $p = 0.001$) and progression-free survival (mPFS, 9.9 *versus* 5.1 months; HR, 0.50; 95% CI, 0.40 to 0.63; $p = 0.003$) when compared to chemotherapy (Modi et al., 2022). Surprisingly, T-DXd further showed significant antitumor activity for patients with HR+ (mOS, 23.9 months; mPFS, 10.1 months) or HR- (mOS, 18.2 months; mPFS, 8.5 months) HER2-low ABC (Modi et al., 2022). Based on these findings, T-DXd was included in the updated Guidelines of the National Comprehensive Cancer Network Clinical Practice (NCCN) as the preferred option for patients with HER2-low, who have received at least one prior line of chemotherapy for metastatic disease or if the tumor is HR+ and refractory to endocrine therapy in 2022(11). Consequently, T-DXd is changing the global landscape in the treatment of HER2-low ABC.

Although the T-DXd treatment is effective and safe for patients with HER2-low ABC, there is still a great need to assess the drug's clinical benefit at a reasonable cost in light of the high price of recently approved novel drugs. Consequently, our investigation aims to evaluate the cost-effectiveness of T-DXd against chemotherapy as a later-line for treating HER2-low ABC and HR status from the economic perspective in the United States.

Materials and methods

Population and treatments

The patient cohort model in this inquiry was adapted from the DESTINY-Breast04 trial and involved 557 patients with HER2-low ABC. The study started on 27 December 2018 and lasted until 31 December 2021 (Modi et al., 2022). Of the 373 (67.0%) patients who were randomly assigned to the T-DXd group and the 184 (33.0%) patients who were assigned to the physician's choice chemotherapy group, 331 (88.7%) and 163 (88.6%), respectively, comprised the HR+ cohort. In addition, the HR- cohort of patients comprised 42 (11.3%) and 21 (11.4%) individuals in the T-DXd and chemotherapy groups, respectively (Modi et al., 2022). The average age of the participants was 55 years, with a body weight of about 74 kg and a body surface area of 1.82 m^2 (Table 1) (Le et al., 2016; Modi et al., 2022). All individuals with HER2-low ABC received at least first-line chemotherapy (Modi et al., 2022). In the T-DXd group, a dose of 5.4 mg T-DXd per kg of body weight was injected directly into the patient's vein once every 3 weeks. Those patients that composed the physician's choice chemotherapy group received anticancer medications such as eribulin (51.1%), capecitabine (20.1%), nab-paclitaxel (10.3%), gemcitabine (10.3%), or paclitaxel (8.2%) (Modi et al., 2022) at doses that complied to the Guidelines of NCCC (National

TABLE 1 Model parameters: baseline values, ranges, and distributions for the sensitivity analysis.

Parameter	Baseline value	Range		References	Distribution
		Minimum	Maximum		
Weibull survival model for OS of chemotherapy					
Overall population	Scale = 0.011708, shape = 1.432,984	—	-	Modi et al. (2022)	-
Population with hormone receptor-positive	Scale = 0.011763, shape = 1.393,105	-	-	Modi et al. (2022)	-
Population with hormone receptor-negative	Scale = 0.050763, shape = 1.129,492	-	-	Modi et al. (2022)	-
Weibull survival model for PFS of chemotherapy					
Overall population	Scale = 0.164,483, shape = 0.903,477	-	-	Modi et al. (2022)	-
Population with hormone receptor-positive	Scale = 0.141,586, shape = 0.945,576	-	-	Modi et al. (2022)	-
Population with hormone receptor-negative	Scale = 0.25686, shape = 0.8906	-	-	Modi et al. (2022)	-
Weibull survival model for OS of trastuzumab deruxtecan					
Overall population	Scale = 0.007249, shape = 1.431,054	-	-	Modi et al. (2022)	-
Population with hormone receptor-positive	Scale = 0.004488, shape = 1.577,038	-	-	Modi et al. (2022)	-
Population with hormone receptor-negative	Scale = 0.026802, shape = 1.097747	-	-	Modi et al. (2022)	-
Weibull survival model for PFS of trastuzumab deruxtecan					
Overall population	Scale = 0.057066, shape = 1.074695	-	-	Modi et al. (2022)	-
Population with hormone receptor-positive	Scale = 0.049346, shape = 1.116,918	-	-	Modi et al. (2022)	-
Population with hormone receptor-negative	Scale = 0.11992, shape = 0.84977	-	-	Modi et al. (2022)	-
Rate of post-discontinuation therapy					
Chemotherapy group	0.081	0.065	0.097	Modi et al. (2022)	Beta
Trastuzumab deruxtecan group	0.162	0.130	0.194	Modi et al. (2022)	Beta
Risk for main AEs in the chemotherapy group					
Risk of neutropenia	0.407	0.326	0.488	Modi et al. (2022)	Beta
Risk of leukopenia	0.192	0.154	0.230	Modi et al. (2022)	Beta
Risk of increased aminotransferase levels	0.081	0.065	0.097	Modi et al. (2022)	Beta
Risk for main AEs in the trastuzumab deruxtecan group					
Risk of neutropenia	0.137	0.110	0.164	Modi et al. (2022)	Beta
Risk of anemia	0.081	0.065	0.097	Modi et al. (2022)	Beta
Risk of fatigue	0.075	0.060	0.090	Modi et al. (2022)	Beta
Risk of leukopenia	0.065	0.052	0.078	Modi et al. (2022)	Beta
Risk of thrombocytopenia	0.051	0.041	0.061	Modi et al. (2022)	Beta
Utility					
Utility PFS	0.700	0.560	0.840	Lloyd et al. (2006); Le et al. (2016)	Beta
Utility PD	0.500	0.400	0.600	Lloyd et al. (2006); Le et al. (2016)	Beta
Disutility					
Neutropenia	0.090	0.072	0.108	Ding et al. (2021)	Beta
Leukopenia	0.090	0.072	0.108	Ding et al. (2021)	Beta
Anemia	0.120	0.096	0.144	Le et al. (2016)	Beta

(Continued on following page)

TABLE 1 (*Continued*) Model parameters: baseline values, ranges, and distributions for the sensitivity analysis.

Parameter	Baseline value	Range		References	Distribution
		Minimum	Maximum		
Thrombocytopenia	0.122	0.098	0.146	Le et al. (2016)	Beta
Fatigue	0.290	0.232	0.348	Liu et al. (2021)	Beta
Increased aminotransferase levels	0.308	0.246	0.370	Wang et al. (2021)	Beta
Drug cost, $/per cycle					
Chemotherapy	7,607	6,086	9,128	CMS (2022)	Gamma
Trastuzumab deruxtecan	20,114	16,091	24,137	CMS (2022)	Gamma
Cost of AEs, $					
Chemotherapy	7,870	6,296	9,444	Le et al. (2016); Wang et al. (2021); Zhu et al. (2021)	Gamma
Trastuzumab deruxtecan	2,585	2,068	3,102	Le et al. (2016); Wang et al. (2021); Zhu et al. (2021)	Gamma
Administration per cycle	352	282	422	Le et al. (2016)	Gamma
Follow-up per cycle	1,980	1,584	2,376	Zhang et al. (2019)	Gamma
Best supportive care per cycle	3,358	2,686	4,029	Wu et al. (2020)	Gamma
Immunohistochemical test per patient	123	98	148	Han et al. (2020)	Gamma
Terminal care per patient	2,844	2,275	3,413	Wang et al. (2021)	Gamma
Weight (kg)	74	59	89	Le et al. (2016)	Normal
Body surface area (meters^2)	1.82	1.46	2.18	Le et al. (2016)	Normal
Discount rate	0.03	0	0.05	Ding et al. (2021)	Uniform

Abbreviation: OS, overall survival; PFS, progression-free survival; PD, disease progressed; AEs, adverse events.

Comprehensive Cancer Network Clinical, 2022). Detailed information on the dosage, method of administration, and price per unit of the drugs are provided in Supplementary Table S2 of Supplementary Material. Tumor measurements were performed every 6 weeks until the progression of the disease or the detection of unacceptable adverse events (AEs). In those two cases, the treatment was replaced with the best supportive care (BSC). In the T-DXd and chemotherapy group, 60 (16.2%) and 14 (8.1%) of the enrolled patients received BSC, respectively (Modi et al., 2022). Finally, every individual who had a treatment-related death received terminal care. This inquiry was guided according to the checklist of the reporting standards regarding the consolidated health economic evaluation (CHEERS) (Supplementary Material Supplementary Table S1).

Model structure and transition probabilities

The three separate health states that established the 6-week cycle of the Markov model were PFS, PD, and death (Supplementary Material Supplementary Figure S1). This model was setup based on the combination of the efficacy of the treatment over time with the estimation of the transition probabilities. The latter was estimated from the DESTINY-Breast04 trial's OS and PFS curves. The time-dependency transition probabilities in each Markov cycle were calculated based on the following formula: $tp(tu) = 1 - \exp\{\lambda(t - u)\gamma - \lambda t\gamma\}$ ($\lambda > 0$, $? > 0$), where u is the Markov cycle and tu represents the arrival at state t after u Markov cycles. Over time, the patient's health status deteriorated and led to mortality—more than 99% of the registered patients had died over the last 15 years. The Kaplan–Meier curves of the two groups were employed to select the points. The latter was combined with two criteria as the estimators of prediction error—that is, the Bayesian information criterion and the Akaike information criterion—to select the Weibull distribution that fitted the T-DXd and chemotherapy groups' survival curve, respectively (Supplementary Material Supplementary Figure S2 and Supplementary eTable S4). Concerning the results from another study, we applied the Kaplan–Meier curves, while the shape and scale parameters for γ and λ distributions were calculated, respectively (Ding et al., 2021) (Table 1). The model was built with the TreeAge Software (TreeAge Pro 2021®, available at: https://www.treeage.com). The points were selected with the GetData Graph Digitizer (version 2.26, available at: http://www.getdata-graph-digitizer.com/index.php). R software (version 4.1.1, available at: http://www.rproject.org) was applied in the statistical data evaluation.

The model's primary outcome was to calculate the overall costs, life years (LYs), quality-adjusted life years (QALYs), and incremental cost-effectiveness ratio (ICER). Based on published research, we determined the maximum price that the US payer is ready to pay for the corresponding therapy—in other words, the threshold of willingness-to-pay (WTP), which was $150,000/QALY (Ding et al., 2021). An annual discount rate of 3% on future medical costs and healthcare benefits was additionally implemented (Ding et al., 2021).

Utility and cost

Health utility preference on a scale of 0 (death) to 1 (perfect health) was used in our analysis to reflect a particular health state, including PFS state, PD state, and death state. Because there were no reports regarding the health utility in the conducted clinical trials, the average health utility for PFS and disease progression statuses were assumed to be 0.70 and 0.50, respectively, which were taken from the published articles (Lloyd et al., 2006; Le et al., 2016). We have also corrected the mean health utility *via* the disutility values due to grade 3/4 AEs (Le et al., 2016; Ding et al., 2021; Liu et al., 2021; Wang et al., 2021) (Table 1).

We only examined direct expenditures, such as drugs, administration, IHC tests, follow-up patient, BSC, terminal care, and AEs (only included those with an incidence of grade 3/4 AEs in ≥5% of the cases) (Table 1). The prices of the drugs that were used were obtained from the official website for drug research (CMS, 2022). The remaining costs were derived come from published literature (Le et al., 2016; Wan et al., 2019; Zhang et al., 2019; Han et al., 2020; Wu et al., 2020; Liu et al., 2021; Wang et al., 2021; Zhu et al., 2021) (Table 1). According to the changes in prices paid by US consumers, the healthcare-related costs have been adjusted to the inflation rate in the United States for 2022 (US Bureau of Labor Statistics, 2022).

Sensitivity analysis

The robustness of our conclusions was evaluated by a series of sensitivity analyses. We examined the value variation of 78 parameters in the employed model (ranging from −20% to 20%) to study the impact of examining individuals during a one-way sensitivity analysis on ICERs (Ding et al., 2021). To understand the employed model, 10000 Monte Carlo simulations were executed during the analysis of probability distribution. Every simulation randomly sampled the input model for the distribution. We have also taken the cost-effectiveness of the subgroup of patients with HR+/HER2-low ABC into consideration. Without reporting the survival curves of each group, the PFS curves of the T-DXd group were reconstructed from the overall PFS curves of the chemotherapy group and HR of each subgroup, as suggested by Ding et al. (2021).

Results

Cost-effectiveness results

T-DXd produced 1.869, 1.994, and 1.684 QALYs (3.275, 3.484, and 2.988 LYs) and chemotherapy gained 1.326, 1.436, and 0.895 QALYs (2.393, 2.598, and 1.626 LYs) for overall, HR+, and HR- HER2-low ABC patients, respectively. The cost of standard chemotherapy was calculated to be $119,970, $127,255, and $76,584, whereas for the T-DXd therapy it was estimated as $281,376, $305,162, and $232,341, respectively, for the aforementioned groups. For the T-DXd group, the ICERs cost was $296,873, $318,944, and $197,355 per QALY. Consequently, our results demonstrate that T-DXd was not the best strategy as a later-line therapy for both groups of patients with overall, HR+ and HR- HER2-low ABC in the US medical space, as illustrated in Table 2.

Sensitivity analyses

The one-way sensitivity analysis revealed that the costs of T-DXd (varying from $16,091 to $24,137 each cycle, with the ICER ranging from $217,191/QALY to $376,576/QALY, $234,608/QALY to $403,302/QALY, and $152,336/QALY to $242,385/QALY in overall, HR+, and HR- HER2-low ABC patients, respectively), body weight (varying from 59 kg to 89 kg, with the ICER ranging from $223,519/QALY to $370,227/QALY, $241,113/QALY to $396,774/QALY, and $154,971/QALY to $239,739/QALY in overall, HR+, and HR- HER2-low ABC patients, respectively), the costs of chemotherapy, the costs of AEs in chemotherapy, and the utility of PFS had a significant impact on the model (Figure 1). In addition, the cost of the IHC test and the cost of terminal care had a small impact on the model.

The probability sensitivity analysis using the cost-effectiveness acceptability curve (Figure 2) and scatter plot (Supplementary Figure S3) revealed that the probability of T-DXd being the dominant strategy is about 1.5%, 0.5%, and 28.0% in overall, HR+, and HR- HER2-low ABC patients, respectively, at the WTP of 150,000/QALY. Furthermore, we found that the benefits at the relevant price of T-DXd treatment changed with the fluctuation of WTP. For example, on the occasion of a two times rise in the threshold of the WTP, namely, 300 000$ per QALY, the T-DXd had a 50% probability to be cost-effective when compared with chemotherapy.

TABLE 2 Cost-effectiveness results.

Treatment	Total cost $	LYs	ICER $/LY[a]	QALYs	ICER $/QALY[b]
Overall population					
Chemotherapy	119,970	2.393	NA	1.326	NA
T-DXd	281,376	3.275	182,944	1.869	296,873
Population with hormone receptor-positive					
Chemotherapy	127,255	2.598	NA	1.436	NA
T-DXd	305,162	3.484	200,796	1.994	318,944
Population with hormone receptor-negative					
Chemotherapy	76,584	1.626	NA	0.895	NA
T-DXd	232,341	2.988	114,300	1.684	197,355

[a]Compared to chemotherapy ($/LY).
[b]Compared to chemotherapy ($/QALY).
Abbreviation: ICER, incremental cost-effectiveness ratio; LY, life year; QALY, quality-adjusted life year.

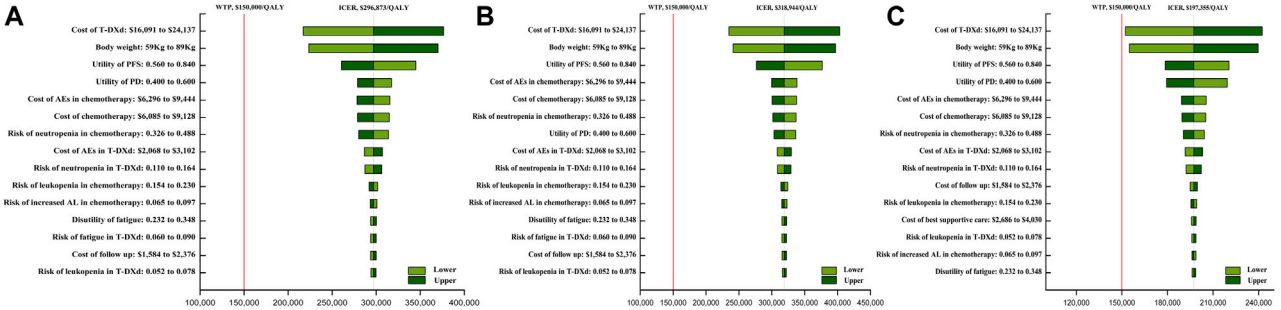

FIGURE 1
One-way sensitivity analyses of trastuzumab deruxtecan (T-DXd) strategy compared to chemotherapy strategy in the overall population **(A)**, population with hormone receptor-positive **(B)**, and population with hormone receptor-negative **(C)**. Abbreviation: ICER, incremental cost-effectiveness ratio; QALY, quality-adjusted life year; T-DXd, trastuzumab deruxtecan; AEs, adverse events; PFS, progression-free survival; PD, disease progressed; BSC, best supportive care; AL, aminotransferase levels.

Interestingly, the T-DXd treatment proved beneficial in decreasing the chance of death in most subgroups. Moreover, the ICERs of the -DXd *vs.* chemotherapy ranged from $193,455/QALY to $486,154/QALY. The probability sensitivity analysis indicated that T-DXd was cost-effective with probabilities ranging between 0% and 35.5% (Supplementary eTable S3).

Discussion

BC has become one of the highest-priced malignant tumors worldwide (Sullivan et al., 2011). The cost of treating women with ABC reached 75.4 billion US dollars in 2020 and has since increased by 4.3%. This puts BC into the category of cancers with the largest increase in healthcare costs (Tartari et al., 2017; Gogate et al., 2021). Currently, patients with HER2-low ABC have limited treatment options after progression during primary therapy. Among them, the available targeted therapies appeared costly with less successful clinical outcomes for these patients (Burris et al., 2011; Cortes et al., 2011; Kaufman et al., 2015; Fehrenbacher et al., 2020; Cook et al., 2021). The development of T-DXd novel drugs has shown great potential in the field of HER2-low expression and has attracted widespread attention. Subsequently, the analysis of the cost-effectiveness of T-DXd has proven to be necessary when the clinical practice guidelines suggest its broad application.

To date, there is no evidence on the assessment of the cost-efficacy of T-DXd in treating subjects with HER2-low BC diagnosis. Only a few studies have been published discussing the cost-effectiveness of trastuzumab emtansin (T-DM1), mostly for the therapeutic purposes of individuals struggling with HER2-positive ABC. Several reports have

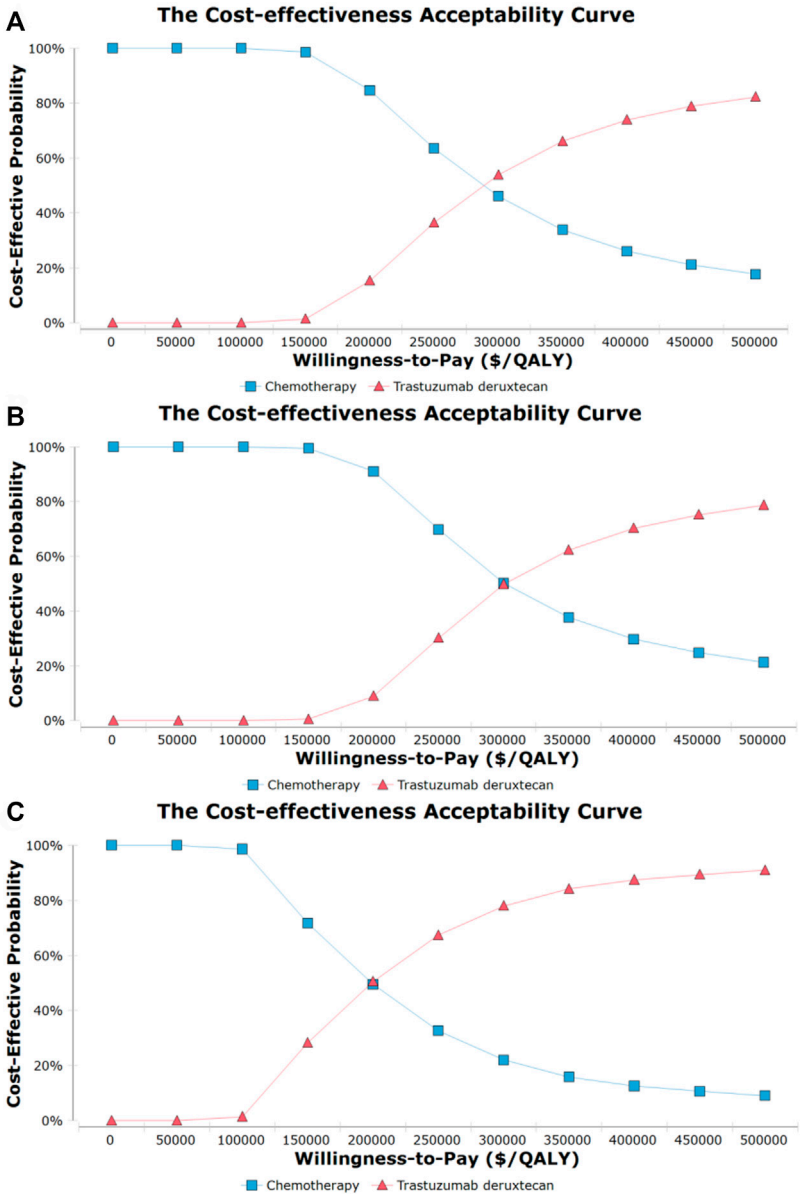

FIGURE 2
Cost-effectiveness acceptability curves for trastuzumab deruxtecan (T-DXd) strategy compared to chemotherapy strategy in the overall population **(A)**, population with hormone receptor-positive **(B)**, and population with hormone receptor-negative **(C)**. Abbreviation: QALY, quality-adjusted life year.

evaluated T-DM1 as a second-approach therapy in contrast with combined chemotherapy from a payer's viewpoint in countries such as the United States, China, United Kingdom, and Spain. These studies reached a consensus that T-DM1 was not a beneficial strategy for the treatment of HER-low BC at a relevant price, probably due to the high price of ADCs (Miranda Romero and Marín Gil, 2015; Le et al., 2016; Squires et al., 2016; Zhang et al., 2021). However, one report confirmed the greater cost-effectiveness of T-DM1 in comparison with chemotherapy alone in the United States (Le et al., 2016). These studies shed light on the possible differences in the cost-effectiveness of ADCs retrieved from the analyses for different payers with the same treatment regimen. The reason for these differences may be that local affordability and market assessment programs differ. Therefore, when an approved drug is widely used in clinical practice, it is equally important for its cost-effectiveness to be proven in different regions.

To our knowledge, this study is the first to build a 15-year Markov model as an instrument to contrast the cost-effectiveness of T-DXd with chemotherapy as later-line treatment for patients with HER2-low ABC from a US payer's perspective. Our study shows that the employment of T-DXd in comparison with physician's choice chemotherapy produced 0.543 QALYs that increased by $161,406, thus leading to an ICER of $296,873/QALY, which was significantly higher than the WTP standard of $150,000/QALY in the United States. The additional costs associated with T-DXd mainly represented the drug price. Therefore, T-DXd was not a dominant strategy from the point of view of US payers. This means that the high prices of innovative drugs widely used in clinical practice are the main problem. Further analysis has shown that T-DXd cost had a pivotal role in the one-sensitivity analysis. T-DXd therapy was considered to be a cost-effective strategy in the case of a more than 40% decrease in the T-DXd price or in the case of a more than 2.5 times increase in the price of chemotherapy. Therefore, considerable price adjustments are required to enable a wider range of acceptable ICERs. Although the cost for specific indications has the potential to maximize the revenue and decrease the buyer's excess benefit, there is an agreement among researchers that the prices of medicines and their potential medical usefulness seem to have no or little correlation to each other (Mailankody and Prasad, 2015; Chandra and Garthwaite, 2017). Subsequently, it is necessary to overcome the administrative challenges in the United States by linking the costs and efficacy of the drugs, and encouraging the development of therapies with high impact. Body weight was another important factor in our study. Surprisingly, the cost-effectiveness of T-DXd was low at the WTP inception at 150 000$/QALY for patients weighing more than 43 kg. Nevertheless, most of the enrolled patients weighed more than 40 kg (Darnis et al., 2012; da Silva et al., 2017), which raised an ethical issue of debiting emaciated individuals less for the same amount of money for a life-prolonging procedure. The potential reasons for this might be the adjustment of the T-DXd dose to the patient's body weight and the number of disposable vials rather than the administered dose when the drug cost was calculated. Heavier patients required more T-DXd, which increased the financial burden. Our recommendation in this case is to arrange the patient's medication bottles on the same day. However, there are some safety concerns about sharing the vials and the US Centers for Disease Control and Prevention claim that each patient should use their vial for single usage (Centers for Disease Control and Prevention, 2022).

Our findings from the executed analysis demonstrate a lack of price-efficacy of the T-DXd in patients with HR+ or HR- HER2-low ABC, with detected ICERs of about $318,944/QALY and $197,355/QALY, respectively. Even though it was not cost-effective, T-DXd provided greater health benefits for patients with HR+/HER2-low ABC. This is consistent with the findings of several previously published studies (Gampenrieder et al., 2021; Horisawa et al., 2022). A recent retrospective study involved 4,977 Japanese patients for comparison of the prognosis of BC disease concerning the HR status among patients with HER2-low BC (Horisawa et al., 2022). The authors found that the HR-/HER2-low cases had a worse prognosis than the HR+/HER2-low cases, with 5-year OS (96.7% and 86.5%, respectively) and 5-year PFS (91.6% and 78.7%, respectively). Another retrospective study that included 1,973 Austrian patients showed that individuals struggling with HR+/HER2-low and HR-/HER2-low metastatic BC had higher 5-year OS (11% and 33%, respectively) and 5-year PFS (37% and 6%, respectively) (Gampenrieder et al., 2021). Due to the high cost of new HER2-ADC drugs, therapeutic strategies for treating patients with HER2-low breast cancer should be considered in the context of HR status in the context of cost-effectiveness and optimal choice, and early testing of such prognostic factors is critical.

As with most cost-effectiveness analyses, our study has observed some limitations. First, we acknowledge that phase III DESTINY-Breast04 is the only trial that randomly compares T-DXd cost-effectiveness with chemotherapy in individuals struggling with HER2-low ABC. This trial is characterized by its large scale and proper plan, However, the model depends on the trial results, which means that any bias in the test will have a serious impact on the outcome of this study. Second, the extended benefit of T-DXd in the current model was inferred from the data retrieved of the Destiny-BREAST04 trial, which was exposed to ambiguity. To assess the ambiguity, we performed a series of sensitivity and subgroup analyses. However, the prolonged benefits of T-DXd remained unclear. Therefore, more data are needed to validate the model *versus* the prolonged survival data. Third, due to the shortage of subgroup survival data and curves for HR+/HER2-low, as well as the reduction of the strength of the results because of the small size of the samples, we have carefully interpreted the results of the subsection analysis. Fourth, due to sparse data on utility values, we have used such values from the published literature. While this estimate cannot be regarded as ideal, we have executed analyses that included utility value variability. Finally, we adjusted the mean health utility using disutility values of AEs but we have only considered disutility with an incidence of grade 3 or higher AEs in ≥5%, which led to the overstatement or understatement of the utility values. However, the conducted analysis showcased the small influence of the disutility of AEs on economic outcomes.

Conclusion

This study has revealed that the widespread use of innovative drugs requires the drug price and drug dosage to be balanced for the most cost-effective treatment to be obtained. From a US payer's perspective, our study showed

that T-DXd was not cost-effective for patients with HER2-low ABC. Furthermore, we have provided evidence that the HR status should be taken into consideration in the price-efficacy evaluation because T-DXd provides additional health benefits for patients with HR+/HER-low ABC.

Data availability statement

The original contributions presented in the study are included in the article/Supplementary Material; further inquiries can be directed to the corresponding author.

Author contributions

YZ, KL, XZ, and HZ designed the experiment. YZ, KL, and XZ performed the experiments. YZ and KL analyzed the data. HZ contributed analysis tools. YZ, KL, XZ, QQ, and HZ wrote the manuscript. HZ and QQ are co-corresponding author. All authors have read and approved the manuscript.

Funding

This work was partly supported by the Clinical Research Project of Xiangya Hospital (grant number, 2016L06 to HZ).

Acknowledgments

We thank HZ for providing us with the analysis tools and funding.

Conflict of interest

The authors declare that the research was conducted in the absence of any commercial or financial relationships that could be construed as a potential conflict of interest.

Publisher's note

All claims expressed in this article are solely those of the authors and do not necessarily represent those of their affiliated organizations, or those of the publisher, the editors, and the reviewers. Any product that may be evaluated in this article, or claim that may be made by its manufacturer, is not guaranteed or endorsed by the publisher.

Supplementary material

The Supplementary Material for this article can be found online at: https://www.frontiersin.org/articles/10.3389/fphar.2022.1025243/full#supplementary-material

References

Burris, H. A., 3rd, Rugo, H. S., Vukelja, S. J., Vogel, C. L., Borson, R. A., Limentani, S., et al. (2011). Phase II study of the antibody drug conjugate trastuzumab-DM1 for the treatment of human epidermal growth factor receptor 2 (HER2)-positive breast cancer after prior HER2-directed therapy. *J. Clin. Oncol.* 29 (4), 398–405. doi:10.1200/JCO.2010.29.5865

Centers for Disease Control and Prevention (2022). *Protect patients against preventable harm from improper use of single-dose/single-use vials*. Available at: https://www.cdc.gov/injectionsafety/CDCposition-SingleUseVial.html.

Chandra, A., and Garthwaite, C. (2017). The economics of indication-based drug pricing. *N. Engl. J. Med.* 377 (2), 103–106. doi:10.1056/NEJMp1705035

Cms (2022). *The Centers for medicare & medicaid services*. United States: CMS. Available at: https://www.cms.gov/medicare/medicare-part-b-drug-average-sales-price/2022-asp-drug-pricing-files (Accessed July, 2022).

Cook, M. M., Al Rabadi, L., Kaempf, A. J., Saraceni, M. M., Savin, M. A., and Mitri, Z. I. (2021). Everolimus plus exemestane treatment in patients with metastatic hormone receptor-positive breast cancer previously treated with CDK4/6 inhibitor therapy. *Oncologist* 26 (2), 101–106. doi:10.1002/onco.13609

Cortes, J., O'Shaughnessy, J., Loesch, D., Blum, J. L., Vahdat, L. T., Petrakova, K., et al. (2011). Eribulin monotherapy versus treatment of physician's choice in patients with metastatic breast cancer (EMBRACE): A phase 3 open-label randomised study. *Lancet* 377 (9769), 914–923. doi:10.1016/S0140-6736(11)60070-6

da Silva, B. R., Mialich, M. S., de Paula, F. J. A., and Jordao, A. A. (2017). Comparison of new adiposity indices for the prediction of body fat in hospitalized patients. *Nutrition* 42, 99–105. doi:10.1016/j.nut.2017.04.008

Darnis, S., Fareau, N., Corallo, C. E., Poole, S., Dooley, M. J., and Cheng, A. C. (2012). Estimation of body weight in hospitalized patients. *Qjm* 105 (8), 769–774. doi:10.1093/qjmed/hcs060

Ding, D., Hu, H., Li, S., Zhu, Y., Shi, Y., Liao, M., et al. (2021). Cost-effectiveness analysis of durvalumab plus chemotherapy in the first-line treatment of extensive-stage small cell lung cancer. *J. Natl. Compr. Canc. Netw.* 19, 1141–1147. doi:10.6004/jnccn.2020.7796

Doi, T., Shitara, K., Naito, Y., Shimomura, A., Fujiwara, Y., Yonemori, K., et al. (2017). Safety, pharmacokinetics, and antitumour activity of trastuzumab deruxtecan (DS-8201), a HER2-targeting antibody-drug conjugate, in patients with advanced breast and gastric or gastro-oesophageal tumours: A phase 1 dose-escalation study. *Lancet. Oncol.* 18 (11), 1512–1522. doi:10.1016/S1470-2045(17)30604-6

Fehrenbacher, L., Cecchini, R. S., Geyer, C. E., Jr., Rastogi, P., Costantino, J. P., Atkins, J. N., et al. (2020). NSABP B-47/NRG oncology phase III randomized trial comparing adjuvant chemotherapy with or without trastuzumab in high-risk invasive breast cancer negative for HER2 by FISH and with IHC 1+ or 2. *J. Clin. Oncol.* 38 (5), 444–453. doi:10.1200/JCO.19.01455

Gampenrieder, S. P., Rinnerthaler, G., Tinchon, C., Petzer, A., Balic, M., Heibl, S., et al. (2021). Landscape of HER2-low metastatic breast cancer (MBC): Results from the Austrian AGMT_MBC-Registry. *Breast Cancer Res.* 23 (1), 112. doi:10.1186/s13058-021-01492-x

Gogate, A., Wheeler, S. B., Reeder-Hayes, K. E., Ekwueme, D. U., Fairley, T. L., Drier, S., et al. (2021). Projecting the prevalence and costs of metastatic breast cancer from 2015 through 2030. *JNCI Cancer Spectr.* 5 (4), 1. doi:10.1093/jncics/pkab063

Han, J., Tian, K., Yang, J., and Gong, Y. (2020). Durvalumab vs placebo consolidation therapy after chemoradiotherapy in stage III non-small-cell lung cancer: An updated PACIFIC trial-based cost-effectiveness analysis. *Lung Cancer* 146, 42–49. doi:10.1016/j.lungcan.2020.05.011

Horisawa, N., Adachi, Y., Takatsuka, D., Nozawa, K., Endo, Y., Ozaki, Y., et al. (2022). The frequency of low HER2 expression in breast cancer and a comparison of prognosis between patients with HER2-low and HER2-negative breast cancer by HR status. *Breast Cancer* 29 (2), 234–241. doi:10.1007/s12282-021-01303-3

Kaufman, P. A., Awada, A., Twelves, C., Yelle, L., Perez, E. A., Velikova, G., et al. (2015). Phase III open-label randomized study of eribulin mesylate versus capecitabine in patients with locally advanced or metastatic breast cancer previously treated with an anthracycline and a taxane. *J. Clin. Oncol.* 33 (6), 594–601. doi:10.1200/JCO.2013.52.4892

Le, Q. A., Bae, Y. H., and Kang, J. H. (2016). Cost-effectiveness analysis of trastuzumab emtansine (T-DM1) in human epidermal growth factor receptor 2 (HER2): Positive advanced breast cancer. *Breast Cancer Res. Treat.* 159 (3), 565–573. doi:10.1007/s10549-016-3958-x

Liu, Q., Luo, X., Yi, L., Zeng, X., and Tan, C. (2021). First-line chemo-immunotherapy for extensive-stage small-cell lung cancer: A United States-based cost-effectiveness analysis. *Front. Oncol.* 11, 699781. doi:10.3389/fonc.2021.699781

Lloyd, A., Nafees, B., Narewska, J., Dewilde, S., and Watkins, J. (2006). Health state utilities for metastatic breast cancer. *Br. J. Cancer* 95 (6), 683–690. doi:10.1038/sj.bjc.6603326

Mailankody, S., and Prasad, V. (2015). Five years of cancer drug approvals: Innovation, efficacy, and costs. *JAMA Oncol.* 1 (4), 539–540. doi:10.1001/jamaoncol.2015.0373

Miranda Romero, P., and Marín Gil, R. (2015). Trastuzumab emtansine in locally advanced or metastatic HER2 positive breast cancer; GENESIS-SEFH drug evaluation report. *Farm. Hosp.* 39 (3), 171–175. doi:10.7399/fh.2015.39.3.8912

Modi, S., Jacot, W., Yamashita, T., Sohn, J., Vidal, M., Tokunaga, E., et al. (2022). Trastuzumab deruxtecan in previously treated HER2-low advanced breast cancer. *N. Engl. J. Med.* 387 (1), 9–20. doi:10.1056/NEJMoa2203690

National Cancer Institute (2021). *Surveillance, epidemiology, and end results program. Cancer stat facts: Female breast cancer*. Available at: https://seer.cancer.gov/statfacts/html/breast.html (Accessed July, 2021).

National comprehensive cancer Network clinical practice guidelines in oncology (NCCN Guidelines®): Breast cancer, Version 4.2022. Available at: https://www.nccn.org/professionals/physician_gls/pdf/breast.pdf. (Accessed June, 2022).

Schettini, F., Chic, N., Brasó-Maristany, F., Paré, L., Pascual, T., Conte, B., et al. (2021). Clinical, pathological, and PAM50 gene expression features of HER2-low breast cancer. *NPJ Breast Cancer* 7 (1), 1. doi:10.1038/s41523-020-00208-2

Siegel, R. L., Miller, K. D., Fuchs, H. E., and Jemal, A. (2022). Cancer statistics, 2016. *Ca. Cancer J. Clin.* 72 (1), 7–30. doi:10.3322/caac.21332

Slamon, D. J., Clark, G. M., Wong, S. G., Levin, W. J., Ullrich, A., and McGuire, W. L. (1987). Human breast cancer: Correlation of relapse and survival with amplification of the HER-2/neu oncogene. *Science* 235 (4785), 177–182. doi:10.1126/science.3798106

Squires, H., Stevenson, M., Simpson, E., Harvey, R., and Stevens, J. (2016). Trastuzumab emtansine for treating HER2-positive, unresectable, locally advanced or metastatic breast cancer after treatment with trastuzumab and a taxane: An evidence review group perspective of a NICE single technology appraisal. *Pharmacoeconomics* 34 (7), 673–680. doi:10.1007/s40273-016-0386-z

Sullivan, R., Peppercorn, J., Sikora, K., Zalcberg, J., Meropol, N. J., Amir, E., et al. (2011). Delivering affordable cancer care in high-income countries. *Lancet. Oncol.* 12 (10), 933–980. doi:10.1016/S1470-2045(11)70141-3

Tarantino, P., Hamilton, E., Tolaney, S. M., Cortes, J., Morganti, S., Ferraro, E., et al. (2020). HER2-Low breast cancer: Pathological and clinical landscape. *J. Clin. Oncol.* 38 (17), 1951–1962. doi:10.1200/JCO.19.02488

Tartari, F., Santoni, M., Pistelli, M., and Berardi, R. (2017). Healthcare cost of HER2-positive and negative breast tumors in the United States (2012-2035). *Cancer Treat. Rev.* 60, 12–17. doi:10.1016/j.ctrv.2017.08.005

Us Bureau of Labor Statistics (2022). *CPI inflation calculator*. Available at: https://www.bls.gov/data/inflation_calculator.htm (Accessed June, 2022).

Wan, X., Zhang, Y., Tan, C., Zeng, X., and Peng, L. (2019). First-line nivolumab plus ipilimumab vs sunitinib for metastatic renal cell carcinoma: A cost-effectiveness analysis. *JAMA Oncol.* 5 (4), 491–496. doi:10.1001/jamaoncol.2018.7086

Wang, Y., Rui, M., Guan, X., Cao, Y., and Chen, P. (2021). Cost-effectiveness analysis of abemaciclib plus fulvestrant in the second-line treatment of women with hr+/HER2- advanced or metastatic breast cancer: A us payer perspective. *Front. Med.* 8, 658747. doi:10.3389/fmed.2021.658747

World Health Organization (2022). *Breast cancer*. France: WHO. Available at: https://gco.iarc.fr/today/data/factsheets/cancers/20-Breast-fact-sheet.pdf (Accessed March, 2022).

Wu, Q., Liao, W., Zhang, M., Huang, J., Zhang, P., and Li, Q. (2020). Cost-effectiveness of tucatinib in human epidermal growth factor receptor 2-positive metastatic breast cancer from the US and Chinese perspectives. *Front. Oncol.* 10, 1336. doi:10.3389/fonc.2020.01336

Zhang, H., Zhang, Y., Huang, C., and Wang, J. (2021). Cost-effectiveness analysis of trastuzumab emtansine as second-line therapy for HER2-positive breast cancer in China. *Clin. Drug Investig.* 41 (6), 569–577. doi:10.1007/s40261-021-01035-4

Zhang, Y., Zeng, X., Deng, H., Ma, F., Peng, Y., Yi, L., et al. (2019). Cost-effectiveness analysis of adding palbociclib as a second-line endocrine therapy for HR(+)/HER2(-) metastatic breast cancer from the US and Chinese perspectives. *Clin. Ther.* 41 (6), 1175–1185. doi:10.1016/j.clinthera.2019.04.033

Zhu, Y., Hu, H., Ding, D., Li, S., Liao, M., Shi, Y., et al. (2021). First-line pembrolizumab plus chemotherapy for extensive-stage small-cell lung cancer: A United States-based cost-effectiveness analysis. *Cost. Eff. Resour. Alloc.* 19 (1), 77. doi:10.1186/s12962-021-00329-w

frontiers | Frontiers in Pharmacology

TYPE Original Research
PUBLISHED 25 November 2022
DOI 10.3389/fphar.2022.1039376

OPEN ACCESS

EDITED BY
Khuloud Bajbouj,
University of Sharjah, United Arab Emirates

REVIEWED BY
Deniz Cansen Kahraman,
Middle East Technical University, Turkey
Alaaeldin Ahmed Hamza,
National Organization for Drug Control and Research (NODCAR), Egypt

*CORRESPONDENCE
Hong-Zin Lee,
hong@mail.cmu.edu.tw

†These authors have contributed equally to this work

SPECIALTY SECTION
This article was submitted to Pharmacology of Anti-Cancer Drugs, a section of the journal Frontiers in Pharmacology

RECEIVED 08 September 2022
ACCEPTED 17 November 2022
PUBLISHED 25 November 2022

CITATION
Lee K-T, Chen L-Y, Li W-S and Lee H-Z (2022), Transcriptome analysis revealed the role of mTOR and MAPK signaling pathways in the white strain of *Hypsizygus marmoreus* extracts-induced cell death of human hepatoma Hep3B cells.
Front. Pharmacol. 13:1039376.
doi: 10.3389/fphar.2022.1039376

Transcriptome analysis revealed the role of mTOR and MAPK signaling pathways in the white strain of *Hypsizygus marmoreus* extracts-induced cell death of human hepatoma Hep3B cells

Kun-Tsung Lee[1,2†], Li-Yun Chen[3†], Wei-Sung Li[4†] and Hong-Zin Lee[3*]

[1]Department of Oral Hygiene, College of Dental Medicine, Kaohsiung Medical University, Kaohsiung, Taiwan, [2]Department of Dentistry, Kaohsiung Medical University Hospital, Kaohsiung Medical University, Kaohsiung, Taiwan, [3]School of Pharmacy, China Medical University, Taichung, Taiwan, [4]Plant Pathology Division, Taiwan Agricultural Research Institute, Council of Agriculture, Executive Yuan, Taichung, Taiwan

The aim of this study was to investigate the anticancer mechanisms of white genius mushroom (WGM). WGM is a popular edible mushroom in Taiwan and has been demonstrated to mediate potent antiproliferation effects against human Hep3B liver cancer cells in our previous study. According to next generation sequencing technology and KEGG pathway enrichment analysis, mTOR and MAPK signaling pathways were markedly changed during treatment with WGM extracts in Hep3B cells. Therefore, this study examined the effects of WGM extracts on the expression of mTOR and MAPK signaling pathway-related proteins, such as PI3K, Akt, mTOR, Ras, Raf, MEK, ERK, p38 and JNK in Hep3B cells. According to the results of immunoblotting, we demonstrated that the protein expression of the members of PI3K/Akt/mTOR and MAPK signaling pathways were involved in WGM extracts-induced cell death. Furthermore, the inhibitors of PI3K/Akt/mTOR and MAPK signaling pathways such as rapamycin, MK2206, LY3214996 and SB202190, blocked the induction of cell death and vacuoles formation induced by WGM extracts. This study also demonstrated that WGM extracts is able to inhibit Hep3B cell migration and colony formation in a dose-dependent manner. In addition to being a very popular food, WGM should be a pharmacologically safe natural agent for cancer treatment. Therefore, WGM might be designed to develop into a dietary chemopreventive agent for the cancer treatment.

KEYWORDS

***Hypsizygus marmoreus*, white genius mushroom, human Hep3B liver cancer cells, next generation sequencing technology, mTOR signaling pathway, MAPK signaling pathway, migration, cancer chemopreventive agent**

Introduction

Cancer is a major public health concern and the leading cause of death in Taiwan. According to the report provided by the Ministry of Health and Welfare in Taiwan, liver cancer is always the second leading cause of cancer death for the past 20 years. Drug resistance continues to be the principal reason for achieving cures in patients with liver cancer. In recent years, an advent of cancer cells develop resistance to anticancer drugs has led researchers to expedite and put in more effort in the development of new and more effective anticancer drugs. Cancer chemoprevention is defined as the use of food supplements or synthetic compounds to suppress, prevent or delay cancer development and progression. Natural products, such as fruits and vegetables, were also receiving renewed attention as the discovery of cancer chemopreventive agents. For prevention the development of the liver cancer by blocking the initiation stage of tumorigenesis, the development of an effective cancer chemopreventive agent derived from the daily intake of food is urgently needed.

Mushrooms have been shown to have numerous biological activities including anticancer activity, antimicrobial effect and immunomodulating effects (Bao and You, 2011; Kim et al., 2011; Kwak et al., 2015). Based on the consideration of anticancer activity and immune-promoting effect, mushrooms are people's favourite food. Anticancer activity of mushrooms against human cancer cells, such as breast, prostate and colorectal cancer cells, involves apoptosis, cell cycle arrest and inhibition of cell proliferation (Hu et al., 2002; Stanley et al., 2005; Hsu et al., 2008). Transcriptome profiling is an effective tool in large-scale investigation of gene expression patterns in distinct cellular states. Next generation sequencing (NGS) refers to massive scale RNA sequencing technology that allows investigation of a transcriptome profiling. Therefore, NGS has been widely used in the detection of changes in gene expression in different groups or treatments. KEGG (Kyoto Encyclopedia of Genes and Genomes) is a collection of databases dealing with metabolism, genetic information processing, environmental information processing, cellular processes, organismal systems, human diseases and drug development (Kanehisa and Goto, 2000). KEGG pathway enrichment facilitates to determine the differential expressed genes involved in the most important signal transduction pathways and metabolic pathways.

Phosphatidylinositol 3-kinase (PI3K)/Akt/mammalian target of rapamycin (mTOR) signaling is one of the most important intracellular signaling pathways that is related to cell proliferation, motility, survival and apoptosis of cancer cells (Katso et al., 2001; Engelman et al., 2006). Many reports have indicated that inhibition of PI3K/Akt/mTOR signaling pathway triggers apoptosis and inhibits the proliferation of tumor cells, which have elevated Akt levels (Hennessy et al., 2005; Mandal et al., 2005). Activation of the PI3K/Akt/mTOR pathway leads to tumor development and anticancer drugs resistance (Hennessy et al., 2005; Martini et al., 2014). The Ras/Raf/ERK signaling and PI3K/Akt signaling pathway are highly interconnected (Castellano and Downward, 2011). MAPK (mitogen-activated protein kinase) cascades plays a key role in the cellular response to extracellular stimuli (Raingeaud et al., 1995; Liu et al., 1996). MAPK signaling pathway has been found to be involved in the proliferation, differentiation and apoptosis of human cancers (You et al., 2011; Guo et al., 2016). Three well-defined subgroups of mammalian MAPKs are extracellular signal-regulated kinase (ERK1/2), jun N-terminal kinase/stress activated protein kinase (JNK/SAPK) and p38. Among all MAPK signal transduction pathways, the Ras/Raf/ERK signaling pathway is the most important signaling cascade and plays an important role in the proliferation and migration of tumor cells (Roberts and Der, 2007; Sun et al., 2015). It has been reported that inhibition of ERK signaling pathway can result in both decreased cellular proliferation and increased cellular death (Liu et al., 2018; Li et al., 2020).

White genius mushroom (WGM) is white strain of *H. marmoreus* and is one of the most important edible mushrooms in Taiwan. In our previous study, we have identified the cytotoxicity of white genius mushroom extracts on Hep3B cells which is partially dependent on the production of ROS in Hep3B cells (Li et al., 2022). In order to get a better understanding of the underlying mechanisms of WGM extracts-produced anticancer activity of Hep3B cells, the differential expressed genes and pathways involved in the WGM extracts-induced cell death of Hep3B cells were identified using the NGS technology and KEGG tool. According to the KEGG pathway enrichment analysis, autophagy, mitophagy and apoptosis pathways were markedly changed by WGM extracts in human Hep3B liver cancer cells (Li et al., 2022). Although WGM extracts were found to have anticancer activities, the exact mechanism of the anticancer effect of WGM extracts is substantially unknown. In this study, WGM extracts was examined for its anticancer activities and exact mechanisms in hepatocellular carcinoma Hep3B cells, and expected to develop into a dietary chemopreventive agent in the future.

Materials and methods

Materials

Chloroquine, MK2206, rapamycin and Temuterkib (LY3214996) were from MedChemExpress (Monmouth Junction, NJ, United States). SB202190 was purchased from Calbiochem (San Diego, CA, United States). Antibodies to various proteins were obtained from the following sources: β-Actin, Akt, Aktp (S473), JNKp(Thr183/Tyr185), MEK, p38p

(Thr180/Tyr182), PI3K, Ras and mTOR were purchased from GeneTex Inc. (Irvine, CA, United States). ERK, p38 and Raf were purchased from BD Biosciences (San Diego, CA, United States). JNK was from Cell Signaling Technology (Danvers, MA, United States). ERK1p(Thr202/Tyr204)/ERK2p(Thr185/Tyr187) was from Thermo Fisher Scientific (Waltham, MA, United States). Horseradish peroxidase (HRP)-conjugated goat anti-mouse and -rabbit IgG were from Abcam (Cambridge, MA, United States).

Preparation of white genius mushroom

White genius mushroom used in this study was harvested in September and purchased form 8329 Farm (Changhua, Taiwan). The voucher specimens of white genius mushroom (CMU-RX-HM-2020021) were deposited in School of Pharmacy, China Medical University, Taichung, Taiwan. The air-dried WGM (122.2 g) was soaked thrice with 1 L of 95% ethanol at room temperature for 3 days. The combined filtrate was then concentrated under reduced pressure at 40°C. The yield of dry extract of WGM was about 5.6%. WGM extracts are dissolved in 100% dimethylsulfoxide (DMSO) and stored at -20°C until use. In our previous study, we have demonstrated that the IC_{50} (half maximal inhibitory concentration) of WGM extracts was about 175 μg/ml (Li et al., 2022). Since the concentration of IC_{50} of WGM was used to treat the cells in the inhibitor experiment, inhibitors had no significant protective effect on the WGM-induced vacuoles formation and cell death. Therefore, IC_{40}, which was about 150 μg/ml WGM, was chosen in this study.

Cell culture

Hepatocellular carcinoma Hep3B, hepatocellular carcinoma HepG2 and lung squamous carcinoma CH27 cells were cultured in Dulbecco's Modified Eagle Medium (Gibco BRL, Gaithersburg, MD, United States) supplemented with 10% fetal bovine serum (HyClone, Logan, UT, United States), 100 U/ml penicillin, 100 μg/ml streptomycin and 2 mM glutamine at 37°C in a humidified atmosphere with 5% CO_2. Breast cancer MCF-7 and prostatic adenocarcinoma PC-3 cells were cultured in Minimum Essential Medium (Gibco BRL, Gaithersburg, MD, United States) and Roswell Park Memorial Institute 1640 Medium (Gibco BRL, Gaithersburg, MD, United States), respectively, supplemented with 10% fetal bovine serum, 100 U/ml penicillin, 100 μg/ml streptomycin and 2 mM glutamine. Hep3B, HepG2, MCF-7 and PC-3 cancer cell lines were purchased from the Food Industry Research and Development Institute (Hsinchu, Taiwan). CH27 cells was kindly provided by Professor Shih-Lan Hsu (Taichung Veterans General Hospital, Taichung, Taiwan).

Total RNA extraction

Total RNA was extracted from Hep3B cells using AllPure Total RNA Isolation Kit (AllBio Science Inc., Taiwan) following the manufacturer's protocol. RNA concentration was detected using a spectrophotometer with wavelength at 260 nm.

Differential expressed genes analysis

Gene expression is measured using read density, with higher read density indicating higher gene expression levels. Gene expression was calculated using Cuffdiff (v2.2.1) software that calculates FPKM (fragments per kilo bases per million reads). The formula is:

$$\mathrm{FPKM} = \frac{\text{total exon fragments}}{\text{mapped read (Millions)} \times \text{exon length (KB)}}$$

Comparison of the expression levels of all genes under different experimental conditions by FPKM profiling. Gene differential analysis was performed using the Cuffdiff (v2.2.1). Based on the criteria of fold change greater than 2 and p-value less than 0.05, the results of the Cuffdiff analysis were further analyzed to identify genes with significantly differential expression. Differential expressed genes (DEGs) of WGM extracts-treated samples compared to controls were analyzed using DESeq (v1.18.0) Bioconductor package, which is a model based on a negative binomial distribution. After adjustment by the Benjamini–Hochberg method for controlling the false discovery rate, p-values for genes were set at < 0.05 to detect differential expressed genes. The raw sequencing data were uploaded to the NCBI Sequence Read Archive (SRA) with the accession ID PRJNA813700.

Cluster analysis of differential expressed genes

Cluster analysis is the calculation and classification of data based on similarity, thereby grouping samples or genes with similar expression patterns into one group. This can predict the function of unknown genes and predict whether they are involved in the same cellular pathway or metabolic process. The FPKM value of different genes under different experimental conditions was taken as the expression level and used for hierarchical clustering. The most obvious feature of this method is the generation of dendrogram. Different clusters are represented by different colored regions. Gene expression patterns are similar within the same cluster and close to each other, and they may have similar biological functions. The gplots in R software were used for cluster analysis, and the data of union_for_cluster were clustered by the log relative expression

value of genes. We used algorithms to obtain the distance between genes, and then calculated the relative distance between the genes through repeated operations. Finally, clustering was performed by dividing genes into different subclusters based on their relative distances.

Kyoto encyclopedia of genes and genomes enrichment analysis of differential expressed genes

KEGG is a collection of databases dealing with metabolism, genetic information processing, environmental information processing, cellular processes, organismal systems, human diseases and drug development (http://en.wikipedia.org/wiki/KEGG). We used scripts in house to enrich significant differential expressed genes in KEGG pathways. KEGG pathway units and a hypergeometric test were used to perform the pathway enrichment analysis and find the pathways of the differentially express genes that are significantly enriched in the transcriptome data. Below is the formula:

$$p = 1 - \sum_{i=0}^{m-1} \frac{\binom{M}{i}\binom{N-M}{n-i}}{\binom{N}{n}}$$

N is the number of genes with pathway annotations, n is the number of differential expressed genes in *N*, *M* is the number of genes annotated for a particular pathway in all genes, and m is the number of differential expressed genes annotated for that pathway. The threshold Q value is ≤ 0.05.

Assessment of morphological changes

Cells were seeded at a density of 5×10^4 cells per well onto 12-well plate 48 h before being treated with drugs. Hep3B cells were incubated without or with indicated various concentrations WGM extracts for 24 h. The morphology of the cells was photographed with an Olympus IX 73 phase contrast microscope at objective ×10 magnification. A field was chosen in the center of each well at approximately the same location for photography.

Mitochondrial reductase activity assay

Mitochondrial reductase activity assay was performed as previously described (Li et al., 2022). The assay is based on the measurement of the reduction of 3-(4,5-dimethylthiazol-2-yl)-2,5-diphenyltetrazolium bromide (MTT) after white genius mushroom extracts treatment.

Protein preparation and western blot analysis

Protein preparation and Western blot analysis were performed as previously described (Lee et al., 2009). The primary antibodies used in this study were as follows. β-Actin, 1:5000; Akt, 1:2000; Aktp (S473), 1:1500; ERK, 1:1000; ERK1p(Thr202/Tyr204)/ERK2p(Thr185/Tyr187), 1:1000; JNK, 1:2000; JNKp(Thr183/Tyr185), 1:1000; MEK, 1:2000; p38, 1:1000; p38p (Thr180/Tyr182), 1:1000; PI3K, 1:3000; Raf, 1:1000; Ras, 1:1000; mTOR, 1:1000. β-Actin was used as an internal control. The secondary antibody was used at a dilution of 1:20,000 of HRP-conjugated goat anti-mouse IgG (for β-actin, ERK, p38 and Raf) or HRP-conjugated goat anti-rabbit IgG (for Akt, Aktp (S473), ERK1p(Thr202/Tyr204)/ERK2p(Thr185/Tyr187), JNK, JNKp(Thr183/Tyr185), MEK, p38p (Thr180/Tyr182), PI3K, Ras and mTOR). The Western blot results of protein were quantified by Lane 1D Gel imaging analysis software (Sagecreation, Beijing, China).

Wound healing assay

The migratory activity of Hep3B cells was assessed using a wounded migration assay. Wounded migration assay was performed as previously described (Liao et al., 2015). As cell reached confluence or near confluence, a linear wound was scratched across each well by a sterile 200 μl pipette tip. After washing, cells were treated with vehicle alone (control) or with 75, 125 or 150 μg/ml WGM extracts for 24 h. Images of wounds at 0 h and 24 h after scratching were obtained with an Olympus IX 73 phase-contrast microscope (Olympus Optical Co., Tokyo, Japan) at objective ×10 magnification.

Transwell migration experiments

In vitro cell migration was also performed using 24-well transwell inserts with a pore size of 8 μm (Corning Life Sciences, NY, United States). The transwell chambers were used according to the manufacturer's protocol. The cell pellets were resuspended in DMEM supplemented with 0.1% FBS at a cell density of 1×10^6 cells/ml. Aliquots of 100 μl cell suspension (1×10^5 cells per well) containing DMSO or WGM extracts were loaded into transwell inserts that were subsequently placed into the 24-well plate, and 600 μl medium supplemented with 10% FBS was used as a chemoattractant in the lower chamber. After incubated for 24 h at 37°C, the cells remaining on the upper surface of the membrane were removed with a cotton swab, and the cells on the lower surface of the membrane are the migrated cells. Filters were fixed with 4% paraformaldehyde solution for 20 min and stained with 0.1% crystal violet for 10 min, then the cells that passed through the filter were photographed by

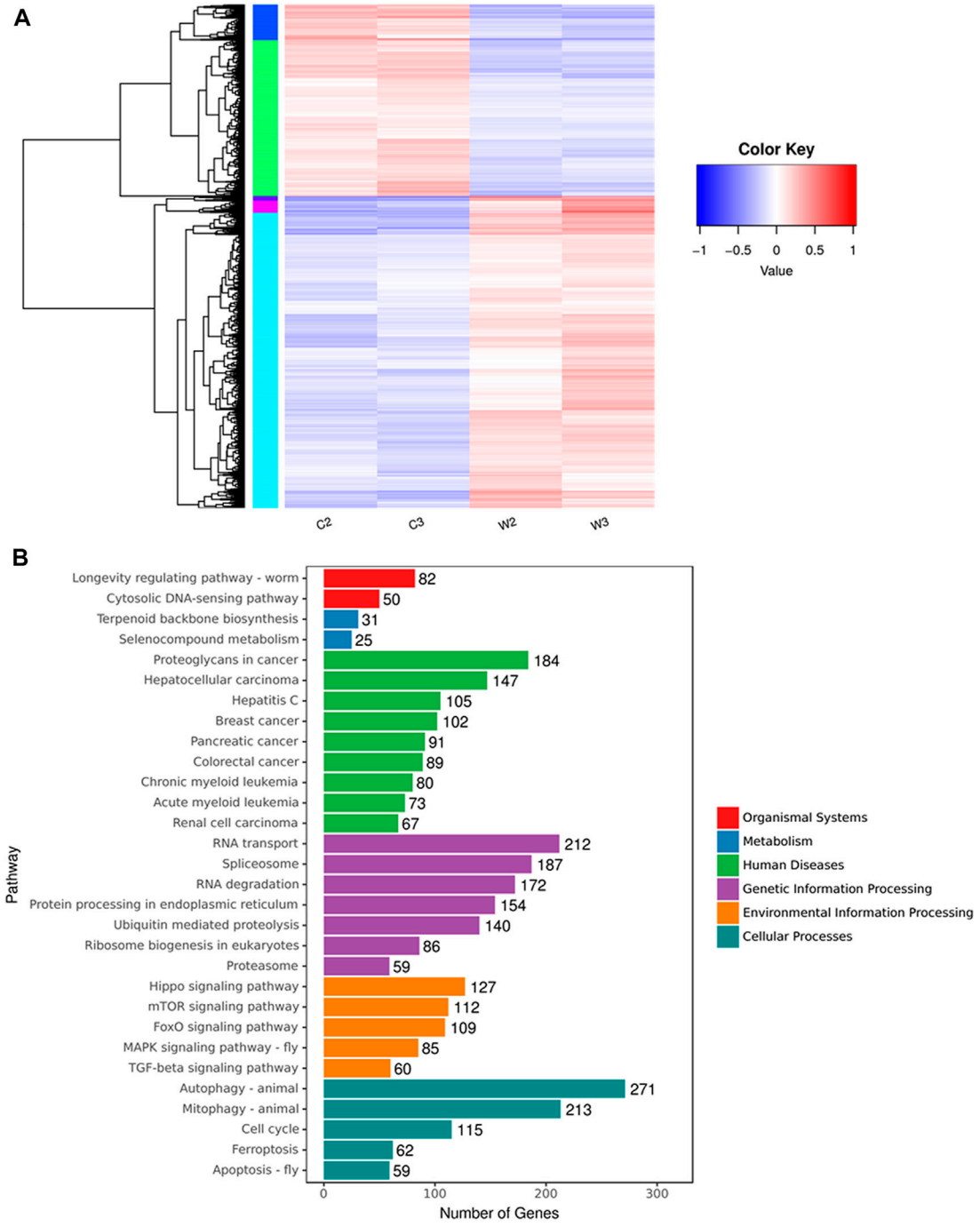

FIGURE 1
Cluster analysis and KEGG pathway enrichment of differential expressed genes between WGM extracts-treated and control groups in Hep3B cells. Cells were treated with vehicle alone or with 150 μg/ml WGM extracts for 24 h. **(A)** Cluster analysis of differential expressed genes between the WGM extracts-treated and control groups. The regions of different colors represent different clusters. The color scale of the heatmap illustrates the $\log_2$ of fold change of the WGM extracts-treated/control samples shown in the heatmap. **(B)** The KEGG pathway enrichments of the DEGs between WGM extracts-treated and control samples. The *y-axis* shows the names of the enriched pathways. The results were analyzed to determine genes with significant differential expression according to the criteria of fold change greater than 2 and FDR less than 0.05.

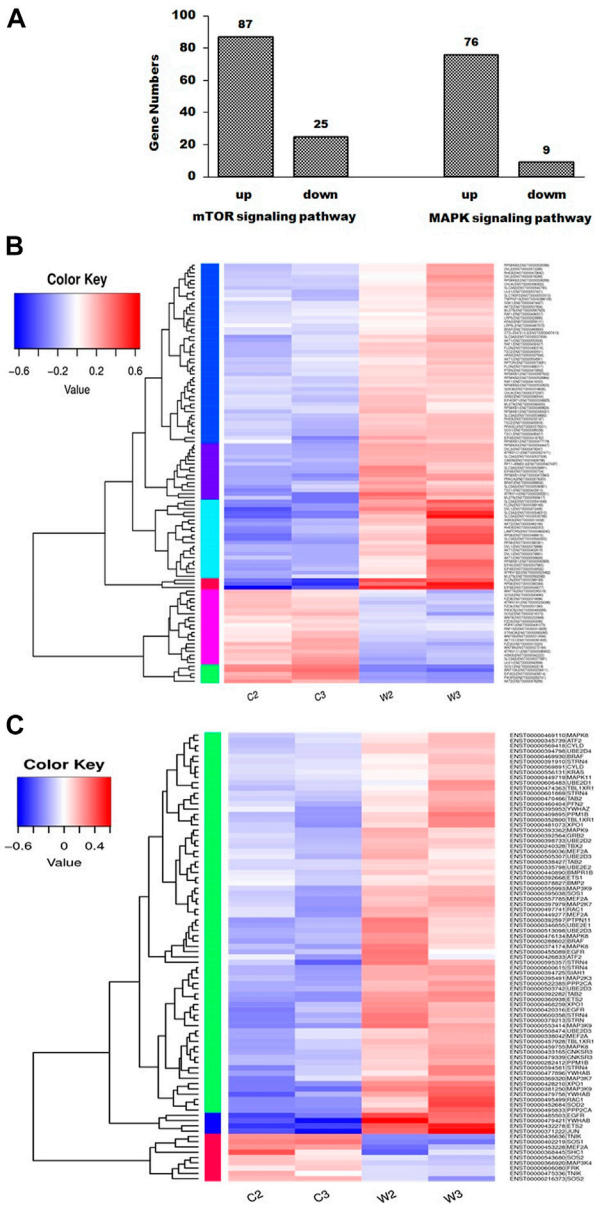

FIGURE 2
mTOR and MAPK signaling pathways were involved in WGM extracts-induced cell death of Hep3B cells. Cells were treated with vehicle alone or with 150 μg/ml WGM extracts for 24 h. **(A)** Summary of gene numbers of mTOR and MAPK signaling pathways that are significantly upregulated or downregulated between WGM extracts-treated and control cells. Differential expressed genes between WGM extracts-treated and control cells were selected based on more than 2-fold expression changes and the *p*-value was <0.05. **(B)** Cluster analysis of DEGs in mTOR signaling pathway of the WGM extracts-treated and control groups. The regions of different colors represent different clusters. The color scale of the heatmap illustrates the $\log_2$ of fold change of the WGM extracts-treated/control samples shown in the heatmap. **(C)** Heatmap displaying hierarchical clustering of DEG involved in MAPK signaling pathway. The regions of different colors represent different clusters. The color scale of the heatmap illustrates the $\log_2$ of fold change of the WGM extracts-treated/control samples shown in the heatmap.

Olympus IX 73 phase-contrast microscope (Olympus Optical Co., Tokyo, Japan) at objective ×20 magnification.

Colony formation assay

To assess the effects of WGM extracts on cell proliferation, the colony formation assay was carried out *in vitro*. Hep3B cells were seeded at a density of 5×10^3 cells per well onto 6-well plate 48 h before drug treatment. Cells were treated with vehicle alone or with 125 or 150 μg/ml WGM extracts for 24 h. After treatment, the media was replaced with fresh complete growth media without the WGM extracts. Treated cells were washed by phosphate-buffered saline and then cultured in culture medium for 3 and 4 days with medium replacement every 2 days. After incubated at 37°C for 3 and 4 days, colonies were fixed with 4% paraformaldehyde solution and then stained with 0.5% crystal violet. Finally, the colonies were photographed.

Data analysis and statistics

One-way ANOVA and Bonferroni post-hoc test were used to analyze differences between each experimental group. A *p*-value less than 0.05 was considered significant.

Results

Processing of next generation sequencing data and differential expressed genes analysis

Since the exact mechanism of the anticancer effect of WGM extracts is substantially unknown, this study takes advantage of NGS technology to compare differences in the transcriptome profiles between control and WGM extracts-treated cells. The software of Cuffdiff (v2.2.1) and HTSEQ (v0.6.1) were used for gene expression calculation. Based on the criteria of fold change greater than 2 and *p*-value less than 0.05, the results of the Cuffdiff analysis were further analyzed to identify genes with significantly differential expression. To directly assess differential expressed genes (DEGs) expression in these samples and confirm the classification, a DEG heat map was drawn using the R package pheatmap (version 1.0.8). Gene expression patterns are similar within the same cluster and close to each other, and they may have similar biological functions. Cluster analysis of differentially expressed genes $\log_{10}$ (FPKM +1) values are used for clustering. Genes of low expression are in blue, and high expressed in red. The heat map clearly indicated the distinct separation of the WGM extracts-treated and control groups (Figure 1A).

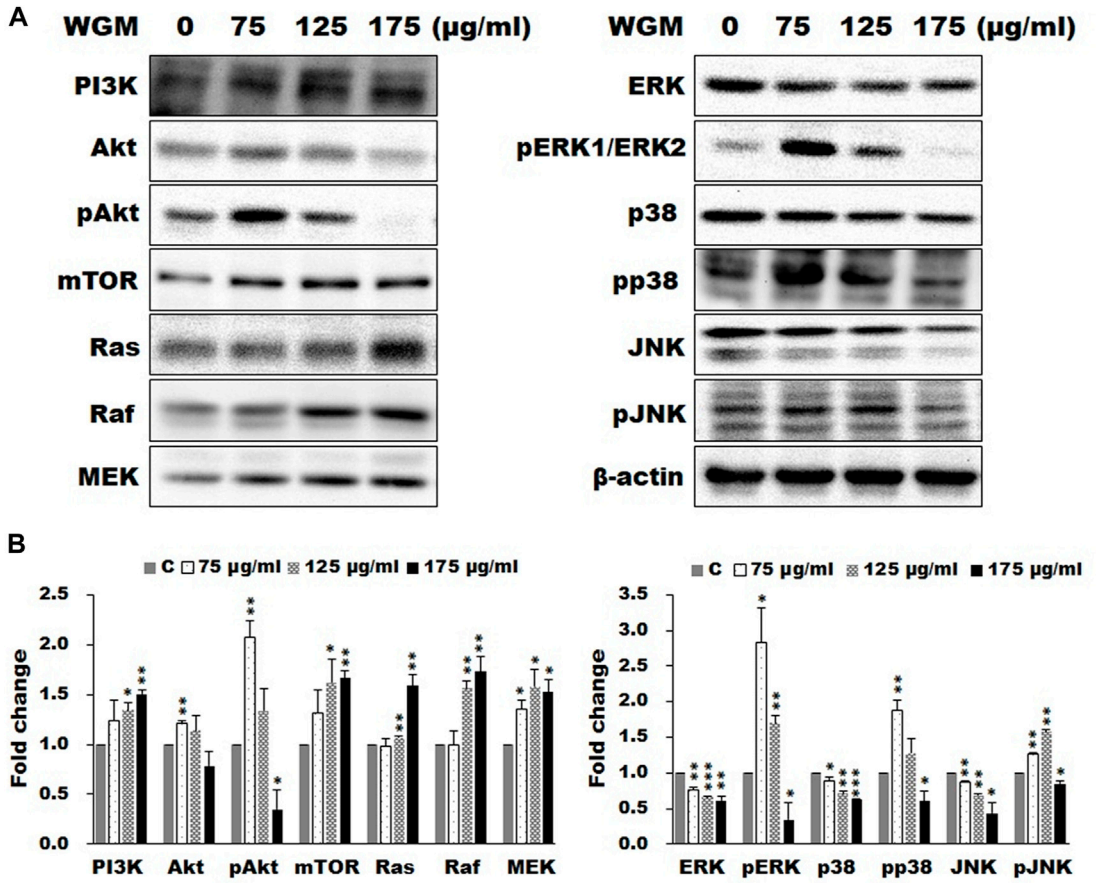

FIGURE 3
Effects of WGM extracts on the protein levels of the members of mTOR and MAP signaling pathways in Hep3B cells. The effects of WGM extracts on mTOR and MAPK signaling pathway-related proteins were analyzed by Western blotting. Cells were treated with vehicle alone or with 75, 125 or 175 μg/ml WGM extracts for 24 h. Protein samples were analyzed by SDS-PAGE (5% for PI3K and mTOR, 8% for Raf, 10% for Akt and Aktp (S473), 12% for β-actin, ERK, ERK1p(Thr202/Tyr204)/ERK2p(Thr185/Tyr187), JNK, JNKp(Thr183/Tyr185), MEK, p38 and p38p (Thr180/Tyr182) and 14% for Ras), and then probed with primary antibodies followed by secondary antibodies. **(A)** Representative blots. **(B)** The blots were quantified by Lane 1D Gel imaging analysis software. Protein expression was normalized using β-actin. Fold change = normalized signal treated/normalized signal control. Results are expressed as the mean ± S.D. of three independent experiments. $*p < 0.05$, $**p < 0.01$, $***p < 0.001$ compared to the control values.

mTOR and mitogen-activated protein kinase signaling pathways were involved in white genius mushroom extracts-induced cell death of Hep3B cells

After screening differential expressed genes, KEGG pathway enrichment analysis was subsequently performed to investigate the function of the identified genes. Pathway functional enrichment facilitates to determine the DEGs involved in the most important signal transduction pathways and metabolic pathways. The top 30 KEGG pathways are presented in Figure 1B. KEGG pathway analysis showed that the DEGs induced by WGM extracts were found to be involved in molecular pathways for organismal systems, metabolism, human diseases, genetic information processing, environmental information processing and cellular processes (Figure 1B). In the cellular processes of KEGG pathway analysis, autophagy, mitophagy and apoptosis pathways were found to be significantly changed in WGM extracts-treated cells (Figure 1B). However, the involvement of autophagy, mitophagy and apoptosis pathways in WGM extracts-induced cell death was investigated in our previously study. Hippo, mTOR, FoxO, MAPK and TGF-beta signaling pathways were significantly altered in the environmental information processing (Figure 1B). The mTOR and MAPK signaling pathways are necessary, however, to promote growth and proliferation in many mammalian cell types. We focused our attention on the investigation of the effects of WGM extracts on the expression of mTOR and MAPK signaling pathways in Hep3B cells in this study. As shown in Figure 2A, 112 genes (87 upregulated and 25 downregulated) were related to mTOR signaling pathway and 85 genes (76 upregulated and

10.3389/fphar.2022.1039376

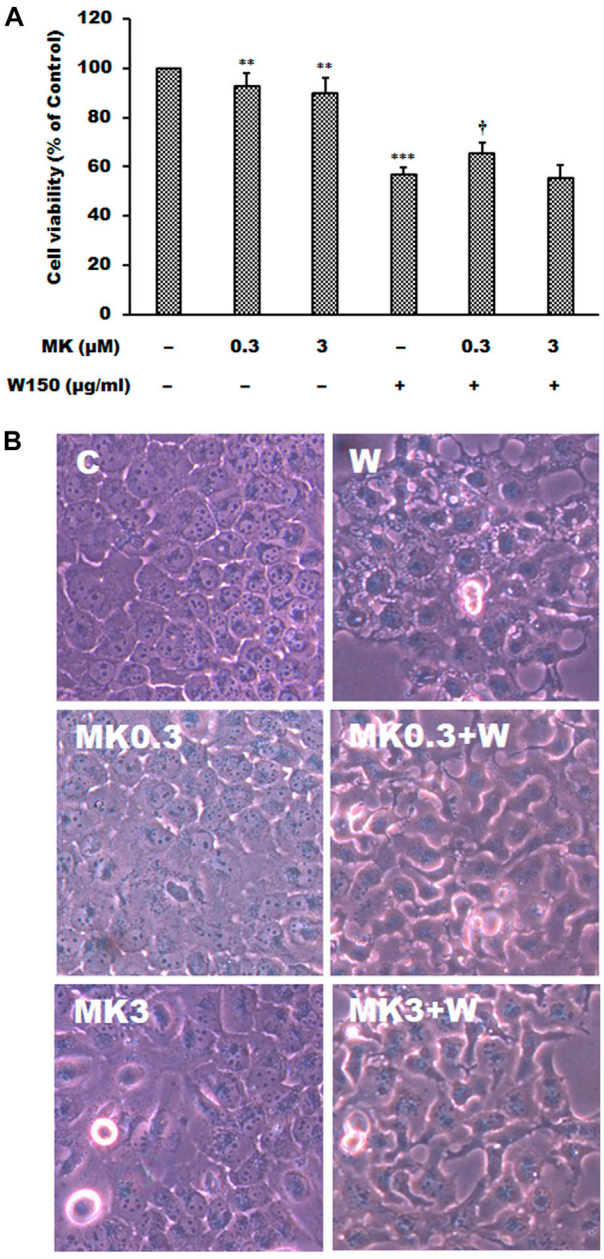

FIGURE 4
The effects of MK2206 on WGM extracts-induced cell death and membrane-enclosed vacuoles of Hep3B cells. Cells were pretreated with 0.3 or 3 μM MK2206 (MK) for 1 h and then treated with 0.1% DMSO or 150 μg/ml WGM extracts (W) for 24 h. **(A)** The effects of MK2206 on WGM extracts-induced cell death of Hep3B cells. After treatment, the viable cells were measured by MTT assay. All determinations are expressed as the mean % control ±S.D. of duplicate from three independent experiments. $^{**}p < 0.01$, $^{***}p < 0.001$ compared to the control values. $^{\dagger}p < 0.05$ compared to the WGM extracts alone. **(B)** The effects of MK2206 on WGM extracts-induced membrane-enclosed vacuoles of Hep3B cells. After treatment, the cells were immediately photographed with an Olympus IX 73 phase-contrast microscope. All results are representative of three independent experiments.

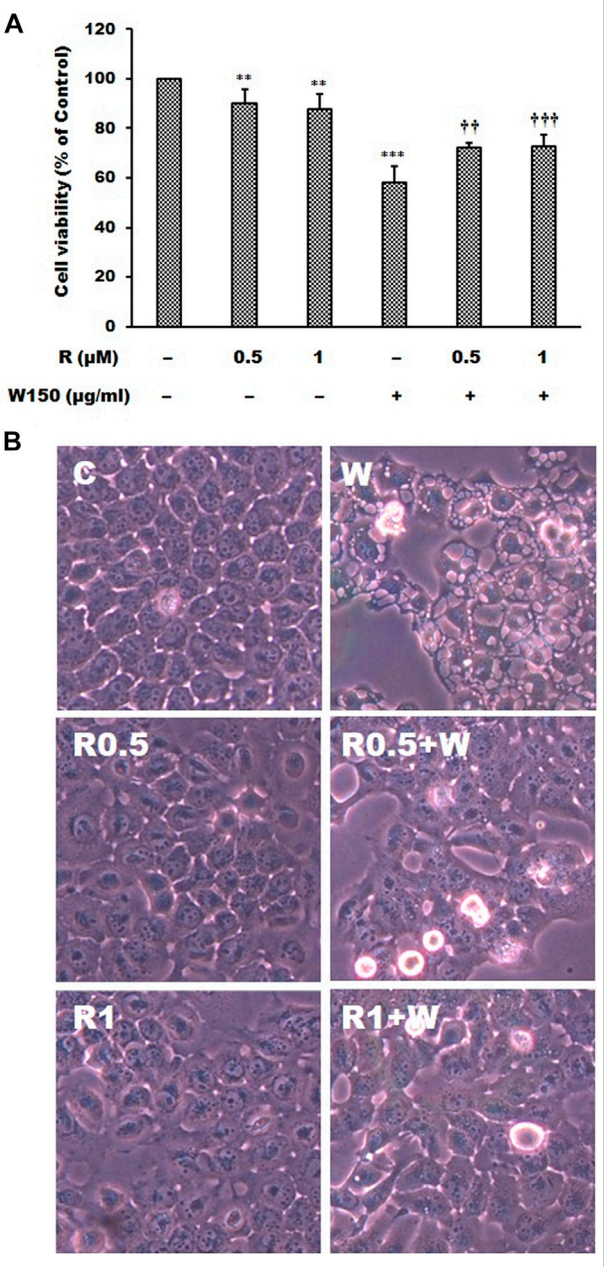

FIGURE 5
The effects of rapamycin on WGM extracts-induced cell death and membrane-enclosed vacuoles of Hep3B cells. Cells were pretreated with 0.5 or 1 μM rapamycin (R) for 1 h and then treated with 0.1% DMSO or 150 μg/ml WGM extracts (W) for 24 h. **(A)** The effects of rapamycin on WGM extracts-induced cell death of Hep3B cells. After treatment, the viable cells were measured by MTT assay. All determinations are expressed as the mean % control ±S.D. of duplicate from three independent experiments. $^{**}p < 0.01$, $^{***}p < 0.001$ compared to the control values. $^{\dagger\dagger}p < 0.01$, $^{\dagger\dagger\dagger}p < 0.001$ compared to the WGM extracts alone. **(B)** The effects of rapamycin on WGM extracts-induced membrane-enclosed vacuoles of Hep3B cells. After treatment, the cells were immediately photographed with an Olympus IX 73 phase-contrast microscope. All results are representative of three independent experiments.

9 downregulated) to MAPK signaling pathway. The differential expressed genes involved in mTOR and MAPK signaling pathways were shown in Supplementary Tables S1, S2, respectively. The results of a hierarchical clustering analysis of DEG involved in mTOR and MAPK signaling pathways are displayed in a heat map as a dendrogram (Figures 2B,C).

The effects of white genius mushroom extracts on the expression of mTOR and mitogen-activated protein kinase signaling pathways-related proteins

According to the KEGG pathway enrichment analysis, the present study examined the effects of WGM extracts on the expression of mTOR and MAPK signaling pathway-related proteins, such as PI3K, Akt, mTOR, Ras, Raf, MEK, ERK, p38 and JNK, in Hep3B cells. The expression of mTOR and MAPK signaling pathway-related proteins during WGM extracts-induced cell death was performed by Western blotting techniques. After treating the Hep3B cells with WGM extracts for 24 h, the protein levels of PI3K and mTOR were increased after treatment with WGM extracts for 24 h (Figure 3A). Cells treated for 24 h with WGM extracts showed a marked dose-dependent decrease in the expression of the ERK and JNK protein, and an upregulation of the Ras, Raf and MEK protein (Figure 3A). The present study also investigated the expression of pERK protein in WGM extracts-induced Hep3B cell death. Treatment with WGM extracts increased pERK protein in Hep3B cells up to 125 μg/ml, but pERK level was decreased after treatment with 175 μg/ml WGM extracts. It is interesting to note that WGM extracts induced a significant increase in the protein expression of Ras, but did not induce ERK activity, in cells exposed to 175 μg/ml WGM extracts for 24 h (Figure 3A). These results indicate that WGM extracts-mediated ERK activation occurs through a Ras-independent pathway. As shown in Figure 3A, the present study also demonstrated that the expression patterns of pERK protein are similar to those seen in Akt and pAkt expression after treatment with WGM extracts for 24 h (Figure 3A). In our study, not only the expression of ERK, which is associated with cell proliferation, but also p38, which is regulated by various environmental stresses, is regulated by WGM extracts. As shown by immunoblotting, WGM extracts caused a marked increase in the protein levels of pp38 in Hep3B cells (Figure 3A). However, the protein levels of p38 were decreased after treatment with WGM extracts (Figure 3A). As shown in Figure 3B, the Western blot results of protein were quantified by Lane 1D Gel imaging analysis software. These results indicate that changes in the expression of PI3K/mTOR and MAPK signaling pathways-related proteins in WGM extracts-treated cells is associated with WGM extracts-induced Hep3B cell death.

The effects of the inhibitors of PI3K/Akt/mTOR signaling pathway on white genius mushroom extracts-induced cell death and membrane-enclosed vacuoles of Hep3B cells

As shown by the Western blotting analysis, we guess that the cell death of WGM extracts treated Hep3B cells is related to PI3K/Akt/mTOR signaling pathway. Therefore, we used Akt inhibitor MK2206 and mTOR inhibitor rapamycin to demonstrate that PI3K/Akt/mTOR signaling pathway is an important intracellular signaling pathway in the WGM extracts-induced cell death. MK2206, a well-known Akt inhibitor, was used to demonstrate whether Akt activity can promote the WGM extracts-induced cell death of Hep3B cells. The present study demonstrated that MK2206 (0.3 μM) was only slightly restore the cell death induced by WGM extracts (Figure 4A). MK2206 (0.3 and 3 μM, pretreatment 1 h) had a significant preventive effect, however, on the WGM extracts (150 μg/ml)-induced membrane-enclosed vacuoles of Hep3B cells (Figure 4B). The mTOR inhibitor rapamycin, an autophagy inducer, was also used in this study. As shown in Figures 5A,B, a significant preventive effect on the WGM extracts (150 μg/ml)-induced cell death and vacuoles formation was observed in Hep3B cells pretreatment with 0.5 or 1 μM rapamycin. Hep3B cells did not show any cytoplasmic vacuolization after 24 h treatment with 0.5 or 1 μM rapamycin alone, but the proliferation of Hep3B cells were slightly inhibited by the presence of rapamycin (Figure 5A). Our previous study has demonstrated that 3-MA, PI3K inhibitor, did not recover the membrane-enclosed vacuoles and cell death induced by 150 μg/ml WGM extracts (data not shown). These results showed that PI3K/Akt/mTOR signaling pathway was involved in the WGM extracts-induced cell death in Hep3B cells. The lysosomotropic agent chloroquine, an autophagy inhibitor, was also used in this study. The WGM extracts (150 μg/ml)-induced vacuoles formation and cell death of Hep3B cells were partially blocked by pretreatment with 10 or 50 μM chloroquine (Figure 6A). It is interesting to note that chloroquine alone had a slight effect on the vacuoles formation in Hep3B cells (Figure 6B).

The effects of extracellular signal-regulated kinase inhibitor LY3214996 and p38 inhibitor SB202190 on white genius mushroom extracts-induced cell death and membrane-enclosed vacuoles of Hep3B cells

It is well known that MAPK signaling pathway was an important intracellular signaling pathway that is related to cell

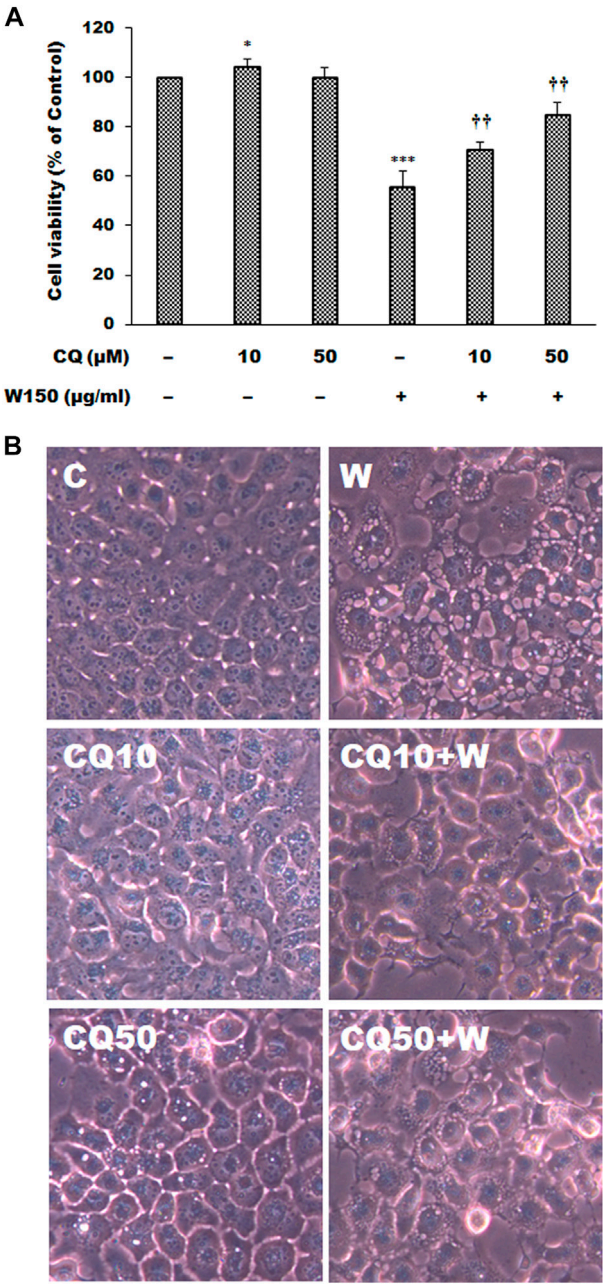

FIGURE 6
The effects of chloroquine on WGM extracts-induced cell death and membrane-enclosed vacuoles of Hep3B cells. Cells were pretreated with 10 or 50 μM chloroquine (CQ) for 1 h and then treated with 0.1% DMSO or 150 μg/ml WGM extracts (W) for 24 h. **(A)** The effects of chloroquine on WGM extracts-induced cell death of Hep3B cells. After treatment, the viable cells were measured by MTT assay. All determinations are expressed as the mean % control ±S.D. of duplicate from three independent experiments. *$p < 0.05$, ***$p < 0.001$ compared to the control values. ††$p < 0.01$ compared to the WGM extracts alone. **(B)** The effects of chloroquine on WGM extracts-induced membrane-enclosed vacuoles of Hep3B cells. After treatment, the cells were immediately photographed with an Olympus IX 73 phase-contrast microscope. All results are representative of three independent experiments.

proliferation, motility, survival and apoptosis of cancer cells. According to the results of immunoblotting, WGM extracts caused a marked increase in the protein levels of pERK in Hep3B cells. The ERK inhibitor LY3214996 was used in this study. Pretreatment with LY3214996 (5 and 10 nM) significantly inhibited the WGM extracts (150 μg/ml)-induced cell death and membrane-enclosed vacuoles of Hep3B cells (Figure 7). In this study, not only the expression of phosphorylation of ERK but also phosphorylation of p38 is regulated by WGM extracts according to the results of immunoblotting. This study determined the effect of p38 inhibitor SB202190 on the WGM extracts-induced cell death of Hep3B cells. Pretreatment with SB202190 (0.5 and 1 μM) for 1 h had a significant preventive effect on the WGM extracts (150 μg/ml)-induced cell death and membrane-enclosed vacuoles of Hep3B cells (Figure 8). Based on the above data, these results indicate that WGM extracts-mediated the activation of ERK and p38 is involved in the WGM extracts-induced membrane-enclosed vacuoles and even cell death.

The effect of white genius mushroom extracts on the migration potential of Hep3B cells

Controlling the invasion and metastasis of cancer cells has been recognized as a new strategy for cancer prevention and treatment. The MAPK and mTOR signaling pathway are most important signaling cascade and play key role in the proliferation and migration of tumor cells. Since cell migration is an essential step in the cancer metastatic process, the present study investigated the effect of WGM extracts on the migration ability of Hep3B cells. For examination of the ability of Hep3B cell migration, a wound-healing assay was performed to examine whether WGM extracts can inhibit Hep3B cell migration. Wound healing experiment was performed on cells treated with 75, 125 and 150 μg/ml WGM extracts for 24 h. As shown in Figure 9A, an increase in the distance of the wound edge indicates that the speed of cell migration is significantly reduced after treatment with WGM extracts. To obtain further support for the inhibition of cell migration by WGM extracts in Hep3B cells, the transwell migration assay, which is used to examine the migratory response of cancer cells to treatments, were performed in this study. The results from that assay showed that WGM extracts had a significant inhibition of the Hep3B cell migration ability in a dose-dependent manner through the transwell membrane compared with those in the control cells (Figure 9B). Based on the above data, we suggested that WGM extracts be able to inhibit Hep3B cell migration in a dose-dependent manner.

10.3389/fphar.2022.1039376

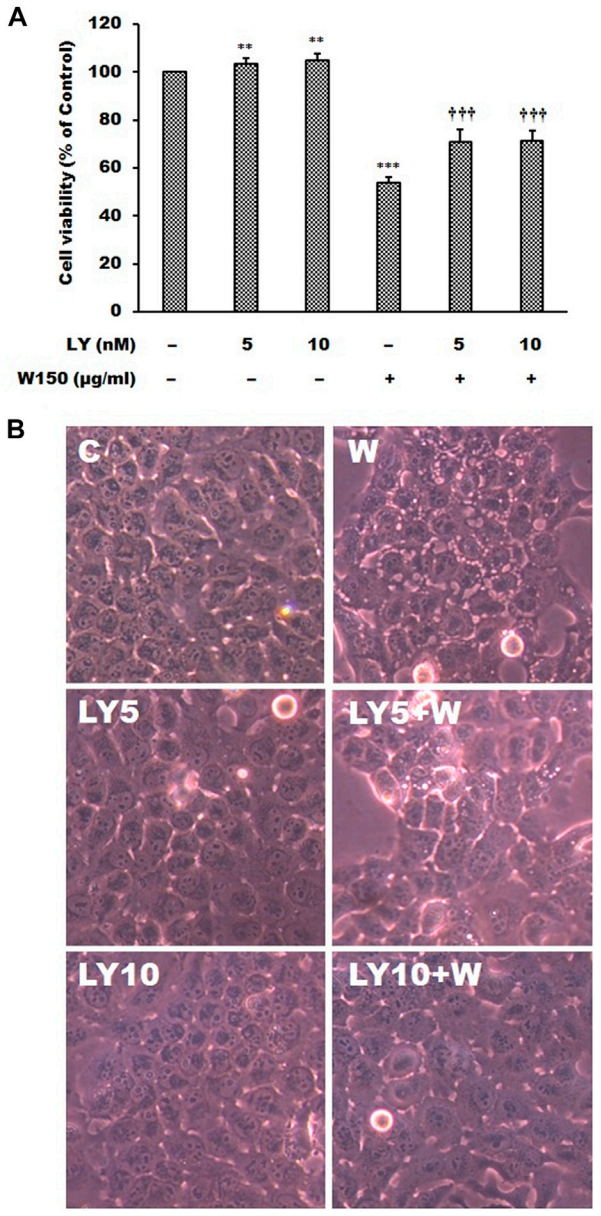

FIGURE 7
The effects of LY3214996 on WGM extracts-induced cell death and membrane-enclosed vacuoles of Hep3B cells. Cells were pretreated with 5 or 10 nM LY3214996 (LY) for 1 h and then treated with 0.1% DMSO or 150 μg/ml WGM extracts (W) for 24 h. **(A)** The effects of LY3214996 on WGM extracts-induced cell death of Hep3B cells. After treatment, the viable cells were measured by MTT assay. All determinations are expressed as the mean % control ±S.D. of duplicate from three independent experiments. $^{**}p < 0.01$, $^{***}p < 0.001$ compared to the control values. $^{\dagger\dagger\dagger}p < 0.001$ compared to the WGM extracts alone. **(B)** The effects of LY3214996 on WGM extracts-induced membrane-enclosed vacuoles of Hep3B cells. After treatment, the cells were immediately photographed with an Olympus IX 73 phase-contrast microscope. All results are representative of three independent experiments.

White genius mushroom extracts inhibits the proliferation of Hep3B cells *in vitro*

Colony formation assay was used to mimic cancer growth from a single cell to grow into a cancer cell colonies or tumor mass. Plate colony formation assay was used to examine the effect of WGM extracts on the colony-forming ability of Hep3B cells. Cells were plated onto 6-well plates and incubated with vehicle alone or with 125 or 150 μg/ml WGM extracts and treated cultures were maintained in culture for an additional 3 or 4 days to allow formation of colonies. As shown in Figure 10A, WGM extracts significantly inhibited the colony-forming ability of Hep3B cells in a dose- and time-dependent manner, as fewer colonies were observed in cells treated with higher concentrations of WGM extracts. In other words, higher doses inhibited colony formation and resulted in a significant decrease in colony numbers in the WGM extracts-treated group. In control group, Hep3B cells grow and form colonies within 3 or 4 days of incubation (Figure 10A). In our previous study, we have confirmed the cytotoxicity of white genius mushroom extracts on human Hep3B liver cancer cells. WGM extracts induced a significant concentration-dependent inhibition of Hep3B cell growth with IC_{50} (half maximal inhibitory concentration) value of 175 μg/ml. We further investigated whether WGM extracts selectively causes cytotoxicity in different cancer cell lines. Therefore, this study evaluated the effects of WGM extracts on cell growth of hepatocellular carcinoma HepG2 cells, human lung squamous carcinoma CH27 cells, breast cancer MCF-7 cells and prostatic adenocarcinoma PC-3 cells. WGM extracts had no significant cytotoxic effect on the HepG2, CH27 and MCF-7 cells after treatment with WGM extracts for 24 h (Figure 10B). Furthermore, WGM extracts treatment leads to an increase in cell viability of MCF-7 cells (Figure 10B). The treatment of PC-3 cells with WGM extracts for 24 h resulted in a slight cytotoxic effect (Figure 10B). The concentration of inducing about 50% cell death by WGM extracts is more than 200 μg/ml for PC-3 cells (Figure 10B). Based on the above data, we demonstrated that the cytotoxic effect of WGM extracts on Hep3B cells was significantly higher than that in PC-3, HepG2, CH27 and MCF-7 cells. Therefore, Hep3B cells were chosen for investigation of the anticancer mechanisms of WGM extracts in this study.

Discussion

Hepatocellular carcinoma (HCC) is one of the most common cancers in Taiwan, with a high incidence and mortality rate. However, the drugs used to treat for liver cancer may appear high toxicity, many side effects and drug resistance, leading to poor quality of life after treated for cancer. Therefore, the search for new drugs or chemoprevention agents with few side effects and

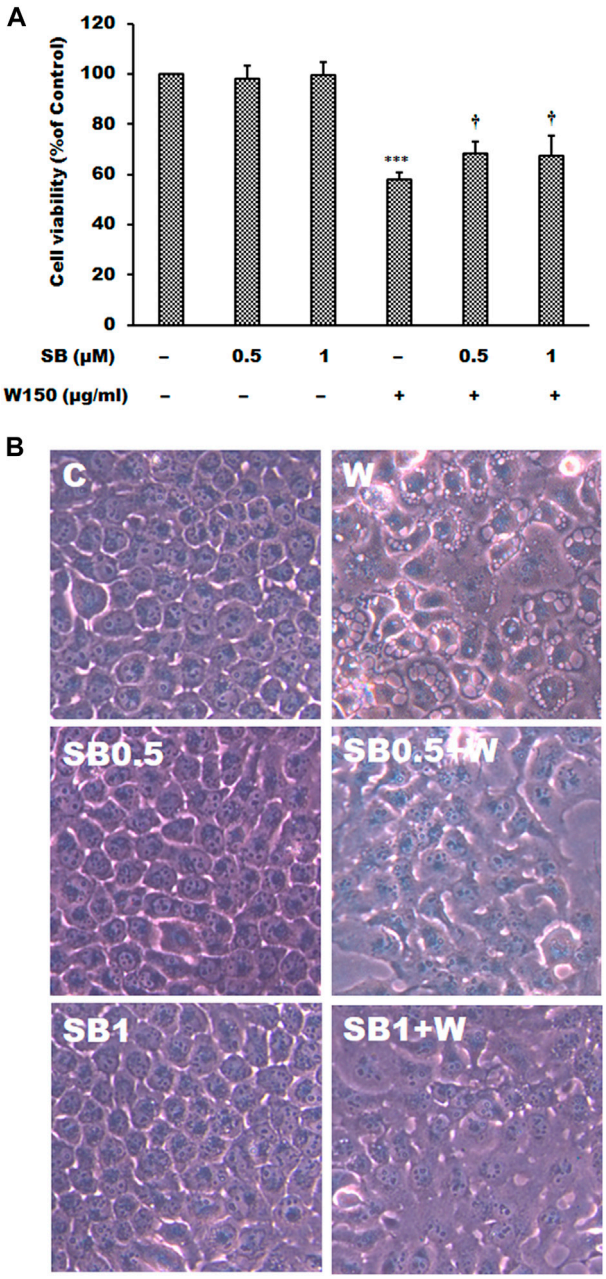

FIGURE 8
The effects of SB202190 on WGM extracts-induced cell death and membrane-enclosed vacuoles of Hep3B cells. Cells were pretreated with 0.5 or 1 μM SB202190 (SB) for 1 h and then treated with 0.1% DMSO or 150 μg/ml WGM extracts (W) for 24 h. **(A)** The effects of SB202190 on WGM extracts-induced cell death of Hep3B cells. After treatment, the viable cells were measured by MTT assay. All determinations are expressed as the mean % control ±S.D. of duplicate from three independent experiments. ***$p < 0.001$ compared to the control values. †$p < 0.05$ compared to the WGM extracts alone. **(B)** The effects of SB202190 on WGM extracts-induced membrane-enclosed vacuoles of Hep3B cells. After treatment, the cells were immediately photographed with an Olympus IX 73 phase-contrast microscope. All results are representative of three independent experiments.

high efficacy is in demand in order to treat liver cancer patients. White genius mushroom (WGM) is a popular edible mushroom whose anticancer activity was demonstrated to be partially dependent on the production of ROS in human Hep3B liver cancer cells in our previous study (Li et al., 2022). Furthermore, autophagy, mitophagy and apoptosis pathways were identified as significant in WGM extracts-treated Hep3B liver cancer cells according to the KEGG pathway enrichment analysis (Li et al., 2022). Although WGM extracts were found to have anticancer activities, the exact mechanisms of the anticancer effect of WGM extracts are not fully understood. In this study, WGM extracts was evaluated for its anticancer activities and exact mechanisms in hepatocellular carcinoma Hep3B cells. Since WGM is a pharmacologically safe natural agent, WGM might be a dietary chemopreventive agent for cancer treatment with an excellent safety profile *in vivo*.

RNA expression profiles produced by NGS technology allow comprehensive investigation of transcribed sequences in distinct cellular states (Wu et al., 2019; Shi et al., 2020). The KEGG pathways database is the comprehensive coverage of a wide range of different biochemical pathways. In general, KEGG pathway enrichment analysis was conducted to identify differential expressed genes (DEGs) into significantly enriched metabolic pathways or signaling pathways. In this study, the KEGG pathway analysis was used to screen the enrichment of dysfunctional signaling pathways of the DEGs in WGM extracts-treated cells. KEGG pathway enrichment analysis showed that the DEGs induced by WGM were found to be involved in organismal systems, metabolism, human diseases, genetic information processing, environmental information processing and cellular process. In the environmental information processing of KEGG pathway analysis, Hippo, mTOR, FoxO, MAPK and TGF-beta signaling pathways were significantly changed. The Hippo signaling pathway is a highly conserved tumor suppressor pathway that exerts a critical role in modulating cell division, cell proliferation and apoptosis. It has been suggested that Hippo signaling pathway is a potent growth and tumor suppressor pathway in the mammalian liver (Lu et al., 2010; Hong et al., 2015). FoxOs (forkhead box class O proteins) are also considered to be tumor suppressors and known to be implicated in the progression of several human cancers (Su et al., 2014; Jiramongkol and Lam, 2020). The mTOR and MAPK signaling pathways are necessary to promote growth and proliferation in many cancer cell types. PI3K/Akt/mTOR and MAPK signaling pathways had been demonstrated to be involve in cell proliferation, motility, survival and apoptosis of cancer cells (Chen, 2010; Ma et al., 2013; Zhang et al., 2016). Recently, PI3K/Akt/mTOR and Ras/Raf/MEK/ERK signaling pathways have also been recognized as a new strategy for cancer therapy (Asati et al., 2016). Therefore, we focused our attention on the investigation of the effects of WGM extracts on the expression of mTOR and MAPK signaling pathways in Hep3B cells in this study.

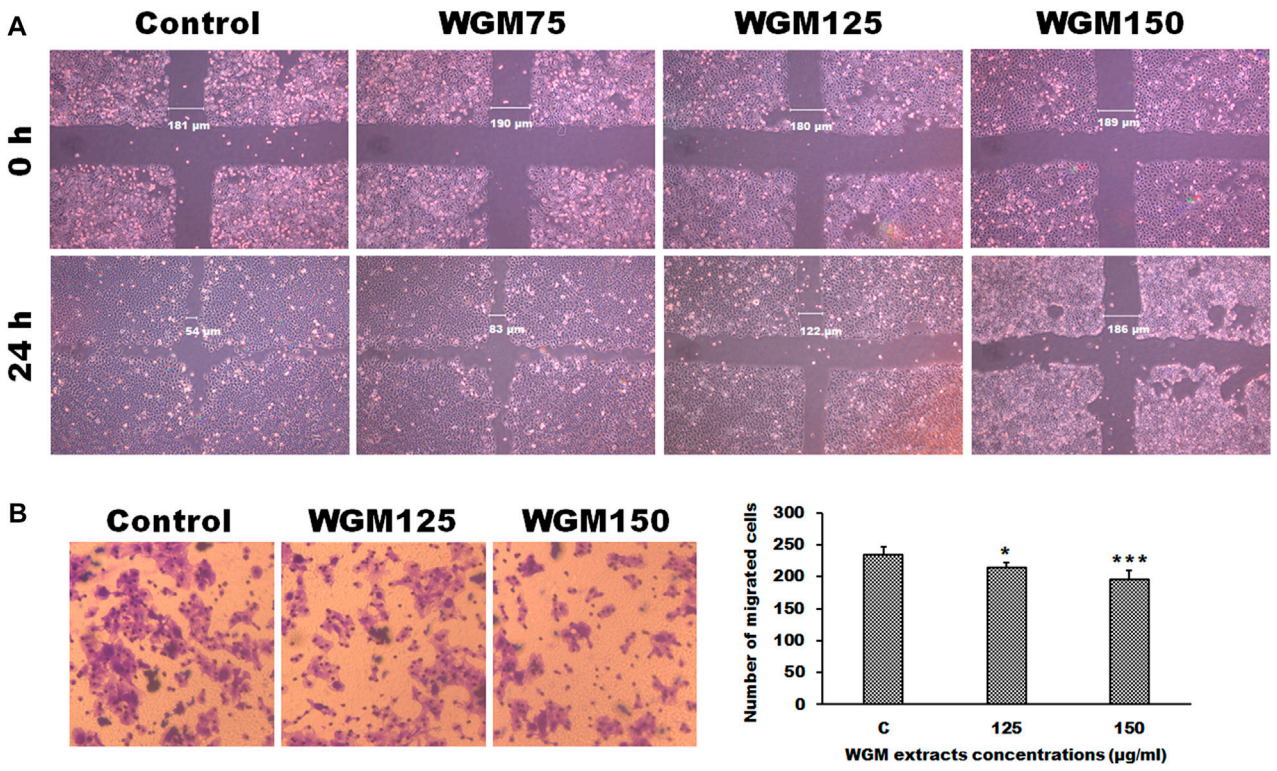

FIGURE 9
The effect of WGM extracts on cell migration of Hep3B cells. **(A)** The migratory activity of Hep3B cells was assessed using a wounded migration assay. A linear wound was made with a sterile 200 μl pipette tip. Cells were treated with vehicle alone (Control) or with 75, 125 or 150 μg/ml WGM extracts for 24 h. Images of wounds at 0 h and 24 h after scratching were obtained with an Olympus IX 73 phase-contrast microscope at objective ×10 magnification. All results are representative of three independent experiments. **(B)** The effects of WGM extracts on cell migration of Hep3B cells were also measured by Transwell assay in the study. Cell migration was also detected using Transwell assay with a pore size of 8 μm the Transwell inserts for 24-well plates. Cells were treated with vehicle alone or with 125 or 150 μg/ml WGM extracts for 24 h. Filters were fixed with 4% paraformaldehyde solution for 20 min and stained with 0.1% crystal violet for 10 min, then the cells that passed through the filter were photographed by Olympus IX 73 phase-contrast microscope at objective ×20 magnification. Left: Representative images of Transwell migration assay. Right: Cells were counted from 4 random microscope fields for each sample in three independent experiments. Results are expressed as the mean ± S.D. $*p < 0.05$, $***p < 0.001$ compared to the control values.

This study demonstrated that PI3K/Akt/mTOR signaling pathway was involved in the WGM extracts-induced cell death in Hep3B cells according to the results of the Western blotting analysis. Wu et al. (2010) demonstrated that PI3K inhibitor 3-MA can block autophagosome formation by inhibiting PI3K, thereby inhibiting autophagy. However, 3-MA did not recover the membrane-enclosed vacuoles and cell death induced by WGM extracts in our previous study (Li et al., 2022). In this study, we demonstrated that Akt inhibitor MK2206 was only slightly restore the cell death induced by WGM extracts. MK2206 had a significant preventive effect, however, on the WGM extracts-induced membrane-enclosed vacuoles of Hep3B cells. Furthermore, pretreatment with the mTOR inhibitor rapamycin abolished the WGM extracts-induced cell death and membrane-enclosed vacuoles of Hep3B cells in this study. It is interesting to note that MK2206 did not have as much effect on the WGM extracts-induced cell death as rapamycin did. In addition to 3-MA, we demonstrated that the inhibitors of PI3K/Akt/mTOR signaling pathway are able to prevent the WGM-induced vacuoles formation and cell death, indicating PI3K/Akt/mTOR signaling pathway is an important intracellular signaling pathway in the WGM extracts-induced cell death. In this study, the Akt and mTOR inhibitor can reverse the WGM extracts-mediated Hep3B cell death of Hep3B cells which are consistent with those of other studies reporting that the dependence of PI3K/Akt/mTOR signaling on the growth and survival of certain tumors has broad implications in cancer therapy (Guertin and Sabatini, 2007; Fasolo and Sessa, 2008; Zhou et al., 2011; Hassan et al., 2013). It is worthy of note that mTOR inhibitor is significantly more effective in preventing the membrane-enclosed vacuoles formation and cell death induced by WGM extracts than PI3K or Akt inhibitors.

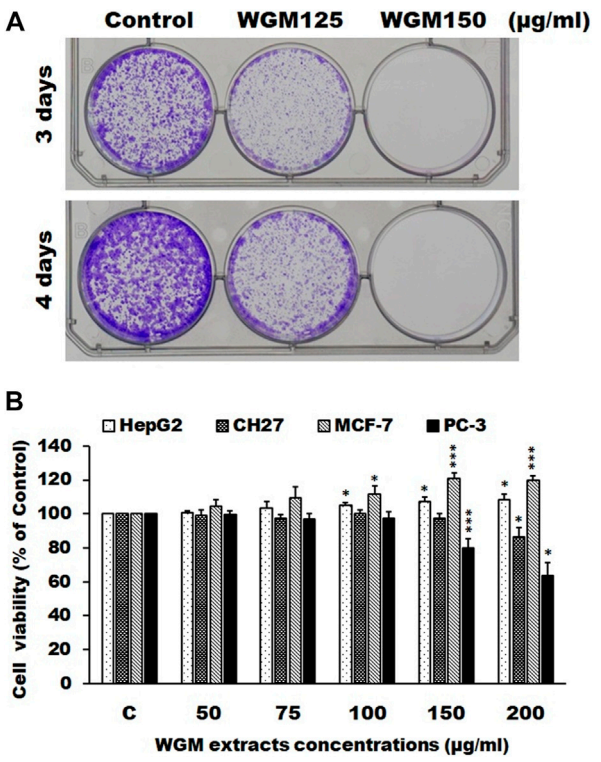

FIGURE 10
(A) WGM extracts inhibits colony forming ability of Hep3B cells in a dose- and time-dependent manner. Representative images of Hep3B colonies after treatment with 125 or 150 μg/ml of WGM extracts. Colonies were fixed with 4% paraformaldehyde solution and then stained with 0.5% crystal violet. Finally, the colonies were photographed. All results are representative of three independent experiments. **(B)** Cytotoxic effects of WGM extracts on HepG2, CH27, MCF-7 and PC-3 cells. HepG2, CH27, MCF-7 and PC-3 cells were incubated with vehicle alone or with various concentrations of WGM extracts for 24 h. After treatment, the viable cells were measured by MTT assay. The data are expressed as the mean % control ±S.D. of three independent experiments performed in duplicate. $*p < 0.05$, $***p < 0.001$ compared to the control values.

In this study, we demonstrated that mTOR inhibitor rapamycin actually reversed WGM-induced cell death and vacuole formation. However, rapamycin is also a well-known autophagy inducer, which activates autophagy by repressing the mechanistic target of mTOR which is associated with lysosomal biogenesis and autophagosome-lysosome fusion (Huang et al., 2021). This study also investigated whether chloroquine could inhibit the induction of cell death and vacuole formation induced by WGM of Hep3B cells. Chloroquine, which is lysosomotropic agent, is a classic inhibitor of autophagy that blocks autophagic processes by inhibiting the binding of autophagosomes to lysosomes (Mushtaque and Shahjahan, 2015). Furthermore, lysosomotropic agents are one of the triggers for cytoplasmic vacuolation caused by lysosomal dysfunction (Zou et al., 2020). The present study showed that chloroquine had a significant preventive effect on the WGM extracts-induced cell death of Hep3B cells. It is interesting to note that both the autophagy inducer rapamycin and the autophagy inhibitor chloroquine prevented WGM-induced membrane-enclosed vacuoles and cell death in Hep3B cells. We also demonstrated that chloroquine was more effective than rapamycin in preventing WGM extract-induced cell death, however the prevention of vacuole formation had the opposite effect. According to the results of immunoblotting, WGM extracts induced a marked increase in the expression of the mTOR protein. It indicated that WGM might attempt to inhibit autophagy process by activating mTOR protein expression. Therefore, we guessed that rapamycin may inhibit WGM-induced cell death through induction autophagy, which is essential for maintaining cell survival. While autophagy is considered as cell survival mechanism, the occurrence of autophagy is also thought to promote apoptosis and even accelerate cell death (Gump and Thorburn, 2011; Rubinstein et al., 2011; Mukhopadhyay et al., 2014; Wei et al., 2014). Since chloroquine prevents WGM extract-induced cell death more efficiently than rapamycin, we further confirmed that Hep3B cells should attempt to survive by inducing autophagy during WGM extracts-induced death cells in this study.

The most important pathway interacting with PI3K/Akt in different types of cancers is the Ras/Raf/ERK pathway (Castellano and Downward, 2011). MAPK signaling pathway signaling pathway was found to be a crucial intracellular signaling pathway, which is closely related to proliferation, apoptosis and metastasis of cancer cells (You et al., 2011; Guo et al., 2016). According to the results of immunoblotting, WGM extracts induced a marked dose-dependent decrease in the expression of the ERK protein, and an upregulation of the Ras, Raf and MEK protein in this study. The expression patterns of pERK protein are similar to those seen in Akt and pAkt expression after treatment with WGM extracts for 24 h in this study. There is abundant evidence that PI3K/Akt has surprisingly extensive cross talk with ERK1/2 (Yang et al., 2019; Duff et al., 2021). Furthermore, PI3K/Akt and ERK1/2 pathways are downstream of EGF-EGFR signaling in many cell types (Zhang et al., 2012; Fan et al., 2015; Li et al., 2019). We also demonstrated that treatment with WGM extracts increased pERK protein in Hep3B cells up to 125 μg/ml, but pERK level was decreased after treatment with 175 μg/ml WGM extracts. It is interesting to note that WGM extracts induced a significant increase in the protein expression of Ras in cells exposed to 175 μg/ml WGM extracts for 24 h. These results indicate that WGM extracts-mediated ERK activation occurs through a Ras-independent pathway. It had also been reported that the crosstalk between ERK and Akt is mediated

by EGFR and independent of Ras or Raf mutation (Klinger et al., 2013). In addition to the ERK, p38 is also an important intracellular signaling pathway in the MAPK signaling pathway. In our study, not only the expression of ERK, which is associated with cell proliferation, but also p38, which is regulated by various environmental stresses, is regulated by WGM extracts. As shown by immunoblotting, WGM extracts caused a marked increase in the protein levels of pp38, but p38 levels decrease in Hep3B cells. According to the results of immunoblotting, the ERK inhibitor LY3214996 and p38 inhibitor SB202190 were used in this study. The present study showed that both inhibitors partially abolished the WGM extracts-induced cell death and membrane-enclosed vacuoles of Hep3B cells. It indicate that WGM extracts-mediated the activation of ERK and p38 is involved in the WGM extracts-induced membrane-enclosed vacuoles and even cell death. Based on the above data, we also demonstrated that MAPK pathway is an important intracellular signaling pathway in the WGM extracts-induced cell death.

Our previous study indicated that only (2*E*,6*E*)-3,7,11,15,19,23,27,31,35-non-amethylhexatriaconta-2,6,34-triene-1,11,15,19,23,27,31-heptol and (18:2) lysophosphatidylcholine (lysoPC) were identified in the WGM alcoholic extracts using UPLC-MS/MS analyses, MS data processing and Molecular networking–GNPS (http://gnps.ucsd.edu) (Li et al., 2022). (2*E*,6*E*)-3,7,11,15,19,23,27,31,35-non-amethylhexatriaconta-2,6,34-triene-1,11,15,19,23,27,31-heptol has been considered to be an inhibitor of the NK-1 (neurokinin-1) and NK-2 (neurokinin-2) receptors (Hegde et al., 1997). Recently, the NK-1 receptor (NK1R) was demonstrated to be involved in the development of the various cancer cells (Muñoz and Coveñas, 2014; Ebrahimi et al., 2020; Isorna et al., 2020). It has also been suggested that NK1R is overexpressed in human liver cancer and can significantly inhibit the proliferation of cancer cells by antagonizing the expression of NK1R (Garnier et al., 2016; Muñoz et al., 2019). All these reports suggest that NK-1R plays an important role in regulation cancer cell proliferation, apoptosis and migration for invasion or metastasis. Furthermore, PI3K/Akt/mTOR and MAPK signaling pathways was demonstrated to have a crucial role in the cell growth inhibition and apoptosis exerted by NK-1R antagonists (Castagliuolo et al., 2000; Garnier et al., 2016; Shi et al., 2021). In general, the cancer cell proliferation, motility, survival and apoptosis associated with PI3K/Akt/mTOR and MAPK signaling pathways have been well documented. Therefore, we guessed that WGM extracts might regulate PI3K/Akt/mTOR and MAPK signaling pathways and induce apoptosis and migration through blocking NK-1R in Hep3B cells.

Migration and invasion are important factors that accelerate the occurrence and progression of malignant tumors. Many cellular signaling pathways are thought to be involved in the proliferation and migration of cancer cells (Guo et al., 2016; Luo et al., 2016; Yang et al., 2016). PI3K/Akt and MAPK signaling pathways have been reported to be important signaling pathways involved in the network regulation on cell migration in many different kinds of cancer (Guo et al., 2016; Luo et al., 2016; Yang et al., 2016). According to the results of immunoblotting and experiments of inhibitors, this study examined whether WGM extracts will yield an inhibitory effect on cell migration of Hep3B cells. To obtain further support for the inhibition of cell migration by WGM extracts in Hep3B cells, the transwell migration and wound healing assays, which are used to examine the migratory response of cancer cells to treatments, were performed in this study. The results from those assays showed that WGM extracts had a significant inhibition of the Hep3B cell migration ability in a dose-dependent manner. Colony formation assay was used to mimic cancer growth from a single cell to grow into a cancer cell colonies or tumor mass. Plate colony formation assay was used to examine the effect of WGM extracts on the colony-forming ability of Hep3B cells. We demonstrated that WGM extracts had a significant inhibitory effect on the colony forming ability of Hep3B cells in a concentration- and time-dependent manner. Based on the above data, we suggest that PI3K/Akt/mTOR and MAPK signaling pathways be involved in the WGM extracts-mediated inhibition of cell colony formation and migration of Hep3B cells. It is worthy to note that WGM extracts selectively induced cytotoxicity in different cancer cell lines. We demonstrated that the cytotoxic effect of WGM extracts on Hep3B cells was significantly higher than that in prostate cancer PC-3 cells, liver cancer HepG2, lung cancer CH27 and breast cancer MCF-7 cells.

Conclusion

According to the KEGG pathway enrichment analysis, the results of immunoblotting and experiments of inhibitors, we demonstrated that PI3K/Akt/mTOR and MAPK signaling pathways were involved in WGM extracts-induced vacuoles formation and cell death. Our results are the first findings to indicate that WGM extracts induces cell death in Hep3B cancer cells and that the induction of vacuoles formation and cell death coincides with the PI3K/Akt/mTOR and MAPK signaling pathways. This study also demonstrated that WGM extracts had a significant inhibition of the Hep3B cell colony formation and migration ability in a dose-dependent manner. The present findings indicate that WGM should be a pharmacologically safe natural agent and might be a dietary chemopreventive agent for the cancer treatment.

Data availability statement

The raw data supporting the conclusions of this article will be made available by the authors, without undue reservation. The RNA sequencing raw data was uploaded to NCBI Sequence Read Archive (SRA), and the accession ID is PRJNA813700.

Author contributions

H-ZL designed this study; L-YC, K-TL, W-SL, and H-ZL performed the experiments; L-YC, K-TL, W-SL, and H-ZL analyzed data; L-YC, K-TL, W-SL, and H-ZL wrote the manuscript. All authors approved the submission of the manuscript.

Funding

This work was supported by the Ministry of Science and Technology Grant of Republic of China [MOST 107-2320-B-039-009-MY3, MOST 107-2813-C-039-285-B, and MOST 109-2813-C-039-036-B] and the China Medical University Grant of the Republic of China [CMU 109-MF-101 and CMU 109-SR-31].

Conflict of interest

The authors declare that the research was conducted in the absence of any commercial or financial relationships that could be construed as a potential conflict of interest.

Publisher's note

All claims expressed in this article are solely those of the authors and do not necessarily represent those of their affiliated organizations, or those of the publisher, the editors and the reviewers. Any product that may be evaluated in this article, or claim that may be made by its manufacturer, is not guaranteed or endorsed by the publisher.

Supplementary material

The Supplementary Material for this article can be found online at: https://www.frontiersin.org/articles/10.3389/fphar.2022.1039376/full#supplementary-material

References

Asati, V., Mahapatra, D. K., and Bharti, S. K. (2016). PI3K/Akt/mTOR and Ras/Raf/MEK/ERK signaling pathways inhibitors as anticancer agents: Structural and pharmacological perspectives. *Eur. J. Med. Chem.* 109, 314–341. doi:10.1016/j.ejmech.2016.01.012

Bao, H., and You, S. (2011). Molecular characteristics of water-soluble extracts from *Hypsizigus marmoreus* and their *in vitro* growth inhibition of various cancer cell lines and immunomodulatory function in Raw 264.7 cells. *Biosci. Biotechnol. Biochem.* 75, 891–898. doi:10.1271/bbb.100825

Castagliuolo, I., Valenick, L., Liu, J., and Pothoulakis, C. (2000). Epidermal growth factor receptor transactivation mediates substance P-induced mitogenic responses in U-373 MG cells. *J. Biol. Chem.* 275, 26545–26550. doi:10.1074/jbc.M003990200

Castellano, E., and Downward, J. (2011). RAS interaction with PI3K: More than just another effector pathway. *Genes Cancer* 2, 261–274. doi:10.1177/1947601911408079

Chen, J. (2010). The Src/PI3K/Akt signal pathway may play a key role in decreased drug efficacy in obesity-associated cancer. *J. Cell. Biochem.* 110, 279–280. doi:10.1002/jcb.22572

Duff, A., Kavege, L., Baquier, J., and Hu, T. (2021). A PI3K inhibitor-induced growth inhibition of cancer cells is linked to MEK-ERK pathway. *Anticancer. Drugs* 32, 517–525. doi:10.1097/CAD.0000000000001024

Ebrahimi, S., Javid, H., Alaei, A., and Hashemy, S. I. (2020). New insight into the role of substance P/neurokinin-1 receptor system in breast cancer progression and its crosstalk with microRNAs. *Clin. Genet.* 98, 322–330. doi:10.1111/cge.13750

Engelman, J. A., Luo, J., and Cantley, L. C. (2006). The evolution of phosphatidylinositol 3-kinases as regulators of growth and metabolism. *Nat. Rev. Genet.* 7, 606–619. doi:10.1038/nrg1879

Fan, J. B., Liu, W., Zhu, X. H., Yuan, K., Xu, D. W., Chen, J. J., et al. (2015). EGFR-AKT-mTOR activation mediates epiregulin-induced pleiotropic functions in cultured osteoblasts. *Mol. Cell. Biochem.* 398, 105–113. doi:10.1007/s11010-014-2210-4

Fasolo, A., and Sessa, C. (2008). mTOR inhibitors in the treatment of cancer. *Expert Opin. Investig. Drugs* 17, 1717–1734. doi:10.1517/13543784.17.11.1717

Garnier, A., Ilmer, M., Kappler, R., and Berger, M. (2016). Therapeutic innovations for targeting hepatoblastoma. *Anticancer Res.* 36, 5577–5592. doi:10.21873/anticanres.11143

Guertin, D. A., and Sabatini, D. M. (2007). Defining the role of mTOR in cancer. *Cancer Cell* 12, 9–22. doi:10.1016/j.ccr.2007.05.008

Gump, J. M., and Thorburn, A. (2011). Autophagy and apoptosis: What is the connection? *Trends Cell Biol.* 21, 387–392. doi:10.1016/j.tcb.2011.03.007

Guo, J. R., Li, W., Wu, Y., Wu, L. Q., Li, X., Guo, Y. F., et al. (2016). Hepatocyte growth factor promotes proliferation, invasion, and metastasis of myeloid leukemia cells through PI3K-AKT and MAPK/ERK signaling pathway. *Am. J. Transl. Res.* 8, 3630–3644. eCollection 2016.

Hassan, B., Akcakanat, A., Holder, A. M., and Meric-Bernstam, F. (2013). Targeting the PI3-kinase/Akt/mTOR signaling pathway. *Surg. Oncol. Clin. N. Am.* 22, 641–664. doi:10.1016/j.soc.2013.06.008

Hegde, V. R., Dai, P., Chu, M., Patel, M., Bryant, R., Terracciano, J., et al. (1997). Neurokinin receptor inhibitors: Fermentation, isolation, physico-chemical properties, structure and biological activity. *J. Antibiot. (Tokyo)* 50, 983–991. doi:10.7164/antibiotics.50.983

Hennessy, B. T., Smith, D. L., Ram, P. T., Lu, Y., and Mills, G. B. (2005). Exploiting the PI3K/AKT pathway for cancer drug discovery. *Nat. Rev. Drug Discov.* 4, 988–1004. doi:10.1038/nrd1902

Hong, L., Cai, Y., Jiang, M., Zhou, D., and Chen, L. (2015). The Hippo signaling pathway in liver regeneration and tumorigenesis. *Acta Biochim. Biophys. Sin.* 47, 46–52. doi:10.1093/abbs/gmu106

Hsu, S. C., Ou, C. C., Li, J. W., Chuang, T. C., Kuo, H. P., Liu, J. Y., et al. (2008). *Ganoderma tsugae* extracts inhibit colorectal cancer cell growth via G(2)/M cell cycle arrest. *J. Ethnopharmacol.* 120, 394–401. doi:10.1016/j.jep.2008.09.025

Hu, H., Ahn, N. S., Yang, X., Lee, Y. S., and Kang, K. S. (2002). *Ganoderma lucidum* extract induces cell cycle arrest and apoptosis in MCF-7 human breast cancer cell. *Int. J. Cancer* 102, 250–253. doi:10.1002/ijc.10707

Huang, H., Ouyang, Q., Zhu, M., Yu, H., Mei, K., and Liu, R. (2021). mTOR-mediated phosphorylation of VAMP8 and SCFD1 regulates autophagosome maturation. *Nat. Commun.* 12, 6622. doi:10.1038/s41467-021-26824-5

Isorna, I., Esteban, F., Solanellas, J., Coveñas, R., and Muñoz, M. (2020). The substance P and neurokinin-1 receptor system in human thyroid cancer: An immunohistochemical study. *Eur. J. Histochem.* 64, 3117. doi:10.4081/ejh.2020.3117

Jiramongkol, Y., and Lam, E. W. (2020). FOXO transcription factor family in cancer and metastasis. *Cancer Metastasis Rev.* 39, 681–709. doi:10.1007/s10555-020-09883-w

Kanehisa, M., and Goto, S. (2000). KEGG: Kyoto encyclopedia of genes and genomes. *Nucleic Acids Res.* 28, 27–30. doi:10.1093/nar/28.1.27

Katso, R., Okkenhaug, K., Ahmadi, K., White, S., Timms, J., and Waterfield, M. D. (2001). Cellular function of phosphoinositide 3-kinases: Implications for development, homeostasis, and cancer. *Annu. Rev. Cell Dev. Biol.* 17, 615–675. doi:10.1146/annurev.cellbio.17.1.615

Kim, S. P., Kang, M. Y., Kim, J. H., Nam, S. H., and Friedman, M. (2011). Composition and mechanism of antitumor effects of *Hericium erinaceus* mushroom extracts in tumor-bearing mice. *J. Agric. Food Chem.* 59, 9861–9869. doi:10.1021/jf201944n

Klinger, B., Sieber, A., Fritsche-Guenther, R., Witzel, F., Berry, L., Schumacher, D., et al. (2013). Network quantification of EGFR signaling unveils potential for targeted combination therapy. *Mol. Syst. Biol.* 9, 673. doi:10.1038/msb.2013.29

Kwak, A. M., Min, K. J., Lee, S. Y., and Kang, H. W. (2015). Water extract from spent mushroom substrate of *Hericium erinaceus* suppresses bacterial wilt disease of tomato. *Mycobiology* 43, 311–318. doi:10.5941/MYCO.2015.43.3.311

Lee, H. Z., Liu, W. Z., Hsieh, W. T., Tang, F. Y., Chung, J. G., and Leung, H. W. (2009). Oxidative stress involvement in *Physalis angulata*-induced apoptosis in human oral cancer cells. *Food Chem. Toxicol.* 47, 561–570. doi:10.1016/j.fct.2008.12.013

Li, K., Hong, S., Lin, S., and Chen, K. (2020). Genistein inhibits the proliferation, migration and invasion of the squamous cell carcinoma cells *via* inhibition of MEK/ERK and JNK signalling pathways. *J. BUON.* 25, 1172–1177.

Li, L., Fan, P., Chou, H., Li, J., Wang, K., and Li, H. (2019). Herbacetin suppressed MMP9 mediated angiogenesis of malignant melanoma through blocking EGFR-ERK/AKT signaling pathway. *Biochimie* 162, 198–207. doi:10.1016/j.biochi.2019.05.003

Li, W. S., Lee, K. D., Chen, L. Y., You, B. J., and Lee, H. Z. (2022). Identification of key pathways involved in white strain of *Hypsizygus marmoreus* extracts-induced cell death of human hepatoma Hep3B cells by next generation sequencing. *Front. Pharmacol.* 13, 888863. doi:10.3389/fphar.2022.888863

Liao, J. C., Lee, K. T., You, B. J., Lee, C. L., Chang, W. T., Wu, Y. C., et al. (2015). Raf/ERK/Nrf2 signaling pathway and MMP-7 expression involvement in the trigonelline-mediated inhibition of hepatocarcinoma cell migration. *Food Nutr. Res.* 59, 29884. doi:10.3402/fnr.v59.29884

Liu, F., Yang, X., Geng, M., and Huang, M. (2018). Targeting ERK, an Achilles' Heel of the MAPK pathway, in cancer therapy. *Acta Pharm. Sin. B* 8, 552–562. doi:10.1016/j.apsb.2018.01.008

Liu, Y., Guyton, K. Z., Gorospe, M., Xu, Q., Lee, J. C., and Holbrook, N. J. (1996). Differential activation of ERK, JNK/SAPK and P38/CSBP/RK map kinase family members during the cellular response to arsenite. *Free Radic. Biol. Med.* 21, 771–781. doi:10.1016/0891-5849(96)00176-1

Lu, L., Li, Y., Kim, S. M., Bossuyt, W., Liu, P., Qiu, Q., et al. (2010). Hippo signaling is a potent *in vivo* growth and tumor suppressor pathway in the mammalian liver. *Proc. Natl. Acad. Sci. U. S. A.* 107, 1437–1442. doi:10.1073/pnas.0911427107

Luo, Y., Wu, J. Y., Lu, M. H., Shi, Z., Na, N., and Di, J. M. (2016). Carvacrol alleviates prostate cancer cell proliferation, migration, and invasion through regulation of PI3K/Akt and MAPK signaling pathways. *Oxid. Med. Cell. Longev.* 2016, 1469693. doi:10.1155/2016/1469693

Ma, Y., Qin, H., and Cui, Y. (2013). MiR-34a targets GAS1 to promote cell proliferation and inhibit apoptosis in papillary thyroid carcinoma via PI3K/Akt/Bad pathway. *Biochem. Biophys. Res. Commun.* 441, 958–963. doi:10.1016/j.bbrc.2013.11.010

Mandal, M., Kim, S., Younes, M. N., Jasser, S. A., El-Naggar, A. K., Mills, G. B., et al. (2005). The Akt inhibitor KP372-1 suppresses Akt activity and cell proliferation and induces apoptosis in thyroid cancer cells. *Br. J. Cancer* 92, 1899–1905. doi:10.1038/sj.bjc.6602595

Martini, M., De Santis, M. C., Braccini, L., Gulluni, F., and Hirsch, E. (2014). PI3K/AKT signaling pathway and cancer: An updated review. *Ann. Med.* 46, 372–383. doi:10.3109/07853890.2014.912836

Mukhopadhyay, S., Panda, P. K., Sinha, N., Das, D. N., and Bhutia, S. K. (2014). Autophagy and apoptosis: Where do they meet? *Apoptosis* 19, 555–566. doi:10.1007/s10495-014-0967-2

Muñoz, M., and Coveñas, R. (2014). Involvement of substance P and the NK-1 receptor in pancreatic cancer. *World J. Gastroenterol.* 20, 2321–2334. doi:10.3748/wjg.v20.i9.2321

Muñoz, M., Rosso, M., and Coveñas, R. (2019). Neurokinin-1 receptor antagonists against hepatoblastoma. *Cancers (Basel)* 11, 1258. doi:10.3390/cancers11091258

Mushtaque, M., and Shahjahan (2015). Reemergence of chloroquine (CQ) analogs as multi-targeting antimalarial agents: A review. *Eur. J. Med. Chem.* 90, 280–295. doi:10.1016/j.ejmech.2014.11.022

Raingeaud, J., Gupta, S., Rogers, J. S., Dickens, M., Han, J., Ulevitch, R. J., et al. (1995). Pro-inflammatory cytokines and environmental stress cause p38 mitogen-activated protein kinase activation by dual phosphorylation on tyrosine and threonine. *J. Biol. Chem.* 270, 7420–7426. doi:10.1074/jbc.270.13.7420

Roberts, P. J., and Der, C. J. (2007). Targeting the Raf-MEK-ERK mitogen-activated protein kinase cascade for the treatment of cancer. *Oncogene* 26, 3291–3310. doi:10.1038/sj.onc.1210422

Rubinstein, A. D., Eisenstein, M., Ber, Y., Bialik, S., and Kimchi, A. (2011). The autophagy protein Atg12 associates with antiapoptotic Bcl-2 family members to promote mitochondrial apoptosis. *Mol. Cell* 44, 698–709. doi:10.1016/j.molcel.2011.10.014

Shi, D., Xin, J., Lu, Y., Ding, W., Jiang, J., Zhou, Q., et al. (2020). Transcriptome profiling reveals distinct phenotype of human bone marrow mesenchymal stem cell-derived hepatocyte-like cells. *Int. J. Med. Sci.* 17, 263–273. doi:10.7150/ijms.36255

Shi, Y., Wang, X., Meng, Y., Ma, J., Zhang, Q., Shao, G., et al. (2021). A novel mechanism of endoplasmic reticulum stress- and c-myc-degradation-mediated therapeutic benefits of antineurokinin-1 receptor drugs in colorectal cancer. *Adv. Sci.* 8, 2101936. doi:10.1002/advs.202101936

Stanley, G., Harvey, K., Slivova, V., Jiang, J., and Sliva, D. (2005). *Ganoderma lucidum* suppresses angiogenesis through the inhibition of secretion of VEGF and TGF-beta1 from prostate cancer cells. *Biochem. Biophys. Res. Commun.* 330, 46–52. doi:10.1016/j.bbrc.2005.02.116

Su, L., Liu, X., Chai, N., Lv, L., Wang, R., Li, X., et al. (2014). The transcription factor FOXO4 is down-regulated and inhibits tumor proliferation and metastasis in gastric cancer. *BMC Cancer* 14, 378. doi:10.1186/1471-2407-14-378

Sun, Y., Liu, W. Z., Liu, T., Feng, X., Yang, N., and Zhou, H. F. (2015). Signaling pathway of MAPK/ERK in cell proliferation, differentiation, migration, senescence and apoptosis. *J. Recept. Signal Transduct. Res.* 35, 600–604. doi:10.3109/10799893.2015.1030412

Wei, M. F., Chen, M. W., Chen, K. C., Lou, P. J., Lin, S. Y., Hung, S. C., et al. (2014). Autophagy promotes resistance to photodynamic therapy-induced apoptosis selectively in colorectal cancer stem-like cells. *Autophagy* 10, 1179–1192. doi:10.4161/auto.28679

Wu, H., Chen, L., Zhu, F., Han, X., Sun, L., and Chen, K. (2019). The cytotoxicity effect of resveratrol: Cell cycle arrest and induced apoptosis of breast cancer 4T1 cells. *Toxins (Basel)* 11, 731. doi:10.3390/toxins11120731

Wu, Y. T., Tan, H. L., Shui, G., Bauvy, C., Huang, Q., Wenk, M. R., et al. (2010). Dual role of 3-methyladenine in modulation of autophagy via different temporal patterns of inhibition on class I and III phosphoinositide 3-kinase. *J. Biol. Chem.* 285, 10850–10861. doi:10.1074/jbc.M109.080796

Yang, J., Nie, J., Ma, X., Wei, Y., Peng, Y., and Wei, X. (2019). Targeting PI3K in cancer: Mechanisms and advances in clinical trials. *Mol. Cancer* 18, 26. doi:10.1186/s12943-019-0954-x

Yang, Y., Ye, Y., Qiu, Q., Xiao, Y., Huang, M., Shi, M., et al. (2016). Triptolide inhibits the migration and invasion of rheumatoid fibroblast-like synoviocytes by blocking the activation of the JNK MAPK pathway. *Int. Immunopharmacol.* 41, 8–16. doi:10.1016/j.intimp.2016.10.005

You, B. J., Wu, Y. C., Wu, C. Y., Bao, B. Y., Chen, M. Y., Chang, Y. H., et al. (2011). Proteomics displays cytoskeletal proteins and chaperones involvement in Hedyotis corymbosa-induced photokilling in skin cancer cells. *Exp. Dermatol.* 20, 653–658. doi:10.1111/j.1600-0625.2011.01290.x

Zhang, Y., Bao, C., Mu, Q., Chen, J., Wang, J., Mi, Y., et al. (2016). Reversal of cisplatin resistance by inhibiting PI3K/Akt signal pathway in human lung cancer cells. *Neoplasma* 63, 362–370. doi:10.4149/304_150806N433

Zhang, Y., Wang, L., Zhang, M., Jin, M., Bai, C., and Wang, X. (2012). Potential mechanism of interleukin-8 production from lung cancer cells: An involvement of EGF-EGFR-PI3K-Akt-Erk pathway. *J. Cell. Physiol.* 227, 35–43. doi:10.1002/jcp.22722

Zhou, Q., Lui, V. W., and Yeo, W. (2011). Targeting the PI3K/Akt/mTOR pathway in hepatocellular carcinoma. *Future Oncol.* 7, 1149–1167. doi:10.2217/fon.11.95

Zou, X., Meng, F., Fu, C., Zhou, J., Zhang, Y., Wang, R., et al. (2020). LZ-106, a potent lysosomotropic agent, causing TFEB-dependent cytoplasmic vacuolization. *Gene* 760, 145017. doi:10.1016/j.gene.2020.145017

frontiers | Frontiers in Pharmacology

TYPE Case Report
PUBLISHED 28 November 2022
DOI 10.3389/fphar.2022.1037646

OPEN ACCESS

EDITED BY
Husain Yar Khan,
Wayne State University School of Medicine, United States

REVIEWED BY
Melania Rivano,
R. Binaghi Hospit, Italy
Alessandro Rizzo,
National Cancer Institute Foundation (IRCCS), Italy

*CORRESPONDENCE
Xianze Xiong,
xianzexiong123@163.com
Hongfeng Gou,
gouhongfeng1977@wchscu.cn

†These authors have contributed equally to this work and share first authorship

SPECIALTY SECTION
This article was submitted to Pharmacology of Anti-Cancer Drugs, a section of the journal Frontiers in Pharmacology

RECEIVED 06 September 2022
ACCEPTED 14 November 2022
PUBLISHED 28 November 2022

CITATION
Tan S, Yu J, Huang Q, Zhou N, Xiong X and Gou H (2022), Durable response to the combination of pembrolizumab and nab-paclitaxel in a metastatic extrahepatic cholangiocarcinoma: A case report and literature review. *Front. Pharmacol.* 13:1037646. doi: 10.3389/fphar.2022.1037646

Durable response to the combination of pembrolizumab and nab-paclitaxel in a metastatic extrahepatic cholangiocarcinoma: A case report and literature review

Sirui Tan[1†], Jing Yu[1†], Qiyue Huang[1], Nan Zhou[1], Xianze Xiong[2*] and Hongfeng Gou[1*]

[1]Department of Medical Oncology, Gastric Cancer Center, West China Hospital, Sichuan University, Chengdu, Sichuan, China, [2]Department of Bile Duct Surgery, West China Hospital, Sichuan University, Chengdu, China

Background: Cholangiocarcinoma (CCA) is a highly aggressive malignant tumor with poor overall survival. Although the first-line standard chemotherapy (gemcitabine plus cisplatin) combined with immunotherapy has yielded positive results with survival prolongation, the efficacy remains unsatisfactory, and new treatment modalities need to be explored.

Case presentation: We report the case of a patient with metastatic extrahepatic CCA who achieved a durable response and good tolerance to the combination treatment of pembrolizumab and nab-paclitaxel following progression on gemcitabine plus capecitabine chemotherapy. The tumor samples of the patient revealed low TMB, MSS, negative PD-L1 expression, and negative $CD8^+$ TIL expression. This patient was treated with 3 cycles of pembrolizumab plus nab-paclitaxel and cisplatin, followed by 5 cycles of pembrolizumab plus nab-paclitaxel. Finally, 10 cycles of pembrolizumab monotherapy were administered. The patient survived for over 27 months after the initiation of combined therapy and was still in continuous remission at the last follow-up.

Conclusion: As far as we know, this is the first report that pembrolizumab plus nab-paclitaxel successfully treated a patient with advanced CCA. This combination therapy might be a potential treatment option for patients with cholangiocarcinoma, and further clinical trials are needed to explore the outcomes.

KEYWORDS

cholangiocarcinoma, immunotherapy, nab-paclitaxel, pembrolizumab, tumor microenvironment

Background

Cholangiocarcinoma (CCA) originates from the bile duct cells and accounts for 3% of digestive system tumors (Rizvi and Gores, 2013). Its morbidity and mortality have risen in recent years (Khan et al., 2019). According to anatomical location, Cholangiocarcinoma is categorized as intrahepatic cholangiocarcinoma (iCCA) and extrahepatic cholangiocarcinoma (eCCA). In addition, eCCA can be divided into perihilar CCA (pCCA) and distal CCA (dCCA) (Rizvi and Gores, 2013). Cholangiocarcinoma is highly aggressive, and surgery is still the primary treatment option. However, more than two-thirds of patients are unsuitable for surgery at the initial diagnosis (Jarnagin et al., 2001). Patients who have undergone radical surgery have a high rate of recurrence and metastasis (Jung et al., 2012). The prognosis of metastatic cholangiocarcinoma is extremely poor, with a 5-year overall survival (OS) rate of about 10% (Everhart and Ruhl, 2009; Tyson and El-Serag, 2011).

For patients with advanced cholangiocarcinoma, systemic chemotherapy is the backbone of palliative care, and commonly used agents include gemcitabine, platinum, and fluoropyrimidines. The United Kingdom ABC-02 study established cisplatin and gemcitabine (CisGem) as the reference first-line regimen, with an improved OS (11.7 vs. 8.1 months) compared with gemcitabine monotherapy (Valle et al., 2010). Recently, in a promising single-arm phase II study, the combination of CisGem plus nab-paclitaxel provided a response rate (RR) of 45% and a median OS of 19.2 months in chemotherapy-naïve patients (Shroff et al., 2019). The median OS with first-line reference doublet is less than one year, and the high incidence of adverse effects of intensified triple-agent cannot be ignored. In the second-line setting, the only phase III trial is the ABC-06 study which assessed the benefit of the regimen of mFOLFOX (oxaliplatin, leucovorin, 5-fluorouracil) compared with active symptomatic control in CisGem-refractory patients. Although the median OS of patients receiving mFOLFOX was statistically significant, the OS improvement was modest (6.2 vs. 5.3 months) (Lamarca et al., 2021). The limited survival benefit of current chemotherapy options highlights the need to develop more effective therapeutic options. The molecular heterogeneities in CCA have been identified with the emergence of next-generation sequencing. The patients carrying fibroblast growth factor

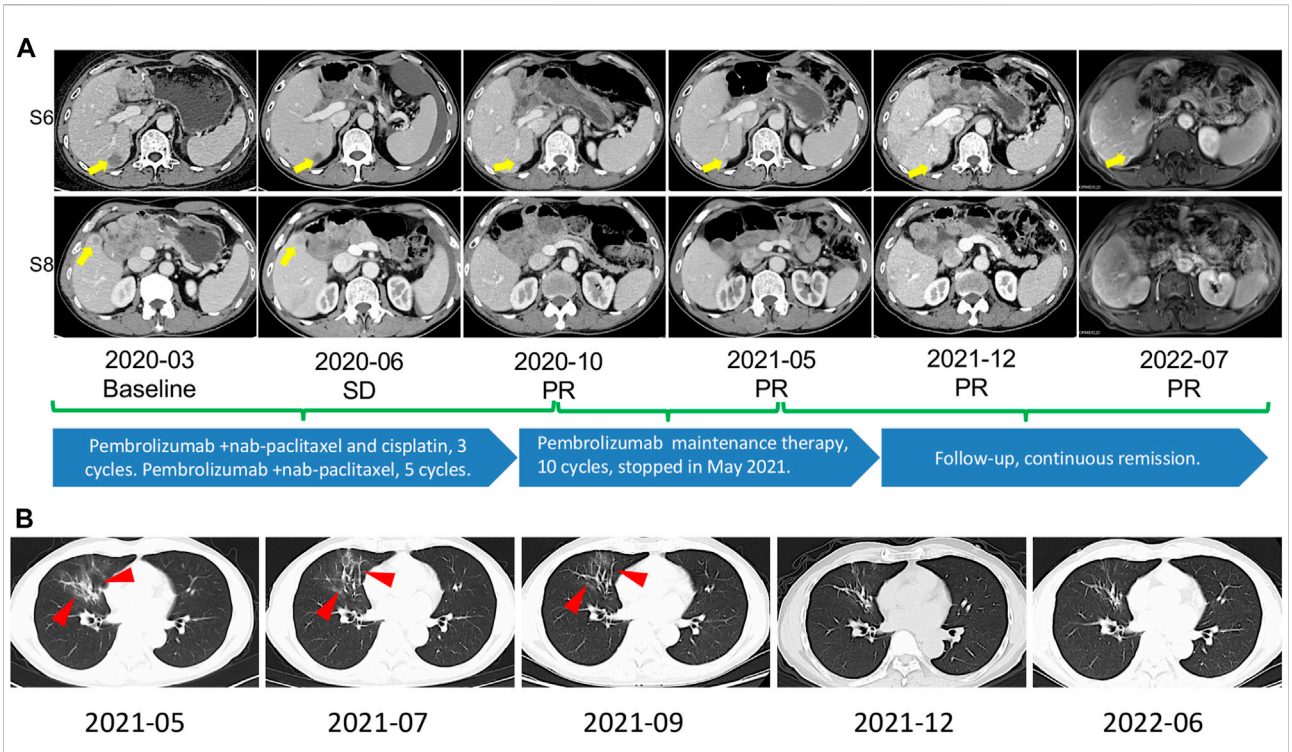

FIGURE 1
(A) The timeline and representative CT and MRI images. CT of March 2020, yellow arrow points toward intrahepatic lesions in S6/S8 at tumor metastasis. CT of June 2020 revealed stable disease was observed after 2 cycles of nab-paclitaxel/cisplatin plus pembrolizumab. CT of October 2020, partial remission was observed after 3 cycles of nab-paclitaxel/cisplatin plus pembrolizumab and 5 cycles of nab-paclitaxel plus pembrolizumab. CT of May 2021, continuous partial remission was observed after 10 cycles of pembrolizumab maintenance therapy. In July 2022, MRI showed durable partial remission. S6, Segment 6; S8, Segment 8; SD, stable disease; PR, partial remission. **(B)** Image changes during prednisolone treatment after the onset of CIP. CIP was significantly relieved, as seen in the images. The red arrow points to the part where CIP occurred. CIP, checkpoint inhibitor pneumonitis.

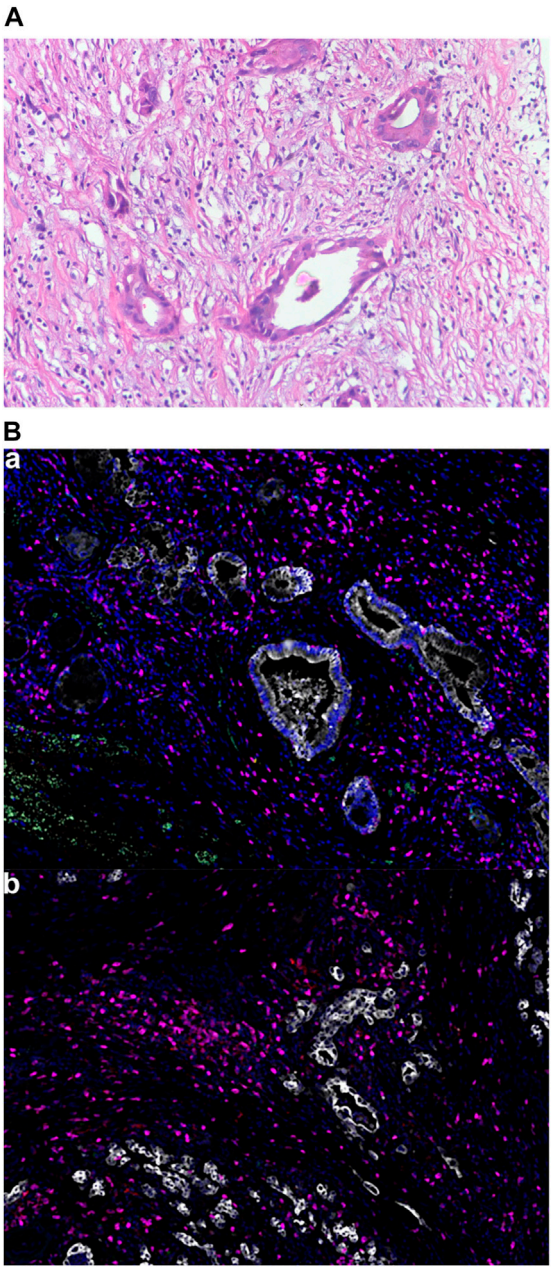

FIGURE 2
Tumor pathological findings. **(A)** Hematoxylin and eosin staining of the patient's tumor. Magnification, x200; **(B)** Multiple immunofluorescence of the TME: (a): Green for PD-1; Yellow for PD-L1; Pink for CD8; Cyan for CD68; Red for CD163. Magnification, x200. (b): Pink for CD3; Red for CD4; Green for CD20; Cyan for CD56; Yellow for FoxP3. Magnification, x200.

receptor 2 (FGFR2) fusion/rearrangement, isocitrate dehydrogenase (IDH) mutation, and neurotrophin receptor tyrosine kinase (NTRK) genes fusion may benefit from the corresponding targeted therapy (Mazzaferro et al., 2019; Abou-Alfa et al., 2020; Bekaii-Saab et al., 2020; Doebele et al., 2020; Lamarca et al., 2020; Rizzo et al., 2021b). However, these actionable molecular alterations usually occur in intrahepatic cholangiocarcinoma (Abou-Alfa et al., 2020; Montal et al., 2020; Rizzo et al., 2020).

In recent years, immune checkpoint inhibitors (ICIs) have shown outstanding efficacy in pan-tumors such as malignant melanoma, lung cancer, urothelial cancer, and liver cancer (Balar et al., 2017; Eggermont et al., 2018; Xu et al., 2018; Mok et al., 2019). The results of early clinical trials of ICIs monotherapy (pembrolizumab, nivolumab, and durvalumab) in unselected patients with biliary tract cancer (BTC) provided limited activity, with response rate (RR) ranging between 3% and 13% (Bang et al., 2019; Ueno et al., 2019; Kim et al., 2020; Rizzo et al., 2021a). A number of different ICIs combinations are under investigation, and the combination of ICIs and chemotherapy (chemoimmunotherapy) has shown promising anti-tumor efficacy. Notably, data from the placebo-controlled, phase III TOPAZ-1 trial demonstrated that durvalumab plus CisGem signficantly improved survival outcomes (12.8 vs. 11.5 months) compared to CisGem alone as a first-line treatment in advanced BTC (Oh et al., 2022). Patients receiving the chemoimmunotherapy also had an improved progression-free survival (7.2 vs. 5.7 months) and RR (26.7% vs. 18.7%). This combination is currently considered a new standard of care in first-line advanced BTC. The first-line, placebo-controlled phase 3 study of pembrolizumab (NCT04003636) in combination with CisGem is underway. Most chemoimmunotherapy trials in advanced BTC applied CisGem or oxaliplatin-based regimens as the chemotherapy backbone. However, the net benefit was not satisfying, and new combinations still need to be investigated. Here, for the first time, we report a patient with metastatic extrahepatic cholangiocarcinoma who had a durable response and good tolerance to pembrolizumab combined with nanoparticle albumin-bound (nab)-paclitaxel in a background of low tumor mutation burden (TMB), microsatellite stable (MSS), negative PD- L1 expression and negative $CD8^+$ tumor-infiltrating lymphocyte (TIL) expression in the tumor microenvironment (TME).

Case presentation

On 15 April 2019, a 66-year-old man was admitted to the West China Hospital with pain in his lower back and jaundice of the skin and sclera. The patient has no other medical, family, or psychosocial history.

Computed tomography (CT) scan showed dilatation of the common bile duct, with thickened lower duct wall and mild enhancement. A radical pancreaticoduodenectomy was performed on 22 April 2019. Postoperative pathology revealed a moderately-poorly differentiated adenocarcinoma, with invasion to the common bile duct

TABLE 1 Cell composition of tumor immune microenvironment.

Cellular components		Tumor parenchyma		Tumor stroma	
		Number/mm^2	%	Number/mm^2	%
T cell related indicators	CD3	227	3.69	790	14.03
	CD4	15	0.25	77	1.37
	CD8	17	0.21	65	1.15
	FoxP3	15	0.24	49	0.88
	PD-1$^+$CD8$^+$	0	0.00	0	0.00
	CD4$^+$FoxP3$^+$	1	0.02	6	0.10
Macrophage related indicators	CD68$^+$CD163$^+$	0	0.00	1	0.02
	CD68$^+$CD163$^-$	36	0.44	166	2.94
	PD-L1$^+$CD68$^+$	1	0.01	4	0.06
NK cell related indicators	CD56bright	7	0.11	43	0.77
	CD56dim	72	1.17	128	2.27
B cell related indicators	CD20	14	0.22	82	1.45

FIGURE 3
PET-CT in August 2020 showed disappeared hypermetabolic activities in the hepatic lesions and no clear sign of tumor recurrence and metastasis throughout the body. S6, Segment 6; S8, Segment 8.

wall, duodenal wall and pancreatic parenchyma. Nerve invasion and intravascular emboli were also observed. There were no regional lymph node metastases. Immunohistochemical (IHC) analysis showed CK7(+), CK19(+), MUC-1 (+), MUC-2 (-), DPC-4 (+/-), CK (focal+), CDX-2 (-). The patient was diagnosed as stage IIIB-T4N0M0. Chest and abdominal CT were performed two months after surgery, showing no signs of tumor recurrence or metastasis. A total of 8 cycles of gemcitabine plus capecitabine (GEMCAP) as adjuvant chemotherapy was performed from 22 June 2019, to 18 December 2019. On 27 March 2020, abdominal CT showed multiple liver metastases with a 22 mm × 27 mm mass forming lesion in segment 6 (S6) and a 9 mm × 13.5 mm mass forming lesion in S8 (Figure 1A). Meanwhile, laboratory examinations showed that the patient's carcinoembryonic antigen (CEA) was 7.69 ng/ml (normal level < 3.4 ng/ml), and the carbohydrate antigen 19–9 (CA 19–9) was 33.10 U/ml (normal level < 22 U/ml). Subsequently, the patient underwent next-generation sequencing (NGS) on surgically resected specimens, and the results showed KRAS and TP53 mutations, TMB of 1 mutation/megabase, and MSS. Multiple immunofluorescence was used to detect TME (Figure 2), indicating that PD-L1 expression was negative (TPS< 1%, CPS< 1) and CD8$^+$ TIL expression was quantified at 0.21% of the tumor parenchyma and 1.15% of the stroma (Table 1). Based on the results of Gainor et al. (2016), the patient was judged "negative" for CD8+TIL expression.

Four months after adjuvant chemotherapy, the patient developed metastasis, and the GEMCAP regimen was

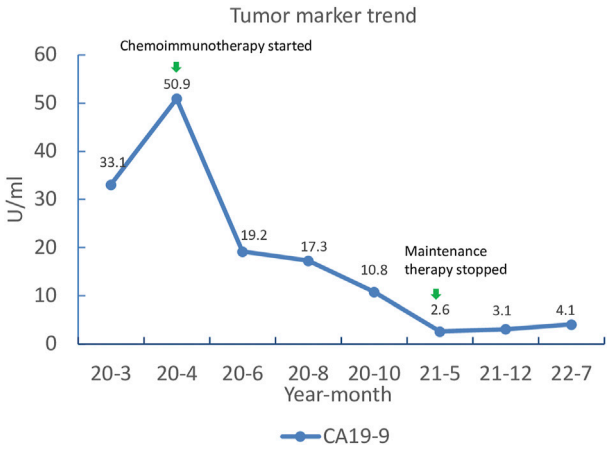

FIGURE 4
The response of tumor marker to chemoimmunotherapy. CA19–9, carbohydrate antigen 19–9.

considered the first-line treatment. Due to the limited benefit of the standard second-line chemotherapy (FOLFOX), a switch to second-line systemic therapy with nab-paclitaxel and cisplatin (AP) plus pembrolizumab was recommended by our tumor conference. Before treatment, written informed consent was obtained from the patient who presented Eastern Cooperative Oncology Group performance score (ECOG) of zero. In April 2020, the treatment with pembrolizumab plus AP was initiated. The first radiological imaging in June 2020 showed a stable disease after two cycles (Figure 1A). Due to grade 3 vomiting and grade 2 nausea (CTCAE5.0), cisplatin was discontinued after three cycles. Five cycles of pembrolizumab plus nab-paclitaxel were performed from July to October 2020. Although the positron emission tomography-computed tomography (PET-CT) in August 2020 showed no hypermetabolic activities in the hepatic lesions and no clear sign of tumor recurrence or metastasis throughout the body (Figure 3), the CT scan in October 2020 indicated a partial response (PR) (Figure 1A), The patient's CEA and CA 19–9 levels also returned to the normal range (Figure 4). The most common adverse events were hematologic toxicities (grade 2 leukopenia, grade 2 neutropenia and grade 1 anemia) during chemoimmunotherapy.

Subsequent ten cycles of pembrolizumab monotherapy (the maintenance therapy) were administered and stopped in May 2021, when grade 2 checkpoint inhibitor pneumonitis (CIP) was observed (Figure 1B). The prednisolone (initial dose at 1 mg/kg/day–2 mg/kg/day) was administered, and the dose was reduced by 5 mg per week. The final therapy was glucocorticosteroid treatment, which started in May 2021 and lasted for six weeks, and the patient did not receive any anti-tumor treatment since then. The patient survived for over 27 months after the chemoimmunotherapy and was still in continuous remission at the last follow-up in July 2022 (Figure 1A).

Discussion

Here, we report on the efficacy and tolerability of a combination of pembrolizumab plus nab-paclitaxel as a second-line therapy after GEMCAP regimen progression in a patient with low TMB, MSS, negative PD-L1 expression, and negative $CD8^+$ TIL expression extrahepatic cholangiocarcinoma.

Recent evidence suggests that cytotoxic agents work synergistically with immunotherapy by boosting anti-tumor immunity. Cytotoxic agents majoring modulate the TME by inducing immunogenic tumor cell death and inhibiting mechanisms utilized by tumor cells for immune evasion (Galluzzi et al., 2015). The TOPAZ-1 phase III trial has shown a benefit for chemoimmunotherapy (durvalumab plus CisGem) compared to chemotherapy alone. Although the survival benefits are limited, the survival curves indicated that 24.9% of patients are still alive after two years and showed unprecedented durable responses that chemotherapy alone couldn't reach (Oh et al., 2022). Based on this encouraging data, many trials comparing the effects of ICI alone or in combination with chemotherapy, such as KEYNOTE-966 (pembrolizumab + CisGem), IMBRAVE 151 (atezolizumab + CisGem), M7824 (bintrafuspare + CisGem), are ongoing. Most trials applied chemoimmunotherapy as the first-line treatment, with CisGem regimen chemotherapy backbone. In this case, the patient was treated with nab-paclitaxel-based chemoimmunotherapy as second-line therapy and achieved a long-lasting response. It is worth mentioning that our patient started with doublet chemotherapy in the second line of treatment but experienced unacceptable adverse effects and declining performance status. Therefore, single-agent chemotherapy combined with immunotherapy might be a good strategy from the perspective of patient tolerance in the second-line setting. The anti-tumor activity of nab-paclitaxel plus immunotherapy has been validated, with acceptable toxicity in backline treatment in other tumors (Schmid et al., 2018; Giannatempo et al., 2020; Wang et al., 2022). Nab-paclitaxel has been widely explored in patients with BTC in previous clinical trials (Sahai et al., 2018; Shroff et al., 2019; Woodford et al., 2021 June 28), while the efficacy of the combination of nab-paclitaxel plus immunotherapy as the second-line treatment in BTC patients has not been studied. Notably, nab-paclitaxel has a synergistic effect in combination with ICIs due to its special nanoparticle carrier (Martin et al., 2020). The underlying mechanisms are associated with enhancing antigen-presenting cells (APCs) antigen presentation ability, affecting the tumor immune microenvironment, and

promoting T lymphocyte activation to kill tumor cells (Martin et al., 2020).

Selecting people who can benefit from immunotherapy remains one of the biggest problems. MSI-H/dMMR, high TMB, PD-L1 positive expression, and high immune cell infiltration are currently considered predictive biomarkers of response to immunotherapy or its combination with chemotherapy (Zhao et al., 2019). Previous studies have demonstrated great clinical activity of ICIs in BTC patients with microsatellite instability-high (MSI-H) or mismatch repair deficiency (dMMR) (Le et al., 2017). However, the incidence of dMMR/MSI-H BTC is less than 5% (Winkelmann et al., 2018; Goeppert et al., 2019). High TMB has been only reported in 5.9% of BTC patients, and the median TMB of BTC is about two mutations/megabase (Nakamura et al., 2015; Lin et al., 2021). A phase II study (JS001-ZS-BC001) of toripalimab (PD-1 inhibitor) plus S-1 and gemcitabine had promising survival benefits in untreated BTC patients with ORR of 27.1% and a median OS of 16 months (Li et al., 2021). Biomarker analysis revealed that TMB was not associated with treatment response or survival outcomes in JS001-ZS-BC001, which was further validated by the phase II study of camrelizumab (PD-1 inhibitor) plus gemcitabine and oxaliplatin in untreated BTC patients (Chen et al., 2020). The efficacy of pembrolizumab on PD-L1-positive and negative CCA was analyzed in the KEYNOTE-158 trial. PD-L1 positivity was not associated with superior survival outcomes, and there were no significant differences in median PFS (1.9 vs. 2.1 months) or OS (7.2 vs. 9.3 months) between PD-L1-positive and negative subgroups (Bang et al., 2019). In the subgroup of TOPAZ-1 trail, the addition of durvalumab to chemotherapy benefited patients with tumors characterized by a PD-L1 tumor area positivity (TAP) of 1% or greater and a TAP of less than 1%, suggesting that PD-L1 status may have limited value in predicting clinical benefit with chemoimmunotherapy in BTC (Oh et al., 2022). Additionally, trials of chemoimmunotherapy have been completed for patients with non-small cell lung cancer (NSCLC), even independent of PD-L1 status. In the KEYNOTE-189 and KEYNOTE-407 trials, NSCLC patients with less than 1% PD-L1 expression also responded to chemoimmunotherapy, and PD-L1 expression did not correlate with the clinical benefit (Gandhi et al., 2018; Yan et al., 2018). It is worth mentioning that the accuracy of these biomarkers is controversial. The biological process of anti-tumor immune response is complicated, involving cancer cells and cells in the TME. The different biomarkers accounted for few aspects of the overall process and, therefore, cannot be used to predict efficiently. For example, in this case, we comprehensively analyzed the genomic alterations and the immune microenvironment and found that our patient, with MSS, low TMB, negative $CD8^+$ TIL and PD-L1 expression, can still benefit from chemoimmunotherapy, even in the second-line treatment. Further exploration of predictive biomarkers of response to immunotherapy for BTC is needed.

The optimal duration of ICI maintenance therapy remains controversial. Currently, the immunotherapy duration designed in most studies for advanced tumors is two years or discontinued when tumor progression or intolerable toxicities appear. However, several studies have shown that patients who were sensitive to immunotherapy but discontinued it due to immune-related adverse events had similar survival outcomes to those who completed the established therapy, indicating that early discontinuation of immunotherapy had no impact on survival (Schadendorf et al., 2017; Horiguchi et al., 2018; Kimura et al., 2019). In the current case, no significant change in tumor size was observed after switching to pembrolizumab monotherapy, but immune-related adverse effects occurred. Interestingly, no considerable tumor changes were observed even 14 months after discontinuing maintenance therapy. Although controllable CIP occurred on this patient, we will consider reintroducing nab-paclitaxel plus pembrolizumab if tumor progression in the following follow-ups because the patient has been off this treatment for more than one year.

Conclusion

ICI combined with nab-paclitaxel might be a potential treatment option for patients with CCA and further clinical trials are needed to explore the outcomes.

Data availability statement

The original contributions presented in the study are included in the article, further inquiries can be directed to the corresponding author.

Ethics statement

The study involving human participant was reviewed and approved by the ethics committee on biomedical research, West China Hospital of Sichuan University. The patient provided written informed consent for the publication of any potentially identifiable images or data included in this article.

Author contributions

All authors participated in the diagnosis and treatment process. ST and JY collected the data and wrote the manuscript. JY, QH, and NZ helped collect literature and participated in the follow-up course.

HG developed the treatment plan and examined the language. All authors approved the submitted version.

Funding

This work was supported by the Health Commission of Sichuan Province Program (21PJ007).

Acknowledgments

We thank the patient and his family for allowing us to publish his clinical case.

Conflict of interest

The authors declare that the research was conducted in the absence of any commercial or financial relationships that could be construed as a potential conflict of interest.

Publisher's note

All claims expressed in this article are solely those of the authors and do not necessarily represent those of their affiliated organizations, or those of the publisher, the editors and the reviewers. Any product that may be evaluated in this article, or claim that may be made by its manufacturer, is not guaranteed or endorsed by the publisher.

References

Abou-Alfa, G. K., Macarulla, T., Javle, M. M., Kelley, R. K., Lubner, S. J., Adeva, J., et al. (2020). Ivosidenib in IDH1-mutant, chemotherapy-refractory cholangiocarcinoma (ClarIDHy): A multicentre, randomised, double-blind, placebo-controlled, phase 3 study. *Lancet. Oncol.* 21 (6), 796–807. doi:10.1016/S1470-2045(20)30157-1

Balar, A. V., Castellano, D., O'Donnell, P. H., Grivas, P., Vuky, J., Powles, T., et al. (2017). First-line pembrolizumab in cisplatin-ineligible patients with locally advanced and unresectable or metastatic urothelial cancer (KEYNOTE-052): A multicentre, single-arm, phase 2 study. *Lancet. Oncol.* 18 (11), 1483–1492. doi:10.1016/S1470-2045(17)30616-2

Bang, Y-J. U., Chung, H. C., Nagrial, A., Kelley, R. K., Kelley, R. K., et al. (2019). Pembrolizumab (pembro) for advanced biliary adenocarcinoma: Results from the KEYNOTE-028 (KN028) and KEYNOTE-158 (KN158) basket studies. *J. Clin. Oncol.* 37, 4079. doi:10.1200/jco.2019.37.15_suppl.4079

Bekaii-Saab, T. S., Valle, J. W., Van Cutsem, E., Rimassa, L., Furuse, J., Ioka, T., et al. (2020). FIGHT-302: First-line pemigatinib vs gemcitabine plus cisplatin for advanced cholangiocarcinoma with FGFR2 rearrangements. *Future Oncol.* 16 (30), 2385–2399. doi:10.2217/fon-2020-0429

Chen, X., Wu, X., Wu, H., Gu, Y., Shao, Y., Shao, Q., et al. (2020). Camrelizumab plus gemcitabine and oxaliplatin (GEMOX) in patients with advanced biliary tract cancer: A single-arm, open-label, phase II trial. *J. Immunother. Cancer* 8 (2), e001240. doi:10.1136/jitc-2020-001240

Doebele, R. C., Drilon, A., Paz-Ares, L., Siena, S., Shaw, A. T., Farago, A. F., et al. (2020). Entrectinib in patients with advanced or metastatic NTRK fusion-positive solid tumours: Integrated analysis of three phase 1-2 trials. *Lancet. Oncol.* 21 (2), 271–282. doi:10.1016/S1470-2045(19)30691-6

Eggermont, A. M. M., Blank, C. U., Mandala, M., Long, G. V., Atkinson, V., Dalle, S., et al. (2018). Adjuvant pembrolizumab versus placebo in resected stage III melanoma. *N. Engl. J. Med.* 378 (19), 1789–1801. doi:10.1056/NEJMoa1802357

Everhart, J. E., and Ruhl, C. E. (2009). Burden of digestive diseases in the United States Part III: Liver, biliary tract, and pancreas. *Gastroenterology* 136 (4), 1134–1144. doi:10.1053/j.gastro.2009.02.038

Gainor, J. F., Shaw, A. T., Sequist, L. V., Fu, X., Azzoli, C. G., Piotrowska, Z., et al. (2016). EGFR mutations and alk rearrangements are associated with low response rates to PD-1 pathway blockade in non-small cell lung cancer: A retrospective analysis. *Clin. Cancer Res.* 22 (18), 4585–4593. doi:10.1158/1078-0432.CCR-15-3101

Galluzzi, L., Buque, A., Kepp, O., Zitvogel, L., and Kroemer, G. (2015). Immunological effects of conventional chemotherapy and targeted anticancer agents. *Cancer Cell* 28 (6), 690–714. doi:10.1016/j.ccell.2015.10.012

Gandhi, L., Rodriguez-Abreu, D., Gadgeel, S., Esteban, E., Felip, E., De Angelis, F., et al. (2018). Pembrolizumab plus chemotherapy in metastatic non-small-cell lung cancer. *N. Engl. J. Med.* 378 (22), 2078–2092. doi:10.1056/NEJMoa1801005

Giannatempo, P., Raggi, D., Marandino, L., Bandini, M., Fare, E., Calareso, G., et al. (2020). Pembrolizumab and nab-paclitaxel as salvage therapy for platinum-treated, locally advanced or metastatic urothelial carcinoma: Interim results of the open-label, single-arm, phase II PEANUT study. *Ann. Oncol.* 31 (12), 1764–1772. doi:10.1016/j.annonc.2020.09.012

Goeppert, B., Roessler, S., Renner, M., Singer, S., Mehrabi, A., Vogel, M. N., et al. (2019). Mismatch repair deficiency is a rare but putative therapeutically relevant finding in non-liver fluke associated cholangiocarcinoma. *Br. J. Cancer* 120 (1), 109–114. doi:10.1038/s41416-018-0199-2

Horiguchi, M., Uno, H., and Wei, L. J. (2018). Patients with advanced melanoma who discontinued treatment with nivolumab and ipilimumab as a result of adverse events lived significantly longer than patients who continued treatment. *J. Clin. Oncol.* 36 (7), 720–721. doi:10.1200/JCO.2017.76.0983

Jarnagin, W. R., Fong, Y., DeMatteo, R. P., Gonen, M., Burke, E. C., Bodniewicz, B. J., et al. (2001). Staging, resectability, and outcome in 225 patients with hilar cholangiocarcinoma. *Ann. Surg.* 234 (4), 507–517. discussion 517-509. doi:10.1097/00000658-200110000-00010

Jung, S. J., Woo, S. M., Park, H. K., Lee, W. J., Han, M. A., Han, S. S., et al. (2012). Patterns of initial disease recurrence after resection of biliary tract cancer. *Oncology* 83 (2), 83–90. doi:10.1159/000339695

Khan, S. A., Tavolari, S., and Brandi, G. (2019). Cholangiocarcinoma: Epidemiology and risk factors. *Liver Int.* 39 (1), 19–31. doi:10.1111/liv.14095

Kim, R. D., Chung, V., Alese, O. B., El-Rayes, B. F., Li, D., Al-Toubah, T. E., et al. (2020). A phase 2 multi-institutional study of nivolumab for patients with advanced refractory biliary tract cancer. *JAMA Oncol.* 6 (6), 888–894. doi:10.1001/jamaoncol.2020.0930

Kimura, H., Araya, T., Yoneda, T., Shirasaki, H., Kurokawa, K., Sakai, T., et al. (2019). Long-lasting responses after discontinuation of nivolumab treatment for reasons other than tumor progression in patients with previously treated, advanced non-small cell lung cancer. *Cancer Commun.* 39 (1), 78. doi:10.1186/s40880-019-0423-3

Lamarca, A., Barriuso, J., McNamara, M. G., and Valle, J. W. (2020). Molecular targeted therapies: Ready for "prime time" in biliary tract cancer. *J. Hepatol.* 73 (1), 170–185. doi:10.1016/j.jhep.2020.03.007

Lamarca, A., Palmer, D. H., Wasan, H. S., Ross, P. J., Ma, Y. T., Arora, A., et al. (2021). Second-line FOLFOX chemotherapy versus active symptom control for advanced biliary tract cancer (ABC-06): A phase 3, open-label, randomised, controlled trial. *Lancet. Oncol.* 22 (5), 690–701. doi:10.1016/s1470-2045(21)00027-9

Le, D. T., Durham, J. N., Smith, K. N., Wang, H., Bartlett, B. R., Aulakh, L. K., et al. (2017). Mismatch repair deficiency predicts response of solid tumors to PD-1 blockade. *Science* 357 (6349), 409–413. doi:10.1126/science.aan6733

Li, W., Yu, Y., Xu, X., Guo, X., Wang, Y., Li, Q., et al. (2021). Toripalimab with chemotherapy as first-line treatment for advanced biliary tract tumors: Update analytic results of an open-label phase II clinical study (JS001-ZS-BC001). *J. Clin. Oncol.* 39 (15), e16170. doi:10.1200/JCO.2021.39.15_suppl.e16170

Lin, J., Cao, Y., Yang, X., Li, G., Shi, Y., Wang, D., et al. (2021). Mutational spectrum and precision oncology for biliary tract carcinoma. *Theranostics* 11 (10), 4585–4598. doi:10.7150/thno.56539

Martin, J. D., Cabral, H., Stylianopoulos, T., and Jain, R. K. (2020). Improving cancer immunotherapy using nanomedicines: Progress, opportunities and challenges. *Nat. Rev. Clin. Oncol.* 17 (4), 251–266. doi:10.1038/s41571-019-0308-z

Mazzaferro, V., El-Rayes, B. F., Droz Dit Busset, M., Cotsoglou, C., Harris, W. P., Damjanov, N., et al. (2019). Derazantinib (ARQ 087) in advanced or inoperable FGFR2 gene fusion-positive intrahepatic cholangiocarcinoma. *Br. J. Cancer* 120 (2), 165–171. doi:10.1038/s41416-018-0334-0

Mok, T. S. K., Wu, Y. L., Kudaba, I., Kowalski, D. M., Cho, B. C., Turna, H. Z., et al. (2019). Pembrolizumab versus chemotherapy for previously untreated, PD-L1-expressing, locally advanced or metastatic non-small-cell lung cancer (KEYNOTE-042): A randomised, open-label, controlled, phase 3 trial. *Lancet* 393 (10183), 1819–1830. doi:10.1016/S0140-6736(18)32409-7

Montal, R., Sia, D., Montironi, C., Leow, W. Q., Esteban-Fabro, R., Pinyol, R., et al. (2020). Molecular classification and therapeutic targets in extrahepatic cholangiocarcinoma. *J. Hepatol.* 73 (2), 315–327. doi:10.1016/j.jhep.2020.03.008

Nakamura, H., Arai, Y., Totoki, Y., Shirota, T., Elzawahry, A., Kato, M., et al. (2015). Genomic spectra of biliary tract cancer. *Nat. Genet.* 47 (9), 1003–1010. doi:10.1038/ng.3375

Oh, D.-Y., He, A. R., Qin, S., Chen, L.-T., Okusaka, T., Vogel, A., et al. (2022). A phase 3 randomized, double-blind, placebo-controlled study of durvalumab in combination with gemcitabine plus cisplatin (GemCis) in patients (pts) with advanced biliary tract cancer (BTC): TOPAZ-1. *J. Clin. Oncol.* 40 (4), 378. doi:10.1200/JCO.2022.40.4_suppl.378

Rizvi, S., and Gores, G. J. (2013). Pathogenesis, diagnosis, and management of cholangiocarcinoma. *Gastroenterology* 145 (6), 1215–1229. doi:10.1053/j.gastro.2013.10.013

Rizzo, A., Ricci, A. D., and Brandi, G. (2021a). Durvalumab: An investigational anti-PD-L1 antibody for the treatment of biliary tract cancer. *Expert Opin. Investig. Drugs* 30 (4), 343–350. doi:10.1080/13543784.2021.1897102

Rizzo, A., Ricci, A. D., and Brandi, G. (2021b). Pemigatinib: Hot topics behind the first approval of a targeted therapy in cholangiocarcinoma. *Cancer Treat. Res. Commun.* 27, 100337. doi:10.1016/j.ctarc.2021.100337

Rizzo, A., Ricci, A. D., Tober, N., Nigro, M. C., Mosca, M., Palloni, A., et al. (2020). Second-line treatment in advanced biliary tract cancer: Today and tomorrow. *Anticancer Res.* 40 (6), 3013–3030. doi:10.21873/anticanres.14282

Sahai, V., Catalano, P. J., Zalupski, M. M., Lubner, S. J., Menge, M. R., Nimeiri, H. S., et al. (2018). Nab-paclitaxel and gemcitabine as first-line treatment of advanced or metastatic cholangiocarcinoma: A phase 2 clinical trial. *JAMA Oncol.* 4 (12), 1707–1712. doi:10.1001/jamaoncol.2018.3277

Schadendorf, D., Wolchok, J. D., Hodi, F. S., Chiarion-Sileni, V., Gonzalez, R., Rutkowski, P., et al. (2017). Efficacy and safety outcomes in patients with advanced melanoma who discontinued treatment with nivolumab and ipilimumab because of adverse events: A pooled analysis of randomized phase II and III trials. *J. Clin. Oncol.* 35 (34), 3807–3814. doi:10.1200/JCO.2017.73.2289

Schmid, P., Adams, S., Rugo, H. S., Schneeweiss, A., Barrios, C. H., Iwata, H., et al. (2018). Atezolizumab and nab-paclitaxel in advanced triple-negative breast cancer. *N. Engl. J. Med.* 379 (22), 2108–2121. doi:10.1056/NEJMoa1809615

Shroff, R. T., Javle, M. M., Xiao, L., Kaseb, A. O., Varadhachary, G. R., Wolff, R. A., et al. (2019). Gemcitabine, cisplatin, and nab-paclitaxel for the treatment of advanced biliary tract cancers: A phase 2 clinical trial. *JAMA Oncol.* 5 (6), 824–830. doi:10.1001/jamaoncol.2019.0270

Tyson, G. L., and El-Serag, H. B. (2011). Risk factors for cholangiocarcinoma. *Hepatology* 54 (1), 173–184. doi:10.1002/hep.24351

Ueno, M., Ikeda, M., Morizane, C., Kobayashi, S., Ohno, I., Kondo, S., et al. (2019). Nivolumab alone or in combination with cisplatin plus gemcitabine in Japanese patients with unresectable or recurrent biliary tract cancer: A non-randomised, multicentre, open-label, phase 1 study. *Lancet. Gastroenterol. Hepatol.* 4 (8), 611–621. doi:10.1016/S2468-1253(19)30086-X

Valle, J., Wasan, H., Palmer, D. H., Cunningham, D., Anthoney, A., Maraveyas, A., et al. (2010). Cisplatin plus gemcitabine versus gemcitabine for biliary tract cancer. *N. Engl. J. Med.* 362 (14), 1273–1281. doi:10.1056/NEJMoa0908721

Wang, J., He, Y., Zhang, B., Lv, H., Nie, C., Chen, B., et al. (2022). The efficacy and safety of sintilimab combined with nab-paclitaxel as a second-line treatment for advanced or metastatic gastric cancer and gastroesophageal junction cancer. *Front. Oncol.* 12, 924149. doi:10.3389/fonc.2022.924149

Winkelmann, R., Schneider, M., Hartmann, S., Schnitzbauer, A. A., Zeuzem, S., Peveling-Oberhag, J., et al. (2018). Microsatellite instability occurs rarely in patients with cholangiocarcinoma: A retrospective study from a German tertiary care hospital. *Int. J. Mol. Sci.* 19 (5), E1421. doi:10.3390/ijms19051421

Woodford, R., Brungs, D., Leighton, C., Grimison, P., Sjoquist, K. M., Becker, T., et al. (2021). Combination chemotherapy with NAB® -paclitaxel and capecitabine for patients with advanced biliary tract cancer (NAP-CAPABIL Pilot Study). *Asia. Pac. J. Clin. Oncol.* 18, e220–e226. doi:10.1111/ajco.13599

Xu, F., Jin, T., Zhu, Y., and Dai, C. (2018). Immune checkpoint therapy in liver cancer. *J. Exp. Clin. Cancer Res.* 37 (1), 110. doi:10.1186/s13046-018-0777-4

Yan, Y., Kumar, A. B., Finnes, H., Markovic, S. N., Park, S., Dronca, R. S., et al. (2018). Combining immune checkpoint inhibitors with conventional cancer therapy. *Front. Immunol.* 9, 1739. doi:10.3389/fimmu.2018.01739

Zhao, P., Li, L., Jiang, X., and Li, Q. (2019). Mismatch repair deficiency/microsatellite instability-high as a predictor for anti-PD-1/PD-L1 immunotherapy efficacy. *J. Hematol. Oncol.* 12 (1), 54. doi:10.1186/s13045-019-0738-1

frontiers | Frontiers in Pharmacology

TYPE Original Research
PUBLISHED 29 November 2022
DOI 10.3389/fphar.2022.1049117

OPEN ACCESS

EDITED BY
Husain Yar Khan,
Wayne State University, United States

REVIEWED BY
Alaaeldin Ahmed Hamza,
National Organization for Drug Control and Research (NODCAR), Egypt
Samson Mathews Samuel,
Weill Cornell Medicine-Qatar, Qatar

*CORRESPONDENCE
Hua Zhu,
zhuhuagx@163.com
Li Long,
longli6662022@163.com
Li-Ba Xu,
xuliba15078772841@163.com

†These authors have contributed equally to this work and share first authorship

SPECIALTY SECTION
This article was submitted to Pharmacology of Anti-Cancer Drugs, a section of the journal Frontiers in Pharmacology

RECEIVED 20 September 2022
ACCEPTED 15 November 2022
PUBLISHED 29 November 2022

CITATION
Lin S, Qin H-Z, Li Z-Y, Zhu H, Long L and Xu L-B (2022), Gallic acid suppresses the progression of triple-negative breast cancer HCC1806 cells *via* modulating PI3K/AKT/EGFR and MAPK signaling pathways.
Front. Pharmacol. 13:1049117.
doi: 10.3389/fphar.2022.1049117

Gallic acid suppresses the progression of triple-negative breast cancer HCC1806 cells *via* modulating PI3K/AKT/EGFR and MAPK signaling pathways

Si Lin[1,2†], Hui-Zhen Qin[1,2†], Ze-Yu Li[2†], Hua Zhu[1,2*], Li Long[3*] and Li-Ba Xu[1,2*]

[1]Guangxi Key Laboratory of Zhuang and Yao Ethnic Medicine, Guangxi University of Chinese Medicine, Nanning, China, [2]Guangxi Scientific Research Center of Traditional Chinese Medicine, Guangxi University of Chinese Medicine, Nanning, China, [3]Guangxi International Zhuang Medicine Hospital, Guangxi University of Chinese Medicine, Nanning, China

Triple-negative breast cancer (TNBC) is a severe threat to women's health because of its aggressive nature, early age of onset, and high recurrence rate. Therefore, in this study, we aimed to evaluate the anti-tumor effects of Gallic acid (GA) on the TNBC HCC1806 cells *in vitro*. The cell proliferation was detected by MTT and plate clone formation assays, cell apoptosis, cell cycle, and mitochondrial membrane potential (MMP) were analyzed by flow cytometry and Hoechst 33258 staining assays, and the intracellular reactive oxygen species (ROS) accumulation were also investigated. Real-Time PCR and western blot were examined to explore the mechanism of action. The results indicated that GA suppressed HCC1806 cells proliferation and promoted HCC1806 cells apoptosis. Meanwhile, GA treatment changed the morphology of the HCC1806 cells. In addition, GA blocked the HCC1806 cells cycle in the S phase, and it induced cells apoptosis accompanied by ROS accumulation and MMP depolarization. Real-Time PCR results suggested that GA increased Bax, Caspase-3, Caspase-9, P53, JINK and P38 mRNA expression, and decreased Bcl-2, PI3K, AKT and EGFR mRNA expression. Western blotting results suggested that GA increased Bax, cleaved-Caspase-3, cleaved-Caspase-9, P53, P-ERK1/2, P-JNK, P-P38 proteins expression, and decreased Bcl-2, P-PI3K, P-AKT, P-EGFR proteins expression. Furthermore, molecular docking suggested that GA has the high affinity for PI3K, AKT, EGFR, ERK1/2, JNK, and P38. In conclusion, GA could suppress HCC1806 cells proliferation and promote HCC1806 cells apoptosis through the mitochondrial apoptosis pathway and induces ROS generation which further inhibits PI3K/AKT/EGFR and activates MAPK signaling pathways. Our study will provide some new references for using GA in the treatment of TNBC.

KEYWORDS

triple-negative breast cancer, gallic acid, proliferation, apoptosis, PI3K/AKT/EGFR signaling pathway, MAPK signaling pathway

Introduction

Breast cancer (BC) is a malignant tumor that seriously threatens women's life and health worldwide (Akram et al., 2017). According to the statistics, an estimated 2.3 million new cases of BC worldwide in 2020 (Sung et al., 2021). Triple-negative breast cancer (TNBC), which accounts for 20% of all BC, is a type of BC that is negative for estrogen receptor (ER), progesterone receptor (PR) and human epidermal growth factor receptor 2 (HER-2), resulting in a meager survival rate due to its aggressiveness, malignancy and poor prognosis (Oh et al., 2017; Hon et al., 2016). Due to its unique molecular phenotype, TNBC is insensitive to endocrine and molecular targeted therapy. Currently, the main treatment methods are local surgical excision and systemic chemotherapy. However, conventional postoperative adjuvant radiotherapy is less effective and has a higher metastasis and recurrence rate, so TNBC has became the most treatment-challenging BC subtype (Denkert et al., 2017). The doxorubicin, represented by adriamycin, is among the most effective drugs used in chemotherapy for TNBC. However, its usage is greatly limited due to its tendency to develop resistance to drugs. (Angelini et al., 2013; Woo et al., 2016; Aydinlik et al., 2017). Therefore, it is urgent to find a novel anti-tumor drug with effective, fewer side effects and less toxicity for the TNBC treatment.

As we all know, an increasing number of studies have demonstrated that plant extracts, especially traditional Chinese medicine (TCM) extracts have apoptosis-promoting effects on a wide range of cancer cells. For example, Chen et al. (2020) revealed that Ethanol Extract of *Brucea javanica* Seed could suppress TNBC cell proliferation and promote cell apoptosis. Li et al. (2020) found that Extracts of Cordyceps sinensis could inhibit BC growth by promoting M1 macrophage polarization *via* NF-κB pathway activation. Therefore, the search for new anti-tumor drugs from plant extracts has attracted the attention of a wide range of researchers.

Gallic acid (GA) is a polyphenol compound with various biological activities such as antioxidant, anti-inflammatory, anti-tumor, anti-viral and anti-bacterial (Lin et al., 2020; Bai et al., 2021). In current times, numerous research studies have confirmed the anti-tumor effect of GA, and it is said to be a potential anti-cancer agent (Zhang N et al., 2019; Zeng et al., 2020; Lin Q et al., 2021; Jiang et al., 2022). At the same time, a growing number of studies reported that inhibition of tumor cell proliferation and induction of apoptosis are the keys to active anti-tumor drugs, and both radiotherapy and chemotherapy are closely related to the induction of apoptosis (Hickman, 1992; Gong et al., 2018; Jan and Chaudhry, 2019; Hu et al., 2021). Apoptosis pathways include the mitochondrial pathway, the death receptor and the endoplasmic reticulum pathway, and the mitochondrial pathway plays a crucial role. Some studies showed a strong link between mitochondrial morphology and cancer disease (Maycotte et al., 2017). B-cell lymphoma 2 (Bcl-2) and Bcl-2-associated X protein (Bax) play an important role in the regulation of the mitochondrial apoptosis pathway (Lv et al., 2020; Ma et al., 2020). In response to various apoptosis stimulus signals, Bax protein conformation changes and translocates to the outer mitochondrial membrane, forming a homodimer with a microporous structure, stimulating the release of pro-apoptotic factors such as cytochrome C into the cytoplasm, forming a multimeric complex with apoptotic protease-activating factor-1, promoting the self-activation of cysteine aspartate protease-9 (caspase-9) precursor, which activates caspase-3 and ultimately leads to apoptosis (Liu et al., 2020; Montero et al., 2020). In addition, several studies have reported that dysregulation of the Phosphoinositide-3-kinase (PI3K)/protein kinase B (AKT) signaling pathway is closely associated with the development of breast cancer (Abdullah et al., 2021; Guo et al., 2021). And activated AKT signaling pathway promotes breast cancer cell growth, survival and metastasis (Lin X et al., 2021; Ock and Kim, 2021; Shin et al., 2021). Epidermal growth factor receptor (EGFR) is a tyrosine kinase that promotes cell proliferation and inhibits apoptosis, and its high expression can promote neovascularization and induce tumorigenesis, invasion and metastasis (Ohmori et al., 2021; Lee et al., 2018). Mitogen-activated protein kinase (MAPK) signaling pathways pathway has three sub-pathways, including the ERK, JNK and p38 MAPK sub-pathways, with the ERK pathway reported to be essential for cell survival. At the same time, JNK and p38 MAPK were associated with apoptosis (Yue and Lopez, 2020). In a word, PI3K/AKT/EGFR and MAPK signaling pathways play a crucial role in cancer cell proliferation and tumor progression, and a previous study has confirmed that EGFR is a target for TNBC treatment (Liao et al., 2019).

Although some studies have confirmed the anti-tumor activity of GA against TNBC, for example, Lee et al. (2017) found that GA induced apoptosis in MDA-MB-231 cells through the P38MAPK/P27/P21 signaling axis, Khorsandi et al. (2020) found that GA induced ferroptosis in MDA-MB-231 cells through the production of ROS, and Moghtaderi et al. (2018) found that GA combined with curcumin induced apoptosis in MDA-MB-231 cells by decreasing the expression of Bcl-2 and increasing the expression of Bax, cleaved-caspase3 and PARP, the exact mechanism of GA action on HCC1806 cells is still unknown. Hence, the current study was conducted to investigate whether GA could inhibit HCC1806 cells progression, and our experiments evaluated the effects of GA on proliferation, apoptosis, cycle, and mitochondrial membrane potential of HCC1806 cells for the first time. In addition, we investigated whether GA could regulate the PI3K/AKT/EGFR and MAPK signaling pathways and thus promote HCC1806 cells apoptosis

TABLE 1 Sequences of real-time polymerase chain reaction (RT-PCR) primer.

	Forward primer 5′ to 3′	Reverse primer 5′ to 3′
Bax	AGCGACTGATGTCCCTGTCTCC	AGATGGTGAGTGAGGCGGTGAG
Bcl-2	TCGCCCTGTGGATGACTGAGTAC	ACAGCCAGGAGAAATCAAACAGAGG
Caspase-3	GTGGAGGCCGACTTCTTGTATGC	TGGCACAAAGCGACTGGATGAAC
Caspase-9	GACCAGAGATTCGCAAACCAGAGG	AAGAGCACCGACATCACCAAATCC
P53	GCCCATCCTCACCATCATCACAC	GCACAAACACGCACCTCAAAGC
PI3K	GGAAGCAGCAACCGAAACAAAGC	TCCACCACTACAGAGCAGGCATAG
AKT	AGATGCAGCCACCATGAAGACATTC	ACCAGTCTACTGCTCGGCCATAG
EGFR	TACTTGGAGGACCGTCGCTTGG	CTCTTCCGCACCCAGCAGTTTG
ERK1/2	TCGCCGAAGCACCATTCAAGTTC	TCCTGGCTGGAATCTAGCAGTCTC
JNK	ACTACAGAGCACCCGAGGTCATC	TTTCTCCCATGATGCACCCAACTG
P38	GCAGAGCGATGAGGCCAAGAAC	GCGTCCAGCACCAGCATCTTC
GAPDH	CAGGAGGCATTGCTGATGAT	GAAGGCTGGGGCTCATTT

by promoting ROS generation, which would provide further references for the use of GA in the treatment of TNBC.

Materials and methods

Reagents

GA with 99% purity was purchased form Shanghai Macklin Biochemical Co., Ltd. (Shanghai, China). RPMI-1640 medium, crystal violet and Cell Cycle Assay Kit were purchased form Jiangsu KeyGEN BioTECH Corp., Ltd. (Nanjing, China). Fetal bovine serum (FBS) was purchased form Gibco (United States). MTT and Hoechst 33258 solution were acquired from Beijing Solarbio Science & Technology Co., Ltd. (Beijing, China). Annexin V-FITC Apoptosis Detection Kit was acquired from BD Biosciences (Becton Dickinson, United States). Mitochondria Staining Kit (JC-1) was acquired from MultiSciences (Lianke) Biotech Co., Ltd. (Hangzhou, China). ROS Assay Kit was acquired from Beyotime Institute of Biotechnology (Shanghai, China). The antibodies against Caspase-3, cleaved-Caspase-3, cleaved-Caspase-9, Bax, Bcl-2, PI3K, P-PI3K, AKT, P-AKT, JNK, P-JNK, ERK1/2, P-ERK1/2, P38, P-P38, EGFR, P-EGFR, GAPDH were obtained from Cell Signaling Technology (CST, United States). The antibodies against Caspase-9 and P53 were obtained from Proteintech Group, Inc. (Wuhan, China).

Cell culture and drug preparation

The human TNBC HCC1806 and MDA-MB-468 cells line were purchased form Jiangsu KeyGEN BioTECH Corp., Ltd. (Nanjing, China). HCC1806 cells were cultured with RPMI-1640 medium supplemented with 10% FBS and 1% penicillin/streptomycin at 37°C in a humidified incubator with 5% CO_2. GA was prepared into a storage solution (1,000 μM/L) with FBS-free RPMI-1640 medium, then stored at -20°C. Dissolve the GA stock solution and dilute it to the appropriate concentration with FBS-free RPMI-1640 medium before using it.

Cell viability detection

HCC1806 cells were (5×10^3 cells/well) seeded into 96-well plates overnight and then treated with GA (0, 200, 250, and 300 μM) for 24, 48, and 72 h. The MTT (5 mg/ml) reagent was added to each well (20 μL) and cultured for another 4 h. Next, dimethyl sulfoxide (DMSO) was added to each well (150 μL), and the absorbance was recorded at 490 nm by a Enzyme labeling instrument (BioTek, United States). MDA-MB-468 cells were (5×10^3 cells/well) seeded into 96-well plates overnight and then treated with GA (0, 3, 6, 12, 24, 48, 96, 192, 288, and 384 μM) for 24 h. Other steps are the same as those of HCC1806 cells (Yu et al., 2016).

Cellular morphology analysis

HCC1806 cells were plated in 6-well plate for 24 h, and then treated with GA (0, 200, 250, and 300 μM) for 24 h. The cell morphology was observed by an inverted microscope (Olympus, Japan) (Zeng et al., 2020).

Plate clone formation assay

HCC1806 cells were (1×10^3 cells/well) seeded into 6-well plates overnight, and then treated with GA (0, 200, 250, and 300 μM) for

24 h. Subsequently, removed the media and added to fresh media, and allowed to grow undisturbed for 10 days. Cells were fixed with 4% paraformaldehyde for 15 min and stained with crystal violet solution for 15 min. The plates were dried and photographed, and ImageJ Software counted the number of colonies (Zeng et al., 2020).

Cell cycle analysis

HCC1806 cells were seeded into 6-well plates overnight, and then treated with GA (0, 200, 250, and 300 μM) for 24 h. Subsequently, cells were digested and collected, washed once in PBS, fixed for 3 h at 4°C in 2 ml of 75% ethanol, then washed once in PBS, 500 μL PI/RNase dye solution was added and incubated for 20 min at room temperature and protected from light, and the fluorescence intensity of HCC1806 cells were detected by flow cytometry (Dakewe Biotech Co., Ltd., Shenzhen, China). (Zeng et al., 2020).

Hoechst 33258 staining

HCC1806 cells were seeded into 6-well plates overnight, and then treated with GA (0, 200, 250, and 300 μM) for 24 h. Next, cells were fixed with 4% paraformaldehyde for 15 min, followed by incubation with Hoechst 33258 solution for 10 min. Cells were observed and photographed under an inverted fluorescence microscope (Nikon, Japan) (Zeng et al., 2020).

Cell apoptosis assay

HCC1806 cells were seeded into 6-well plates overnight, and then treated with GA (0, 200, 250, and 300 μM) for 24 h. Subsequently, cells were digested and collected, then washed with cold PBS. Moreover, add 500 μL of Binding Buffer to each tube, resuspension by centrifugation, add 5 μL of Annexin V-FITC and 10 μL of PI staining solution to each tube, and incubate for 15 min at 25°C, protected from light, and the apoptosis rate of HCC1806 cells were detected by flow cytometry (Dakewe Biotech Co., Ltd., Shenzhen, China). (Zeng et al., 2020).

MMP level assessment

HCC1806 cells were seeded into 6-well plates overnight, and then treated with GA (0, 200, 250, and 300 μM) for 24 h. Subsequently, cells were digested and collected, and washed with PBS. Then add 1 ml JC-1 Staining Buffer to each tube and incubated for 30 min at room temperature and protected from light, and the depolarization rate of HCC1806 cells were detected by flow cytometry (Dakewe Biotech Co., Ltd., Shenzhen, China) (Zeng et al., 2020).

Intracellular ROS production

HCC1806 cells were seeded into 6-well plates overnight, and then treated with GA (0, 200, 250, and 300 μM) for 24 h. Subsequently, 1 ml DCFH-DA working solution was added to each well and incubation at 37°C for 30 min. Finally, cells were observed and photographed under an inverted fluorescence microscope (Nikon, Japan), and fluorescence intensity was detected by ImageJ Software (Zeng et al., 2020).

Quantitative Real-Time polymerase chain reaction (QRT-PCR) analysis

HCC1806 cells were seeded into 6-well plates overnight, and then treated with GA (0, 200, 250, and 300 μM) for 24 h. Cells were processed and harvested according to the manufacturer's instructions, total RNA was extracted using a TRIzol reagent kit (Thermo Fisher Scientific, United States). RNA was reverse-transcribed with cDNA reverse transcription kits (Thermo Fisher Scientific, United States). The sequences of PCR primers were design and synthesis form Sangon Biotech (Shanghai, China) Co., Ltd. (Shanghai, China). And the sequences as followed in Table 1. The relative mRNA expression levels were analyzed by $2^{-\Delta\Delta CT}$ method and normalized to GAPDH (Zeng et al., 2020).

Western blotting

HCC1806 cells were seeded into 6-well plates overnight, and then treated with GA (0, 200, 250, 300 μM) for 24 h. After that, The culture solution was removed and the 6-well plates were transferred to ice and washed 3 times with PBS. Then 300 μL RIPA lysis buffer solution was added to each well, lysed on ice for 30 min and then transferred to EP tubes and centrifuged. Protein concentrations were detected by the Enhanced BCA Protein Assay Kit (Beyotime Institute of Biotechnology, Shanghai, China). The protein samples were separated by 10% or 8% SDS-PAGE and then transferred to a polyvinylidene difluoride (PVDF) membrane (Millipore, United States). BSA (5%) (Beijing Solarbio Science & Technology Co., Ltd., Beijing, China) was used to block the membrane for 1 h, and then the primary antibodies Caspase-3 (1:1000), cleaved-Caspase-3 (1:500), cleaved-Caspase-9 (1:1000), Bax (1:1000), Bcl-2 (1:500), PI3K (1:1000), P-PI3K (1:1000), AKT (1:1000), P-AKT (1:1000), JNK (1:1000), P-JNK (1:500), ERK1/2 (1:1000), P-ERK1/2 (1:1000), P38 (1:1000), P-P38 (1:1000), EGFR (1:1000), P-EGFR (1:500), P53 (1:1000), Caspase-9 (1:1000) and GAPDH (1:1000) were incubated overnight at 4°C, followed by incubation with the secondary antibodies (1:3000, Proteintech Group, Inc., Wuhan, China) at room temperature for 1 h. Protein bands were visualized using the ECL Plus western blotting detection

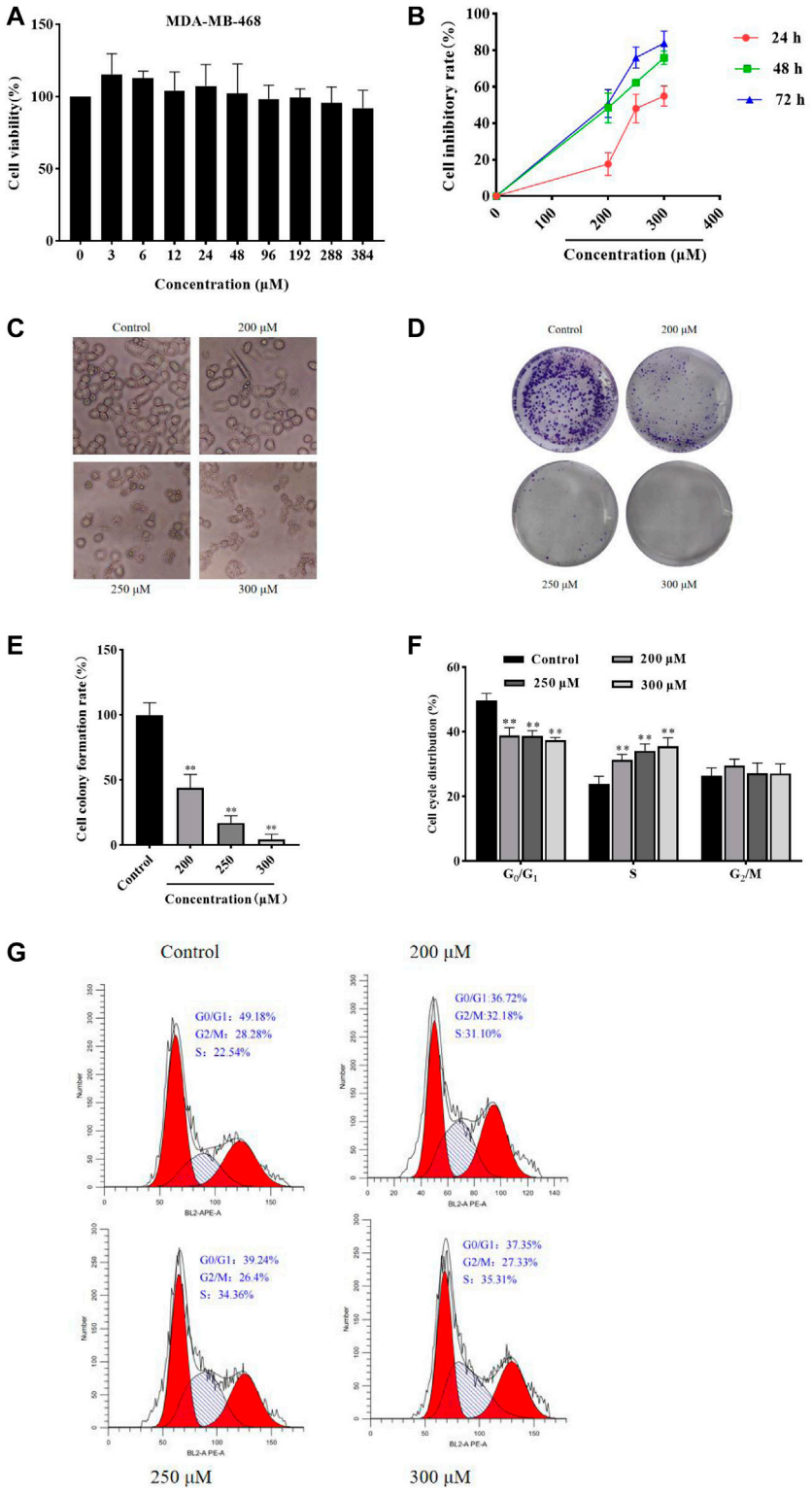

FIGURE 1
GA inhibited HCC1806 cells viability and affected cells morphology, and affected HCC1806 cells proliferation and cycle distribution. **(A)** The MDA-MB-468 cells viability was detected by MTT assay. **(B)**The HCC1806 cell inhibitory rate was detected by MTT assay. **(C)** The morphology changes of HCC1806 cells treated with different concentrations of GA were observed under an inverted microscope. **(D,E)** Effect of GA on the colony formation rate of HCC1806 cells. **(F,G)** The cell cycle distribution of HCC1806 were assessed by flow cytometry. Date were expressed as means ± SD. Compared with the control group, $^{**}p < 0.01$.

reagents (Shanghai Epizyme Biomedical Technology Co., Ltd., Shanghai, China) following the manufacturer's instructions. The relative expression of proteins were analyzed by ImageJ Software (Zeng et al., 2020).

Molecular docking

To further explore the molecular target of GA in TNBC cells, The molecular docking of GA with PI3K, ERK1/2, JNK, EGFR, AKT and P38 were carried out by autodock 4.2.6 software. It is generally believed that the binding energy <0 indicates that the small molecule components of the ligand and the target protein of the receptor can bind independently. The lower the binding energy, the more stable the molecular conformation, the greater the possibility of action, and the greater the absolute value of the binding energy, the better the binding between the ligand and the receptor.

Statistical analysis

The results were shown as the mean ± standard deviation (SD). Each experiment was repeated at least six times. All the data of this paper were analyzed with SPSS 22.0 (IBM, United States). Comparison between groups using one-way ANOVA followed by Tukey's test. $p < 0.05$ was defined as statistically significant.

Results

GA inhibits HCC1806 cells viability

MTT assay was performed to detect the MDA-MB-468 and HCC1806 cells viability. As shown in Figure 1A, GA has no obvious inhibitory effect in MDA-MB-468 cells after GA treatment for 24 h. While GA has notable inhibitory effect in HCC1806 cells. As shown in Figure 1B, compared with the control group, GA treatment significantly increased the cell inhibitory rate. These results suggested that GA notably inhibited HCC1806 cell viability.

GA changes HCC1806 cells morphology

After different concentrations of GA (0, 200, 250, and 300 μM) treatment HCC1806 cells for 24 h, the changes in cell morphology could be observed under an inverted microscope. As shown in Figure 1C, the control group cells still adhered to the wall, with clear cell contour, high cell density and in a great condition. However, the cells in GA treatment groups were shrank, the nucleus was fragmented, the cell density decreased and cells were in a state of apoptosis.

GA increases HCC1806 cells cytotoxic activity

The plate clone formation assay was performed to assess the effect of GA on HCC1806 cells cytotoxic activity. As shown in Figures 1D,E, compared with the control group, GA treatment was significantly decreased the number of colonies of HCC1806 cells, and the number of colonies decreased with increasing GA concentration. These results suggested that GA notably enhanced HCC1806 cells cytotoxic activity.

GA blocked HCC1806 cells cycle in S phase

The flow cytometry was performed to assess the effects of GA on HCC1806 cells cycle. As shown in Figures 1F,G, in the control group, the percentage of HCC1806 cells in G_0/G_1 phase was 50.47% ± 1.63%, in S phase was 23.32% ± 2.25%, and in G_2/M phase was 25.88% ± 2.13%. Compared with the control group, the percentage of G_0/G_1 phase in GA treatment groups (200, 250, 300 μM) were 39.18% ± 0.30%, 37.27% ± 0.22%, 36.87% ± 0.14%, respectively, the percentage of G_0/G_1 phase in GA treatment groups were significantly decreased. Compared with the control group, the percentage of S phase in GA treatment groups (200, 250, 300 μM) were 31.37% ± 1.07%, 34.06% ± 1.03%, 34.16% ± 1.27%, respectively, the percentage of S phase in GA treatment groups were significantly increased. These results suggested that GA blocked HCC1806 cells cycle in S phase.

GA induces HCC1806 cells apoptosis

Hoechst 33258 Staining and flow cytometry were performed to assess the effect of GA on HCC1806 cells apoptosis. As shown in Figure 2A, compared with the control group, cells in the GA intervention groups showed a strong fluorescence response, cytoplasmic condensation and nuclear incorporation, indicating an increased number of cells in an apoptotic state. Furthermore, as shown in Figures 2B,C, flow cytometry results indicated that GA induced HCC1806 cells apoptosis. Compared with the control group, the apoptotic cell rate of HCC1806 cells in GA treatment groups were significantly increased. The apoptotic rate in the control group was 4.43%, while in the GA treatment groups were 29%, 38.6% and 56.2%, respectively. In addition, the proportion of late apoptosis was higher than early apoptosis, these data indicated that GA-induced apoptosis was mainly achieved through late apoptosis.

GA reduces intracellular MMP level

The JC-1 staining method was used to detect the cell MMP level. As shown in Figures 2D,E, the upper right quadrant represented the

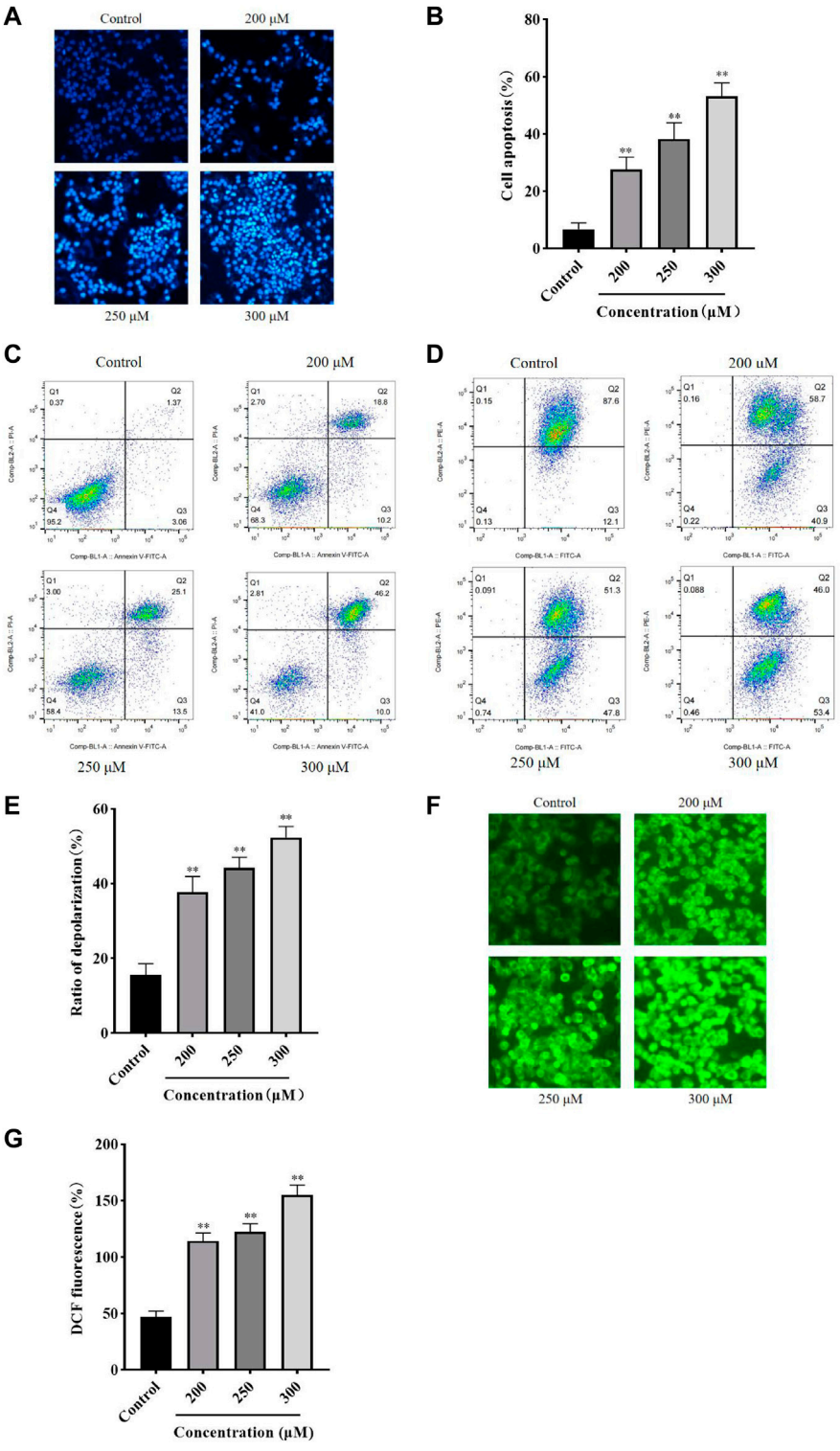

FIGURE 2
GA induced HCC1806 cells apoptosis accompanied by ROS accumulation and MMP depolarization. **(A–C)** Hoechst 33258 staining and flow cytometry were performed to assess the effect of GA on HCC1806 cells apoptosis. **(D,E)** The depolarization ratio of HCC1806 cells were detected by flow cytometry. **(F,G)** The ROS level of HCC1806 cells were assessed by a fluorescence microscope. Date were expressed as means ± SD. Compared with the control group, $^{**}p < 0.01$.

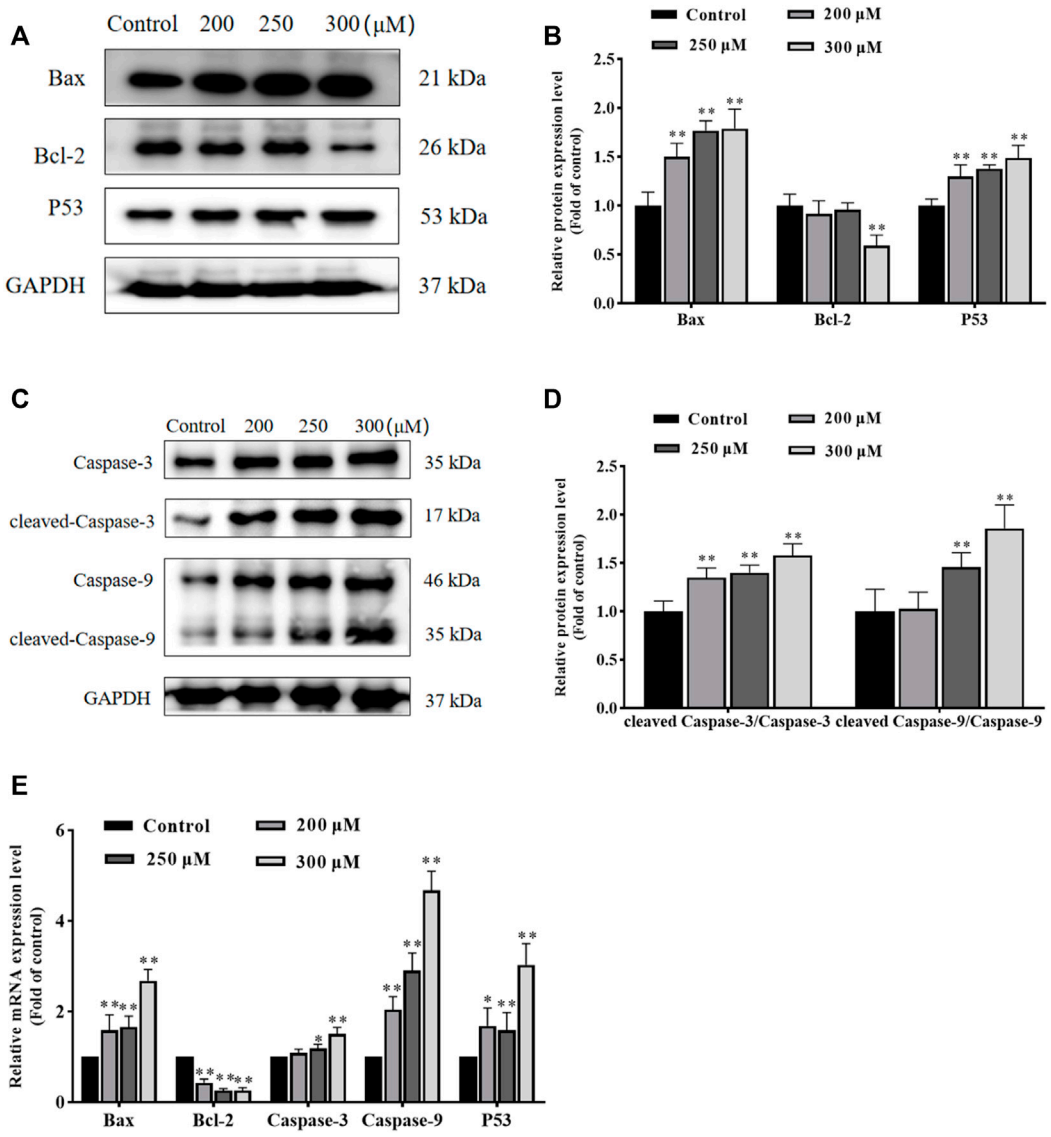

FIGURE 3
GA induces HCC1806 cells apoptosis *via* the mitochondrial pathway. **(A–D)** Effect of GA on the expression of Bax, Bcl-2, cleaved-Caspase-3, cleaved-Caspase-9 and P53 proteins in HCC1806 cells. **(E)** Effect of GA on the expression of Bax, Bcl-2, Caspase-3, Caspase-9 and P53 mRNA in HCC1806 cells. Date were expressed as means ± SD. Compared with the control group, $*p < 0.05$,$**p < 0.01$.

proportion of cells that did not depolarized, while the lower right quadrant represented the proportion of cells that depolarized. These results indicated that GA induced MMP depolarization. Compared with the control group, the MMP depolarization rate of HCC1806 cells in GA treatment groups were significantly increased. The MMP depolarization rate in the control group was 12.1%, while in the GA treatment groups were 40.9%, 47.8% and 53.4%, respectively. These results indicated that GA could decrease the MMP levels in HCC1806 cells and implied GA-induced apoptosis might be related to the mitochondrial apoptosis pathway.

GA promotes intracellular ROS generation

The DCFH-DA fluorescent probe was used to detect intracellular ROS accumulation and assess cellular damage's extent. As shown in Figures 2F,G, the green fluorescence of cells in GA treatment groups significantly increased compared with the control group. The levels of ROS in the control group was 46.94%, while in the GA treatment groups were 117.34%, 122.44%, and 154.72%, respectively. These results suggested that GA induced oxidative stress in HCC1806 cells.

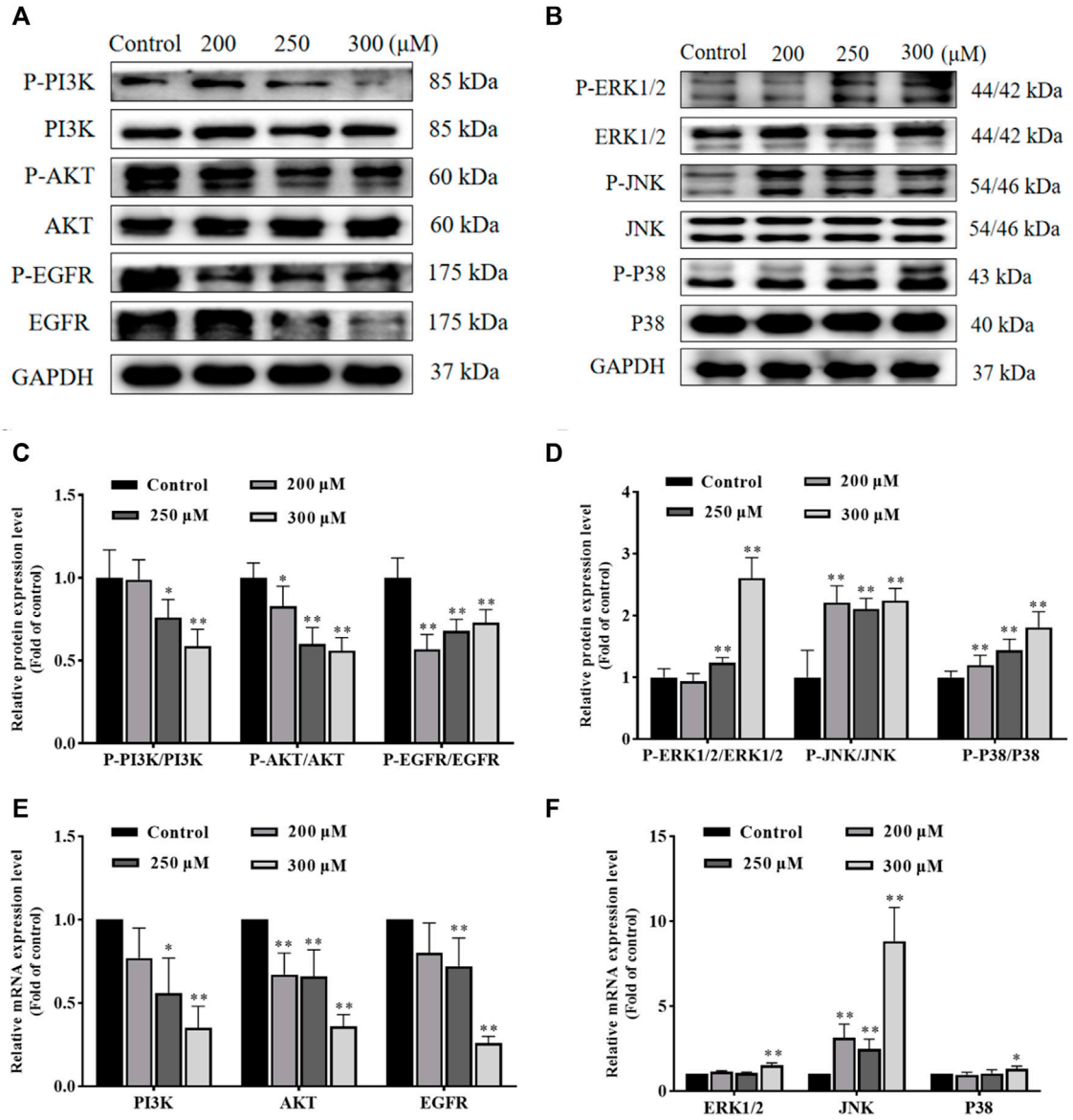

FIGURE 4
GA induces HCC1806 cells apoptosis *via* the PI3K/Akt/EGFR and MAPK signaling pathways. **(A–D)** Effect of GA on the expression of P-PI3K, P-AKT, P-EGFR, P-ERK1/2, P-JNK, and P-P38 proteins in HCC1806 cells. **(E,F)** Effect of GA on the expression of PI3K, AKT, EGFR, ERK1/2, JNK and P38 mRNA in HCC1806 cells. Date were expressed as means ± SD. Compared with the control group, $^{*}p < 0.05$, $^{**}p < 0.01$.

GA induces HCC1806 cells apoptosis *via* the mitochondrial pathway

To further investigate the effect of GA in promoting apoptosis and to assess whether this effect was associated with mitochondrial functional impairment, we examined the expression of related proteins and genes. As shown in Figures 3A–E, compared with the control group, the expression of Bax and P53 proteins in GA treatment groups were significantly increased, and the ratio of cleaved-Caspase-3/Caspase-3 and cleaved-Caspase-9/Caspase-9 were significantly increased, while the expression of Bcl-2 protein was significantly decreased. Meanwhile, compared with the control group, the expression of Bax, Caspase-3, Caspase-9 and P53 mRNA in GA treatment groups were significantly increased, while the expression of Bcl-2 mRNA was significantly decreased. These data indicated that GA induced HCC1806 cells apoptosis was related to the mitochondrial apoptosis pathway.

TABLE 2 Information of molecular docking analysis.

Protein name	PDB ID	Hydrogen bond (bond length)	Docking binding energy/kcal·mol^{-1}
PI3K	3APC	GLN-1071 (1.9, 3.3), GLU-981 (3.0)	−7.32
AKT	1GZK	TYR-417 (1.9)	−5.61
EGFR	3IKA	THR-710 (2.1, 2.2)	−4.64
ERK1/2	5LCJ	LEU-294 (2.0, 2.2)	−9.21
JNK	3V6R	GLU-369 (2.2, 2.4)	−4.39
P38	2GHL	ASP-324 (2.6), PRO-322 (1.9), ARG-73 (2.9, 3.0, 3.2)	−7.63

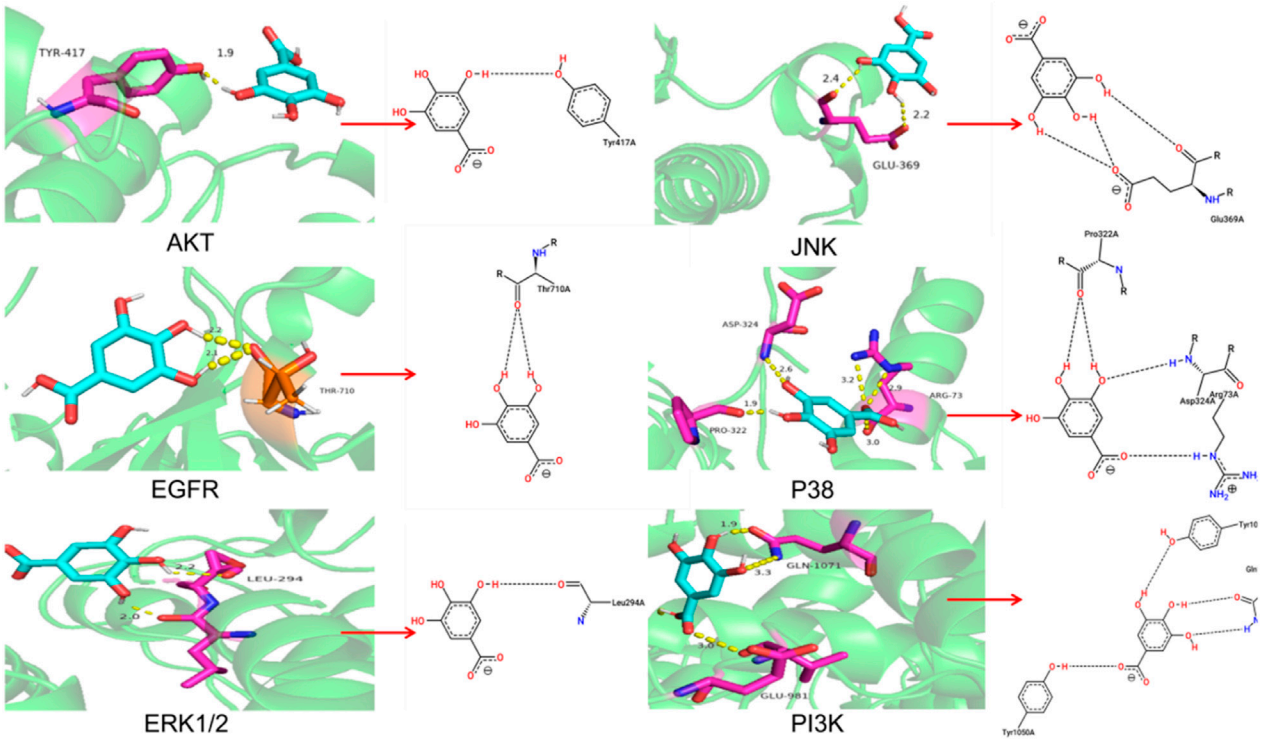

FIGURE 5
(A) Molecular docking diagram of GA and PI3K, AKT, EGFR, ERK1/2, JNK, and P38.

GA induces HCC1806 cells apoptosis *via* the PI3K/AKT/EGFR and MAPK signaling pathways

In order to investigate the possible molecular mechanisms of GA-induced apoptosis, we examined the expression of PI3K, P-PI3K, AKT, P-AKT, EGFR, P-EGFR, ERK1/2, P-ERK1/2, JNK, P-JNK, P38 and P-P38 proteins. As shown in Figures 4A–D, compared with the control group, the ratio of P-PI3K/PI3K, P-AKT/AKT and P-EGFR/EGFR in GA treatment groups were significantly decreased, while the ratio of P-ERK1/2/ERK1/2, P-JNK/JNK and P-P38/P38 in GA treatment groups were significantly increased. Furthermore, as shown in Figures 4E,F, the expression of PI3K, AKT and EGFR mRNA in GA treatment groups significantly decreased, while the expression of JNK, ERK1/2 and P38 mRNA in GA treatment groups significantly increased. These data suggested that GA induced HCC1806 cells apoptosis *via* modulating PI3K/AKT/EGFR and MAPK signaling pathways.

Molecular docking showed high binding of GA with PI3K, AKT, EGFR, ERK1/2, JNK, and P38

The molecular docking results were shown in Table 2 and Figure 5A. And the specific information of protein name, PDB ID, hydrogen bond (bond length) and docking binding energy were shown in Table 2. The binding energy of PI3K, AKT, EGFR, ERK1/2, JNK, and P38 are −7.32 kcal mol^{-1}, −5.61 kcal mol^{-1}, −4.64 kcal mol^{-1}, −9.21 kcal mol^{-1}, −4.39 kcal mol^{-1} and −7.63 kcal mol^{-1}, respectively. These molecular docking results showed that GA and each target protein had good docking activity, which could stably dock in the active capsule of the receptor protein and form hydrogen bonds. Therefore, it could be suggested that GA has a high affinity for PI3K, AKT, EGFR, ERK1/2, JNK, and P38 from the docking studies.

Discussion

BC is one of the most prevalent malignancies in women worldwide and the leading cause of cancer deaths in women (Sung et al., 2021). TNBC is more prone to distant metastases and recurrence than other breast cancers, and the risk of recurrence is highest in the third year (Shah et al., 2012). Currently, surgery, chemotherapy and radiotherapy are commonly used to treat TNBC, but these methods have serious adverse effects and do not reduce the recurrence rate of TNBC (Kim et al., 2012; Beggs et al., 2014). Therefore, it is essential to find a safe and effective drug to treat TNBC. Previous studies have shown that GA can block the MDA-MB-231 cell cycle in the G_1 phase, induce apoptosis through the P38/P21/P27 signaling axis, activate the ferroptosis pathway by inducing ROS production in MDA-MB-231 cells, and also promote cellular ROS generation and depolarization of mitochondrial membrane potential in combination with curcumin, thereby inducing MDA-MB-231 cells apoptosis (Lee et al., 2017; Moghtaderi et al., 2018; Khorsandi et al., 2020). In the present study, the effect of GA on the proliferation and apoptosis of HCC1806 cells was systematically investigated for the first time. We indicated that GA could inhibit viability and induce apoptosis of HCC1806 cells. Furthermore, it was also found that inhibition of the PI3K/AKT/EGFR signaling pathway and activation MAPK signaling pathway, which relied on the generation of ROS were involved in GA-induced apoptosis. To our knowledge, this is the first study to demonstrate that GA inhibits the viability and induces apoptosis of HCC1806 cells.

We first assessed the effect of GA on the proliferation of HCC1806 cells by MTT and plate clone formation assays. The results showed that GA could inhibit HCC1806 cells proliferation in a dose-and time-dependent manner (Zeng et al., 2020; Chen et al., 2021). Meanwhile, we found that the morphology of HCC1806 cells changed significantly after GA treatment, the number of HCC1806 cells decreased and the cells were in an apoptotic state. Furthermore, we found that GA blocked HCC1806 cells cycle in S phase. Therefore, we speculated that the inhibitory effect of GA on the proliferation of HCC1806 cells was related to the induction of apoptosis. Subsequently, we assessed the effect of GA on apoptosis of HCC1806 cells by Hoechst 33258 Staining and flow cytometry. Surprisingly, GA could induce apoptosis in HCC1806 cells. Therefore, the following experiments mainly explored the molecular mechanism of GA promoting apoptosis of HCC1806 cells.

Mitochondria plays a decisive role in cell apoptosis, and the mitochondrial apoptosis pathway is often accompanied by ROS accumulation and MMP depolarization (Song et al., 2016; Burke, 2017; Wen et al., 2019; Hengartner, 2020). We detected the ROS and MMP levels, and as we had expected, the ROS level significantly increased and the MMP significantly decreased after GA treatment. Bax is a pro-apoptotic protein that promotes apoptosis by disrupting mitochondrial membranes and creating permeable pores. Bcl-2 is an anti-apoptotic protein that inhibits apoptosis by maintaining the integrity of mitochondrial membranes. Both Bax and Bcl-2 work together to regulate cell apoptosis (Zhao et al., 2018; Estaphan et al., 2020). The Caspases family is a key target of the mitochondrial apoptosis pathway, Caspase-9 activated by mitochondria-associated proteins triggers a cascade of Caspases and further activates Caspase-3, ultimately leading to cell apoptosis (Hadisaputri et al., 2021). Accumulating evidence indicated that P53 plays a crucial role in cell apoptosis by regulating the expression of apoptosis-related proteins and activating the mitochondrial apoptosis pathway to induce apoptosis (Amaral et al., 2010; Kanapathipillai, 2018; Stein et al., 2019). Our data indicated that the ratio of cleaved-Caspase-3/Caspase-3, cleaved-Caspase-9/Caspase-9 were significantly increased, and the expression of Bax and P53 were also significantly increased, while the expression of Bcl-2 was significantly decreased after GA treatment. Moreover, the expression of Bax, P53, Caspase-3 and Caspase-9 mRNA were significantly increased, while the expression of Bcl-2 mRNA was significantly decreased after GA treatment. These results showed that GA promotes HCC1806 cells apoptosis is associated with the mitochondrial apoptosis pathway. And our research has proved that the apoptosis-promoting effect of GA on HCC1806 cells is related to mitochondrial apoptosis pathway for the first time.

PI3K/Akt signaling pathway is ubiquitous in a variety of organisms. It can regulate the cell cycle, participate in angiogenesis, promote the transition of epithelial cells to mesenchymal cells, influence chemoresistance and many other biological processes (Xu and Davis, 2017). This signaling pathway often over-express in a variety of malignancies such as breast, ovarian and lung cancers (Zhang et al., 2018; Guo et al., 2019; Zhang T et al., 2019). EGFR is a large molecular weight transmembrane glycoprotein with multiple structural regions that plays an essential role in tumor formation and growth, and it has became the critical target for targeted therapies in various tumors (Chong and Janne, 2013; Sabbah et al., 2020). MAPK

signaling pathways, including ERK, JNK, and P38, regulate nearly all cellular functions and are frequently deregulated in various human cancers (Dhillon et al., 2007). Several types of research have proved that activation of ERK1/2 signaling could cause DNA damage and induce cell apoptosis (Cagnol and Chambard, 2010; Dubey et al., 2018). Abnormal P38MAPK function is associated with cancer development and patient survival time, it mediates the Fas/Fas L apoptosis pathway by promoting p53 and c-jun phosphorylation, which induces Bax translocation, thereby activating the mitochondrial apoptosis pathway and ultimately promoting apoptosis (Feng et al., 2018; Fei et al., 2020). JNK signaling pathway plays a key role in cell proliferation, apoptosis and tumor development, and activation of the JNK signaling pathway is an effective way to induce apoptosis and is closely linked to apoptosis (Xu and Davis, 2017; Zhou et al., 2021). Tumor cells are in a state of high ROS levels and show a higher sensitivity to changes in ROS, which could induce apoptosis when stimulated by internal and external factors to produce excessive ROS (Bekhet and Eid, 2015). Amounting evidence confirmed that excessive ROS accumulation can inhibit the PI3K/AKT signaling pathway and activate the MAPK signaling pathway, ultimately resulting in cell apoptosis. For example, Zhu et al. (2020) proved ROS accumulation could induce tumor cell apoptosis by inhibiting PI3K/Akt/mTOR signaling pathway. In addition, Isoliensinine was shown to induce apoptosis in TNBC MDA-MB-231 cells by increasing ROS generation and activating P38/JNK signaling pathway (Zhang et al., 2015). And Liu et al. (2015) demonstrated that palmitate induces H9c2 cell death by activating ROS/MAPK signaling pathway. Our data showed that the expression of P-PI3K, P-AKT, and P-EGFR proteins were significantly decreased, while the expression of P-ERK1/2, P-JNK, and P-P38 proteins were significantly increased after GA treatment. In addition, the expression of PI3K, AKT and EGFR mRNA were significantly decreased, the expression of JNK and P38 mRNA were significantly increased after GA treatment. Furthermore, molecular docking results indicated that GA highly affinity for PI3K, AKT, EGFR, ERK1/2, JNK, and P38. These results provided the first evidence that GA promotes HCC1806 cells apoptosis and is associated with the PI3K/AKT/EGFR and MAPK signaling pathways, and we found that ROS generation induced by GA is crucial for the inhibition of PI3K/AKT signaling pathway and activation of MAPK signaling pathway.

In conclusion, our study provided the first evidence that GA inhibited HCC1806 cells proliferation and induced HCC1806 cells apoptosis *via* the mitochondrial apoptosis pathway and induced ROS generation, which further inhibits PI3K/AKT/EGFR and activates MAPK signaling pathways. Hence, our study initially revealed the mechanism of GA-induced apoptosis in HCC1806 cells, and it is different from previous studies on the mechanism of GA action on TNBC cells, and it will provide some new references for GA to treat TNBC. Moreover, in combination with previous studies, we know that GA has a pro-apoptotic effect on many TNBC cells and can promote apoptosis through multiple signaling pathways, which suggests that GA is a promising drug for treating TNBC. However, the present study only preliminarily validated the effect of GA on HCC1806 cells *in vitro*. Therefore, the effects and the mechanisms of action *in vivo* (animals) need to be explored in further studies.

Data availability statement

The original contributions presented in the study are included in the article/supplementary material, further inquiries can be directed to the corresponding authors.

Author contributions

HZ and LL conceived the study. SL and H-ZQ implemented the experiments and constructed the Figs. L-BX and Z-YL analyzed the data. All authors read and approved the final manuscript.

Funding

This study was supported by the National Natural Science Foundation of China (No. 8206095); Guangxi Distinguished Expert Project (Standard Research of Zhuang and Yao Ethnic Medicine, Gui Talent Tong Zi (2019) No. 13); GuangXi Key Laboratory of Zhuang and Yao Ethnic Medicine [Gui Ke Ji Zi (2014) No. 32]; Collaborative Innovation Center of Zhuang and Yao Ethnic Medicine [Gui Jiao Ke Yan (2013) No. 20]; Joint Laboratory of Zhuang and Yao Ethnic Medicine from Guangxi University of Chinese Medicine and Central South University [Gui Ke Ji Zi (2021) No. 238]; GuangXi Ethnic Medicine Resources and Application Research Center of Engineering [Gui Fa Gai Gao Ji Han (2020) No. 2605].

Conflict of interest

The authors declare that the research was conducted in the absence of any commercial or financial relationships that could be construed as a potential conflict of interest.

Publisher's note

References

Abdullah, M. L., Al-Shabanah, O., Hassan, Z. K., and Hafez, M. M. (2021). Eugenol-induced autophagy and apoptosis in breast cancer cells via PI3K/AKT/FOXO3a Pathway Inhibition. *Int. J. Mol. Sci.* 22 (17), 9243. doi:10.3390/ijms22179243

Akram, M., Iqbal, M., Daniyal, M., and Khan, A. U. (2017). Awareness and current knowledge of breast cancer. *Biol. Res.* 50 (1), 33. doi:10.1186/s40659-017-0140-9

Amaral, J, D., Xavier, J, M., Steer, C, J., and Rodrigues, C, M. (2010). The role of p53 in apoptosis. *Discov. Med.* 9 (45), 145–152.

Angelini, A., Conti, P., Ciofani, G., Cuccurullo, F., and Di Ilio, C. (2013). Modulation of multidrug resistance P-glycoprotein activity by antiemetic compounds in human doxorubicin-resistant sarcoma cells (MES-SA/Dx-5): Implications on cancer therapy. *J. Biol. Regul. Homeost. Agents* 27 (4), 1029–1037.

Aydinlik, S., Erkisa, M., Cevatemre, B., Sarimahmut, M., Dere, E., Ari, F., et al. (2017). Enhanced cytotoxic activity of doxorubicin through the inhibition of autophagy in triple negative breast cancer cell line. *Biochim. Biophys. Acta. Gen. Subj.* 1861 (2), 49–57. doi:10.1016/j.bbagen.2016.11.013

Bai, J. R., Zhang, Y. S., Tang, C., Hou, Y., Ai, X. P., Chen, X. R., et al. (2021). Gallic acid: Pharmacological activities and molecular mechanisms involved in inflammation-related diseases. *Biomed. Pharmacother.* 133, 110985. doi:10.1016/j.biopha.2020.110985

Beggs, A, D., Dilworth, M, P., Powell, S, L., Atherton, H., and Griffiths, E. A. (2014). A systematic review of transarterial embolization versus emergency surgery in treatment of major nonvariceal upper gastrointestinal bleeding. *Clin. Exp. Gastroenterol.* 7, 93–104. doi:10.2147/CEG.S56725

Bekhet, O, H., and Eid, M, E. (2015). The interplay between reactive oxygen species and antioxidants in cancer progression and therapy: A narrative review. *Transl. Cancer Res.* 10 (9), 4196–4206. doi:10.21037/tcr-21-629

Burke, P. J. (2017). Mitochondria, bioenergetics and apoptosis in cancer. *Trends Cancer* 3 (12), 857–870. doi:10.1016/j.trecan.2017.10.006

Cagnol, S., and Chambard, J, C. (2010). ERK and cell death: Mechanisms of ERK-induced cell death-apoptosis, autophagy and senescence. *FEBS J.* 277 (1), 2–21. doi:10.1111/j.1742-4658.2009.07366.x

Chen, X. H., Li, S., Li, D., Li, M. X., Su, Z. R., Lai, X. P., et al. (2020). Ethanol extract of Brucea javanica seed inhibit triple-negative breast cancer by restraining autophagy via PI3K/Akt/mTOR pathway. *Front. Pharmacol.* 11, 606. doi:10.3389/fphar.2020.00606

Chen, Y, W., Zhang, F., Du, Z, C., Xie, J, L., Xia, L., Hou, X, T., et al. (2021). Proteome analysis of camellia nitidissima chi revealed its role in colon cancer through the apoptosis and ferroptosis pathway. *Front. Oncol.* 11, 727130. doi:10.3389/fonc.2021.727130

Chong, C, R., and Jänne, P, A. (2013). The quest to overcome resistance to EGFR-targeted therapies in cancer. *Nat. Med.* 19 (11), 1389–1400. doi:10.1038/nm.3388

Denkert, C., Liedtke, C., Tutt, A., and von Minckwitz, G. (2017). Molecular alterations in triple-negative breast cancer-the road to new treatment strategies. *Lancet* 389 (10087), 2430–2442. doi:10.1016/S0140-6736(16)32454-0

Dhillon, A, S., Hagan, S., Rath, O., and Kolch, W. (2007). MAP kinase signalling pathways in cancer. *Oncogene* 26 (22), 3279–3290. doi:10.1038/sj.onc.1210421

Dubey, N, K., Peng, B, Y., Lin, C, M., Wang, P, D., Wang, J, R., Chan, C, H., et al. (2018). NSC 95397 suppresses proliferation and induces apoptosis in colon cancer cells through MKP-1 and the ERK1/2 pathway. *Int. J. Mol. Sci.* 19 (6), 1625. doi:10.3390/ijms19061625

Estaphan, S., Abdel-Malek, R., Rashed, L., and Mohamed, E, A. (2020). Cimetidine a promising radio-protective agent through modulating Bax/Bcl2 ratio: An *in vivo* study in male rats. *J. Cell. Physiol.* 235 (11), 8495–8506. doi:10.1002/jcp.29692

Fei, T., Guo, C, X., Zhang, J., Wang, L, N., and Fan, W, W. (2020). The role of p38MAPK signaling pathway in hepatocellular carcinoma recurrence. *J. Biol. Regul. Homeost. Agents* 34 (2), 647–654. doi:10.23812/20-118-L-56

Feng, Y., Wang, Y, R., Liu, H, L., Liu, Z, S., Mills, C., Owzar, K., et al. (2018). Novel genetic variants in the P38MAPK pathway gene ZAK and susceptibility to lung cancer. *Mol. Carcinog.* 57 (2), 216–224. doi:10.1002/mc.22748

Gong, Y., Zhang, L., Zhang, A. Q., Chen, X., Gao, P., and Zeng, Q. (2018). GATA4 inhibits cell differentiation and proliferation in pancreatic cancer. *PLoS One* 13 (8), e0202449. doi:10.1371/journal.pone.0202449

Guo, C. L., Li, S., Liang, A., Cui, M. C., Lou, Y., and Wang, H. (2021). PPA1 Promotes breast cancer proliferation and metastasis through PI3K/AKT/GSK3β signaling pathway. *Front. Cell Dev. Biol.* 9, 730558. doi:10.3389/fcell.2021.730558

Guo, Q., Zhu, L, C., Wang, C, X., Wang, S., Nie, X., Liu, J, J., et al. (2019). SERPIND1 affects the malignant biological behavior of epithelial ovarian cancer via the PI3K/AKT pathway: A mechanistic study. *Front. Oncol.* 9, 954. doi:10.3389/fonc.2019.00954

Hadisaputri, Y, E., Andika, R., Sopyan, I., Zuhrotun, A., Maharani, R., Rachmat, R., et al. (2021). Caspase cascade activation during apoptotic cell death of human lung carcinoma Cells A549 induced by marine sponge callyspongia aerizusa. *Drug Des. devel. Ther.* 15, 1357–1368. doi:10.2147/DDDT.S282913

Hengartner, M, O. (2000). The biochemistry of apoptosis. *Nature* 407 (6805), 770–776. doi:10.1038/35037710

Hickman, J. A. (1992). Apoptosis induced by anticancer drugs. *Cancer Metastasis Rev.* 11 (2), 121–139. doi:10.1007/BF00048059

Hon, J. D. C., Singh, B., Sahin, A., Du, G., Wang, J., Wang, V. Y., et al. (2016). Breast cancer molecular subtypes: From TNBC to QNBC. *Am. J. Cancer Res.* 6 (9), 1864–1872.

Hu, J. H., Song, J., Tang, Z. S., Wei, S. M., Chen, L., and Zhou, R. (2021). Hypericin-mediated photodynamic therapy inhibits growth of colorectal cancer cells via inducing S phase cell cycle arrest and apoptosis. *Eur. J. Pharmacol.* 900, 174071. doi:10.1016/j.ejphar.2021.174071

Jan, R., and Chaudhry, G. E. (2019). Understanding apoptosis and apoptotic pathways targeted cancer therapeutics. *Adv. Pharm. Bull.* 9 (2), 205–218. doi:10.15171/apb.2019.024

Jiang, Y., Pei, J., Zheng, Y., Miao, Y. J., Duan, B. Z., and Huang, L. F. (2022). Gallic acid: A potential anti-cancer agent. *Chin. J. Integr. Med.* 28 (7), 661–671. doi:10.1007/s11655-021-3345-2

Kanapathipillai, M. (2018). Treating p53 mutant aggregation-associated cancer. *Cancers (Basel)* 10 (6), 154. doi:10.3390/cancers10060154

Khorsandi, K., Kianmehr, Z., Hosseinmardi, Z., and Hosseinzadeh, R. (2020). Anti-cancer effect of gallic acid in presence of low level laser irradiation: ROS production and induction of apoptosis and ferroptosis. *Cancer Cell Int.* 20, 18. doi:10.1186/s12935-020-1100-y

Kim, J, H., Byun, S, J., Park, S, G., Oh, Y, K., and Baek, S, K. (2012). Interval between surgery and radiation therapy is an important prognostic factor in treatment of rectal cancer. *Cancer Res. Treat.* 44 (3), 187–194. doi:10.4143/crt.2012.44.3.187

Lee, H. L., Lin, C. S., Kao, S. H., and Chou, M. C. (2017). Gallic acid induces G1 phase arrest and apoptosis of triple-negative breast cancer cell MDA-MB-231 via p38 mitogen-activated protein kinase/p21/p27 axis. *Anticancer. Drugs* 28 (10), 1150–1156. doi:10.1097/CAD.0000000000000565

Lee, J. Y., Kim, J. M., Jeong, D. S., and Kim, M. H. (2018). Transcriptional activation of EGFR by HOXB5 and its role in breast cancer cell invasion. *Biochem. Biophys. Res. Commun.* 503 (4), 2924–2930. doi:10.1016/j.bbrc.2018.08.071

Li, J., Cai, H. W., Sun, H. H., Qu, J. B., Zhao, B., Hu, X. F., et al. (2020). Extracts of Cordyceps sinensis inhibit breast cancer growth through promoting M1 macrophage polarization via NF-κB pathway activation. *J. Ethnopharmacol.* 260, 112969. doi:10.1016/j.jep.2020.112969

Liao, W. S., Ho, Y., Lin, Y. W., Naveen Raj, E., Liu, K. K., Chen, C., et al. (2019). Targeting EGFR of triple-negative breast cancer enhances the therapeutic efficacy of paclitaxel- and cetuximab-conjugated nanodiamond nanocomposite. *Acta Biomater.* 86, 395–405. doi:10.1016/j.actbio.2019.01.025

Lin Q, Q., Fang, X. L., Liang, G. H., Luo, Q., Cen, Y. H., Shi, Y., et al. (2021). Silencing CTNND1 mediates triple-negative breast cancer bone metastasis via upregulating CXCR4/CXCL12 axis and neutrophils infiltration in bone. *Cancers* 13 (22), 5703. doi:10.3390/cancers13225703

Lin X, X. M., Wang, G. F., Liu, P., Han, L., Wang, T., Chen, K. L., et al. (2021). Gallic acid suppresses colon cancer proliferation by inhibiting SRC and EGFR phosphorylation. *Exp. Ther. Med.* 21 (6), 638. doi:10.3892/etm.2021.10070

Lin, Y. Q., Luo, T. Y., Weng, A. L., Huang, X. D., Yao, Y. Q., Fu, Z., et al. (2020). Gallic Acid Alleviates gouty arthritis by inhibiting NLRP3 inflammasome activation and pyroptosis through enhancing Nrf2 signaling. *Front. Immunol.* 11, 580593. doi:10.3389/fimmu.2020.580593

Liu, J., Chang, F., Li, F., Fu, H., Wang, J., Zhang, S., et al. (2015). Palmitate promotes autophagy and apoptosis through ROS-dependent JNK and p38 MAPK. *Biochem. Biophys. Res. Commun.* 463 (3), 262–267. doi:10.1016/j.bbrc.2015.05.042

Liu, S. H., Guo, R. J., Liu, F., Yuan, Q. J., Yu, Y., and Ren, F. F. (2020). Gut microbiota regulates depression-like behavior in rats through the neuroendocrine-immune-mitochondrial pathway. *Neuropsychiatr. Dis. Treat.* 16, 859–869. doi:10.2147/NDT.S243551

Lv, J., Guan, W. K., You, Q., Deng, L., Zhu, Y., Guo, K., et al. (2020). RIPC provides neuroprotection against ischemic stroke by suppressing apoptosis via the mitochondrial pathway. *Sci. Rep.* 10 (1), 5361. doi:10.1038/s41598-020-62336-w

Ma, Y. H., Li, Y. H., Zhang, H. Z., Wang, Y., Wu, C. E., and Huang, W. Y. (2020). Malvidin induces hepatic stellate cell apoptosis via the endoplasmic reticulum stress pathway and mitochondrial pathway. *Food Sci. Nutr.* 8 (9), 5095–5106. doi:10.1002/fsn3.1810

Maycotte, P., Marín-Hernández, A., Goyri-Aguirre, M., Anaya-Ruiz, M., Reyes-Leyva, J., and Cortés-Hernández, P. (2017). Mitochondrial dynamics and cancer. *Tumour Biol.* 39 (5), 1010428317698391. doi:10.1177/1010428317698391

Moghtaderi, H., Sepehri, H., Delphi, L., and Attari, F. (2018). Gallic acid and curcumin induce cytotoxicity and apoptosis in human breast cancer cell MDA-MB-231. *Bioimpacts* 8 (3), 185–194. doi:10.15171/bi.2018.21

Montero, J. A., Lorda-Diez, C. I., and Hurle, J. M. (2020). Confluence of cellular degradation pathways during interdigital tissue remodeling in embryonic tetrapods. *Front. Cell Dev. Biol.* 8, 593761. doi:10.3389/fcell.2020.593761

Ock, C. W., and Kim, G. D. (2021). Harmine hydrochloride mediates the induction of G2/M cell cycle arrest in breast cancer cells by regulating the MAPKs and AKT/FOXO3a signaling pathways. *Molecules* 26 (21), 6714. doi:10.3390/molecules26216714

Oh, S., Kim, H., Nam, K., and Shin, I. (2017). Glut1 promotes cell proliferation, migration and invasion by regulating epidermal growth factor receptor and integrin signaling in triple-negative breast cancer cells. *BMB Rep.* 50 (3), 132–137. doi:10.5483/bmbrep.2017.50.3.189

Ohmori, T., Yamaoka, T., Ando, K., Kusumoto, S., Kishino, Y., Manabe, R., et al. (2021). Molecular and clinical features of EGFR-TKI-Associated lung injury. *Int. J. Mol. Sci.* 22 (2), 792. doi:10.3390/ijms22020792

Sabbah, D, A., Hajjo, R., and Sweidan, K. (2020). Review on epidermal growth factor receptor (EGFR) structure, signaling pathways, interactions, and recent updates of EGFR inhibitors. *Curr. Top. Med. Chem.* 20 (10), 815–834. doi:10.2174/1568026620666200303123102

Shah, S, P., Roth, A., Goya, R., Oloumi, A., Ha, G., Zhao, Y, J., et al. (2012). The clonal and mutational evolution spectrum of primary triple-negative breast cancers. *Nature* 486 (7403), 395–399. doi:10.1038/nature10933

Shin, S. W., Choi, C., Kim, H., Kim, Y., Park, S., Kim, S. Y., et al. (2021). MnTnHex-2-PyP^{5+}, coupled to radiation, suppresses metastasis of 4T1 and MDA-MB-231 breast cancer via AKT/snail/EMT pathways. *Antioxidants (Basel)* 10 (11), 1769. doi:10.3390/antiox10111769

Song, B., Li, J., and Li, J. (2016). Pomegranate peel extract polyphenols induced apoptosis in Human hepatoma cells by mitochondrial pathway. *Food Chem. Toxicol.* 93, 158–166. doi:10.1016/j.fct.2016.04.020

Stein, Y., Rotter, V., and Aloni-Grinstein, R. (2019). Gain-of-function mutant p53: All the roads lead to tumorigenesis. *Int. J. Mol. Sci.* 20 (24), 6197. doi:10.3390/ijms20246197

Sung, H., Ferlay, J., Siegel, R. L., Laversanne, M., Soerjomataram, I., Jemal, A., et al. (2021). Global cancer statistics 2020: GLOBOCAN estimates of incidence and mortality worldwide for 36 cancers in 185 countries. *Ca. Cancer J. Clin.* 71 (3), 209–249. doi:10.3322/CAAC.21660

Wen, H., Zhou, S., and Song, J. (2019). Induction of apoptosis by magnolol via the mitochondrial pathway and cell cycle arrest in renal carcinoma cells. *Biochem. Biophys. Res. Commun.* 508 (4), 1271–1278. doi:10.1016/j.bbrc.2018.12.087

Woo, S. M., Kim, A. J., Choi, Y. K., Shin, Y. C., Cho, S. G., and Ko, S. G. (2016). Synergistic Effect of SH003 and doxorubicin in triple-negative breast cancer. *Phytother. Res.* 30 (11), 1817–1823. doi:10.1002/ptr.5687

Xu, P., and Davis, R, J. (2017). Correction for Xu and Davis, "c-Jun NH2-terminal kinase is required for lineage-specific differentiation but not stem cell self-Renewal. *Mol. Cell. Biol.* 37 (17), e002800–17. doi:10.1128/MCB.00280-17

Yu, R., Yu, B, X., Chen, J, F., Lv, X, Y., Yan, Z, J., Cheng, Y., et al. (2016). Anti-tumor effects of Atractylenolide I on bladder cancer cells. *J. Exp. Clin. Cancer Res.* 35, 40. doi:10.1186/s13046-016-0312-4

Yue, J, C., and López, J. M. (2020). Understanding MAPK signaling pathways in apoptosis. *Int. J. Mol. Sci.* 21 (7), 2346. doi:10.3390/ijms21072346

Zeng, M. L., Su, Y., Li, K. Y., Jin, D., Li, Q., Li, Y. L., et al. (2020). Gallic Acid inhibits bladder cancer T24 cell progression through mitochondrial dysfunction and PI3K/Akt/NF-κB signaling suppression. *Front. Pharmacol.* 11, 1222. doi:10.3389/fphar.2020.01222

Zhang, H., Xu, H, L., Wang, Y, C., Lu, Z, Y., Yu, X, F., and Sui, D, Y. (2018). 20(S)-Protopanaxadiol-induced apoptosis in MCF-7 breast cancer cell line through the inhibition of PI3K/AKT/mTOR signaling pathway. *Int. J. Mol. Sci.* 19 (4), 1053. doi:10.3390/ijms19041053

Zhang N, N., Yan, Q, Q., Lu, L., Shao, J, B., and Sun, Z, G. (2019). The KLF6 splice variant KLF6-SV1 promotes proliferation and invasion of non-small cell lung cancer by up-regultating PI3K-AKT signaling pathway. *J. Cancer* 10 (22), 5324–5331. doi:10.7150/jca.34212

Zhang T, T. X., Ma, L. J., Wu, P. F., Li, W., Li, T., Gu, R., et al. (2019). Gallic acid has anticancer activity and enhances the anticancer effects of cisplatin in non-small cell lung cancer A549 cells via the JAK/STAT3 signaling pathway. *Oncol. Rep.* 41 (3), 1779–1788. doi:10.3892/or.2019.6976

Zhang, X., Wang, X., Wu, T., Li, B., Liu, T., Wang, R., et al. (2015). Isoliensinine induces apoptosis in triple-negative human breast cancer cells through ROS generation and p38 MAPK/JNK activation. *Sci. Rep.* 5, 12579. doi:10.1038/srep12579

Zhao, D, X., Zhang, M, L., Yuan, H, P., Meng, C, Y., Zhang, B, Y., and Wu, H. (2018). Ginsenoside Rb1 protects against spinal cord ischemia-reperfusion injury in rats by downregulating the Bax/Bcl-2 ratio and caspase-3 and p-Ask-1 levels. *Exp. Mol. Pathol.* 105 (3), 229–235. doi:10.1016/j.yexmp.2018.09.001

Zhou, N., Wei, Z, X., Qi, Z, X., and Chen, L. (2021). Abscisic acid-induced autophagy selectively via MAPK/JNK signalling pathway in glioblastoma. *Cell. Mol. Neurobiol.* 41 (4), 813–826. doi:10.1007/s10571-020-00888-1

Zhu, S., Zhou, J., Sun, X., Zhou, Z., and Zhu, Q. (2020). ROS accumulation contributes to abamectin-induced apoptosis and autophagy via the inactivation of PI3K/AKT/mTOR pathway in TM3 Leydig cells. *J. Biochem. Mol. Toxicol.* 34 (8), e22505. doi:10.1002/jbt.22505

frontiers | Frontiers in Oncology

TYPE Mini Review
PUBLISHED 29 November 2022
DOI 10.3389/fonc.2022.1013902

OPEN ACCESS

EDITED BY
Cyril Corbet,
Fonds National de la Recherche Scientifique (FNRS), Belgium

REVIEWED BY
Aaron Hobbs,
Medical University of South Carolina, United States
Boshi Wang,
Shanghai Cancer Institute, China

*CORRESPONDENCE
Asfar S. Azmi
azmia@karmanos.org

SPECIALTY SECTION
This article was submitted to Pharmacology of Anti-Cancer Drugs, a section of the journal Frontiers in Oncology

RECEIVED 08 August 2022
ACCEPTED 08 November 2022
PUBLISHED 29 November 2022

CITATION
Bannoura SF, Khan HY and Azmi AS (2022) KRAS G12D targeted therapies for pancreatic cancer: Has the fortress been conquered?
Front. Oncol. 12:1013902.
doi: 10.3389/fonc.2022.1013902

KRAS G12D targeted therapies for pancreatic cancer: Has the fortress been conquered?

Sahar F. Bannoura[1], Husain Yar Khan[2] and Asfar S. Azmi[2*]

[1]Cancer Biology Graduate Program, Wayne State University School of Medicine, Karmanos Cancer Institute, Detroit, MI, United States, [2]Department of Oncology, Karmanos Cancer Institute, Wayne State University School of Medicine, Detroit, MI, United States

KRAS mutations are among the most commonly occurring mutations in cancer. After being deemed undruggable for decades, KRAS G12C specific inhibitors showed that small molecule inhibitors can be developed against this notorious target. At the same time, there is still no agent that could target KRAS G12D which is the most common KRAS mutation and is found in the majority of KRAS-mutated pancreatic tumors. Nevertheless, significant progress is now being made in the G12D space with the development of several compounds that can bind to and inhibit KRAS G12D, most notably MRTX1133. Exciting advances in this field also include an immunotherapeutic approach that uses adoptive T-cell transfer to specifically target G12D in pancreatic cancer. In this mini-review, we discuss recent advances in KRAS G12D targeting and the potential for further clinical development of the various approaches.

KEYWORDS

KRAS, KRAS G12C, KRAS G12D, sotorasib, adagrasib, MRTX1133, adoptive cell therapy, immunotherapy

Introduction

RAS genes (KRAS, HRAS, NRAS) are the most commonly mutated oncogenes in cancers, resulting in increased downstream signaling that drives incessant proliferation and tumorigenesis. Certain tumors are more dependent on KRAS mutation, especially pancreatic ductal adenocarcinoma (PDAC) which remains one of the most lethal cancers, with a 5-year survival rate of 11% in the United States (1). Advances in our understanding of PDAC molecular pathology and subtypes have not translated into significant improvements in patient outcomes (2). Genetic alterations in the oncogene KRAS, and the tumor suppressors CDKN2A, SMAD4, and TP53 are the most common mutational drivers in PDAC, in addition to various genes identified at low mutation frequency. This complex genetic landscape has created a tremendous challenge for therapeutic targeting.

KRAS mutations in PDAC

Mutations in KRAS, CDKN2A, TP53, and SMAD4 are the major genetic mutations that underly PDAC development (Figure 1A). The KRAS oncogene is the major oncogenic driver of PDAC (86 – 91%) (3), and is considered a master oncogenic regulator that drives cancer hallmarks including sustained proliferative signaling and evading growth suppression. KRAS mutations are found at the earliest stage of PDAC development in patient samples, and are required for the initiation and maintenance of PDAC in genetically engineered mouse models, suggesting that KRAS mutations are important for both PDAC initiation and progression (4–6). The most predominant KRAS mutation site in PDAC occurs at codon 12; most commonly G12D (45%), followed by G12V (35%), and G12R at 17% (Figure 1B) (3). Other mutations such as G12C and G12F occur at a lower frequency.

Mutant KRAS is notoriously difficult to target. It had been deemed undruggable until the recent success of inhibitors that target KRAS with a G12C mutation, AMG510 (sotorasib) and

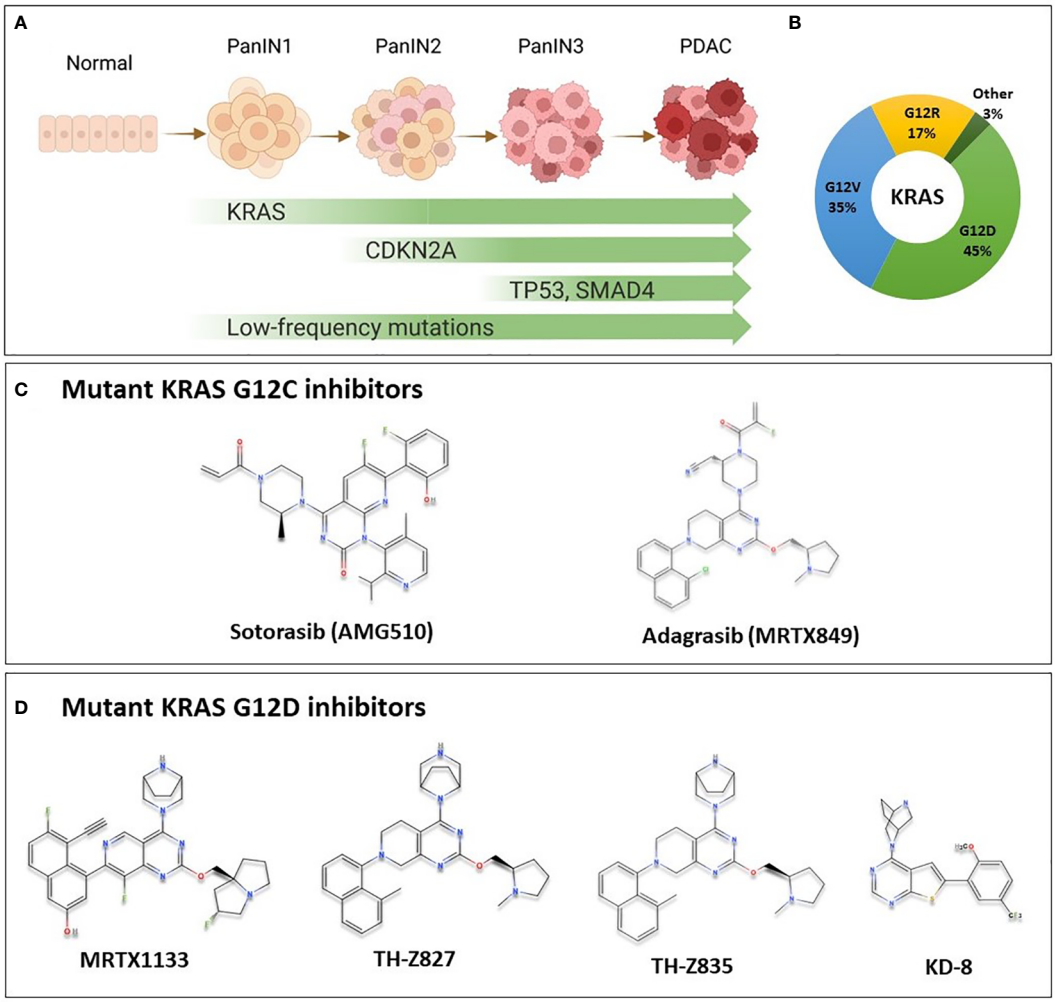

FIGURE 1
KRAS Oncogene in PDAC and the chemical structure of some of mutant KRAS small molecule inhibitors. **(A)** Multi-stage development model of KRAS-mutated PDAC. As cells acquire mutations in KRAS, CDKN2A, SMAD4 and TP53 in addition to less commonly mutated genes, the lesion progresses from low grade pancreatic intraepithelial neoplasia (PanIN1), through PanIN2, and high grade PanIN3 to become invasive carcinoma. **(B)** Most common KRAS mutations in PDAC are G12D (45%), G12V (35%), G12R (17%) representing important targets for PDAC patients. Other mutations such as G12C, G12A and others are less common (3%). **(C)** Sotorasib and adagrasib are mutant KRAS G12C inhibitors. They bind specifically to the mutant form by making covalent interactions with Cys12 in the switch-II pocket of mutant KRAS, locking it in the inactive state, and preventing downstream signaling. These agents have been investigated in clinical trials, and sotorasib is currently FDA approved for the treatment of KRAS G12C-mutated NSCLC. **(D)** Novel KRAS G12D inhibitors with available chemical structures, MRTX1133, TH-Z827, TH-Z835, and KD-8. These agents bind specifically and non-covalently to mutant KRAS G12D, thereby inhibiting proliferation in mutated cells. These agents are currently in preclinical development, and details on further clinical development are not currently known.

MRTX849 (adagrasib) (Figure 1C) (7). Sotorasib has been granted approval by the US Food and Drug Administration (FDA) for the treatment of certain patients with KRAS-mutated non-small cell lung cancer (NSCLC); and adagrasib has been given a breakthrough therapy designation by the FDA also for NSCLC (8). For PDAC patients, however, a mutation that replaces Glycine at codon 12 with Aspartic Acid (G12D) is the most common mutational event in KRAS, representing approximately 45% of KRAS mutations, as previously mentioned (3), and only a very modest proportion of patients would benefit from G12C targeted therapy. Nonetheless, since KRAS was found to be potentially druggable, multiple groups have aptly been working to develop inhibitors targeting the most common KRAS G12D mutation.

Overview of KRAS oncogene and targeting efforts

KRAS is a small GTPase protein that is encoded by the *KRAS* proto-oncogene (9). It is activated by extracellular growth signaling that is transmitted by growth receptors such as EGFR family (10). Growth signaling allows KRAS to exchange its GDP for GTP, thereby affecting conformational change and further transmission of downstream signals. KRAS is upstream of critical signaling pathways, such as RAF/MEK/ERK MAPK, and PI3K signaling pathways.

KRAS cycles between GDP and GTP with the activity of guanine exchange factors (GEFs) that catalyze the exchange of GDP for GTP, and GTPase activating proteins (GAPs) that enhance the intrinsic KRAS GTPase activity. Son of Sevenless 1 (SOS1) is the main GEF to act on KRAS, and together with GAPs, it is responsible for the regulation of the guanine exchange cycle, and maintenance of KRAS in an inactive state in the absence of proper growth signaling (11). Mutations in KRAS change the dynamics of the guanine exchange cycle, resulting in hyperactive KRAS and increased pools of GTP-bound KRAS. This leads to the constant activation of downstream signaling cascades such as MAPK and PI3K, and consequently incessant cellular proliferation.

KRAS is frequently mutated in pancreatic cancer, colorectal cancer (CRC), and lung cancer (3). Therefore, looking for ways to target KRAS, whether directly or indirectly, has garnered great attention from researchers (12). Directly targeting KRAS had been elusive for decades. KRAS lacks a suitable deep hydrophobic binding pocket to design small molecule inhibitors, other than the GTP/GDP binding pocket. However, GTP is highly abundant in the cell, thus precluding efficacious nucleotide competitive inhibitors. Additionally, indirect targeting of KRAS through upstream or downstream regulators or effectors was either ineffective or caused major toxicities (13). The major breakthrough in the field came when undruggable KRAS was finally drugged with the discovery of the first KRAS G12C inhibitors.

The Discovery of KRAS G12C inhibitors and its targetable pocket

Pioneering work by Shokat and colleagues paved the way for the clinical development of mutant KRAS G12C inhibitors (14). They were able to identify a druggable pocket termed the switch II pocket, which contains a reactive cysteine as a result of the G12C mutation in mutant KRAS (14). The co-crystal structure of hit compound and KRAS showed the compound binding in a pocket that lies beneath the switch II region of KRAS protein (14). Within the switch II allosteric pocket Cys12 is present, which contains a nucleophilic thiol group, making it a prime target for covalent drugs (15). It also affords the inhibitor high specificity over the other RAS isoforms (HRAS and NRAS) as well as wild-type KRAS, thereby reducing off-target effects and toxicities.

The early G12C inhibitor, compound 12, is a covalent inhibitor that binds in the switch II pocket of KRAS G12C in its GDP-bound form. Several other compounds were subsequently discovered and reported to have activity against cancer cells with KRAS G12C mutations (16, 17). An early compound, ARS-1620, was shown to inhibit tumor growth in cell-derived and patient-derived xenograft models (18). These efforts provided proof of concept for targeting KRAS G12C, which culminated in the development of the clinical agents sotorasib and adagrasib (19–23). Based on the safety, tolerability, and efficacy results of a phase 1/2 study of sotorasib (CodeBreaK 100, NCT03600883), it has received FDA approval for advanced NSCLC with KRAS G12C mutations. Results from the trial demonstrated an 80.6% disease control rate, with four patients achieving a complete response, and a median progression free survival of 6.3 months (22). A phase III trial (CodeBreaK 200, NCT04303780) is ongoing, which compares sotorasib with docetaxel chemotherapy in previously treated NSCLC patients. Sotorasib is also being investigated clinically as first-line therapy for stage 4 NSCLC patients (NCT04933695).

Adagrasib is being investigated in a phase I/II clinical trial (KRYSTAL-1, NCT03785249). In patients with measurable disease at baseline, the objective response rate was 42.9%, median progression free survival of 6.5 months, and overall survival of 12.6 months after 15.6 months of follow-up (23).

The limitation of any single agent treatment is the inevitable emergence of resistance. Studies have shown that resistance to G12C inhibitors could be inherent or acquired (24). Mechanisms of resistance include activation of receptor tyrosine kinase (RTKs), resulting in downstream activation of KRAS *via* SHP2 (25). Several mechanisms of resistance have been reported in

patient samples treated with adagrasib including secondary activating mutations in KRAS, amplification of KRAS(G12C), and mutations in compensatory pathways that bypass KRAS such as MET amplification, and NRAS, BRAF, MAP2K1, and RET mutations (26). To combat resistance to G12C inhibitors, several trials are looking to combine mutation specific inhibitors with other agents. In CodeBreaK 101 (NCT04185883) several drugs are being investigated in combination with sotorasib, such as trametinib, TNO155, everolimus, palbociclib, pembrolizumab or several other agents. Adagrasib is also being evaluated in combination with other agents, such as pembrolizumab (NCT04613596), and TNO155 (NCT04330664). Although these trials would primarily benefit lung cancer patients, they provide valuable strategies for future targeting of non-G12C mutations.

As discussed, sotorasib has been given FDA approval for the treatment of certain patients with NSCLC (27). Despite encouraging results from the trials, and FDA approval, these drugs have provided little hope for the majority of PDAC patients. While KRAS G12C mutations are more prevalent in lung cancer, KRAS G12D mutation is the most common in PDAC as well as CRC. Available G12C inhibitors rely on the reactivity of the thiol group in Cys12 of mutant KRAS. To benefit PDAC patients and target the G12D mutation, an approach that does not rely on a reactive cysteine is required.

Small molecule inhibitors targeting KRAS G12D

Discovery of KRAS G12D inhibitor MRTX1133

As previously mentioned, G12D mutations are present in a large proportion of PDAC patients. The covalent G12C inhibitors relied on the presence of a strongly nucleophilic cysteine in the switch II pocket, as well as the unique biochemical properties of the KRAS G12C mutant, which has a higher rate of GTP hydrolysis compared to other mutants (28). The switch II pocket in KRAS G12D, however, lacks a reactive cysteine to target with a covalent inhibitor, and aspartic acid is not considered a good target for covalent attack.

A structure-based medicinal chemistry approach has been employed to identify compounds that can react through a salt bridge with Asp12 of the switch II pocket in KRAS G12D (29). Using adagrasib as a starting point, chemical modifications to the reactive warhead and various other groups in the compound were introduced to increase the binding affinity within the pocket. Optimization of hit compounds resulted in the discovery of MRTX1133 (Figure 1D), which selectively and reversibly binds KRAS G12D with low nanomolar affinity in cellular assays (30).

Binding of MRTX1133 to KRAS G12D prevents downstream signaling through inhibition of nucleotide exchange and binding of downstream effector RAF1 (30). This compound was shown to inhibit oncogenic KRAS signaling selectively in tumor cells (30). In a xenograft mouse model, MRTX1133 was able to significantly reduce tumor growth and decrease the phosphorylation of downstream signaling molecule ERK in a dose-dependent manner (30). So far, this agent remains an *in vitro* tool compound, and its clinical progress is not known.

Other KRAS G12D inhibitors

Besides MRTX1133 described above, other groups have been pursuing the development of KRAS G12D inhibitors as well. For example, using a medicinal chemistry approach to find inhibitors that bind to Asp12 in KRAS G12D, two inhibitors TH-Z827 and TH-Z835 were discovered (Figure 1D) (31). These inhibitors form a salt bridge with Asp12 within the switch-II pocket resulting in the inhibition of KRAS signaling in G12D mutant PDAC cell lines (31). These compounds were able to bind the G12D mutant specifically, and not KRAS G12C or WT. The compounds also showed *in vivo* inhibition of tumor growth in xenograft tumor mouse models (31). Another set of inhibitors was discovered using virtual combinatorial chemistry and compound screening approach (32). In this approach, they used the backbone of G12C inhibitors in combination with piperazine-based compounds as building blocks for the compound library, followed by molecular docking to discover compounds with predicted selective binding. Compound 'KD-8' was discovered, which resulted in the inhibition of cellular and tumor growth of KRAS G12D mutated cells (32). However, further development of these compounds is required to increase their potency and minimize off-target effects. While these agents are not yet ready for clinical development, they provide further proof of principle that several classes of G12D inhibitors could be potentially discovered as clinical anti-cancer agents.

A tricomplex inhibitor, RMC-9805, is a novel covalent KRAS G12D inhibitor that binds KRAS in the GTP-bound state, thus termed a KRAS-G12D(ON) inhibitor (33). Tricomplex inhibitors bind a chaperone protein, Cyclophilin A, which is ubiquitously found inside the cell (34), which then binds the target protein, creating a target-inhibitor-Cyclophilin-A complex. RMC-9805 reacts covalently with Asp12, thereby attenuating KRAS G12D downstream signaling specifically over KRAS WT and other KRAS mutants, and it restricts tumor growth in xenograft PDAC and CRC mouse models (33). Within this class of inhibitors, there are several other compounds being developed to target various KRAS mutants, as well.

An emerging strategy to target oncogenic RAS is using monobodies to target the α4-α5 interface of KRAS, thus preventing its dimerization and downstream signaling (35–37). A monobody termed NS-1 was able to inhibit growth of G12D mutated PDAC in mice (35). However, the limitation of this strategy is the low cellular permeability of these large molecules.

Therefore, further optimization is required for this approach prior to clinical testing.

Various efforts are now focused on research and discovery of novel KRAS G12D inhibitors. The development of agents, such as MRTX1133, is exciting for the field of PDAC research and provides evidence that KRAS G12D can be effectively targeted with a small molecule inhibitor. As with the G12C inhibitors, perhaps this discovery could lead to more small molecules entering the arsenal against G12D. As we await to see further clinical development of MRTX1133, the optimization of hits and potential discovery of more targeted compounds is anticipated. These efforts are critical for patients with KRAS G12D mutations, which make up a large subset of Ras-mutated cancers, especially for PDAC where the therapeutics currently available are providing meager benefits in the majority of cases.

Immunotherapy targeting KRAS G12D in PDAC

Immunotherapeutic approaches have not had great success for PDAC patients (38). In other Ras-mutated cancers, immune checkpoint inhibitors (ICIs) have improved patient outcomes in clinical trials and thus have been approved by the FDA for the treatment of NSCLC and melanoma (39). However, ICIs did not achieve similar success in PDAC, even in combinatorial approaches. PDAC is characterized by a desmoplastic tumor microenvironment (TME) with low numbers of tumor-infiltrating lymphocytes (TILs) and is largely considered to be immunosuppressive (40). Immune cells that are found within the PDAC TME include tumor-associated macrophages (TAMs), myeloid-derived suppressive cells (MDSCs), and regulatory T cells (Tregs) which contribute to immune evasion, PDAC progression, and resistance to immunotherapies (38, 41). These factors could explain the observed low response of PDAC to ICIs in clinical trials (42–44). The exception is a small subset of PDAC patients with high microsatellite instability (MSI-H) tumors or mismatch repair deficiency (<1%) who can benefit from anti-PD-1 therapy (45, 46). Nevertheless, attempts are being made to identify targets that could reinvigorate the immune suppressive tumor microenvironment to become more immunogenic and better responsive to immunotherapy.

Mutant KRAS modulates tumor immune microenvironment

Several studies have highlighted the role of oncogenic KRAS in establishing a pro-inflammatory microenvironment that enables PDAC tumorigenesis and progression (47–50). Oncogenic KRAS G12D signaling in tumor cells regulates the signaling of surrounding stromal cells and establishes reciprocal signaling between tumor and stromal cells (49, 51). PD-L1 expression is also suppressed by oncogenic KRAS G12D, and patients with G12D mutation have lower PD-L1 expression compared to other KRAS mutants (52, 53). Additional evidence for the role of oncogenic KRAS in modulating the TME comes from a recent study utilizing the anti-KRAS G12C agent AMG510 (19); where treatment with AMG510 increased the number of cytotoxic CD8+ T cells that infiltrated tumors in mice. Anti-KRAS therapy also synergized with anti-PD-1 treatment and produced durable anti-tumor responses (19). This provides strong evidence that KRAS signaling is involved in modulating the TME and maintaining an immune evasive environment, which hinders the development of ICIs as monotherapy in PDAC. Nevertheless, it also shows that using the right tools, the TME can be modulated and PDAC can potentially become responsive to immunotherapeutic approaches.

T cell therapy targeting KRAS G12D

Adoptive cell therapy utilizes the patient's own lymphocytes which may be engineered to express receptors that specifically target tumor neoantigens (54). This immunotherapeutic approach may be suitable to target KRAS neoantigens for PDAC therapy and to address the challenge of targeting KRAS, as well as the challenge of implementation of immunotherapies in PDAC. A study identified HLA-A*11:01 to be able to present KRAS neoantigens, and then generated murine T cells that recognize G12D mutated PDAC in an HLA-A*11:01 restricted manner and could inhibit the growth of tumors *in vivo*. (55). An ongoing phase I/II clinical trial is investigating transfer of T-cells engineered to express a G12D specific murine T-cell receptor (TCR) in HLA-A*11:01 patients with solid tumors, including pancreatic cancer, harboring the KRAS G12D mutation (NCT03745326).

In a recent report, a patient with metastatic G12D-mutated PDAC received adoptive cell transfer therapy using engineered autologous T cells that target KRAS G12D mutant protein in the tumor, resulting in regression of metastases in the patient (Figure 2) (56). A patient with CRC had been previously reported to receive an infusion of ex-vivo expanded T cells with HLA-C*08:02 restriction and KRAS G12D reactivity, resulting in the regression of metastatic lung lesions (57). Based on the previous success of this approach, a heavily pretreated PDAC patient with lung metastases was treated with T-cells that were engineered to express HLA-C*08:02 restricted TCRs with specificity against KRAS G12D (56). A single infusion of 16.2×10^9 T-cells was given to the patient, which contained 85% CD8+ T-cells, and 15% CD4+ T cells, with high-dose interleukin-2 therapy to support T-cell expansion. One month follow-up revealed regression of metastatic lung lesions, which continued to regress at the 6-month follow-up with an overall objective partial response of 72% according to RECIST, version 1.1, criteria (56). Additionally, the infused T-cells were found to persist in circulation at 6 months, making up 2.4% of total circulating T cells.

This reported case shows that engineered TCRs could be beneficial to some patients with metastatic PDAC. The drawback

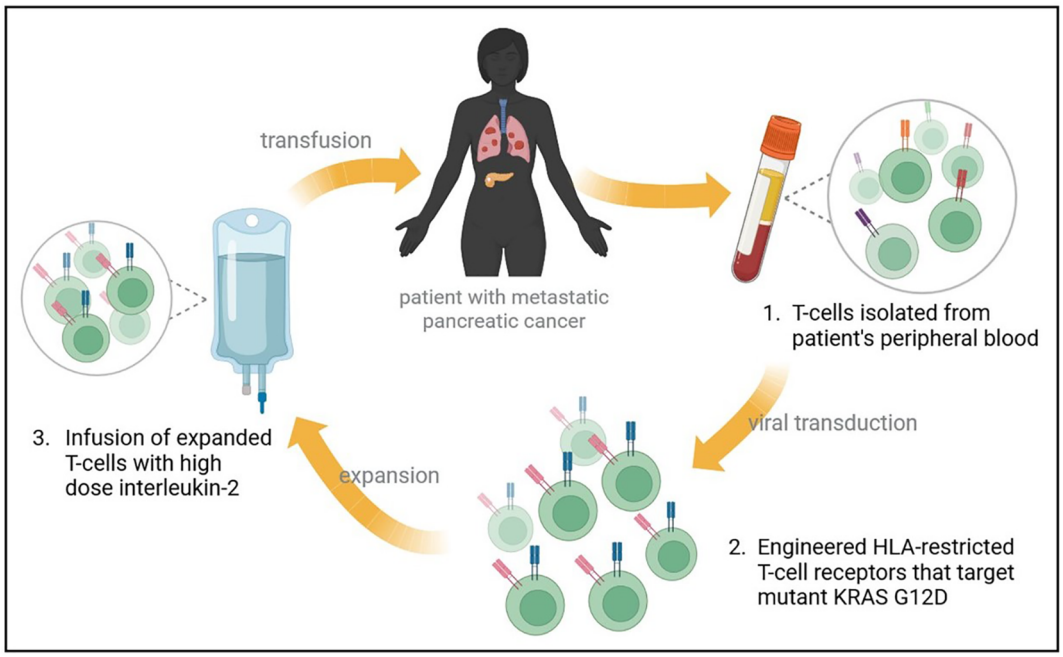

FIGURE 2
Treatment of metastatic PDAC with mutant KRAS-targeting genetically engineered T-cells. A heavily pretreated patient with metastatic PDAC to the lungs underwent an expiremental immunotherapy that targets mutant KRAS. Autologous T-cells were isolated and transfected with genes encoding two HLA-restricted T-cell receptors targeting KRAS G12D epitopes. The infusion product contained $16.2x10^9$ T cells, and supportive high dose interleukin-2 therapy was administered. Metastatic lung lesions regressed at 1 month follow up, with continued regression at 6-months and an overall partial response rate of 72%.

of this therapy is that TCRs were restricted by a specific HLA-C*08:02, which is expressed by a small subset of patients. Further studies and clinical trials are needed to investigate this therapy on a larger scale, and to identify other KRAS-G12D-reactive TCRs which could be utilized for similar therapies (58, 59). Meanwhile, results from the ongoing clinical trial for HLA-A*11:01+ patients are eagerly awaited.

Targeting KRAS mutations beyond G12D

Since the discovery of G12C inhibitors, there has been growing interest in finding novel mutant-specific inhibitors to other common KRAS mutants. For a more detailed review, Nagasaka and colleagues have recently published an article highlighting novel strategies to target KRAS beyond G12C inhibitors including cancer vaccines, adoptive cell therapy, PROTACs and CRISPR/Cas9 (60).

KRAS G12R mutation is present in 17% of PDAC cases (Figure 1) and is therefore an important target for PDAC. Recent work has shown that the mutant arginine 12 in KRAS G12R can be targeted covalently with small molecule electrophiles (61). Although the molecules that target G12R have not shown activity in mutant cells, they could be further optimized to develop more potent molecules, and thus this presents an important proof of concept for targeting G12R. Less prevalent in PDAC, the G12S mutation in KRAS has also been targeted recently with compounds that acylate the noncatalytic mutant serine 12 residue (62). These compounds have shown selectivity for cells harboring the G12S mutation, but currently remain *in vitro* tools that require further optimization. Another class of drugs mentioned previously, is the tricomplex Ras(On) inhibitors, which are being developed against various KRAS mutants including G12C, G12D, and G13C, in addition to a G12X inhibitor that targets several G12 mutants (63).

Conclusion

RAS genes are the most commonly mutated oncogenes in cancers. A mutation in KRAS is the most common oncogenic driver in PDAC and is also a known driver of NSCLC and CRC. Until the recent discovery of KRAS G12C inhibitors, KRAS had been considered an undruggable target for decades (64). Given the success of translating this discovery to the clinic, research efforts are focusing on drugging KRAS G12D, the most common hotspot mutation. The discovery of the preclinical agent

MRTX1133 is an exciting advance for pancreatic cancer research. MRTX1133 binds potently and reversibly in the switch II pocket of mutant KRAS G12D. We hope that this discovery will lead to precipitous efforts by various groups to introduce optimized agents that can be tested clinically for PDAC patients.

The switch-II pocket seems to be a druggable pocket in various KRAS mutants and is susceptible to reversible non-covalent inhibition. Additionally, this pocket could potentially be targeted in both the GDP as well as the GTP-bound states of KRAS (31, 65), meaning it is possible to develop inhibitors that target KRAS mutants with low intrinsic GTPase activity (28).

Cancer immunotherapy using ICIs and the observed durable responses with limited toxicities has generated a lot of excitement within the cancer research field. Despite many approvals for various cancers, immunotherapeutic approaches are yet to be approved for the treatment of PDAC. Targeting KRAS G12D using engineered T cells is an exciting development for immunotherapy in the PDAC KRAS G12D space.

To answer the question, has the KRAS G12D fortress been conquered? At this point in time, there are definitely exciting advances towards that goal, but G12D agents have a few more hurdles to overcome. The fortress may not have been conquered yet, but the walls we once thought were impervious have certainly been breached.

Author contributions

SB researched and drafted the article. HK and AA supervised the content. All authors contributed to the article and approved the submitted version.

Funding

Work in the lab of AA is supported by NIH NCI R01CA24060701 and R37CA215427

Acknowledgments

AA acknowledges support from SKY Foundation Inc and U CAN-CER VIVE foundation. SB is supported by WSU Thomas C. Rumble Fellowship.

Conflict of interest

The remaining authors declare that the research was conducted in the absence of any commercial or financial relationships that could be construed as a potential conflict of interest.

AA received funding from Karyopharm Therapeutics Inc and Purple Biotech. AA serves as a consultant for GLG and Guidepoint.

Publisher's note

References

1. Siegel RL, Miller KD, Fuchs HE, Jemal A. Cancer statistic. *CA Cancer J Clin* (2022) 72:7–33. doi: 10.3322/caac.21708

2. Torres C, Grippo PJ. Pancreatic cancer subtypes: A roadmap for precision medicine. *Ann Med* (2018) 50:277–87. doi: 10.1080/07853890.2018.1453168

3. Moore AR, Rosenberg SC, Mccormick F, Malek S. RAS-targeted therapies: Is the undruggable drugged? *Nat Rev Drug Discov* (2020) 19:533–52. doi: 10.1038/s41573-020-0068-6

4. Kanda M, Matthaei H, Wu J, Hong SM, Yu J, Borges M, et al. Presence of somatic mutations in most early-stage pancreatic intraepithelial neoplasia. *Gastroenterology* (2012) 142:730–733.e9. doi: 10.1053/j.gastro.2011.12.042

5. Hingorani SR, Petricoin EF, Maitra A, Rajapakse V, King C, Jacobetz MA, et al. Preinvasive and invasive ductal pancreatic cancer and its early detection in the mouse. *Cancer Cell* (2003) 4:437–50. doi: 10.1016/s1535-6108(03)00309-x

6. Collins MA, Bednar F, Zhang Y, Brisset JC, Galban S, Galban CJ, et al. Oncogenic kras is required for both the initiation and maintenance of pancreatic cancer in mice. *J Clin Invest* (2012) 122:639–53. doi: 10.1172/JCI59227

7. Huang L, Guo Z, Wang F, Fu L. KRAS mutation: From undruggable to druggable in cancer. *Signal Transduction Targeted Ther* (2021) 6:386. doi: 10.1038/s41392-021-00780-4

8. Arbour KC, Lito P. Expanding the arsenal of clinically active KRAS G12C inhibitors. *J Clin Oncol* (2022) 40:2609–11. doi: 10.1200/JCO.22.00562

9. Hobbs GA, Der CJ, Rossman KL. RAS isoforms and mutations in cancer at a glance. *J Cell Sci* (2016) 129:1287–92. doi: 10.1242/jcs.182873

10. Buday L, Downward J. Many faces of ras activation. *Biochim Biophys Acta (BBA) - Rev Cancer* (2008) 1786:178–87. doi: 10.1016/j.bbcan.2008.05.001

11. Hennig A, Markwart R, Esparza-Franco MA, Ladds G, Rubio I. Ras activation revisited: Role of GEF and GAP systems. *Biol Chem* (2015) 396:831–48. doi: 10.1515/hsz-2014-0257

12. Bannoura SF, Uddin MH, Nagasaka M, Fazili F, Al-Hallak MN, Philip PA, et al. Targeting KRAS in pancreatic cancer: New drugs on the horizon. *Cancer Metastasis Rev* (2021) 40:819–35. doi: 10.1007/s10555-021-09990-2

13. Nollmann FI, Ruess DA. Targeting mutant KRAS in pancreatic cancer: Futile or promising? *Biomedicines* (2020) 8(8):281. doi: 10.3390/biomedicines8080281

14. Ostrem JM, Peters U, Sos ML, Wells JA, Shokat KM. K-Ras(G12C) inhibitors allosterically control GTP affinity and effector interactions. *Nature* (2013) 503:548–51. doi: 10.1038/nature12796

15. Potashman MH, Duggan ME. Covalent modifiers: An orthogonal approach to drug design. *J Med Chem* (2009) 52:1231–46. doi: 10.1021/jm8008597

16. Lito P, Solomon M, Li LS, Hansen R, Rosen N. Allele-specific inhibitors inactivate mutant KRAS G12C by a trapping mechanism. *Science* (2016) 351:604–8. doi: 10.1126/science.aad6204

17. Patricelli MP, Janes MR, Li LS, Hansen R, Peters U, Kessler LV, et al. Selective inhibition of oncogenic KRAS output with small molecules targeting the inactive state. *Cancer Discov* (2016) 6:316–29. doi: 10.1158/2159-8290.CD-15-1105

18. Janes MR, Zhang J, Li LS, Hansen R, Peters U, Guo X, et al. Targeting KRAS mutant cancers with a covalent G12C-specific inhibitor. *Cell* (2018) 172:578–589.e17. doi: 10.1016/j.cell.2018.01.006

19. Canon J, Rex K, Saiki AY, Mohr C, Cooke K, Bagal D, et al. The clinical KRAS(G12C) inhibitor AMG 510 drives anti-tumour immunity. *Nature* (2019) 575:217–23. doi: 10.1038/s41586-019-1694-1

20. Lanman BA, Allen JR, Allen JG, Amegadzie AK, Ashton KS, Booker SK, et al. Discovery of a covalent inhibitor of KRAS(G12C) (AMG 510) for the treatment of solid tumors. *J Med Chem* (2020) 63:52–65. doi: 10.1021/acs.jmedchem.9b01180

21. Hallin J, Engstrom LD, Hargis L, Calinisan A, Aranda R, Briere DM, et al. The KRAS(G12C) inhibitor MRTX849 provides insight toward therapeutic susceptibility of KRAS-mutant cancers in mouse models and patients. *Cancer Discovery* (2020) 10:54–71. doi: 10.1158/2159-8290.CD-19-1167

22. Hong DS, Fakih MG, Strickler JH, Desai J, Durm GA, Shapiro GI, et al. KRAS(G12C) inhibition with sotorasib in advanced solid tumors. *N Engl J Med* (2020) 383:1207–17. doi: 10.1056/NEJMoa1917239

23. Jänne PA, Riely GJ, Gadgeel SM, Heist RS, Ou SI, Pacheco JM, et al. Adagrasib in non-Small-Cell lung cancer harboring a KRAS(G12C) mutation. *N Engl J Med* (2022) 387:120–31. doi: 10.1056/NEJMoa2204619

24. Liu J, Kang R, Tang D. The KRAS-G12C inhibitor: activity and resistance. *Cancer Gene Ther* (2022) 29:875–8. doi: 10.1038/s41417-021-00383-9

25. Xue JY, Zhao Y, Aronowitz J, Mai TT, Vides A, Qeriqi B, et al. Rapid non-uniform adaptation to conformation-specific KRAS(G12C) inhibition. *Nature* (2020) 577:421–5. doi: 10.1038/s41586-019-1884-x

26. Awad MM, Liu S, Rybkin II, Arbour KC, Dilly J, Zhu VW, et al. Acquired resistance to KRASG12C inhibition in cancer. *N Engl J Med* (2021) 384:2382–93. doi: 10.1056/NEJMoa2105281

27. Nakajima EC, Drezner N, Li X, Mishra-Kalyani PS, Liu Y, Zhao H, et al. FDA Approval summary: Sotorasib for KRAS G12C-mutated metastatic NSCLC. *Clin Cancer Res* (2022) 28:1482–6. doi: 10.1158/1078-0432.CCR-21-3074

28. Hunter JC, Manandhar A, Carrasco MA, Gurbani D, Gondi S, Westover KD. Biochemical and structural analysis of common cancer-associated KRAS mutations. *Mol Cancer Res* (2015) 13:1325–35. doi: 10.1158/1541-7786.MCR-15-0203

29. Zheng Q, Peacock DM, Shokat KM. Drugging the next undruggable KRAS allele-Gly12Asp. *J Medicinal Chem* (2022) 65:3119–22. doi: 10.1021/acs.jmedchem.2c00099

30. Wang X, Allen S, Blake JF, Bowcut V, Briere DM, Calinisan A, et al. Identification of MRTX1133, a noncovalent, potent, and selective KRAS(G12D) inhibitor. *J Med Chem* (2022) 65:3123–33. doi: 10.1021/acs.jmedchem.1c01688

31. Mao Z, Xiao H, Shen P, Yang Y, Xue J, Yang Y, et al. KRAS(G12D) can be targeted by potent inhibitors *via* formation of salt bridge. *Cell Discov* (2022) 8:5. doi: 10.1038/s41421-021-00368-w

32. Li L, Liu J, Yang Z, Zhao H, Deng B, Ren Y, et al. Discovery of Thieno[2,3-d] pyrimidine-based KRAS G12D inhibitors as potential anticancer agents *via* combinatorial virtual screening. *Eur J Med Chem* (2022) 233:114243. doi: 10.1016/j.ejmech.2022.114243

33. Knox J, Jiang J, Burnett L, Liu Y, Weller C, Wang Z, et al. Abstract 3596: RM-036, a first-in-class, orally-bioavailable, tri-complex covalent KRASG12D(ON) inhibitor, drives profound anti-tumor activity in KRASG12D mutant tumor models. *Cancer Res* (2022) 82(12_Supplement):3596. doi: 10.1158/1538-7445.AM2022-3596

34. Wang P, Heitman J. The cyclophilins. *Genome Biol* (2005) 6:226. doi: 10.1186/gb-2005-6-7-226

35. Khan I, Marelia-Bennet C, Lefler J, Zuberi M, Denbaum E, Koide A, et al. Targeting the KRAS α4-α5 allosteric interface inhibits pancreatic cancer tumorigenesis. *Small GTPases* (2021), 1–14. doi: 10.1080/21541248.2021.1906621

36. Khan I, Spencer-Smith R, O'bryan JP. Targeting the α4-α5 dimerization interface of K-RAS inhibits tumor formation *in vivo*. *Oncogene* (2019) 38:2984–93. doi: 10.1038/s41388-018-0636-y

37. Spencer-Smith R, Li L, Prasad S, Koide A, Koide S, O'bryan JP. Targeting the α4-α5 interface of RAS results in multiple levels of inhibition. *Small GTPases* (2019) 10:378–87. doi: 10.1080/21541248.2017.1333188

38. Leinwand J, Miller G. Regulation and modulation of antitumor immunity in pancreatic cancer. *Nat Immunol* (2020) 21:1152–9. doi: 10.1038/s41590-020-0761-y

39. Darvin P, Toor SM, Sasidharan Nair V, Elkord E. Immune checkpoint inhibitors: recent progress and potential biomarkers. *Exp Mol Med* (2018) 50:1–11. doi: 10.1038/s12276-018-0191-1

40. Feig C, Gopinathan A, Neesse A, Chan DS, Cook N, Tuveson DA. The pancreas cancer microenvironment. *Clin Cancer Res* (2012) 18:4266–76. doi: 10.1158/1078-0432.CCR-11-3114

41. Johnson BA3rd, Yarchoan M, Lee V, Laheru DA, Jaffee EM. Strategies for increasing pancreatic tumor immunogenicity. *Clin Cancer Res* (2017) 23:1656–69. doi: 10.1158/1078-0432.CCR-16-2318

42. Royal RE, Levy C, Turner K, Mathur A, Hughes M, Kammula US, et al. Phase 2 trial of single agent ipilimumab (anti-CTLA-4) for locally advanced or metastatic pancreatic adenocarcinoma. *J Immunother* (2010) 33:828–33. doi: 10.1097/CJI.0b013e3181eec14c

43. O'reilly EM, Oh DY, Dhani N, Renouf DJ, Lee MA, Sun W, et al. Durvalumab with or without tremelimumab for patients with metastatic pancreatic ductal adenocarcinoma: A phase 2 randomized clinical trial. *JAMA Oncol* (2019) 5:1431–8. doi: 10.1001/jamaoncol.2019.1588

44. Kamath SD, Kalyan A, Kircher S, Nimeiri H, Fought AJ, Benson A3rd, et al. Ipilimumab and gemcitabine for advanced pancreatic cancer: A phase ib study. *Oncologist* (2020) 25:e808–15. doi: 10.1634/theoncologist.2019-0473

45. Le DT, Durham JN, Smith KN, Wang H, Bartlett BR, Aulakh LK, et al. Mismatch repair deficiency predicts response of solid tumors to PD-1 blockade. *Science* (2017) 357:409–13. doi: 10.1126/science.aan6733

46. Das S, Berlin J, Cardin D. Harnessing the immune system in pancreatic cancer. *Curr Treat Options Oncol* (2018) 19:48. doi: 10.1007/s11864-018-0566-5

47. Mcallister F, Bailey JM, Alsina J, Nirschl CJ, Sharma R, Fan H, et al. Oncogenic kras activates a hematopoietic-to-Epithelial IL-17 signaling axis in preinvasive pancreatic neoplasia. *Cancer Cell* (2014) 25:621–37. doi: 10.1016/j.ccr.2014.03.014

48. Dey P, Li J, Zhang J, Chaurasiya S, Strom A, Wang H, et al. Oncogenic KRAS-driven metabolic reprogramming in pancreatic cancer cells utilizes cytokines from the tumor microenvironment. *Cancer Discov* (2020) 10:608–25. doi: 10.1158/2159-8290.CD-19-0297

49. Tape CJ, Ling S, Dimitriadi M, Mcmahon KM, Worboys JD, Leong HS, et al. Oncogenic KRAS regulates tumor cell signaling *via* stromal reciprocation. *Cell* (2016) 165:910–20. doi: 10.1016/j.cell.2016.03.029

50. Pylayeva-Gupta Y, Lee KE, Hajdu CH, Miller G, Bar-Sagi D. Oncogenic kras-induced GM-CSF production promotes the development of pancreatic neoplasia. *Cancer Cell* (2012) 21:836–47. doi: 10.1016/j.ccr.2012.04.024

51. Wang HC, Lin YL, Hsu CC, Chao YJ, Hou YC, Chiu TJ, et al. Pancreatic stellate cells activated by mutant KRAS-mediated PAI-1 upregulation foster pancreatic cancer progression *via* IL-8. *Theranostics* (2019) 9:7168–83. doi: 10.7150/thno.36830

52. Liu C, Zheng S, Wang Z, Wang S, Wang X, Yang L, et al. KRAS-G12D mutation drives immune suppression and the primary resistance of anti-PD-1/PD-L1 immunotherapy in non-small cell lung cancer. *Cancer Commun (Lond)* (2022) 42(9):828–47. doi: 10.1002/cac2.12327

53. Falk AT, Yazbeck N, Guibert N, Chamorey E, Paquet A, Ribeyre L, et al. Effect of mutant variants of the KRAS gene on PD-L1 expression and on the immune microenvironment and association with clinical outcome in lung adenocarcinoma patients. *Lung Cancer* (2018) 121:70–5. doi: 10.1016/j.lungcan.2018.05.009

54. Wang Z, Cao YJ. Adoptive cell therapy targeting neoantigens: A frontier for cancer research. *Front Immunol* (2020) 11:176. doi: 10.3389/fimmu.2020.00176

55. Wang QJ, Yu Z, Griffith K, Hanada K, Restifo NP, Yang JC. Identification of T-cell receptors targeting KRAS-mutated human tumors. *Cancer Immunol Res* (2016) 4:204–14. doi: 10.1158/2326-6066.CIR-15-0188

56. Leidner R, Sanjuan Silva N, Huang H, Sprott D, Zheng C, Shih YP, et al. Neoantigen T-cell receptor gene therapy in pancreatic cancer. *N Engl J Med* (2022) 386:2112–9. doi: 10.1056/NEJMoa2119662

57. Tran E, Robbins PF, Lu YC, Prickett TD, Gartner JJ, Jia L, et al. T-Cell transfer therapy targeting mutant KRAS in cancer. *N Engl J Med* (2016) 375:2255–62. doi: 10.1056/NEJMoa1609279

58. Cafri G, Yossef R, Pasetto A, Deniger DC, Lu YC, Parkhurst M, et al. Memory T cells targeting oncogenic mutations detected in peripheral blood of epithelial cancer patients. *Nat Commun* (2019) 10:449. doi: 10.1038/s41467-019-08304-z

59. Bear AS, Blanchard T, Cesare J, Ford MJ, Richman LP, Xu C, et al. Biochemical and functional characterization of mutant KRAS epitopes validates this oncoprotein for immunological targeting. *Nat Commun* (2021) 12:4365. doi: 10.1038/s41467-021-24562-2

60. Nagasaka M, Potugari B, Nguyen A, Sukari A, Azmi AS, Ou SI. KRAS inhibitors- yes but what next? direct targeting of KRAS- vaccines, adoptive T cell therapy and beyond. *Cancer Treat Rev* (2021) 101:102309. doi: 10.1016/j.ctrv.2021.102309

61. Zhang Z, Morstein J, Ecker AK, Guiley KZ, Shokat KM. Chemoselective covalent modification of K-Ras(G12R) with a small molecule electrophile. *J Am Chem Soc* (2022) 144:15916–21. doi: 10.1021/jacs.2c05377

62. Zhang Z, Guiley KZ, Shokat KM. Chemical acylation of an acquired serine suppresses oncogenic signaling of K-Ras(G12S). *Nat Chem Biol* (2022) 18 (11):1177–83. doi: 10.1038/s41589-022-01065-9

63. Koltun E, Rice M, Gustafson WC, Wilds D, Jiang J, Lee B, et al. Abstract 3597: Direct targeting of KRASG12X mutant cancers with RMC-6236, a first-in-class, RAS-selective, orally bioavailable, tri-complex RASMULTI(ON) inhibitor. *Cancer Res* (2022) 82:3597–7. doi: 10.1158/1538-7445.AM2022-3597

64. Ostrem JM, Shokat KM. Direct small-molecule inhibitors of KRAS: From structural insights to mechanism-based design. *Nat Rev Drug Discov* (2016) 15:771–85. doi: 10.1038/nrd.2016.139

65. Gentile DR, Rathinaswamy MK, Jenkins ML, Moss SM, Siempelkamp BD, Renslo AR, et al. Ras binder induces a modified switch-II pocket in GTP and GDP states. *Cell Chem Biol* (2017) 24:1455–1466.e14. doi: 10.1016/j.chembiol.2017.08.025

frontiers | Frontiers in Pharmacology

TYPE Original Research
PUBLISHED 19 January 2023
DOI 10.3389/fphar.2023.1016967

OPEN ACCESS

EDITED BY
Khuloud Bajbouj,
University of Sharjah, United Arab Emirates

REVIEWED BY
Yuhe Lei,
Shenzhen Hospital of Guangzhou University of Chinese Medicine, China
Wilfred W. K. Lin,
HerbMiners Informtics Limited, Hong Kong SAR, China
Shakeel Ahmad Khan,
Daegu Gyeongbuk Institute of Science and Technology (DGIST), South Korea

*CORRESPONDENCE
Xiongwen Wang,
awen681029@163.com

†These authors have contributed equally to this work and share first authorship

SPECIALTY SECTION
This article was submitted to Pharmacology of Anti-Cancer Drugs, a section of the journal Frontiers in Pharmacology

RECEIVED 11 August 2022
ACCEPTED 05 January 2023
PUBLISHED 19 January 2023

CITATION
Yang M, Yan Q, Luo Y, Wang B, Deng S, Luo H, Ye B and Wang X (2023), Molecular mechanism of Ganji Fang in the treatment of hepatocellular carcinoma based on network pharmacology, molecular docking and experimental verification technology.
Front. Pharmacol. 14:1016967.
doi: 10.3389/fphar.2023.1016967

Molecular mechanism of Ganji Fang in the treatment of hepatocellular carcinoma based on network pharmacology, molecular docking and experimental verification technology

Miaolun Yang[1†], Qian Yan[1†], Yuehua Luo[1†], Boqing Wang[1], Shicong Deng[1], Huiyan Luo[1], Baoqian Ye[1] and Xiongwen Wang[2*]

[1]The First Clinical Medical School, Guangzhou University of Chinese Medicine, Guangzhou, China, [2]The First Affiliated Hospital, Guangzhou University of Chinese Medicine, Guangzhou, China

Background: Hepatocellular carcinoma (HCC) is a malignant tumor harmful to human health. Ganji Fang (GJF) has good clinical efficacy in the treatment of HCC, but its mechanism is still unclear.

Objective: The aim of this study was to investigate the mechanism of action of GJF in the treatment of HCC through network pharmacology, molecular docking and *in vitro* experiments.

Methods: A series of network pharmacology methods were used to identify the potential targets and key pathways of GJF in the treatment of HCC. Then, molecular docking technology was used to explore the binding ability of key active ingredients and targets in GJF. Multiple external databases were used to validate the key targets. In in vitro experiments, we performed MTT assays, wound-healing assays, cell cycle assays, apoptosis assays and RT–qPCR to verify the inhibitory effect of GJF on the Human hepatoma G2 (HepG2) cells.

Result: A total of 162 bioactive components and 826 protein targets of GJF were screened, and 611 potential targets of HCC were identified. Finally, 63 possible targets of GJF acting on HCC were obtained. KEGG enrichment analyses showed that the top five pathways were the cell cycle, cellular senescence, p53 signaling pathway, PI3K/Akt signaling pathway, and progesterone-mediated oocyte maturation. Among them, we verified the PI3K/Akt signaling pathway. CCNE1, PKN1, CCND2, CDK4, EPHA2, FGFR3, CDK6, CDK2 and HSP90AAI were enriched in the PI3K/Akt pathway. The molecular docking results showed that the docking scores of eight active components of GJF with the two targets were all less than -5.0, indicating that they had certain binding activity. *In vitro* cell experiments showed that GJF could inhibit the proliferation and migration of HepG2 cells, block the cell cycle and induce apoptosis of HepG2 cells, which may be related to the PI3K/Akt signaling pathway. In summary, EPHA2 may be an important target of GJF in HCC, and pachymic acid may be an important critical active compound of GJF that exerts anticancer activity.

Conclusion: In general, we demonstrated, for the first time, that the molecular mechanism of GJF in HCC may involve induction of G0/G1 phase cycle arrest through inhibition of the PI3K/Akt signaling pathway and promote apoptosis of

hepatoma cell lines. This study provides a scientific basis for the subsequent clinical application of GJF and the in-depth study of its mechanism.

KEYWORDS

Ganji Fang, hepatocellular carcinoma, network pharmacology, HepG2 cells, PI3K/Akt signaling pathway, EPHA2

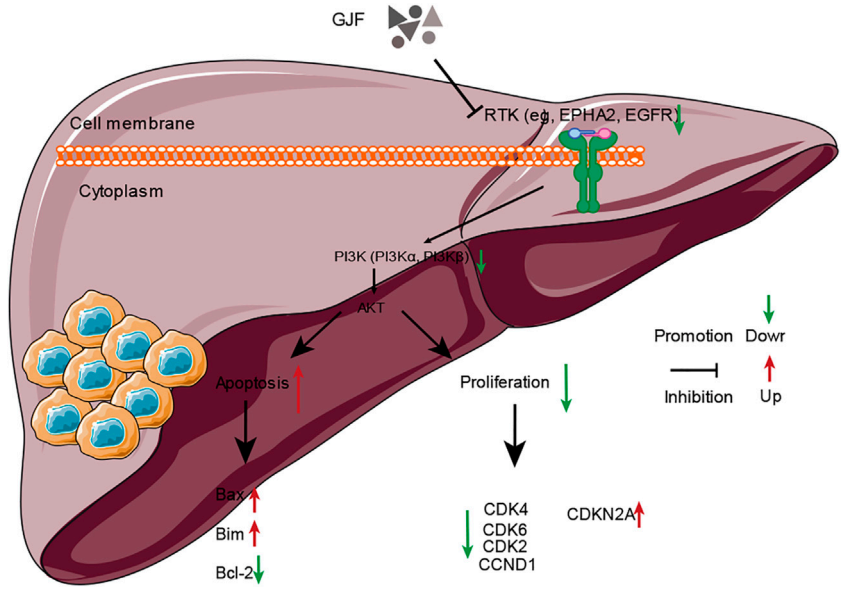

GRAPHICAL ABSTRACT

1 Introduction

Primary liver cancer (PLC) includes hepatocellular carcinoma (HCC) and intrahepatic cholangiocarcinoma as well as other rare types (Bray et al., 2018). HCC, the most prevalent type of PLC, accounts for approximately 90% of cases (Gunasekaran et al., 2020). HCC ranks fifth in terms of global cases and second in terms of deaths for males (Bray et al., 2018). Studies have shown that the incidence of HCC has stabilized in men after decades of steep increase but continues to rise in women by >2% annually (Siegel et al., 2021). Surgical removal involving resection and transplantation remains the only curative treatment for most types of liver tumors (Petrowsky et al., 2020). In addition, chemotherapy, radiotherapies, radiofrequency ablation (RFA), percutaneous ethanol injection (PEI), transarterial chemoembolization (TACE), targeted therapy, and immunological therapy are also important treatment methods (Petrowsky et al., 2020). However, all of these treatments have side effects that affect patients' lives. As the use of immune checkpoint inhibitors continues to expand, this treatment will become more crucial than early detection, and management of these side effects becomes paramount to maximize the duration of treatment while minimizing toxicity for patients (Hussaini et al., 2021).

Although the effect of traditional Chinese medicine (TCM) on tumor shrinkage is not as obvious as that of modern Western medicine, reducing toxicity and increasing the efficacy of TCM can help to reduce the side effects, improve the curative effect and improve the quality of life of patients (Z. Ma et al., 2019; Ye et al., 2015). Evidence-based functions of Chinese herbal medicines against cancer can be summarized as enhancement of natural killer (NK) cell activity or relative percentage; prevention of tumor growth and metastasis; relief of side effects or complications of therapeutic strategies (i.e., chemotherapy, radiotherapy, and resection) (H. Liu et al., 2021). Some studies have shown that adjuvant therapy with TCM may prolong the median overall survival time and reduce the mortality of HCC patients (X. Liu et al., 2019). GJF is an established prescription drug with beneficial gas spleen detoxification and anticancer functions. GJF is commonly used to treat HCC in clinical practice, and some patients with advanced liver cancer even choose to be treated with pure Chinese medicine. Previous clinical and animal studies have preliminarily explored whether GJF may have anti-inflammatory effects, protect the liver, inhibit tumor cell proliferation, and induce tumor cell apoptosis. Therefore, this study will further explore the clinical application value and possible mechanism of GJF along the lines of previous research. TCM compounds are difficult to study because they are composed of multiple herbs, contain complex components, and their mechanism of action is unclear.

Network pharmacology uses drug, compound, gene, and disease database information to construct drug-target, target-disease, and drug-disease interaction networks to reveal the complex mechanisms of TCM formulations that have multiple targets and multicomponent characteristics (S. Li & Zhang, 2013), which provides a new strategy for the study of complex traditional Chinese medicine

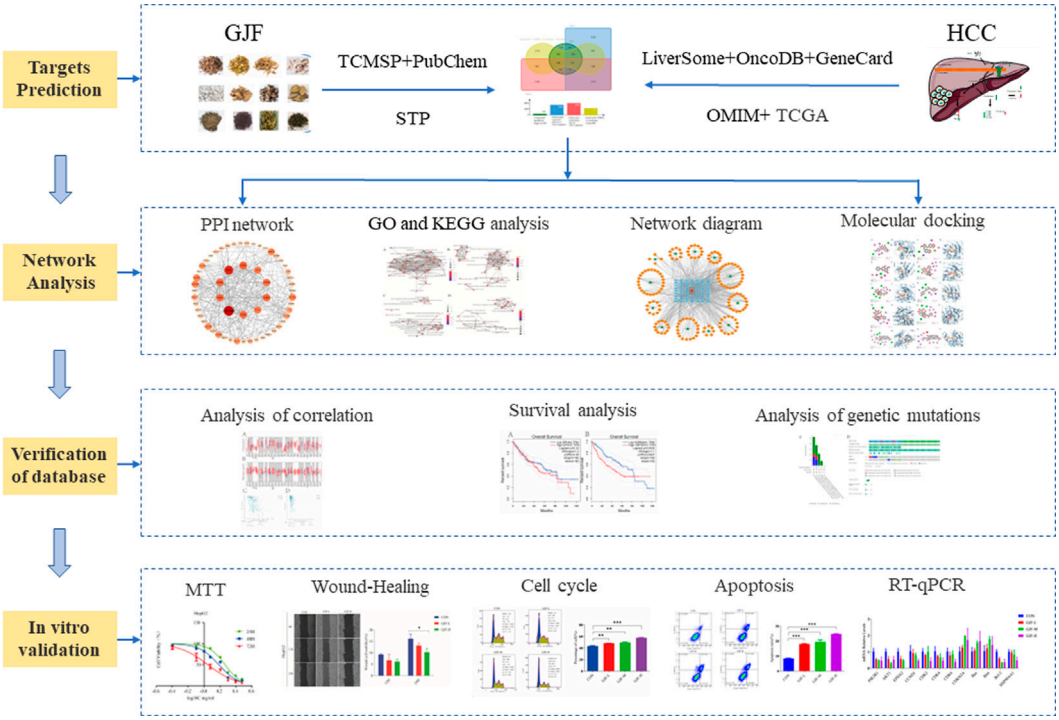

FIGURE 1
Overall workflow of this study (GJF, Ganji Fang; TCMSP, Traditional Chinese Medicine System Pharmacology database; STP, SwissTargetPrediction database; HCC, Hepatocellular carcinoma).

systems. The comprehensive, systematic and holistic nature of network pharmacology are consistent with the multicompound, multitarget and multipathway characteristics of Chinese medicine (Luo et al., 2020). Many researchers use network pharmacology to predict the active phytochemicals and molecular mechanisms of traditional Chinese medicine in the treatment of HCC. Many researchers use network pharmacology to predict the active phytochemicals and molecular mechanisms of traditional Chinese medicine in the treatment of HCC (Khan & Lee, 2022). In this paper, the possible pathways and targets of GIF for HCC treatment were predicted mainly through network pharmacology methods and then verified by molecular docking, external databases, experimental research and other methods. The detailed flow chart of the study is shown in Figure 1.

2 Materials and methods

2.1 Screening active compounds GJF

We obtained the compounds of each drug of GJF from the Traditional Chinese Medicine System Pharmacology Database and Analysis Platform (TCMSP, http://lsp.nwu.edu.cn/tcmsp.php, accessed on 12 May 2020). In addition, the potential active compounds of each Chinese medicine were also supplemented through a literature search. Oral bioavailability (OB) and drug-likeness (DL) are some of the most important pharmacokinetic parameters in the process of absorption, distribution, metabolism, and excretion (ADME). We screened compounds on the condition that oral utilization of compounds OB ≥ 30% and DL ≥ 0.18.

2.2 Prediction of drug targets for GJF

The 3D structures of the active ingredients of each compound and canonical SMILES format were downloaded from the PubChem database (https://pubchem.ncbi.nlm.nih.gov/, accessed on 20 May 2020). The potentially effective action targets of GJF were obtained using the SwissTargetPrediction database (STP, http://www.swisstargetprediction, accessed on 20 May 2020) (Daina et al., 2019). We chose the target probability to be greater than 0, and if there were too many predicted targets, we chose the top 100 targets ranked according to the target probability. When SwissTargetPrediction could not predict relevant targets, we used the TMSCP database to make a supplement prediction.

2.3 Extracting the targets of hepatocellular carcinoma

We consolidated HCC-related targets through the Databases Liverome (http://liverome.kobic.re.kr/index.php, accessed on 23 May 2020), OncoDB. HCC databases (http://www.oncodb.hcc.ibms.sinica.edu.org/, accessed on 23 May 2020), GeneCards databases (https://www.genecards.org/, accessed on 23 May 2020), and OMIM databases (http://www.ncbi.nlm.nih.gov/, accessed on 23 May 2020) (Su et al., 2007; Lee et al., 2011; Paolacci et al., 2019).

Additionally, the mRNA sequencing data of HCC were downloaded for the PI3K/Akt signaling pathway on The Cancer Genome Atlas (TCGA) dataset (http://cancergenome.nih.gov/, accessed on 23 May 2020), including 370 primary HCC tissues and 50 normal tissues and the corresponding clinical follow-up data. To

improve the accuracy of the data, we preprocessed the dataset, including deleting the sites where 70% methylation levels were unavailable and samples expressing more than 30% missing values. Genes with zero RPKM expression in the sample were also excluded (J. Xu et al., 2015).

The data were standardized using the RMA algorithm in the "Limma" package in R software (Smyth, 2004; Law et al., 2014; Ritchie et al., 2015). A false detection rate (FDR) method was used to regulate the *p-value*. The screening criteria for differentially methylated genes (DMGs) were FDR <0.05 and β values >0.2, HCC in cancerous tissue and normal liver tissue differentially expressed genes (Differentially expressed genes, DEGs) in line with|1og $_2$ (fold change)|> 1 and FDR <0.05 standard. We intersected HCC-related targets in the public database with DMGS and DEGs in the TCGA database, regarded this intersection as possible key targets in HCC, and mapped these targets to related targets predicted by compounds in GJF as potential targets of GJF for HCC.

2.4 Construction of networks and analysis

The key targets of GJF for HCC were imported into the STRING database to construct a PPI network, and the confidence level was set as ≥0.70. Cytoscape (Version: 3.9.1) software was used for visualization. The key genes and their relationship network of TCM, drug active ingredient, and drug and disease crossing were imported into Cytoscape 3.9.1 software to construct a herb-compound-target network of GJF.

2.5 Gene ontology and pathway enrichment analysis for HCC-Related targets of GJF

Gene Ontology (GO) and Kyoto Encyclopedia of Genes and Genomes (KEGG) enrichment analyses were performed using the "cluster profile" package in R software for better biological interpretation (Yu et al., 2012). GO and KEGG enrichment analyses of the potential targets were performed using the database for annotation, visualization, and integrated discovery (DAVID, https://david.ncifcrf.gov/, accessed on 26 May 2021). GO enrichment analysis included biological processes (BP), molecular functions (MF), and cellular components (CC).

2.6 Molecular docking

The RCSB PDB database (https://www.rcsb. org/, accessed on 10 June 2021) to retrieve and download 3D structure files for key target proteins, while using the PubChem database (https://pubchem.ncbi.nlm.nih.gov/, accessed on 12 June 2021) to download 3D structure files for active compounds. For docking analysis, all protein and molecular files were converted into PDBQT format with all water molecules excluded, and polar hydrogen atoms were added. The grid box was centered to cover the domain of each protein and to accommodate free molecular movement. The grid box was set to 30 Å × 30 Å × 30 Å, and the grid point distance was 0.05 nm. Molecular docking studies were performed by Autodock Vina 1.2.2 (http://autodock.scripps.edu/, accessed on 12 June 2021).

2.7 Validation of external databases

For the above key targets, we performed a series of validations in the TCGA database. The cBioPortal (http://cbioportal.org, accessed on 16 June 2021) genomics database (J. Gao et al., 2013) demonstrated the association of genetic mutation status, mRNA, and DNA methylation. The GEPIA (Gene Expression Profiling Interactive Analysis, http://gepia.cancer-pku.cn/, accessed on 16 June 2021) database was used to examine the prognostic differences between high and low gene levels. The (T. Li et al., 2017) database was used to verify the difference in mRNA level expression.

2.8 *In Vitro* validation cell culture

The HCC cell line HepG2, which was purchased from Guangzhou Cellcook Biotech Co., Ltd., was routinely cultured in DMEM (Gibco, Grand Island, NY, United States) containing 10% FBS (Thermo Fisher Scientific, Rochester, NY, United States). Cells were cultured at 37 °C in a 5% CO^2 incubator, subcultured at a ratio of 1:2, and used for subsequent experiments after reaching the logarithmic growth phase. In this study, we set the 72-hour IC_{50} to a medium dose, half the 72-hour IC_{50} to a low dose, and two times the 72-hour IC_{50} to a high dose.

2.9 The source of GJF and preparation of lyophilized powder

GJF was purchased from the Outpatient Pharmacy of the First Affiliated Hospital of Guangzhou University of Traditional Chinese Medicine. The dose of 1 fu of GJF was 241 g (12 g bupleurum, 12 g paeoniae, 30 g codonopsis, 15 g poria, 15 g atractylodes, 20 g Rhizoma lucidum, 30 g ligustrum scutellariae, 12 g Scutellaria scutellariae, 20 g Rhizoma barbiliae, 30 g Augustaloza, 15 g Zedoary Zedoaria, 30 g Pellucidaria). Deionized water was added at 10x (approximately 2400 ml), sampled was cooked twice and centrifuged at 1000 r for 5 min. The supernatant was collected and refrigerated at -80 °C for 6–8 h until it was completely frozen. Then, the samples were quickly put into a lyophilized powder machine. After the preparation of lyophilized powder, complete culture medium was used to prepare 50 mg/ml liver-product solution.

2.10 MTT assay

The logarithmic phase cells were collected, the cell density was adjusted to 5 * 10^4/ml, and the cells were inoculated in three 96-well plates. Then, 100 μL of GJF solution with different concentration gradients was added to the cell culture box. One plate was removed at 24 h, 48 h, and 72 h, and a mixture of MTT solution and basic medium (ratio: 1:4) was added under closed light conditions, 100 μL for each well. After further incubation for 4 h, 150 μL DMSO solution was added to each well. The wavelength of the enzyme plate analyzer was set at 490 nm, and the OD values of 3 96-well plates were measured at different times.

2.11 Wound-healing assay

HepG2 cells in logarithmic growth were cultured in a 6-well plate (2×10^5 cells/well). After the cells reached a subconfluency state (approximately 80%), a 2-mm scratch was made along the midline of the plate. Cells were assigned to the blank serum group (blank serum) (cells cultured with normal culture medium supplemented with blank serum), GJF low-dose group (GJF-L), and GJF high-dose group (GJF-H), with two replicate wells set up for each group. When cells were cultured for 0, 12, and 24 h in drug-containing or drug-free media, they were photographed under an inverted microscope (Olympus, Tokyo, Japan), and the rate of cell migration was calculated.

2.12 Cell cycle detection

The cells were inoculated in a 6-well plate, divided into control group, GJF of low, medium, and high concentration group, allowed to adhere and grown to a certain density, and then a different concentration of GJF frozen-dried powder solution was added to each well. Twenty-four hours later the cells were added to 1 ml of ice bath precooled with 70% ethanol and fixed at 4 °C for 2 h or more. Then, the cells were precipitated and resuspended. Next, 0.5 ml of cyclosome iodide dyeing liquid was added to each group, incubated at 37 °C in a bath for 30 min in the dark, and stored at 4 °C or on an ice bath for 24 h to complete the flow test.

2.13 Apoptosis detection

The cells at several stages were inoculated in a 6-well plate, divided into control group, GJF of low, medium, and high concentration group, 24 h after taking 5–10 million suspended cells, the cells were centrifuged at 1000r for 5 min, after discarding, 195 μL Annexin V-FITC binding fluid was added to gently resuspend the cells, 5 μL Annexin V-FITC was added, 10u1 iodide dye was added, and cells were incubated at room temperature (20°C–25°C) for 10–20 min, then placed in an ice bath. The cells were tested on a flow cytometer as soon as possible within an hour.

2.14 RT–qPCR microarray analysis

Total RNA was extracted from experimental cells using a universal RNA extraction kit. Then, EVO-M-MLVRT Master Mix was used for reverse transcription into cDNA. The reaction system was prepared according to the instructions of the SYBR premixed RT–qPCR kit for RT–qPCR amplification. The RT–qPCR conditions were as follows: pre-denaturation at 95 °C for 30 s, denaturation at 95°C for 30 s, and annealing at 60 °C for 30 s, for a total of 40 cycles. The experiment was repeated 3 times. Gene expression was evaluated by RT-qPCR, using the 2 -ΔΔCT method.

2.15 Statistical analysis

Measurement data are expressed as the mean taxi standard deviation (X ± S) and were statistically processed using SPSS (version: 26.0) software. When the experimental data met the normal distribution and the variance was consistent, one-way analysis of variance and two-way analysis of variance were used, and a non-parametric test was used if the data did not meet the normal distribution. $p < 0.05$ indicates that the difference is statistically significant. The above experiments were repeated three times, with the results of the cell cycle and apoptosis experiments presented in FlowJo (version 10.7.1) and the rest in GraphPad Prism (version 8.0).

3 Results

3.1 Active ingredients and prediction of a protein target of GJF

A total of 162 bioactive components and 826 protein targets of GJF were obtained from both TCMSP databases and a literature search (Supplementary Table S1). Radix Bupleuri was supplemented with Saponin A (Wen-Sheng, 2003) and Saponin D (Ren et al., 2019), Atractylodide I, Atractylodide II, and Atractylodide III were added to Atractylodes macrocephala Koidz (Zhu et al., 2018), raffinose was added to Codonopsitis Radix (S. Gao et al., 2019), Paeoniae Radix Alba was supplemented with oxypaeoniflorin, (M. Lu et al., 2019), Eclalbasaponin I and ursolic acid were added to Eclipse Herba (Q. M. Liu et al., 2012), oleanic acid was added to Fructus Ligustri Lucidi, Phytodolor and rosmarinic acid were added to Herba Sarcandrae, Scutellariae Barbatae Herba was supplemented with scutellarin, curcumin was added to Curcumae Rhizoma, and Akebiae Frucyus was added to Calceolarioside B.

3.2 Prediction results of hepatocellular carcinoma targets

We screened 5,714 genes in four public databases. The mRNA and methylation sites differentially expressed in the TCGA were further screened. According to the screening criteria for the differentially expressed genes, we obtained 7645 differentially expressed genes, and after the conversion of the differentially methylated sites, we identified 8938 differentially methylated genes, which we display in the form of heatmaps and volcano plots. (Figures 2A–C).

3.3 GO and KEGG enrichment analyses

The 611 potential targets associated with HCC were mapped to the targets predicted by GJF (Figure 2D), and 63 intersections were obtained, which were the possible targets of GJF acting on HCC. The 63 genes were analyzed by GO and KEGG (Figure 3). According to the number of genes enriched in each item, the results showed that the top five biological processes involved in these genes were epithelial cell proliferation, regulation of epithelial cell proliferation, regulation of cell cycle phase transition, gland development, and embryonic organ development; in terms of cell composition, they were mainly involved in cell-substrate junction, cell-substrate adherens junction, focal adhesion, adherens junction, and extracellular matrix composition. In the molecular function category, they were mainly associated with cell adhesion molecule binding, proximal promoter sequence-specific DNA binding, chromatin binding, RNA polymerase

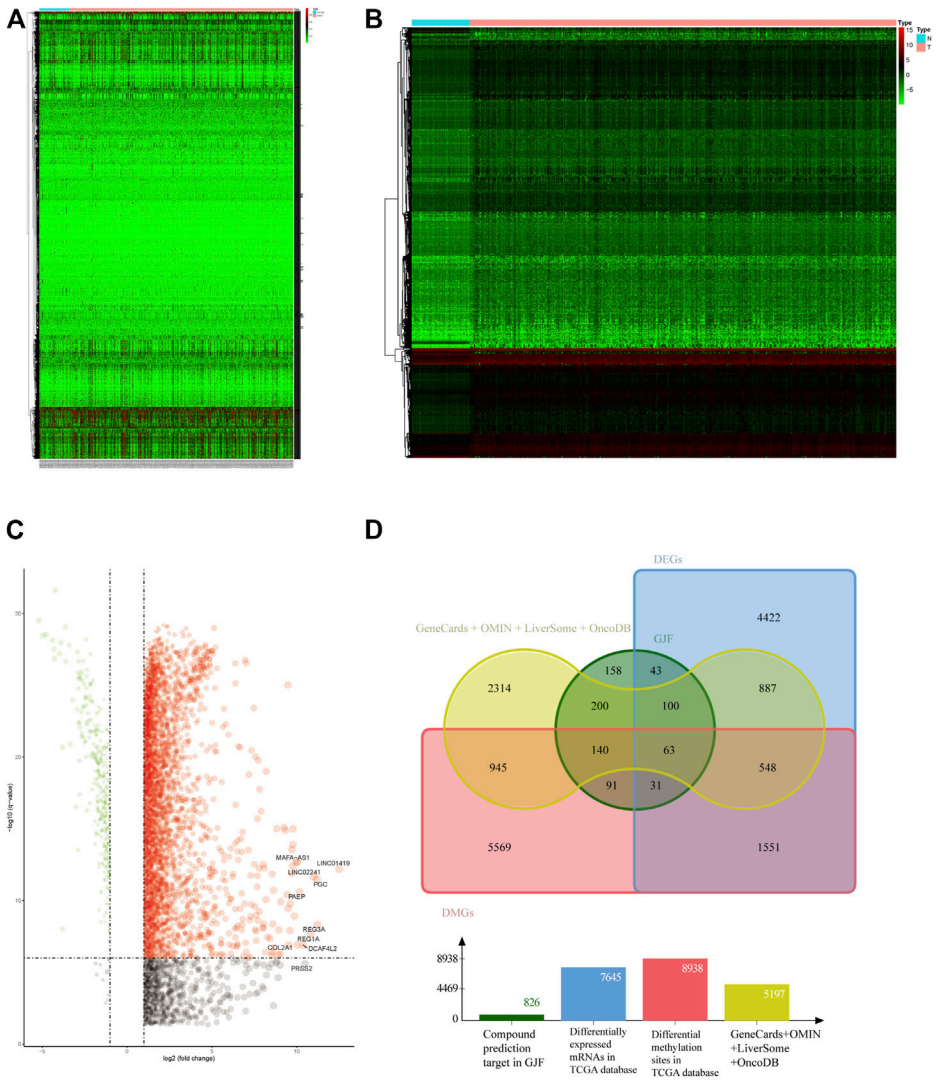

FIGURE 2
(A) Heatmap of HCC-associated differential methylation sites in the TCGA database **(B)** Heatmap of HCC-related differentially expressed genes in the TCGA database **(C)** Volcano plot of HCC-related differentially expressed genes in the TCGA **(D)** Venn diagram of the intersection of HCC-related targets (DEGs, differentially expressed genes; DMGs, differentially methylated genes).

II proximal promoter sequence-specific DNA binding and laminin binding. In addition, the top five pathways were the cell cycle (Gotoh et al., 2003), cellular senescence, p53, signaling pathway, PI3K/Akt signaling pathway, and progesterone-mediated oocyte maturation (Supplementary Table S2).

3.4 PPI network and herb-compound-target network of GJF

We performed PPI network analysis of 63 intersection genes between HCC (Figure 4A). GJF and the top 10 genes were HSP90AA1, SRC, CDK1, CCNA2, CDK4, PLK1, CDK2, TOP2A, AURKB and CDK6. Based on the results of the KEGG analysis, we verified the role of the PI3K/Akt signaling pathway in GJF. KEGG analysis showed that CCNE1, PKN1, CCND2, CDK4, EPHA2, FGFR3, CDK6, CDK2, and HSP90AA1 were enriched in the PI3K/Akt pathway. We constructed a network diagram of "TCM-compound-target-pathway" (Figure 4B). The network consisted of 235 nodes (12 TCM name nodes, 162 active ingredient nodes, 63 gene target nodes) and 1225 edges.

3.5 Molecular docking

We conducted a molecular docking analysis between HSP90AA1, anhydroicaritin, cubebin, (2R)-7-hydroxy-5-methoxy-2-phenylchroman-4-one, paeoniflorin (PF), albiflorin_qt, and bisdemethoxycurcumin to screen the compounds with the strongest binding ability to HSP90AA1. In addition, PF, albiflorin_qt, pachymic acid (PA), and (7,9 (11)-dehydropachymic acid were used to screen the compounds that acted most closely with EPHA2. The results showed that the docking scores of the eight active components of GJF with the two targets were all less than -4.0, indicating that they had

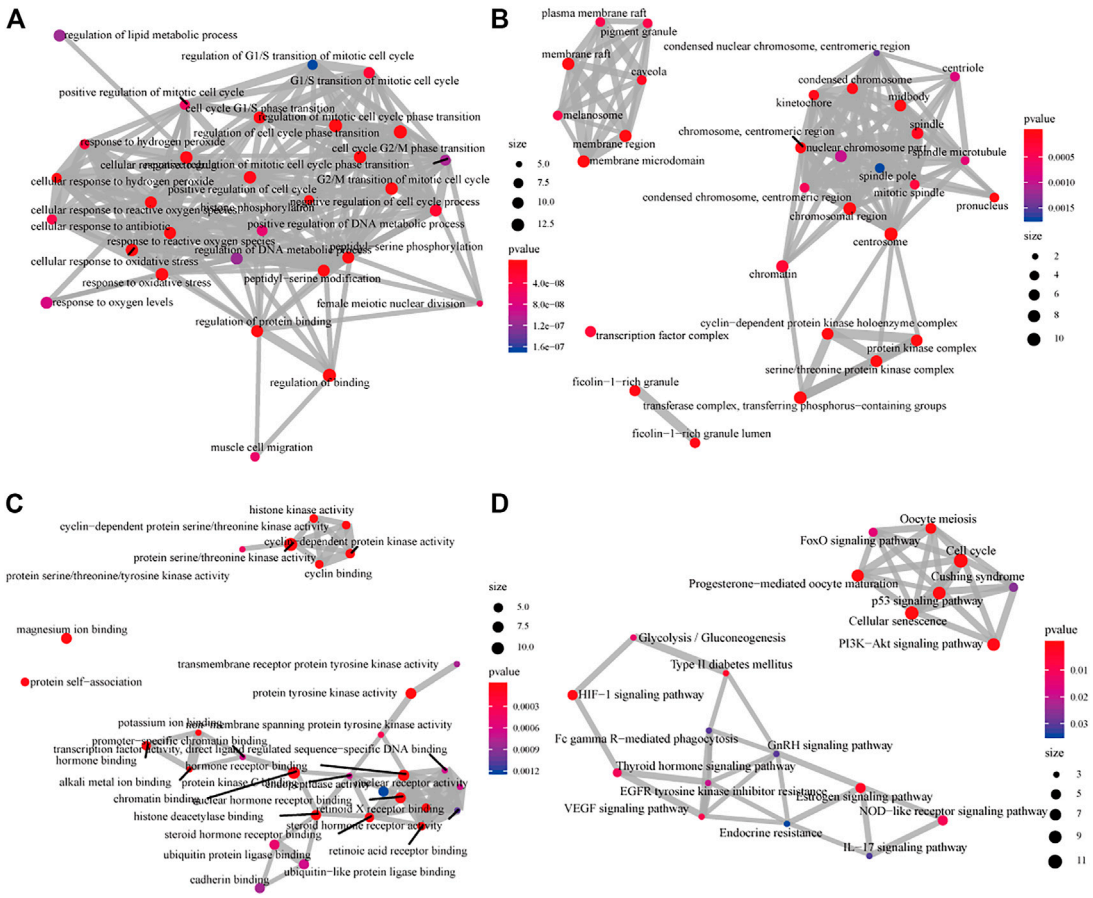

FIGURE 3
GO and KEGG analysis diagram of the intersection of targets of GJF in HCC **(A)** The analysis diagrams of the biological process **(B)** Diagrams of the analysis of cell components **(C)** The analysis diagrams of molecular functions **(D)** KEGG analysis diagram (GO, gene ontology; KEGG, Kyoto Encyclopedia of Genes and Genomes).

certain binding activity. As shown in Table 1, the strongest binding energy between PF and HSP90AA1 is -7.3 and that between PA and EPHA2 was -8.8. Therefore, these key components may be potential active compounds of GJF in the treatment of HCC (Figure 5).

3.6 Validation of EPHA2 and HAP90AA1 in the TCGA database

The TIMER database showed that EPHA2 and HSP90AA1 were differentially expressed in multiple tumors, and EPHA2 was expressed at low levels in HCC. The mRNA expression levels of EPHA2 and HSP90AA1 were strongly correlated with the DNA methylation level (Figure 6), suggesting that the regulatory effect of GJF on EPHA2 and HSP90AA1 might be caused by the regulation of their methylation status by methyltransferase and then the regulation of their expression. However, HSP90AA1 was hypermethylated and highly expressed in HCC, and there was a negative correlation between the two, which may require further experimental confirmation. Our study showed that low expression of EPHA2 may have a better prognosis, but the difference was not statistically significant (Figure 7A, $p = 0.35$). In multiple TCGA datasets, the mutation rate of EPHA2 was 1.9% and that of HSP90AA1 was 1.4% (Figures 7C, D), suggesting that these two molecules have a certain application value, but further basic experiments may be needed to confirm this.

3.7 Effects on cell proliferation and migration

The MTT experiment results showed that a certain concentration of GJF freeze-dried powder solution inhibited the proliferation of HepG2 cell strains. With increasing drug concentration and time, the inhibition gradually increased in a time- and concentration-dependent manner (Figure 8A). The IC_{50} values of 24H, 48H, and 72H in the HepG2 cell line were 1.91 mg/ml, 1.56 mg/ml, and 1.12 mg/ml, respectively. The GJF freeze-dried powder solution was divided into a low concentration group (0.5 mg/ml), medium concentration group (1.0 mg/ml), and high concentration group (3.0 mg/ml).

The wound healing assay showed that compared with the control group, the cell mobility of the high concentration group and the low concentration group showed a downward trend in the HepG2 cell line. After 24 h of treatment, the inhibitory effect of the high concentration group was significantly stronger than that of the control group (Figure 8B).

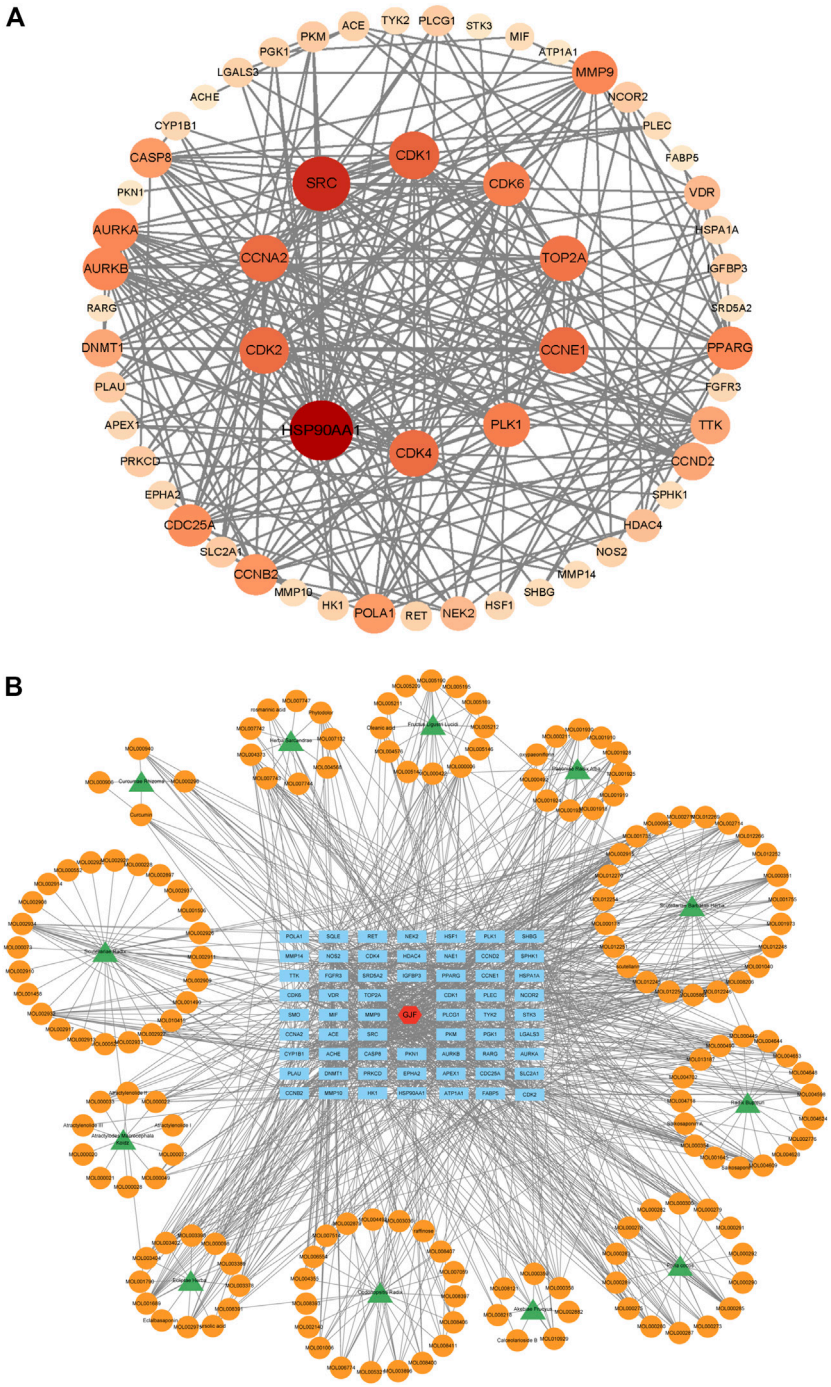

FIGURE 4
(A) The PPI network of 63 nodes (genes) (The darker the color, the larger the circle, the more connected; The 10 targets in the innermost layer are the key targets with the highest connection degree) **(B)** Herb-compound-target network of GJF (green represents the name of traditional Chinese medicine, orange represents the active ingredient, blue represents the key gene target, and red represents Ganji Fang).

3.8 Effects of the cell cycle and apoptosis

The cell cycle can be divided into the GOG1 phase, G phase, and G2/M phase, and the ratio of the GOG1 phase is usually used to represent its inhibitory effect on proliferation. As shown in the figure below, GJF blocked HepG2 cell lines in the GOG1 phase in a concentration-dependent manner (Figure 8C). Compared with the control group, the difference between the low-dose, medium-dose, and high-dose groups and the control group was statistically significant.

As shown in Figure 8D, GJF blocked HepG2 cell lines in the G0/G1 phase in a concentration-dependent manner. In the HepG2 cell line, the apoptosis rate of the medium-dose group was higher than that of the high-dose group. Compared with the control group, the differences between the low-dose group, medium-dose group, and high-dose group and the control group were statistically significant.

TABLE 1 Docking scores of key compounds and targets in hepatocellular formulas.

Molecule name	Molecule ID	Receptor	PDB ID	Binding affinity (kcal/mol)
Anhydroicaritin	MOL004373	HSP90AA1	6lr9	−6.2
Cubebin	MOL013187	HSP90AA1	6lr9	−7
(2R)-7-hydroxy-5-methoxy-2-phenylchroman-4-one	MOL000228	HSP90AA1	6lr9	−6
Paeoniflorin	MOL001924	HSP90AA1	6lr9	−7.3
Albiflorin_qt	MOL001928	HSP90AA1	6lr9	−6.4
Bisdemethoxycurcumin	MOL000940	HSP90AA1	6lr9	−5.5
Paeoniflorin	MOL001924	EPHA2	6q7e	−8.4
Albiflorin_qt	MOL001928	EPHA2	6q7e	−8.4
Pachymic acid	MOL000289	EPHA2	6q7e	−8.8
7,9 (11)-dehydropachymic acid	MOL000276	EPHA2	6q7e	−8.5

3.9 Validation of related indicators in the PI3K/Akt signaling pathway

We verified the relevant molecules in the PI3K/Akt signaling pathway in the HepG2 cell line (Supplementary Table S3). According to the RT–qPCR results (Figure 8E), we observed that GJF reduced the expression levels of PIK3R1 and Akt1 in the HepG2 cell line, and the difference was statistically significant. These results suggest that GJF may inhibit the expression level of the PI3K/Akt signaling axis in HCC. On the other hand, GJF decreased the levels of cycling-related proteins (CCND1, CDK2, CDK4, and CDK6) in HepG2 cell lines and increased the expression of the tumor suppressor gene CDKN2A. For apoptosis-related proteins, GJF increased the expression levels of Bax and Bim while decreased the expression level of Bel-2. In the HepG2 cell line, GJF decreased the expression levels of EPHA2.

4 Discussion

HCC, the most prevalent type of PLC, is a common malignant tumor threatening human health and life (Siegel et al., 2020). Clinically, the combination of traditional Chinese and Western medicine is very important in the treatment of HCC. Preliminary clinical and animal studies have explored the effects of GJF on anti-inflammatory, antitumor, liver protection, inhibition of tumor cell proliferation, and induction of tumor cell apoptosis. Therefore, this study further explored the clinical application value and possible mechanism of action of GJF along with previous research ideas.

To further explore the mechanism of GJF intervention in the HCC process, we first screened the potential active compounds of GJF acting on HCC and clarified the molecular mechanism of GJF intervention in HCC through the PI3K/Akt signaling axis using network pharmacology. A total of 63 key targets of GJF acting on HCC were obtained, and the results showed that the top five BPs involved in these genes were epithelial cell proliferation, regulation of epithelial cell proliferation, regulation of cell cycle phase transition, gland development, and embryonic organ development, respectively; In terms of CC, the targets were mainly involved in cell-substrate junction, cell-substrate adherens junction, focal adhesion, adherens junction, and extracellular matrix composition. In the category of MF, they were mainly associated with cell adhesion molecule binding, proximal promoter sequence-specific DNA binding, chromatin binding, RNA polymerase II proximal promoter sequence-specific DNA binding and laminin-binding are related. In addition, the top five pathways were the cell cycle, cellular senescence, p53 signaling pathway, PI3K/Akt signaling pathway, and progesterone-mediated oocyte maturation. Studies have shown that telomere shortening and cell cycle checkpoint inactivation are characteristic of the development of human liver cancer (Plentz et al., 2007). Cellular senescence is the process leading to end-of-life growth arrest with characteristic morphological features, mediated by telomere dependent, oncogene-induced, and ROS-induced pathways, but persistent DNA damage is the most common cause. Aging arrest is mediated by p16-and p21-dependent pathways that both lead to retinoblastoma protein activation. p53 acts as a relay between DNA damage detection and p21 activation, and aging arrest and cellular immortality are likely to significantly promote the development of HCC. Aging in oncogene-induced precancerous lesions and reversible immortality of cancer cells, including HCCs, offer new potential for tumor prevention and treatment (Ozturk et al., 2009). Yan Wang et al. showed that circulating neutrophils can predict low HCC survival and promote HCC progression through the p53 and STAT3 signaling pathways (Wang et al., 2020). Several studies have shown that progestin-mediated oocyte maturation is strongly associated with the progression of HCC, but further experimental confirmation is needed (B. Jin et al., 2015; Ma et al., 2020). Xiao-Lu Ma et al. showed that CD73 could promote the progression and metastasis of HCC by inducing RAP1-mediated P110β membrane localization to activate PI3K/Akt signaling, which was associated with poor prognosis of HCC(X. L. Ma et al., 2019). Similarly, the results showed that GJF may regulate the mRNA expression levels of relevant molecules in the PI3K/Akt signaling pathway and play a role in regulating the mRNA expression levels of proteins related to proliferation and apoptosis downstream of the pathway.

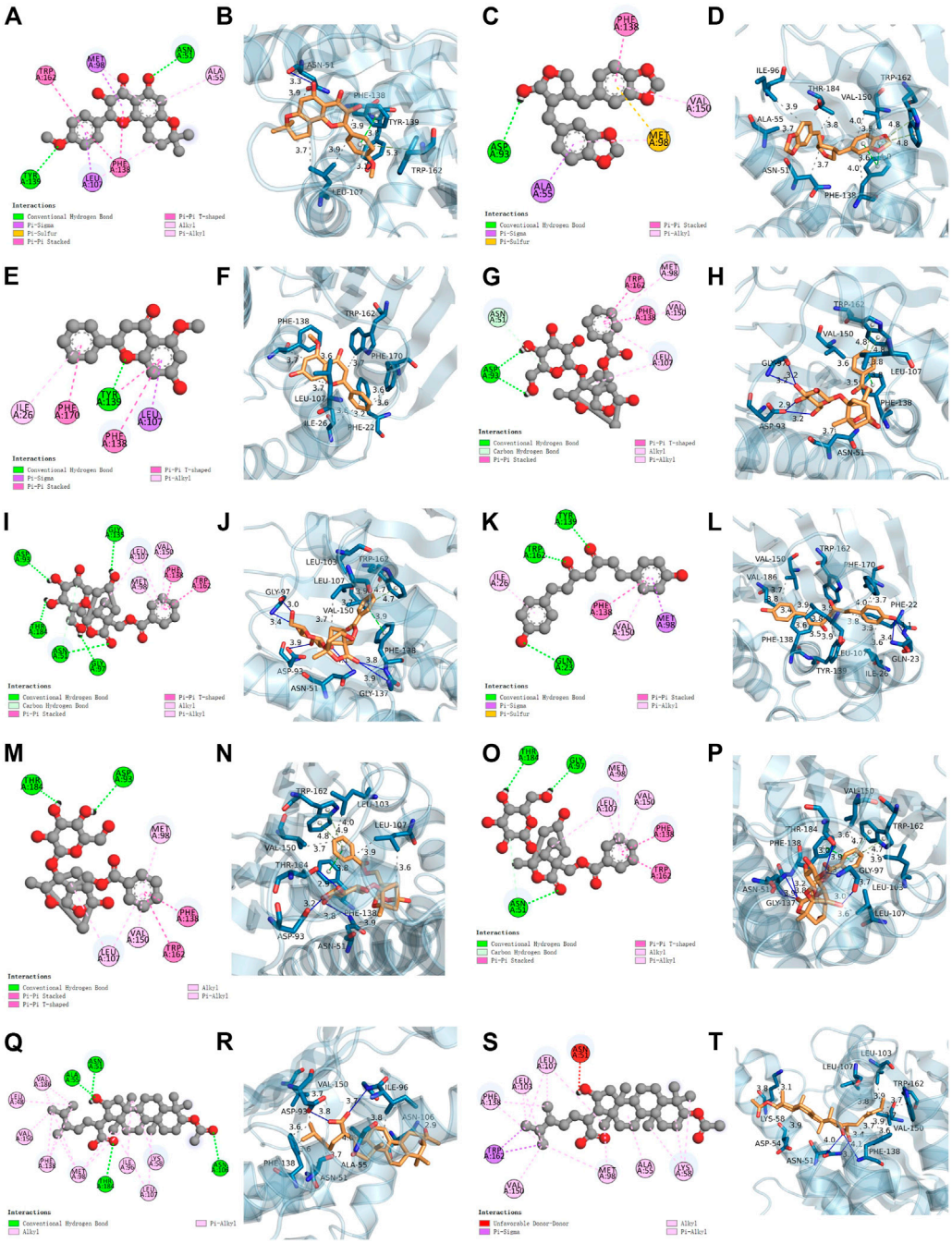

FIGURE 5
Molecular docking results. HSP90AA1 binds with MOL004373 (2D and 3D) **(A, B)**, MOL013187 (2D and 3D) **(C, D)**, MOL000228 (2D and 3D) **(E, F)**, MOL001924 (2D and 3D) **(G, H)**, MOL001928 (2D and 3D) **(I, J)**, MOL000940 (2D and 3D) **(K, L)**. EPHA2 binds with MOL001924 (2D and 3D) **(M, N)**, MOL001928 (2D and 3D) **(O, P)**, MOL000289 (2D and 3D) **(Q, R)**, MOL000276 (2D and 3D) **(S, T)**.

HSP90AA1 plays an important role in the proliferation, differentiation, survival, and angiogenesis of tumor cells (Jego et al., 2013). HSP90AA1 is highly expressed in a variety of malignancies, including breast, endometrial, ovarian, colon, lung, and prostate cancers (Kang et al., 2010; Y; Li et al., 2011; Soroka et al., 2012), which is consistent with our conclusion based on the TCGA database. Qiuran Xu et al. showed that Hsp90 can regulate the abundance of PKM2 through phosphorylation of Thr-328 to promote cell glycolysis and proliferation and inhibit apoptosis of HCC cells (Q. Xu et al., 2017). Xiao Xiang et al. showed that the VEGF/VEGFR2 pathway may be related to the recurrence of HCC in patients with high expression of HSP90AA1 (Xiang et al., 2018). EPHA2 overexpression is associated with tumor progression, metastasis and prognosis of HCC. Pu Yang et al. showed that EPHA2 is involved in key mediators of angiogenesis and invasion (Yang et al., 2009). Qiao Jin et al. showed that EPHA2 can

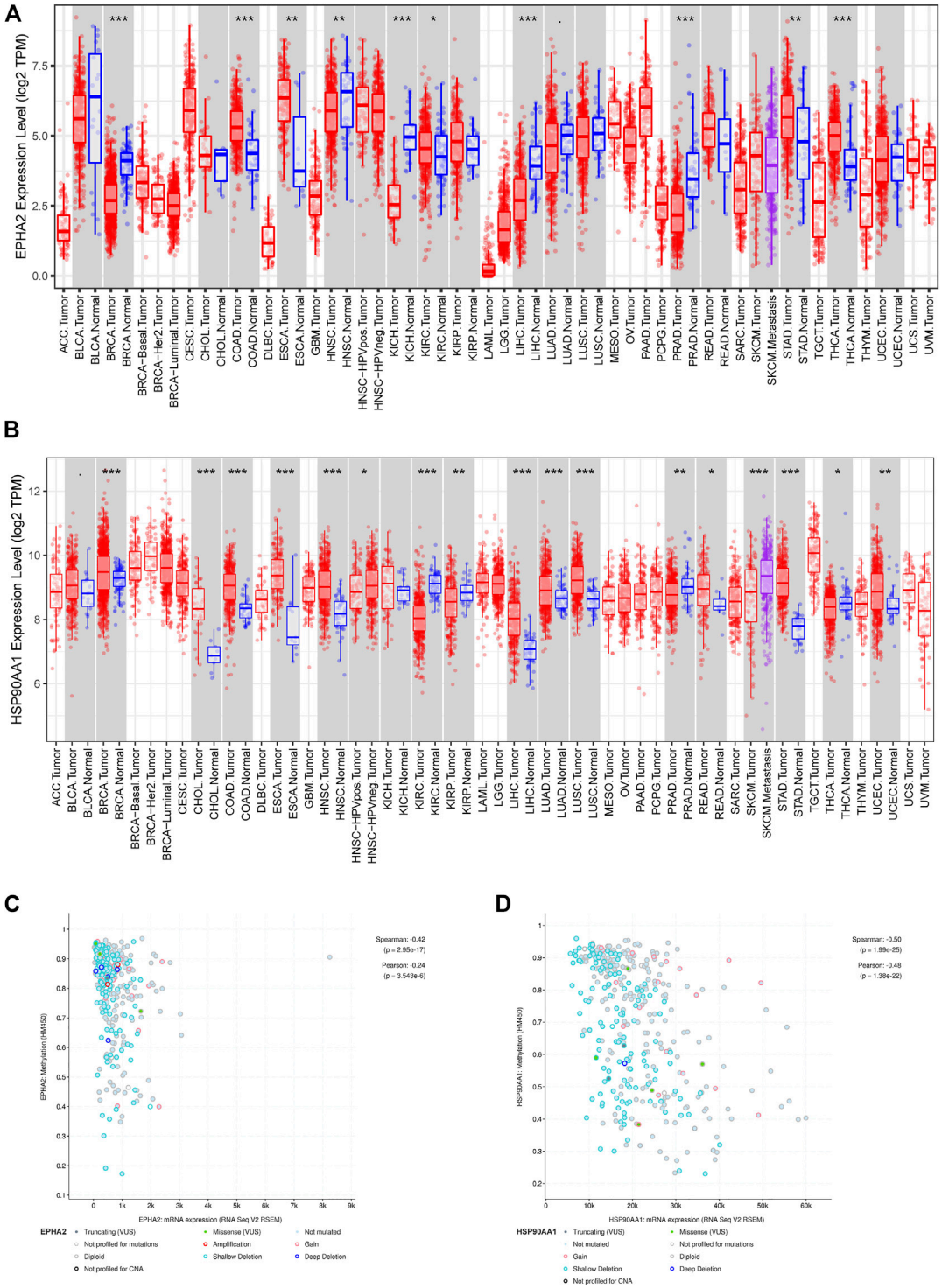

FIGURE 6
(A, B) Differential expression of EPHA2 and HSP90AA1 in various tumors. **(C, D)** Correlation analysis of mRNA expression levels and DNA methylation of EPHA2 and HSP90AA1 in HCC.

negatively regulate the radiosensitivity of MHCC97H cells (Jin et al., 2015), which is consistent with our findings. We verified the application value of EPHA2 by analyzing data from the TCGA database, and the results showed that EPHA2 was differentially expressed in a variety of tumors, and its high expression was associated with poor prognosis in HCC, but the difference between the high and low expression of EPHA2 was not statistically significant. The RT–qPCR results showed that GJF decreased the mRNA expression levels of EPHA2 in HepG2 cells, and the expression levels decreased

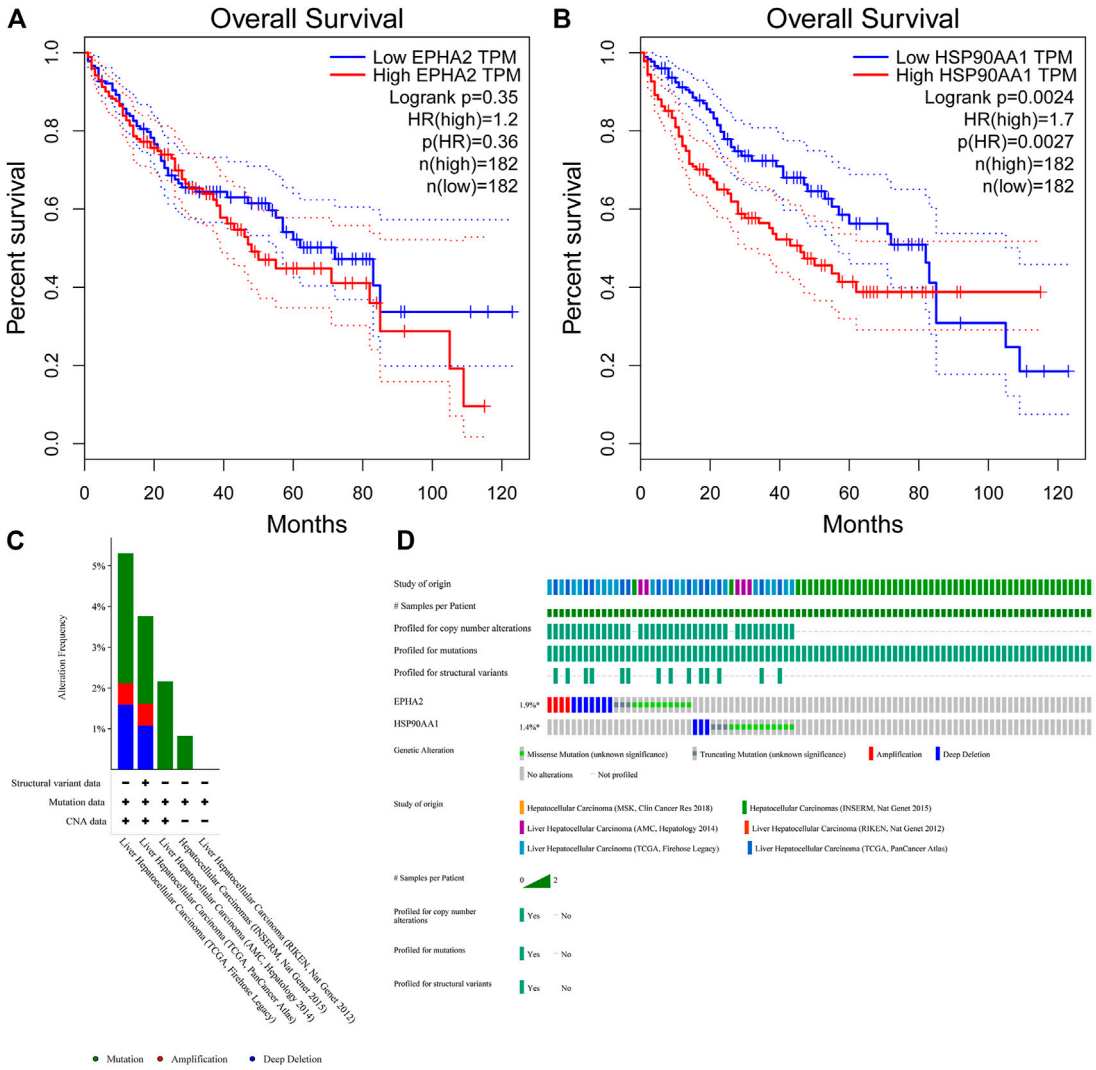

FIGURE 7
(A, B) Survival analysis of high and low expression populations of EPHA2 and HSP90AA1. (In the figure, the red curve refers to the population with high expression in the TCGA database, and the blue curve refers to the population with low expression in the TCGA database. The P value represents the statistical difference in the survival curve between the two groups). **(C, D)** Genetic mutation analysis of EPHA2 and HSP90AA1 in various TCGA datasets. **(C)** The percentage of total mutations of EPHA2 and HSP90AA1. **(D)** The mutations of EPHA2 and HSP90AA1 in each sample.

gradually with increasing hepatocellular formula concentration. The mRNA expression level of HSP90AA1 in HepG2 cells decreased gradually with increasing GJF concentration but only in the high-dose group ($p < 0.05$). Our hypothesis was further verified by RT–qPCR results. GJF may inhibit the mRNA expression levels of related molecules in the PI3K/Akt signaling pathway and regulate the mRNA expression levels of proliferation- and apoptosis-related proteins downstream of the pathway. Combined with molecular docking technology, EPHA2 may be the key target of GJF in HCC through the PI3K/Akt signaling pathway.

Molecular docking results showed that PF and PA might be the key compounds in hepatocellular formation and have anticancer activity. PF is an important compound that protects the liver, reduces cholestasis, alleviates liver fibrosis, and prevents HCC(X. Ma et al., 2020). Yang Zhou et al. showed that PF may block the expression of the Wnt/β-catenin pathway by downregulating the expression of 5-HT1D, thus inhibiting the occurrence of HCC(Zhou et al., 2020). In addition, PF is an effective antimetastatic and anti-invasive agent for inhibiting HCC invasion and metastasis (J. T. Lu et al., 2014). PA is a triterpenoid compound with anticancer activity that has anti-inflammatory, anticancer, anti-aging, and insulin-like properties and other pharmacological effects (Miao et al., 2019). It induces apoptosis in human prostate cancer (Gapter et al., 2005), lung cancer (C. Lu et al., 2018), and bladder cancer (Jeong et al., 2015) cells. In conclusion, our results suggest that PA and PF may be the key compounds of hepatocellular development that exert anticancer activity.

However, our study had certain limitations. Because TCM has the characteristics of multitarget and multipathway effects, the pathway we verified is likely to be only one way for GJF to exert its effects. In

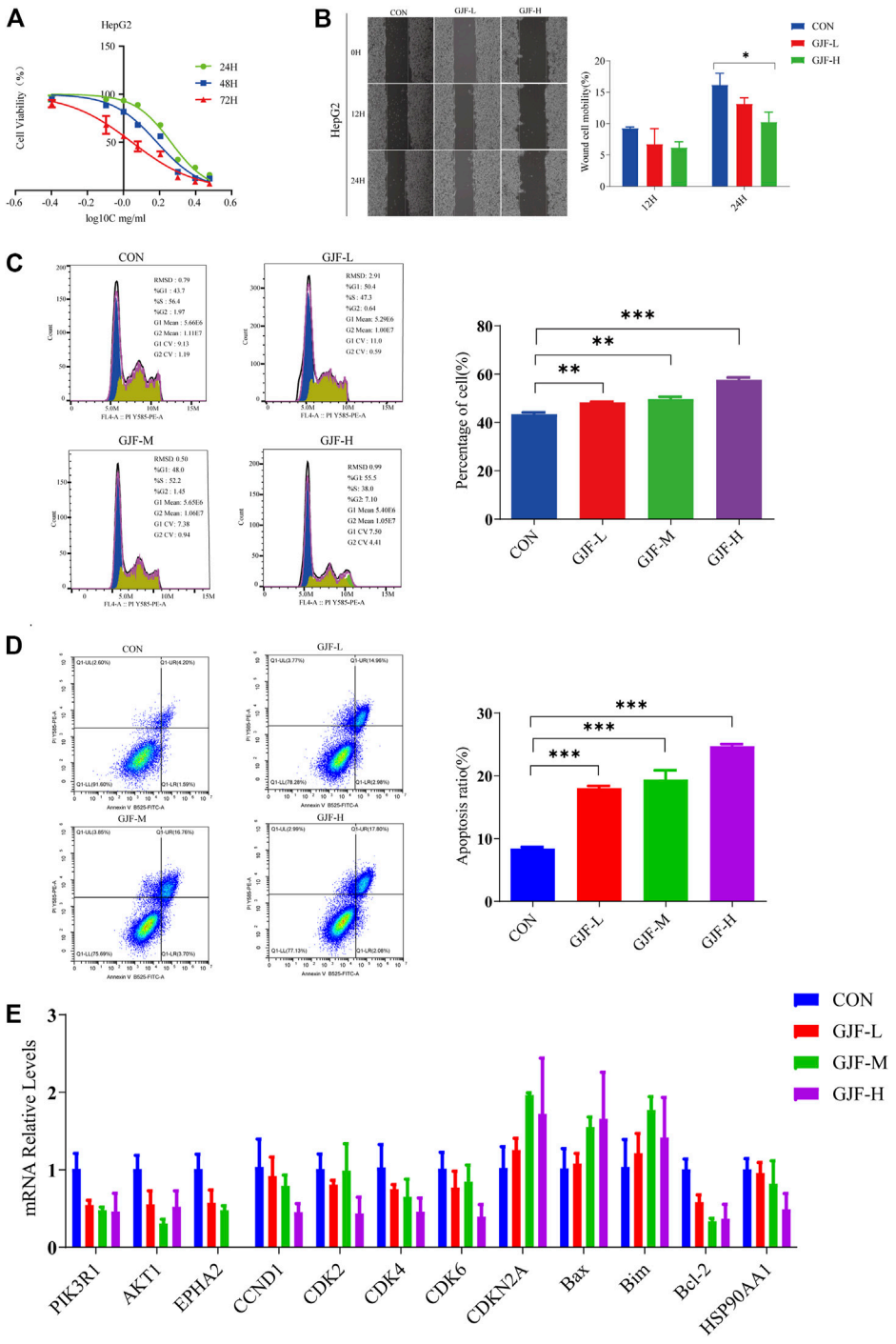

FIGURE 8
GJF inhibited HepG2 cells growth *in vitro*. **(A)** The effect of GJF on the survival rate of HepG2 cells. **(B)** Effect of GJF on the cell mobility of HepG2 cells. **(C)** GJF induces hepatocellular arrest of HepG2 cells cycles. **(D)** GJF induces apoptosis in HepG2 cells. **(E)** Changes in the mRNA expression levels of related molecules in the PI3K/Akt pathway in HepG2 cell lines. Gene expression was evaluated by RT-qPCR, using the 2 −ΔΔCT method. (CON, negative control treatment; GJF-L, treated with low concentrations (0.5 mg/ml) of GJF; GJF-M, treated with medium concentrations (1.0 mg/ml) of GJF; GJF-H, treated with medium concentrations (1.5 mg/ml) of GJF. Data are presented as the mean ± SD, and analysis of variance was used to determine the significance. *p < 0.05; **p < 0.01; ***p < 0.001 compared with the control group).

this study, we made predictions based on data analysis and a small number of *in vitro* experiments. GJF is a well-known prescription with beneficial properties. Therefore, further *in vivo* and *in vitro* experimental verification is still necessary.

5 Conclusion

In conclusion, this study revealed a potential pharmacological mechanism by which GJF can treat HCC at the systemic level, possibly

involving the synergistic effects of multiple mechanisms, such as cell proliferation, apoptosis, cell migration, immune regulation, and inflammatory induction. Our results suggested that GJF may induce G0/G1 phase cycle arrest by inhibiting the PI3K/Akt signaling pathway and promoting the apoptosis of liver cancer cell lines. EPHA2 may be an important target of GJF in HCC, and pachymic acid may be an important active compound of GJF that exerts anticancer activity. This study can provide a scientific basis for the subsequent clinical application of GJF and the in-depth study of its mechanism. Given that the study is primarily based on data analysis, further biological experiments are crucial to verify the results.

Data availability statement

The datasets presented in this study can be found in online repositories. The names of the repository/repositories and accession number(s) can be found in the article/Supplementary Material.

Author contributions

Part of the data in this paper are from the dissertation of co-first author QY. The data presented in the current study were previously deposited as a dissertation in the archives of Guangzhou University of Chinese Medicine, accession number 20171101040. The first author MY participated in the main writing, modification and experimental assistance of this study. XW and QY put forward the idea of the study and supervised the study. MY, QY, and YL carried out the data preparation network construction. BW and SC participated in the experiment. LL and BY analyzed the results. MY and QY wrote the manuscript. XW participated and directed the revision of the manuscript. All authors read and approved the final version of the manuscript.

Funding

This work was supported by the General Project of National Natural Science Foundation of China (Receive No. 8227152807, Grant No. 82274605).

Conflict of interest

The authors declare that the research was conducted in the absence of any commercial or financial relationships that could be construed as a potential conflict of interest.

Publisher's note

All claims expressed in this article are solely those of the authors and do not necessarily represent those of their affiliated organizations, or those of the publisher, the editors and the reviewers. Any product that may be evaluated in this article, or claim that may be made by its manufacturer, is not guaranteed or endorsed by the publisher.

Supplementary material

The Supplementary Material for this article can be found online at: https://www.frontiersin.org/articles/10.3389/fphar.2023.1016967/full#supplementary-material

SUPPLEMENTARY TABLE 1
Top 5 compounds in GJF (ranked by OB %).

SUPPLEMENTARY TABLE 2
Top 10 KEGG Pathways in which GJF acted on the key targets of HCC (ranked by number of genes enriched).

SUPPLEMENTARY TABLE 3
mRNA expression level of each molecule in HepG2 cell line.

References

Bray, F., Ferlay, J., Soerjomataram, I., Siegel, R. L., Torre, L. A., and Jemal, A. (2018). Global cancer statistics 2018: GLOBOCAN estimates of incidence and mortality worldwide for 36 cancers in 185 countries. *CA Cancer J. Clin.* 68 (6), 394–424. doi:10.3322/caac.21492

Daina, A., Michielin, O., and Zoete, V. (2019). SwissTargetPrediction: Updated data and new features for efficient prediction of protein targets of small molecules. *Nucleic Acids Res.* 47 (W1), W357–W364. doi:10.1093/nar/gkz382

Gao, J., Aksoy, B. A., Dogrusoz, U., Dresdner, G., Gross, B., Sumer, S. O., et al. (2013). Integrative analysis of complex cancer genomics and clinical profiles using the cBioPortal. *Sci. Signal* 6 (269), pl1. doi:10.1126/scisignal.2004088

Gao, S., Liu, J., Wang, M., Liu, Y., Meng, X., Zhang, T., et al. (2019). Exploring on the bioactive markers of Codonopsis Radix by correlation analysis between chemical constituents and pharmacological effects. *J. Ethnopharmacol.* 236, 31–41. doi:10.1016/j.jep.2019.02.032

Gapter, L., Wang, Z., Glinski, J., and Ng, K.-y. (2005). Induction of apoptosis in prostate cancer cells by pachymic acid from Poria cocos. *Biochem. Biophysical Res. Commun.* 332 (4), 1153–1161. doi:10.1016/j.bbrc.2005.05.044

Gotoh, J., Obata, M., Yoshie, M., Kasai, S., and Ogawa, K. (2003). Cyclin D1 over-expression correlates with beta-catenin activation, but not with H-ras mutations, and phosphorylation of Akt, GSK3 beta and ERK1/2 in mouse hepatic carcinogenesis. *Carcinogenesis* 24 (3), 435–442. doi:10.1093/carcin/24.3.435

Gunasekaran, G., Bekki, Y., Lourdusamy, V., and Schwartz, M. (2020). Surgical treatments of hepatobiliary cancers. *Hepatology* 73 (S1), 128–136. doi:10.1002/hep.31325

Hussaini, S., Chehade, R., Boldt, R. G., Raphael, J., Blanchette, P., Maleki Vareki, S., et al. (2021). Association between immune-related side effects and efficacy and benefit of immune checkpoint inhibitors - a systematic review and meta-analysis. *Cancer Treat. Rev.* 92, 102134. doi:10.1016/j.ctrv.2020.102134

Jego, G., Hazoumé, A., Seigneuric, R., and Garrido, C. (2013). Targeting heat shock proteins in cancer. *Cancer Lett.* 332 (2), 275–285. doi:10.1016/j.canlet.2010.10.014

Jeong, J.-W., Lee, W. S., Go, S.-i., Nagappan, A., Baek, J. Y., Lee, J.-D., et al. (2015). Pachymic acid induces apoptosis of EJ bladder cancer cells by DR5 up-regulation, ROS generation, modulation of bcl-2 and IAP family members. *Phytotherapy Res.* 29 (10), 1516–1524. doi:10.1002/ptr.5402

Jin, B., Wang, W., Du, G., Huang, G. Z., Han, L. T., Tang, Z. Y., et al. (2015). Identifying hub genes and dysregulated pathways in hepatocellular carcinoma. *Eur. Rev. Med. Pharmacol. Sci.* 19 (4), 592–601.

Jin, Q., Li, X., and Cao, P. (2015). EphA2 modulates radiosensitive of hepatocellular carcinoma cells via p38/mitogen-activated protein kinase-mediated signal pathways. *Kaohsiung J. Med. Sci.* 31 (10), 510–517. doi:10.1016/j.kjms.2015.09.001

Kang, G. H., Lee, E. J., Jang, K. T., Kim, K. M., Park, C. K., Lee, C. S., et al. (2010). Expression of HSP90 in gastrointestinal stromal tumours and mesenchymal tumours. *Histopathology* 56 (6), 694–701. doi:10.1111/j.1365-2559.2010.03550.x

Khan, S. A., and Lee, T. K. W. (2022). Network-pharmacology-based study on active phytochemicals and molecular mechanism of cnidium monnieri in treating hepatocellular carcinoma. *Int. J. Mol. Sci.* 23 (10), 5400. doi:10.3390/ijms23105400

Law, C. W., Chen, Y., Shi, W., and Smyth, G. K. (2014). voom: Precision weights unlock linear model analysis tools for RNA-seq read counts. *Genome Biol.* 15 (2), R29. doi:10.1186/gb-2014-15-2-r29

Lee, L., Wang, K., Li, G., Xie, Z., Wang, Y., Xu, J., et al. (2011). Liverome: A curated database of liver cancer-related gene signatures with self-contained context information. *BMC Genomics* 12, S3. doi:10.1186/1471-2164-12-S3-S3

Li, S., and Zhang, B. (2013). Traditional Chinese medicine network pharmacology: Theory, methodology and application. *Chin. J. Nat. Med.* 11 (2), 110–120. doi:10.1016/s1875-5364(13)60037-0

Li, T., Fan, J., Wang, B., Traugh, N., Chen, Q., Liu, J. S., et al. (2017). Timer: A web server for comprehensive analysis of tumor-infiltrating immune cells. *Cancer Res.* 77 (21), e108–e110. doi:10.1158/0008-5472.can-17-0307

Li, Y., Zhang, T., Schwartz, S. J., and Sun, D. (2011). Sulforaphane potentiates the efficacy of 17-allylamino 17-demethoxygeldanamycin against pancreatic cancer through enhanced abrogation of Hsp90 chaperone function. *Nutr. cancer* 63 (7), 1151–1159. doi:10.1080/01635581.2011.596645

Liu, H., Wang, Z. Y., Zhou, Y. C., Song, W., Ali, U., and Sze, D. M. (2021). Immunomodulation of Chinese herbal medicines on NK cell populations for cancer therapy: A systematic review. *J. Ethnopharmacol.* 268, 113561. doi:10.1016/j.jep.2020.113561

Liu, Q. M., Zhao, H. Y., Zhong, X. K., and Jiang, J. G. (2012). Eclipta prostrata L. Phytochemicals: Isolation, structure elucidation, and their antitumor activity. *Food Chem. Toxicol.* 50 (11), 4016–4022. doi:10.1016/j.fct.2012.08.007

Liu, X., Li, M., Wang, X., Dang, Z., Yu, L., Wang, X., et al. (2019). Effects of adjuvant traditional Chinese medicine therapy on long-term survival in patients with hepatocellular carcinoma. *Phytomedicine* 62, 152930. doi:10.1016/j.phymed.2019.152930

Lu, C., Cai, D., and Ma, J. (2018). Pachymic acid sensitizes gastric cancer cells to radiation therapy by upregulating Bax through hypoxia. *Am. J. Chin. Med.* 46 (4), 875–890. doi:10.1142/s0192415x18500465

Lu, J. T., He, W., Song, S. S., and Wei, W. (2014). Paeoniflorin inhibited the tumor invasion and metastasis in human hepatocellular carcinoma cells. *Bratisl. Lek. Listy* 115 (7), 427–433. doi:10.4149/bll_2014_084

Lu, M., Hu, Q., Zhang, Y., Zhai, Y., Zhou, Y., and Jiang, J. (2019). Comparative chemical profiling of three TCM drugs in the Paeoniaceae family by UPLC-MS/MS combined with chemometric methods. *Biochem. Syst. Ecol.* 83, 121–129. doi:10.1016/j.bse.2019.02.002

Luo, T. T., Lu, Y., Yan, S. K., Xiao, X., Rong, X. L., and Guo, J. (2020). Network pharmacology in research of Chinese medicine formula: Methodology, application and prospective. *Chin. J. Integr. Med.* 26 (1), 72–80. doi:10.1007/s11655-019-3064-0

Ma, C., Kang, W., Yu, L., Yang, Z., and Ding, T. (2020). AUNIP expression is correlated with immune infiltration and is a candidate diagnostic and prognostic biomarker for hepatocellular carcinoma and lung adenocarcinoma. *Front. Oncol.* 10, 590006. doi:10.3389/fonc.2020.590006

Ma, X. L., Shen, M. N., Hu, B., Wang, B. L., Yang, W. J., Lv, L. H., et al. (2019). CD73 promotes hepatocellular carcinoma progression and metastasis via activating PI3K/AKT signaling by inducing Rap1-mediated membrane localization of P110β and predicts poor prognosis. *J. Hematol. Oncol.* 12 (1), 37. doi:10.1186/s13045-019-0724-7

Ma, X., Zhang, W., Jiang, Y., Wen, J., Wei, S., and Zhao, Y. (2020). Paeoniflorin, a natural product with multiple targets in liver diseases-A mini review. *Front. Pharmacol.* 11, 531. doi:10.3389/fphar.2020.00531

Ma, Z., Fan, Y., Wu, Y., Kebebe, D., Zhang, B., Lu, P., et al. (2019). Traditional Chinese medicine-combination therapies utilizing nanotechnology-based targeted delivery systems: A new strategy for antitumor treatment. *Int. J. Nanomedicine* 14, 2029–2053. doi:10.2147/IJN.S197889

Miao, G., Han, J., Zhang, J., Wu, Y., and Tong, G. (2019). Targeting pyruvate kinase M2 and hexokinase II, pachymic acid impairs glucose metabolism and induces mitochondrial apoptosis. *Biol. Pharm. Bull.* 42 (1), 123–129. doi:10.1248/bpb.b18-00730

Ozturk, M., Arslan-Ergul, A., Bagislar, S., Senturk, S., and Yuzugullu, H. (2009). Senescence and immortality in hepatocellular carcinoma. *Cancer Lett.* 286 (1), 103–113. doi:10.1016/j.canlet.2008.10.048

Paolacci, S., Precone, V., Acquaviva, F., Chiurazzi, P., Fulcheri, E., Pinelli, M., et al. (2019) Genetics of lipedema: New perspectives on genetic research and molecular diagnoses. *Eur. Rev. Med. Pharmacol. Sci.* 23 (13), 5581–5594. doi:10.26355/eurrev_201907_18292

Petrowsky, H., Fritsch, R., Guckenberger, M., De Oliveira, M. L., Dutkowski, P., and Clavien, P. A. (2020). Modern therapeutic approaches for the treatment of malignant liver tumours. *Nat. Rev. Gastroenterol. Hepatol.* 17 (12), 755–772. doi:10.1038/s41575-020-0314-8

Plentz, R. R., Park, Y. N., Lechel, A., Kim, H., Nellessen, F., Langkopf, B. H., et al. (2007). Telomere shortening and inactivation of cell cycle checkpoints characterize human hepatocarcinogenesis. *Hepatology* 45 (4), 968–976. doi:10.1002/hep.21552

Ren, M., McGowan, E., Li, Y., Zhu, X., Lu, X., Zhu, Z., et al. (2019). Saikosaponin-d suppresses COX2 through p-STAT3/C/EBPβ signaling pathway in liver cancer: A novel mechanism of action. *Front. Pharmacol.* 10, 623. doi:10.3389/fphar.2019.00623

Ritchie, M. E., Phipson, B., Wu, D., Hu, Y., Law, C. W., Shi, W., et al. (2015). Limma powers differential expression analyses for RNA-sequencing and microarray studies. *Nucleic Acids Res.* 43 (7), e47. doi:10.1093/nar/gkv007

Siegel, R. L., Miller, K. D., Fuchs, H. E., and Jemal, A. (2021). Cancer statistics, 2021. *CA Cancer J. Clin.* 71 (1), 7–33. doi:10.3322/caac.21654

Siegel, R. L., Miller, K. D., and Jemal, A. (2020). Cancer statistics, 2020. *CA Cancer J. Clin.* 70 (1), 7–30. doi:10.3322/caac.21590

Smyth, G. K. (2004). Linear models and empirical bayes methods for assessing differential expression in microarray experiments. *Stat. Appl. Genet. Mol. Biol.* 3, Article3. doi:10.2202/1544-6115.1027

Soroka, J., Wandinger, S. K., Mäusbacher, N., Schreiber, T., Richter, K., Daub, H., et al. (2012). Conformational switching of the molecular chaperone Hsp90 via regulated phosphorylation. *Mol. Cell* 45 (4), 517–528. doi:10.1016/j.molcel.2011.12.031

Su, W. H., Chao, C. C., Yeh, S. H., Chen, D. S., Chen, P. J., and Jou, Y. S. (2007). OncoDB.HCC: An integrated oncogenomic database of hepatocellular carcinoma revealed aberrant cancer target genes and loci. *Nucleic Acids Res.* 35, D727–D731. doi:10.1093/nar/gkl845

Wang, Y., Yao, R., Zhang, D., Chen, R., Ren, Z., and Zhang, L. (2020). Circulating neutrophils predict poor survival for HCC and promote HCC progression through p53 and STAT3 signaling pathway. *J. Cancer* 11 (13), 3736–3744. doi:10.7150/jca.42953

Wen-Sheng, W. (2003). ERK signaling pathway is involved in p15INK4b/p16INK4a expression and HepG2 growth inhibition triggered by TPA and Saikosaponin a. *Oncogene* 22 (7), 955–963. doi:10.1038/sj.onc.1206237

Xiang, X., You, X. M., and Li, L. Q. (2018). Expression of HSP90AA1/HSPA8 in hepatocellular carcinoma patients with depression. *Onco Targets Ther.* 11, 3013–3023. doi:10.2147/ott.s159432

Xu, J., Li, Y., Lu, J., Pan, T., Ding, N., Wang, Z., et al. (2015). The mRNA related ceRNA-ceRNA landscape and significance across 20 major cancer types. *Nucleic Acids Res.* 43 (17), 8169–8182. doi:10.1093/nar/gkv853

Xu, Q., Tu, J., Dou, C., Zhang, J., Yang, L., Liu, X., et al. (2017). HSP90 promotes cell glycolysis, proliferation and inhibits apoptosis by regulating PKM2 abundance via Thr-328 phosphorylation in hepatocellular carcinoma. *Mol. Cancer* 16 (1), 178. doi:10.1186/s12943-017-0748-y

Yang, P., Yuan, W., He, J., Wang, J., Yu, L., Jin, X., et al. (2009). Overexpression of EphA2, MMP-9, and MVD-CD34 in hepatocellular carcinoma: Implications for tumor progression and prognosis. *Hepatol. Res.* 39 (12), 1169–1177. doi:10.1111/j.1872-034X.2009.00563.x

Ye, L., Jia, Y., Ji, K. E., Sanders, A. J., Xue, K., Ji, J., et al. (2015). Traditional Chinese medicine in the prevention and treatment of cancer and cancer metastasis. *Oncol. Lett.* 10 (3), 1240–1250. doi:10.3892/ol.2015.3459

Yu, G., Wang, L. G., Han, Y., and He, Q. Y. (2012). clusterProfiler: an R package for comparing biological themes among gene clusters. *OMICS* 16 (5), 284–287. doi:10.1089/omi.2011.0118

Zhou, Y., Liu, X., Gao, Y., Tan, R., Wu, Z., Zhong, Q., et al. (2020). Paeoniflorin affects hepatocellular carcinoma progression by inhibiting Wnt/β-catenin pathway through downregulation of 5-HT1D. *Curr. Pharm. Biotechnol.* 22, 1246–1253. doi:10.2174/1389201021666201009153808

Zhu, B., Zhang, Q. L., Hua, J. W., Cheng, W. L., and Qin, L. P. (2018). The traditional uses, phytochemistry, and pharmacology of atractylodes macrocephala Koidz.: A review. *J. Ethnopharmacol.* 226, 143–167. doi:10.1016/j.jep.2018.08.023

frontiers | Frontiers in Pharmacology

TYPE Original Research
PUBLISHED 17 February 2023
DOI 10.3389/fphar.2023.1108992

OPEN ACCESS

EDITED BY
Khuloud Bajbouj,
University of Sharjah, United Arab Emirates

REVIEWED BY
Ankit P. Laddha,
University of Connecticut, United States
Hassan Mubarak Ishqi,
University of Miami Health System, United States

*CORRESPONDENCE
Maha R. A. Abdollah,
maha.abdollah@bue.edu.eg

SPECIALTY SECTION
This article was submitted to Pharmacology of Anti-Cancer Drugs, a section of the journal Frontiers in Pharmacology

RECEIVED 27 November 2022
ACCEPTED 06 February 2023
PUBLISHED 17 February 2023

CITATION
Abdollah MRA, Ali AA, Elgohary HH and Elmazar MM (2023), Antiangiogenic drugs in combination with seaweed fucoidan: A mechanistic *in vitro* and *in vivo* study exploring the VEGF receptor and its downstream signaling molecules in hepatic cancer.
Front. Pharmacol. 14:1108992.
doi: 10.3389/fphar.2023.1108992

Antiangiogenic drugs in combination with seaweed fucoidan: A mechanistic *in vitro* and *in vivo* study exploring the VEGF receptor and its downstream signaling molecules in hepatic cancer

Maha R. A. Abdollah[1,2]*, Aya A. Ali[2], Hassnaa H. Elgohary[2] and Mohamed M. Elmazar[1,2]

[1]Department of Pharmacology, Faculty of Pharmacy, The British University in Egypt, El Sherouk City, Egypt, [2]Center for Drug Research and Development (CDRD), Faculty of Pharmacy, The British University in Egypt, El Sherouk City, Egypt

Hepatocellular carcinoma (HCC) is one of the most common cancers reported worldwide with poor morbidity and high mortality rates. HCC is a very vascular solid tumour as angiogenesis is not only a key driver for tumour progression but also an exciting therapeutic target. Our research investigated the use of fucoidan, a sulfated polysaccharide readily abundant in edible seaweeds commonly consumed in Asian diet due to their extensive health benefits. Fucoidan was reported to possess a strong anti-cancer activity, but its anti-angiogenic potential is still to be fully unraveled. Our research investigated fucoidan in combination with sorafenib (an anti-VEGFR tyrosine kinase inhibitor) and Avastin® (bevacizumab, an anti-VEGF monoclonal antibody) in HCC both *in vitro* and *in vivo*. *In vitro* on HUH-7 cells, fucoidan had a potent synergistic effect when combined with the anti-angiogenic drugs and significantly reduced HUH-7 cell viability in a dose dependent manner. Using the scratch wound assay to test cancer cell motility, sorafenib, A + F (Avastin and fucoidan) or S + F (sorafenib and fucoidan) treated cells consistently showed an unhealed wound and a significantly smaller %wound closure (50%–70%) *versus* untreated control (91%–100%) ($p < 0.05$, one-way ANOVA). Using RT-qPCR; fucoidan, sorafenib, A + F and S + F significantly reduced the expression of the pro-angiogenic PI3K/AKT/mTOR and KRAS/BRAF/MAPK pathways by up to 3 folds ($p < 0.05$, one-way ANOVA *versus* untreated control). While ELISA results revealed that in fucoidan, sorafenib, A + F and S + F treated cells, the protein levels of caspases 3, 8, and 9 was significantly increased especially in the S + F group showing 40- and 16-times higher caspase 3 and 8 protein levels, respectively ($p < 0.05$, one-way-ANOVA *versus* untreated control). Finally, in a DEN-HCC rat model, H&E staining revealed larger sections of apoptosis and necrosis in the tumour nodules of rats treated with the combination therapies and immunohistochemical analysis of the apoptotic marker caspase 3, the proliferation marker Ki67 and the marker for angiogenesis CD34 showed significant improvements when the combination therapies were used. Despite the promising findings reported herein that highlighted a promising

chemomodulatory effect of fucoidan when combined with sorafenib and Avastin, further investigations are required to elucidate potential beneficial or adversary interactions between the tested agents.

KEYWORDS

angiogenesis, fucoidan, sorafenib, avastin, hepatocellular carcinoma, VEGF, VEGFR

1 Introduction

Hepatocellular carcinoma (HCC) is the third most common cause of cancer mortality and thus considered a major global health problem (El-Serag and Rudolph, 2007; Tawfik et al., 2022). Eighty percent of HCC cases are reported in the developing countries in East Asia and sub-Saharan Africa representing a major economic burden (El-Serag and Rudolph, 2007; Abdelmageed et al., 2016).

HCC is a highly vascular tumour and therefore represents an attractive candidate for the development of anti-angiogenic drugs (Sampat and O'Neil, 2013; Morse et al., 2019). The process by which new blood vessels are formed from existing ones is called angiogenesis, one of the main hallmarks of cancer (Hanahan and Weinberg, 2011) and a key tumorigenic driver responsible for delivering the essential nutrients and oxygen needed by the tumour to continue its uncontrolled proliferation as well as the removal of unwanted metabolic waste (Nishida et al., 2006). The ability of cancer cells to travel to distant organs *via* the newly formed blood vessels, i.e. metastasis, is one of the inherent dangers associated with angiogenesis as well as one of the main causes of mortality from cancer (Nishida et al., 2006). Therefore, both tumorigenesis and metastatic spread rely mainly on angiogenesis which is triggered by a variety of angiogenic factors secreted from tumor cells (Sampat and O'Neil, 2013).

The main goal of anti-angiogenic therapies is to turn cancer into a "dormant" disease by cutting off the blood supply thus "starving" tumour cells to death. Despite years of research dedicated to developing potent therapies to halt angiogenesis, the full therapeutic potential of anti-angiogenic drugs is yet to be fulfilled. Modest overall survival benefits accompanied with the emergence of resistance are few of the challenges that stop anti-angiogenic drugs from reaching their full therapeutic potential (Yang et al., 2017). Sorafenib, an oral multi-kinase inhibitor, and Avastin, an anti-VEGF monoclonal antibody, are two anti-angiogenic agents currently approved for treating unresectable or metastatic HCC (Morse et al., 2019). Unfortunately, clinical data revealed patients' non-compliance caused by severe side effects, toxicity and tumour relapse (Bonam et al., 2018). This highlights the urgency to develop adjuvant new agents to improve the therapeutic outcome of anti-angiogenic agents.

Medicinal plant-based herbal products have gained a lot of momentum in pursue of safer as well as more efficient anti-cancer therapies. They are mainly used as adjuvant therapies to reduce the toxic side effect of standard chemotherapies (Atashrazm et al., 2015; Bonam et al., 2018; Mahmoud et al., 2022). Natural polysaccharides obtained from algae and marine plants have drawn a lot of attention in recent years owing to their potential anti-cancer effect as well as their diverse biological activities (Atashrazm et al., 2015). Of these polysaccharides, fucoidan (a natural seaweed extract) has been under intense research due to its versatile biological activities (Fitton, 2011). Some of the reported biological activities of fucoidan include antiviral, anticoagulant, anti-inflammatory, antioxidant and antihyperlipidemic (Cumashi et al., 2007; Li et al., 2008; Lira et al., 2011; Abdollah et al., 2018). Fucoidan was also evaluated for potential therapeutic action in liver and kidney diseases, osteoarthritis and stem cell modulation (Fitton, 2011).

Fucoidan is a sulphated polysaccharide consisting mainly of fucose and sulfate ester groups (Cumashi et al., 2007; Li et al., 2008). It is extracted from different species of brown seaweed (e.g., *Laminaria japonica*, *Undaria pinnatifida*, *Fucus vesiculosus*, and *Macrocystis pyrifera*) and some marine invertebrates (e.g., sea urchins and sea cucumbers) (Li et al., 2008; Fitton, 2011; Atashrazm et al., 2015). In addition to being consumed in traditional Asian diet (particularly in China, Korea and Japan), it is commercially available as an over the counter (OTC) herbal food supplement in many western countries (Fitton, 2011; Atashrazm et al., 2015). Therefore, it is considered an exciting agent for clinical development owing to its relative safety and bioavailability.

The diverse pharmacological actions of fucoidan are still under investigation but it has been reported to affect many pathophysiological processes, such angiogenesis, carcinogenesis, oxidative stress, immune modulation and inflammation (Kwak, 2014; Jin et al., 2022). Both *in vitro* and *in vivo* studies have consistently confirmed the anti-cancer potential of fucoidan *via* the inhibition of angiogenesis, induction of cell cycle arrest and apoptosis (Aisa et al., 2005; Zhang et al., 2011; Atashrazm et al., 2015) and down regulation of CDK4, cyclin D1 and cyclin D2 in cancer cells (Banafa et al., 2013; Boo et al., 2013) [reviewed in more details in (Atashrazm et al., 2015) and (Jin et al., 2022)]. Fucoidan also modulated a number of oncogenic signaling pathways known to be upregulated in cancer and involved in promoting tumour progression, for instance, the extracellular signal-regulated kinase (ERK) pathway (or RAS/RAF/MAPK pathway) (Aisa et al., 2005), PI3K/AKT/mTOR pathway (Lee et al., 2012) as well as the GSK and Wnt pathways (Boo et al., 2013).

The aim of our study was to investigate the chemomodulatory effect of fucoidan, as an adjuvant therapy, in combination with two FDA-approved antiangiogenic agents: sorafenib and Avastin (bevacizumab) to potentiate their pharmacological action and potentially reduce their toxic side effects. A limited number of anti-angiogenic agents demonstrated efficacy in the treatment of advanced HCC despite decades of research (Raoul et al., 2017). Furthermore, very limited studies have reported the combination of anti-angiogenic agents with fucoidan, thus, our research might help better elucidate the interaction of fucoidan with the angiogenic pathways and unravel the potential molecular pathways and pharmacological mechanisms involved. A graphical abstract explaining our experimental approach is shown in Figure 1.

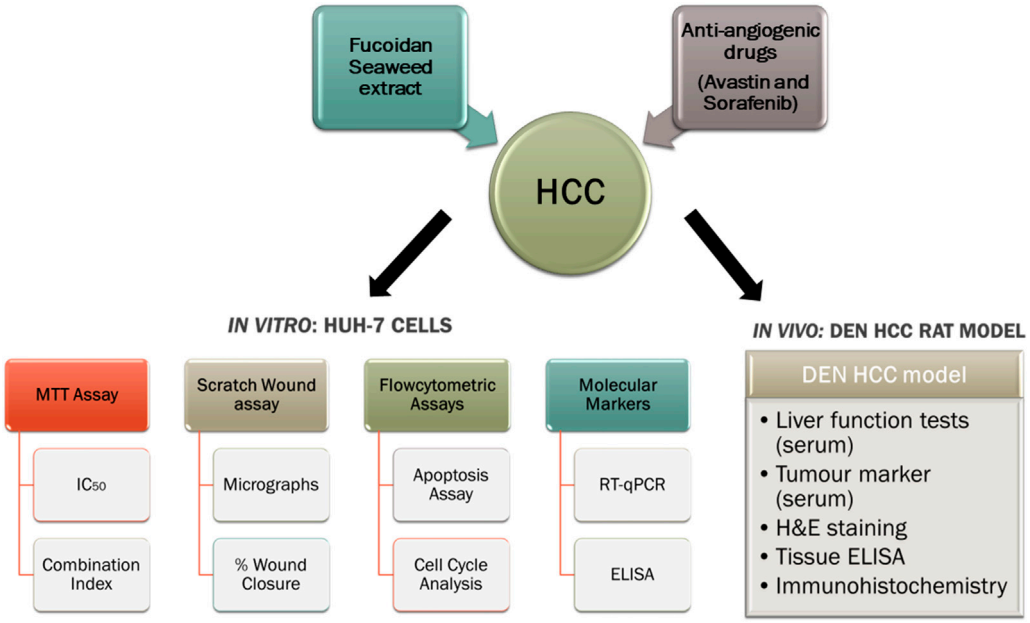

FIGURE 1
A graphical summary of our experimental design.

2 Materials and methods

2.1 Materials

Human hepatocellular carcinoma cell line HUH-7 was purchased from Vacsera (Giza, Egypt), sorafenib p-Toluenesulfonate salt was purchased from LC Laboratories (Woburn, MA, United States), Avastin® (bevacizumab, Genentech, United States) was purchased, in its formulated commercial preparation, from a community Pharmacy (Cairo, Egypt) and fucoidan extracted from *Laminaria Japonica* was purchased as a crude extract from Buchem BV (Holland). Dulbecco's modified Eagle's medium (DMEM) medium and fetal bovine serum (FBS) were purchased from Gibco®, Thermo Fisher Scientific, United States. Antibiotic-antimycotic mixture (100 U/ml of penicillin, 0.1 U/ml streptomycin and 0.25 µg/ml of Amphotericin B) was purchased from Lonza®, Walkersville, MD, United States. All other chemicals were purchased from Sigma Aldrich, United States unless otherwise specified.

2.2 Cell culture

HUH-7 cells were maintained in culture media consisting of DMEM supplemented with 10% fetal bovine serum (FBS), 100 U/ml of penicillin, 0.1 U/ml streptomycin, 0.25 µg/ml of Amphotericin B at 37°C in a humidified incubator containing 5% CO_2. All cell culture procedures were performed in a class II laminar flow hood and incubations were done inside the incubator at 37°C, unless otherwise specified.

2.3 Cell viability (MTT) assay

Cytotoxicity was evaluated using the MTT (3-(4,5-Dimethylthiazol-2-yl)-2,5-diphenyltetrazolium bromide) cell viability assay. 20,000 cells/well were seeded in a 96-well plate and left to attach overnight (o/n). Next day, the cells were treated with increasing concentrations of Avastin (0.94–30 µM), sorafenib (0.3–20 µM) and fucoidan (0.15—5 mg/ml) for 72 h. Next, media was discarded and replaced with 100 µl/well of fresh DMEM containing 12 mM (5 mg/ml) MTT stock in complete media and further incubated for 2 h inside the incubator at 37°C. Finally, the media was discarded and replaced with 100 µl of DMSO to dissolve the formed formazan crystals and then the absorbance was measured at 570 nm. Inhibitory concentration 50 (IC_{50}) was calculated using GraphPad Prism Software using the non-linear regression analysis.

For combination therapies, cells were seeded as previously described then next day treated with increasing concentrations of Avastin (0.94–30 µM), sorafenib (0.3–20 µM) either alone or in combination with IC_3 of fucoidan (55 µg/ml) for 72 h. The pharmacological interaction between fucoidan and sorafenib or Avastin when used in combination was evaluated by applying the isobologram equation shown below to calculate the combination indices (Chou, 2006).

$$\text{Combination index (CI)} = (D)1 / (D_n)1 + (D)2 / (D_n)2$$

Where $(D_n)1$ and $(D_n)2$ are the concentrations of each drug alone to exert n% effect, while (D)1 and (D)2 are the drug concentrations when used in combination to exert the same effect. The pharmacological interaction of the combination is estimated to be synergistic if CI < 0.8; additive if CI ranges from 0.8 to 1.264 or antagonistic if CI > 1.2.

TABLE 1 List of primers' sequences used in the RT-qPCR experiments.

Gene	Forward primer	Reverse primer
PI3K	ACCTTGTTCCAATCCCAGGT	TCGGCCTTTAACAGAGCAAA
AKT1	TATGGCGCTGAGATTGTGTC	AAAGGTCTTCATGGTGGCAC
mTOR	CCCTACTTTGCTTGAGGTGC	TGGATTCTGACAGGCTGACA
KRAS	TACAGTGCAATGAGGGACCA	TCCTGAGCCTGTTTTGTGTC
BRAF	ATTTGGGCAACGAGACCGAT	GTTGATCCTCCATCACCACGA
MAPK1	CCCCATCACAAGAAGACCTG	CTCGTCACTCGGGTCGTAAT
β-actin	AGCACAGAGCCTCGCCTTT	CACGATGGAGGGGAAGAC

2.4 Scratch wound assay

Briefly, 10^6 HUH-7 cells were seeded in six 6-well plates and allowed to attach overnight (o/n). Once cells reached confluency, the cell monolayer was scratched using a 200 µL pipette tip held vertically followed by washing twice with PBS to remove floating cells. The cells in each plate were then treated with complete DMEM medium alone (untreated control) or added to it either 5 µM sorafenib, 25.22 µM Avastin, 55 µg/ml fucoidan or the combinations of sorafenib and fucoidan (S + F) or Avastin and fucoidan (A + F). The wound area was imaged on day 0, 1, 2, 3 and 4 post treatment using an inverted microscope (Labomed Inc., LA, CA, United States) connected to a digital camera. Wound width was calculated using a wound healing size plugin for ImageJ® (NIH, United States) as described by (Suarez-Arnedo et al., 2020).

2.5 Annexin V/propidium iodide (PI) apoptosis assay on HUH-7 cells

HUH-7 cells were seeded in T-25 flasks and allowed to attached o/n. Next day, cells were treated with 5 µM sorafenib, 25.22 µM Avastin, 55 µg/ml fucoidan or the combinations of sorafenib and fucoidan (S + F) or Avastin and fucoidan (A + F) for 72 h. Next, cells were detached using trypsin, rinsed with cold 1x PBS, centrifuged twice at 280 x g for 5 min, resuspended in cold PBS and kept on ice until analysis. To a 100 µl aliquot of each cell suspension, 1 µl of PI stock (prepared at 100 µg/ml) and 5 µl Annexin V-FITC were added for 15 min at room temperature in the dark. Finally, 400 µl of 1x Annexin binding buffer was added to each sample and analyzed by CytoFlex flow cytometer (Beckman Coulter, CA, United States) according to the manufacturers' instructions. A minimum of 10,000 events were recorded for each sample. Data analysis was done using FlowJo software (Treestar Inc., San Carlos, CA, United States).

2.6 Cell cycle analysis

Cells were grown in six 6-well plates and each plate was subsequently treated with either 5 µM sorafenib, 25.22 µM Avastin, 55 µg/ml fucoidan or the combinations of sorafenib and fucoidan (S + F) or Avastin and fucoidan (A + F) for 48 h. Next, cells were harvested, washed with cold 1x PBS, centrifuged twice at 280 x g for 5 min and resuspended in cold PBS and kept on ice until analysis. Cell pellets were fixed by being re-suspended in 2 ml of 60% ice-cold ethanol at 4°C for 1 h. Fixed cells were subsequently washed at least twice with PBS (pH 7.4). The cell pellet was then re-suspended in 1 ml of nuclei acid staining mixture (10 µg/ml propidium iodide (PI) and 50 µg/ml RNAase A in PBS) for 20 min in the dark at 37°C. Cells were analyzed for DNA contents using flow cytometry analysis using CytoFlex flow cytometer (Beckman Coulter, CA, United States) according to the manufacturers' instructions. For each sample, 10,000 events were acquired. Cell cycle distribution was calculated using CytExpert software (Beckman Coulter, CA, United States).

2.7 Real time quantitative polymerase chain rection (RT-qPCR)

HUH-7 cells were seeded in T-75 flasks overnight at a seeding density of 5×10^6 cells/flask. Next day, the media was discarded and replaced with DMEM medium alone (untreated control) or added to it either 5 µM sorafenib, 25.22 µM Avastin, 55 µg/ml fucoidan or the combinations of sorafenib and fucoidan (S + F) or Avastin and fucoidan (A + F) and the cells were incubated for 72 h. Next, total RNA was isolated using RNeasy® Kits (Qiagen, Hilden, Germany) according to the manufacturer's protocol. RNA samples were then assessed to detect purity by measuring the absorbance of the RNA samples using NanoDrop Spectrophotometer (BMG LABTECH, Ortenberg, Germany) at 260 nm (ng/µl) and calculating the A260/280 ratio. cDNA was synthesized using the Revertaid cDNA synthesis kit (K1621; Thermo Fisher Scientific, MA, United States), according to the manufacturer's instructions. Primers used were purchased from Thermo Fisher (MA, United States). Gene expression levels were calculated as follows: $2^{-\Delta\Delta CT} \pm$ standard deviation. Full list of primers' sequences is shown in Table 1.

2.8 Protein extraction for ELISA

HUH-7 cells were seeded in T-75 flasks overnight at a seeding density of 5×10^6 cells/flask. Next day, the media was discarded and replaced with DMEM medium alone (untreated control) or added to it either 5 µM sorafenib, 25.22 µM Avastin, 55 µg/ml fucoidan or the combinations of sorafenib and fucoidan (S + F) or Avastin and fucoidan (A + F) and the cells were incubated for 72 h. Next, cells were collected *via* trypsinization and then washed twice with cold PBS

and re-pelleted. The cell pellet was resuspended in 100 µl cell lysis buffer (1 ml of RIPA lysis buffer (Thermo Scientific, United States, Catalogue number: 89,900) + 10 µl of HALT™ protease inhibitor (Thermo Scientific, United States, Catalogue number: 78,410) + 10 µl of HALT™ phosphatase inhibitor (Thermo Scientific, Catalogue number: 78,420) and incubated for 30 min on a rotor at 4°C. Next, the samples were centrifuged at 280 x g for 10 min at 4°C and the supernatants were transferred to fresh tubes and placed on ice. Total protein concentration was measured using BCA protein assay as per the manufacturer's protocol (Thermo Scientific, United States). The samples were stored at −80°C until processing.

2.9 VEGF, caspase 3, 8, and 9 quantification in whole cell lysates using ELISA

Total protein was quantified in whole cell lysates as described above; all samples were diluted with dH_2O to contain 1 mg/ml total protein. 80 µl of each sample (whole cell lysate) was used in each ELISA and the manufacturer's protocol was followed. All ELISA kits used were from Invitrogen, Thermo Scientific, United States as follows: human VEGF ELISA kit (catalogue number KHG0111); human caspase 3 (active) ELISA kit (catalogue number KHO1091), human caspase 8 ELISA kit (catalogue number BMS2024) and human caspase 9 ELISA kit (catalogue number BMS2025).

2.10 Diethyl nitrosamine (DEN) HCC rat model

All animal procedures met the Animals (Scientific Procedures) Act 1986/ASPA Amendment Regulations 2012 and were done after the approval of the Ethical Review committee at the British University in Egypt (Ethics approval number: EX-2218).

46 Sprague Dawley male rats, 5–6 weeks old (100–150 g) were injected intraperitonially (I.P) with 50 mg/kg DEN dissolved in saline once a week for 16 weeks (Schiffer et al., 2005). At the beginning of the 17th week, rats were randomly divided into 6 groups (n = 7–8): Group 1: Untreated control, group 2: Received 200 µg per rat Avastin I.P once per week. Group 3: Received sorafenib at 10 mg/kg *via* oral gavage once per day for five consecutive days. Group 4: Received fucoidan at 20 mg/kg I.P once per day for five consecutive days while Group 5 received the combination of Avastin and fucoidan and Group 6 received the combination of sorafenib and fucoidan. Treatments were continued for 4 weeks then mice were sacrificed by cervical dislocations. Blood and tissue samples were collected and stored appropriately until further analysis.

2.11 Measuring serum levels of ALT, AST, and AFP

Alanine aminotransferase (ALT) and aspartate aminotransferase (AST) were assessed in the serum samples taken from rats using colorimetric commercial kits from Spectrum diagnostics, Cairo, Egypt as per the manufacturer's protocol. Serum alpha fetoprotein (AFP) was measured using rat AFP ELISA kit (Elabscience, United States, catalogue number E-EL-R01047) as per the manufacturer's protocol.

2.12 Histopathological analysis of tissues extracted from DEN HCC model

For histopathological examination, liver tissues were preserved in 10% formalin solution for at least 48 h. Samples were then rinsed with tap water and treated with serial dilutions of methanol, ethanol and absolute ethanol for tissue dehydration followed by xylene. Tissue samples were embedded in paraffin wax and kept at 56°C for 24 h in a hot air oven. Next, the tissue blocks were sliced into 4 µm thick sections and placed on glass slides, deparaffinized, subsequently stained with hematoxylin & eosin (H&E) and examined with light microscopy (Banchroft et al., 1996).

2.13 Measuring the levels of VEGF, VEGFR and AFP in liver tissues using ELISA

Liver tissue homogenates extracted from rats of the different treatment groups were prepared and evaluated for the levels of VEGF, VEGFR and AFP using ELISA kits as per the manufacturer's protocol. ELISA kits used were rat VEGFR1/FLT1 ELISA kit (Elabscience, United States, catalogue number E-EL-R011108); rat VEGF ELISA kit (Creative Diagnostics, United States, catalogue number DEIA1173) and rat AFP ELISA kit (Elabscience, United States, catalogue number E-EL-R01047).

2.14 Immunohistochemistry analysis of CD34, caspase 3 and Ki67

Avidin-Biotin immunoperoxidase complex technique (ABC) was used (Hsu et al., 1981). Briefly, paraffin embedded tissues were deparaffinized and rehydrated through graded alcohol series. Antigen retrieval was done by incubating tissue sections in an antigen retrieval citrate buffer in a microwave oven for 5 min at 700 w, then sections were left to cool. To quench endogenous peroxidase activity, 2 drops of peroxidase blocking serum was added for 10 min, then slides were rinsed with PBS (pH 7.4). Next, two drops of protein blocking serum were added for 10 min followed by incubation with either of the following primary antibodies: caspase-3 rabbit polyclonal antibody (catalogue number A2156, ABclonal, Woburn, MA, United States), CD34 rabbit monoclonal antibody (catalogue number A19015, ABclonal, Woburn, MA, United States) or Ki67 rabbit monoclonal antibody (Clone QR015, Quartett, Berlin, Germany) for 30 min at room temperature. Next, pre-diluted biotinylated secondary antibody was added to each section for 45 min followed by rinsing with PBS. Horseradish peroxidase conjugated streptavidin was added for 20 min followed by rinsing with PBS. Substrate/chromogen (DAB) mixture (which was prepared immediately before use) was added and slides were incubated for 5–10 min followed by rinsing with dH_2O. Finally counterstaining was done with Harris's hematoxylin and sections were dehydrated with graded alcohol series, cleared in xylene, and

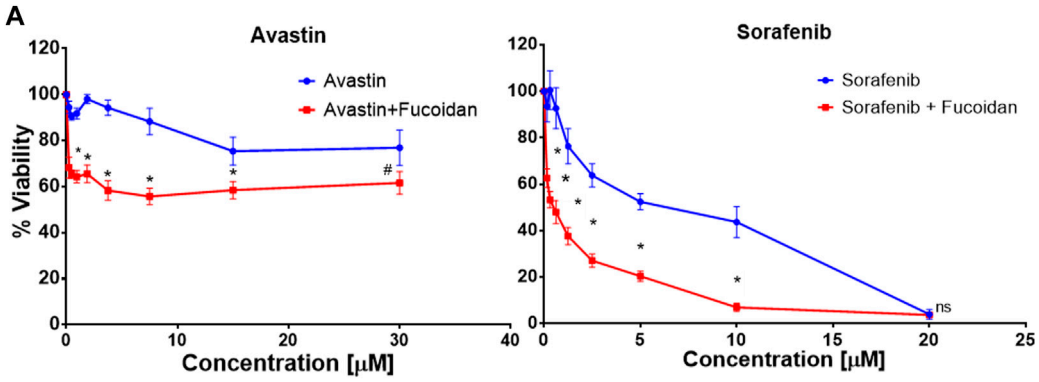

B

Drug	IC50 [μM]	Combination index
Sorafenib	5	0.2 (Strong Synergism)
Sorafenib + Fucoidan	0.44	
Avastin	25.22	0.6 (Synergism)
Avastin+ Fucoidan	11.55	

FIGURE 2
(A) MTT cell viability assay after 72 h of incubating HUH-7 cells with either sorafenib or Avastin monotherapies or in combination with the IC_3 of fucoidan (55 μg/ml) (n = 6 per treatment, experiment was repeated at least 4 times, *$p < 0.0001$ and #$p = 0.002$, Student's two-tailed T-test *versus* monotherapies). **(B)** Summary table showing the calculated IC_{50} of each drug alone or in combination with IC_3 of fucoidan (55 μg/ml) as well as the combination indices indicating a synergistic interaction between fucoidan and the 2 anti-angiogenic drugs.

finally mounted by DPX. Sections were imaged using Leica Application software for tissue sections analysis (Leica Microsystems GmbH, Germany).

2.15 Statistical analysis

Experimental results were plotted as mean values ±standard error of mean (SEM) unless otherwise specified. Statistical analysis for multiple experimental groups was done using one-way analysis of variance (ANOVA) followed by *post hoc* Tukey-Kramer test (unless otherwise specified) with p values considered statistically significant if less than or equal 0.05. All statistical analyses and data plotting were done using GraphPad Prism software, version 5.00 (GraphPad Software, Inc. La Jolla, CA, United States). All experiments were repeated at least 3 times with 3-6 replicates per treatment. Representative data is shown.

3 Results

3.1 Cell viability (MTT) assay

HUH-7 cells were treated with various concentrations of Avastin, sorafenib and fucoidan as single therapies for 72 h. Inhibitory concentrations 50 (IC_{50}) were calculated for each drug individually (data not shown). Next, fucoidan was combined with the anti-angiogenic drugs and results showed a reduction in the IC_{50} of sorafenib from 4.9 to 0.4439 μM and Avastin from 25.22 to 11.55 μM when combined with fucoidan with a calculated combination indices of 0.2 and 0.6, respectively. These findings suggest a synergistic interaction between the anti-angiogenic drugs and fucoidan (Chou, 2006). (As shown in Figure 2)

3.2 Scratch wound assay

The ability of sorafenib, Avastin and fucoidan and their respective combinations to alter HUH-7 cells migration was analyzed *via* the scratch wound healing assay.

Throughout the span of the experiment (4 days); sorafenib, A + F and S + F treated cells consistently showed an unhealed wound indicating the inhibition of cancer cell proliferation and migration unlike the untreated control and fucoidan treated cells where the wound rapidly disappeared throughout the span of the experiment (Figure 3). While Avastin treated cells had a small wound remaining on day 1 and 2 with an almost completely healed wound on day 4. The group S + F followed by sorafenib then A + F showed the best results with almost a slightly smaller wound area observed on day 4 compared to day 0. Next, wound width was quantified using ImageJ software and a plugin designed by (Suarez-Arnedo et al., 2020). Sorafenib, A + F or S + F treated cells consistently showed a significantly smaller % wound closure (sorafenib: 59%–63%; A + F: 69%–70% and S + F: 51%–58%) throughout the incubation period *versus* the untreated control in which the wound almost completely healed (91%–100%) ($p < 0.05$, two-way-ANOVA, Tukey's *post hoc*).

3.3 Annexin V/PI apoptosis assay

To examine the role of apoptosis in the cytotoxic effect of the drugs, the percentage of apoptotic cells was detected *via* Annexin

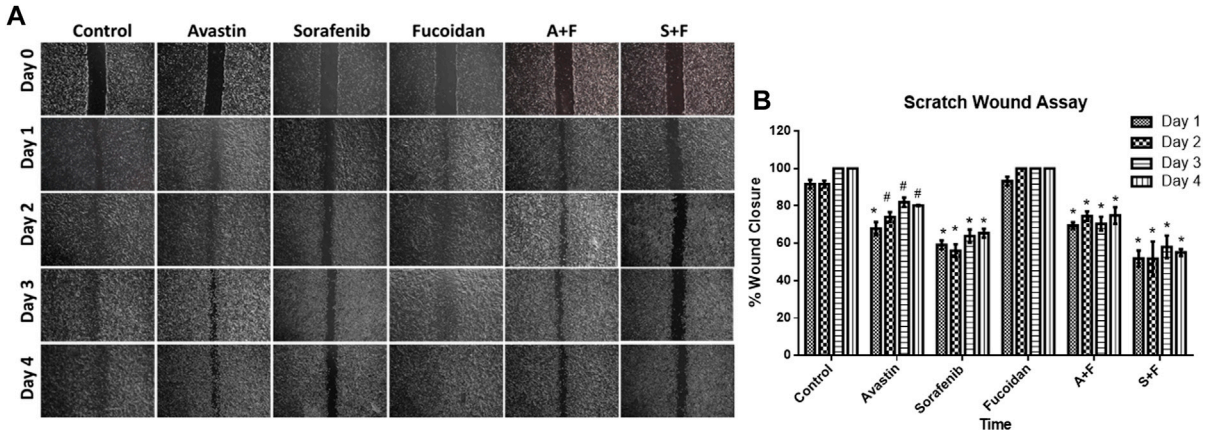

FIGURE 3
(A) Scratch wound assay showing photomicrographs of HUH-7 cells after 1–4 days of drug incubations. **(B)** Percentage wound closure calculated from the photomicrographs of the scratch wound assay using ImageJ. Sorafenib, A + F and S + F treated cells consistently showed an unhealed wound and a significantly smaller % wound closure (sorafenib: 59%–63%; A + F: 69%–70% and S + F: 51%–58%) throughout the incubation period *versus* the untreated control in which the wound almost completely healed (91%–100%) (n = 3 wells/treatment, #$p < 0.05$, *$p < 0.001$ *versus* untreated control at equal time points, two-way ANOVA, Tukey's *post hoc*).

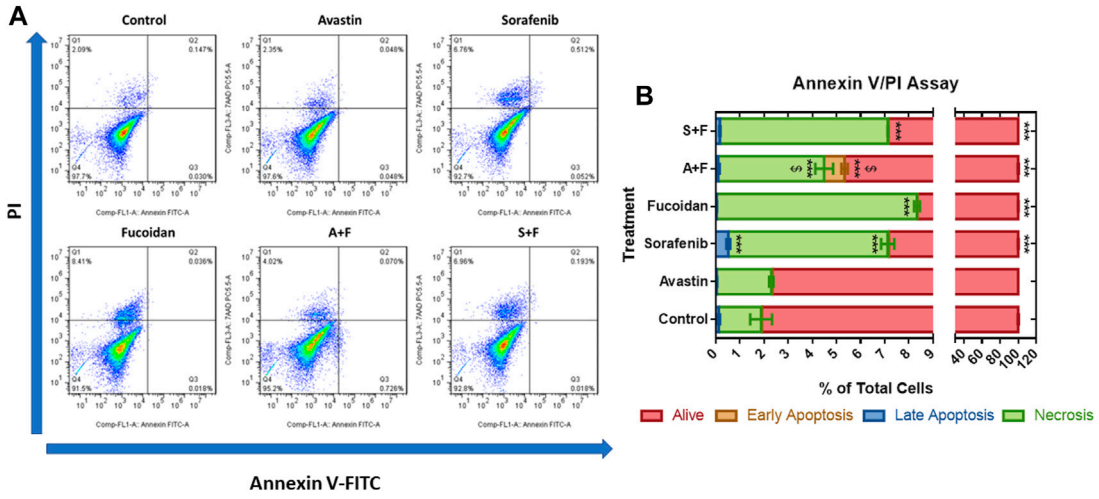

FIGURE 4
Annexin V/PI apoptosis assay showing the effect of Avastin, sorafenib, fucoidan monotherapies or in combination on the percentage of apoptosis in HUH-7 cells **(A)** Dot plots of Annexin V-FITC *versus* PI signal detected (representative data is shown). **(B)** Stacked bar chart showing the percentage of cells detected in each quadrant. 98.1% and 97.66% of the cell population was alive in the untreated control and Avastin with no significant difference between both groups. Sorafenib monotherapy caused a significant increase in the percentage of cells in late apoptosis (0.52%) and necrosis (6.6%) and a significant decrease in the percentage of live cells (92.8%) compared to untreated control. Fucoidan, A + F and S + F showed similar patterns with a significant decrease in live cells to 91.6%, 94.66% and 92.83%, respectively, with an increase of necrotic cells to 8.3%, 4.4% and 6.9%, respectively compared to untreated control. A + F was significantly better than Avastin monotherapy as higher percentage of cells were detected in early apoptosis and necrosis. While the S + F combination showed very similar findings to sorafenib monotherapy (n = 3 wells/treatment, ***$p < 0.0001$ *versus* untreated control and $$p < 0.0001$ compared to monotherapy, one-way ANOVA, Tukey's *post hoc*).

V/PI staining that was measured by flow cytometry. In the untreated control and Avastin, 98.1% and 97.66% of the cell population was alive with no significant difference between both groups. Sorafenib monotherapy caused a significant increase in the percentage of cells in late apoptosis (0.52%) and necrosis (6.6%) and a significant decrease in the percentage of live cells (92.8%) compared to untreated control ($p < 0.0001$). While fucoidan, A + F and S + F showed similar patterns with a significant decrease in live cells to 91.6%, 94.66%, and 92.83%, respectively ($p < 0.0001$) with an increase of necrotic cells to 8.3%, 4.4%, and 6.9%, respectively ($p < 0.0001$) compared to untreated control. The combination of A + F was significantly better than the Avastin monotherapy as it showed higher percentage of cells in early apoptosis and necrosis. While the

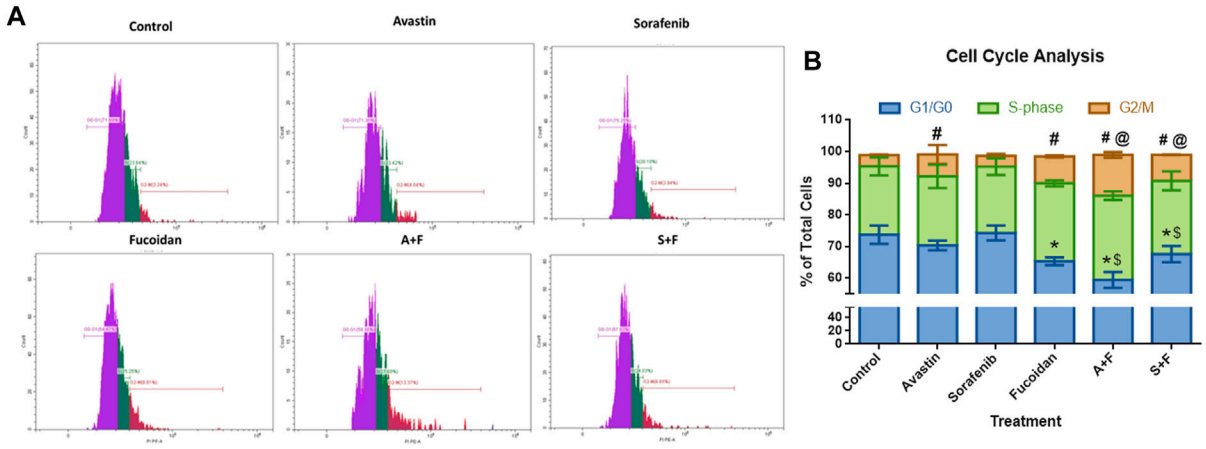

FIGURE 5
Cell cycle analysis showing the effect of Avastin, sorafenib and fucoidan as monotherapies or in combination on the cell cycle progression of HUH-7 cells. **(A)** Representative histograms showing the cell population distribution in each cell cycle phase after the various treatments. **(B)** Stacked bar chart showing the % of total cells detected in G0/G1, S-Phase and G2/M phases. No significant differences between the untreated control and sorafenib treated cells were observed with around 74% of the cells in the G0/G1 phase, 21% in S-phase and 3.5% in the G2/M phase. Avastin treated cells significantly had higher portion of cells arrested in the G2/M phase compared to the untreated control (7% versus 3.5%) while 70.4 % and 21.7% of the cells were detected in the G0/G1 and S-phases, respectively. In fucoidan, A+F and S+F treated cells, a different pattern was observed, with more cells arrested in the S-phase and G2/M phases compared to the untreated control. This pattern appears to be induced by fucoidan as both A+F and S+F had a significantly higher percentage of cells in the S-phase (26.6% and 23.1%, respectively) and G2/M phase (12.9% and 8.2%, respectively) versus the monotherapies. G0/G1: *$p \leq 0.01$ versus untreated control and $ $p < 0.05$ compared to monotherapy; G2/M: #$p < 0.05$ versus untreated control and @ $p < 0.05$ compared to monotherapy, One-way ANOVA, Tukey's Post-Hoc.

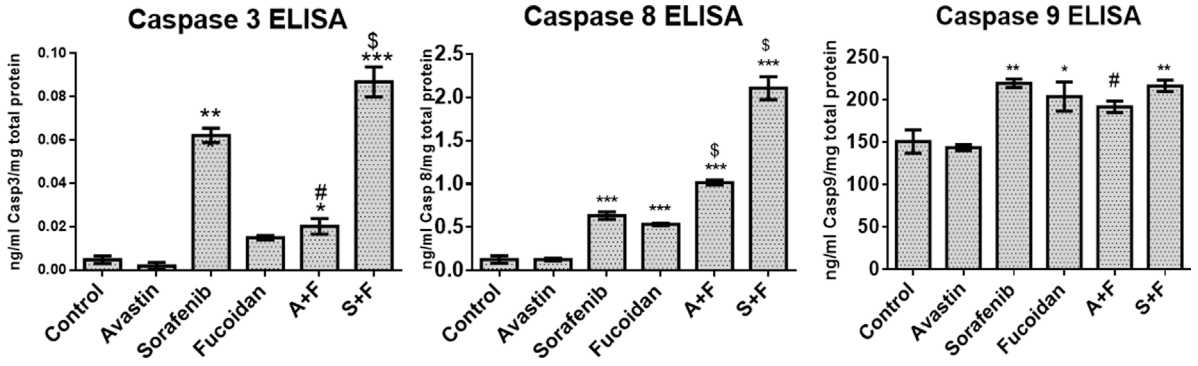

FIGURE 6
Caspase 3, 8, or 9 ELISA results done on HUH-7 whole cell lysates following treatment with Avastin, sorafenib and fucoidan as monotherapies or in combination. Results revealed that all drugs and combinations, except Avastin monotherapy, significantly increased the levels of caspases 3, 8, and 9 with the highest effect observed in the S + F group for caspase 3 and 8. (n = 3–4, *$p < 0.05$, **$p < 0.005$, ***$p < 0.001$ *versus* untreated control or $^{\$}p \leq 0.005$ and $^{\#}p < 0.05$ compared to monotherapy, one-way ANOVA with Tukey's *post hoc*).

S + F combination showed very similar findings to sorafenib monotherapy (Figure 4).

3.4 Cell cycle analysis

We used this assay to examine the effect of the different drugs on the progression of the cell cycle. Results (Figure 5) revealed no significant differences between the untreated control and sorafenib treated cells with around 74% of the cells in the G0/G1 phase, 21% in S-phase and 3.5% in the G2/M phase. In the Avastin monotherapy group, significantly higher portion of cells were arrested in the G2/M phase compared to the untreated control (7% *versus* 3.5%, $p < 0.05$) while 70.4% and 21.7% were detected in the in G0/G1 and S-phases, respectively. In the fucoidan, A + F and S + F treated cells the pattern was different, with more cells arrested in the S-phase and G2/M phases compared to the untreated control. This pattern appears to be induced by fucoidan as both A + F and S + F had a significantly higher percentage of cells in the S-phase (26.6% and 23.1%, respectively) and G2/M phase (12.9% and 8.2%, respectively) *versus* the monotherapies ($p < 0.05$).

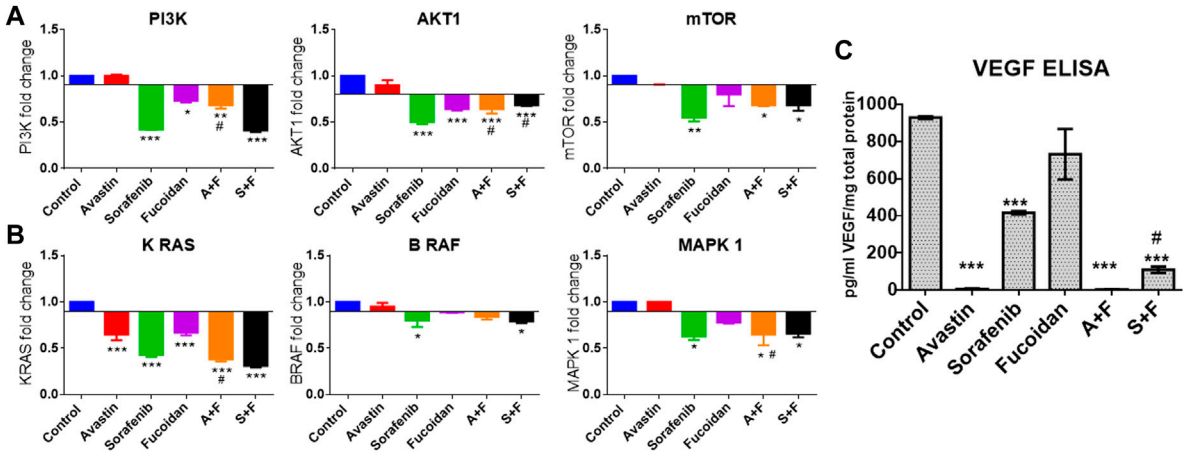

FIGURE 7
Effect of the drug combinations on VEGF and its downstream signaling molecules. **(A, B)** RT-qPCR results showing the fold change in mRNA levels (calculated using $2^{-\Delta\Delta}$CT method) of the key angiogenic genes: PI3K, AKT, mTOR, KRAS, BRAF and MAPK in HUH-7 cells. Sorafenib, A + F and S + F significantly reduced the expression of the oncogenic PI3K/AKT/mTOR and the KRAS/BRAF/MAPK pathways. The most affected were PI3K and KRAS with a decreased mRNA levels of 1.5 and 2.4 folds with A + F or 2.6 and 3.2 folds with S + F, respectively. **(C)** VEGF ELISA results showing a significant reduction in intracellular VEGF levels. Cells treated with Avastin and A + F showed the strongest reduction followed by S + F, sorafenib and fucoidan. *p < 0.05, **p < 0.005, ***p < 0.001 *versus* untreated control or $^{\#}p$ < 0.05 compared to monotherapy, one-way ANOVA with Tukey's *post hoc*.

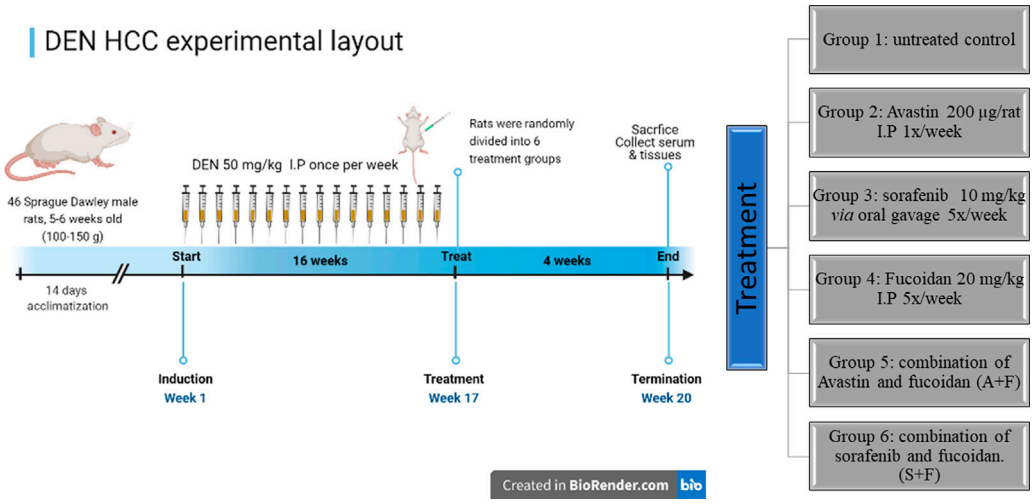

FIGURE 8
A diagram depicting the *in vivo* experimental timeline used to develop the DEN HCC rat model as well as the different treatment groups (created in Biorender.com).

3.5 Effect of the combination therapy on the key apoptotic proteins using ELISA

The effect of the drugs was investigated on the three caspases that are the key players in both the intrinsic and extrinsic pathways of apoptosis (Van Opdenbosch and Lamkanfi, 2019). ELISA results (Figure 6) revealed that all drugs and their combinations, except Avastin monotherapy, significantly increased caspases 3 and 8 with S + F group showing 40- and 16-times higher protein levels, respectively (p < 0.05, *versus* untreated control). While for caspase 9, a similar pattern was observed but to a lesser extent.

3.6 RT-qPCR results of PI3K/AKT/mTOR, KRAS/BRAF/MAPK pathways and VEGF ELISA

Next, we evaluated the effect of the drug alone and in combinations on the key pro-angiogenic pathways: VEGF (using ELISA) and its downstream signaling molecules, PI3K/AKT/mTOR and KRAS/BRAF/MAPK pathways *via* mRNA expression levels by RT-qPCR. Fucoidan, sorafenib, A + F and S + F significantly reduced the expression of the pro-angiogenic PI3K/AKT/mTOR and KRAS/BRAF/MAPK pathways by up to 3 folds (p < 0.05 *versus* untreated control). The most affected were PI3K and KRAS with a significantly

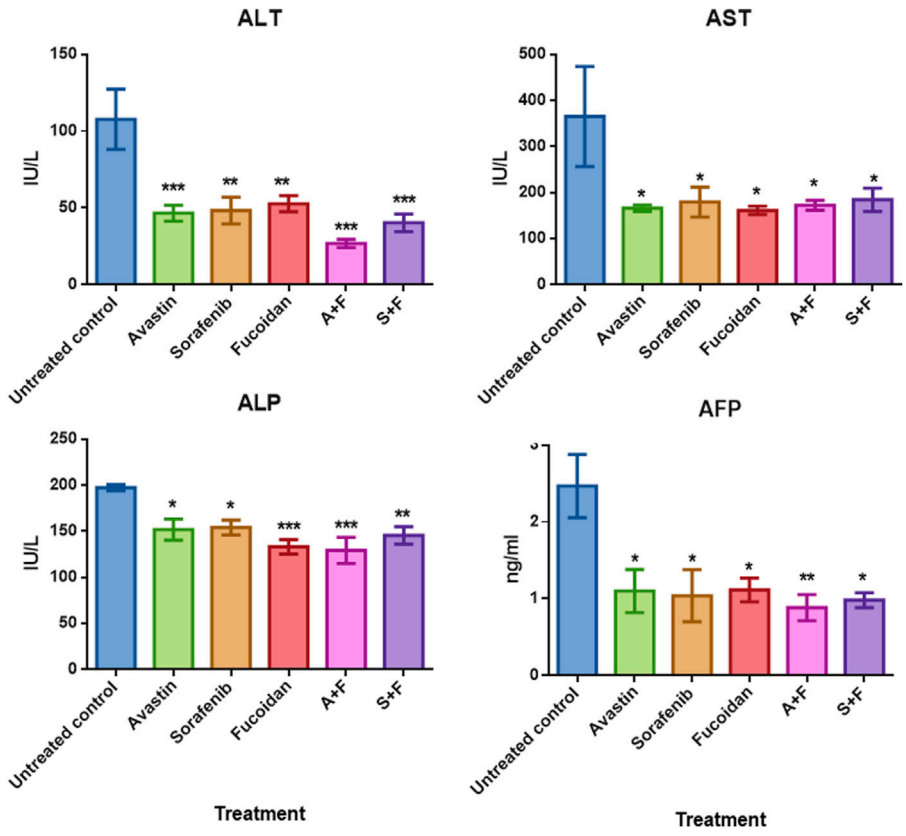

FIGURE 9
The effect of the different treatments on the levels of serum transaminases, ALP and AFP in DEN-HCC rat models. All drug treatments significantly reduced the levels of ALT, AST, ALP and AFP with no significant difference detected amongst the treatment groups. n = 3–5/group, *$p < 0.05$, **$p < 0.005$, ***$p < 0.001$, one-way-ANOVA with Tukey's *post hoc versus* untreated control.

decreased mRNA levels of 1.5 and 2.4 folds with A + F or 2.6 and 3.2 folds with S + F, respectively ($p < 0.05$ *versus* untreated control) (see Figure 7).

3.7 Diethyl nitrosamine (DEN) HCC rat model

As previously described in the methodology, rats were given weekly injections of DEN for 16 weeks then treated for a month with the different drugs and respective combinations. At the end of the experiment, rats were sacrificed, and blood and tissue samples were collected (summary of experimental timeline is shown in Figure 8).

Assessment of liver function was done by measuring aspartate aminotransferase (AST), alanine aminotransferase (ALT) and alkaline phosphatase (ALP) in the rats' serum samples using commercially available colorimetric kits. While Alpha fetoprotein (AFP), a key marker of tumour burden and prognosis (Morse et al., 2019), was assessed using ELISA. Results (Figure 9) showed that the untreated controls had the highest level of ALT, AST, ALP and AFP indicating liver damage and high tumour burden. While all treated groups showed significantly lower levels of these biomarkers compared to the untreated control with no significant difference amongst the different treatments.

3.8 Histological analysis of the liver tissues and other organs of DEN HCC rat model

Next, the histopathological changes induced by DEN was evaluated using hematoxylin and eosin staining (H&E) done on livers, kidneys and lungs tissue sections. All DEN treated rats developed at least cirrhosis with 25 out of 35 rats progressing to HCC, therefore, the success rate of this model was 71.4%. Both acinar (grade I) (Figures 10A, B) and trabecular (grade II) (Figures 10C, D) HCC nodules were observed within the liver tissues with acinar HCC nodules being the most common. Metastatic tumour masses were also observed in the lungs and kidneys of DEN-treated rats regardless of the treatment given (Figure 11).

Upon evaluation of the tumour sections of the untreated control, we observed large nodules of HCC with markedly pleomorphic cells accompanied by prominent nucleoli, scattered apoptosis, mild inflammatory infiltrate, mildly congested blood vessels and marked areas of hemorrhage and inflammatory infiltrate. While smaller tumour nodules as well as marked areas of apoptosis and necrosis were observed in the tumour nodules of rats treated with the different drugs with more prominent apoptotic and necrotic areas observed in the combination treated groups (Figure 12A).

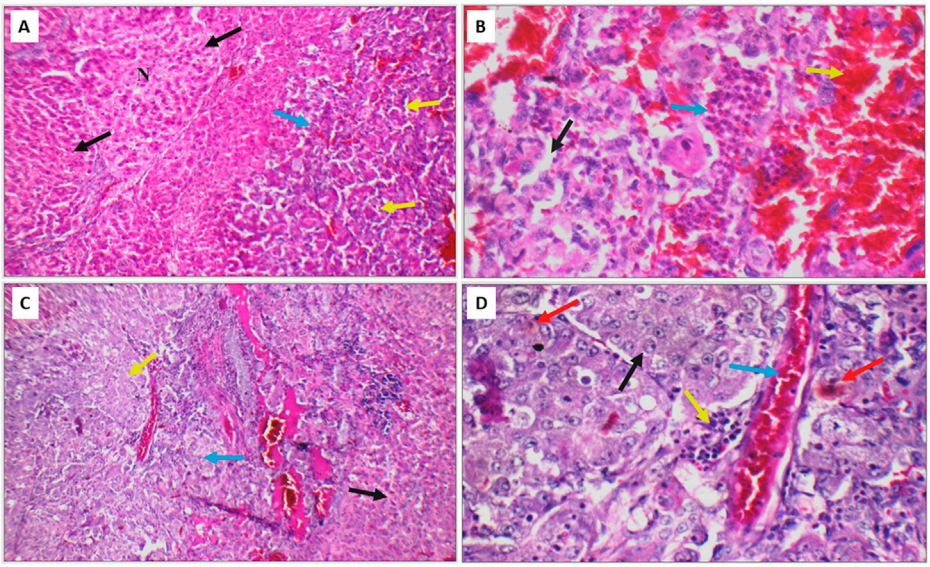

FIGURE 10
(A) DEN-treated positive control liver sections showing area of cirrhosis with well-defined nodules (black arrow), and area of HCC (blue arrow) with acinar formation (yellow arrow) (H&E X 200). **(B)** Another high-power view of the same positive control liver section showing HCC with markedly pleomorphic cells and acinar formation (black arrow), marked areas of hemorrhage (yellow arrow) and inflammatory infiltrate (blue arrow) (H&E X 400). **(C)** Liver section of another positive control showing areas of cirrhosis (black arrow), and area of HCC (blue arrow) with trabecular pattern (yellow arrow) (H&E X 200). **(D)** High power view of the positive control shown in C revealing trabecular HCC with markedly pleomorphic cells and prominent nuclei (black arrow), markedly congested blood vessels (blue arrow), mild inflammatory infiltrate (yellow arrow), and scattered apoptosis (red arrow) (H&E X 400).

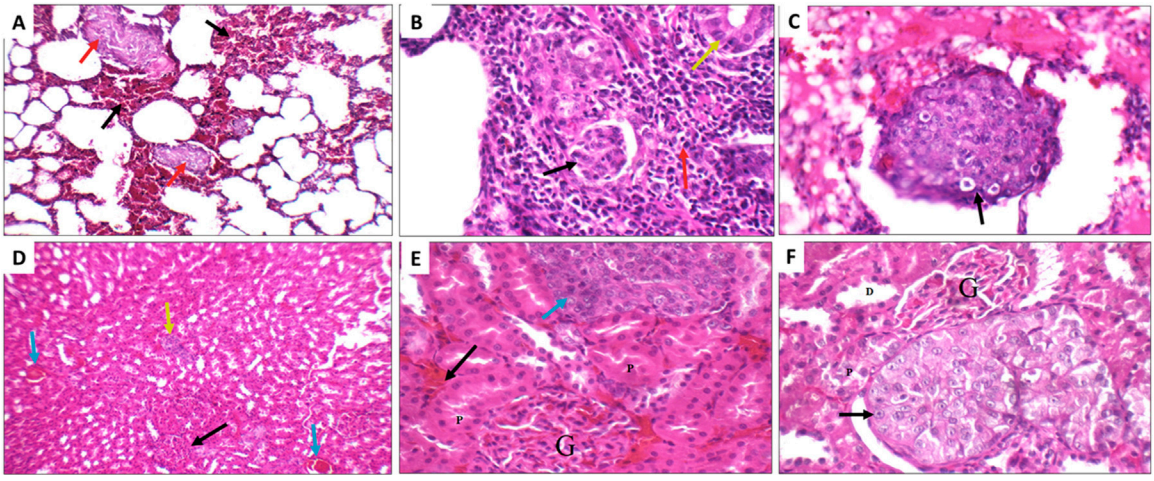

FIGURE 11
Metastatic nodules detected in the lungs **(A–C)** and kidneys **(D–F)** of the DEN rats from the different treatment groups. **(A)** Positive control lung showing marked interstitial hemorrhage (black arrow) with small metastatic nodules (red arrow) (H&E X 200). **(B)** Sorafenib treated rat showing metastatic adenocarcinoma (yellow arrow), with marked inflammatory infiltrate (red arrow), and scattered tumour emboli (black arrow) (H&E X 400. **(C)** Fucoidan treated rats showing vascular tumour emboli (black arrow) (H&E X 400). **(D)** Sorafenib treated rat kidney showing average glomeruli (black arrow), areas of interstitial hemorrhage (blue arrow), and metastatic nodule (yellow arrow) (H&E X 200). **(E)** Avastin treated rat showing average glomeruli (G), and average proximal tubules (P), areas of interstitial hemorrhage (black arrow), and metastatic nodule (blue arrow) (H&E X 400). **(F)** Avastin treated rat showing average glomeruli (G), distal tubules (D) and average proximal tubules (P), and metastatic nodule of malignant cells with prominent nucleoli (black arrow) (H&E X 400).

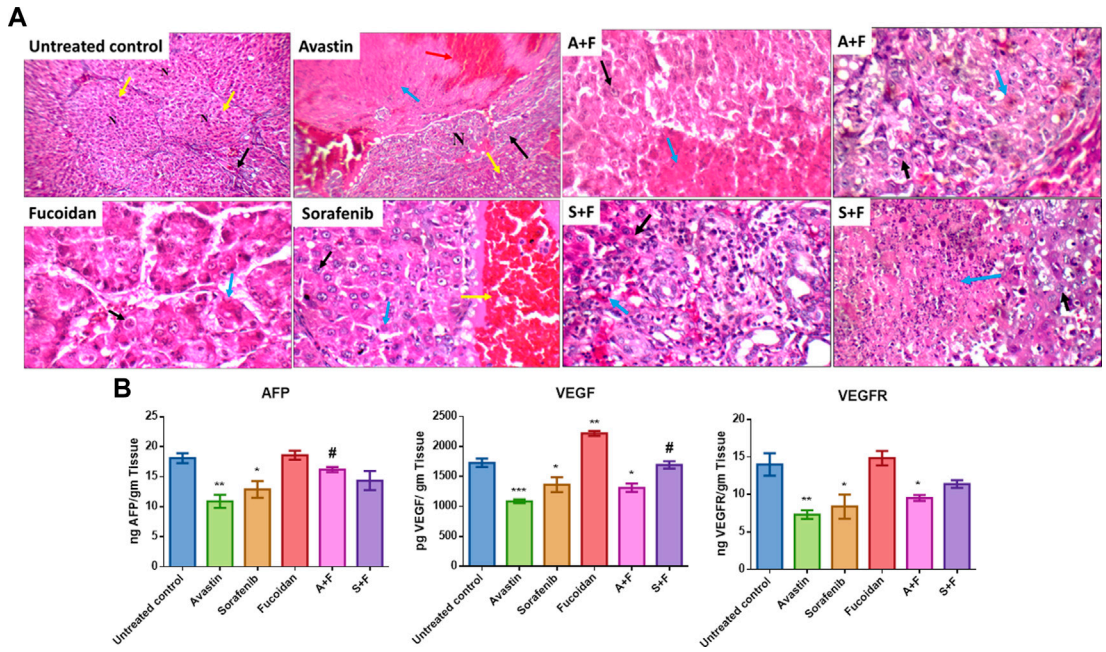

FIGURE 12
(A) Liver sections of DEN treated rats after treatment with the various drugs and their respective combination. Positive control showing fibrotic portal tract (black arrow), with well-defined nodules (yellow arrow, N) (H&E X 200). Avastin treated group showing incomplete nodules and mild micro-vesicular steatosis (yellow arrow) and large nodule of HCC (black arrow) with marked areas of necrosis (blue arrow) and hemorrhage (red arrow) (H&E X 200). Sorafenib treated group showing acinar HCC composed of mildly pleomorphic cells with prominent nucleoli (black arrow) and scattered apoptotic cells (blue arrow) and marked areas of hemorrhage (yellow arrow) (H&E X 400). Fucoidan treated group showing trabecular HCC composed of markedly pleomorphic cells with prominent nucleoli (black arrow) with marked apoptosis (blue arrow) (H&E X 400). A + F slide showing trabecular HCC composed of mildly pleomorphic cells with prominent nucleoli (black arrow) with marked areas of necrosis (blue arrow) (H&E X 400) a second slide of A + F showing large nodule of HCC composed of mildly pleomorphic cells with prominent nucleoli (black arrow) with marked apoptosis (blue arrow) (H&E X 400). S + F showing large nodule of acinar HCC composed of markedly pleomorphic cells (black arrow) with large areas of necrosis (blue arrow) (H&E X 400) a second slide of S + F showing large nodule of acinar HCC composed of mildly pleomorphic cells (black arrow) with marked apoptosis (blue arrow) (H&E X 400). **(B)** Levels of VEGF, VEGFR and AFP in liver tissues as detected with ELISA. Avastin and sorafenib monotherapies significantly decreased the levels of AFP while fucoidan was similar to the untreated control. Although the combination therapies decreased the levels of AFP, the results were not statistically significant compared to the untreated control. VEGF and its receptor VEGFR were significantly reduced by Avastin, sorafenib and A + F compared to the untreated control. While S + F also markedly reduced their levels, but the results were statistically insignificant. For VEGF, fucoidan alone slightly but significantly increased its levels compared to the control unlike VEGFR as fucoidan had very similar levels to the control. n = 3–5, $*p < 0.05$, $**p < 0.005$, $***p < 0.001$, one-way-ANOVA with Tukey's *post hoc versus* untreated control, $\#p < 0.05$ *versus* monotherapies.

3.9 Measuring the levels of VEGF, VEGFR and AFP in liver tissues using ELISA

Liver tissues extracted from DEN HCC model were analyzed using ELISA for the levels of AFP, VEGF, and VEGFR.

AFP, a key marker of liver tumour burden (Morse et al., 2019), was assessed in the different treatment groups. Results (Figure 12B) revealed that Avastin and sorafenib monotherapies significantly decreased the levels of AFP while fucoidan was similar to the untreated control. Although the combination therapies decreased the levels of AFP, the results were not statistically significant compared to the untreated control.

The key angiogenic protein VEGF and its receptor VEGFR were also assessed (Figure 12B). In both instances Avastin, sorafenib and A + F significantly reduced their levels compared to the untreated control. While S + F also markedly reduced their levels, but the results were insignificant. Surprisingly, for VEGF, fucoidan alone slightly but significantly increased its levels compared to the control unlike VEGFR as fucoidan had very similar levels to the control.

3.10 Immunohistochemistry analysis of caspase 3, CD34 and Ki67

Liver tissues were stained for the key apoptotic executioner caspase 3, one of the main proliferation markers (Ki67) (Morse et al., 2019) and CD34, the highly sensitive marker for endothelial cells and is generally used as a marker of angiogenesis in tumours (Vieira et al., 2005).

Caspase 3 reactivity was predominantly cytoplasmic with some nuclear staining. The interpretation of the results considered both the staining intensity (Figure 13A) and the percentage of positive cells (Figure 13B). The reactivity was classified as: negative (0), weak (+), moderate (++) or marked (+++). In the untreated control, liver showed moderate cytoplasmic reactivity (++) for caspase-3 in cirrhotic and tumor nodules. The most significant findings were observed in rats treated with Avastin and S + F, liver tissues showed moderate cytoplasmic reactivity (++) for caspase-3 in liver tissue and marked reactivity (+++) in tumor nodules. While Avastin, fucoidan and A + F were very similar to the untreated control with moderate cytoplasmic reactivity (++) for caspase-3 in tumor nodules and sorafenib alone showing weak reactivity (+) in tumor

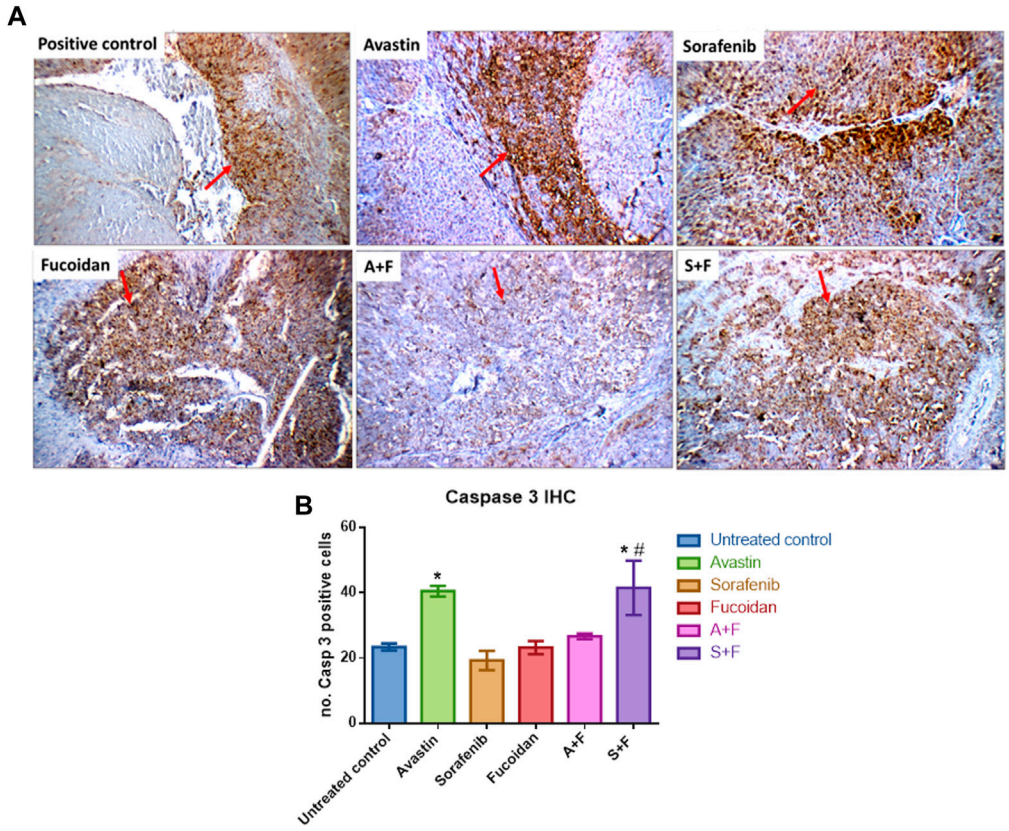

FIGURE 13
Immunohistochemistry analysis of caspase 3 (red arrows) in tumor nodules within liver tissues. **(A)** Photomicrographs of livers extracted from rats treated with the different drugs. Positive control liver view showing moderate cytoplasmic reactivity (++) for caspase 3. Avastin treated liver tissue showing marked cytoplasmic reactivity (+++). Sorafenib treated liver showing moderate cytoplasmic reactivity (++). Fucoidan and A + F showing moderate cytoplasmic reactivity (++) for caspase-3 in tumor tissue and finally S + F liver showing marked cytoplasmic reactivity (+++) for caspase-3 in tumor tissue. (Caspase 3 immunostaining (red arrows) and Hematoxylin counterstain, x 200). **(B)** Number of caspase 3 positive cells showing that the combination of S + F was significantly better than sorafenib alone, but an opposite pattern was observed for Avastin. Avastin monotherapy showed significantly higher levels of caspase 3. (n = 3–5, $*p < 0.05$ *versus* untreated control, $\#p < 0.05$ *versus* monotherapies, one-way-ANOVA with Tukey's *post hoc*).

nodules. The results indicate that the combination of S + F was significantly better than sorafenib alone, but an opposite pattern was observed for Avastin (Figure 13B).

Ki67 positivity was evaluated according to percentage of positive cells into four degree: (-) < 24%, (+) 25%–50% (Isolated), (++) 51%–74% (Focal) or (+++) > 75% (Diffuse) (Mocanu et al., 2012). In the untreated control, liver showed focal reactivity (++) for Ki67 in cirrhotic and tumor nodules. This pattern was reduced in all treatment groups to various degrees. In Avastin treated groups, liver tissues showed isolated reactivity (+) for Ki67 in cirrhotic nodules and negative reactivity (-) in tumor nodules. For sorafenib, liver showed isolated reactivity (+) for Ki67 in cirrhotic and tumor nodules. In fucoidan, negative reactivity (-) for Ki67 in tumor nodules was detected. In the combination groups, A + F liver showed isolated reactivity (+) for Ki67 in tumor nodules, while S + F liver showed negative reactivity (-) for Ki67 in cirrhotic nodules, and isolated reactivity (+) in tumor nodules (as shown in Figure 14A).

Finally, for CD34 staining, the number of positive cells was evaluated as follows: (0 = 0%, 1 = 1–25%, 2 = 26–50%, 3 = 51–75%, and 4 = 76–100% of cells) as described by (Kamat et al., 2006). Untreated control liver showed moderate reactivity (2) for CD34 in cirrhotic and tumor nodules while in the treated groups weak or negative reactivity was detected. For Avastin and sorafenib weak reactivity (1) for CD34 was observed in cirrhotic and tumor nodules. Fucoidan showed negative reactivity (0) for CD34 in tumor nodules. For the combinations, A + F liver showed negative reactivity (0) for CD34 in cirrhotic nodules, and weak reactivity (+) in tumor nodules while S + F showed an opposite pattern with weak reactivity (+) for CD34 in cirrhotic nodules, and negative reactivity (0) in tumor nodules (as shown in Figure 14B).

4 Discussion

Interestingly, 90% of cancer patients have reported the use of complementary and alternative medicines during their treatment, with 70% of patients not discussing the use of such agents with their healthcare professionals (Bahall, 2017; Wu et al., 2022). Being an herbal medicinal product, fucoidan is a particularly popular agent

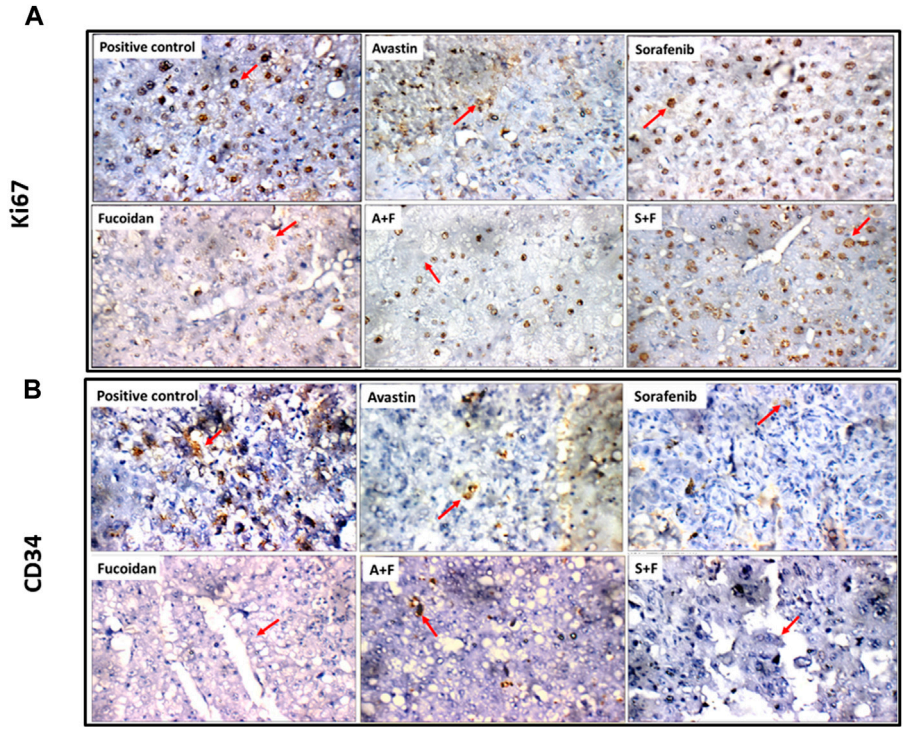

FIGURE 14
(A) Photomicrographs showing immunohistochemical staining for Ki67 in tumor nodules (red arrows) within liver tissues extracted from rats treated with the different drugs. Ki67 positivity was evaluated according to percentage of positive cells into four degree: (-) < 24%, (+) 25%–50% (Isolated), (++) 51%–74% (Focal), (+++) > 75% (Diffuse) (Mocanu et al., 2012). Positive control showing focal reactivity (++), Avastin showing negative reactivity (-), Sorafenib showing isolated reactivity (+) while fucoidan showing negative reactivity (-) for Ki67. A + F showing negative reactivity (-) for Ki67 and S + F showing isolated reactivity (+) (Ki67 immunostaining (red arrows), x 400). **(B)** Photomicrographs showing immunohistochemical staining for CD34 in endothelial cells in tumor nodules (red arrows) within liver tissues extracted from rats treated with the different drugs. The number of positive cells for CD34 staining was evaluated as follows: (0 = 0%, 1 = 1–25%, 2 = 26–50%, 3 = 51–75%, and 4 = 76–100% of cells) as described by (Kamat et al., 2006). Positive control showing moderate reactivity (2) for CD34 in tumor nodules. Avastin and sorafenib showing weak reactivity (1) while fucoidan showing negative reactivity (0) for CD34 in tumor nodules. A + F showing weak reactivity (+) while S + F showing negative reactivity (0) for CD34 in tumor nodules (red arrow) (CD34 immunostaining (red arrows), x 400).

that is readily available as an over the counter (OTC) herbal supplement in many countries around the globe with many cancer patients reporting its use (Wu et al., 2022). Moreover, fucoidan have attracted a lot of attention in recent years with a 100,000,000$ worth of fucoidan related supplements being produced annually (Tsai et al., 2017). This highlights the importance of our research that is studying the combination of fucoidan, which has a proven anti-cancer potential as reported in many preclinical studies (Jin et al., 2022), with 2 clinically approved anti-angiogenic agents (Avastin and sorafenib) in HCC.

HCC is a highly vascular tumour and thus represents an exciting target for the development of anti-angiogenic drugs. Nonetheless, to date, sorafenib and Avastin are the only anti-angiogenic agents that are clinically used in the treatment of HCC. This highlights, the challenges of targeting this key process for the treatment of HCC.

Fucoidan has been investigated before in combination with Avastin but for the treatment of exudative age-related macular degeneration, results showed an *in vitro* reduction in the expression of VEGF (Dithmer et al., 2014). While the combination of fucoidan with sorafenib has been recently reported *in vitro* in a sorafenib resistant cell line (HepG2-SR) and *in vivo* using tumour xenograft in nude mice (Luo et al., 2022). The results of this study focused on the epidermal growth factor receptor (EGFR) pathway and showed that fucoidan could help overcome sorafenib resistance in HCC *via* binding to EGFR (Luo et al., 2022). Nonetheless, despite these previously reported promising findings, our research explores a poorly investigated area of research which is the interaction between fucoidan and the key angiogenic pathway especially in combination with sorafenib and Avastin in HCC.

Published reports have revealed contradicting data about the interaction of fucoidan with the angiogenic pathways, specifically with the key angiogenic promotor: the vascular endothelial growth factor (VEGF). It was reported that fucoidan inhibited binding of VEGF to its receptor (VEGFR) (Koyanagi et al., 2003) and reduced VEGF expression both *in vitro* and *in vivo* in mouse breast cancer cells (Xue et al., 2012). On the contrary, another study reported that fucoidan had a potent growth inhibitory effect on HCC tumorigenesis without interfering with angiogenesis and VEGF expression both *in vitro* and *in vivo* (Zhu et al., 2013). These discrepancies have been attributed to the differences in the molecular weight and chemical structures (such as the degree of sulfation) of the tested fucoidans (Kwak, 2014; Atashrazm et al., 2015).

First, we investigated the combination of fucoidan with sorafenib and Avastin *in vitro* on a human HCC cell line; HUH-7. Results revealed

a strong synergistic interaction between fucoidan, and the 2 anti-angiogenic drugs as measured with the MTT assay. Next, we did several functional assays to assess the effect of the combination therapy on cancer cell motility, induction of apoptosis and cell cycle progression. The results were not as clear as the cell viability assay, even though in most of these assays the drugs and their combinations were significantly better than the untreated control, the differences between the monotherapies and the combination therapies were not always as striking or statistically significant. In the scratch wound assay, results revealed that sorafenib and the combination therapies significantly inhibited wound healing as a significantly smaller % wound closure was observed (50%–70%) *versus* untreated control (91%–100%). Nonetheless, A + F showed slightly better but insignificant difference to Avastin alone while sorafenib and S + F showed very similar patterns. However, in the apoptosis Annexin V/PI assay, A + F showed significantly less viable cells as well as higher percentage of cells in early apoptosis and necrosis compared to Avastin monotherapy which was very similar to the control. Both sorafenib and S + F were significantly better than the untreated control, but both showed very similar patterns to each other. In the cell cycle analysis, both Avastin and sorafenib monotherapies were similar to the untreated control but again fucoidan appeared to direct the cells towards a G2/M arrest. S + F and A + F had a significantly higher percentage of cells in the G2/M phase as compared to their monotherapies.

Next, we embarked on searching for the potential mechanistic interactions between the drugs under investigation. We evaluated the VEGFR pathway and two of its main downstream signaling cascades: the PI3K/AKT/mTOR and the RAS/RAF/MAPK pathways (Dimri and Satyanarayana, 2020). These pathways are commonly dysregulated in HCC and are downstream from many growth factor receptors (e.g. VEGFR, EGFR, fibroblast growth factor receptor (FGFR) and the platelet-derived growth factor receptor (PDGF)) (Dimri and Satyanarayana, 2020). Moreover, the hyperactivation of the PI3K/AKT/mTOR and the RAS/RAF/ERK/MAPK pathways and the overexpression of growth factors (e.g., fibroblast growth factor (FGF)) combined with the overactivation of processes like angiogenesis and epithelial to mesenchymal transition (EMT) are the main culprits in the tumorigeneses of HCC (Lamarca et al., 2016). Therefore, it was crucial to elucidate the effect of our drug combinations on these pathways.

VEGF ELISA done on cell lysates revealed that Avastin, as expected, completely depletes VEGF and similarly A + F showed similar findings. These results are very encouraging because the interaction of fucoidan with VEGF has been a point of controversary in the literature as previously mentioned. Based on the findings presented herein, it is important to highlight that a) fucoidan alone deceased the levels of VEGF (although the results were statistically insignificant compared to the untreated control). (b) It did not interfere with the binding of Avastin to VEGF as similar to Avastin alone, A + F significantly reduced VEGF levels and (c) it strongly potentiated the effect of sorafenib as S + F treated cells had significantly lower VEGF levels. For the PI3K/AKT/mTOR axis, Avastin alone did not induce significant changes compared to the untreated control while A + F significantly reduced the mRNA levels of all three genes. In both sorafenib and S + F groups, the PI3K/AKT/mTOR mRNA levels were also reduced compared to the untreated control with no statistically significant difference between sorafenib and S + F for the PI3K and mTOR.

In summary, it appears that fucoidan potentiated the effect of Avastin in inhibiting the PI3K/AKT/mTOR and the RAS/RAF/MAPK pathways but neither potentiated nor significantly negated the effect of sorafenib on these pathways.

Finally, we evaluated the effect of the drugs on three key apoptosis related proteins, caspase 3, 8, and 9. Fucoidan significantly potentiated the levels of caspase 3 and 8 when combined with the anti-angiogenic drugs (A + F and S + F) either when compared to the untreated control or the monotherapies. While for caspase 9, all drugs and combinations (except Avastin) increased its level but to a lesser extent compared to caspase 3 and 8. Fucoidan was previously reported to induce cell death in HCC cell lines. In a recent study by (Duan et al., 2020), fucoidan induced cell death in LM3 HCC cell line when measured using the Annexin V/PI assay where a higher percentage of cells were detected in early and late apoptosis phases while our study showed cells to be mostly in the necrotic phase. They also reported that this was mediated *via* the promotion of the phosphorylation of p38 MAPK, the reduction of ERK, PI3K and AKT phosphorylation as well as the activation of caspase 3, 8, and 9. These findings are similar to ours except for MAPK which we reported the suppression of its mRNA levels by fucoidan and the combination therapy while (Duan et al., 2020) reported their findings on a protein level.

In vivo, we established the DEN HCC tumour model by a weekly injection of DEN for 16 weeks (Schiffer et al., 2005) and then rats were treated with the drugs and combinations for 4 extra weeks. Generally, we noticed a lot of variations amongst the rats of the same group, a major drawback for carcinogen induced cancer models along with undefined genetic backgrounds detected in the tumours (Macek Jilkova et al., 2019). Microscopically, areas of marked apoptosis and necrosis were observed within the tumour nodules of the treated mice with more areas detected in the combination therapies. Results of the liver function tests (ALT, AST, and ALP) and liver tumour marker (AFP) revealed a significant improvement in all treatment groups but no clear advantage of fucoidan was detected. Surprisingly, tissue levels of AFP, VEGF and VEGFR were slightly elevated with fucoidan alone, but the results were only statistically significant for VEGF. For the combination therapies, the results were always significantly less than the untreated control but when compared to monotherapies variable patterns were detected. For AFP, A + F and S + F showed slightly higher levels but only A + F was significantly higher than Avastin. For VEGF, no significant difference was observed in the Avastin *versus* A + F group unlike the S + F group which was slightly higher than sorafenib. Finally, in VEGFR, no significant difference was observed between the monotherapies and the combination therapies. Finally, we performed IHC to assess the levels of the apoptotic marker caspase 3, the proliferation marker Ki67 and the marker for angiogenesis CD34. We only quantitively assessed caspase 3 as it has the clearest and strongest staining. Results revealed that only Avastin and S + F significantly increased the levels of caspase 3 with fucoidan potentiating the effect of sorafenib but antagonizing the effect of Avastin. Unlike for Ki67 and CD34 as the staining was semiquantitative; analysis revealed weak or negative reactivity in all treatment groups unlike the untreated control. In summary, the *in vivo* results appear to show neither a clear benefit of fucoidan nor a strong antagonistic effect. We found limited data reporting the use of fucoidan in DEN HCC. In a study by (Suresh et al., 2013) they reported that fucoidan inhibited the metabolic activation of DEN and consequently

protected against DEN-induced hepatocarcinogenesis (Suresh et al., 2013; Jin et al., 2022).

5 Summary and conclusions

In summary, we believe that our findings emphasize the importance of studying the combination of commonly used herbal medicinal products with clinically approved drugs. Numerous patients are particularly interested in consuming fucoidan in hope of potentiating the effect of anti-cancer drugs. Our research highlighted a promising chemomodulatory effect of fucoidan when combined with sorafenib and Avastin although further investigations are required to elucidate potential beneficial or adversary interactions between the tested therapies.

Data availability statement

The original contributions presented in the study are included in the article/supplementary material, further inquiries can be directed to the corresponding author.

Ethics statement

The animal study was reviewed and approved by The British University in Egypt (BUE) Ethical Review Committee (Approval Number EX-2218).

Author contributions

MA is the project principal investigator and contributed to the design, execution, and analyses of all the experiments as well as the preparation and submission of this manuscript. AA and HE are the project's research associates as well as postgraduate students. They contributed to the design, execution and analyses of some of the experiments as well as manuscript revision. ME is the project consultant, he helped in the interpretation of the experimental results and statistical analyses of the data as well as manuscript revision.

Funding

This project was funded by the Egyptian Science and Technology Development Fund (STDF)- Reintegration grant number 35965.

Acknowledgments

The authors would like to thank Professor Sayed Abdel Raheem, Department of Pathology, Faculty of Medicine, Al-Azhar University, (Cairo, Egypt) for his technical assistance in the histopathological assessments and Mostafa Darawy, Department of Biochemistry, Faculty of Pharmacy, Ain Shams University (Cairo, Egypt) for his technical help in tissue ELISA.

Conflict of interest

The authors declare that the research was conducted in the absence of any commercial or financial relationships that could be construed as a potential conflict of interest.

Publisher's note

References

Abdelmageed, M. M., El-Naga, R. N., El-Demerdash, E., and Elmazar, M. M. (2016). Indole-3- carbinol enhances sorafenib cytotoxicity in hepatocellular carcinoma cells: A mechanistic study. *Sci. Rep.* 6, 32733. doi:10.1038/srep32733

Abdollah, M. R. A., Carter, T. J., Jones, C., Kalber, T. L., Rajkumar, V., Tolner, B., et al. (2018). Fucoidan prolongs the circulation time of dextran-coated iron oxide nanoparticles. *ACS Nano* 12 (2), 1156–1169. doi:10.1021/acsnano.7b06734

Aisa, Y., Miyakawa, Y., Nakazato, T., Shibata, H., Saito, K., Ikeda, Y., et al. (2005). Fucoidan induces apoptosis of human HS-sultan cells accompanied by activation of caspase-3 and down-regulation of ERK pathways. *Am. J. Hematol.* 78 (1), 7–14. doi:10.1002/ajh.20182

Atashrazm, F., Lowenthal, R. M., Woods, G. M., Holloway, A. F., and Dickinson, J. L. (2015). Fucoidan and cancer: A multifunctional molecule with anti-tumor potential. *Mar. Drugs* 13 (4), 2327–2346. doi:10.3390/md13042327

Bahall, M. (2017). Prevalence, patterns, and perceived value of complementary and alternative medicine among cancer patients: A cross-sectional, descriptive study. *BMC complementary Altern. Med.* 17 (1), 345–349. doi:10.1186/s12906-017-1853-6

Banafa, A. M., Roshan, S., Liu, Y. Y., Chen, H. J., Chen, M. J., Yang, G. X., et al. (2013). Fucoidan induces G1 phase arrest and apoptosis through caspases-dependent pathway and ROS induction in human breast cancer MCF-7 cells. *J. Huazhong Univ. Sci. Technol. Med. Sci.* 33 (5), 717–724. doi:10.1007/s11596-013-1186-8

Banchroft, J., Stevens, A., and Turner, D. (1996). *Theory and practice of histological techniques Fourth*. New York: Churchil Livingstone.

Bonam, S. R., Wu Yuan, S., Tunki, L., Chellian, R., Halmuthur, M. S., Muller, S., et al. (2018). What has come out from phytomedicines and herbal edibles for the treatment of cancer? *ChemMedChem* 13, 1854–1872. doi:10.1002/cmdc.201800343

Boo, H. J., Hong, J. Y., Kim, S. C., Kang, J. I., Kim, M. K., Kim, E. J., et al. (2013). The anticancer effect of fucoidan in PC-3 prostate cancer cells. *Mar. Drugs* 11 (8), 2982–2999. doi:10.3390/md11082982

Chou, T.-C. (2006). Theoretical basis, experimental design, and computerized simulation of synergism and antagonism in drug combination studies. *Pharmacol. Rev.* 58 (3), 621–681. doi:10.1124/pr.58.3.10

Cumashi, A., Ushakova, N. A., Preobrazhenskaya, M. E., D'Incecco, A., Piccoli, A., Totani, L., et al. (2007). A comparative study of the anti-inflammatory, anticoagulant, antiangiogenic, and antiadhesive activities of nine different fucoidans from Brown seaweeds. *Glycobiology* 17 (5), 541–552. doi:10.1093/glycob/cwm014

Dimri, M., and Satyanarayana, A. (2020). Molecular signaling pathways and therapeutic targets in hepatocellular carcinoma. *Cancers* 12 (2), 491. doi:10.3390/cancers12020491

Dithmer, M., Fuchs, S., Shi, Y., Schmidt, H., Richert, E., Roider, J., et al. (2014). Fucoidan reduces secretion and expression of vascular endothelial growth factor in the

retinal pigment epithelium and reduces angiogenesis *in vitro*. *PloS one* 9 (2), e89150. doi:10.1371/journal.pone.0089150

Duan, Y., Li, J., Jing, X., Ding, X., Yu, Y., and Zhao, Q. (2020). Fucoidan induces apoptosis and inhibits proliferation of hepatocellular carcinoma via the p38 MAPK/ERK and PI3K/Akt signal pathways. *Cancer Manag. Res.* 12, 1713–1723. doi:10.2147/CMAR.S243495

El-Serag, H. B., and Rudolph, K. L. (2007). Hepatocellular carcinoma: Epidemiology and molecular carcinogenesis. *Gastroenterology* 132 (7), 2557–2576. doi:10.1053/j.gastro.2007.04.061

Fitton, J. H. (2011). Therapies from fucoidan; multifunctional marine polymers. *Mar. drugs* 9 (10), 1731–1760. doi:10.3390/md9101731

Hanahan, D., and Weinberg, R. A. (2011). Hallmarks of cancer: The next generation. *Cell* 144 (5), 646–674. doi:10.1016/j.cell.2011.02.013

Hsu, S.-M., Raine, L., and Fanger, H. (1981). Use of avidin-biotin-peroxidase complex (ABC) in immunoperoxidase techniques: A comparison between ABC and unlabeled antibody (PAP) procedures. *J. Histochem. Cytochem.* 29 (4), 577–580. doi:10.1177/29.4.6166661

Jin, J.-O., Yadav, D., Madhwani, K., Puranik, N., Chavda, V., and Song, M. (2022). Seaweeds in the oncology arena: Anti-cancer potential of fucoidan as a drug—a review. *Molecules* 27 (18), 6032. doi:10.3390/molecules27186032

Kamat, A. A., Fletcher, M., Gruman, L. M., Mueller, P., Lopez, A., Landen, C. N., Jr, et al. (2006). The clinical relevance of stromal matrix metalloproteinase expression in ovarian cancer. *Clin. Cancer Res.* 12 (6), 1707–1714. doi:10.1158/1078-0432.CCR-05-2338

Koyanagi, S., Tanigawa, N., Nakagawa, H., Soeda, S., and Shimeno, H. (2003). Oversulfation of fucoidan enhances its anti-angiogenic and antitumor activities. *Biochem. Pharmacol.* 65 (2), 173–179. doi:10.1016/S0006-2952(02)01478-8

Kwak, J.-Y. (2014). Fucoidan as a marine anticancer agent in preclinical development. *Mar. drugs* 12 (2), 851–870. doi:10.3390/md12020851

Lamarca, A., Mendiola, M., and Barriuso, J. (2016). Hepatocellular carcinoma: Exploring the impact of ethnicity on molecular biology. *Crit. Rev. oncology/hematology* 105, 65–72. doi:10.1016/j.critrevonc.2016.06.007

Lee, H., Kim, J. S., and Kim, E. (2012). Fucoidan from seaweed Fucus vesiculosus inhibits migration and invasion of human lung cancer cell via PI3K-Akt-mTOR pathways. *PLoS One* 7 (11), e50624. doi:10.1371/journal.pone.0050624

Li, B., Lu, F., Wei, X., and Zhao, R. (2008). Fucoidan: Structure and bioactivity. *Molecules* 13 (8), 1671–1695. doi:10.3390/molecules13081671

Lira, M., Santos-Magalhães, N., Nicolas, V., Marsaud, V., Silva, M., Ponchel, G., et al. (2011). Cytotoxicity and cellular uptake of newly synthesized fucoidan-coated nanoparticles. *Eur. J. Pharm. Biopharm.* 79 (1), 162–170. doi:10.1016/j.ejpb.2011.02.013

Luo, J., Li, L., Zhu, Z., Chang, B., Deng, F., Wang, D., et al. (2022). Fucoidan inhibits EGFR redistribution and potentiates sorafenib to overcome sorafenib-resistant hepatocellular carcinoma. *Biomed. Pharmacother.* 154, 113602. doi:10.1016/j.biopha.2022.113602

Macek Jilkova, Z., Kurma, K., and Decaens, T. (2019). Animal models of hepatocellular carcinoma: The role of immune system and tumor microenvironment. *Cancers* 11 (10), 1487. doi:10.3390/cancers11101487

Mahmoud, M., Abdollah, M. R., Elsesy, M. E., Abou El Ella, D. A., Zada, S. K., and Tolba, M. F. (2022). The natural isoflavone Biochanin-A synergizes 5-fluorouracil anticancer activity *in vitro* and *in vivo* in Ehrlich solid-phase carcinoma model. *Phytotherapy Res.* 36 (3), 1310–1325. doi:10.1002/ptr.7388

Mocanu, E., Broască, V., and Severin, B. (2012). Ki-67 expression in hepatocellular carcinoma developed on a liver cirrhosis. *ARS Medica Tomitana* 18 (1), 33–37. doi:10.2478/v10307-012-0006-x

Morse, M. A., Sun, W., Kim, R., He, A. R., Abada, P. B., Mynderse, M., et al. (2019). The role of angiogenesis in hepatocellular carcinoma. *Clin. Cancer Res.* 25 (3), 912–920. doi:10.1158/1078-0432.CCR-18-1254

Nishida, N., Yano, H., Nishida, T., Kamura, T., and Kojiro, M. (2006). Angiogenesis in cancer. *Vasc. Health Risk Manag.* 2 (3), 213–219. doi:10.2147/vhrm.2006.2.3.213

Raoul, J. L., Gilabert, M., Adhoute, X., and Edeline, J. (2017). An in-depth review of chemical angiogenesis inhibitors for treating hepatocellular carcinoma. *Expert Opin. Pharmacother.* 18 (14), 1467–1476. doi:10.1080/14656566.2017.1378346

Sampat, K. R., and O'Neil, B. (2013). Antiangiogenic therapies for advanced hepatocellular carcinoma. *Oncologist* 18, 430–438. doi:10.1634/theoncologist.2012-0388

Schiffer, E., Housset, C., Cacheux, W., Wendum, D., Desbois-Mouthon, C., Rey, C., et al. (2005). Gefitinib, an EGFR inhibitor, prevents hepatocellular carcinoma development in the rat liver with cirrhosis. *Hepatology* 41 (2), 307–314. doi:10.1002/hep.20538

Suarez-Arnedo, A., Figueroa, F. T., Clavijo, C., Arbeláez, P., Cruz, J. C., and Muñoz-Camargo, C. (2020). An image J plugin for the high throughput image analysis of *in vitro* scratch wound healing assays. *PloS one* 15 (7), e0232565. doi:10.1371/journal.pone.0232565

Suresh, V., Anbazhagan, C., Thangam, R., Senthilkumar, D., Senthilkumar, N., Kannan, S., et al. (2013). Stabilization of mitochondrial and microsomal function of fucoidan from Sargassum plagiophyllum in diethylnitrosamine induced hepatocarcinogenesis. *Carbohydr. Polym.* 92 (2), 1377–1385. doi:10.1016/j.carbpol.2012.10.038

Tawfik, S. M., Abdollah, M. R., Elmazar, M. M., El-Fawal, H. A., and Abdelnaser, A. (2022). Effects of metformin combined with antifolates on HepG2 cell metabolism and cellular proliferation. *Front. Oncol.* 12, 828988. doi:10.3389/fonc.2022.828988

Tsai, H.-L., Tai, C.-J., Huang, C.-W., Chang, F.-R., and Wang, J.-Y. (2017). Efficacy of low-molecular-weight fucoidan as a supplemental therapy in metastatic colorectal cancer patients: A double-blind randomized controlled trial. *Mar. drugs* 15 (4), 122. doi:10.3390/md15040122

Van Opdenbosch, N., and Lamkanfi, M. (2019). Caspases in cell death, inflammation, and disease. *Immunity* 50 (6), 1352–1364. doi:10.1016/j.immuni.2019.05.020

Vieira, S. C., Silva, B. B., Pinto, G. A., Vassallo, J., Moraes, N. G., Santana, J. O., et al. (2005). CD34 as a marker for evaluating angiogenesis in cervical cancer. *Pathology-Research Pract.* 201 (4), 313–318. doi:10.1016/j.prp.2005.01.010

Wu, C.-J., Yeh, T.-P., Wang, Y.-J., Hu, H.-F., Tsay, S.-L., and Liu, L.-C. (2022). Effectiveness of fucoidan on supplemental therapy in cancer patients: A systematic review. *Healthc. MDPI* 10, 923. doi:10.3390/healthcare10050923

Xue, M., Ge, Y., Zhang, J., Wang, Q., Hou, L., Liu, Y., et al. (2012). Anticancer properties and mechanisms of fucoidan on mouse breast cancer *in vitro* and *in vivo*. *PLoS One* 7 (8), e43483. doi:10.1371/journal.pone.0043483

Yang, W. H., Xu, J., Mu, J. B., and Xie, J. (2017). Revision of the concept of anti-angiogenesis and its applications in tumor treatment. *Chronic Dis. Transl. Med.* 3 (1), 33–40. doi:10.1016/j.cdtm.2017.01.002

Zhang, Z., Teruya, K., Eto, H., and Shirahata, S. (2011). Fucoidan extract induces apoptosis in MCF-7 cells via a mechanism involving the ROS-dependent JNK activation and mitochondria-mediated pathways. *PLoS One* 6 (11), e27441. doi:10.1371/journal.pone.0027441

Zhu, C., Cao, R., Zhang, S.-X., Man, Y.-N., and Wu, X.-Z. (2013). Fucoidan inhibits the growth of hepatocellular carcinoma independent of angiogenesis. *Evidence-Based Complementary Altern. Med.* 2013, 692549. doi:10.1155/2013/692549

frontiers | Frontiers in Pharmacology

TYPE Original Research
PUBLISHED 03 March 2023
DOI 10.3389/fphar.2023.1122890

OPEN ACCESS

EDITED BY
Khuloud Bajbouj,
University of Sharjah, United Arab Emirates

REVIEWED BY
Md. Asaduzzaman Khan,
Southwest Medical University, China
Yunhui Chen,
Chengdu University of Traditional Chinese Medicine, China

*CORRESPONDENCE
Bo Qin,
qinbozf@163.com
Zhen Liang,
liang.zhen@szhospital.com

†These authors have contributed equally to this work

SPECIALTY SECTION
This article was submitted to Pharmacology of Anti-Cancer Drugs, a section of the journal *Frontiers in Pharmacology*

RECEIVED 13 December 2022
ACCEPTED 03 February 2023
PUBLISHED 03 March 2023

CITATION
Yuan R, Tan Y, Sun P-H, Qin B and Liang Z (2023), Emerging trends and research foci of berberine on tumor from 2002 to 2021: A bibliometric article of the literature from WoSCC.
Front. Pharmacol. 14:1122890.
doi: 10.3389/fphar.2023.1122890

Emerging trends and research foci of berberine on tumor from 2002 to 2021: A bibliometric article of the literature from WoSCC

Runzhu Yuan[1†], Yao Tan[2†], Ping-Hui Sun[3†], Bo Qin[2*] and Zhen Liang[4*]

[1]School of Medicine, The First Affiliated Hospital of Southern University of Science and Technology, Shenzhen People's Hospital, Shenzhen, China, [2]Shenzhen Aier Eye Hospital, Aier Eye Hospital, Jinan University, Shenzhen, China, [3]Department of Thoracic Surgery, The Second Clinical Medical College of Jinan University, Shenzhen People's Hospital, Shenzhen, China, [4]Department of Geriatrics, The Second Clinical Medical College, Jinan University, Shenzhen People's Hospital, Shenzhen, China

Background: Cancer, also known as a malignant tumor, is caused by the activation of oncogenes, which leads to the uncontrolled proliferation of cells that results in swelling. According to the World Health Organization (WHO), cancer is one of the main causes of death worldwide. The main variables limiting the efficacy of anti-tumor treatments are side effects and drug resistance. The search for natural, safe, low toxicity, and efficient chemical compounds in tumor research is essential. Berberine is a pentacyclic isoquinoline quaternary ammonium alkaloid isolated from Berberis and Coptis that has long been used in clinical settings. Studies in recent years have reported the use of berberine in cancer treatment. In this study, we performed a bibliometric analysis of berberine- and tumor-related research.

Materials and methods: Relevant articles from January 1, 2002, to December 31, 2021, were identified from the Web of Science Core Collection (WOSCC) of Clarivate Analytics. Microsoft Excel, CiteSpace, VOSviewer, and an online platform were used for the literary metrology analysis.

Results: A total of 1368 publications had unique characteristics. Publications from China were the most common (783 articles), and Y. B. Feng (from China) was the most productive author, with the highest total citations. China Medical University (Taiwan) and Sun Yat-sen University (China) were the two organizations with the largest numbers of publications (36 each). *Frontiers in Pharmacology* was the most commonly occurring journal (29 articles). The present body of research is focused on the mechanism, molecular docking, and oxidative stress of berberine in tumors.

Conclusion: Research on berberine and tumors was thoroughly reviewed using knowledge map and bibliometric methods. The results of this study reveal the dynamic evolution of berberine and tumor research and provide a basis for strategic planning in cancer research.

KEYWORDS

berberine, tumor, pharmacology, bibliometric analysis, Web of Science

1 Introduction

In every nation worldwide, cancer ranks as a primary cause of mortality and a significant roadblock to increasing life expectancy (Sung et al., 2021). The mortality and incidence rates of malignant tumors have increased globally (Mullard, 2020). The World Health Organization (WHO) estimates for 2019 suggest that cancer is the third or fourth leading cause of death before the age of 70 years in 23 countries (among 183 nations in total) and the first or second leading cause in 112 countries (Sung et al., 2021). The development of cancer treatments has faced significant obstacles. While both traditional and modern approaches (surgery, radiation, chemotherapy, targeted therapy, and immunotherapy) have good efficacy, these treatment modalities also have negative consequences on patient quality of life, including the development of simultaneous resistance to multiple drugs and dermatologic toxicities (Szakacs et al., 2006; Nastiuk and Krolewski, 2016; Lacouture and Sibaud, 2018). One of the main clinical therapies for cancer is chemotherapy; however, cancer is prone to relapse and drug resistance, and most chemotherapy treatments fail; therefore, efforts to develop anti-cancer drugs are needed. Additionally, toxic side effects caused by chemotherapy also affect the quality of life of patients with cancer. Therefore, identifying anti-tumor medicines with minimal toxicity and high efficacy is crucial for the treatment of tumors.

In recent decades, scientists have conducted numerous clinical and laboratory studies on traditional Chinese medicine. Natural compounds have many medicinal properties, including multiple action targets, low toxicity, low side effects, few adverse reactions, and high safety and effectiveness. These compounds have been gradually applied to cancer treatment due to their safety, availability, accessibility, and low cost. Natural compounds have a variety of anti-cancer effects, including suppression of tumor cell growth, induction of tumor cell death, prevention of tumor spread and angiogenesis, regulation of tumor autophagy, reversal of tumor drug resistance, regulation of body immunity, and influence on tumor metabolic reprogramming (Yang et al., 2021). In addition, natural therapy can prevent many issues, increase tumor cell sensitivity to conventional treatment, reduce side effects, enhance patient quality of life, and extend patient lives to cure cancer (Sun et al., 2022a; Sun et al., 2022b). Therefore, natural medicines are receiving increasing attention. Berberine (BBR) is an isoquinoline alkaloid obtained from the Chinese herb *Coptis chinensis* and other *Berberis* species (Song et al., 2020). It is the main component of Coptidis Rhizome (CR), known as Huanglian in Chinese. Because of its pharmacological characteristics, BBR has been used as a drug to treat diseases. As a secondary metabolite of plants, it has several pharmacological characteristics (Song et al., 2020), including treatment efficacy for cardiovascular and metabolic disease (Feng et al., 2019), polycystic ovary syndrome (Zhang et al., 2021b), and non-alcoholic fatty liver disease (Koperska et al., 2022), in addition to anti-inflammatory (Kuo et al., 2004), antioxidant (Zhuang et al., 2018), and antibacterial (Li et al., 2019) properties. In recent years, BBR has also been used in the research of cancers. For example, BBR binds RXRα to suppress β-catenin signaling, leading to the inhibition of colorectal cancer proliferation (Ruan et al., 2017); BBR also regulates the HMGB1–TLR4 axis to repress the metastasis of breast cancer *in vitro* and *in vivo* (Zheng et al., 2021). Moreover, BBR exerts therapeutic actions on gastric cancer by multi-step actions such as inhibiting cell proliferation, migration, and angiogenesis (Liu et al., 2022a); BBR also combines with cisplatin to induce necroptosis and apoptosis in ovarian cancer (Liu et al., 2019). In recent years, more studies on BBR have been conducted *in vitro* and *in vivo*, which have largely proved the reproducibility and transformation potential of BBR's anti-tumor effect in *in vitro* cell and *in vivo* animal models.

Using measurement techniques from mathematics and statistics, bibliometrics analysis assesses and forecasts the current state of science and technology by utilizing the features of the literature system as its research subject (Chen et al., 2014; Yu et al., 2020). By examining and evaluating the quantity and quality of scientific literature associated with a specific topic, bibliometric evaluation can objectively assess the state and level of development of that field (Musbahi et al., 2022). Bibliometrics assists researchers in swiftly identifying the information context in the target field, including the annual publishing trends of the literature, catalog of publishing institutes or journals, and popular research (Yin et al., 2022). The knowledge structure can be understood more methodically and intuitively using this approach, and frontiers or hotspots in a particular research area can be identified (Musbahi et al., 2022). Therefore, the present bibliometrics study aimed to investigate the role of BBR in tumors and to offer a broad perspective and roadmap for future research on BBR in pan-carcinoma treatment.

2 Materials and methods

2.1 Data source and searching strategies

Published studies from January 1, 2002, to December 31, 2021, related to BBR and tumors were collected from the Science Citation Index Expanded (SCI-E) of the Web of Science (WoS) Core Collection (WOSCC) of Clarivate Analytics. To guarantee the reliability and accuracy of the findings, we performed pertinent pretests and improved the retrieval method. The retrieval method is illustrated in Figure 1. We used the WoS engine to search for terms related to BBR and cancer that were obtained from the Medical Subject Headings (MeSH) in PubMed. The search formula was TS = (Berberine or Umbellatine) and TS = (Tumor or Neoplasm or Tumors or Neoplasia or Neoplasias or Cancer or Cancers or "Malignant Neoplasm" or Malignancy or Malignancies or "Malignant Neoplasms" or "Neoplasm, Malignant" or "Neoplasms, Malignant" or "Benign Neoplasms" or "Benign Neoplasm" or "Neoplasms Benign" or "Neoplasm Benign"). Only publications written in English were included. The reasons for exclusion from the study were 1) no connection between BBR and tumors of any kind; 2) meeting abstract, correction, editorial material, proceeding paper, retracted publication, book chapters, early access, retraction, *etc.*; and 3) publications in a language other than English. A total of 1,368 papers were obtained.

2.2 Data collection

All retrieved documents were used for the bibliometric analysis. We extracted information including titles, annual publications, countries and institutes, authors, references, keywords, and

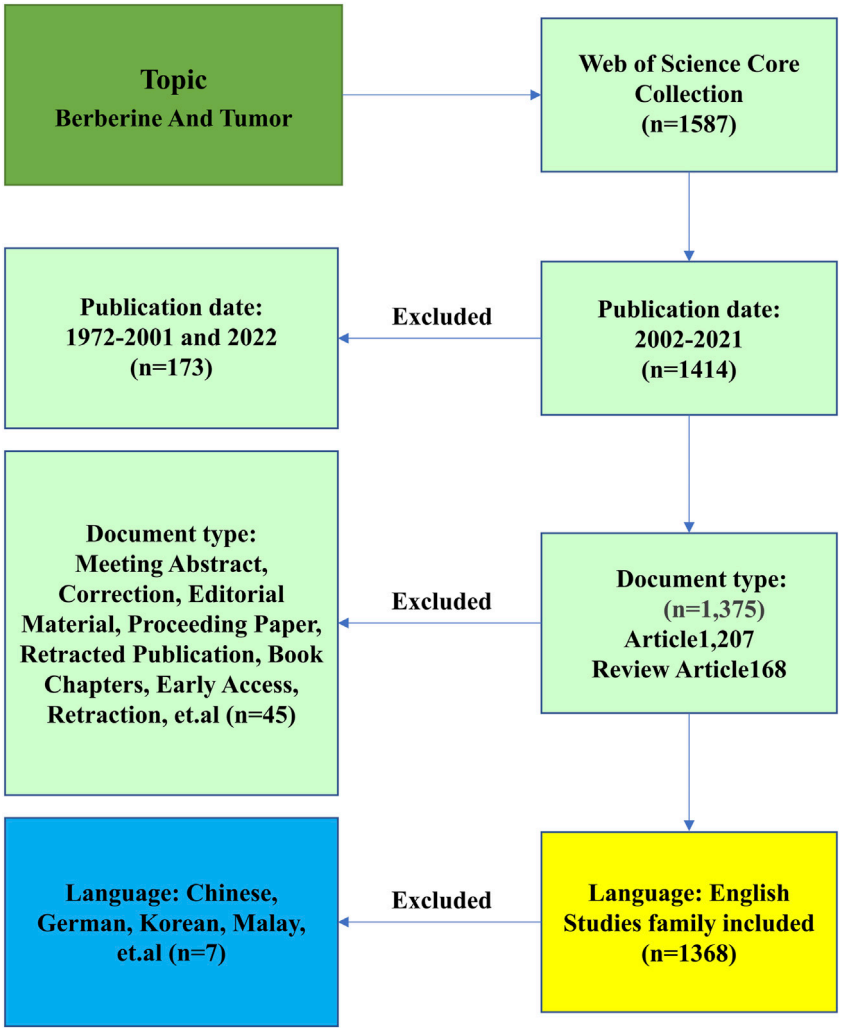

FIGURE 1
Flowchart of the screening process.

scientific cooperation analysis. Data were independently extracted from a set of articles by TY and YRZ. SP-H mediated the outcomes if a disagreement arose.

2.3 Data analysis and visualization

We used CiteSpace (version 6.3. R3), VOSviewer (version 1.6.18), Bibliometrix (version 3.1.4), R language (version 3.6.3), and Microsoft Excel 365 for data analysis and presentation.

CiteSpace, developed by Prof. Chao-mei Chen, is a bibliometric mapping analytical tool used worldwide, most predominantly in China (Qin et al., 2022). It is a free program for analyzing, identifying, and visualizing trends and patterns in scientific literature and was chosen as the analysis target (Pan et al., 2017). In our investigation, the specifics of the CiteSpace settings were as follows: time slices of 1 year each were taken from 2002 to 2021. The links (strength: cosine; scope: inside slices) and term sources (title, abstract, author keywords, and keywords plus) were set to the default values. Items with a g-index citation or occurrence were selected for this study. Links that were not necessary were removed using Pathfinder.

VOSviewer, developed by van Eck and Waltman, creates visual network maps of scientific information, including bibliometric network analysis (van Eck and Waltman, 2010). We used VOSviewer to create network, overlay, and density visualization maps. We chose the "full counting" method for our analysis. For keywords and co-cited journals, the thresholds for the minimum numbers were set at 100 and 5, respectively. Keywords or co-cited journals are displayed as nodes in the form of a network through a visualization diagram.

Visualization of the annual publication numbers; country, institute, author, and journal rankings; cited reference bursts; and most globally and locally cited Local Cited Documents, was performed using Microsoft Excel 365. Additionally, we performed a descriptive study

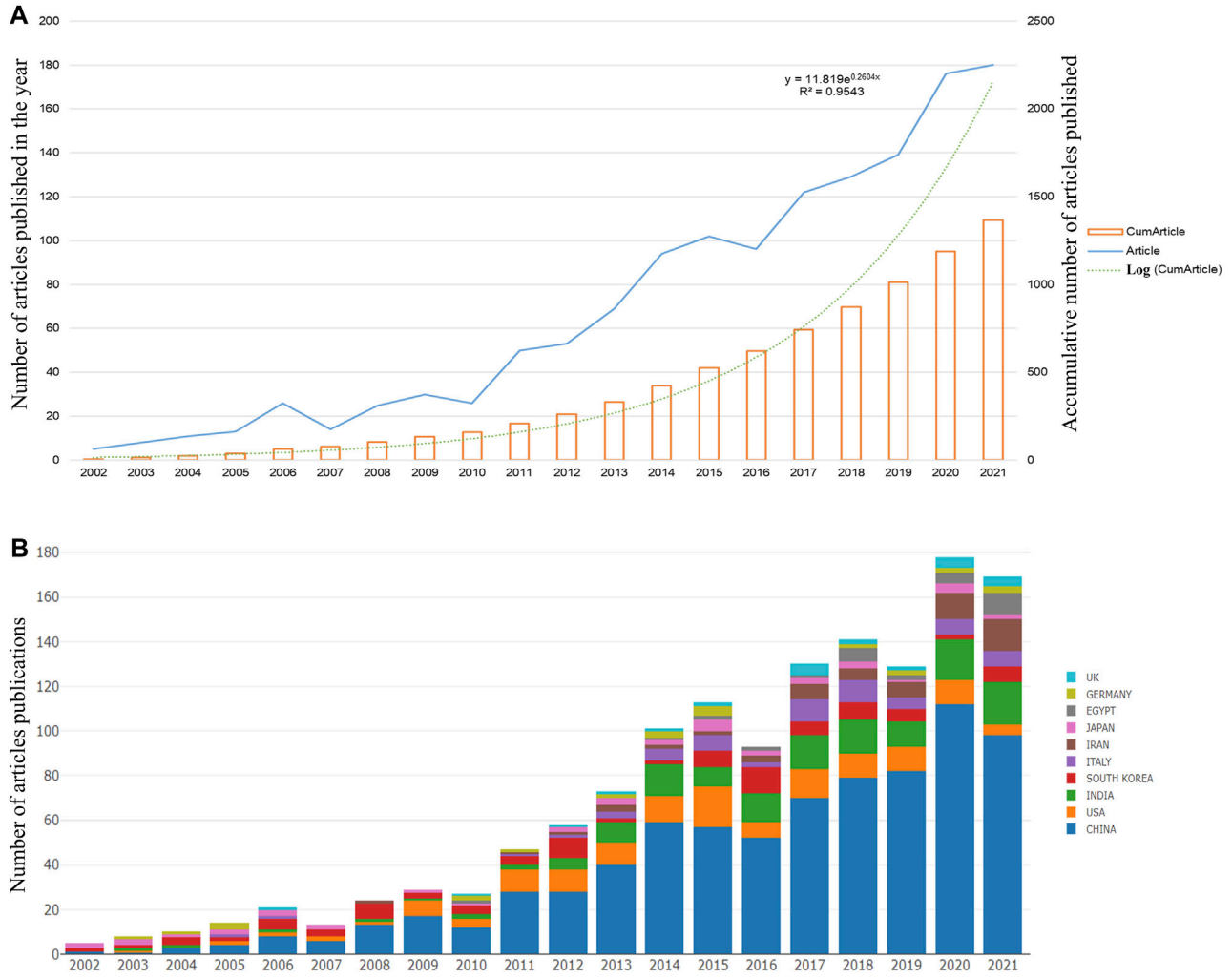

FIGURE 2
Global trends of publications about berberine and tumor. **(A)** The number of articles published each year and the accumulative number of articles from 2002 to 2021. **(B)** The annual number of papers published by nations from 2002 to 2021.

of writer output over time and keyword evolution in Bibliometrix (Cheng et al., 2022). Bibliometrix (https://www.bibliometrix.org) is an open-source instrument for quantitative scient-metric research. Machine-learning software was used to evaluate the distribution of each component examined in the bibliometric investigation. The variables were annual scientific production, average citations per year, most impactful journals by H-index or total citations (TC), top journals' production over time, most relevant authors, most globally and locally cited documents, most pertinent affiliations, country-level scientific output, international collaboration network, country of origin of the corresponding author, top producing nations over time, historical direct citation network, most widely cited publications, most pertinent keywords, and keyword cluster analysis. Impact factor (IF) and partition information for the journals referred to the "Journal Citation Report (JCR) 2022." These analytical methods offer unbiased and varied viewpoints on the function of berberine in tumor formation. The variables are presented as numbers and percentages in the descriptive study. *p*-values were not reported because no comparisons were made.

3 Results

3.1 Global publication outputs

We assessed the historical development process, current research conditions, and forecasted future trends in development by statistically analyzing the general usage of BBR pharmacological functions in the number of publications over time.

We counted the number of papers related to "berberine and tumors" from 1972 to 2021 and collected 1,587 articles for bibliographic records from the WOSCC. Ultimately, 1,368 articles were eligible for the next stage of analysis based on the exclusion criteria of publication time, document type, and language. Figure 2A shows the number of articles published each year and the cumulative number of articles published from 2002 to 2021. The overall trend has increased over the past 20 years. The greatest number of papers was published in 2021, with 180 research articles. The exponential curve equation for the rise in literature production was y =

TABLE 1 Top 10 countries that contributed publications on BBR and tumors.

Rank	Countries	Article count	Percentage (n/1368)	H-index	Total citations	Average citation per article
1	China	783	57.24%	70	23,603	30.14
2	United States	142	10.38%	48	6,886	48.49
3	India	142	10.38%	35	4,137	29.13
4	Republic of Korea	97	7.09%	34	3,198	32.97
5	Italy	61	4.46%	25	2,257	37.00
6	Iran	60	4.39%	22	1,800	30.00
7	Japan	42	3.07%	22	1,403	33.40
8	Egypt	30	2.19%	14	615	20.50
9	Germany	26	1.90%	16	1,117	42.96
10	Poland	24	1.75%	14	539	22.46

$11.819e^{0.2604x}$, which conforms to Price's law. The simulation curve had a relatively strong coefficient of determination (R^2 = 0.9543), which fitted the annual literature growth trend well. Based on this curve, we predicted that the number of annual articles will steadily increase, indicating increased interest in research on BBR and tumors.

3.2 Distributions of countries/regions

Statistics on the research countries reporting on publications related to "berberine and tumors" showed the stages of BBR pharmacology development in each country and made comparisons easier. According to WoS, many countries have participated in research in the last 20 years. Table 1 lists the top 10 productive countries. China had the most publications (783 articles), accounting for 57.24% of the total, followed by the United States and India (142 articles each, accounting for 10.38% each, respectively), South Korea (n = 97), Italy (n = 61), Iran (n = 60), Japan (n = 42), Egypt (n = 30), Germany (n = 26), and Poland (n = 24).

Publications from China ranked first in total number of citations, but the average number of citation per paper was very low, only 30.14%, compared to the top 10 countries. Although the number of articles published by Germany was limited compared to China, the average citation per article ranked second among the top 10 countries. This finding suggested that the publications were of very high quality and had certain reference values. The H-index is a mixed quantitative indicator that considers both the number of posts and the required number of citations and can be used to identify influential researchers (Hirsch, 2005). China's researchers had the highest H-indexes, demonstrating the significant impact of their publications. After 2008, most global publications came from China. Figure 2B shows the total number of papers published worldwide from 2002 to 2021.

Using an online bibliometric analysis platform, we evaluated the significance of nations in the visualization of cooperative networks. Katz and Martin, two scientists, defined scientific cooperation as the study of academics collaborating to create new scientific knowledge, known as scientific collaboration (Katz and Martin, 1997). Figure 3A shows partnerships between countries, among which articles from China showed the most aggressive cooperation with other countries; most often between China and the United States. We conducted a visual analysis using VOSviewer (Figure 3B). The circles in the map represent countries and the lines indicate the connections between them. The larger the area of the circle, the larger the contribution of these countries to this field. We found that China made significant contributions to research on BBR and cancer. A density map can be used to determine the number of publications in each nation. The lighter the color, the greater the number of publications. The density map was used to determine the number of publications in each nation (Figure 3C). As shown in Figure 3C, China had the highest number of publications. Figure 3D shows that American publications were generally concentrated before 2016, whereas Chinese, Indian, Italian, and Iranian articles were concentrated after 2016.

3.3 Distribution of institutes

The top 10 productive institutes are listed in Table 2. China Medical University (Taiwan) and Sun Yat-Sen University (China) had the most publications, with 36 articles each. China Medical University (Taiwan) showed the highest total number of citations (1,417) and H-index (21), with an average number of citations of 39.26, demonstrating a high level of acclaim for its articles. We used VOSviewer to depict the cooperation between institutes in Figure 4A. Figure 4B shows each institute's cooperation timeline from 2002 to 2021; the node color on this map corresponds to each institute's cooperation respective average appearing year (AAY). Jilin University and Mashhad University of Medical Sciences had

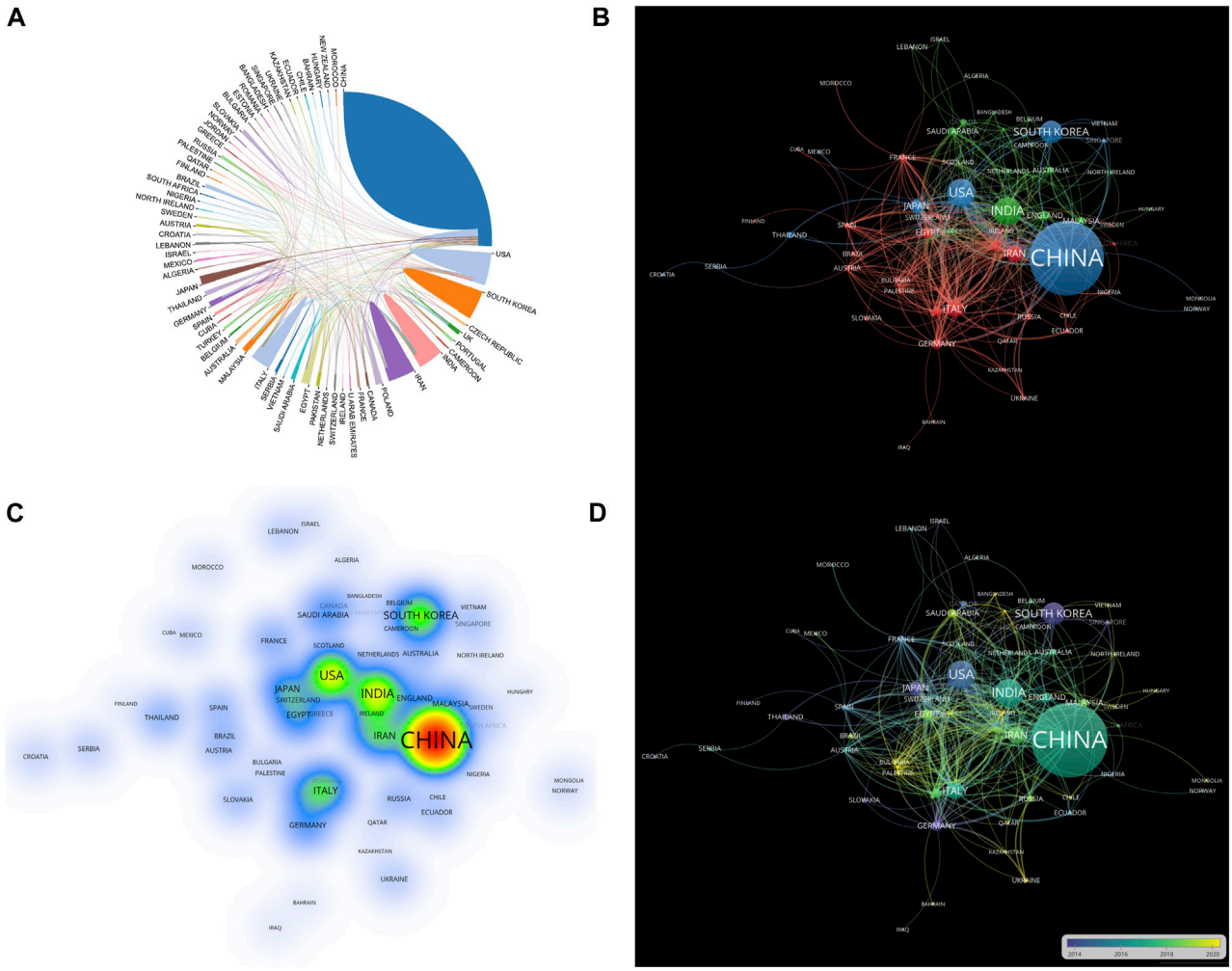

FIGURE 3
Overview of national publications. **(A)** The scientific collaborations among worldwide countries. **(B)** Visual analysis of cooperation between countries based on VOSviewer. **(C)** A density visualization map of number of publications in each nation. **(D)** Median time chart of the number of articles issued by each country.

TABLE 2 Top 10 institutes that contributed publications on BBR and tumors.

Rank	Institute	Country	Article count	H-index	Total number of citations	Average number of citations per article
1	China Medical University (Taiwan)	China	36	21	1,417	39.36
2	Sun Yat-Sen University	China	36	20	1,204	33.44
3	Council of Scientific Industrial Research	India	34	17	898	26.41
4	Shanghai University of Traditional Chinese Medicine	China	31	16	878	28.32
5	Chinese Academy of Sciences	China	29	18	755	26.03
6	Egyptian Knowledge Bank	Egyptian	28	14	606	21.64
7	University of Hong Kong	China	24	18	1,401	58.38
8	Guangzhou University of Chinese Medicine	China	24	14	587	24.46
9	Jilin University	China	24	14	562	23.42
10	Jinan University	China	24	14	484	20.17

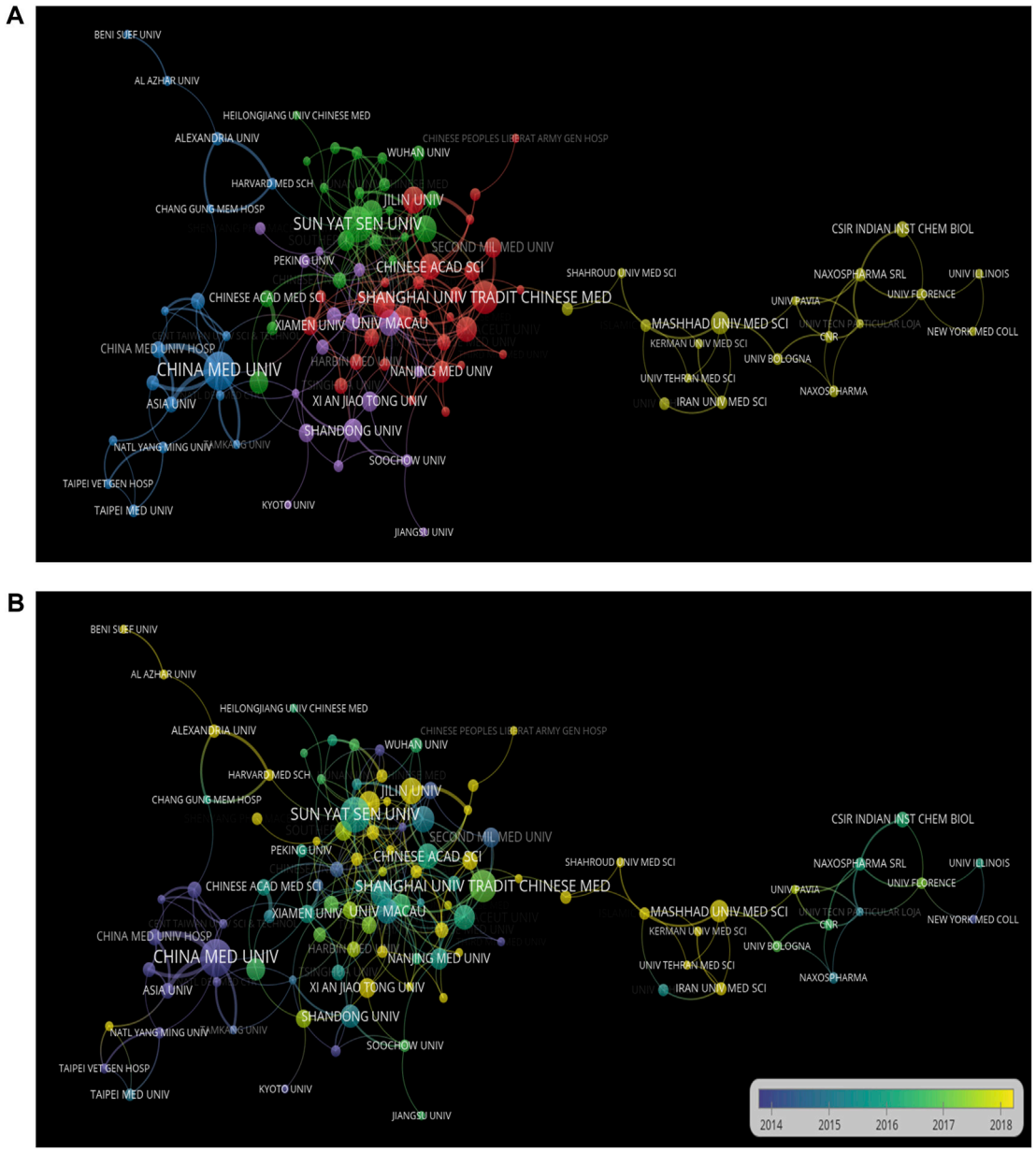

FIGURE 4
Cooperation networks between institutes based on VOSviewer. **(A)** Cooperative relationship of various institutions using network map. **(B)** Cooperative time of various institutions using network map.

relatively fresh entries compared to the nations shown in purple, such as China Medical University (Taiwan), according to the color gradient in the lower right corner.

3.4 Authors

The top 10 authors in terms of the number of articles in the past 20 years are listed in Table 3. Y. B. Feng of the University of Hong Kong, was the most prolific author (21 articles) and also received the highest number of total citations (1,281) and had an H-index of 17, demonstrating his significant contributions to the field. O Paolo from Naxospharma published 17 articles, while L Paolo and K Gopinatha Suresh (Indian Institution of Chemical Biology) both had H-index values of 12.

3.5 Journals and co-cited journals

The top 10 journals according to the number of publications are shown in Table 4 and Figure 5. The top 10 journals published 252 papers, or 18.42% of all the included publications. *Frontiers in Pharmacology* (IF = 5.9879) was the most popular journal with 29 articles, followed by *Molecules* (IF = 4.9269) with 28 articles.

TABLE 3 Top 10 authors that contributed publications on BBR and tumors.

Rank	Author	Article count	H-index	Country	Total number of citations	Average number of citations per article	Institution
1	Feng, Y. B	21	17	China	1,281	61.00	University of Hong Kong
2	Paolo. L	17	12	Italy	879	51.71	Naxospharma
3	Gopinatha Suresh. K	16	12	Indian	510	31.88	Indian Institute of Chemical Biology
4	Tan, H.-Y	13	9	China	408	31.38	Hong Kong Baptist University
5	Wang, Y. T	11	11	China	1,094	99.45	University of Macau
6	Zheng, X	11	9	China	275	25.00	Jilin University
7	Bhupendra M. M	10	8	Republic of Korea	129	12.90	Konkuk University
8	Shao, D	10	9	China	256	25.60	Jilin University
9	Chen, L	10	8	China	297	29.70	Jilin University
10	Doo Hwan. K	10	8	Republic of Korea	129	12.90	Konkuk University

TABLE 4 Top 10 journals and co-cited journals that published articles on BBR and tumors.

Rank	Journal	Count	Total number of citations	Average citation per article	IF and JCR division (2021)	Co-cited journal	Total number of co-citations
1	*Frontiers in Pharmacology*	29	835	28.79	5.9879, Q1	PLOS One	1394
2	*Molecules*	28	690	24.64	4.9269, Q2	*Cancer Research*	1101
3	*PLOS One*	28	1,388	49.57	3.7521, Q2	*Journal of Biological Chemistry*	1037
4	*Evidence-Based Complementary and Alternative Medicine*	27	415	15.37	2.6498, Q3	*Cancer Letters*	973
5	*Molecular Medicine Reports*	25	484	19.36	3.4232, Q3	*Journal of Ethnopharmacology*	910
6	*Biomedicine and Pharmacotherapy*	24	954	39.75	7.4194, Q1	*European Journal of Pharmacology*	827
7	*European Journal of Pharmacology*	24	814	33.92	5.1948, Q2	*Proceedings of the National Academy of Sciences of the United States of America*	717
8	*International Journal of Molecular Sciences*	23	453	19.70	6.2082, Q1/Q2	*Nature*	687
9	*Journal of Ethnopharmacology*	23	1,234	53.65	5.1948, Q1/Q2	*Oncogene*	598
10	*Oncology Reports*	21	483	23.00	4.1361, Q3	*Biochemical and Biophysical Research Communications*	594

PLOS One (IF = 3.7521) was the most frequently cited journal (1,388 citations). The distribution of journals across fields, evolution of citation trajectories, and drift of scientific research centers can be displayed using the dual-map overlay of journals (Chen and Leydesdorff, 2014; Zhang et al., 2021a). In our dual-map overlay analysis (Figure 5E), the left side shows the distribution of the journals where the citing documents were located, representing the main disciplines of science mapping, while the right side shows the distribution of the journals corresponding to the cited literature, representing which disciplines were mainly cited by science mapping. The results showed that research related to BBR and tumors was mainly associated with the areas of molecular/biology/immunology and was often cited by molecular/biology/genetics researchers.

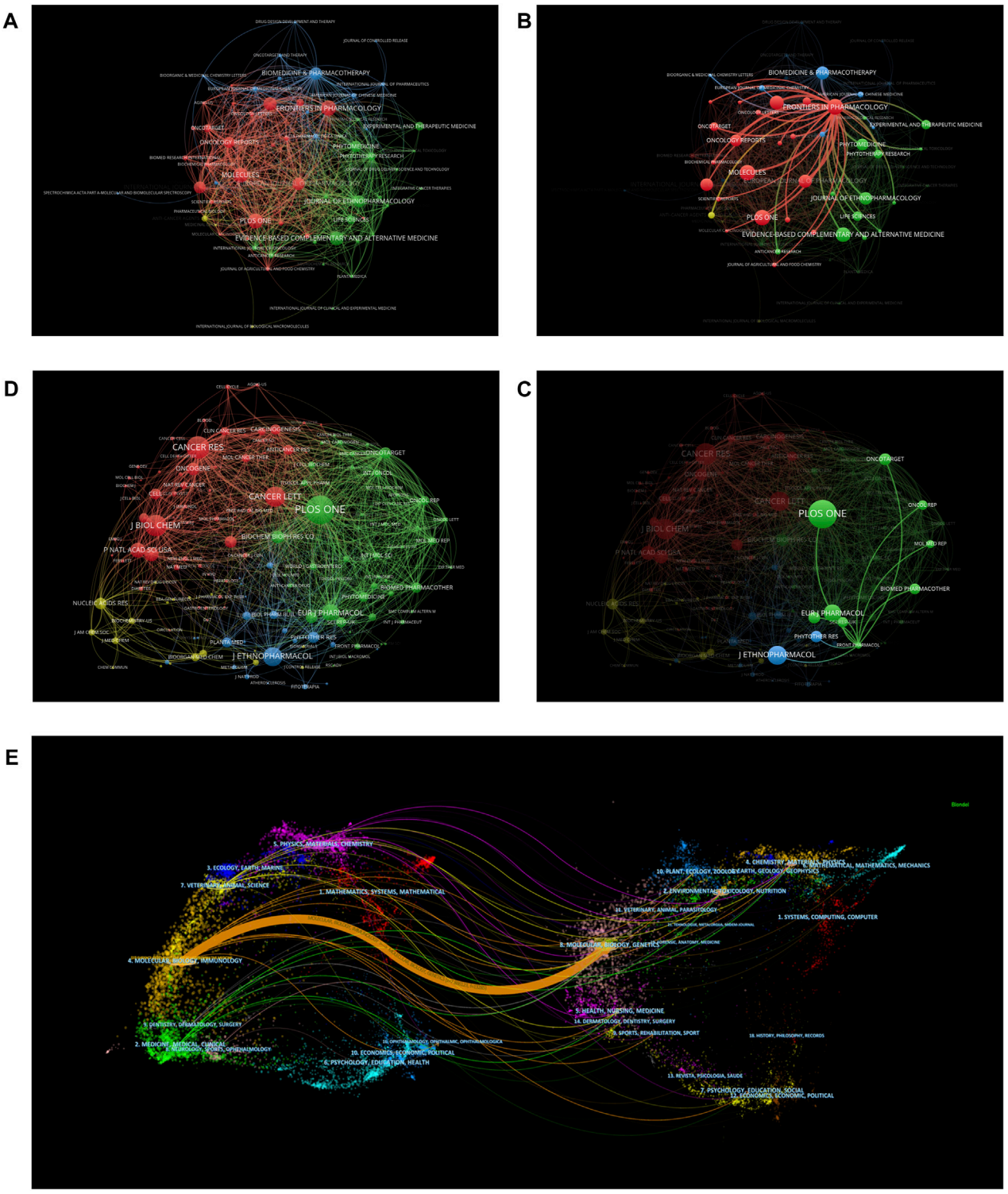

FIGURE 5
The co-cited map of journals. **(A,B)** The map of journals that published papers about berberine and tumor. **(C,D)** The map of the cited journals based on Vosviewer. **(E)** The dual-map overlay of journals.

3.6 Co-cited references

We quantified the knowledge and development of research on a particular topic by evaluating the significant nodes and clusters in the co-cited reference network (Yin et al., 2022). We used CiteSpace to create a timeline-visualized diagram network map of the co-cited articles, which was divided into 19 clusters (Table 5). The co-cited reference network is shown in Figure 6A, in which the node size is

TABLE 5 Major clusters of co-cited references.

Cluster ID	Size	Silhouette	Mean (year)	Top terms (LSI)	Top terms (LLR)	Terms (MI)
0	96	0.842	2015	Berberine; ERK1/2; and glioma	Invasion; migration; and glioma	Triptolide; RT-R breast cancer cells; and chemoprotective agents
1	86	0.884	2008	Breast cancer; signaling pathways; and leukemia	Daxx; side population; and invasiveness	Daxx; side population; and invasiveness
2	85	0.935	2003	Berberine; thermodynamics; and non-cooperative binding	Interleukin-1 beta; ARPE-19 cells; and interleukin-8	Berberine; berberine interleukin-1 beta; and cooperative binding
3	78	0.887	2016	Berberine; carrier-free; and gram-scale	Photodynamic therapy; and epithelial–mesenchymal transition	Transforming growth factor; rat; and reverse pharmacophore mapping
4	70	0.907	2017	Berberine; doxorubicin; and neurotoxicity	Non-small-cell lung cancer; liquid crystalline nanoparticles; and neurotoxicity	Demethyleneberberine; modern science; and top2b
5	69	0.95	2006	Berberine; apoptosis; and ATF3	P53; apoptosis; and *Coscinium fenstratum*	Human liver microsomes; anti-metastasis; and *Tinospora cordifolia*
6	59	0.878	2012	Berberine; IL-8; and adhesion	Prostate cancer; evodiamine; and epigenetics	Interleukin-8; traditional Chinese medicine; and gemcitabine
7	51	0.914	2012	Tumor necrosis factor-alpha; brain inflammation; and interleukin-1 beta	TNF-α; lipopolysaccharide; and NF-κB	Berberine intestinal mucosal barrier; interleukin-1; and interleukin-6
8	45	0.903	2011	Cervical cancer; gastrointestinal disorders; and antitumor	Antioxidant; piperazine; and cervical cancer	RNA triplex; g-quadruplexes; and catenin
9	45	0.971	2000	Human topoisomerase; anti-cancer drugs; and structure-based molecular modeling	Structure-based molecular modeling; interleukin-12; p38 MAPK; and anti-cancer drugs	Berberine; apoptosis; and structure-based molecular modeling
10	43	0.994	2000	Anticancer activity; anticancer effects; and colorectal cancer	Herb; colon 26/clone 20 cells; and pancreatic cancer	Berberine; apoptosis; and colon 26/clone 20 cells
11	30	0.97	2017	Gut microbiota; pharmacokinetic study; and amino acid	Gut microbiota; atherosclerosis; and metabolomics	Metabolomics; fecal metabolites; and functional nano-vector
12	22	0.942	2007	Berberine; barrier function; plant alkaloid; and lipid mediators	Atherogenesis; anti-microbial; and acute intestinal symptoms	Berberine; atherogenesis; and anti-microbial
13	16	0.997	2017	Lung cancer; inhalable nanocomposites; and drug nanosuspension	Lung cancer; lactoferrin targeting; and drug nanosuspension	Berberine; apoptosis; and lactoferrin targeting
14	13	0.957	2010	Replication stress; H_2AX phosphorylation; DNA damage; and ribosomal protein S6 phosphorylation	Rapamycin; replication stress; and salicylate	Berberine; salicylate; and ribosomal protein S6 phosphorylation
15	10	0.995	2016	Alkylated; HeLa cell; and carbohydrate	Carbohydrate; alkylated; and anticancer	Berberine; carbohydrate; and alkylated
17	8	0.983	2014	Kainic acid; status epilepticus; and oxidative stress	Natural toxin; chronic unpredictable mild stress; and temporal lobe epilepsy	Berberine; natural toxin; and chronic unpredictable mild stress
18	7	0.998	2004	Berberine; ATF3; and apoptosis	ATF3; nag-1; p53; and apoptosis	Berberine; apoptosis; cancer; and breast cancer
20	4	0.99	2011	AMPK; aspirin; and berberine	Aspirin; metformin; AMPK; and resveratrol	Berberine; apoptosis; and cancer

the proportion of the research frequency, color is the proportion of the time slice, and the connections are represented by lines. We further conducted cluster analysis on these co-cited articles based on the keywords in those articles (Figure 6B). By removing phrases from the titles of the cited publications, we identified the main research hotspots. Figure 6C shows a timeline of references in the field of BBR and tumors, as determined by CiteSpace. We observed a shift in the focus of research over time. The development of clusters 2 (interleukin 1 beta), 9 (structure-based molecular modeling), and 10 (herb) occurred the earliest, indicating that early research focused more on BBR structure and pharmacology. Clusters 1 (Daxx), 6 (prostate cancer), and 7 (tumor necrosis factor-alpha) occurred

D

Top 10 References with the Strongest Citation Bursts

References	Year	Strength	Begin	End	2002 - 2021
Kuo CL, 2004, CANCER LETT, V203, P127, DOI 10.1016/j.canlet.2003.09.002, DOI	2004	22.15	2005	2009	
Lin JP, 2006, WORLD J GASTROENTERO, V12, P21, DOI 10.3748/wjg.v12.i1.21, DOI	2006	18.47	2007	2011	
Mantena SK, 2006, CARCINOGENESIS, V27, P2018, DOI 10.1093/carcin/bgl043, DOI	2006	16.88	2007	2011	
Mantena SK, 2006, MOL CANCER THER, V5, P296, DOI 10.1158/1535-7163.MCT-05-0448, DOI	2006	16.88	2007	2011	
Hwang JM, 2006, ARCH TOXICOL, V80, P62, DOI 10.1007/s00204-005-0014-8, DOI	2006	15.81	2007	2011	
Meeran SM, 2008, TOXICOL APPL PHARM, V229, P33, DOI 10.1016/j.taap.2007.12.027, DOI	2008	15.71	2009	2013	
Tang J, 2009, J ETHNOPHARMACOL, V126, P5, DOI 10.1016/j.jep.2009.08.009, DOI	2009	20.29	2010	2014	
Sun YY, 2009, ANTI-CANCER DRUG, V20, P757, DOI 10.1097/CAD.0b013e328330d95b, DOI	2009	15.93	2010	2014	
Tillhon M, 2012, BIOCHEM PHARMACOL, V84, P1260, DOI 10.1016/j.bcp.2012.07.018, DOI	2012	20.07	2013	2017	
Ortiz LMG, 2014, MOLECULES, V19, P12349, DOI 10.3390/molecules190812349, DOI	2014	16.5	2015	2019	

FIGURE 6
Analysis of co-cited references. **(A)** Visualized network diagram of co-cited documents. **(B)** Cluster Analysis of the co-cited articles. **(C)** Timeline view of the co-cited articles. **(D)** The top 10 references with the strongest citation bursts.

between 2007 and 2011, indicating a focus on the anti-cancer molecular mechanism of BBR. Clusters 15 (carbohydrate), 3 (photodynamic therapy), 4 (non-small cell lung cancer), and 11 (gut microbiota) are current research hotspots. Figure 6D shows the top 10 references with the strongest citation bursts, highlighting their significance in the fields of BBR and tumor-related research. In

TABLE 6 Total article citations.

Rank	Title	DOI	Total number of citations	TC per year	Normalized TC
1	Regulation of survival, proliferation, invasion, angiogenesis, and metastasis of tumor cells through modulation of inflammatory pathways by nutraceuticals	10.1007/s10555-010-9235-2	570	43.85	7.15
2	The anti-inflammatory potential of berberine *in vitro* and *in vivo*	10.1016/j.canlet.2003.09.002	515	27.11	5.91
3	Pharmacological and therapeutic effects of *Berberis vulgaris* and its active constituent, berberine	10.1002/ptr.2399	430	28.67	5.26
4	Berberine and Coptidis rhizoma as novel antineoplastic agents: A review of traditional use and biomedical investigations	10.1016/j.jep.2009.08.009	394	28.14	5.20
5	A systematic review of the anticancer properties of berberine, a natural product from Chinese herbs	10.1097/CAD.0b013e328330d95b	309	22.07	4.08
6	Berberine, a natural product, induces G1-phase cell cycle arrest and caspase-3-dependent apoptosis in human prostate carcinoma cells	10.1158/1535-7163.MCT-05-0448	285	16.76	3.59
7	Berberine: New perspectives for old remedies	10.1016/j.bcp.2012.07.018	284	25.82	6.05
8	Anti-cancer natural products isolated from Chinese medicinal herbs	10.1186/1749-8546-6-27	264	22.00	5.03
9	Targeting apoptosis pathways in cancer by Chinese medicine	10.1016/j.canlet.2010.07.015	220	22.00	5.41
10	Cancer prevention and therapy through the modulation of the tumor microenvironment	10.1016/j.semcancer.2015.02.007	212	26.50	6.11

addition, we list the total citations of articles and local citations of articles in Tables 6 and Table 7, respectively.

3.7 Analysis of keywords

Keywords are generally regarded as a significant index to reflect research frontiers and hotspots in a certain topic (Zhong And Song, 2008; Wu et al., 2021). We produced a map showing the co-occurrence of keywords using VOSviewer. The cooperation network (Figure 7A) clearly shows keywords changing from 2002 to 2021. At present, the keywords are main focused on “berberine”, “apoptosis” and “cancer”, and so on. Figure 7B shows the evolution of keywords in a typical publishing year. Initially,research on BBR mainly focused on “alkaloid”, and “tumor necrosis factor-alpha”; then, the research keywords shifted towards “prostate cancer”, “rapamycin” and “p53”; finally, the most recent keywords have become more diverse, with topics including “mechanism”, “cancer” and “gut microbiota”, and so on. Figure 7C shows the frequency of keywords in different time periods, the larger the size of the node, the higher the search frequency. In conclusion, “apoptosis”, “non-small cell lung cancer”, and “gut microbiota” were the most frequently searched terms.

4 Discussion

Chemotherapy and radiation therapy are standard treatments for patients with cancer. However, the resistance of malignant tumors to these treatments and the occurrence of major organ damage severely restrict the clinical outcomes of this disease (35). Moreover, current cancer treatments are inefficient, and the surgical prognosis is poor because tumor cells can invade and spread after treatment with a variety of chemical medications (Colagiuri et al., 2013). Natural herbal nutraceuticals have recently gained increased attention among popular clinical medications owing to their safety, adaptability to overcome therapeutic resistance, potential to reduce the adverse side effects of cancer treatments, low cost, and wide availability (Choudhari et al., 2019). Natural remedies can not only prevent drug resistance (38) but also have anti-tumor effects through various signaling pathways (Kumar and Adki, 2018; Al-Bari et al., 2021; Hashem et al., 2022). The prognosis of patients with malignant tumors can be improved by combining Chinese herbal therapies with other therapies (Mignani et al., 2018; Rejhová et al., 2018). BBR is a multi-target Chinese medicine monomer compound that not only regulates the growth of cancer cells but also acts as a combination chemotherapy drug for the treatment of tumors.

In this study, we conducted a bibliometric analysis to evaluate the hotspots and development trends of research on disciplines connected to BBR and tumors. We analyzed a total of 1,368 studies published from January 1, 2001, to December 31, 2021, and found that research on BBR and tumors has become increasingly frequent, suggesting that BBR may be a natural medication for treating tumors. China had the most relevant publications in the last 20 years, but the average number of citations per article was only 30.14%, significantly lower than that of other nations in terms of publications, suggesting that articles from China still have room for improvement. Among the top 10 countries with the greatest number

TABLE 7 The local citations of articles.

Rank	Document	DOI	Year	Local Citations	Global Citations	LC/GC Ratio (%)	Normalized Local Citations	Normalized Global Citations
1	The anti-inflammatory potential of berberine *in vitro* and *in vivo*	10.1016/j.canlet.2003.09.002	2004	155	515	30.10	6.25	5.91
2	Berberine, a natural product, induces G1-phase cell cycle arrest and caspase-3-dependent apoptosis in human prostate carcinoma cells	10.1158/1535-7163.MCT-05-0448	2006	124	285	43.51	4.61	3.59
3	A systematic review of the anticancer properties of berberine, a natural product from Chinese herbs	10.1097/CAD.0b013e328330d95b	2009	121	309	39.16	4.63	4.08
4	Berberine and Coptidis rhizoma as novel antineoplastic agents: a review of traditional use and biomedical investigations	10.1016/j.jep.2009.08.009	2009	115	394	29.19	4.40	5.20
5	Berberine: new perspectives for old remedies	10.1016/j.bcp.2012.07.018	2012	103	284	36.27	7.57	6.05
6	Berberine induces apoptosis through a mitochondria/caspase's pathway in human hepatoma cells	10.1007/s00204-005-0014-8	2006	86	170	50.59	3.20	2.14
7	Berberine induces autophagic cell death and mitochondrial apoptosis in liver cancer cells: the cellular mechanism	10.1002/jcb.22869	2010	85	200	42.50	5.44	2.51
8	Berberine inhibits growth, induces G1 arrest and apoptosis in human epidermoid carcinoma A431 cells by regulating Cdki-Cdk-cyclin cascade, disruption of mitochondrial membrane potential and cleavage of caspase 3 and PARP	10.1093/carcin/bgl043	2006	83	161	51.55	3.09	2.03
9	Pharmacological and therapeutic effects of Berberis vulgaris and its active constituent, berberine	10.1002/ptr.2399	2008	83	430	19.30	3.31	5.26
10	Berberine, an epiphany against cancer	10.3390/molecules190812349	2014	79	165	47.88	10.53	4.19

of articles, China engages the most in international collaborations, primarily with the United States. China Medical University (Taiwan) published the most studies related to BBR and tumors worldwide. However, the University of Hong Kong ranked first in terms of average citations per article. Y. B. Feng, an author based in China, was the most productive and had the highest total citations. The journal that published the most articles was *Frontiers in Pharmacology* (29 articles), followed by *Molecules* (28 articles). We also analyzed the reference with the strongest citation burst; the latest literature of the co-cited reference was "Berberine, an epiphany against cancer," which was published in *Molecules* in 2014. This article summarizes the molecular targets of BBR, several mechanisms by which BBR inhibits cancer, and the potential discovery of BBR derivatives for anti-cancer drugs (Ortiz et al., 2014). Our analysis of cooperation between countries, institutes,

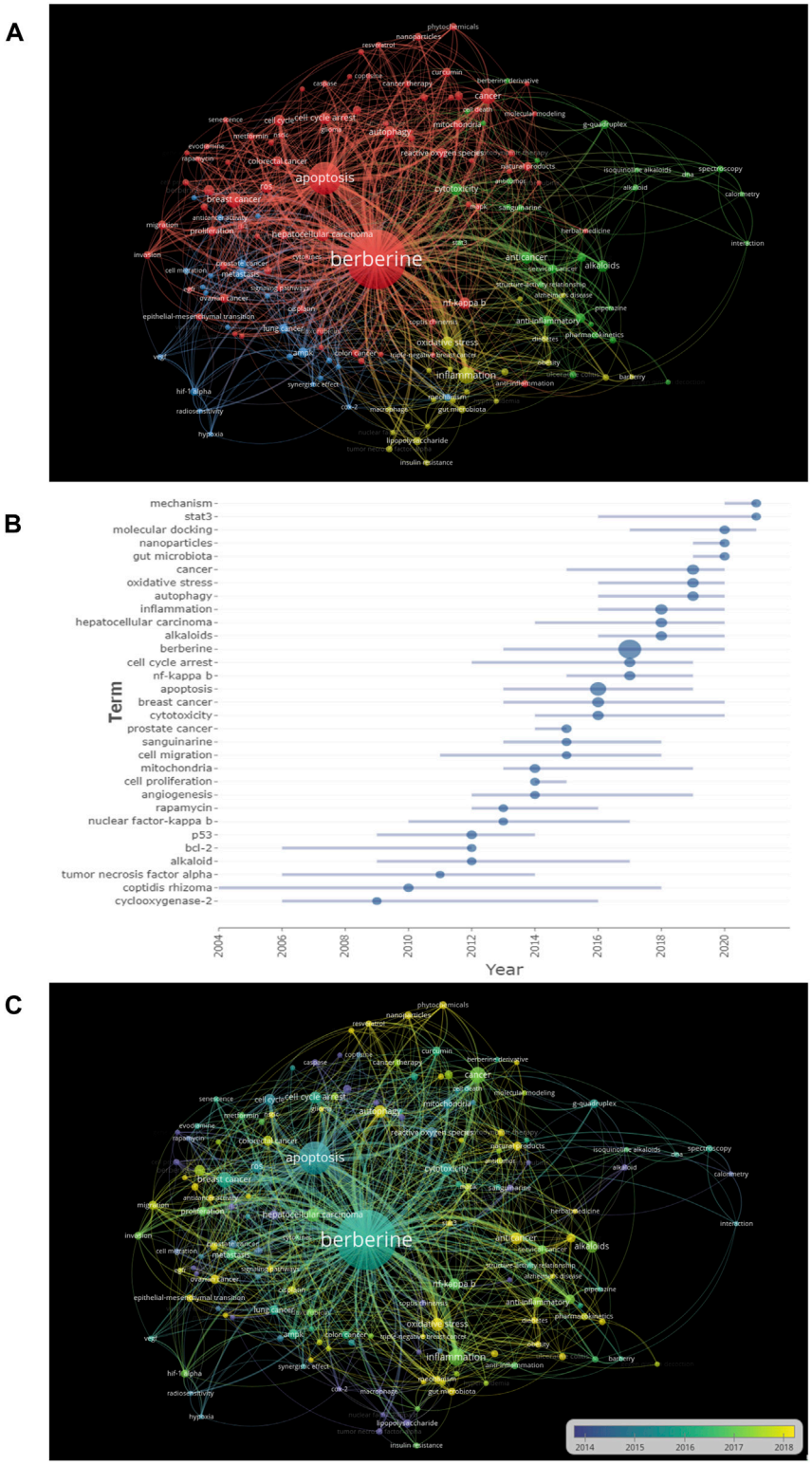

FIGURE 7
Analysis of keywords **(A)** the changing trend of research keywords from 2002 to 2021. **(B)** The evolution of keyword frequency. **(C)** The network map of keywords. Minimum number of occurrences of keywords ≥5.

and institutes, showed that academic cooperation can promote the development of clinical and academic research.

4.1 Mechanism of berberine on cancers

As shown in Figure 6B, BBR has been used in the treatment of lung cancer (#13), prostate cancer (#6), and non-small-cell lung cancer, and has been a research hotspot in recent years (Figure 6C). The mechanisms of action of BBR in cancer have also been studied and mainly consist of inhibiting migration and invasion, inducing apoptosis, arresting the cell cycle, inhibiting proliferation, and promoting autophagy in tumors.

4.1.1 Berberine can inhibit the migration and invasion of tumors

In clinical practice, most patients experience the invasion and migration of cancer cells from a single focus to other distant tissues. In 2015, research on migration and invasion became a hot topic (Figure 7B). A wide variety of migratory and invasion mechanisms are involved in cancer (Figure 6C). In triple-negative breast cancer cells, BBR reduces interleukin-8 (IL-8) expression by blocking the EGFR/MEK/ERK signaling pathway to prevent cell invasion and metastasis (Kim et al., 2018). BBR also affected cell migration and invasion in the human hepatoma HepG2 cell line by inhibiting the transforming growth factor (TGF-beta/Smad) signaling pathway (Du et al., 2021). Understanding cellular and molecular changes in these various migration/invasion programs will enable us to develop novel therapeutic approaches and provide insights into the spread of cancer cells.

4.1.2 Berberine can promote tumor cell apoptosis

Apoptosis was the main keyword in BBR-related research (Figure 7A) and the median time of the research boom occurred around 2016 (Figure 7C). Apoptosis is an evolutionarily conserved cell death system responsible for eliminating cells during embryonic development and maintaining organismal homeostasis (Singh et al., 2019). The pathways of apoptosis are divided into the exogenous pathway, endogenous pathway, caspase cascade reaction, and caspase effects. Many biochemical processes, such as a loss of mitochondrial membrane potential, release of cytochrome C into the cytoplasm, expression of Bcl-2 family and caspase family proteins, and cleavage of poly ADP ribose polymerase, induced apoptosis in the skin squamous cell carcinoma A431 cell line after treatment with BBR (Wartenberg et al., 2003). Moreover, BBR induced apoptosis involved in the caspase-related mitochondrial pathway compared to normal liver HL-7702 cells, which was mediated by adenosine monophosphate-activated protein kinase (AMPK) and reduced the survival of human hepatoma HepG2, SMMC-7721, and Bel-7402 cells (Mitani et al., 2001). To reach the goal of treatment, researchers are currently modeling small molecules with apoptosis-promoting protein activity, which renders cells susceptible to mitochondrial apoptosis and triggers apoptosis.

4.1.3 Berberine can block the cell cycle of tumor cells

Research on the effect of BBR on cell cycle arrest started around 2012 but was mainly concentrated in 2017 (Figure 7B). To some degree, changes in the cell cycle can either slow or accelerate cancer development. Previous studies demonstrated that BBR inhibits the growth of certain tumor cells by regulating their cell cycle. A study on the mechanism of BBR in breast cancer showed that the alkaloid BBR prevented breast cancer cells from entering the S phase and increased cancer cell sensitivity to treatment (Kim et al., 2010). In a human chondrosarcoma cell HBT-94 model, BBR activated the PI3K/Akt and p38 signaling pathways, increased the protein levels of p53 and p21, and triggered G2/M phase arrest, thus demonstrating anti-cancer effects (Eo et al., 2014). Gene stability is maintained by cell cycle arrest and cancer formation is significantly influenced by the incidence of cell cycle-regulated gene alterations. If DNA is damaged during a healthy cell cycle, the cell cycle stalls at a relevant checkpoint. Cell cycle arrest gives cells more time to repair damage, which lowers the likelihood of mutations and prevents tumor development. Therefore, targeting cell cycle checkpoints may significantly enhance cancer treatment.

4.1.4 Berberine can inhibit tumor proliferation

Numerous studies have reported that BBR regulates cell signal transduction by inhibiting tumor cell proliferation. As shown in Figure 7B, the keyword "tumor proliferation" mainly appeared in 2014. BBR inhibited the growth of human colon cancer cell lines Caco-2 and Lovo by reducing citrate synthase activity (Mantena et al., 2006). Moreover, BBR inhibited melanoma by increasing miRNA-582-5p and miRNA-188-5p levels and decreasing the expression of cell cycle-related proteins in melanoma A375 cells (Lin et al., 2005). Research on the mechanism associated with tumor proliferation mainly focuses on material metabolism; therefore, a deeper understanding of the molecular connections between cellular metabolism and growth regulation may ultimately result in more effective cancer treatments.

4.1.5 Berberine can induce autophagy of tumor cells

The cooperation network shown in Figure 7A shows that the keyword "autophagy" is closely connected with BBR. Autophagy, a type of programmed cell death, is crucial for preserving intracellular homeostasis. BBR induces autophagy by inhibiting the ERK1/2 signaling pathway in glioblastoma and further reduces temozolomide resistance (Qu et al., 2020). By inducing cytostatic autophagy and regulating the MAPK/mTOR/p70S6K and Akt signaling pathways, BBR inhibits the development of human gastric cancer cells both *in vitro* and *in vivo* (Zhang et al., 2020a). Despite substantial research on the regulation of autophagy by BBR in recent years, the precise mechanism remains unclear.

4.2 Applications of berberine

Figure 6 and Figure 7 list several conditions that can be regulated by BBR, including non-small-cell lung cancer, breast cancer, colorectal cancer, gut microbiota, and photodynamic therapy. Among these, the application of BBR in cancer has been the focus of research in recent years. The results are summarized in Table 8.

TABLE 8 BBR applications.

Application	Cell line	Effect	Reference
Non-small-cell lung cancer	A549, PC9, H1650, and H1299	Activation of the p38α MAPK signaling pathway	Wu et al. (2021)
		Induction of the protein expression of p53 and FOXO3a	
		Inhibit proliferation and induce apoptosis	
	A549, H157, H358, H460, H1299, H1975, and Lewis cells	Enhance tumor-infiltrating T-cell immunity and attenuate the activation of MDSCs and Tregs	Yang et al. (2021)
		Trigger PD-L1 degradation through the ubiquitin (Ub)/proteasome-dependent pathway	
	A549, NCI-H1299, and BEAS-2B	Suppression of epithelial–mesenchymal transition	Yin et al. (2022)
		Trigger cell cycle arrest	
		Suppression of HIF-1α expression	
	HCC827/AR, HCC827/AR0.5, HCC827/AR2, HCC827/ER, PC-9/AR, and PC-9/GR/AR	Act as a naturally existing MET inhibitor	Yu et al. (2020)
		Enhance induction of apoptosis through Bim elevation and Mcl-1 reduction	
Breast cancer	HEK293, SMCC-7721, and ZR-75-30	Decrease the expression of ephrin-B2 and its PDZ-binding proteins	Zhang et al. (2021a)
		Downregulate the phosphorylation of VEGFR2 and downstream signaling members (AKT and Erk1/2)	
		Downregulate the expression of MMP-2 and MMP-9	
	MCF-7 and MCF-7/MDR	Enhance sensitivity in drug-resistance breast cancer cells	Zhang et al. (2020a), Zhang et al. (2021b)
		Induce apoptosis	
	MDA-MB-231 and BT549	Induce DSB	Zhang et al. (2020b)
		Increase the release of cytochrome c	
		Trigger the caspase-9-dependent apoptosis	
Colorectal cancer	HT-29, SW480, and NIH3T3-Light2 cell lines	Suppression of the paracrine sonic hedgehog (SHH) signaling	Zhang et al. (2020c)
		Inhibition of the secretion and expression of SHH protein	
	HCT116 and SW480	Inhibit proliferation and induce G0/G1 phase arrest	Zhao et al. (2017)
		Knockdown of IGF2BP3 could suppress the PI3K/AKT pathway to inhibit cell proliferation and cycle transition	
	HCT-8, HCT-116, and HT-29	Suppress lipogenesis *via* promotion of PLZF-mediated SCAP ubiquitination	Zhao et al. (2022)
	HCT116, SW48, RKO, Caco-2, SW480, and HT-29	Suppression of DNA replication	Zheng et al. (2014)
Gut microbiota	Brain neuron cells	Accelerate the production of L-DOPA by intestinal bacteria	Zheng et al. (2021)
	P. mirabilis, *S. boydii*, and *B. fragilis* (intestinal bacterial strains)	Reduce the biosynthesis of TMAO by interacting with the enzyme/coenzyme containing (CutC) and (FMO)	Zhong and Song (2008)
	β-cells	Inhibit the biotransformation of DCA by *Ruminococcus bromii*	Zhuang et al. (2018)
Photodynamic therapy	ACHN, 786-O, and HK-2	Increase reactive oxygen species	[71]
		Increase autophagy levels and apoptosis by caspase 3 activity	
	A375, M8, SK-Mel-19, and the cisplatin-resistant cell lines A375/DDP, M8/DDP, and SK-Mel-19/DDP	Activate the P38 MAPK signaling pathway	[72]

4.2.1 Non-small-cell lung cancer

Figure 6C shows a research hotspot focused on non-small cell lung cancer. Several mechanisms by which BBR inhibits non-small cell lung cancer have been reported. For example, Zheng et al. (2014) reported that BBR induces apoptosis of NSCLC cells to prevent growth and is involved in activating the p38α MAPK signaling pathway and subsequent increased protein expression of p53 and FOXO3a. BBR plays also an anti-tumor role from the perspective of

immunity, as it can specifically bind to glutamic acid 76 of constitutive photomorphogenic-9 signalosome 5 (CSN5) and inhibit the PD-1/PD-L1 axis through its deubiquitylation activity, leading to the PD-L1 ubiquitination and destruction (Liu et al., 2020). In addition, BBR and its derivatives are considered potential drugs for the treatment of NSCLC. Liu et al. (2021) demonstrated that the derivative of BBR, demethyleneberberine (DMB), exerts an anti-tumor effect leading to cell arrest and cellular senescence in NSCLC. In addition, BBR can be combined with other drugs such as osimertinib (Chen et al., 2022). These findings demonstrate that BBR exerts anti-tumor effects through various mechanisms.

4.2.2 Breast cancer

According to the keyword analysis (Figure 7A), "breast cancer" is also an aspect of BBR research. Ma et al. (2017) reported that BBR prevents the proliferation and migration of breast cancer ZR-75-30 cells by regulating ephrin-B2. BBR also increases chemosensitivity, reverses hypoxia-induced chemoresistance, and further induces apoptosis in breast cancer (Pan et al., 2017b; Pan et al., 2017c). Moreover, Zhao et al. (2017) reported that BBR inhibits triple-negative breast cancer. BBR induces caspase-9/cytochrome c-mediated apoptosis both *in vitro* and *in vivo* to inhibit the proliferation of TNBC cells. Thus, BBR has been used to treat breast cancer.

4.2.3 Colorectal cancer

BBR inhibits colorectal tumor development A previous study showed that BBR reduces paracrine sonic hedgehog (SHH) signaling, which in turn reduces colon cancer growth *in vitro* and *in vivo* (Shen et al., 2021). This revealed a novel molecular mechanism for the anti-cancer effects of BBR. BBR inhibits proliferation through cell cycle arrest-related pathways. BBR has been reported to induce G0/G1 phase arrest in colorectal cancer cells by downregulating the targeted gene *IGF2BP3* (Zhang et al., 2020c). Moreover, BBR showed potential anti-migration and anti-invasion properties in cell lines including HCT-8, HCT-116, and HT-29. BBR reduces lipogenesis and the spread of colon cancer cells by promoting PLZF-mediated SCAP ubiquitination (Liu et al., 2022b). Meanwhile, several studies have reported on BBR combined with other drugs, for example, the combination with *Andrographis* to treat colorectal cancer (Zhao et al., 2022). BBR is well known as a potential drug for the treatment of colon cancer.

4.2.4 Gut microbiota

Figure 6C shows that cluster 11 (gut microbiota) is a current research hotspot. The gut microbiota includes a large number and a wide range of species that are interdependent and interact with the host. The occurrence, development, and prognosis of many human diseases are closely related to intestinal flora. In 2021, Wang et al. (2021b) introduced oral BBR to accelerate the production of L-dopa by intestinal bacteria. The L-DOPA produced by intestinal bacteria enters the brain through circulation and is converted to dopamine, significantly increasing the brain dopamine levels of mice and improving PD expression. Ma et al. (2022) demonstrated that oral BBR reduced the biosynthesis of trimethylamine-N-oxide (TMAO), an atherogenic metabolite derived from the gut microbiota in the intestine, by interacting with the enzyme/coenzyme containing choline trimethylamine lyase (CutC) and lutein monooxygenase (FMO) in the intestinal microbiota, thus playing a role in the treatment of atherosclerosis. In addition, the human intestinal microbiome is a promising target for the treatment of type 2 diabetes. BBR reduces blood sugar levels by inhibiting the biotransformation of DCA by *Ruminococcus bromii* (Zhang et al., 2020b). Intestinal microorganisms affect the occurrence and development of metabolic diseases by regulating the metabolism of sugars, lipids, and amino acids and are inextricably linked with diseases of the neuropsychiatric, cardiovascular, urinary, and other systems. Therefore, it is of great significance to study the correlation between intestinal flora and diseases for the prevention and treatment of diseases and the maintenance of human health.

4.2.5 Photodynamic therapy

BBR is well known for its anti-inflammatory, antioxidant, anti-diabetes, anti-obesity, and anti-cancer properties; however, little is known about its photosensitive properties, and it might serve as a new kind of photodynamic therapeutic agent. Our analysis of co-cited references (Figure 6C) showed that photodynamic therapy is a hotspot of current research in BBR. For example, a study that assessed the effects of BBR on PDT in renal cancer cell lines reported increased reactive oxygen species (ROS) levels after treatment with BBR associated with PDT, which was accompanied by increased autophagy levels and apoptosis due to caspase 3 activity (Lopes et al., 2020). Wang et al. (2021a) reported that a combination of cisplatin and BBR-PDT played a role in cisplatin-resistant melanoma cells. The experimental findings showed that mitochondrial apoptotic pathways that depend on caspases were the mode of cell death and that BBR photodynamic therapy modulated apoptosis by activating the P38 MAPK signaling pathway. The number of articles on BBR photosensitivity therapy is currently small, and most have focused on the treatment and application of cancer, which may suggest that photosensitivity therapy could provide a new method for cancer treatment.

BBR is a natural compound with great biological activity that is effective against various diseases. The literature review showed that increasing numbers of BBR derivatives have been created and used in disease research. BBR can be used as a combination drug in the study of drug-resistant cell lines and has shown significant effects. The ability of BBR to disrupt intracellular pathways and its intrinsic features has been the subject of numerous investigations in recent years. More importantly, BBR has been investigated as a curative medication in both animal models and human cell lines. However, there remain many issues to resolve; for example, BBR alone has not been tested in humans and it has weak water solubility, reduced oral absorption, and low bioavailability. Therefore, future studies should focus on the clinical use of BBR.

5 Conclusion

This study analyzed publications, research topics, research hotspots, and development trends of research in the field of BBR and tumors through systematic bibliometric analysis. Chinese researchers have produced the most publications; however, articles published in the United States ranked first in terms of

average citations per article. The most prolific universities are China Medical University (Taiwan) and Sun Yat-sen University. The terms "mechanism," "molecular docking," and "oxidative stress" are now popular study topics related to BBR in tumors.

Data availability statement

The original contributions presented in the study are included in the article/Supplementary Material; further inquiries can be directed to the corresponding authors.

Author contributions

All authors contributed significantly to the work that was published, whether it was in ideation, study design, data collection, analysis, etc. All authors also participated in writing, revising, or critically evaluating the article; gave their final approval for the published version; decided on the journal to which the article would be submitted; and agreed to be responsible for all aspects of the work.

Funding

This study was supported by the Shenzhen Natural Science Foundation (KCXFZ20201221173600001).

Conflict of interest

The authors declare that the research was conducted in the absence of any commercial or financial relationships that could be construed as a potential conflict of interest.

Publisher's note

All claims expressed in this article are solely those of the authors and do not necessarily represent those of their affiliated organizations, or those of the publisher, the editors and the reviewers. Any product that may be evaluated in this article, or claim that may be made by its manufacturer, is not guaranteed or endorsed by the publisher.

References

Al-Bari, M. A. A., Ito, Y., Ahmed, S., Radwan, N., Ahmed, H. S., and Eid, N. (2021). Targeting autophagy with natural products as a potential therapeutic approach for cancer. *Int. J. Mol. Sci.* 22, 9807. doi:10.3390/ijms22189807

Chen, C., Dubin, R., and Kim, M. C. (2014). Emerging trends and new developments in regenerative medicine: A scientometric update (2000 - 2014). *Expert Opin. Biol. Ther.* 14, 1295–1317. doi:10.1517/14712598.2014.920813

Chen, C., and Leydesdorff, L. (2014). Patterns of connections and movements in dual-map overlays: A new method of publication portfolio analysis. *J. Assoc. Inf. Sci. Technol.* 65, 334–351. doi:10.1002/asi.22968

Chen, Z., Vallega, K. A., Chen, H., Zhou, J., Ramalingam, S. S., and Sun, S.-Y. (2022). The natural product berberine synergizes with osimertinib preferentially against MET-amplified osimertinib-resistant lung cancer via direct MET inhibition. *Pharmacol. Res.* 175, 105998. doi:10.1016/j.phrs.2021.105998

Cheng, K., Guo, Q., Yang, W., Wang, Y., Sun, Z., and Wu, H. (2022). Mapping knowledge landscapes and emerging trends of the links between bone metabolism and diabetes mellitus: A bibliometric analysis from 2000 to 2021. *Front. Public Health* 10, 918483. doi:10.3389/fpubh.2022.918483

Choudhari, A. S., Mandave, P. C., Deshpande, M., Ranjekar, P., and Prakash, O. (2019). Phytochemicals in cancer treatment: From preclinical studies to clinical practice. *Front. Pharmacol.* 10, 1614. doi:10.3389/fphar.2019.01614

Colagiuri, B., Dhillon, H., Butow, P. N., Jansen, J., Cox, K., and Jacquet, J. (2013). Does assessing patients' expectancies about chemotherapy side effects influence their occurrence? *J. Pain Symptom Manag.* 46, 275–281. doi:10.1016/j.jpainsymman.2012.07.013

Dalian (2008). *Peoples R China*, 11529–11532.

Du, H., Gu, J., Peng, Q., Wang, X., Liu, L., Shu, X., et al. (2021). Berberine suppresses EMT in liver and gastric carcinoma cells through combination with TGFR regulating TGF-/smad pathway. *Oxidative Med. Cell. Longev.* 2021, 2337818. doi:10.1155/2021/2337818

Eo, S.-H., Kim, J.-H., and Kim, S.-J. (2014). Induction of G2/M arrest by berberine via activation of PI3K/Akt and p38 in human chondrosarcoma cell line. *Oncol. Res.* 22, 147–157. doi:10.3727/096504015X14298122915583

Feng, X. J., Sureda, A., Jafari, S., Memariani, Z., Tewari, D., Annunziata, G., et al. (2019). Berberine in cardiovascular and metabolic diseases: From mechanisms to therapeutics. *Theranostics* 9, 1923–1951. doi:10.7150/thno.30787

Hashem, S., Ali, T. A., Akhtar, S., Nisar, S., Sageena, G., Ali, S., et al. (2022). Targeting cancer signaling pathways by natural products: Exploring promising anti-cancer agents. *Biomed. Pharmacother. = Biomedecine Pharmacother.* 150, 113054. doi:10.1016/j.biopha.2022.113054

Hirsch, J. E. (2005). An index to quantify an individual's scientific research output. *Proc. Natl. Acad. Sci. U. S. A.* 102, 16569–16572. doi:10.1073/pnas.0507655102

Katz, J. S., and Martin, B. R. (1997). What is research collaboration? *Res. Policy* 26, 1–18. doi:10.1016/s0048-7333(96)00917-1

Kim, J. B., Yu, J. H., Ko, E., Lee, K. W., Song, A. K., Park, S. Y., et al. (2010). The alkaloid Berberine inhibits the growth of Anoikis-resistant MCF-7 and MDA-MB-231 breast cancer cell lines by inducing cell cycle arrest. *Phytomedicine Int. J. Phytotherapy Phytopharm.* 17, 436–440. doi:10.1016/j.phymed.2009.08.012

Kim, S., You, D., Jeong, Y., Yu, J., Kim, S. W., Nam, S. J., et al. (2018). Berberine down-regulates IL-8 expression through inhibition of the EGFR/MEK/ERK pathway in triple-negative breast cancer cells. *Phytomedicine Int. J. Phytotherapy Phytopharm.* 50, 43–49. doi:10.1016/j.phymed.2018.08.004

Koperska, A., Wesołek, A., Moszak, M., and Szulińska, M. (2022). Berberine in non-alcoholic fatty liver disease-A review. *Nutrients* 14, 3459. doi:10.3390/nu14173459

Kumar, M. S., and Adki, K. M. (2018). Marine natural products for multi-targeted cancer treatment: A future insight. *Biomed. Pharmacother. = Biomedecine Pharmacother.* 105, 233–245. doi:10.1016/j.biopha.2018.05.142

Kuo, C.-L., Chi, C.-W., and Liu, T.-Y. (2004). The anti-inflammatory potential of berberine *in vitro* and *in vivo*. *Cancer Lett.* 203, 127–137. doi:10.1016/j.canlet.2003.09.002

Lacouture, M., and Sibaud, V. (2018). Toxic side effects of targeted therapies and immunotherapies affecting the skin, oral mucosa, hair, and nails. *Am. J. Clin. Dermatology* 19, 31–39. doi:10.1007/s40257-018-0384-3

Li, T., Wang, P., Guo, W., Huang, X., Tian, X., Wu, G., et al. (2019). Natural berberine-based Chinese herb medicine assembled nanostructures with modified antibacterial application. *ACS Nano* 13, 6770–6781. doi:10.1021/acsnano.9b01346

Lin, S. S., Chung, J. G., Lin, J. P., Chuang, J. Y., Chang, W. C., Wu, J. Y., et al. (2005). Berberine inhibits arylamine N-acetyltransferase activity and gene expression in mouse leukemia L 1210 cells. *Phytomedicine Int. J. Phytotherapy Phytopharm.* 12, 351–358. doi:10.1016/j.phymed.2003.11.008

Liu, J., Huang, X., Liu, D., Ji, K., Tao, C., Zhang, R., et al. (2021). Demethyleneberberine induces cell cycle arrest and cellular senescence of NSCLC cells via c-Myc/HIF-1α pathway. *Phytomedicine Int. J. Phytotherapy Phytopharm.* 91, 153678. doi:10.1016/j.phymed.2021.153678

Liu, L., Fan, J., Ai, G., Liu, J., Luo, N., Li, C., et al. (2019). Berberine in combination with cisplatin induces necroptosis and apoptosis in ovarian cancer cells. *Biol. Res.* 52, 37. doi:10.1186/s40659-019-0243-6

Liu, Q., Tang, J., Chen, S., Hu, S., Shen, C., Xiang, J., et al. (2022a). Berberine for gastric cancer prevention and treatment: Multi-step actions on the Correa's cascade underlie its therapeutic effects. *Pharmacol. Res.* 184, 106440. doi:10.1016/j.phrs.2022.106440

Liu, Y., Fang, X., Li, Y., Bing, L., Li, Y., Fang, J., et al. (2022b). Berberine suppresses the migration and invasion of colon cancer cells by inhibition of lipogenesis through modulation of promyelocytic leukemia zinc finger-mediated sterol-regulatory element binding proteins cleavage-activating protein ubiquitination. *J. Pharm. Pharmacol.* 74, 1353–1363. doi:10.1093/jpp/rgac026

Liu, Y., Liu, X., Zhang, N., Yin, M., Dong, J., Zeng, Q., et al. (2020). Berberine diminishes cancer cell PD-L1 expression and facilitates antitumor immunity *via*

inhibiting the deubiquitination activity of CSN5. *Acta Pharm. Sin. B* 10, 2299–2312. doi:10.1016/j.apsb.2020.06.014

Lopes, T. Z., De Moraes, F. R., Tedesco, A. C., Arni, R. K., Rahal, P., and Calmon, M. F. (2020). Berberine associated photodynamic therapy promotes autophagy and apoptosis via ROS generation in renal carcinoma cells. *Biomed. Pharmacother. = Biomedecine Pharmacother.* 123, 109794. doi:10.1016/j.biopha.2019.109794

Ma, S.-R., Tong, Q., Lin, Y., Pan, L.-B., Fu, J., Peng, R., et al. (2022). Berberine treats atherosclerosis via a vitamine-like effect down-regulating Choline-TMA-TMAO production pathway in gut microbiota. *Signal Transduct. Target. Ther.* 7, 207. doi:10.1038/s41392-022-01027-6

Ma, W., Zhu, M., Zhang, D., Yang, L., Yang, T., Li, X., et al. (2017). Berberine inhibits the proliferation and migration of breast cancer ZR-75-30 cells by targeting Ephrin-B2. *Phytomedicine Int. J. Phytotherapy Phytopharm.* 25, 45–51. doi:10.1016/j.phymed.2016.12.013

Mantena, S. K., Sharma, S. D., and Katiyar, S. K. (2006). Berberine, a natural product, induces G1-phase cell cycle arrest and caspase-3-dependent apoptosis in human prostate carcinoma cells. *Mol. Cancer Ther.* 5, 296–308. doi:10.1158/1535-7163.MCT-05-0448

Mignani, S., Rodrigues, J., Tomas, H., Zablocka, M., Shi, X., Caminade, A.-M., et al. (2018). Dendrimers in combination with natural products and analogues as anti-cancer agents. *Chem. Soc. Rev.* 47, 514–532. doi:10.1039/c7cs00550d

Mitani, N., Murakami, K., Yamaura, T., Ikeda, T., and Saiki, I. (2001). Inhibitory effect of berberine on the mediastinal lymph node metastasis produced by orthotopic implantation of Lewis lung carcinoma. *Cancer Lett.* 165, 35–42. doi:10.1016/s0304-3835(00)00710-2

Mullard, A. (2020). Addressing cancer's grand challenges. *Nat. Rev. Drug Discov.* 19, 825–826. doi:10.1038/d41573-020-00202-0

Musbahi, A., Rao, C. B., and Immanuel, A. (2022). A bibliometric analysis of robotic surgery from 2001 to 2021. *World J. Surg.* 46, 1314–1324. doi:10.1007/s00268-022-06492-2

Nastiuk, K. L., and Krolewski, J. J. (2016). Opportunities and challenges in combination gene cancer therapy. *Adv. Drug Deliv. Rev.* 98, 35–40. doi:10.1016/j.addr.2015.12.005

Ortiz, L. M. G., Lombardi, P., Tillhon, M., and Scovassi, A. I. (2014). Berberine, an epiphany against cancer. *Mol. (Basel, Switz.* 19, 12349–12367. doi:10.3390/molecules190812349

Pan, X. L., Cui, M., Yu, X. T., and Hua, W. N. (2017). "How is CiteSpace used and cited in the literature? An analysis of the articles published in English and Chinese core journals," in 16th International Conference on Scientometrics and Informetrics (ISSI), Oct 16-20 2017a Wuhan Univ (Wuhan, PEOPLES R CHINA: ISSI), 158–165.

Pan, Y., Shao, D., Zhao, Y., Zhang, F., Zheng, X., Tan, Y., et al. (2017b). Berberine reverses hypoxia-induced chemoresistance in breast cancer through the inhibition of AMPK- HIF-1α. *Int. J. Biol. Sci.* 13, 794–803. doi:10.7150/ijbs.18969

Pan, Y., Zhang, F., Zhao, Y., Shao, D., Zheng, X., Chen, Y., et al. (2017c). Berberine enhances chemosensitivity and induces apoptosis through dose-orchestrated AMPK signaling in breast cancer. *J. Cancer* 8, 1679–1689. doi:10.7150/jca.19106

Qin, Y.-F., Ren, S.-H., Shao, B., Qin, H., Wang, H.-D., Li, G.-M., et al. (2022). The intellectual base and research fronts of IL-37: A bibliometric review of the literature from WoSCC. *Front. Immunol.* 13, 931783. doi:10.3389/fimmu.2022.931783

Qu, H., Song, X., Song, Z., Jiang, X., Gao, X., Bai, L., et al. (2020). Berberine reduces temozolomide resistance by inducing autophagy via the ERK1/2 signaling pathway in glioblastoma. *Cancer Cell Int.* 20, 592. doi:10.1186/s12935-020-01693-y

Rejhová, A., Opattová, A., Čumová, A., SlíVA, D., and Vodička, P. (2018). Natural compounds and combination therapy in colorectal cancer treatment. *Eur. J. Med. Chem.* 144, 582–594. doi:10.1016/j.ejmech.2017.12.039

Ruan, H., Zhan, Y. Y., Hou, J., Xu, B., Chen, B., Tian, Y., et al. (2017). Berberine binds RXRα to suppress β-catenin signaling in colon cancer cells. *Oncogene* 36, 6906–6918. doi:10.1038/onc.2017.296

Shen, Z.-Q., Wang, J., Tan, W.-F., and Huang, T.-M. (2021). Berberine inhibits colorectal tumor growth by suppressing SHH secretion. *Acta Pharmacol. Sin.* 42, 1190–1194. doi:10.1038/s41401-020-00514-2

Singh, R., Letai, A., and Sarosiek, K. (2019). Regulation of apoptosis in health and disease: The balancing act of BCL-2 family proteins. *Nat. Rev. Mol. Cell Biol.* 20, 175–193. doi:10.1038/s41580-018-0089-8

Song, D., Hao, J., and Fan, D. (2020). Biological properties and clinical applications of berberine. *Front. Med.* 14, 564–582. doi:10.1007/s11684-019-0724-6

Sun, Q., Gong, T., Liu, M. L., Ren, S., Yang, H., Zeng, S., et al. (2022a). Shikonin, a naphthalene ingredient: Therapeutic actions, pharmacokinetics, toxicology, clinical trials and pharmaceutical researches. *Phytomedicine* 94, 153805. doi:10.1016/j.phymed.2021.153805

Sun, Q., Yang, H., Liu, M. L., Ren, S., Zhao, H., Ming, T. Q., et al. (2022b). Berberine suppresses colorectal cancer by regulation of Hedgehog signaling pathway activity and gut microbiota. *Phytomedicine* 103, 154227. doi:10.1016/j.phymed.2022.154227

Sung, H., Ferlay, J., Siegel, R. L., Laversanne, M., Soerjomataram, I., Jemal, A., et al. (2021). Global cancer statistics 2020: GLOBOCAN estimates of incidence and mortality worldwide for 36 cancers in 185 countries. *Ca-a Cancer J. Clin.* 71, 209–249. doi:10.3322/caac.21660

Szakacs, G., Paterson, J. K., Ludwig, J. A., Booth-Genthe, C., and Gottesman, M. M. (2006). Targeting multidrug resistance in cancer. *Nat. Rev. Drug Discov.* 5, 219–234. doi:10.1038/nrd1984

Van Eck, N. J., and Waltman, L. (2010). Software survey: VOSviewer, a computer program for bibliometric mapping. *Scientometrics* 84, 523–538. doi:10.1007/s11192-009-0146-3

Wang, X., Gong, Q., Song, C., Fang, J., Yang, Y., Liang, X., et al. (2021a). Berberine-photodynamic therapy sensitizes melanoma cells to cisplatin-induced apoptosis through ROS-mediated P38 MAPK pathways. *Toxicol. Appl. Pharmacol.* 418, 115484. doi:10.1016/j.taap.2021.115484

Wang, Y., Tong, Q., Ma, S.-R., Zhao, Z.-X., Pan, L.-B., Cong, L., et al. (2021b). Oral berberine improves brain dopa/dopamine levels to ameliorate Parkinson's disease by regulating gut microbiota. *Signal Transduct. Target. Ther.* 6, 77. doi:10.1038/s41392-020-00456-5

Wartenberg, M., Budde, P., De MareéS, M., GrüNHECK, F., Tsang, S. Y., Huang, Y., et al. (2003). Inhibition of tumor-induced angiogenesis and matrix-metalloproteinase expression in confrontation cultures of embryoid bodies and tumor spheroids by plant ingredients used in traditional Chinese medicine. *Laboratory Investigation; a J. Tech. Methods Pathology* 83, 87–98. doi:10.1097/01.lab.0000049348.51663.2f

Wu, H., Zhou, Y., Wang, Y., Tong, L., Wang, F., Song, S., et al. (2021). Current state and future directions of intranasal delivery route for central nervous system disorders: A scientometric and visualization analysis. *Front. Pharmacol.* 12, 717192. doi:10.3389/fphar.2021.717192

Yang, X.-H., Zhang, L.-J., Luo, M.-J., Luo, S., Gong, Y.-Y., and Chen, T. (2021). Research progress in mechanism of berberine's antitumor action. *Zhongguo Zhong Yao Za Zhi = Zhongguo Zhongyao Zazhi = China J. Chin. Materia Medica* 46, 2449–2455. doi:10.19540/j.cnki.cjcmm.20210209.601

Yin, H., Zhang, F., Yang, X., Meng, X., Miao, Y., Hussain, M. S. N., et al. (2022). Research trends of artificial intelligence in pancreatic cancer: A bibliometric analysis. *Front. Oncol.* 12, 973999. doi:10.3389/fonc.2022.973999

Yu, Y. T., Li, Y. J., Zhang, Z. H., Gu, Z. C., Zhong, H., Zha, Q. F., et al. (2020). A bibliometric analysis using VOSviewer of publications on COVID-19. *Ann. Transl. Med.* 8, 816. doi:10.21037/atm-20-4235

Zhang, J., Song, L., Xu, L., Fan, Y., Wang, T., Tian, W., et al. (2021a). Knowledge domain and emerging trends in ferroptosis research: A bibliometric and knowledge-map analysis. *Front. Oncol.* 11, 686726. doi:10.3389/fonc.2021.686726

Zhang, Q., Wang, X., Cao, S., Sun, Y., He, X., Jiang, B., et al. (2020a). Berberine represses human gastric cancer cell growth *in vitro* and *in vivo* by inducing cytostatic autophagy via inhibition of MAPK/mTOR/p70S6K and Akt signaling pathways. *Biomed. Pharmacother. = Biomedecine Pharmacother.* 128, 110245. doi:10.1016/j.biopha.2020.110245

Zhang, S.-W., Zhou, J., Gober, H.-J., Leung, W. T., and Wang, L. (2021b). Effect and mechanism of berberine against polycystic ovary syndrome. *Biomed. Pharmacother. = Biomedecine Pharmacother.* 138, 111468. doi:10.1016/j.biopha.2021.111468

Zhang, Y., Gu, Y., Ren, H., Wang, S., Zhong, H., Zhao, X., et al. (2020b). Gut microbiome-related effects of berberine and probiotics on type 2 diabetes (the PREMOTE study). *Nat. Commun.* 11, 5015. doi:10.1038/s41467-020-18414-8

Zhang, Y., Liu, X., Yu, M., Xu, M., Xiao, Y., Ma, W., et al. (2020c). Berberine inhibits proliferation and induces G0/G1 phase arrest in colorectal cancer cells by downregulating IGF2BP3. *Life Sci.* 260, 118413. doi:10.1016/j.lfs.2020.118413

Zhao, Y., Jing, Z., Lv, J., Zhang, Z., Lin, J., Cao, X., et al. (2017). Berberine activates caspase-9/cytochrome c-mediated apoptosis to suppress triple-negative breast cancer cells *in vitro* and *in vivo*. *Biomed. Pharmacother. = Biomedecine Pharmacother.* 95, 18–24. doi:10.1016/j.biopha.2017.08.045

Zhao, Y., Roy, S., Wang, C., and Goel, A. (2022)., 15. Pharmaceuticals (Basel, Switzerland), 262. doi:10.3390/ph15030262A combined treatment with berberine and andrographis exhibits enhanced anti-cancer activity through suppression of DNA replication in colorectal cancer*Pharmaceuticals*

Zheng, F., Tang, Q., Wu, J., Zhao, S., Liang, Z., Li, L., et al. (2014). p38α MAPK-mediated induction and interaction of FOXO3a and p53 contribute to the inhibited-growth and induced-apoptosis of human lung adenocarcinoma cells by berberine. *J. Exp. Clin. Cancer Res. CR* 33, 36. doi:10.1186/1756-9966-33-36

Zheng, X., Zhao, Y., Jia, Y., Shao, D., Zhang, F., Sun, M., et al. (2021). Biomimetic co-assembled nanodrug of doxorubicin and berberine suppresses chemotherapy-exacerbated breast cancer metastasis. *Biomaterials* 271, 120716. doi:10.1016/j.biomaterials.2021.120716

Zhong, Q., and Song, J. (2008). "The developing trend research of knowledge management overseas based on word frequency analysis," in 4th International Conference on Wireless Communications, Networking and Mobile Computing (IEEE).

Zhuang, W., Li, T., Wang, C., Shi, X., Li, Y., Zhang, S., et al. (2018). Berberine exerts antioxidant effects via protection of spiral ganglion cells against cytomegalovirus-induced apoptosis. *Free Radic. Biol. Med.* 121, 127–135. doi:10.1016/j.freeradbiomed.2018.04.575

Frontiers in Pharmacology

Explores the interactions between chemicals and living beings

The most cited journal in its field, which advances access to pharmacological discoveries to prevent and treat human disease.

Discover the latest Research Topics

See more →

Frontiers

Avenue du Tribunal-Fédéral 34
1005 Lausanne, Switzerland
frontiersin.org

Contact us

+41 (0)21 510 17 00
frontiersin.org/about/contact